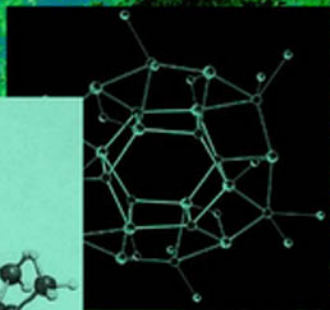
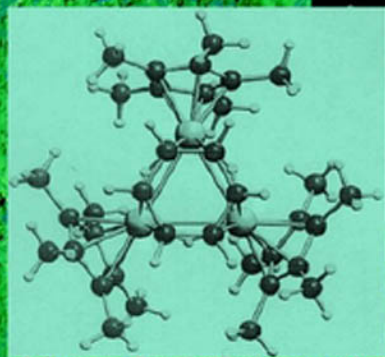


PHYSICAL ORGANOMETALLIC CHEMISTRY



WILEY

UNUSUAL STRUCTURES AND PHYSICAL PROPERTIES IN ORGANOMETALLIC CHEMISTRY



Edited by Marcel Gielen
Rudolph Willem
Bernd Wrackmeyer

PHYSICAL ORGANOMETALLIC
CHEMISTRY VOLUME 3

Unusual Structures and
Physical Properties in
Organometallic
Chemistry

Edited by

MARCEL GIELEN

Free University of Brussels, Belgium

RUDOLPH WILLEM

Free University of Brussels, Belgium

BERND WRACKMEYER

Universität Bayreuth, Germany



JOHN WILEY & SONS, LTD

Physical Organometallic Chemistry

Editorial Board

Marcel Gielen, Free University of Brussels, Belgium
Rudolph Willem, Free University of Brussels, Belgium
Bernd Wrackmeyer, Universität Bayreuth, Germany

Books previously published in this Series

Volume 1 **Advanced Applications of NMR to Organometallic Chemistry**

Edited by

Marcel Gielen, Free University of Brussels, Belgium
Rudolph Willem, Free University of Brussels, Belgium
Bernd Wrackmeyer, Universität Bayreuth, Germany
ISBN 0 471 95938 3

Volume 2 **Solid State Organometallic Chemistry: Methods and Applications**

Edited by

Marcel Gielen, Free University of Brussels, Belgium
Rudolph Willem, Free University of Brussels, Belgium
Bernd Wrackmeyer, Universität Bayreuth, Germany
ISBN 0 471 97920 1

PHYSICAL ORGANOMETALLIC
CHEMISTRY VOLUME 3

Unusual Structures and
Physical Properties in
Organometallic
Chemistry

Edited by

MARCEL GIELEN

Free University of Brussels, Belgium

RUDOLPH WILLEM

Free University of Brussels, Belgium

BERND WRACKMEYER

Universität Bayreuth, Germany



JOHN WILEY & SONS, LTD

Copyright © 2002 John Wiley & Sons, Ltd, The Atrium
West Sussex PO19 1UD, England

Phone (+44) 1243 779777

Email (for orders and customer service enquiries): cs-books@wiley.co.uk
Visit our Home Page on www.wiley.co.uk or www.wiley.com

All Rights Reserved. No part of this publication may be reproduced, stored in a retrieval system or transmitted in any form or by any means, electronic, mechanical, photocopying, recording, scanning or otherwise, except under the terms of the Copyright, Designs and Patents Act 1988 or under the terms of a licence issued by the Copyright Licensing Agency Ltd., 90 Tottenham Court Road, London W1P 0LP, UK, without the permission in writing of the Publisher. Requests to the Publisher should be addressed to the Permissions Department, John Wiley & Sons, Ltd., The Atrium, Southern Gate, Chichester, West Sussex P019 8SQ, England, or emailed to permreq@wiley.co.uk, or faxed to (+44) 1243 770571.

This publication is designed to provide accurate and authoritative information in regard to the subject matter covered. It is sold on the understanding that the Publisher is not engaged in rendering professional services. If professional advice or other expert assistance is required, the services of a competent professional should be sought.

Other Wiley Editorial Offices

John Wiley & Sons, Inc., 111 River Street, Hoboken, NJ 07030, USA

Jossey-Bass, 989 Market Street, San Francisco, CA 94103-1741, USA

Wiley-VCH Verlag GmbH, Pappelallee 3, D-69469 Weinheim, Germany

John Wiley & Sons Australia, Ltd., 33 Park Road, Milton, Queensland 4064, Australia

John Wiley & Sons (Asia) Pte Ltd., 2 Clementi Loop # 02-01, Jin Xing Distripark, Singapore 129809

John Wiley & Sons Canada, Ltd., 22 Worcester Road, Etobicoke, Ontario, Canada M9W 1L1

British Library Cataloguing in Publication Data

A catalogue record for this book is available from the British Library

ISBN 0-471-49635-9

Typeset in 10/12pt Times by Kolam Information Services Pvt. Ltd, Pondicherry, India.

Printed and bound in Great Britain by Biddles Ltd, Guildford, Surrey.

This book is printed on acid-free paper responsibly manufactured from sustainable forestry in which at least two trees are planted for each one used for paper production.

Contents

Contributors	xv
Series Preface	xvii
Preface	xix
1 Structure and Electrochemistry of Transition Metal Carbonyl Clusters with Interstitial or Semi-Interstitial Atoms: Contrast between Nitrides or Phosphides and Carbides	
<i>Piero Zanello</i>	
1 Introduction	2
2 Homonuclear Clusters	6
2.1 Homonuclear Iron Clusters	6
2.1.1 $\text{Fe}_4(\text{C})(\text{CO})_{13}$ and $[\text{Fe}_4(\text{C})(\text{CO})_{12}]^{2-}$ versus $[\text{Fe}_4(\text{N})(\text{CO})_{12}]^-$	6
2.1.2 $\text{Fe}_5(\text{C})(\text{CO})_{15}$ and $[\text{Fe}_5(\text{C})(\text{CO})_{14}]^{2-}$ versus $[\text{Fe}_5(\text{N})(\text{CO})_{14}]^-$	11
2.1.3 $[\text{Fe}_6(\text{C})(\text{CO})_{16}]^{2-}$ versus $[\text{Fe}_6(\text{N})(\text{CO})_{15}]^{3-}$	13
2.2 Homonuclear Ruthenium Clusters	15
2.2.1 $\text{Ru}_5(\text{C})(\text{CO})_{15}$ versus $[\text{Ru}_5(\text{N})(\text{CO})_{14}]^-$	15
2.2.2 $[\text{Ru}_8(\text{P})(\text{CO})_{22}]^-$	15
2.2.3 $[\text{Ru}_{10}(\text{C})(\text{CO})_{24}]^{2-}$	16
2.2.4 Further Structural Data	18
2.3 Homonuclear Osmium Clusters	18
2.3.1 $[\text{Os}_5(\text{C})(\text{CO})_{14}]^{2-}$ and $\text{Os}_5(\text{C})(\text{CO})_{15}$	18
2.3.2 $[\text{Os}_6(\text{P})(\text{CO})_{18}]^-$	18
2.3.3 $[\text{Os}_{10}(\text{C})(\text{CO})_{24}]^{2-}$	19
2.3.4 Further Structural Data	20
2.4 Homonuclear Cobalt Clusters	21
2.4.1 $[\text{Co}_6(\text{C})(\text{CO})_{15}]^{2-}$ versus $[\text{Co}_6(\text{N})(\text{CO})_{15}]^-$ and $[\text{Co}_6(\text{P})(\text{CO})_{16}]^-$; $[\text{Co}_6(\text{C})_2(\text{CO})_{18}]$	21
2.4.2 $[\text{Co}_7(\text{N})(\text{CO})_{15}]^{2-}$	22
2.4.3 $[\text{Co}_8(\text{C})(\text{CO})_{18}]^{2-}$	24
2.4.4 $[\text{Co}_9(\text{P})(\text{CO})_{21}]^{2-}$ and $[\text{Co}_{10}(\text{P})(\text{CO})_{22}]^{3-}$	24
2.4.5 $[(\text{Co}_{13}(\text{C})_2(\text{CO})_{24})]^{4-}$ versus $[\text{Co}_{13}(\text{N})_2(\text{CO})_{24}]^{3-}$	24

2.4.6	Further Structural Data	27
2.5	Homonuclear Rhodium Clusters	29
2.5.1	$[\text{Rh}_6(\text{C})(\text{CO})_{15}]^{2-}$ versus $[\text{Rh}_6(\text{N})(\text{CO})_{15}]^-$	29
2.5.2	$[\text{Rh}_7(\text{N})(\text{CO})_{15}]^{2-}$	30
2.5.3	$[\text{Rh}_{12}(\text{C})_2(\text{CO})_{24}]^{2-}$	30
2.5.4	Further Structural Data	31
2.6	Homonuclear Nickel Clusters	32
2.6.1	$[\text{Ni}_9(\text{C})(\text{CO})_{17}]^{2-}$	32
2.6.2	$[\text{Ni}_{32}(\text{C})_6(\text{CO})_{36}]^{6-}$	32
2.6.3	$[\text{Ni}_{38}(\text{C})_6(\text{CO})_{42}]^{6-}$	34
2.6.4	Further Structural Data	34
2.7	Homonuclear Rhenium Clusters	35
2.7.1	$[\text{Re}_7(\text{C})(\text{CO})_{21}]^{3-}$ and $[\text{Re}_8(\text{C})(\text{CO})_{24}]^{2-}$	35
2.7.2	Further Structural Data	36
3	Heteronuclear Clusters	36
3.1	Heteronuclear Iron Clusters	36
3.1.1	Heteronuclear Iron–Molybdenum Clusters	36
3.1.2	Heteronuclear Iron–Ruthenium Clusters	36
3.1.3	Heteronuclear Iron–Rhodium Clusters	36
3.1.3.1	$[\text{Fe}_5\text{Rh}(\text{N})(\text{CO})_{15}]^{2-}$ and $[\text{Fe}_4\text{Rh}_2(\text{N})(\text{CO})_{15}]^-$	36
3.1.3.2	Further Structural Data	36
3.1.4	Heteronuclear Iron–Iridium Clusters	38
3.1.5	Heteronuclear Iron–Nickel clusters	38
3.1.5.1	$[\text{Fe}_6\text{Ni}_6(\text{N})_2(\text{CO})_{24}]^{2-}$	38
3.1.6	Heteronuclear Iron–Platinum Clusters	39
3.1.7	Heteronuclear Iron–Mercury Clusters	39
3.1.7.1	$\{\mu_4\text{-Hg}[\text{Fe}_5(\text{C})(\text{CO})_{14}]_2\}^{2-}$	39
3.2	Heteronuclear Ruthenium Clusters	40
3.2.1	Heteronuclear Ruthenium–Platinum Clusters	40
3.2.2	Heteronuclear Ruthenium–Mercury Clusters	40
3.3	Heteronuclear Osmium Clusters	40
3.3.1	Heteronuclear Osmium–Mercury Clusters: $[\text{Os}_{18}\text{Hg}_3(\text{C})_2(\text{CO})_{42}]^{2-}$, $[\text{Os}_{18}\text{Hg}_2(\text{C})_2(\text{CO})_{42}]^{4-}$ and $[\text{Os}_{18}\text{Hg}_2(\text{C})_2(\text{CO})_{42}]^{2-}$	40
3.4	Heteronuclear Cobalt Clusters	41
3.4.1	Heteronuclear Cobalt–Nickel Clusters: $[\text{Co}_2\text{Ni}_{10}(\text{C})(\text{CO})_{20}]^{2-}$, $[\text{Co}_3\text{Ni}_9(\text{C})(\text{CO})_{20}]^{2-}$ and $[\text{Co}_6\text{Ni}_2(\text{C})_2(\text{CO})_{16}]^{2-}$	41
3.5	Heteronuclear Rhodium Clusters	44
3.5.1	Heteronuclear Rhodium–Platinum Clusters	44
3.5.2	Heteronuclear Rhodium–Cobalt Clusters	45
3.5.3	Heteronuclear Rhodium–Iridium Clusters	45
3.5.4	Heteronuclear Rhodium–Silver Clusters	45

4	Acknowledgements	45
5	References	45
2	Unusual Nuclear Magnetic Shielding and Coupling Constants Related to Unusual Bonding Situations <i>Bernd Wrackmeyer</i>	
1	Introduction	51
1.1	General	51
1.2	Chemical Shifts, δX	54
1.3	Coupling Constants, ${}^nJ(A, X)$	57
2	Hydrides	58
2.1	Boron Hydrides	58
2.2	Unusual Chemical Shifts, δ^1H , of Hydrocarbons	59
2.3	Carbocations	60
2.4	Hydrogen Bonding Involving Nitrogen, Oxygen and Fluorine	60
2.5	Transition Metal Hydrides	62
3	Alkali Metal Compounds	65
3.1	Alkalide anions	65
3.2	Organolithium Compounds	65
4	${}^{11}B$ and ${}^{27}Al$ NMR Spectroscopy	66
4.1	The Structures of Boron Compounds	66
4.2	Complexes with Transition Metal–Boron Bonds	72
4.3	Pentamethylcyclopentadienyl (Cp*) Aluminium Compounds	74
5	Group 14 Element Chemistry in the Light of NMR.	74
5.1	Carbon Atoms in Unusual Surroundings	74
5.2	Organosilicon, -germanium, -tin and -lead Compounds: An Almost Perfect Playing Field for NMR Spectroscopy	79
6	Nitrogen Compounds. What Can We Learn from Nitrogen NMR?	87
6.1	Some Simple Nitrogen Compounds: N_2 , N_2O , $[N_3]^-$, $[N_5]^+$ and Others	89
6.2	Lithium Amides	90
6.3	Boron–Nitrogen Compounds	90
6.4	Carbon–Nitrogen Compounds	92
6.5	Complexes with Transition Metal–Nitrogen Bonds	93
7	Phosphorus, An Element Made for NMR Studies	94
8	Oxygen Compounds: ${}^{17}O$ NMR	98
8.1	Some Simple Oxygen Compounds: Water, Ozone, Sulfur Dioxide and Others	98
8.2	Complexes with Transition Metal–Oxygen Bonds.	101
9	Selenium and Tellurium Compounds: ${}^{77}Se$ and ${}^{125}Te$ NMR	101

10	Fluorine Compounds: ^{19}F , A Nucleus with Excellent NMR Properties	104
10.1	Some Simple Molecules: F_2 , Cl-F , OF_2 , XeF_2 , NF_3 and Others	104
10.2	Transition Metal Fluorides	105
11	Chemistry of Xenon: ^{129}Xe NMR.	105
12	Organotransition Metal Complexes—A Wide Field of NMR.	106
12.1	Vanadium Complexes: ^{51}V NMR	107
12.2	^{95}Mo and ^{183}W NMR.	107
12.3	^{55}Mn and ^{99}Tc NMR	109
12.4	^{57}Fe , ^{99}Ru and ^{187}Os NMR	112
12.5	^{59}Co and ^{103}Rh NMR.	114
12.6	^{195}Pt NMR.	115
12.7	$^{63/65}\text{Cu}$ and $^{107/109}\text{Ag}$ NMR.	118
12.8	$^{111/113}\text{Cd}$ and ^{199}Hg NMR	119
13	Lanthanides and Actinides	121
14	Conclusions.	121
15	Acknowledgements	122
16	References	123

3 Deuterium Spin–Lattice Relaxation and Deuterium Quadrupole Coupling Constants. A Novel Strategy for Characterization of Transition Metal Hydrides and Dihydrogen Complexes in Solution

Vladimir I. Bakhmutov

1	Introduction. Hydride Ligands from a Concept of Protons Buried in Metal Orbitals to Hydrides Showing Quantum Mechanical Behaviour	145
2	Applications of ^1H NMR in the Chemistry of Transition Metal Hydride Complexes	147
3	Deuterium NMR Approach to Studies of Transition Metal Hydride Complexes	149
3.1	Deuterium as a Quadrupole Nucleus.	149
3.2	Methods for DQCC Determination	151
3.2.1	^2H Solid-State NMR Spectroscopy	151
3.2.2	Molecular Orbital Calculations	153
3.2.3	^2H Spin–Lattice Relaxation (T_1) in Solution.	153
3.3	Deuterium Quadrupole Coupling Constants in Terminal Transition Metal Hydrides: Results and Interpretation	154
4	Concluding Remarks	161
5	Acknowledgements	162
6	References	162

4 NMR Studies of Ligand Nuclei in Organometallic Compounds—New Information from Solid-State NMR Techniques

Guy M. Bernard and Roderick E. Wasylshen

1	Introduction	165
2	Theoretical Background	166
2.1	Ligand–Metal Bonding	166
2.2	The Chemical Shift Tensor	167
2.2.1	Nuclear Magnetic Shielding and Chemical Shift	167
2.2.2	Ramsey’s Theory	168
2.3	Notation	168
2.4	<i>Ab Initio</i> Calculations of Magnetic Shielding Tensors	169
3	Experimental Techniques	170
3.1	The Principal Components of a CS Tensor for an Isolated Spin- $\frac{1}{2}$ Nucleus	171
3.2	The Dipolar Chemical Shift Method	171
3.3	CS Tensors from Spectra of MAS Samples	173
3.4	Sample Size	174
4	Experimental Results	174
4.1	Metal Carbides	174
4.1.1	Carbon CS Tensors for the Alkali-Metal Carbides	174
4.1.2	Carbon CS Tensors for the Alkaline-Earth Metal Carbides	175
4.1.3	Comparison of CS Tensors for Metal Carbides	176
4.1.4	Solid-State NMR Studies of Fullerenes	176
4.2	Metal–Olefin and Metal–Acetylene Complexes	177
4.2.1	Carbon-13 NMR Studies	178
4.2.1.1	Platinum–olefin complexes	180
4.2.1.2	Carbon chemical shift tensors of some copper–olefin complexes	182
4.2.1.3	Carbon chemical shift tensors for η^4 -coordinated transition-metal–olefin complexes	183
4.2.1.4	Carbon chemical shift tensors for some transition-metal–acetylene complexes	184
4.2.2	Solid-State NMR Studies of Internal Dynamics	185
4.3	Metallocenes	185
4.3.1	Carbon CS Tenors	186
4.3.1.1	Carbon-13 NMR studies of cyclopentadienyl–metal complexes	188
4.3.1.2	Carbon-13 NMR studies of η^6 -coordinated complexes	191
4.3.2	Other Solid-State NMR Studies	191

4.4	Adsorbed Olefins and Acetylenes	193
4.4.1	Solid-State NMR Studies of Adsorbed Olefins	194
4.4.2	Carbon-13 NMR Studies of Adsorbed Acetylene	197
4.4.3	Solid-State NMR Studies of Other Adsorbed η -Coordinated Organometallics	198
5	Conclusions	198
6	Acknowledgements	198
7	References and Notes	199
5	Metal Atom Motion in Some Iron Organometallics <i>Rolfe H. Herber</i>	
1	Introduction	207
2	Baseline Studies.	208
2.1	Hydroxymethylferrocene	209
2.2	Decamethylferrocene	210
2.3	Nonamethylferrocene and Nonamethylferrocenium Hexafluorophosphate	211
2.4	Ethynyloctamethylferrocene and Ethynyloctamethylferrocenium Hexafluorophosphate	214
3	Experimental.	216
4	Acknowledgements	216
5	References.	217
6	Magnetic Communication in Binuclear Organometallic Complexes Mediated by Carbon-Rich Bridges <i>Frédéric Paul and Claude Lapinte</i>	
1	Introduction	220
2	General Notions Regarding Magnetic Interactions in Polyradicals	223
2.1	Antiferro- and Ferromagnetic Exchange Interactions	223
2.2	The Heisenberg–Dirac–van Vleck Hamiltonian	223
2.3	Rules for Deriving the Ground State	225
2.4	Structural Changes Between Spin States in Ditopic Diradicals	227
2.5	Experimental Determinations of Magnetic Interactions in Di- or Tritopic Polyradicals	229
2.5.1	NMR and the Evans Method.	230
2.5.2	Electronic Spin Resonance.	231
2.5.3	Solid-State Magnetic Susceptibility Measurements	233
3	Magnetic Interactions in Cationic Organoiron Di- and Trinuclear Metal-Centered Polyradicals Containing [[η^2 -Diphos](η^5 -C ₅ Me ₅)Fe] ⁺ End Groups	237

3.1	The $[(\eta^2\text{-Diphos})(\eta^5\text{-C}_5\text{Me}_5)\text{Fe}]^{+/}$ Radical Cation Fragment	237
3.1.1	The $[(\eta^5\text{-Diphos})(\eta^5\text{-C}_5\text{Me}_5)\text{Fe}]^+$ Fragment in Mononuclear Complexes	237
3.1.2	The $[(\eta^5\text{-Diphos})(\eta^5\text{-C}_5\text{Me}_5)\text{Fe}]^+$ Fragment(s) in Polynuclear Complexes	239
3.2	Magnetic Interactions in Polynuclear Mono-, Di- and Triradicals	240
3.2.1	Magnetic Interactions in Polynuclear Monoradicals	240
3.2.2	Magnetic Interactions in Polynuclear Diradicals	241
3.2.3	Magnetic Interactions in Polynuclear Triradicals	248
3.3	Intramolecular Magnetic Exchange Between Metal-Centered Spins in the Organoiron Polynuclear Diradicals	250
4	Structural Implications of the Magnetic Exchange in Polytopic Organometallic Polyradicals Featuring Carbon-Rich Bridges	251
4.1	All Carbon(C_{2n})-Bridged Organometallic Metal-Centered Diradicals.	252
4.1.1	Structure of the Spin Isomers in C_{2n} -Bridged Organometallic Diradicals	252
4.1.2	Bonding and Superexchange in C_{2n} -Bridged Organometallic Diradicals	256
4.1.3	Magnitude of the S/T Gap in C_{2n} -Bridged Organometallic Diradicals	262
4.1.4	Some Results Regarding the C_{2n} -Bridged Organometallic Ditopic Triradicals	264
4.1.5	Redox Chemistry of the C_{2n} -Bridged Organometallic Diradicals	266
4.2	End-On Polyene-Diyl-Bridged Organometallic Metal-Centered Diradicals	270
4.2.1	Structure of the Spin Isomers in $(\text{RC}=\text{CR}')_n$ - Bridged Organometallic Ditopic Polyradicals	270
4.2.2	Bonding and Superexchange in $(\text{RC}=\text{CR}')_n$ - Bridged Organometallic Diradicals	272
4.2.3	Considerations on the Spin Transition in $(\text{RC}=\text{CR}')_n$ -Bridged Organometallic Diradicals	276
4.2.4	Redox Chemistry of the $d^5-d^5(\text{RC}=\text{CR}')_n$ - Bridged Organometallic Diradicals	276
4.3	Organometallic Diradicals Bridged by Carbon-Rich Spacers Featuring (Hetero)Aryl Units	277

4.3.1	Simple Aryl-Bridged Ditopic Polyradicals	278
4.3.2	Ditopic Polyradicals Incorporating the 1,4-Diethynylphenyl Units	279
4.3.3	Diradicals Incorporating the 2,5-Diethynylthienyl Unit	280
4.3.4	Diradicals Incorporating the 1,3-Diethynylphenyl Unit	281
4.3.5	Bonding and Toplogy-Dependant Superexchange Interaction in Diethynyl-(Hetero)aryl Diradicals	282
4.3.6	Triradicals Featuring a 1,3,5-Phenylene Unit	285
4.4	Spin-Exchange-Induced Structural Changes of the Bridging Ligand	287
5	Conclusions	289
6	Acknowledgements	291
7	References.	291
7	Molecular Cluster Complexes with Facial Arene Ligands <i>Hubert Wadepohl</i>	
1	Introduction	297
2	Syntheses	299
3	Molecular Structure and Dynamic Behaviour	304
4	Electronic Structure	312
5	Reactivity	314
6	Conclusions	316
7	References and Notes	316
8	Cobaltifulvenes and Cobaltapentalenes: Highly Polar Metallacyclic Π-Systems with Unusual Properties <i>Hubert Wadepohl</i>	
1	Introduction	321
2	Cobaltifulvene Complexes.	323
3	Cobaltapentalene Complexes	328
4	Conclusions	332
5	Acknowledgements	335
6	References.	335
9	Novel Highly Nucleophilic Ylidic Ligands for the Preparation of Unusually Stable Metal Complexes <i>Norbert Kuhn, Martin Göhner, Gernot Frenking and Yu Chen</i>	
1	Introduction	337
2	Iminoimidazolines	338
2.1	Synthesis and Structure	338
2.2	Bonding in 2-Iminoimidazolines	339
2.3	Metalation and Silylation.	343

2.4	Bonding in 2-Imidoimidazolines	343
2.5	The Structure of $[\text{Li}_{12}\text{O}_2\text{Cl}_2(\text{ImN})_8]$	345
2.6	Iminoimidazoline Phosphanes	346
2.7	Bonding in Iminoimidazoline Phosphanes	348
2.8	Aluminium and Titanium Iminoimidazolides	351
2.9	Bonding in Titanium Iminoimidazolides	352
2.10	Alkylation and Acylation	352
2.11	Coordination of 2-Iminoimidazolines at Metal Centers.	358
3	Methyleneimidazolines	362
3.1	Synthesis and Structure.	362
3.2	Bonding in 2-Methyleneimidazolines and Related Compounds.	365
3.3	Reactions with Main Group Element Electrophiles	369
3.4	Bonding in Iodine Complexes	372
3.5	Transition Metal Complexes	373
3.6	C-Substituted 2-Methyleneimidazolines	376
3.7	Bonding in Im-CS_2 and Im-CS_2^{2-}	379
4	Conclusions	380
5	Acknowledgements	384
6	References and Notes	384
10	Supramolecular Interactions in Structures of Organic Antimony and Bismuth Compounds <i>Gabor Balázs and Hans Joachim Breunig</i>	
1	Introduction	387
2	Diorganoelement Halides and Related Ionic Compounds.	389
3	Organoelement Dihalides	393
4	Organometallic Compounds with Sb–Sb or Bi–Bi Bonds	401
5	Organometallic Chalcogen and Nitrogen Derivatives of Sb or Bi	404
6	References	408
	Index	411

Contributors

Vladimir I. Bakhmutov, Department of Chemistry, PO Box 30012, College Station, TX 77842-3012, USA

Gabor Balázs, Institut für Anorganische und Physikalische Chemie der Universität Bremen, Fb 2, D-28334 Bremen, Germany

Guy M. Bernard, Department of Chemistry, University of Alberta, Edmonton, Alberta, Canada, T6G 2G2

Hans Joachim Breunig, Institut für Anorganische und Physikalische Chemie der Universität Bremen, Fb 2, D-28334 Bremen, Germany

Yu Chen, Fachbereich Chemie, Philipps-Universität Marburg, Hans-Meerwein-Strasse, D-35032 Marburg, Germany

Gernot Frenking, Fachbereich Chemie, Philipps-Universität Marburg, Hans-Meerwein-Strasse, D-35032 Marburg, Germany

Martin Göhner, Institut für Anorganische Chemie der Universität Tübingen, Tübingen, Germany

Rolfe H. Herber, Racah Institute of Physics, The Hebrew University of Jerusalem, 99904 Jerusalem, Israel

Norbert Kuhn, Institut für Anorganische Chemie der Universität Tübingen, Tübingen, Germany

Claude Lapinte, Institut de Chimie de Rennes, UMR CNRS 6509 Organometalliques et Catalyse, Université de Rennes I, Campus de Beaulieu, 35042 Rennes, Cedex France

Frédéric Paul, Institut de Chimie de Rennes, UMR CNRS 6509 Organometalliques et Catalyse, Université de Rennes I, Campus de Beaulieu, 35042 Rennes, Cedex France

Hubert Wadepohl, Anorganisch-Chemisches Institut der Ruprecht-Karls-Universität, Im Neuenheimer Feld 270, D-69120 Heidelberg, Germany

Roderick E. Wasylishen, Department of Chemistry, University of Alberta, Edmonton, Alberta, Canada, T6G 2G2

Bernd Wrackmeyer, Laboratorium für Anorganische Chemie, Universität Bayreuth, D-95440 Bayreuth, Germany

Piero Zanello, Dipartimento di Chimica dell'Università di Siena, Via Aldo Moro, 53100 Siena, Italy

Series Preface

Physical organic chemistry, the study of the basic physical principles of organic reactions, is not a new field: in 1940, Hammett had already written a book with this title. This area has developed during the last 20 years mainly because of the explosive growth of sophisticated analytical instrumentation and computational techniques, going from the simple Hückel molecular orbital theory to *ab initio* calculations of increasing accuracy enabled by the advent of fast supercomputers.

An analogous genesis characterized physical organometallic chemistry. Understanding the basis of chemical reactivity and the detailed pathways of reactions of organometallic compounds is now one of the major goals of physical organometallic chemists. Correlation of structure with reactivity, increasing in sophistication, contributes powerfully to the understanding of electronic transmission, as well as of steric and conformational properties, including solvent effects. Homogeneous catalysis has reached a development stage making it a wide, complex topic deserving special consideration. Chiral induction is also becoming increasingly important, considering the economic importance of asymmetric syntheses in the design of pharmaceuticals: organometallic compounds play a key role in this area; understanding this role is the key to further progress.

Accordingly, the major developments of physical organometallic chemistry are not only relevant to *ab initio* calculations of metal-based organic compounds or new spectroscopic tools like multidimensional high-resolution NMR. They also involve new ingenious technologies to study reaction mechanisms, group-theoretical approaches to investigate the fluxionality of organometallic molecules, photochemical reactions on organometallic substrates, and, last but not least, experimental highlights like unstable organometallic compounds in matrices, piezochemistry, and sonochemistry.

The main goal of this series 'Physical Organometallic Chemistry' is to offer to post-graduates and researchers leading contributions written by well-known scientists reviewing the state-of-the-art of hot topics animating this wide research area, in order to develop new insights and to promote novel interest and investigations.

Preface

The term ‘unusual’ is often misused in chemistry with the purpose of (over?)-emphasizing structural or property originality of novel chemical compounds. Organometallic chemistry does not escape from this trend, but paradoxically, suffers also from the insufficient scientific exploitation of really unusual techniques, tools, properties or parameters to investigate really unusual chemical features or structures. This can be traced to a vast extent to a quite traditional, albeit respectable, strategy of conducting research in organometallic chemistry consisting basically of a classical scheme involving sequentially synthesis, purification, basic characterization, structure determination by X-ray diffraction, and, if any, chemical applications in synthesis or catalysis. Apart maybe from X-ray diffraction, the characterization tools remain often at routine level, e.g. in proton and carbon-13 NMR or IR spectroscopy, elemental analysis and mass spectrometry, with the identity of chemical structures in crystalline and solution states being taken too often for granted. In this way other properties—electronic, magnetic, fluxional—are sometimes overlooked or insufficiently addressed. Starting from this standpoint, the idea came up to conceive a book offering a selection of unusual properties, tools or structures that could serve as a source of new challenges in broader fields of organometallic chemistry than those in which they have been presently created, implemented or applied.

This present book is intended for a vast majority of scientists working in various areas of organometallic chemistry. This statement looks trivial at first glance, but is less so when considering the ever-increasing speed of development of novel physical methods and the diversity of their real or potential applications to organometallic chemistry, even though, as stated above, they are not widespread. Actually, it becomes more and more difficult to keep track in exploiting the full potential of these methods, especially when unusual structures or physical properties are concerned. Hence, the principal idea of this book is to offer in this particular context a *Capita Selecta* of unconventional and thought-provoking topics in organometallic chemistry, presented by experts in each field at state-of-the-art level. As intended in this book, this approach leads either to reviews covering a specific uncommon class of organometallic compounds or to overviews which relate uncommon physical properties with various classes of organometallic compounds. Thus, extended cross-linking of useful information is provided, even for people working in rather different areas of organometallic chemistry. Clearly, it is not possible to

cover the theme of such a book in an exhaustive manner. However, the *Capita Selecta* offered are representative of this original approach and serve as examples which should stimulate the reader to consider one or other physical method or structural pattern for his own special interests. He/she should also find unusual structural features for systems, apparently not related to his own field, which however possess familiar physical data. In this way, this book should help the reader to understand relevant physical data in a more general way. The text is streamlined into two main axes, namely unusual properties reflecting structures and bonding situations, on the one hand, and uncommon structural features or structure–reactivity relationships, on the other hand. The first axis consists of six chapters: the electrochemistry–structure relationship in transition metal carbonyl clusters with interstitial atoms, with special emphasis on the contrast between carbides and nitrides; unusual nuclear shielding and coupling constants in organometallic compounds, with contrast between data of unusual bonding situations and data from the basic simple chemical molecules involved; deuterium relaxation times and quadrupolar coupling constants in metal hydrides and metal–dihydrogen complexes in solution; novel aspects of solid-state NMR spectroscopy of organometallic compounds; Mössbauer spectroscopy addressing metal atom motions in iron organometallics; magnetic communication and spin equilibria of organometallic complexes, and spin transitions in binuclear organometallic complexes. The second axis consists of four contributions: molecular clusters with facial arene ligands; cobaltfulvenes and cobaltapentalenes, as highly polar metallic π -systems with unusual properties; highly nucleophilic ylidic ligands for the preparation of unusually stable metal complexes; supramolecular interactions in solid organo-antimony and -bismuth chemistry.

In this way, it is hoped to provide of a broad overview of unusual techniques, research tools, structures and properties that can stimulate novel research axes in areas of organometallic chemistry where they have never previously been addressed.

1 Structure and Electrochemistry of Transition Metal Carbonyl Clusters with Interstitial or Semi-Interstitial Atoms: Contrast between Nitrides or Phosphides and Carbides

PIERO ZANELLO

Dipartimento di Chimica dell'Università di Siena, Via Aldo Moro, 53100 Siena, Italy

Transition-metal carbonyl clusters containing *interstitial* or *semi-interstitial* atoms have been the subject of many studies, particularly in view of the fact that the insertion of interstitial atoms inside the metal cage of the clusters often increases the number of valence electrons (hence affecting to some extent the reactivity), leaving essentially unaltered the molecular geometry with respect to the original species. Their preparative [1,2], structural [1,2], spectroscopic (NMR) [3] and theoretical [4] aspects have been elucidated and their possible use as catalysts has been proposed [5]. In addition, their electrochemical behaviour has been mostly reviewed in a series of articles devoted to a systematic examination of the electrochemical behaviour of homo- [6] and hetero-metal [7] carbonyl clusters.

In this present paper, we should like to focus more specifically on the different, and in some cases contrasting, electrochemical behaviour of *homo-leptic* transition-metal carbonyl clusters containing interstitial or exposed *N*, *P* atoms with respect to the *C*-containing analogues. Since these nitride or phosphide carbonyl clusters can be considered as a link between *organometallic* and *coordination* compounds, it is hoped that a detailed comparison of their redox aptitude can help theoreticians in understanding more and more the extent to which the nature of such interstitial heteroatoms might affect the electron mobility inside such compounds.

We will examine here only those complexes for which the X-ray structures have been solved—discussions of the structural details are given in the relevant literature references, or mostly in References [5] and [6]. Even if in many cases there are not sufficient electrochemical data to allow comparisons to be made

between *nitride/phosphide*-containing metal clusters and their *carbide* analogues, we think it is useful to give literature references to the X-ray structures of all of the complexes known so far.

The molecular structures and electrochemical responses presented here are adapted from the original figures quoted in the text. Unless otherwise specified, all the electrode potentials are referred to the saturated-calomel electrode.

1 INTRODUCTION

Although *carbide*-containing transition-metal carbonyl clusters have been known for a long time [1,2], delays were experienced before electrochemists began to deal with them, so that their redox chemistry was adequately, although roughly explored by chemical routes. In fact, the use of chemical reagents does not allow the redox properties of a molecule to be finely tuned. For instance, Chini's group in Milan pioneeringly investigated not only the synthetic and structural aspects of metal clusters, but also their redox chemistry. Thus, one can find in the literature the structural characterization of a few redox couples of metal carbonyl clusters obtained 'blindly' by using chemical reagents. In this connection, Figures 1–3 show the molecular

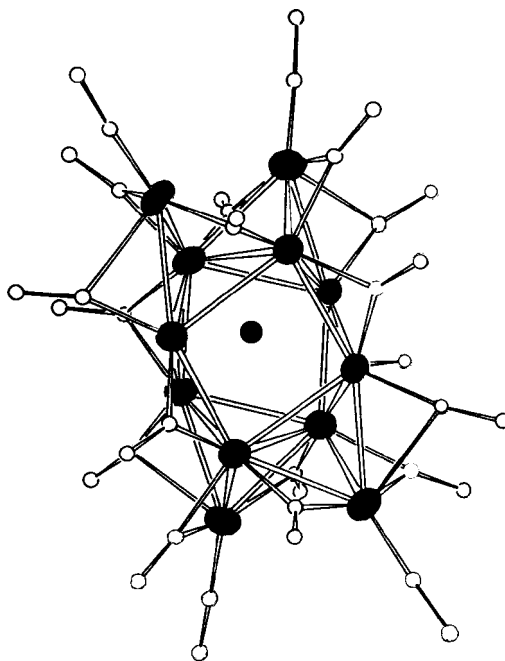


Figure 1 Molecular structure of the tetraanion $[\text{Co}_3\text{Ni}_9(\text{C})(\text{CO})_{20}]^{3-}$

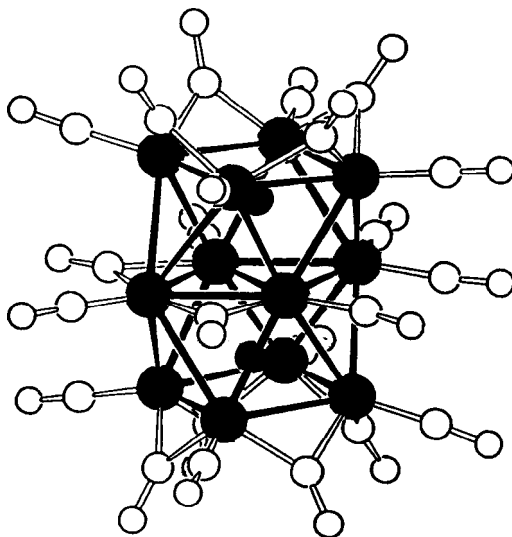


Figure 2 Molecular structure of the trianion $[\text{Rh}_{12}(\text{C})_2(\text{CO})_{23}]^{4-}$

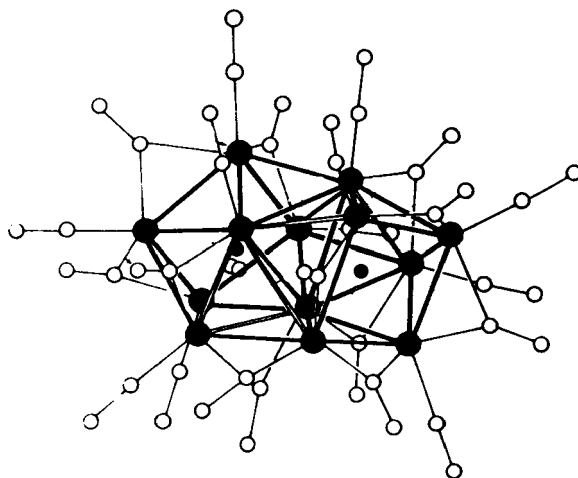


Figure 3 Molecular structure of the tetraanion $[\text{Co}_{13}(\text{C})_2(\text{CO})_{24}]^{4-}$

structures of one member of each of the couples, $[\text{Co}_3\text{Ni}_9(\text{C})(\text{CO})_{20}]^{3-/2-}$ [8,9], $[\text{Rh}_{12}(\text{C})_2(\text{CO})_{23}]^{4-/3-}$ [10,11], and $[\text{Co}_{13}(\text{C})_2(\text{CO})_{24}]^{4-/3-}$ [12,13].

In all of these cases, the redox congeners are isostructural with each other and only minor variations in the metal-metal, metal-carbon_(carbonyl), and metal-carbon_(carbide) bonding distances occur upon addition/removal of one electron.

As previously mentioned, the use of chemical reagents does not allow the multiple redox states of a molecule to be adequately determined. For instance, $[\text{Co}_3\text{Ni}_9(\text{C})(\text{CO})_{20}]^{3-}$ not only undergoes the chemically reversible one-electron removal process, $[\text{Co}_3\text{Ni}_9(\text{C})(\text{CO})_{20}]^{3-/2-}$ ($E^{0'} = -0.30$ V), but it is also able to add two electrons in a single step ($E^{0'} = -1.71$ V), affording the pentaanion $[\text{Co}_3\text{Ni}_9(\text{C})(\text{CO})_{20}]^{5-}$, which, however, is a transient species ($t_{1/2} \approx 1$ s) (Figure 4) [14].

Analogously, the chemical picture concerned with the redox change $[\text{Rh}_{12}(\text{C})_2(\text{CO})_{23}]^{4-/3-}$ appears to be correct as far as the full stability within the family is concerned. Indeed, as Figure 5 illustrates [5], the redox ability is more extended in that $[\text{Rh}_{12}(\text{C})_2(\text{CO})_{23}]^{4-}$ not only undergoes reversibly the cited one-electron oxidation ($E^{0'} = -0.46$ V), but also exhibits a second irreversible one-electron removal ($E_p = -0.16$ V), as well as a single two-electron reduction to the corresponding hexaanion $[\text{Rh}_{12}(\text{C})_2(\text{CO})_{23}]^{6-}$ ($E^{0'} = -1.62$ V), which, however, is relatively short-lived ($t_{1/2} \approx 1$ s).

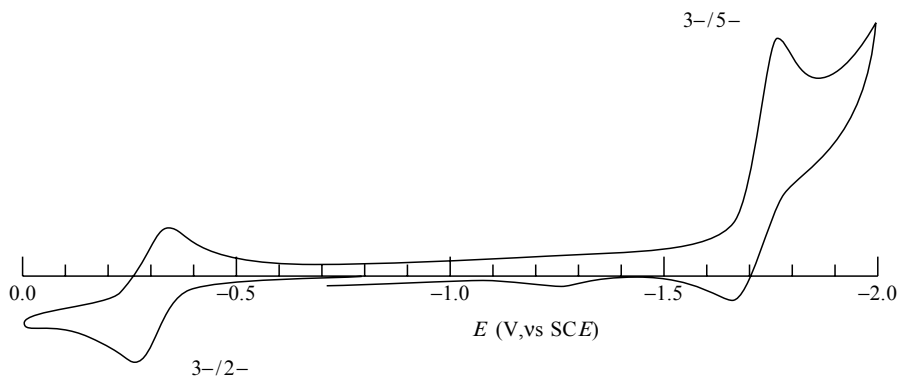


Figure 4 Cyclic voltammogram recorded at a platinum electrode for a Me_2CO solution containing $[\text{Co}_3\text{Ni}_9(\text{C})(\text{CO})_{20}]^{3-}$ (scan rate, 0.2 V s^{-1})

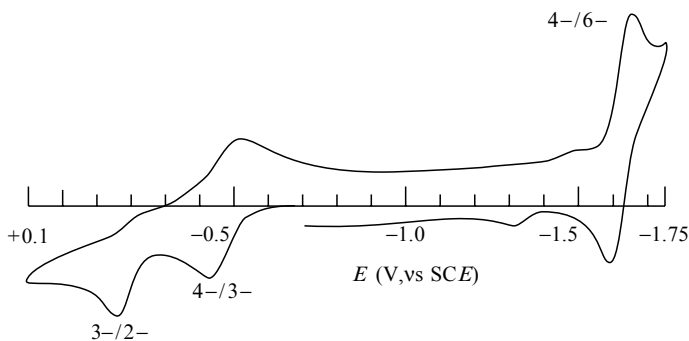


Figure 5 Cyclic voltammetric response exhibited by $[\text{Rh}_{12}(\text{C})_2(\text{CO})_{23}]^{4-}$ in MeCN solution, with a platinum working electrode (scan rate, 0.2 V s^{-1})

Even more instructive is the case of the redox family of $[\text{Co}_{13}(\text{C})_2(\text{CO})_{24}]^{4-}$. As Figure 6 proves, the tetraanion not only undergoes reversible one-electron oxidation to the trianion $[\text{Co}_{13}(\text{C})_2(\text{CO})_{24}]^{3-}$ ($E^0 = -0.54$ V), but it also exhibits the chemically reversible sequential access to the corresponding penta- ($E^0 = -1.06$ V) and hexa- ($E^0 = -1.68$ V) anions, $[\text{Co}_{13}(\text{C})_2(\text{CO})_{24}]^{5-/6-}$, respectively [5].

Furthermore, the usefulness of electrochemical studies in the present field is not limited to the discovery of multiple, stable or unstable, redox states of clusters, but also to the eventual conversion of a molecule to a somewhat related species by simple redox processes [15].

For instance, the dianion $[\text{Ru}_6(\text{C})(\text{CO})_{16}]^{2-}$, the octahedral geometry of which is shown in Figure 7(a) [16] undergoes an irreversible two-electron oxidation ($E_p = +0.48$ V, vs Ag/AgCl) to the neutral more carbonylated congener $\text{Ru}_6(\text{C})(\text{CO})_{17}$, which in turn undergoes an irreversible reduction ($E_p = -0.47$ V) (Figure 7(b)) [17].

As confirmation, $\text{Ru}_6(\text{C})(\text{CO})_{17}$, the octahedral geometry of which is shown in Figure 8(a) [18], exhibits a quite complementary voltammetric response (Figure 8(b)), thus pointing out that, upon two-electron addition, it converts again to the decarbonylated dianion $[\text{Ru}_6(\text{C})(\text{CO})_{16}]^{2-}$ [17].

By way of comparison, the isostructural and isoelectronic non-carbide dianion $[\text{Ru}_6(\text{CO})_{18}]^{2-}$ (Figure 9) [19] also exhibits in dichloromethane solution a two-electron oxidation coupled to fast chemical complicated behaviour, although this it occurs at a notably lower potential value ($E_p = -0.36$ V, vs Ag/AgCl) [20].

Finally, as an alternative to the thermally induced phosphine substitution, which affords a series of not easily separable products, the anodic oxidation of

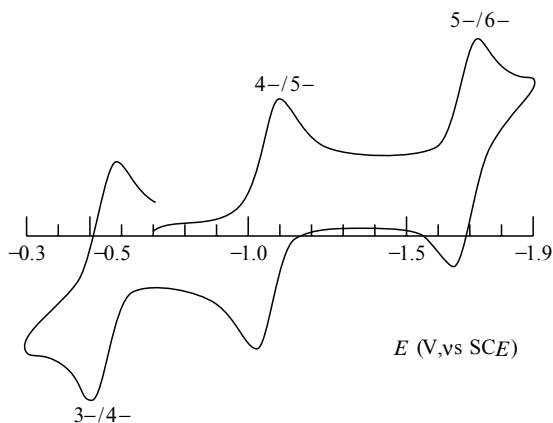


Figure 6 Cyclic voltammetric response exhibited by $[\text{Co}_{13}(\text{C})_2(\text{CO})_{24}]^{4-}$ in MeCN solution, with a platinum working electrode (scan rate, 0.2 V s^{-1})

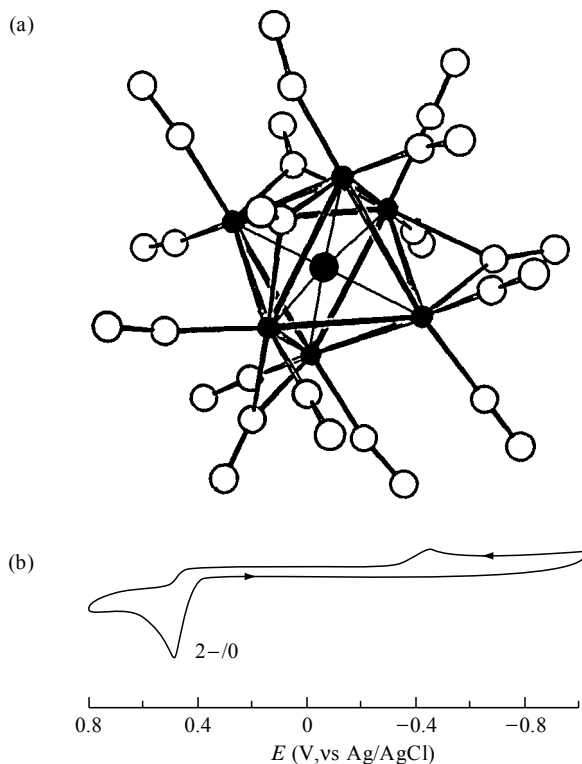


Figure 7 (a) Molecular structure of $[\text{Ru}_6(\text{C})(\text{CO})_{16}]^{2-}$, and (b) its cyclic voltammetric profile in CH_2Cl_2 solution

$[\text{Ru}_6(\text{C})(\text{CO})_{16}]^{2-}$ in the presence of phosphines selectively leads to the mono-substituted neutral species $\text{Ru}_6(\text{C})(\text{CO})_{16}(\text{PR}_3)$ [17]. In this connection, Figure 10 shows the molecular structure of $\text{Ru}_6(\text{C})(\text{CO})_{16}(\text{PPh}_2\text{Et})$ [21].

2 HOMONUCLEAR CLUSTERS

2.1 HOMONUCLEAR IRON CLUSTERS

2.1.1 $\text{Fe}_4(\text{C})(\text{CO})_{13}$ and $[\text{Fe}_4(\text{C})(\text{CO})_{12}]^{2-}$ versus $[\text{Fe}_4(\text{N})(\text{CO})_{12}]^{-}$

As Figure 11 illustrates, the three 62-cluster-valence-electron (CVE) complexes $[\text{Fe}_4(\text{C})(\text{CO})_{12}]^{2-}$, $\text{Fe}_4(\text{C})(\text{CO})_{13}$ and $[\text{Fe}_4(\text{N})(\text{CO})_{12}]^{-}$ possess a butterfly geometry [22–24].

It has been briefly reported that the dianion $[\text{Fe}_4(\text{C})(\text{CO})_{12}]^{2-}$ undergoes, in nonaqueous solvents, four oxidation steps, with only the first two of these having features of transient chemical reversibility [25]. This means that the

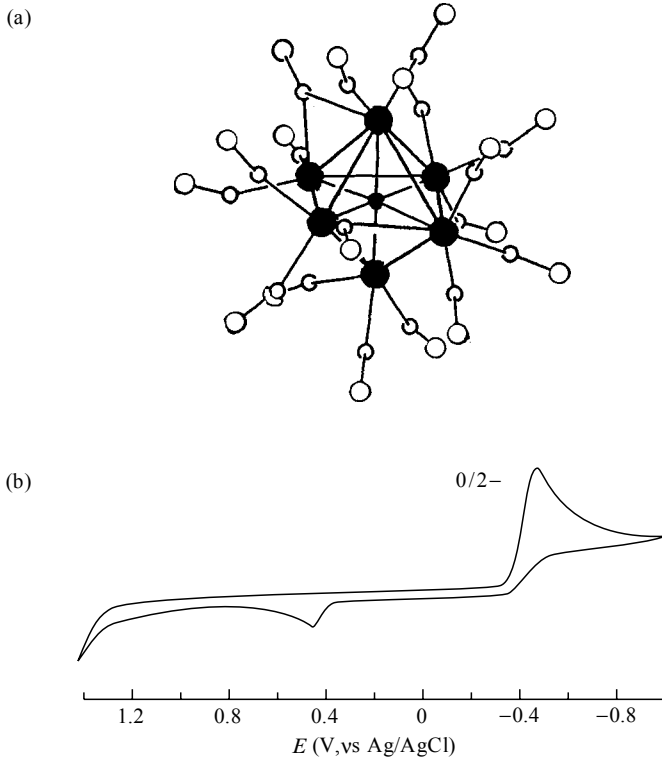


Figure 8 (a) Molecular structure of $\text{Ru}_6(\text{C})(\text{CO})_{17}$, and (b) its cyclic voltammetric profile in CH_2Cl_2 solution

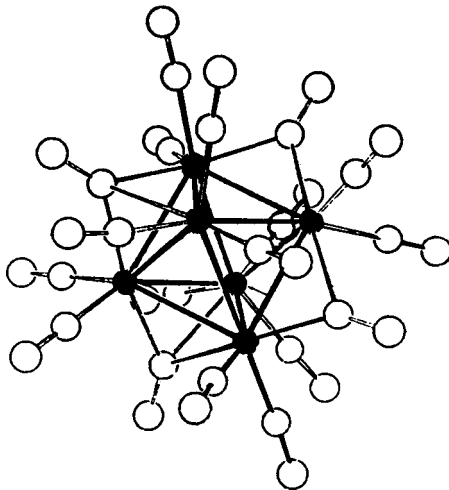


Figure 9 Molecular structure of $[\text{Ru}_6(\text{CO})_{18}]^{2-}$

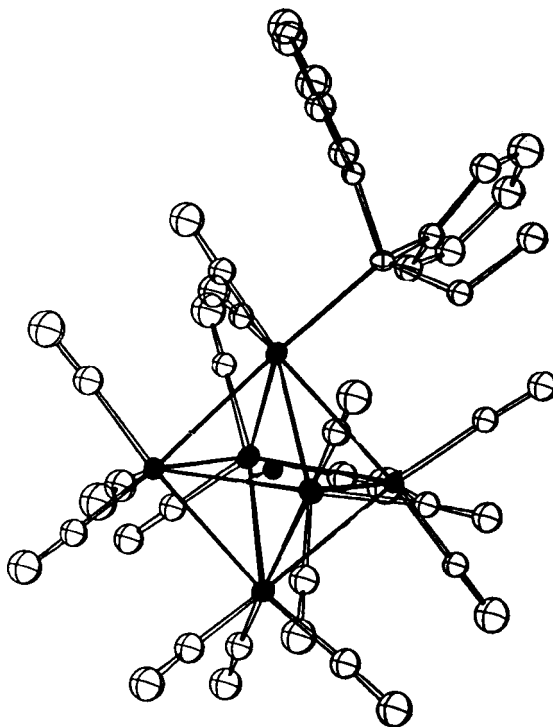


Figure 10 Molecular structure of $\text{Ru}_6(\text{C})(\text{CO})_{16}(\text{PPh}_2\text{Et})$

corresponding 61/60-CVE congeners $[\text{Fe}_4(\text{C})(\text{CO})_{12}]^{-,0}$ are only partially stable and tend to decompose. As a matter of fact, oxidation under CO atmosphere affords $\text{Fe}_4(\text{C})(\text{CO})_{13}$ [26].

Quite opposite is the redox ability of the monoanion $[\text{Fe}_4(\text{N})(\text{CO})_{12}]^-$. As Figure 12 shows, this undergoes in acetonitrile solution two sequential one-electron reductions at $E^{0'} = -1.23$ V and -1.58 V, respectively, with both having features of chemical reversibility [27].

Indeed, over the long time-scales of macroelectrolysis only the 63-CVE dianion $[\text{Fe}_4(\text{N})(\text{CO})_{12}]^{2-}$ remains quite stable. Furthermore, in the presence of triphenylphosphine, the electrochemical reduction triggers the electrocatalytic substitution of one carbonyl ligand, affording $[\text{Fe}_4(\text{N})(\text{CO})_{11}(\text{PPh}_3)]^-$ [27]. The electrochemical pathway quite parallels the thermal one, which also allowed the obtainment and consequent structural characterization of $[\text{Fe}_4(\text{N})(\text{CO})_{11}(\text{PMe}_2\text{Ph})]^-$ [28]. The molecular structures of these substituted complexes are shown in Figure 13. In both cases, the phosphine ligand replaces one carbonyl on the wingtip, i.e. the less coordinated iron vertex of the Fe_4 butterfly.

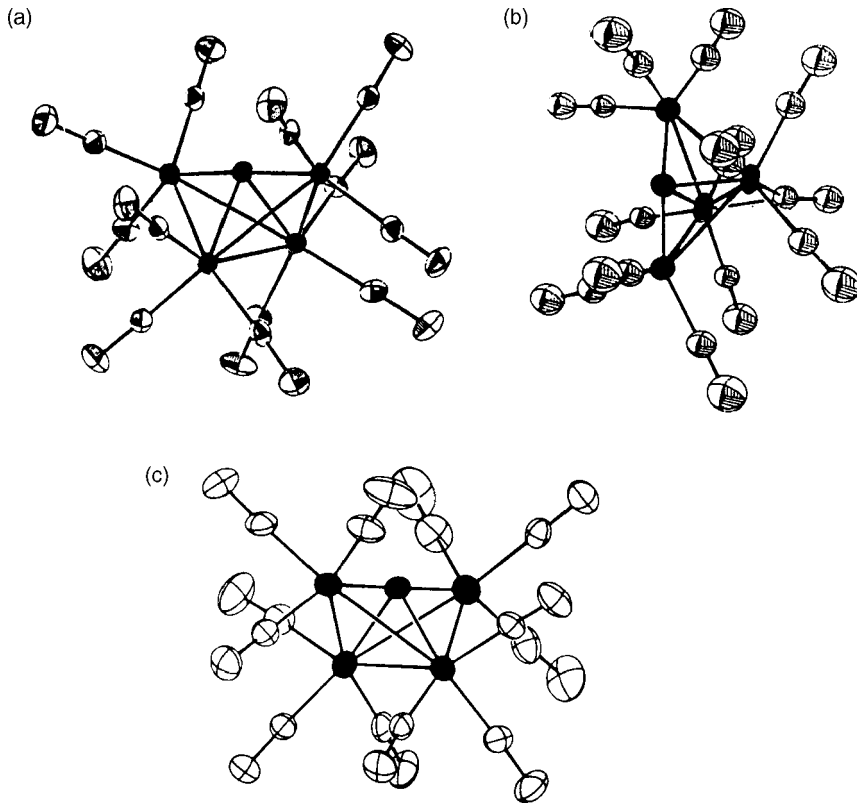


Figure 11 Molecular structures of (a) $[\text{Fe}_4(\text{C})(\text{CO})_{12}]^{2-}$, (b) $\text{Fe}_4(\text{C})(\text{CO})_{13}$, and (c) $[\text{Fe}_4(\text{C})(\text{CO})_{12}]^-$

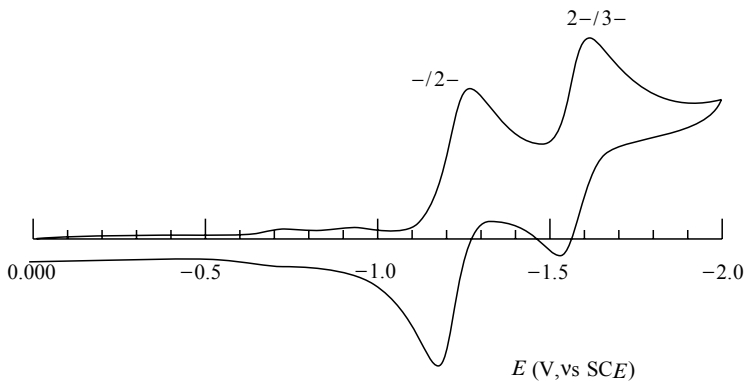


Figure 12 Cyclic voltammetric response exhibited by $[\text{Fe}_4(\text{C})(\text{CO})_{12}]^-$ in MeCN solution, with a mercury working electrode (scan rate, 0.2 V s^{-1})

On the other hand, it seems useful to take into account that the electrocatalytic substitution does not proceed in the presence of diferrocenylphosphine, whereas the thermal activation remains operative, affording $[\text{Fe}_4(\text{N})(\text{CO})_{11}(\text{PPh}(\text{C}_5\text{H}_4\text{FeC}_5\text{H}_5)_2)]^-$, the molecular structure of which is shown in Figure 14 [29].

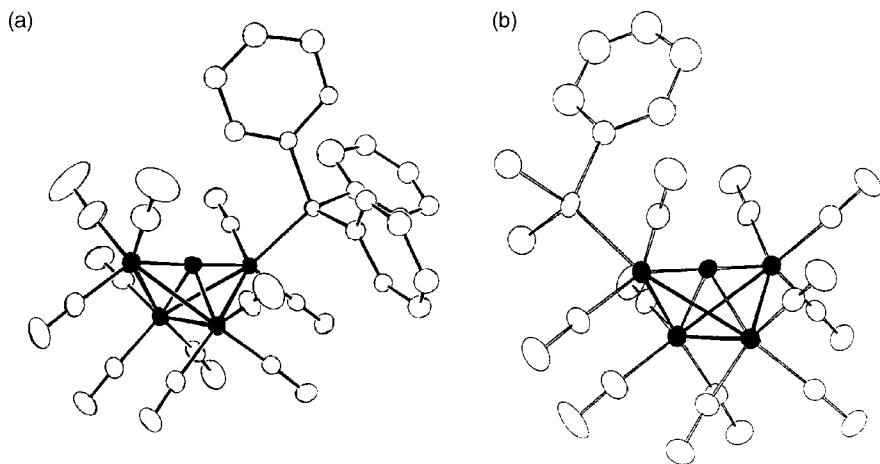


Figure 13 Molecular structures of (a) $[\text{Fe}_4(\text{N})(\text{CO})_{11}(\text{PPh}_3)]^-$, and (b) $[\text{Fe}_4(\text{N})(\text{CO})_{11}(\text{PMe}_2\text{Ph})]^-$

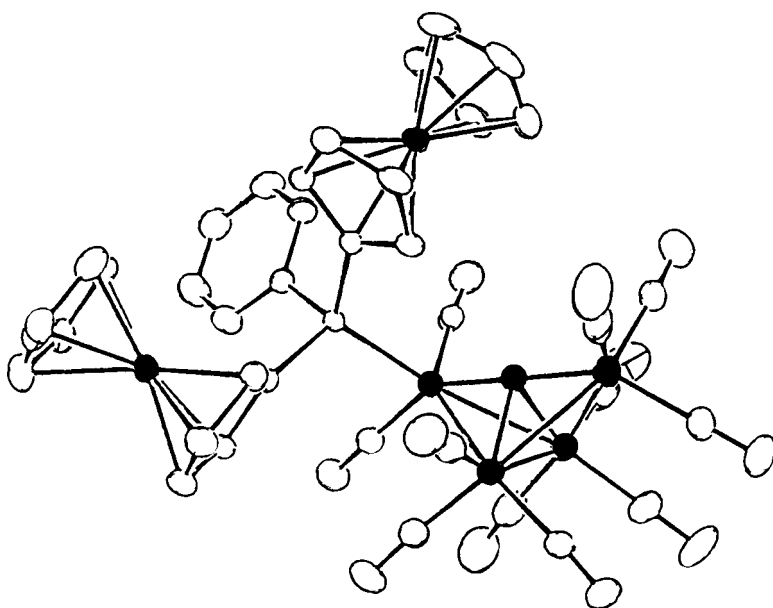


Figure 14 Molecular structure of $[\text{Fe}_4(\text{N})(\text{CO})_{11}(\text{PPh}(\text{C}_5\text{H}_4\text{FeC}_5\text{H}_5)_2)]^-$

2.1.2 $\text{Fe}_5(\text{C})(\text{CO})_{15}$ and $[\text{Fe}_5(\text{C})(\text{CO})_{14}]^{2-}$ versus $[\text{Fe}_5(\text{N})(\text{CO})_{14}]^-$

$[\text{Fe}_5(\text{C})(\text{CO})_{14}]^{2-}$, $\text{Fe}_5(\text{C})(\text{CO})_{15}$ and $[\text{Fe}_5(\text{N})(\text{CO})_{14}]^-$ constitute the object of the first comparative electrochemical study of isoelectronic and isostructural carbide and nitride clusters [30]. The square pyramidal geometries of the 74-CVE clusters $\text{Fe}_5(\text{C})(\text{CO})_{15}$, $[\text{Fe}_5(\text{C})(\text{CO})_{14}]^{2-}$ and $[\text{Fe}_5(\text{N})(\text{CO})_{14}]^-$ are illustrated in Figure 15 [30].

As Figure 16 shows, $\text{Fe}_5(\text{C})(\text{CO})_{15}$ in dichloromethane solution, at low temperature ($-15\text{ }^\circ\text{C}$), undergoes a single, uncomplicated, two-electron reduction ($E^{0'} = -0.11\text{ V}$) to the 76-CVE dianion $[\text{Fe}_5(\text{C})(\text{CO})_{15}]^{2-}$. Increasing the temperature, the current ratio $i_{\text{pa}}/i_{\text{pc}}$ decreases and a new re-oxidation wave appears at higher potential values ($E_{\text{p}} = +0.13\text{ V}$), which proved to be due to the oxidation of the decarbonylated dianion $[\text{Fe}_5(\text{C})(\text{CO})_{14}]^{2-}$, formed as a consequence of the chemical complication following the two-electron addition [30].

As a matter of fact, $[\text{Fe}_5(\text{C})(\text{CO})_{14}]^{2-}$ exhibits in dichloromethane solution either a single two-electron oxidation ($E^{0'} = +0.07\text{ V}$) or a single two-electron reduction ($E^{0'} = -1.58\text{ V}$) [30].

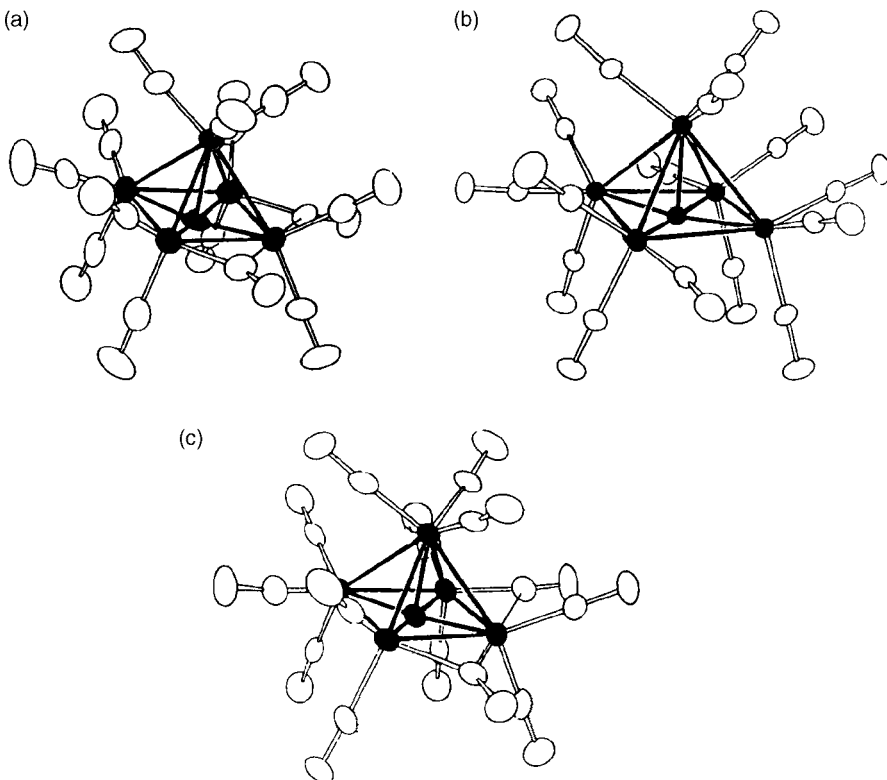


Figure 15 Molecular structures of (a) $[\text{Fe}_5(\text{C})(\text{CO})_{14}]^{2-}$, (b) $\text{Fe}_5(\text{C})(\text{CO})_{15}$, and (c) $[\text{Fe}_5(\text{N})(\text{CO})_{14}]^-$

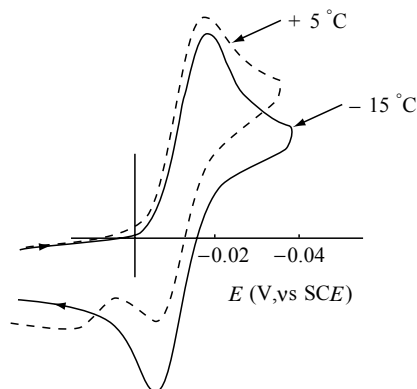


Figure 16 Cyclic voltammetric responses exhibited by $\text{Fe}_5(\text{C})(\text{CO})_{15}$ in CH_2Cl_2 solution, at different temperatures, with a carbon working electrode (scan rate, 0.1 V s^{-1})

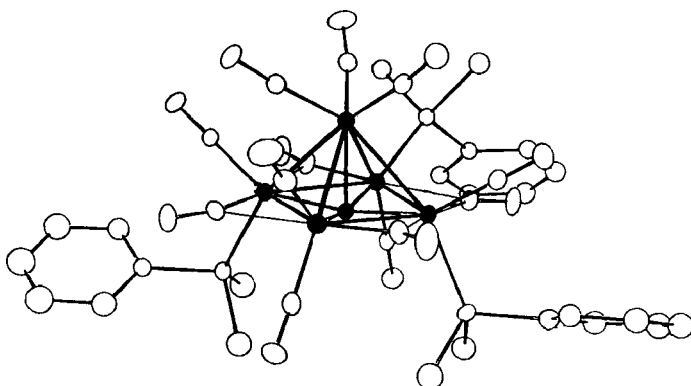


Figure 17 Molecular structure of $\text{Fe}_5(\text{C})(\text{CO})_{12}(\text{PMe}_2\text{Ph})_3$

The easy reduction of $\text{Fe}_5(\text{C})(\text{CO})_{15}$ and the instability of its dianion are likely to be responsible for the fact that simple reaction of $\text{Fe}_5(\text{C})(\text{CO})_{15}$ with PMe_2Ph affords the trisubstituted species $\text{Fe}_5(\text{C})(\text{CO})_{12}(\text{PMe}_2\text{Ph})_3$. The molecular structure of this latter species shows that replacement of carbonyl ligands takes place at the basal iron atoms (Figure 17) [31].

In its turn, $[\text{Fe}_5(\text{N})(\text{CO})_{14}]^-$ undergoes two separate one-electron reductions, with only the first one being chemically reversible (Figure 18) [32].

The 74/75/76-CVE $[\text{Fe}_5(\text{N})(\text{CO})_{14}]^{-2-/-3-}$ redox sequence occurs in acetonitrile solution at $E^0 = -0.90 \text{ V}$ and $E_p = -1.40 \text{ V}$, respectively, whereas in dichloromethane solution it occurs at $E^0 = -1.04 \text{ V}$ and $E_p = -1.50 \text{ V}$, respectively.

As in the case of $[\text{Fe}_4(\text{N})(\text{CO})_{12}]^-$, evidence has been gained that in the presence of phosphines the first cathodic reduction of $[\text{Fe}_5(\text{N})(\text{CO})_{14}]^-$ affords

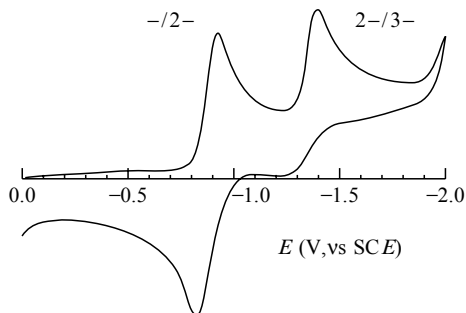


Figure 18 Cyclic voltammogram recorded at a mercury electrode for a MeCN solution of $[\text{Fe}_5(\text{N})(\text{CO})_{14}]^-$ (scan rate, 0.2 V s^{-1})

the monosubstituted species $[\text{Fe}_5(\text{N})(\text{CO})_{13}(\text{PR}_3)]^-$ via an electron-transfer chain catalytic process [5].

2.1.3 $[\text{Fe}_6(\text{C})(\text{CO})_{16}]^{2-}$ versus $[\text{Fe}_6(\text{N})(\text{CO})_{15}]^{3-}$

The octahedral geometries of the 86-CVE cluster dianions $[\text{Fe}_6(\text{C})(\text{CO})_{16}]^{2-}$ and $[\text{Fe}_6(\text{N})(\text{CO})_{15}]^{3-}$ are illustrated in Figure 19 [29,33]. In these cases, the carbide or nitride atoms are fully encapsulated inside the Fe_6 cage.

As deducible from Figure 20, $[\text{Fe}_6(\text{C})(\text{CO})_{16}]^{2-}$ undergoes in dichloroethane solution essentially irreversible redox changes [34]. Only the first one-electron oxidation ($E_p = +0.20 \text{ V}$) has some features of chemical reversibility, indicating that the 85-CVE monoanion $[\text{Fe}_6(\text{C})(\text{CO})_{16}]^-$, even if short-lived, is able to exist. In contrast, both of the 84-CVE neutral species $\text{Fe}_6(\text{C})(\text{CO})_{16}$, or the tetranion $[\text{Fe}_6(\text{C})(\text{CO})_{16}]^{4-}$, immediately decompose.

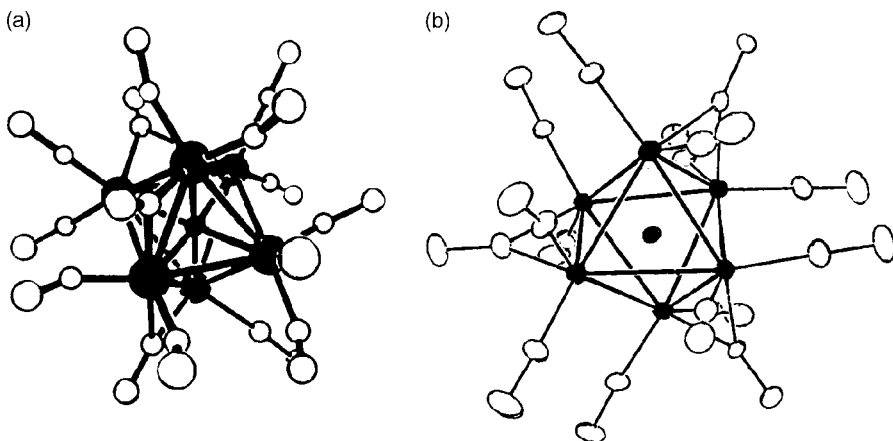


Figure 19 Molecular structures of (a) $[\text{Fe}_6(\text{C})(\text{CO})_{16}]^{2-}$, and (b) $[\text{Fe}_6(\text{N})(\text{CO})_{15}]^{3-}$

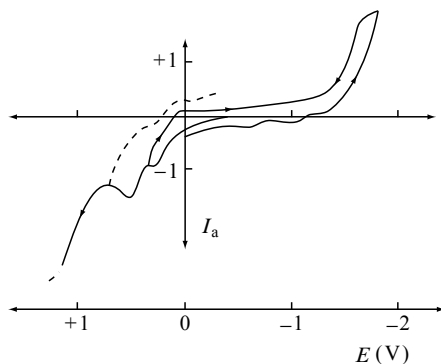


Figure 20 Cyclic voltammogram recorded at a platinum electrode for a C₂H₄Cl₂ solution of $[\text{Fe}_6(\text{C})(\text{CO})_{16}]^{2-}$ (scan rate, 0.1 V s⁻¹)

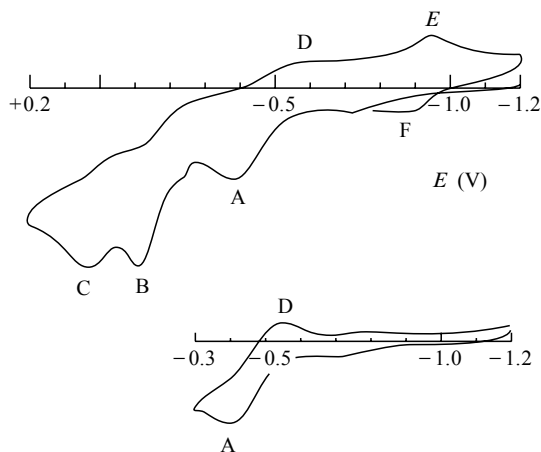


Figure 21 Cyclic voltammograms recorded at a platinum electrode for a MeCN solution of $[\text{Fe}_6(\text{N})(\text{CO})_{15}]^{3-}$ (scan rate, 0.2 V s⁻¹)

As illustrated in Figure 21, the redox ability of the nitride $[\text{Fe}_6(\text{N})(\text{CO})_{15}]^{3-}$ is also characterized by three, substantially irreversible, one-electron anodic steps [29].

In addition, in this case the corresponding 85-CVE dianion $[\text{Fe}_6(\text{N})(\text{CO})_{15}]^{2-}$ is able to exist for short periods of time ($t_{1/2} \approx 15$ s). It is, however, interesting to note that it has been proved that, upon exhaustive three-electron oxidation, the original octahedral trianion releases one Fe(CO) group and converts to the previously examined square-pyramidal pentairon species $[\text{Fe}_5(\text{N})(\text{CO})_{14}]^-$ [29].

2.2 HOMONUCLEAR RUTHENIUM CLUSTERS

2.2.1 $\text{Ru}_5(\text{C})(\text{CO})_{15}$ versus $[\text{Ru}_5(\text{N})(\text{CO})_{14}]^-$

The only possible structural comparison between carbide and nitride complexes of ruthenium can be found in the 74-CVE clusters $\text{Ru}_5(\text{C})(\text{CO})_{15}$ and $[\text{Ru}_5(\text{N})(\text{CO})_{14}]^-$, the square pyramidal structures of which are shown in Figure 22 [35,36].

$\text{Ru}_5(\text{C})(\text{CO})_{15}$ undergoes in dichloromethane solution either an irreversible two-electron oxidation ($E_p = +0.49$ V, vs Ag/Ag^+), or two sequential irreversible one-electron reductions ($E_p = -0.58$ and -1.04 V, respectively), which induce reorganization to the isoelectronic (and likely isostructural) dianion $[\text{Ru}_5(\text{C})(\text{CO})_{14}]^{2-}$. This latter, in turn, undergoes an irreversible oxidation ($E_p = +0.2$ V) to the neutral carbonylated congener $\text{Ru}_5(\text{C})(\text{CO})_{15}$ [36].

As happens for $\text{Fe}_5(\text{C})(\text{CO})_{15}$, $\text{Ru}_5(\text{C})(\text{CO})_{15}$ also easily reacts with phosphines to afford the decarbonylated species $\text{Ru}_5(\text{C})(\text{CO})_{15-n}(\text{PR}_3)_n$ ($n = 1, 2$) [37].

Unfortunately, no electrochemical comparison is possible with $[\text{Ru}_5(\text{N})(\text{CO})_{14}]^-$, in that no electrochemical investigations have so far been carried out on this system.

2.2.2 $[\text{Ru}_8(\text{P})(\text{CO})_{22}]^-$

The square antiprismatic assembly of the eight ruthenium atoms in the 114-CVE phosphide monoanion $[\text{Ru}_8(\text{P})(\text{CO})_{22}]^-$ is illustrated in Figure 23 [38].

At room temperature, $[\text{Ru}_8(\text{P})(\text{CO})_{22}]^-$ undergoes, in dichloromethane solution, two subsequent one-electron reductions with apparent features of chemical reversibility ($E_{-1/2}^{0'} = -0.24$ V, $E_{2-/3-}^{0'} = -0.37$ V, vs Ag/AgCl), followed by a third two-electron reduction which is irreversible in character

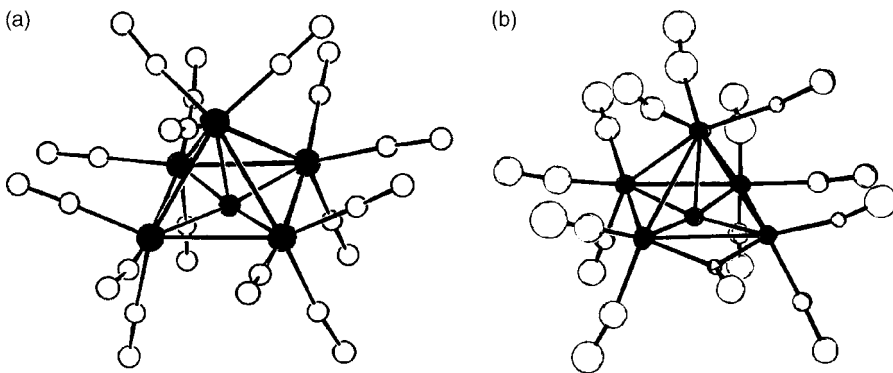


Figure 22 Molecular structures of (a) $\text{Ru}_5(\text{C})(\text{CO})_{15}$, and (b) $[\text{Ru}_5(\text{N})(\text{CO})_{14}]^-$

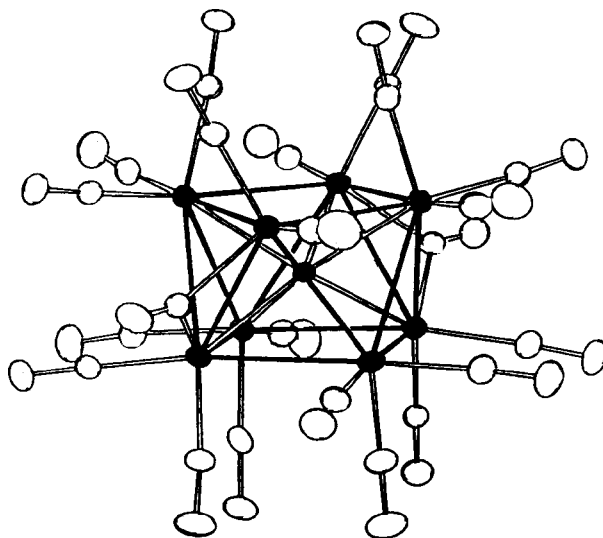


Figure 23 Molecular structure of $[\text{Ru}_8(\text{P})(\text{CO})_{22}]^-$

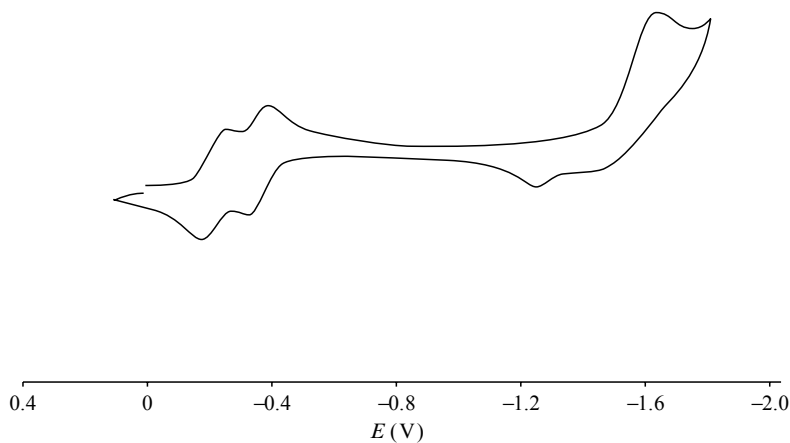


Figure 24 Cyclic voltammogram recorded at a platinum electrode for a CH_2Cl_2 solution of $[\text{Ru}_8(\text{P})(\text{CO})_{22}]^-$ (scan rate, 0.1 V s^{-1})

($E_{\text{p}3-/5-} = -1.63 \text{ V}$) (Figure 24). In fact, it has been hypothesized that some structural change occurs inside the molecular framework of the electrogenerated trianion $[\text{Ru}_8(\text{P})(\text{CO})_{22}]^{3-}$ [38].

2.2.3 $[\text{Ru}_{10}(\text{C})(\text{CO})_{24}]^{2-}$

The supertetrahedral geometry of the 134-CVE dianion $[\text{Ru}_{10}(\text{C})(\text{CO})_{24}]^{2-}$ is shown in Figure 25 [39–41].

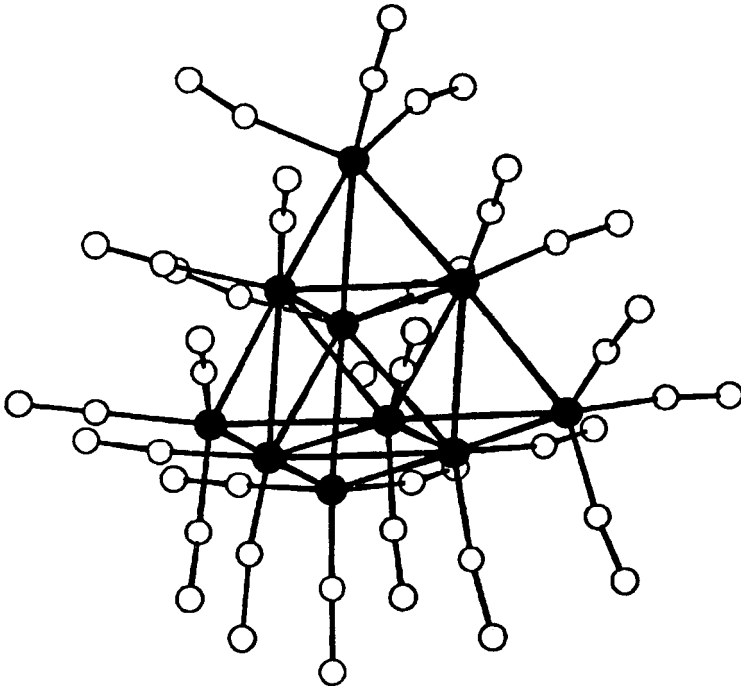


Figure 25 Molecular structure of $[\text{Ru}_{10}(\text{C})(\text{CO})_{24}]^{2-}$

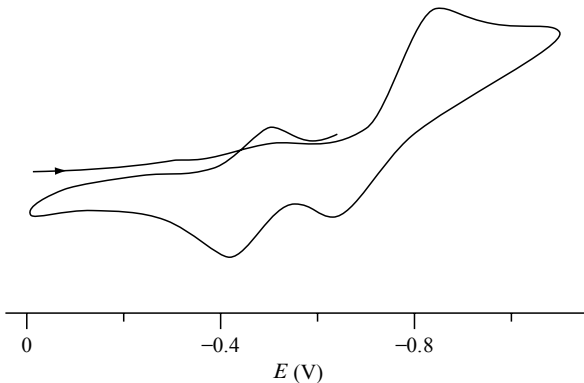


Figure 26 Cyclic voltammogram recorded at a platinum electrode for a CH_2Cl_2 solution of $[\text{Ru}_{10}(\text{C})(\text{CO})_{24}]^{2-}$ (scan rate, 0.1 V s^{-1})

As Figure 26 shows, $[\text{Ru}_{10}(\text{C})(\text{CO})_{24}]^{2-}$ undergoes, in dichloromethane solution a quasi-reversible two-electron reduction ($E_{\text{p}2-/4-} = -0.84 \text{ V}$, vs Ag/AgCl), complicated by subsequent reactions which generate a new, unidentified species which is able to be oxidized reversibly at $E^0 = -0.46 \text{ V}$ [42].

2.2.4 Further Structural Data

We have already discussed in the introductory section the electrochemical behaviour and the structural geometries of the 86-CVE species $[\text{Ru}_6(\text{C})(\text{CO})_{16}]^{2-}$ and $\text{Ru}_6(\text{C})(\text{CO})_{17}$.

The solid-state structure of the 138-CVE dianion $[\text{Ru}_{10}(\text{C})_2(\text{CO})_{24}]^{2-}$ is also available [43].

In the field of nitride clusters, the X-ray structures of both the tetranuclear 62-CVE $[\text{Ru}_4(\text{N})(\text{CO})_{12}]^-$ and the decanuclear 134-CVE $[\text{Ru}_{10}(\text{N})(\text{CO})_{24}]^-$ monoanions are known [41,44].

2.3 HOMONUCLEAR OSMIUM CLUSTERS

As far as osmium clusters having interstitial atoms are concerned, no comparative analysis among isonuclear complexes is possible.

2.3.1 $[\text{Os}_5(\text{C})(\text{CO})_{14}]^{2-}$ and $\text{Os}_5(\text{C})(\text{CO})_{15}$

The square pyramidal assembly of the 74-CVE complexes $\text{Os}_5(\text{C})(\text{CO})_{15}$ and $[\text{Os}_5(\text{C})(\text{CO})_{14}]^{2-}$ are illustrated in Figure 27 [37,45].

As occurs for the iron and ruthenium analogues, the neutral species undergoes in dichloromethane solution an irreversible two-electron reduction ($E_p = -1.50$ V, vs Ag/Ag^+) to the decarbonylated dianion [37].

2.3.2 $[\text{Os}_6(\text{P})(\text{CO})_{18}]^-$

The trigonal prismatic geometry of the 90-CVE phosphide-encapsulating monoanion $[\text{Os}_6(\text{P})(\text{CO})_{18}]^-$ is shown in Figure 28 [46].

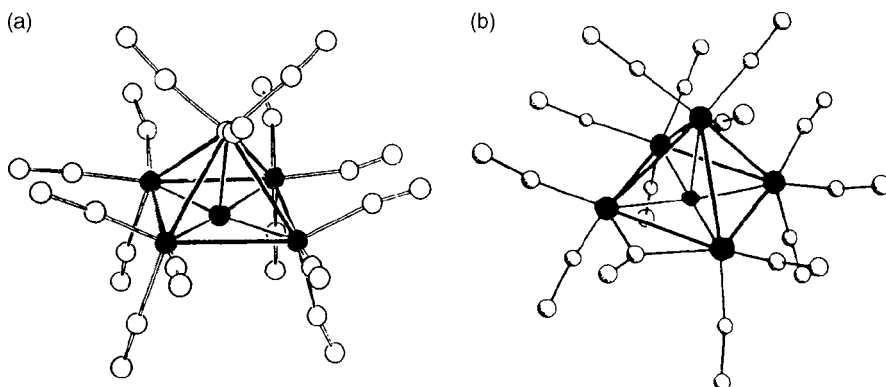


Figure 27 Molecular structures of (a) $\text{Os}_5(\text{C})(\text{CO})_{15}$, and (b) $[\text{Os}_5(\text{C})(\text{CO})_{14}]^{2-}$

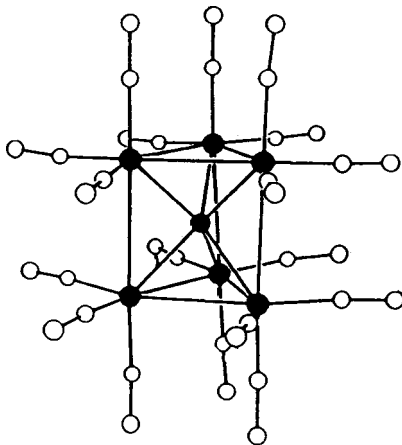


Figure 28 Molecular structure of $[\text{Os}_6(\text{P})(\text{CO})_{18}]^-$

It has been briefly reported that $[\text{Os}_6(\text{P})(\text{CO})_{18}]^-$ undergoes an irreversible two-electron reduction to the corresponding 92-CVE trianion $[\text{Os}_6(\text{P})(\text{CO})_{18}]^{3-}$ [47]. This result indeed sounds rather unlikely, in that the electrochemical irreversibility not only precludes significant structural changes, but also variations in chemical composition.

2.3.3 $[\text{Os}_{10}(\text{C})(\text{CO})_{24}]^{2-}$

The tetra-capped octahedral geometry of the 134-CVE dianion $[\text{Os}_{10}(\text{C})(\text{CO})_{24}]^{2-}$ is shown in Figure 29 [48].

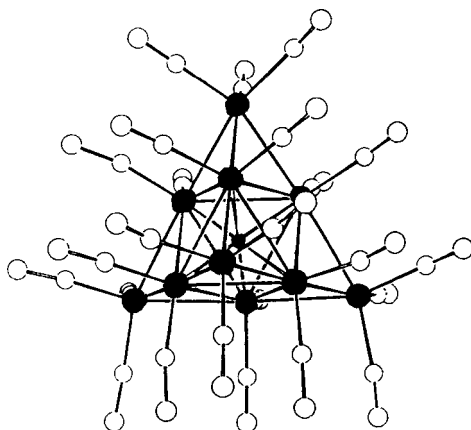


Figure 29 Molecular structure of $[\text{Os}_{10}(\text{C})(\text{CO})_{24}]^{2-}$

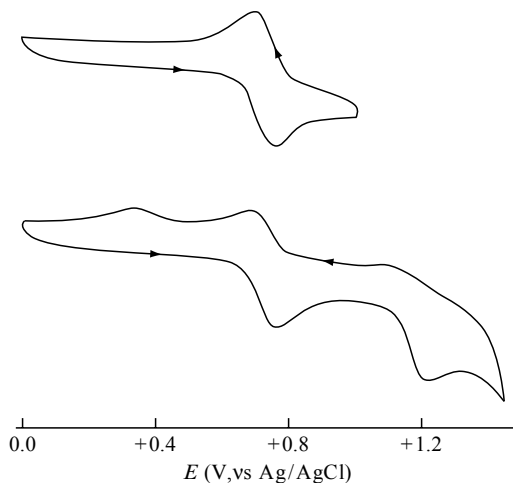


Figure 30 Cyclic voltammograms recorded at a platinum electrode for a CH_2Cl_2 solution of $[\text{Os}_{10}(\text{C})(\text{CO})_{24}]^{2-}$ (scan rate, 0.1 V s^{-1})

The complex undergoes, in dichloromethane solution, either a first reversible one-electron removal ($E^{0'} = +0.74 \text{ V}$), followed by a second irreversible one-electron oxidation ($E_p = +1.16 \text{ V}$) (Figure 30) [49], or two almost overlapping one-electron additions, with only the first one of these possessing features of chemical reversibility ($E^{0'} = -1.39 \text{ V}$) [50].

It is interesting to note that the isoelectronic and isostructural hydride dianion $[\text{Os}_{10}(\text{H})_4(\text{CO})_{24}]^{2-}$ (Figure 31) [51] exhibits a quite similar redox pattern, but is shifted towards less positive potential values ($E_{2-/1}^{0'} = +0.35 \text{ V}$; $E_{p-/0} = +0.57 \text{ V}$) [49].

This result, together with what has been previously illustrated for $[\text{Ru}_6(\text{C})(\text{CO})_{16}]^{2-}/[\text{Ru}_6(\text{CO})_{18}]^{2-}$, suggests that within isostructural and isoelectronic species the presence of interstitial carbide atoms makes the removal of electrons more difficult.

It must also be taken into account that, as previously noted, the isostructural and isoelectronic $[\text{Ru}_{10}(\text{C})(\text{CO})_{24}]^{2-}$ species only undergoes a single two-electron reduction, accompanied by additional complicated chemical reactions [42].

2.3.4 Further Structural Data

The solid-state structures of the 62-CVE $[\text{Os}_4(\text{N})(\text{CO})_{12}]^-$ and the 76-CVE $\text{Os}_5(\text{C})(\text{CO})_{16}$ species are known [36,52].

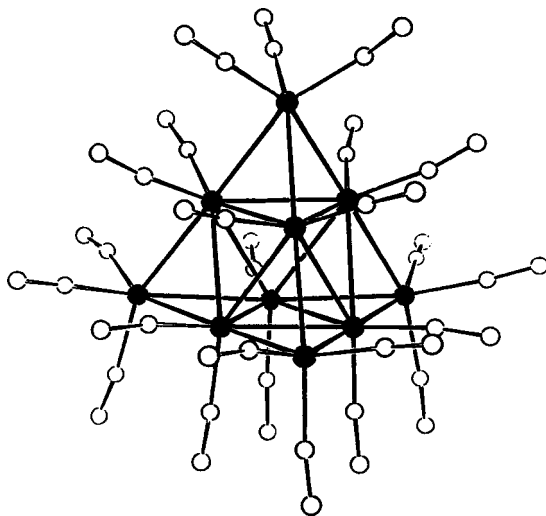


Figure 31 Molecular structure of $[\text{Os}_{10}(\text{H})_4(\text{CO})_{24}]^{2-}$

2.4 HOMONUCLEAR COBALT CLUSTERS

2.4.1 $[\text{Co}_6(\text{C})(\text{CO})_{15}]^{2-}$ versus $[\text{Co}_6(\text{N})(\text{CO})_{15}]^-$ and $[\text{Co}_6(\text{P})(\text{CO})_{16}]^-$; $[\text{Co}_6(\text{C})_2(\text{CO})_{18}]$

Figure 32 shows the molecular structures of the 90-CVE $[\text{Co}_6(\text{C})(\text{CO})_{15}]^{2-}$ and $[\text{Co}_6(\text{N})(\text{CO})_{15}]^-$, plus that of the 92-CVE $[\text{Co}_6(\text{P})(\text{CO})_{16}]^-$ species [53–55].

It is interesting to note that the 90-CVE species $[\text{Co}_6(\text{C})(\text{CO})_{15}]^{2-}$ and $[\text{Co}_6(\text{N})(\text{CO})_{15}]^-$ possess the trigonal prismatic geometry already observed for the isoelectronic complex $[\text{Os}_6(\text{P})(\text{CO})_{16}]^-$ (but for the disposition of a few carbonyl ligands), whereas the 92-CVE $[\text{Co}_6(\text{P})(\text{CO})_{16}]^-$ possesses an open structure. It could be naively thought that the two additional electrons cause breakage of the bonds within the basal metal atoms of the trigonal prism.

From the electrochemical viewpoint, the carbide species $[\text{Co}_6(\text{C})(\text{CO})_{15}]^{2-}$ in dichloromethane solution undergoes two sequential one-electron oxidations, irreversible in character ($E_p = 0.00$ and $+0.15$ V, respectively) [34], which cause decarbonylation followed by geometrical reorganization to the 87-CVE octahedral $[\text{Co}_6(\text{C})(\text{CO})_{14}]^-$ (Figure 33) [56].

In its turn, $[\text{Co}_6(\text{N})(\text{CO})_{15}]^-$ is more difficult to oxidize, in that it undergoes in acetonitrile solution an irreversible two-electron oxidation at $E_p = +0.64$ V [57]. From a speculative viewpoint, it might be convenient to think that such a step is the preliminary approach to the final decarbonylated 86-CVE mono-anion $[\text{Co}_6(\text{N})(\text{CO})_{13}]^-$, which possesses an octahedral geometry. [58]

$[\text{Co}_6(\text{C})_2(\text{CO})_{18}]$ consists of two tetrahedral $\text{Co}_3(\text{C})(\text{CO})_9$ sub-units, connected to one another through the carbide–carbide bond (Figure 34(a)) [59,60].

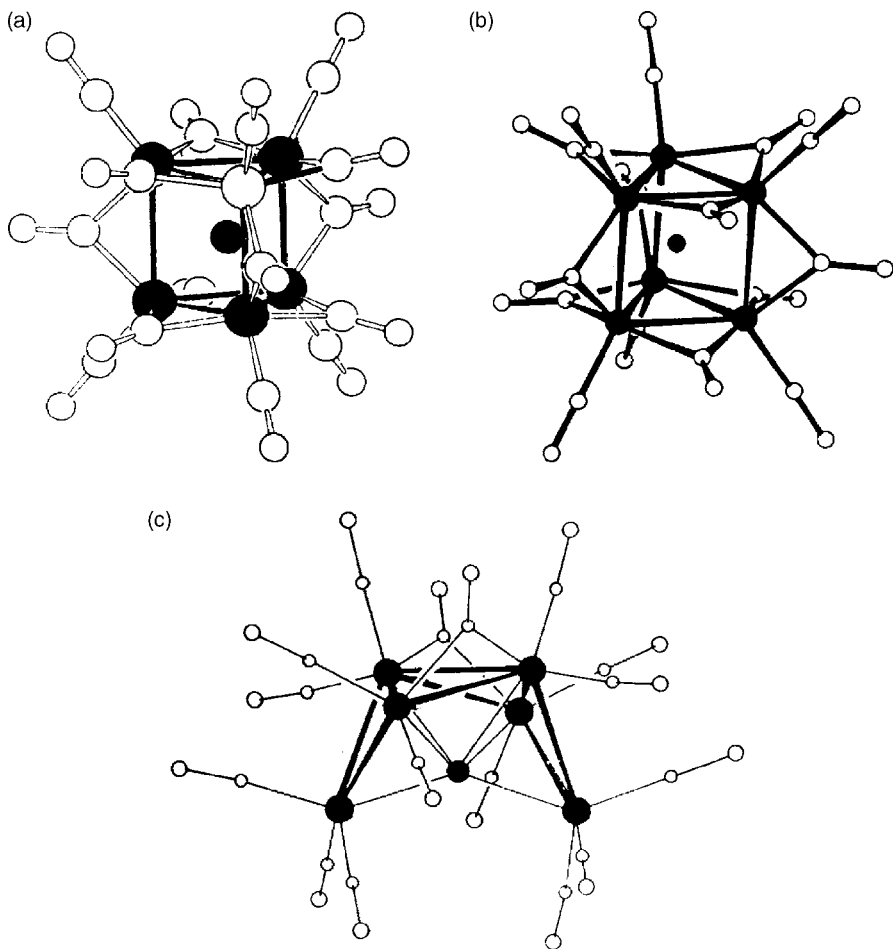


Figure 32 Molecular structures of (a) $[\text{Co}_6(\text{C})(\text{CO})_{15}]^{2-}$, (b) $[\text{Co}_6(\text{N})(\text{CO})_{15}]^{-}$, and (c) $[\text{Co}_6(\text{P})(\text{CO})_{16}]^{-}$

As illustrated in Figure 34(b), at -40°C , this species undergoes two one-electron reductions with features of partial chemical reversibility. At higher temperatures, the electrogenerated radical anion $[\text{Co}_6(\text{C})_2(\text{CO})_{18}]^{\bullet-}$ undergoes fast complicated chemical reactions [61].

2.4.2 $[\text{Co}_7(\text{N})(\text{CO})_{15}]^{2-}$

The 100-CVE $[\text{Co}_7(\text{N})(\text{CO})_{15}]^{2-}$ possesses a trigonal prismatic geometry, one square face of which is capped by a seventh cobalt atom (Figure 35) [62]. To date the corresponding carbide species is not known.

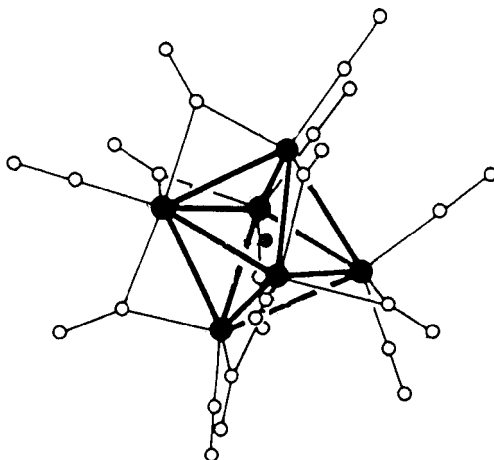


Figure 33 Molecular structure of $[\text{Co}_6(\text{C})(\text{CO})_{14}]^-$

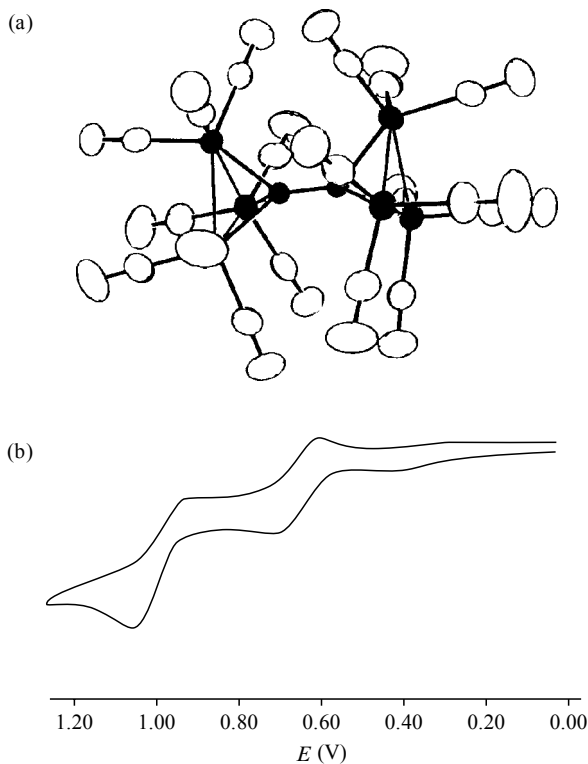


Figure 34 (a) Molecular structure of $[\text{Co}_6(\text{C})_2(\text{CO})_{18}]$, and (b) its cyclic voltammetric profile in CH_2Cl_2 solution at -40°C (scan rate, 0.05 V s^{-1})

As illustrated in Figure 36, $[\text{Co}_7(\text{N})(\text{CO})_{15}]^{2-}$ undergoes in acetonitrile solution two separate one-electron reductions with features of chemical reversibility ($E_{2-/3-}^{0'} = -1.04 \text{ V}$; $E_{3-/4-}^{0'} = -1.52 \text{ V}$). Indeed, over the longer time-scale of macroelectrolysis, only the 101-CVE trianion $[\text{Co}_7(\text{N})(\text{CO})_{15}]^{3-}$ proved to be stable [57].

2.4.3 $[\text{Co}_8(\text{C})(\text{CO})_{18}]^{2-}$

Figure 37 briefly shows the tetragonal antiprismatic geometry of the 114-CVE dianion $[\text{Co}_8(\text{C})(\text{CO})_{18}]^{2-}$ [63] and its voltammetric behaviour [34].

In spite of the apparent chemical reversibility of the redox changes $2 -/-$ ($E^{0'} = -0.01 \text{ V}$), $2 -\beta -$ ($E^{0'} = -0.81 \text{ V}$), and $3 -/4 -$ ($E^{0'} = -1.35 \text{ V}$), exhaustive macroelectrolysis tests proved that such redox congeners are not long-lived [34].

2.4.4 $[\text{Co}_9(\text{P})(\text{CO})_{21}]^{2-}$ and $[\text{Co}_{10}(\text{P})(\text{CO})_{22}]^{3-}$

As shown in Figure 38, the two anions $[\text{Co}_9(\text{P})(\text{CO})_{21}]^{2-}$ and $[\text{Co}_{10}(\text{P})(\text{CO})_{22}]^{3-}$ have geometries related to one another in that the Co_9P core is comprised of a monocapped squared antiprism, whereas the Co_{10}P core consists of a bicapped square antiprism, in both cases encapsulating a phosphide atom [64].

The 130-CVE Co_9P dianion displays an interesting redox behaviour, in that, as shown in Figure 39, it undergoes, in acetonitrile solution, either a one-electron oxidation ($E^{0'} = +0.16 \text{ V}$), or a two-electron reduction ($E^{0'} = -1.00 \text{ V}$), both of which are accompanied by degradation to a so far unidentified new species able to support reversibly two redox changes at intermediate potential values ($E^{0'} = -0.06$ and -0.51 V , respectively).

In its turn, the 142-CVE Co_{10}P trianion exhibits somewhat similar redox pathways, in that it also undergoes either a one-electron oxidation ($E^{0'} = -0.10 \text{ V}$), or a two-electron reduction. In this case, however, the two-electron reduction proceeds through two slightly separated one-electron steps ($E^{0'} = -1.32$ and -1.47 V , respectively) (Figure 40). The electrogenerated congeners in this case too are not stable, although the degradation seems to follow a different pathway in that there is no trace of the previously cited peak systems at -0.06 and -0.51 V , respectively [64].

2.4.5 $[\text{Co}_{13}(\text{C})_2(\text{CO})_{24}]^{4-}$ versus $[\text{Co}_{13}(\text{N})_2(\text{CO})_{24}]^{3-}$

The molecular structure and electrochemical behaviour of the 177-CVE tetraanion $[\text{Co}_{13}(\text{C})_2(\text{CO})_{24}]^{4-}$ have been discussed in the introduction to this chapter.

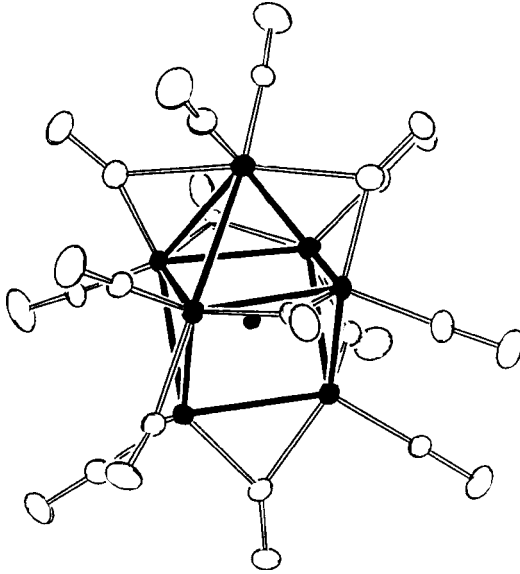


Figure 35 Molecular structure of $[\text{Co}_7(\text{N})(\text{CO})_{15}]^{2-}$

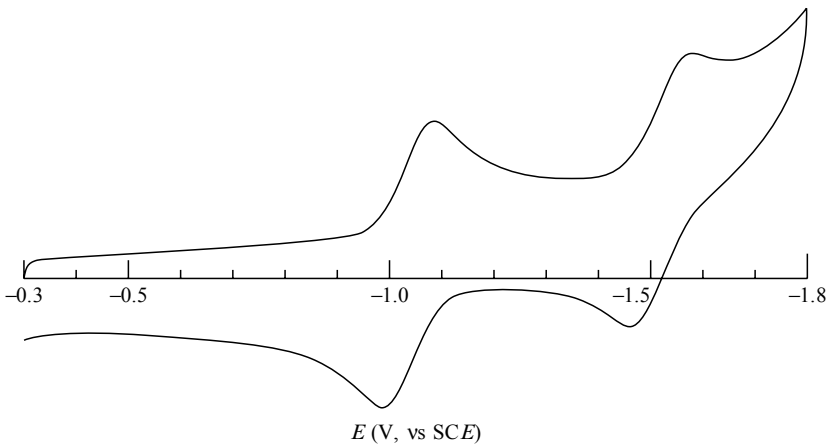


Figure 36 Cyclic voltammogram recorded at a platinum electrode for a MeCN solution of $[\text{Co}_7(\text{N})(\text{CO})_{15}]^{2-}$ (scan rate, 10.0 V s^{-1})

As seen, the dicarbide undergoes reversibly either a one-electron oxidation or two discrete one-electron reductions. Quite interestingly, as illustrated in Figure 41, the isostructural 178-CVE dinitride $[\text{Co}_{13}(\text{N})_2(\text{CO})_{24}]^{3-}$ undergoes reversibly only two separated one-electron reductions at $E^0 = -0.74$ and

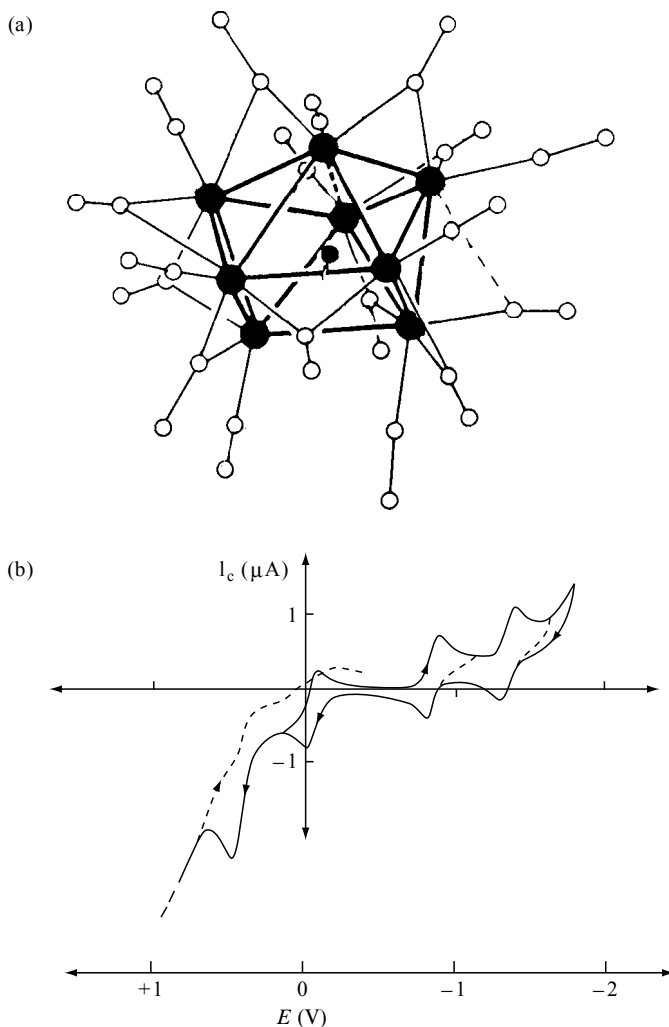


Figure 37 (a) Molecular structure of $[\text{Co}_8(\text{C})(\text{CO})_{18}]^{2-}$, and (b) its cyclic voltammogram profile in 1,2- $\text{C}_2\text{H}_4\text{Cl}_2$, recorded at a platinum electrode (scan rate, 0.1 V s^{-1})

$E^0 = -1.29 \text{ V}$, respectively. A further reduction at $E_p = -1.68 \text{ V}$ also occurs but it does not possess any features of chemical reversibility [65].

It is therefore evident that, in spite of the isostructural geometrical frameworks, the Co_{13}C_2 assembly is able to shuttle from the 176-CVE to 179-CVE forms without any important structural modifications, whereas the Co_{13}N_2 assembly reversibly supports the sequential changes from 178-CVE to 180-CVE.

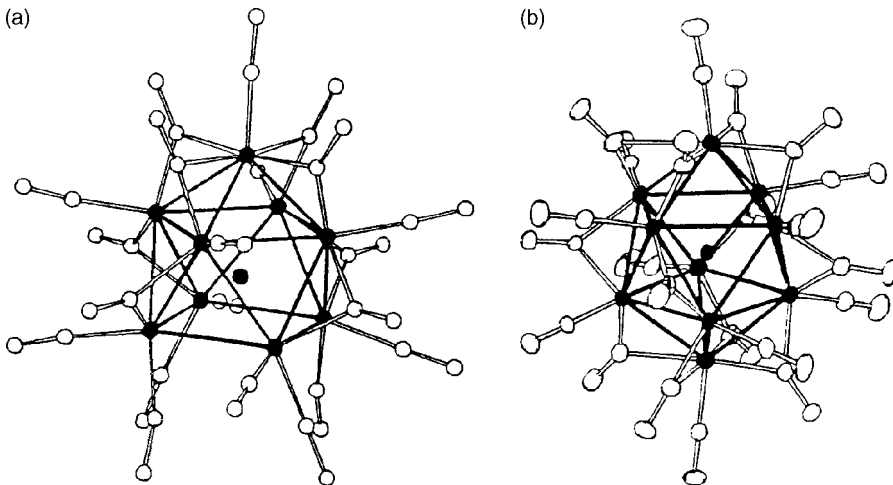


Figure 38 Molecular structures of (a) $[\text{Co}_9(\text{P})(\text{CO})_{21}]^{2-}$, and (b) $[\text{Co}_{10}(\text{P})(\text{CO})_{22}]^{3-}$

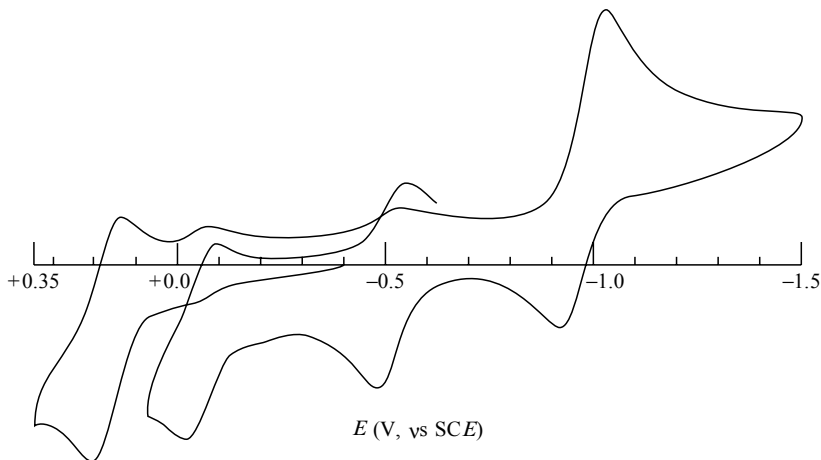


Figure 39 Cyclic voltammogram recorded at a platinum electrode for a MeCN solution of $[\text{Co}_9(\text{P})(\text{CO})_{21}]^{2-}$ (scan rate, 0.2 V s^{-1})

2.4.6 Further Structural Data

A few more cobalt clusters with interstitial carbide atoms have been prepared and structurally characterized, although their electrochemical behaviours are unknown. We recall here the 86-CVE $[\text{Co}_6(\text{C})(\text{CO})_{13}]^{2-}$ [66], the 129-CVE $[\text{Co}_9(\text{C})_2(\text{CO})_{19}]^{2-}$ [67], and the 154-CVE $[\text{Co}_{11}(\text{C})_2(\text{CO})_{22}]^{2-}$ [68] species.

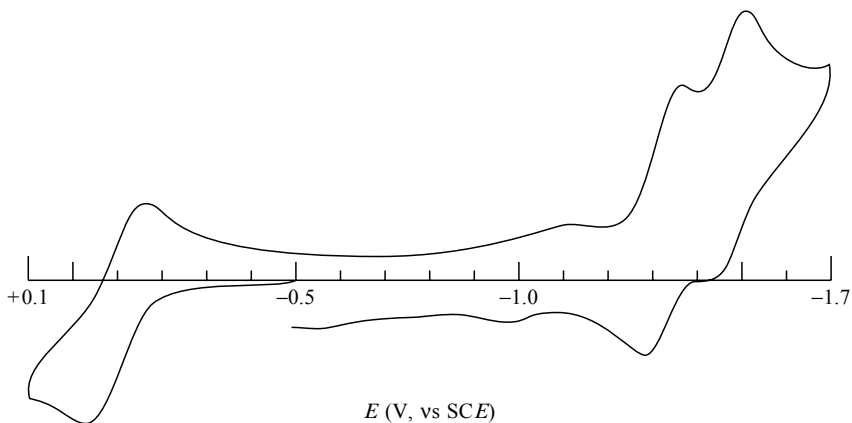


Figure 40 Cyclic voltammogram recorded at a platinum electrode for a MeCN solution of $[\text{Co}_{10}(\text{P})(\text{CO})_{22}]^{3-}$ (scan rate, 0.2 V s^{-1})

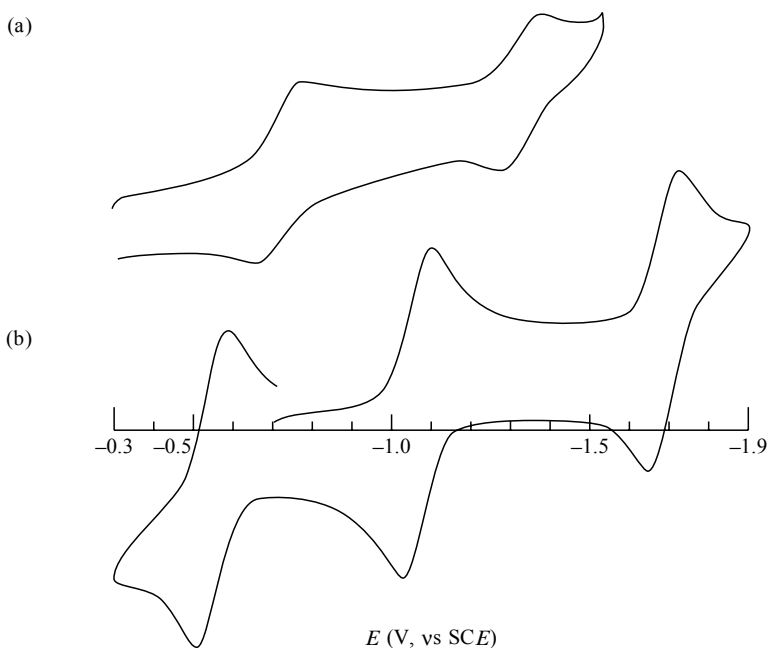


Figure 41 Cyclic voltammograms recorded at a platinum electrode for MeCN solutions of (a) $[\text{Co}_{13}(\text{N})_2(\text{CO})_{24}]^{3-}$, and (b) $[\text{Co}_{13}(\text{C})_2(\text{CO})_{24}]^{4-}$ (scan rates, 0.2 V s^{-1})

Finally, as far as the nitride clusters are concerned, we can cite the 142-CVE $[\text{Co}_{10}(\text{N})_2(\text{CO})_{29}]^{4-}$ [69] and the 196-CVE $[\text{Co}_{14}(\text{N})_3(\text{CO})_{26}]^{3-}$ [70] systems.

2.5 HOMONUCLEAR RHODIUM CLUSTERS

2.5.1 $[\text{Rh}_6(\text{C})(\text{CO})_{15}]^{2-}$ versus $[\text{Rh}_6(\text{N})(\text{CO})_{15}]^-$

Like the cobalt analogues, the 90-CVE species $[\text{Rh}_6(\text{C})(\text{CO})_{15}]^{2-}$ and $[\text{Rh}_6(\text{N})(\text{CO})_{15}]^-$ possess a trigonal prismatic geometry (Figure 42) [71,72].

$[\text{Rh}_6(\text{C})(\text{CO})_{15}]^{2-}$ undergoes, in dichloroethane solution, an irreversible two-electron oxidation ($E_p = +0.34$ V), which, under a CO atmosphere, affords the dimer-like dianion $[\text{Rh}_{12}(\text{C})_2(\text{CO})_{24}]^{2-}$ (Figure 43) [34].

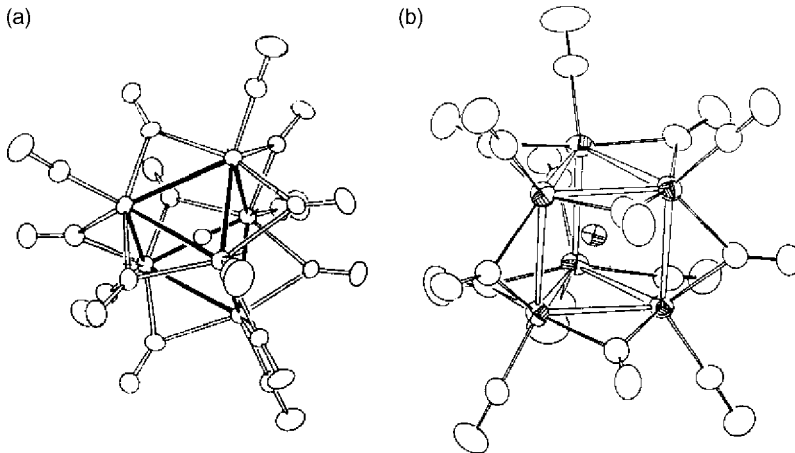


Figure 42 Molecular structures of (a) $[\text{Rh}_6(\text{C})(\text{CO})_{15}]^{2-}$, and (b) $[\text{Rh}_6(\text{N})(\text{CO})_{15}]^-$

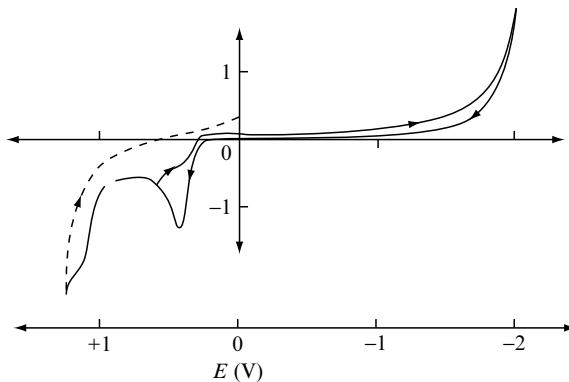


Figure 43 Cyclic voltammogram recorded at a platinum electrode for a 1,2- $\text{C}_2\text{H}_4\text{Cl}_2$ solution of $[\text{Rh}_6(\text{C})(\text{CO})_{15}]^{2-}$ (scan rate, 0.1 V s^{-1})

As happens for the cobalt analogues, the nitride cluster is harder to oxidize; in acetonitrile solution it undergoes a multielectron oxidation at $E_p = +0.93$ V [57].

2.5.2 $[\text{Rh}_7(\text{N})(\text{CO})_{15}]^{2-}$

Figure 44 shows the mono-capped trigonal prismatic geometry of the 100-CVE $[\text{Rh}_7(\text{N})(\text{CO})_{15}]^{2-}$ species [73].

In contrast to the isostructural and isoelectronic $[\text{Co}_7(\text{N})(\text{CO})_{15}]^{2-}$ system, the rhodium cluster undergoes either an irreversible reduction ($E_p = -1.48$ V), or an irreversible oxidation ($E_p = +0.07$ V) [57].

2.5.3 $[\text{Rh}_{12}(\text{C})_2(\text{CO})_{24}]^{2-}$

The above-mentioned 166-CVE dianion $[\text{Rh}_{12}(\text{C})_2(\text{CO})_{24}]^{2-}$ is isoelectronic and substantially isostructural with the tetraanion $[\text{Rh}_{12}(\text{C})_2(\text{CO})_{23}]^{4-}$ discussed above in the Introduction. As a matter of fact, these derivatives possess a geometry which can be seen as two edge-sharing prismatic Rh_6C cores, capped on opposite sides by two extra rhodium atoms (Figure 45) [74].

The redox behaviour of the dianion cluster is illustrated in Figure 46 [75].

In spite of some features of chemical reversibility for the

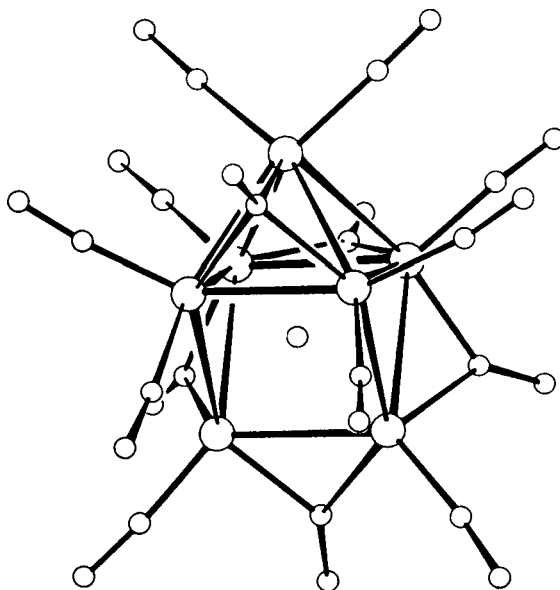


Figure 44 Molecular structure of $[\text{Rh}_7(\text{N})(\text{CO})_{15}]^{2-}$

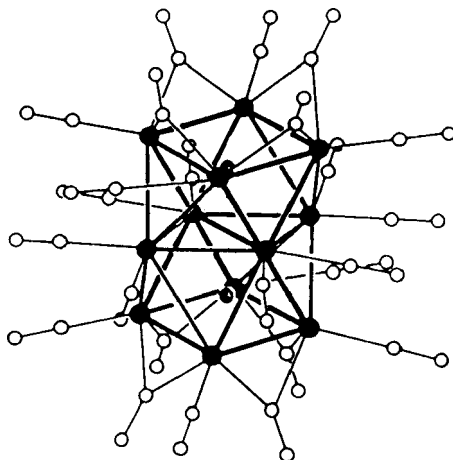


Figure 45 Molecular structure of $[\text{Rh}_{12}(\text{C})_2(\text{CO})_{24}]^{2-}$

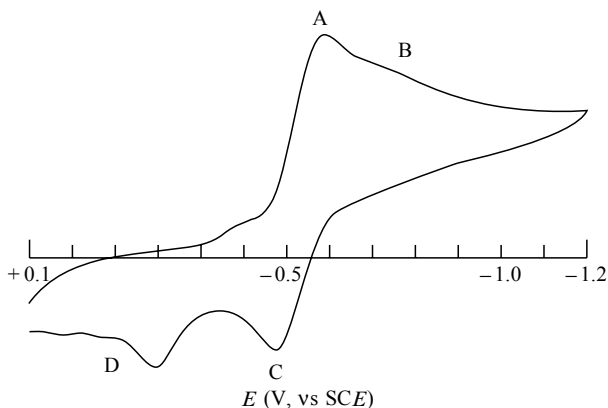


Figure 46 Cyclic voltammogram recorded at a platinum electrode for a MeCN solution of $[\text{Rh}_{12}(\text{C})_2(\text{CO})_{24}]^{2-}$ (scan rate, 0.02 V s^{-1})

$[\text{Rh}_{12}(\text{C})_2(\text{CO})_{24}]^{2-/3-}$ main reduction ($E^0 = -0.54 \text{ V}$), exhaustive reduction affords the decarbonylated species $[\text{Rh}_{12}(\text{C})_2(\text{CO})_{23}]^{4-}$. As a matter of fact, the return peaks C and D are quite reminiscent of the oxidation steps exhibited by the decarbonylated tetraanion (see Figure 5 above).

2.5.4 Further Structural Data

The carbide clusters for which the structures are actually available are the 86-CVE $[\text{Rh}_6(\text{C})(\text{CO})_{13}]^{2-}$ [76], the 114-CVE $\text{Rh}_8(\text{C})(\text{CO})_{19}$ [77], the 166-CVE

$\text{Rh}_{12}(\text{C})_2(\text{CO})_{25}$ [78], the 202-CVE $[\text{Rh}_{14}(\text{C})_2(\text{CO})_{33}]^{2-}$ [79], and the 200-CVE $[\text{Rh}_{15}(\text{C})_2(\text{CO})_{28}]^{2-}$ [80].

In addition to the above cited 100-CVE $[\text{Rh}_7(\text{N})(\text{CO})_{15}]^{2-}$, a number of nitride clusters are also available, namely the 168-CVE $[\text{Rh}_{12}(\text{N})_2(\text{H})(\text{CO})_{23}]^{3-}$ [81], the 188-CVE $[\text{Rh}_{14}(\text{N})_2(\text{CO})_{25}]^{2-}$ [82], the 306-CVE $[\text{Rh}_{23}(\text{N})_4(\text{CO})_{38}]^{3-}$ [83], and the 360-CVE $[\text{Rh}_{28}(\text{N})_4(\text{H})_2(\text{CO})_{41}]^{4-}$ [84] species.

Finally, as far as the phosphide clusters are concerned, the X-ray structures of the 130-CVE $[\text{Rh}_9(\text{P})(\text{CO})_{21}]^{2-}$ and the 142-CVE $[\text{Rh}_{10}(\text{P})(\text{CO})_{22}]^{3-}$ are available [85,86].

2.6 HOMONUCLEAR NICKEL CLUSTERS

2.6.1 $[\text{Ni}_9(\text{C})(\text{CO})_{17}]^{2-}$

Like the isoelectronic $[\text{Co}_9(\text{P})(\text{CO})_{21}]^{2-}$, the 130-CVE dianion $[\text{Ni}_9(\text{C})(\text{CO})_{17}]^{2-}$ is comprised of a mono-capped squared antiprism species (Figure 47) [87].

In acetonitrile solution, the present dianion undergoes either an irreversible oxidation ($E_p = +0.67$ V), or a one-electron reduction ($E^0 = -0.41$ V), along with further complicated chemical reactions [88].

2.6.2 $[\text{Ni}_{32}(\text{C})_6(\text{CO})_{36}]^{6-}$

The spectacular truncated-octahedral assembly of the 386-CVE hexacarbide dianion $[\text{Ni}_{32}(\text{C})_6(\text{CO})_{36}]^{6-}$ is shown in Figure 48. It can be seen as being

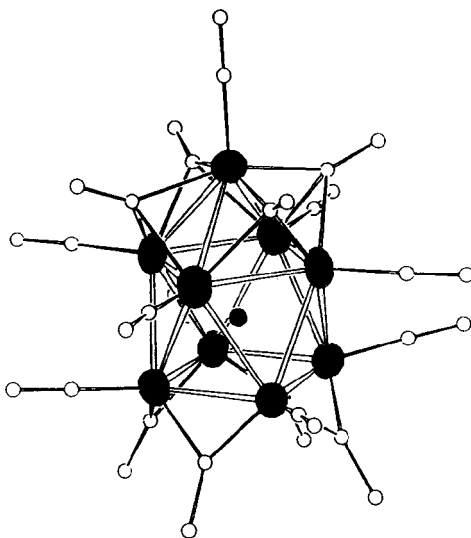


Figure 47 Molecular structure of $[\text{Ni}_9(\text{C})(\text{CO})_{17}]^{2-}$

comprised of a central empty Ni_8 cube, each of the six square faces of which are fused with a square-antiprismatic Ni_8 assembly bearing an interstitial carbide atom [89].

As Figure 49 illustrates, such a hexaanion supercluster exhibits, in acetonitrile solution, a rich redox propensity in that it undergoes reversibly either four sequential one-electron additions or a one-electron removal [90].

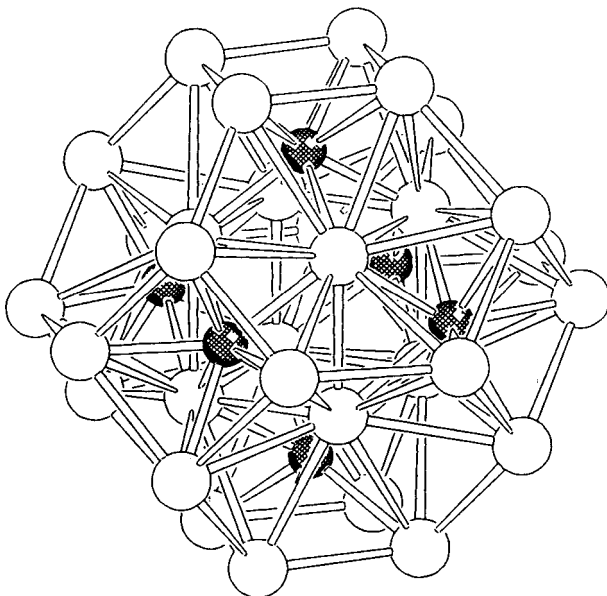


Figure 48 Molecular structure of the metal-carbide core of $[\text{Ni}_{32}(\text{C})_6(\text{CO})_{36}]^{6-}$

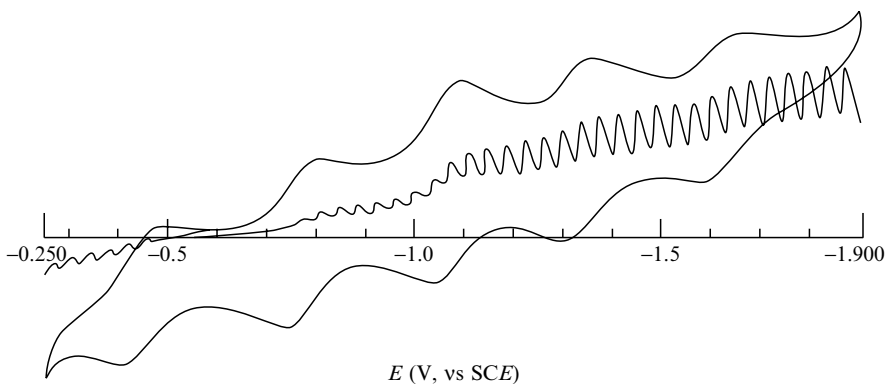


Figure 49 Voltammetric (cyclic and single-sweep hydrodynamic) responses recorded at a platinum electrode for a MeCN solution of $[\text{Ni}_{32}(\text{C})_6(\text{CO})_{36}]^{6-}$ (Scan rates: cyclic voltammogram, 0.2Vs^{-1} ; d.c. voltammogram, 0.02Vs^{-1})

Indeed, over the long time-scales of macroelectrolysis only the heptaanion $[\text{Ni}_{32}(\text{C})_6(\text{CO})_{36}]^{7-}$ remained quite stable.

2.6.3 $[\text{Ni}_{38}(\text{C})_6(\text{CO})_{42}]^{6-}$

Figure 50 shows the molecular structure of the 456-CVE hexacarbide protonated pentaanion $[\text{Ni}_{38}(\text{H})(\text{C})_6(\text{CO})_{42}]^{5-}$ [91]. This derives from the μ_3 -capping of six nickel atoms to the Ni_{32}C_6 core illustrated above.

Figure 51 shows that, somewhat paralleling the electrochemical behaviour of the Ni_{32} precursor, the deprotonated hexaanion $[\text{Ni}_{38}(\text{C})_6(\text{CO})_{42}]^{6-}$ displays three reversible one-electron reductions, as well as a one-electron oxidation [90].

Controlled potential coulometry shows that the corresponding $[\text{Ni}_{38}(\text{C})_6(\text{CO})_{42}]^{7-}$ and $[\text{Ni}_{38}(\text{C})_6(\text{CO})_{42}]^{8-}$ species are both stable.

2.6.4 Further Structural Data

Structural data for further nickel carbide clusters are available, namely the 100-CVE $[\text{Ni}_7(\text{C})(\text{CO})_{12}]^{2-}$ [92], the 118-CVE $[\text{Ni}_8(\text{C})(\text{CO})_{16}]^{2-}$ [87], the 142-CVE $[\text{Ni}_{10}(\text{C})_2(\text{CO})_{16}]^{2-}$ [93], the 152-CVE $[\text{Ni}_{11}(\text{C})_2(\text{CO})_{15}]^{4-}$ [92], the 164-CVE $[\text{Ni}_{12}(\text{C})_2(\text{CO})_{16}]^{4-}$ [92] and the 226-CVE $[\text{Ni}_{16}(\text{C})_4(\text{CO})_{23}]^{4-}$ [94].

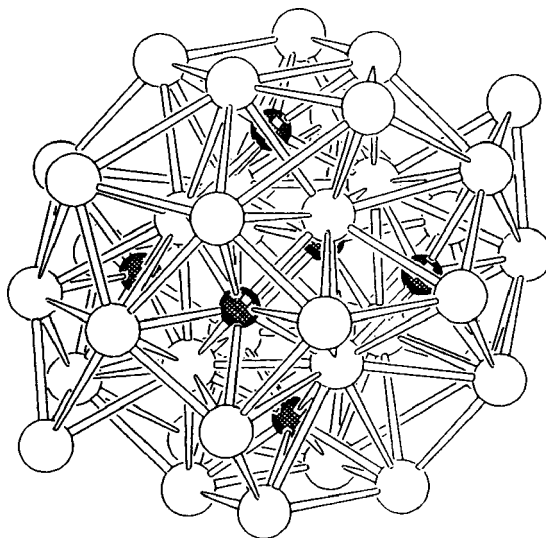


Figure 50 Molecular structure of the metal-carbide core of $[\text{Ni}_{38}(\text{H})(\text{C})_6(\text{CO})_{42}]^{5-}$

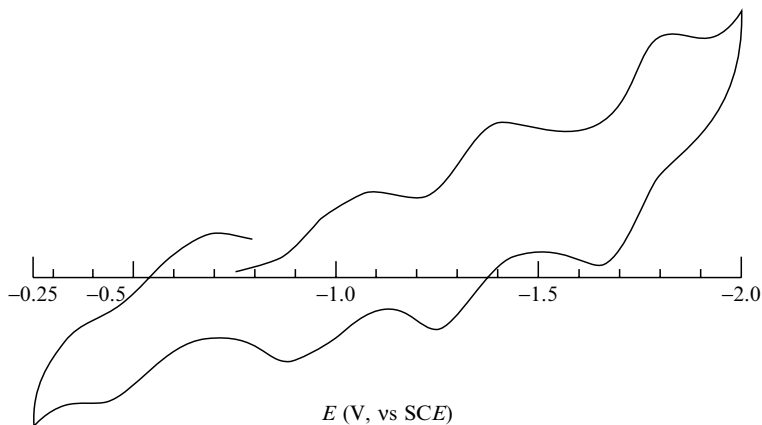


Figure 51 Cyclic voltammetric response recorded at a platinum electrode for a MeCN solution of $[\text{Ni}_{38}(\text{C})_6(\text{CO})_{42}]^{6-}$ (Scan rate, 0.2Vs^{-1})

2.7 HOMONUCLEAR RHENIUM CLUSTERS

2.7.1 $[\text{Re}_7(\text{C})(\text{CO})_{21}]^{3-}$ and $[\text{Re}_8(\text{C})(\text{CO})_{24}]^{2-}$

The mono-capped and bi-capped octahedral assemblies of the 98-CVE and 110-CVE carbide clusters, $[\text{Re}_7(\text{C})(\text{CO})_{21}]^{3-}$ and $[\text{Re}_8(\text{C})(\text{CO})_{24}]^{2-}$, are illustrated in Figure 52 [95,96].

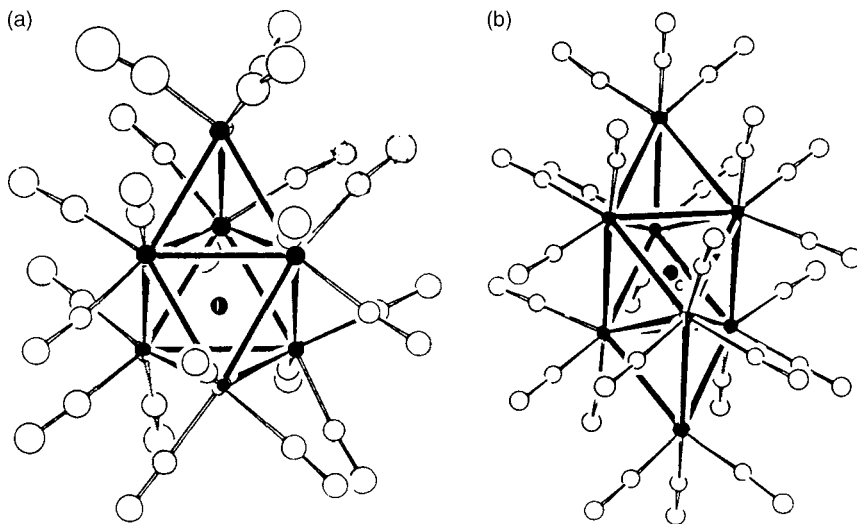


Figure 52 Molecular structures of (a) $[\text{Re}_7(\text{C})(\text{CO})_{21}]^{3-}$, and (b) $[\text{Re}_8(\text{C})(\text{CO})_{24}]^{2-}$

Both complexes undergo, in dichloromethane solution, two one-electron oxidations to the corresponding congeners ($[\text{Re}_7(\text{C})(\text{CO})_{21}]^{3-/2-}$, $E^0 = +0.04 \text{ V}$; $[\text{Re}_7(\text{C})(\text{CO})_{21}]^{2-/1-}$, $E^0 = +0.38 \text{ V}$; $[\text{Re}_8(\text{C})(\text{CO})_{24}]^{2-/1-}$, $E^0 = +0.80 \text{ V}$; $[\text{Re}_8(\text{C})(\text{CO})_{24}]^{-/0}$, $E^0 = +1.05 \text{ V}$) [97,98].

2.7.2 Further Structural Data

Additional structural data for carbide complexes of rhenium are limited to the octahedral 86-CVE $[\text{Re}_6(\text{C})(\text{CO})_{19}]^{2-}$ [99] which comprises the parent octahedral cluster of the above-mentioned species.

3 HETERONUCLEAR CLUSTERS

3.1 HETERONUCLEAR IRON CLUSTERS

3.1.1 Heteronuclear Iron–Molybdenum Clusters

The X-ray structure of the nitride trianion $[\text{Fe}_3\text{Mo}_3(\text{N})(\text{CO})_{18}]^{3-}$ is known [100], but no electrochemical studies have yet been carried out.

3.1.2 Heteronuclear Iron–Ruthenium Clusters

The X-ray structure of the nitride monoanion $[\text{FeRu}_3(\text{N})(\text{CO})_{12}]^{-}$ is known [101], but no electrochemical studies have so far been reported.

3.1.3 Heteronuclear Iron–Rhodium Clusters

3.1.3.1 $[\text{Fe}_5\text{Rh}(\text{N})(\text{CO})_{15}]^{2-}$ and $[\text{Fe}_4\text{Rh}_2(\text{N})(\text{CO})_{15}]^{-}$

The octahedral geometries of the 86-CVE nitride clusters $[\text{Fe}_5\text{Rh}(\text{N})(\text{CO})_{15}]^{2-}$ and $[\text{Fe}_4\text{Rh}_2(\text{N})(\text{CO})_{15}]^{-}$ are illustrated in Figure 53 [102].

In spite of their structural and electron-content analogies, their electrochemical behaviours are rather different, in that, as shown in Figure 54, $[\text{Fe}_5\text{Rh}(\text{N})(\text{CO})_{15}]^{2-}$ undergoes, in THF solution, two anodic and one cathodic processes, with the first anodic and the cathodic one-electron steps being chemically reversible in cyclic voltammetry, whereas $[\text{Fe}_4\text{Rh}_2(\text{N})(\text{CO})_{15}]^{-}$ undergoes only a partially reversible, two-electron reduction [102].

3.1.3.2 Further structural data

The X-ray structures of the 74-CVE $[\text{Fe}_4\text{Rh}(\text{C})(\text{CO})_{14}]^{2-}$ and the 86-CVE $[\text{Fe}_3\text{Rh}_3(\text{C})(\text{CO})_{15}]^{-}$ and $[\text{Fe}_5\text{Rh}(\text{C})(\text{CO})_{16}]^{-}$ carbide clusters are known [103–105].

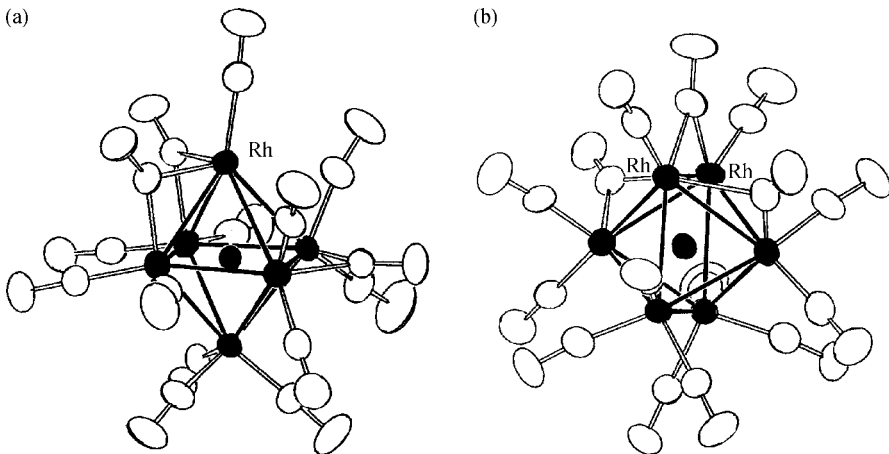


Figure 53 Molecular structures of (a) $[\text{Fe}_5\text{Rh}(\text{N})(\text{CO})_{15}]^{2-}$, and (b) $[\text{Fe}_4\text{Rh}_2(\text{N})(\text{CO})_{15}]^{-}$

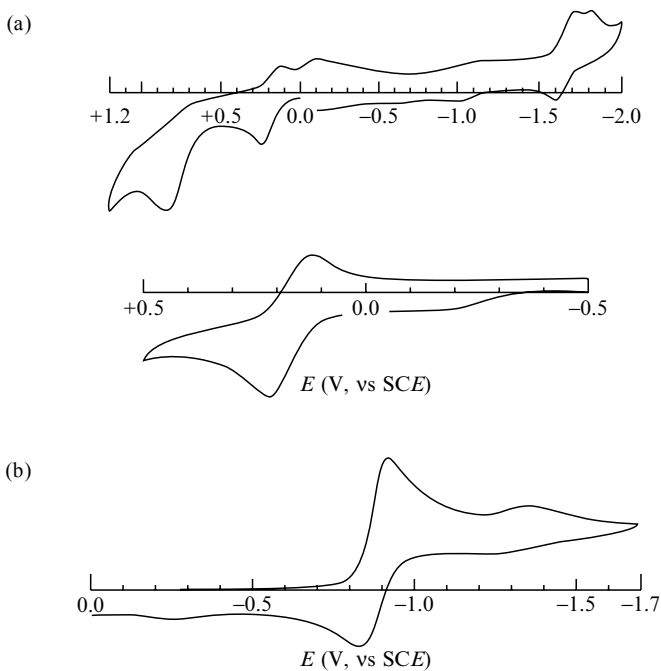


Figure 54 Cyclic voltammetric responses recorded at a platinum electrode for THF solutions of (a) $[\text{Fe}_5\text{Rh}(\text{N})(\text{CO})_{15}]^{2-}$ (scan rates: top, 0.2 V s^{-1} ; bottom, 0.05 V s^{-1}), and (b) $[\text{Fe}_4\text{Rh}_2(\text{N})(\text{CO})_{15}]^{-}$ (scan rate, 0.05 V s^{-1})

3.1.4 Heteronuclear Iron–Iridium Clusters

$[\text{Fe}_5\text{Ir}(\text{N})(\text{CO})_{15}]^{2-}$ is isostructural and isoelectronic with the preceding $[\text{Fe}_5\text{Rh}(\text{N})(\text{CO})_{15}]^{2-}$ species, and also displays a similar electrochemical behaviour [102].

3.1.5 Heteronuclear Iron–Nickel Clusters

3.1.5.1 $[\text{Fe}_6\text{Ni}_6(\text{N})_2(\text{CO})_{24}]^{2-}$

A quite rich redox propensity is exhibited by the 168-CVE dinitride dianion $[\text{Fe}_6\text{Ni}_6(\text{N})_2(\text{CO})_{24}]^{2-}$, the molecular structure of which is shown in Figure 55 [106].

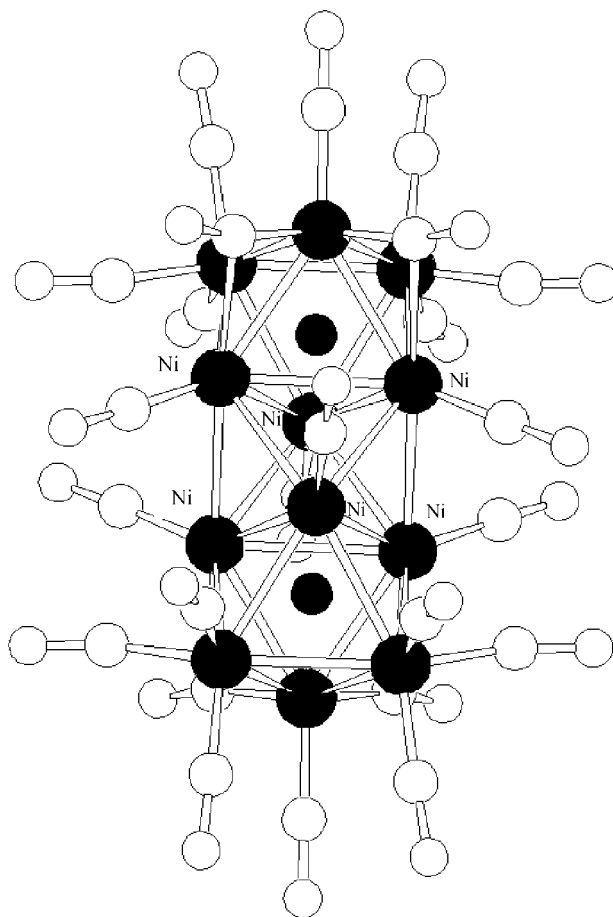


Figure 55 The molecular structure of $[\text{Fe}_6\text{Ni}_6(\text{N})_2(\text{CO})_{24}]^{2-}$

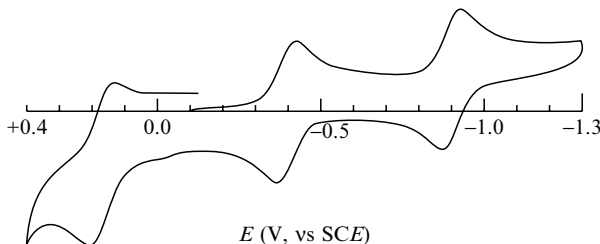


Figure 56 Cyclic voltammogram recorded at a platinum electrode for a MeCN solution of $[\text{Fe}_6\text{Ni}_6(\text{N})_2(\text{CO})_{24}]^{4-}$ (scan rate, 0.2 V s^{-1})

It can be seen as consisting of four parallel triangles forming three fused octahedra sharing one face. The two outer octahedra enclose one nitride atom, whereas the central cavity, consisting only of nickel atoms, is empty.

As illustrated in Figure 56, the dianion exhibits two chemically reversible one-electron reductions ($E_{2-/3-}^{0'} = -0.39 \text{ V}$; $E_{3-/4-}^{0'} = -0.89 \text{ V}$), as well as a one-electron oxidation ($E_{2-/-}^{0'} = +0.17 \text{ V}$), which, in spite of the features of chemical reversibility in the cyclic voltammetric time-scale, resulted in being partially reversible over the long time-scales of macroelectrolysis.

It is interesting to note that preliminary structural data on the anions $[\text{Fe}_6\text{Ni}_6(\text{N})_2(\text{CO})_{24}]^{3-}$ and $[\text{Fe}_6\text{Ni}_6(\text{N})_2(\text{CO})_{24}]^{4-}$ confirm the substantial maintenance of the original geometry [106].

3.1.6 Heteronuclear Iron–Platinum Clusters

The X-ray structure of the 86-CVE carbide dianion $[\text{Fe}_5\text{Pt}(\text{C})(\text{CO})_{15}]^{2-}$ is known [107].

3.1.7 Heteronuclear Iron–Mercury Clusters

3.1.7.1 $\{\mu_4\text{-Hg}[\text{Fe}_5(\text{C})(\text{CO})_{14}]_2\}^{2-}$

Figure 57 shows the molecular structure of the dianion $\{\mu_4\text{-Hg}[\text{Fe}_5(\text{C})(\text{CO})_{14}]_2\}^{2-}$, in which two square pyramidal $\text{Fe}_5(\text{C})(\text{CO})_{14}$ fragments are each other connected through a tetrahedral mercury atom [108].

In dichloromethane solution, the dianion undergoes an irreversible oxidation ($E_p = +0.81 \text{ V}$), as well as two discrete one-electron reductions ($\{\text{Hg}[\text{Fe}_5(\text{C})(\text{CO})_{14}]_2\}^{2-/3-}$, $E^{0'} = -0.81 \text{ V}$; $\{\text{Hg}[\text{Fe}_5(\text{C})(\text{CO})_{14}]_2\}^{3-/4-}$, $E^{0'} = -1.56 \text{ V}$), both accompanied by slow complicated chemical reactions [108]. It is interesting to note that, pointing out the significant and not easily predictable electronic effects played by the connecting mercury atom, the building block unit $[\text{Fe}_5(\text{C})(\text{CO})_{14}]^{2-}$ exhibits a single two-electron reduction ($E^{0'} = -1.58 \text{ V}$) [30]. It would therefore have been expected that the presence of two Fe_5C sub-units

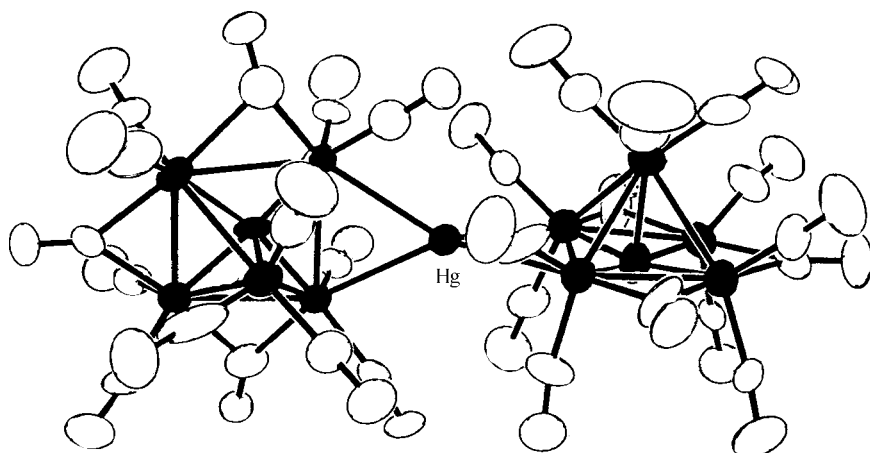


Figure 57 Molecular structure of $\{\mu_4\text{-Hg}[\text{Fe}_5(\text{C})(\text{CO})_{14}]_2\}^{2-}$

in the present heteronuclear cluster should afford one four-electron reduction if they are non-communicating, or two separated two-electron reductions if they communicate.

3.2 HETERONUCLEAR RUTHENIUM CLUSTERS

In addition to the already cited $[\text{FeRu}_3(\text{N})(\text{CO})_{12}]^-$ anion, a few other heteronuclear complexes are known.

3.2.1 Heteronuclear Ruthenium–Platinum Clusters

The X-ray structure of the 86-CVE neutral carbide $\text{PtRu}_5(\text{C})(\text{CO})_{16}$ has been reported [109].

3.2.2 Heteronuclear Ruthenium–Mercury Clusters

The X-ray structures of the 182-CVE $\{\mu_4\text{-Hg}[\text{Ru}_6(\text{C})(\text{CO})_{16}]_2\}^{2-}$ and the 274-CVE $\{\text{Hg}_3[\text{Ru}_9(\text{C})(\text{CO})_{21}]_2\}^{2-}$ carbide dianions are known [110,111].

3.3 HETERONUCLEAR OSMIUM CLUSTERS

3.3.1 Heteronuclear Osmium–Mercury Clusters: $[\text{Os}_{18}\text{Hg}_3(\text{C})_2(\text{CO})_{42}]^{2-}$, $[\text{Os}_{18}\text{Hg}_2(\text{C})_2(\text{CO})_{42}]^{4-}$ and $[\text{Os}_{18}\text{Hg}_2(\text{C})_2(\text{CO})_{42}]^{2-}$

As Figure 58 shows, the structure of the 274-CVE carbide supercluster $\{\text{Hg}_3[\text{Os}_9(\text{C})(\text{CO})_{21}]_2\}^{2-}$ (isostructural with the above-mentioned $\{\text{Hg}_3[\text{Ru}_9(\text{C})(\text{CO})_{21}]_2\}^{2-}$) consists of two tri-capped octahedral $\text{Os}_9(\text{C})(\text{CO})_{21}$ units sandwiching an Hg_3 triangle [112].

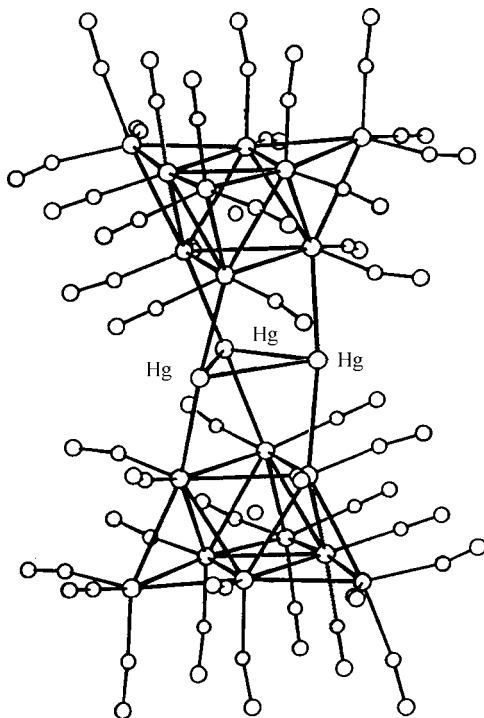


Figure 58 Molecular structure of $[\text{Os}_{18}\text{Hg}_3(\text{C})_2(\text{CO})_{42}]^{2-}$

Such a dianion undergoes, in dichloromethane solution, an irreversible two-electron reduction ($E_p = -0.84$ V, vs Ag/AgCl), which upon releasing a mercury atom affords the 264-CVE tetraanion $\{\text{Hg}_2[\text{Os}_9(\text{C})(\text{CO})_{21}]_2\}^{4-}$. In its turn, such a tetraanion undergoes reversibly the two sequential one-electron oxidations $[\text{Os}_{18}\text{Hg}_2(\text{C})_2(\text{CO})_{42}]^{4-/3-}$ ($E^0 = +0.13$ V), and $[\text{Os}_{18}\text{Hg}_2(\text{C})_2(\text{CO})_{42}]^{3-/2-}$ ($E^0 = +0.30$ V) (Figure 59) [113].

The geometry of the tetraanion $\{\text{Hg}_2[\text{Os}_9(\text{C})(\text{CO})_{21}]_2\}^{4-}$ (which is substantially similar to that of the corresponding dianion $\{\text{Hg}_2[\text{Os}_9(\text{C})(\text{CO})_{21}]_2\}^{2-}$) [114] is illustrated in Figure 60 [113].

The X-ray structure of the 278-CVE dianion $\{\text{Hg}[\text{Os}_{10}(\text{C})(\text{CO})_{24}]_2\}^{2-}$ has been also reported [112].

3.4 HETERONUCLEAR COBALT CLUSTERS

3.4.1 Heteronuclear Cobalt–Nickel Clusters: $[\text{Co}_2\text{Ni}_{10}(\text{C})(\text{CO})_{20}]^{2-}$, $[\text{Co}_3\text{Ni}_9(\text{C})(\text{CO})_{20}]^{2-}$ and $[\text{Co}_6\text{Ni}_2(\text{C})_2(\text{CO})_{16}]^{2-}$

The geometry and electrochemistry of the 164-CVE trianion $[\text{Co}_3\text{Ni}_9(\text{C})(\text{CO})_{20}]^{3-}$ have been discussed above in the Introduction.

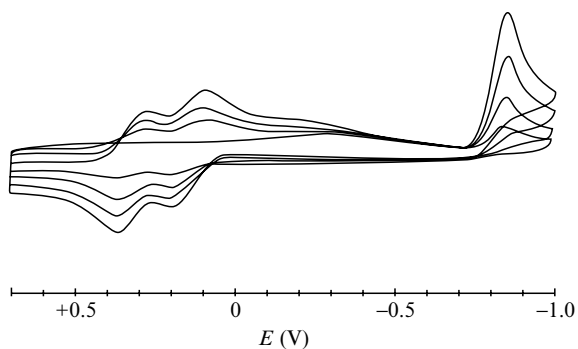


Figure 59 Cyclic voltammetric responses recorded at a platinum electrode for a CH_2Cl_2 solution of $[\text{Os}_{18}\text{Hg}_3(\text{C})_2(\text{CO})_{42}]^{2-}$

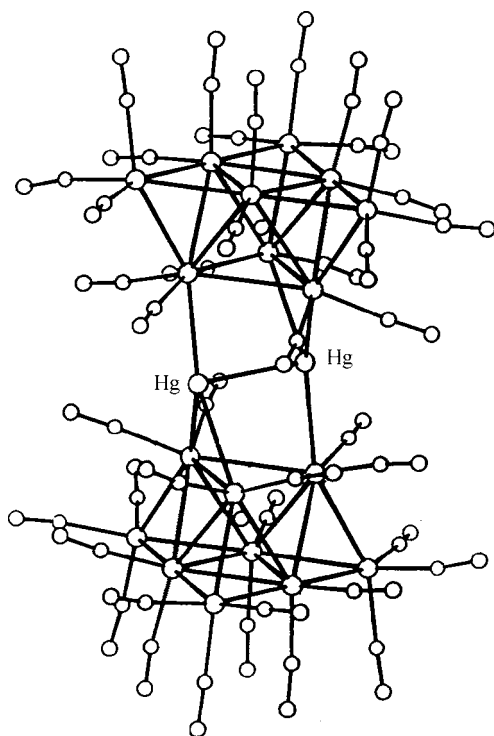


Figure 60 Molecular structure of $[\text{Os}_{18}\text{Hg}_2(\text{C})_2(\text{CO})_{42}]^{4-}$

The tetra-capped triangulated dodecahedral geometry of the 164-CVE dianion $[\text{Co}_2\text{Ni}_{10}(\text{C})(\text{CO})_{20}]^{2-}$ is shown in Figure 61 [9].

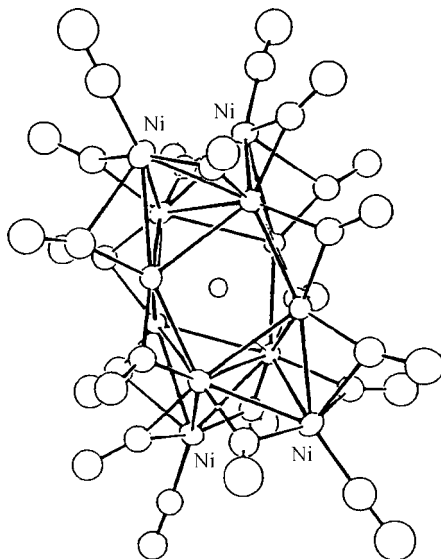


Figure 61 Molecular structure of $[\text{Co}_2\text{Ni}_{10}(\text{C})(\text{CO})_{20}]^{2-}$

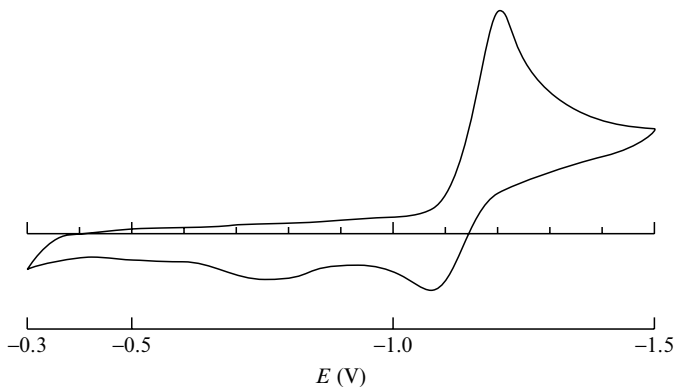


Figure 62 Cyclic voltammogram recorded at a platinum electrode for a THF solution of $[\text{Co}_2\text{Ni}_{10}(\text{C})(\text{CO})_{20}]^{2-}$ (scan rate, 0.05 V s^{-1})

In tetrahydrofuran solution, $[\text{Co}_2\text{Ni}_{10}(\text{C})(\text{CO})_{20}]^{2-}$ undergoes a one-electron reduction ($E^0 = -1.14 \text{ V}$) to the short-lived 117-CVE trianion $[\text{Co}_2\text{Ni}_{10}(\text{C})(\text{CO})_{20}]^{3-}$ (Figure 62) [115].

Figure 63 illustrates the rhombohedral geometry of the 116-CVE dianion $[\text{Co}_6\text{Ni}_2(\text{C})_2(\text{CO})_{16}]^{2-}$ [116].

As Figure 64 shows, such a dianion undergoes, in tetrahydrofuran solution, either a one-electron oxidation ($E^0 = -0.04 \text{ V}$), or two sequential one-electron reductions ($E^0 = -1.24$ and -1.48 V , respectively) [117].

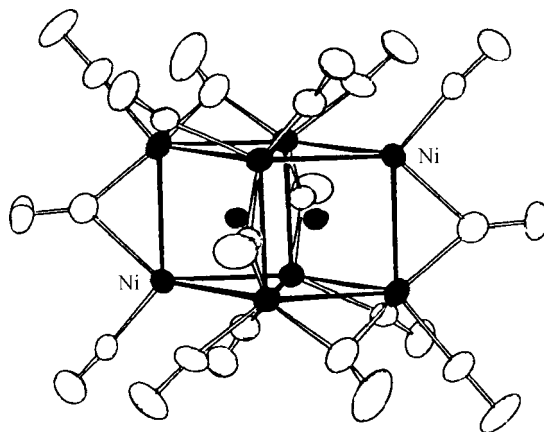


Figure 63 Molecular structure of $[\text{Co}_6\text{Ni}_2(\text{C})_2(\text{CO})_{16}]^{2-}$

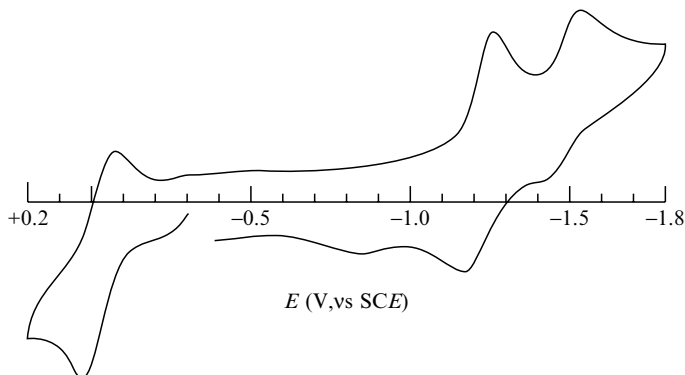


Figure 64 Cyclic voltammogram recorded at a platinum electrode for a THF solution of $[\text{Co}_6\text{Ni}_2(\text{C})_2(\text{CO})_{16}]^{2-}$ (scan rate, 0.2 V s^{-1})

In spite of the apparent chemical reversibility of these redox changes, over the long time-scales of macroelectrolysis no redox congeners remain stable indefinitely.

The X-ray structures of the 138-CVE $[\text{Co}_3\text{Ni}_7(\text{C})_2(\text{CO})_{15}]^{3-}$ and the 139-CVE $[\text{Co}_3\text{Ni}_7(\text{C})_2(\text{CO})_{16}]^{2-}$ carbide clusters have been reported [107,118].

3.5 HETERONUCLEAR RHODIUM CLUSTERS

3.5.1 Heteronuclear Rhodium–Platinum Clusters

In addition to the above-mentioned heteronuclear iron–rhodium clusters, the X-ray structure of the 150-CVE nitride trianion $[\text{Rh}_{10}\text{Pt}(\text{N})(\text{CO})_{21}]^{3-}$ has been reported [119].

3.5.2 Heteronuclear Rhodium–Cobalt Clusters

The 100-CVE $[\text{Rh}_6\text{Co}(\text{N})(\text{CO})_{15}]^{2-}$ is isostructural with the $[\text{Co}_7(\text{N})(\text{CO})_{15}]^{2-}$ species illustrated above in Figure 35 [62].

3.5.3 Heteronuclear Rhodium–Iridium Clusters

The 100-CVE $[\text{Rh}_6\text{Ir}(\text{N})(\text{CO})_{15}]^{2-}$ is also isostructural with the $[\text{Co}_7(\text{N})(\text{CO})_{15}]^{2-}$ species illustrated above in Figure 35 [62].

3.5.4 Heteronuclear Rhodium–Silver Clusters

The X-ray structure of the 190-CVE carbide trianion $\{\text{Ag}[\text{Rh}_6(\text{C})(\text{CO})_{15}]_2\}^{3-}$ has been solved [120].

4 ACKNOWLEDGEMENTS

The financial support of MURST (Cofin 2000) is gratefully acknowledged.

5 REFERENCES

1. (a) G. Longoni and M. C. Iapalucci, in *Clusters and Colloids. From Theory to Applications*, G. Schmid (Ed.), VCH, Weinheim, 1994, Chapter 3.2, p. 91. (b) G. Longoni, C. Femoni, M. C. Iapalucci and P. Zanello, in *Metal Clusters in Chemistry*, vol. 2, P. Braunstein, L. A. Oro and P. R. Raithby (Eds), Wiley-VCH, Weinheim, 1999, pp. 1137–1158.
2. (a) A. Ceriotti, R. Della Pergola, and L. Garlaschelli, in *Physics and Chemistry of Materials with Low-Dimensional Structures. Model Systems for Small Metal Particles*, L. J. De Jongh (Ed.), Kluwer Academic Publishers, Dordrecht, The Netherlands, 1994, Chapter 2, p. 41. (b) A. Fumagalli and R. Della Pergola, in *Metal Clusters in Chemistry*, vol. 1, P. Braunstein, L. A. Oro and P. R. Raithby (Eds), Wiley-VCH, Weinheim, 1999, pp. 323–347.
3. B. T. Heaton, J. A. Iggo, G. Longoni and S. Mulley, *J. Chem. Soc., Dalton Trans.*, 1985 (1995).
4. A. Sironi, *J. Chem. Soc., Dalton Trans.*, 173 (1993).
5. G. Süß-Fink and G. Meister, *Adv. Organomet. Chem.*, **19**, 896 (1993).
6. P. Zanello, in *Stereochemistry of Organometallic and Inorganic Compounds*, vol. 5, P. Zanello (Ed.), Elsevier, Amsterdam, 1994, p. 163.
7. P. Zanello, *Struct. Bonding (Berlin)*, **79**, 101 (1992).
8. A. Ceriotti, R. Della Pergola, G. Longoni, M. Manassero and M. Sansoni, *J. Chem. Soc., Dalton Trans.*, 1181 (1984).
9. A. Ceriotti, R. Della Pergola, G. Longoni, M. Manassero, N. Masciocchi and M. Sansoni, *J. Organomet. Chem.*, **330**, 237 (1987).
10. V. G. Albano, D. Braga, D. Strumolo, C. Seregni and S. Martinengo, *J. Chem. Soc., Dalton Trans.*, 1309 (1985).
11. D. Strumolo, C. Seregni, S. Martinengo, V. G. Albano and D. Braga, *J. Organomet. Chem.*, **252**, C93 (1983).

12. V. G. Albano, D. Braga, P. Chini, G. Ciani and S. Martinengo, *J. Chem. Soc., Dalton Trans.*, 645 (1982).
13. V. G. Albano, D. Braga, A. Fumagalli and S. Martinengo, *J. Chem. Soc., Dalton Trans.*, 1137 (1985).
14. P. Zanello and R. Della Pergola, unpublished results.
15. S. R. Drake, B. F. G. Johnson and J. Lewis, *J. Chem. Soc., Chem. Commun.*, 1033 (1988).
16. B. F. G. Johnson, J. Lewis, S. W. Sankey, K. Wong, M. McPartlin and W. J. H. Nelson, *J. Organomet. Chem.*, **191**, C3 (1980).
17. S. R. Drake, B. F. G. Johnson and J. Lewis, *J. Chem. Soc., Dalton Trans.*, 243 (1989).
18. A. Sirigu, M. Bianchi and E. Benedetti, *J. Chem. Soc., Chem. Commun.*, 596 (1969).
19. P. F. Jackson, B. F. G. Johnson, J. Lewis, M. McPartlin and W. J. H. Nelson, *J. Chem. Soc., Chem. Commun.*, 735 (1979).
20. A. J. Downard, B. H. Robinson, J. Simpson and A. M. Bond, *J. Organomet. Chem.*, **320**, 363 (1987).
21. S. C. Brown, J. Evans and M. Webster, *J. Chem. Soc., Dalton Trans.*, 2263 (1981).
22. R. F. Boehme and P. Coppens, *Acta Cryst., B*, **37**, 1914 (1981).
23. J. S. Bradley, G. B. Ansell, M. E. Leonowicz and E. W. Hill, *J. Am. Chem. Soc.*, **103**, 4968 (1981).
24. D. E. Fjare and W. L. Gladfelter, *Inorg. Chem.*, **20**, 3533 (1981).
25. M. Tachikawa and E. L. Muettterties, *J. Am. Chem. Soc.*, **102**, 4541 (1980).
26. J. H. Davis, M. A. Beno, J. M. Williams, J. Zimmil, M. Tachikawa and E. L. Muettterties, *Proc. Natl. Acad. Sci. USA*, **78**, 668 (1981).
27. P. Zanello, F. Laschi, A. Cinquantini, R. Della Pergola, L. Garlaschelli, M. Cucco, F. Demartin and T. R. Spalding, *Inorg. Chim. Acta*, **226**, 1 (1994).
28. A. Gourdon and Y. Jeannin, *J. Organomet. Chem.*, **440**, 353 (1992).
29. R. Della Pergola, C. Bandini, F. Demartin, E. Diana, L. Garlaschelli, P. L. Stanghellini and P. Zanello, *J. Chem. Soc., Dalton Trans.*, 747 (1996).
30. A. Gourdon and Y. Jeannin, *J. Organomet. Chem.*, **290**, 199 (1985).
31. A. Gourdon and Y. Jeannin, *J. Organomet. Chem.*, **388**, 195 (1990).
32. R. Hourihane, T. R. Spalding, G. Ferguson, T. Deeney and P. Zanello, *J. Chem. Soc., Dalton Trans.*, 43 (1993).
33. M. R. Churchill and J. Wormald, *J. Chem. Soc., Dalton Trans.*, 2410 (1974).
34. J. Rimmelin, P. Lemoine, M. Gross, R. Mathieu and D. de Montauzon, *J. Organomet. Chem.*, **309**, 355 (1986).
35. B. F. G. Johnson, J. Lewis, J. N. Nicholls, J. Puga, P. R. Raithby, M. J. Rosales, M. McPartlin and W. Clegg, *J. Chem. Soc., Dalton Trans.*, 277 (1983).
36. D. S. Shephard, B. F. G. Johnson, A. Harrison, S. Parsons, S. P. Smidt, L. J. Yellowlees and D. Reed, *J. Organomet. Chem.*, **563**, 113 (1998).
37. R. A. Burrow, D. H. Farrar, J. Hao, A. Lough, O. Mourad, A. J. Poë and Y. Zheng, *Polyhedron*, **17**, 2907 (1998).
38. M. P. Cifuentes, S. M. Waterman, M. G. Humphrey, G. A. Heath, B. W. Skelton, A. H. White, M. P. Seneka Perera and M. L. Williams, *J. Organomet. Chem.*, **565**, 193 (1998).
39. T. Chihara, R. Komoto, K. Kobayashi, H. Yamazaki and Y. Matsumura, *Inorg. Chem.*, **28**, 964 (1989).
40. P. J. Bailey, B. F. G. Johnson, J. Lewis, M. McPartlin and H. R. Powell, *J. Organomet. Chem.*, **377**, C17 (1989).
41. P. J. Bailey, G. Conole, B. F. G. Johnson, J. Lewis, M. McPartlin, A. Moule, H. R. Powell and D. A. Wilkinson, *J. Chem. Soc., Dalton Trans.*, 741 (1995).
42. M. P. Cifuentes, M. G. Humphrey and G. A. Heath, *Inorg. Chim. Acta*, **259**, 273 (1997).

43. C.-M. T. Hayward, J. R. Shapley, M. R. Churchill, C. Bueno and A. L. Rheingold, *J. Am. Chem. Soc.*, **104**, 7347 (1982).
44. M. L. Blohm and W. L. Gladfelter, *Organometallics*, **4**, 45 (1985).
45. P. F. Jackson, B. F. G. Johnson, J. Lewis, J. N. Nicholls, M. McPartlin and W. J. H. Nelson, *J. Chem. Soc., Chem. Commun.*, 564 (1980).
46. S. B. Colbran, F. J. Lahoz, P. R. Raithby, J. Lewis, B. F. G. Johnson and C. J. Cardin, *J. Chem. Soc., Dalton Trans.*, 173 (1988).
47. M. H. Barley, C. E. Anson, B. F. G. Johnson and J. Lewis, *J. Organomet. Chem.*, **339**, 151 (1988).
48. P. F. Jackson, B. F. G. Johnson, J. Lewis, W. J. H. Nelson and M. McPartlin, *J. Chem. Soc., Dalton Trans.*, 2099 (1982).
49. S. R. Drake, B. F. G. Johnson, J. Lewis and R. S. C. McQueen, *J. Chem. Soc., Dalton Trans.*, 1051 (1987).
50. S. R. Drake, M. H. Barley, B. F. G. Johnson and J. Lewis, *Organometallics*, **7**, 806 (1988).
51. D. Braga, J. Lewis, B. F. G. Johnson, M. McPartlin, W. J. H. Nelson and M. D. Vargas, *J. Chem. Soc., Chem. Commun.*, 241 (1983).
52. M. A. Collins, B. F. G. Johnson, J. Lewis, J. M. Mace, J. Morris, M. McPartlin, W. J. H. Nelson, J. Puga and P. R. Raithby, *J. Chem. Soc., Chem. Commun.*, 689 (1983).
53. S. Martinengo, D. Strumolo, P. Chini, V. G. Albano and D. Braga, *J. Chem. Soc., Dalton Trans.*, **35** (1985).
54. S. Martinengo, G. Ciani, A. Sironi, B. T. Heaton and J. Mason, *J. Am. Chem. Soc.*, **101**, 7095 (1979).
55. G. Ciani and A. Sironi, *J. Organomet. Chem.*, **241**, 385 (1983).
56. V. G. Albano, P. Chini, G. Ciani, M. Sansoni and S. Martinengo, *J. Chem. Soc., Dalton Trans.*, 163 (1980).
57. P. Zanello and A. Fumagalli, unpublished results.
58. G. Ciani and S. Martinengo, *J. Organomet. Chem.*, **306**, C49 (1986).
59. B. R. Penfold and M. D. Brice, *Inorg. Chem.*, **11**, 1381 (1972).
60. U. Geiser and A. M. Kini, *Acta Cryst., C*, **49**, 1322 (1993).
61. P. A. Brooksby, N. W. Duffy, A. J. McQuillan, B. H. Robinson and J. Simpson, *J. Organomet. Chem.*, **582**, 183 (1999).
62. G. Ciani, N. Masciocchi, A. Sironi, A. Fumagalli and S. Martinengo, *Inorg. Chem.*, **31**, 331 (1992).
63. V. G. Albano, P. Chini, G. Ciani, S. Martinengo and M. Sansoni, *J. Chem. Soc., Dalton Trans.*, 463 (1978).
64. G. Ciani, A. Sironi, S. Martinengo, L. Garlaschelli, R. Della Pergola, P. Zanello, F. Laschi and N. Masciocchi, *Inorg. Chem.*, **40**, 3905 (2001).
65. A. Fumagalli, S. Martinengo, M. Tasselli, R. Della Pergola, P. Zanello, F. Fabrizi de Biani, P. Macchi and A. Sironi, unpublished.
66. V. G. Albano, D. Braga and S. Martinengo, *J. Chem. Soc., Dalton Trans.*, 981 (1986).
67. S. Martinengo, L. Noziglia, A. Fumagalli, V. G. Albano, D. Braga and F. Grepioni, *J. Chem. Soc., Dalton Trans.*, 2493 (1998).
68. V. G. Albano, D. Braga, G. Ciani and S. Martinengo, *J. Organomet. Chem.*, **213**, 293 (1981).
69. A. Fumagalli, S. Martinengo, M. Tasselli, G. Ciani, P. Macchi and A. Sironi, *Inorg. Chem.*, **37**, 2826 (1992).
70. S. Martinengo, G. Ciani and A. Sironi, *J. Organomet. Chem.*, **358**, C23 (1988).
71. V. G. Albano, M. Sansoni, P. Chini and S. Martinengo, *J. Chem. Soc., Dalton Trans.*, 651 (1973).

72. R. Bonfichi, G. Ciani, A. Sironi and S. Martinengo, *J. Chem. Soc., Dalton Trans.*, 253 (1983).
73. S. Martinengo, G. Ciani and A. Sironi, *J. Chem. Soc., Chem. Commun.*, 1577 (1984).
74. V. G. Albano, D. Braga, P. Chini, D. Strumolo and S. Martinengo, *J. Chem. Soc., Dalton Trans.*, 249 (1983).
75. P. Zanello and L. Garlaschelli, unpublished results.
76. V. G. Albano, D. Braga and S. Martinengo, *J. Chem. Soc., Dalton Trans.*, 717 (1981).
77. V. G. Albano, M. Sansoni, P. Chini, S. Martinengo and D. Strumolo, *J. Chem. Soc., Dalton Trans.*, 305 (1975).
78. V. G. Albano, P. Chini, S. Martinengo, M. Sansoni and D. Strumolo, *J. Chem. Soc., Dalton Trans.*, 459 (1978).
79. S. Martinengo, D. Strumolo, P. Chini, V. G. Albano and D. Braga, *J. Chem. Soc., Dalton Trans.*, 1837 (1984).
80. V. G. Albano, M. Sansoni, P. Chini, S. Martinengo and D. Strumolo, *J. Chem. Soc., Dalton Trans.*, 970 (1976).
81. S. Martinengo, G. Ciani and A. Sironi, *J. Chem. Soc., Chem. Commun.*, 1742 (1986).
82. S. Martinengo, G. Ciani and A. Sironi, *J. Chem. Soc., Chem. Commun.*, 26 (1991).
83. S. Martinengo, G. Ciani and A. Sironi, *J. Chem. Soc., Chem. Commun.*, 1405 (1992).
84. A. Fumagalli, S. Martinengo, G. Bernasconi, G. Ciani, D. M. Proserpio and A. Sironi, *J. Am. Chem. Soc.*, **119**, 1450 (1997).
85. J. L. Vidal, W. E. Walker, R. L. Pruett and R. C. Schoening, *Inorg. Chem.*, **18**, 129 (1979).
86. J. L. Vidal, W. E. Walker and R. C. Schoening, *Inorg. Chem.*, **20**, 238 (1981).
87. A. Ceriotti, G. Longoni, M. Manassero, M. Perego and M. Sansoni, *Inorg. Chem.*, **24**, 117 (1985).
88. P. Zanello and L. Garlaschelli, unpublished results.
89. F. Calderoni, F. Demartin, M. C. Iapalucci, and G. Longoni, *Angew. Chem. Int. Ed. Engl.*, **35**, 2225 (1996).
90. F. Calderoni, F. Demartin, F. Fabrizi de Biani, C. Femoni, M. C. Iapalucci, G. Longoni and P. Zanello, *Eur. J. Inorg. Chem.*, 663 (1999).
91. A. Ceriotti, A. Fait, G. Longoni, G. Piro, F. Demartin, M. Manassero, N. Masciocchi and M. Sansoni, *J. Am. Chem. Soc.*, **108**, 8091 (1986).
92. A. Ceriotti, G. Piro, G. Longoni, M. Manassero, N. Masciocchi and M. Sansoni, *New J. Chem.*, **12**, 501 (1988).
93. A. Ceriotti, G. Longoni, M. Manassero, N. Masciocchi, L. Resconi and M. Sansoni, *J. Chem. Soc., Chem. Commun.*, 181 (1985).
94. A. Ceriotti, G. Longoni, M. Manassero, N. Masciocchi, G. Piro, L. Resconi and M. Sansoni, *J. Chem. Soc., Chem. Commun.*, 1402 (1985).
95. G. Ciani, G. D'Alfonso, M. Freni, P. Romiti and A. Sironi, *J. Chem. Soc., Chem. Commun.*, 339 (1982).
96. G. Ciani, G. D'Alfonso, M. Freni, P. Romiti and A. Sironi, *J. Chem. Soc., Chem. Commun.*, 705 (1982).
97. C.-M. T. Hayward and J. R. Shapley, *Organometallics*, **7**, 448 (1988).
98. T. J. Henly, J. R. Shapley, A. L. Rheingold and S. J. Gelb, *Organometallics*, **7**, 441 (1988).
99. T. Beringhelli, G. D'Alfonso, H. Molinari and A. Sironi, *J. Chem. Soc., Dalton Trans.*, 689 (1992).

100. R. Della Pergola, M. Branchini, A. Fumagalli, L. Garlaschelli, M. Manassero and M. Sansoni, *Eur. J. Inorg. Chem.*, 1759 (2000).
101. D. E. Fjare and W. L. Gladfelter, *J. Am. Chem. Soc.*, **106**, 4799 (1984).
102. R. Della Pergola, A. Cinquantini, E. Diana, L. Garlaschelli, F. Laschi, P. Luzzini, M. Manassero, A. Repposi, M. Sansoni, P. L. Stanghellini and P. Zanello, *Inorg. Chem.*, **36**, 3761 (1997).
103. M. Tachikawa, A. C. Sievert, E. L. Muetterties, M. R. Thompson, C. S. Day and V. W. Day, *J. Am. Chem. Soc.*, **102**, 1725 (1980).
104. M. K. Alami, F. Dahan and R. Mathieu, *J. Chem. Soc., Dalton Trans.*, 1983 (1987).
105. Yu. L. Slovokhotov, Yu. T. Struchkov, V. E. Lopatin and S. P. Gubin, *J. Organomet. Chem.*, **266**, 139 (1984).
106. R. Della Pergola, V. Betti, A. Ceriotti, M. Fontani, M. Manassero, M. Sansoni and P. Zanello, in *Proceedings of the XX National Conference of the Italian Chemical Society*, Rimini, Italy, June 4–9, 2000, Centro Audiovisivi e Stampa dell' Università degli Studi di Camerino, Italy, 2000, p. IN-ORO13.
107. G. Longoni, A. Ceriotti, R. Della Pergola, M. Manassero, M. Perego, G. Piro and M. Sansoni, *Phil. Trans. R. Soc. London, A*, **308**, 47 (1982).
108. R. Reina, O. Riba, O. Rossell, M. Seco, P. Gómez-Sal, A. Martín, D. de Montauzon and A. Mari, *Organometallics*, **17**, 4127 (1998).
109. R. D. Adams and W. Wu, *J. Cluster Sci.*, **2**, 271 (1991).
110. B. F. G. Johnson, W.-L. Kwik, J. Lewis, P. R. Raithby and V. P. Saharan, *J. Chem. Soc., Dalton Trans.*, 1037 (1991).
111. P. J. Bailey, B. F. G. Johnson, J. Lewis, M. McPartlin and H. R. Powell, *J. Chem. Soc., Chem. Commun.*, 1513 (1989).
112. L. H. Gade, B. F. G. Johnson, J. Lewis, M. McPartlin and H. R. Powell, *J. Chem. Soc., Chem. Commun.*, 110 (1990).
113. L. H. Gade, B. F. G. Johnson, J. Lewis, G. Conole and M. McPartlin, *J. Chem. Soc., Dalton Trans.*, 3249 (1992).
114. E. Charalambous, L. H. Gade, B. F. G. Johnson, T. Kotch, A. J. Lees, J. Lewis and M. McPartlin, *Angew. Chem. Int. Ed. Engl.*, **29**, 1137 (1990).
115. L. Garlaschelli and P. Zanello, unpublished results.
116. A. Arrigoni, A. Ceriotti, R. Della Pergola, G. Longoni, M. Manassero, N. Masciocchi and M. Sansoni, *Angew. Chem. Int. Ed. Engl.*, **23**, 322 (1984).
117. A. Ceriotti, R. Della Pergola, L. Garlaschelli, G. Longoni, M. Manassero, N. Masciocchi, M. Sansoni and P. Zanello, *Gazz. Chim. It al.*, **122**, 365 (1992).
118. A. Arrigoni, A. Ceriotti, R. Della Pergola, G. Longoni, M. Manassero and M. Sansoni, *J. Organomet. Chem.*, **296**, 243 (1985).
119. S. Martinengo, G. Ciani, and A. Sironi, *J. Am. Chem. Soc.*, **104**, 328 (1982).
120. B. T. Heaton, L. Strona, S. Martinengo, D. Strumolo, V. G. Albano and D. Braga, *J. Chem. Soc., Dalton Trans.*, 2175 (1983).

2 Unusual Nuclear Magnetic Shielding and Coupling Constants Related to Unusual Bonding Situations

BERND WRACKMEYER

Laboratorium für Anorganische Chemie, Universität Bayreuth, D-95440 Bayreuth, Germany

1 INTRODUCTION

1.1 GENERAL

The decade following the first successful NMR experiments in 1945/46 on water [1] and paraffin [2] had witnessed numerous pioneering discoveries of NMR phenomena. Around 1955, with the growing availability of easy-to-handle commercial NMR spectrometers, it had become clear to many chemists that structural assignments of organic compounds in solution would be greatly improved by ^1H NMR spectroscopy; attractive applications of the method had also been demonstrated for problems in inorganic chemistry (e.g. by ^{31}P NMR of phosphorus compounds, as early as 1951 [3]), and even in the still young research area of organometallic chemistry NMR had already some impact (e.g. the simple ^1H NMR spectrum of ferrocene, dicyclopentadienyliron [$(\eta^5\text{-C}_5\text{H}_5)_2\text{Fe}$], had provided one of the numerous arguments in favour of the sandwich structure [4], ruling out the originally proposed structure with Fe–C σ bonds [5]). Thus, NMR spectroscopy had been transformed from the realms of physics into the hands of chemists. This process might have retarded some developments—it had even led to some misinterpretation of NMR spectroscopic results—however, as a whole, it has been a story of amazing success for the scientific community, and the event of 50 years of NMR has been widely celebrated [6].

Prominent solution-state NMR parameters like chemical shifts δX of nuclei X and indirect nuclear spin–spin coupling constants $^nJ(\text{A},\text{X})$ serve very well for the characterization of a particular compound or for the qualitative and even quantitative analysis of more or less complex mixtures (Figure 1). These parameters can also be used to monitor the formation of new compounds, including the detection of intermediates, as well as the decomposition or rearrangement

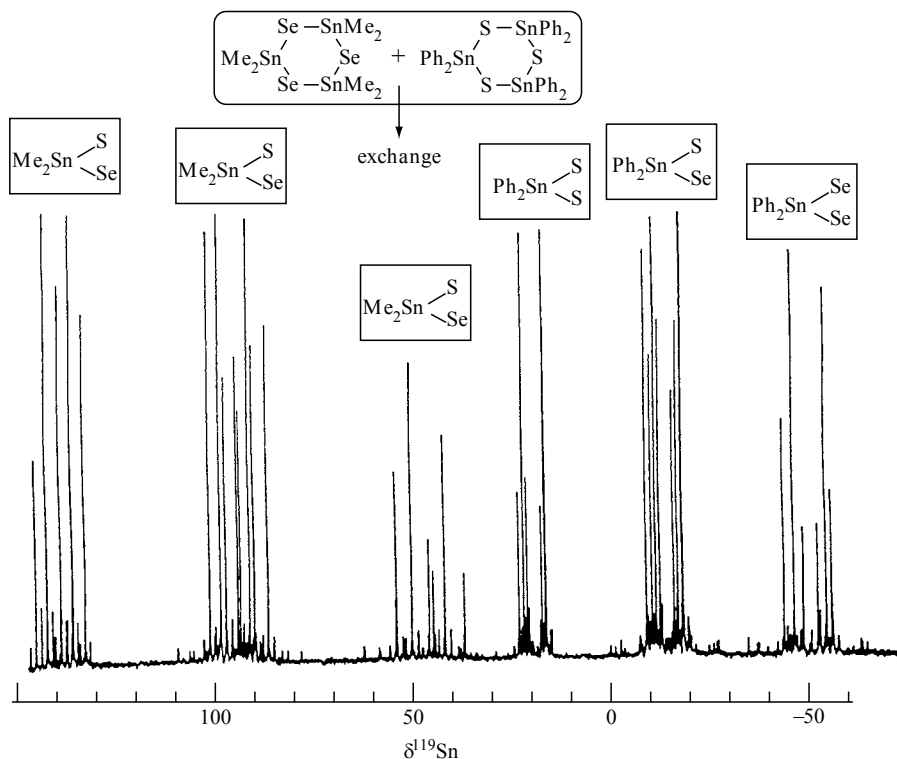


Figure 1 74.6 MHz $^{119}\text{Sn}\{^1\text{H}\}$ NMR spectrum of an equilibrated mixture containing 20 different tin compounds, formed by exchange reactions between $[\text{Me}_2\text{SnSe}_3]$ and $[\text{Ph}_2\text{SnS}_3]$ in CDCl_3 ; of the 40 expected signals, 39 are resolved. The low-intensity signals can be assigned to the coupling constants $^1J(^{119}\text{Sn}, ^{77}\text{Se})$, $^2J(^{119}\text{Sn}, ^{117}\text{Sn})$, and $^2J(^{119}\text{Sn}, ^{119}\text{Sn})$, in addition to $^1J(^{119}\text{Sn}, ^{13}\text{C})$

of products. Very often, an empirical treatment of the NMR data is sufficient for these purposes [7–11].

A most intriguing feature of NMR spectroscopy is its potential in studying intramolecular and/or intermolecular dynamic processes [12]. The comparison of information on structures and dynamics evaluated by NMR experiments with calculated parameters, e.g. by a force field approach [13,14], is possible and successful in many cases. This involves determination and analysis of exchange processes [15,16], nuclear Overhauser effect measurements [17], and/or pulsed field gradient spin-echo experiments [18–20], to name just a few techniques. Such studies usually involve additional NMR parameters such as the nuclear spin relaxation times ($T_1(\text{X}) =$ longitudinal or spin-lattice relaxation time, and $T_2(\text{X}) =$ transversal or spin-spin relaxation time; $T^{\text{Q}}(\text{X}) =$ quadrupolar relaxation time) which are of principal importance for all NMR experiments. However, since these parameters are in general not directly accessible from routine

NMR spectra, they have received (unjustifiably) less attention when compared to δX and ${}^nJ(A,X)$. It can be said that relaxation rates are related to unusual bonding situations in a simple way only in rare cases (see Chapter 3 of this present volume for some exceptions). Therefore, T_1 and T_2 values will be highlighted only in a few cases throughout this current chapter.

The NMR properties are described by the Hamiltonians in equation (1) below (H_Z and H_{RF} arise from the Zeeman effect and the radiofrequency as external Hamiltonians, while H_S , H_{SR} , H_{DD} , H_J , and H_Q represent the shielding, spin rotation, dipolar, scalar coupling and quadrupole interactions, respectively, as the internal Hamiltonians. In solution, the majority of anisotropic interactions are almost completely averaged by molecular motion. Nevertheless, both the chemical shifts δX and coupling constants ${}^nJ(A,X)$ depend on the structure, and in most cases, these parameters are obtained for diamagnetic compounds in solution in a straightforward manner from routine NMR spectra. In the case of solids (see Chapter 4 of this present volume) and also of paramagnetic compounds, this situation is somewhat different. The experimentally determined solution-state isotropic chemical shifts δX of diamagnetic compounds can be analysed for their tensor components δ_{xx} , δ_{yy} , and δ_{zz} by solid-state NMR measurements of powders or single crystals, and all of these data can be reproduced with reasonable accuracy, at least for lighter nuclei, by appropriate MO calculations [21]. MO calculations can also be carried out for coupling constants ${}^nJ(A,X)$ [22,23]. Dealing with more heavy nuclei means that careful extrapolations of simple models are required in order to interpret the experimental data, and that relativistic effects have to be taken into account.

$$H_{NMR} = H_Z + H_{RF} + H_S + H_{SR} + H_{DD} + H_J + H_Q \quad (1)$$

The phenomena of NMR spectroscopy accompany many disciplines in chemistry and related sciences. This is easy to realize by an inspection of Tables 1 and 2. Almost any element has at least one NMR-suitable isotope in appreciable natural abundance. It is sensible to distinguish between spin-1/2 nuclei and quadrupolar nuclei ($I \geq 1$). In the latter cases, nuclear spin relaxation is governed mainly by efficient relaxation owing to quadrupolar interactions with the electric field gradient at the site of the nucleus. This leads often to severely broadened NMR signals, and therefore, the appearance of NMR spectra for quadrupolar nuclei, and also experimental conditions for obtaining their NMR spectra, are considerably different when compared with spin-1/2 nuclei.

The selection of topics in this chapter was governed by the theme of the series which deals mainly with organometallic compounds. In order to keep the balance, some examples of inorganic or organic chemistry are included. Clearly, from the NMR point of view, such borderlines between chemical disciplines are not meaningful. The emphasis here is on solution-state NMR spectroscopy.

Table 1 NMR Properties of spin-1/2 nuclei^a

Nucleus	Natural abundance (%)	R^{Cb}	$\gamma(10^7 \text{ rad s}^{-1} T^{-1})$	Ξ (MHz)	Reference standard
¹ H	99.985	5.67×10^3	26.7522	100.000 000	SiMe ₄ , 1 % in CDCl ₃
³ H	— ^c	—	28.5350	106.666 398 4	T ₁ -SiMe ₄
³ He	0.000 14	3.51×10^{-3}	-20.3801	76.178 972	He gas
¹³ C	1.108	1.00	6.7283	25.145 020	SiMe ₄ 1 % in CDCl ₃
¹⁵ N	0.37	2.19×10^{-2}	-2.7126	10.136 767	MeNO ₂ (neat)
¹⁹ F	100	4.73×10^3	25.1815	94.094 003	CFCl ₃ (neat)
²⁹ Si	4.70	2.10	-5.3190	19.867 187	SiMe ₄ 1 % in CDCl ₃
³¹ P	100	3.77×10^2	10.8394	40.480 747	H ₃ PO ₄ , 85 % aq.
⁵⁷ Fe	2.19	4.25×10^{-3}	0.8687	3.237 798	Fe(CO) ₅ (neat)
⁷⁷ Se	7.58	3.02	5.1214	19.071 523	Me ₂ Se (neat)
⁸⁹ Y	100	0.676	-1.3163	4.900 200	Y ³⁺ aq. (H ₂ O, D ₂ O)
¹⁰³ Rh	100	0.180	-0.8468	3.160 000	No compound
¹⁰⁷ Ag	51.82	0.198	-1.0878	4.047 898	Ag ⁺ ∞aq.
¹⁰⁹ Ag	48.18	0.280	-1.2519	4.653 623	Ag ⁺ ∞aq.
¹¹¹ Cd	12.75	7.01	-5.7046	21.201 877	Cd(ClO ₄) ₂ , 0.1 M aq.
¹¹³ Cd	12.26	7.69	-5.9609	22.193 173	CdMe ₂ (neat)
¹¹⁵ Sn	0.35	0.707	-8.8014	32.718 780	SnMe ₄ (neat)
¹¹⁷ Sn	7.61	19.9	-9.589	35.632 295	SnMe ₄ (neat)
¹¹⁹ Sn	8.58	25.7	-10.0318	37.290 665	SnMe ₄ (neat)
¹²³ Te	0.87	0.906	-7.0576	26.169 773	Me ₂ Te (neat)
¹²⁵ Te	6.99	12.8	-8.5087	31.549 802	Me ₂ Te (neat)
¹²⁹ Xe	26.44	32.4	-7.4521	27.811 008	XeOF ₄ (neat)
¹⁷¹ Yb	14.31	4.50	4.7348	17.499 306	[Yb(Cp*) ₂ (THF) ₂] in THF, 0.171 M
¹⁸³ W	14.28	6.08×10^{-2}	1.1283	4.166 398	Na ₂ WO ₄ in D ₂ O, 1 M
¹⁸⁷ Os	1.64	1.15×10^{-3}	0.6193	2.282 343	OsO ₄ (CDCl ₃)
¹⁹⁵ Pt	33.8	19.9	5.8383	21.400 000	No compound $\delta^{195}\text{Pt}([\text{PtCl}_6]^{2-}) = +4533$
¹⁹⁹ Hg	16.84	5.68	4.8458	17.910 841	HgMe ₂ (neat) ^d
²⁰³ Tl	29.5	3.28×10^2	15.5394	57.072 641	Tl ⁺ aq. ^e
²⁰⁵ Tl	70.5	8.07×10^2	15.6922	57.633 833	Tl ⁺ aq. ^e
²⁰⁷ Pb	22.6	11.9	5.6264	20.920 597	PbMe ₄ (neat)

^a Most data are taken from Reference [6] (vol. 5, p. 3301) and References [7] and [10]; some data are my own unpublished measurements.

^b Receptivity relative to that of ¹³C in natural abundance.

^c (12 years).

^d $\Xi(^{199}\text{Hg}) = 17:870\ 535$ MHz for Hg(ClO₄)₂ (0.1 M in 0.1 M HClO₄)

^e $\Xi(^{203}\text{Tl}) = 57:123\ 200$ MHz for Tl(NO₃)₃ aq. and $\Xi(^{205}\text{Tl}) = 57:683\ 838$ MHz for Tl(NO₃)₃ aq.

1.2 CHEMICAL SHIFTS, δX

The chemical shift data δX are given with respect to $\delta X = 0$ for a particular X-compound and/or a particular X-frequency (e.g. for $\delta^{103}\text{Rh}$ or $\delta^{195}\text{Pt}$), as shown in Tables 1 and 2, and a positive sign of δX indicates a shift of the X NMR

Table 2 NMR Properties of some quadrupolar nuclei^a

Nucleus	Natural abundance (%)	Spin <i>I</i>	<i>Q</i> (10 ⁻²⁸ m ²) ^b	γ (10 ⁷ rad s ⁻¹ T ⁻¹)	Ξ (MHz)	Reference standard
² H	0.015	1	2.87×10^{-3}	4.1066	15.350 609	Si(CD ₃) ₄ (D ₁₂ -TMS)
⁶ Li	7.42	1	-6.4×10^{-4}	3.9371	14.716 106	LiCl, in D ₂ O, \approx 9.7 M
⁷ Li	92.58	3/2	-3.7×10^{-3}	10.3976	38.863 790	LiCl, in D ₂ O \approx 9.7 M
⁹ Be	100	3/2	5.3×10^{-2}	-3.7606	14.051 820	BeSO ₄ , D ₂ O, \approx 0.45 M
¹⁰ B	19.58	3	8.5×10^{-2}	2.8747	10.743 657	F ₃ B-OEt ₂ (CDCl ₃)
¹¹ B	80.42	3/2	4.1×10^{-2}	8.5847	32.083 971	F ₃ B-OEt ₂ (CDCl ₃)
¹⁴ N	99.63	1	1.67×10^{-2}	1.9338	7.226 324	MeNO ₂ (neat)
¹⁷ O	0.037	5/2	6.11×10^{-2}	-3.6280	13.556 430	D ₂ O (liquid)
²³ Na	100	3/2	0.10	7.0704	26.451 921	NaBr, in D ₂ O, \approx 10 M
²⁵ Mg	10.13	5/2	0.22	-1.6389	6.121 643	MgCl ₂ , in D ₂ O, \approx 15 M
²⁷ Al	100	5/2	0.14	6.9762	26.056 890	A(NO ₃) ₃ , in D ₂ O, 1.1 M
³³ S	0.76	3/2	-6.4×10^{-2}	2.0557	7.676 020	(NH ₄) ₂ SO ₄ , in D ₂ O (sat.)
³⁵ Cl	75.53	3/2	-8.2×10^{-2}	2.6242	9.797 931	KCl, in D ₂ O, \approx 2.2 M
³⁷ Cl	24.47	3/2	-6.5×10^{-2}	2.1844	8.155 764	KCl, in D ₂ O, \approx 2.2 M
³⁹ K	93.1	3/2	5.5×10^{-2}	1.2499	4.666 423	KI, in D ₂ O, \approx 3.8 M
⁴³ Ca	0.145	7/2	-5×10^{-2}	-1.8028	6.729 996	CaCl ₂ , in D ₂ O
⁴⁵ Sc	100	7/2	-0.22	6.5088	24.291 702	ScCl ₃ , in D ₂ O, 1 M
⁴⁷ Ti	7.28	5/2	0.29	-1.5106	5.637 587	TiCl ₄ (neat)
⁴⁹ Ti	5.51	7/2	0.24	-1.5110	5.639 095	TiCl ₄ (neat)
⁵¹ V	99.76	7/2	-5.2×10^{-2}	7.0492	26.302 963	VOCl ₃ (neat)
⁵³ Cr	9.55	3/2	-0.15	-1.5077	5.652 511	(NH ₄) ₂ CrO ₄ , in D ₂ O, 1 M
⁵⁵ Mn	100	5/2	0.40	6.6453	24.789 290	MnO ₄ ⁻ aq. (sat.)
⁵⁹ Co	100	7/2	0.42	6.3015	23.727 074	K ₃ [Co(CN) ₆], in D ₂ O, 0.56 M
⁶¹ Ni	1.19	3/2	0.16	-2.3948	8.936 050	Ni(CO) ₄ (neat)
⁶³ Cu	69.09	3/2	-0.22	7.1088	26.515 473	[Cu(NCMe) ₄]BF ₄ , in MeCN, 0.1 M
⁶⁵ Cu	30.91	3/2	-0.195	7.6104	28.403 659	[Cu(NCMe) ₄]BF ₄ , in MeCN, 0.1 M
⁶⁷ Zn	4.11	5/2	0.15	1.6778	6.256 782	Zn(ClO ₄) ₂ ∞ aq.
⁷¹ Ga	39.6	3/2	0.11	8.1812	30.496 579	Ga(NO ₃) ₃ , in D ₂ O, 1.1 M
⁷³ Ge	7.76	9/2	-0.17	-0.9360	3.488 315	GeMe ₄ (neat)
⁷⁵ As	100	3/2	0.29	4.5961	17.122 712	NaAsF ₆ , in MeCN
⁸¹ Br	49.46	3/2	0.27	7.2498	27.007 028	NaBr, in D ₂ O, \approx 10 M
⁸⁷ Rb	27.85	3/2	0.13	8.7851	32.721 218	RbCl, in D ₂ O, \approx 6 M
⁹¹ Zr	11.23	5/2	-0.21	-2.4975	9.296 298	[Zr(η^5 -Cp) ₂ Cl ₂], in CH ₂ Cl ₂
⁹³ Nb	100	9/2	-0.32	6.5674	24.476 195	KNbCl ₆ , in MeCN, sat.
⁹⁵ Mo	15.72	5/2	-0.015	-1.7514	6.516 943	Na ₂ MoO ₄ , in D ₂ O, 2 M
⁹⁹ Tc ^c	— ^d	9/2	-0.13	6.0503	22.508 311	TcO ₄ ⁻ aq.
⁹⁹ Ru	12.72	5/2	7.6×10^{-2}	-1.2286	4.605 151	K ₄ [Ru(CN) ₆], in D ₂ O, 0.3 M
¹¹⁵ In	95.72	9/2	0.86	5.8971	21.912 527	In(NO ₃) ₃ , in D ₂ O, 0.1 M
¹²¹ Sb	57.25	5/2	-0.33	6.4442	23.930 691	KSBCl ₆ , in MeCN (sat.)
¹²⁷ I	100	5/2	-0.79	5.3896	20.008 632	KI, in D ₂ O, \approx 6 M

(continued)

Table 2 (continued)

Nucleus	Natural abundance (%)	Spin I	Q (10^{-28} m ²) ^b	γ (10^7 rad s ⁻¹ T ⁻¹)	Ξ (MHz)	Reference standard
¹³³ Cs	100	7/2	-3×10^{-3}	3.5339	13.116 208	CsNO ₃ , in D ₂ O, \approx 1.7 M
¹³⁹ La	99.91	7/2	0.51	3.8085	14.125 606	LaCl ₃ , aq.
¹⁷⁷ Hf	18.5	7/2	3.3	1.086	4.059	—
¹⁸¹ Ta	99.988	7/2	3.3	3.2445	11.989 601	KTaCl ₆ , in MeCN (sat.)
¹⁸⁷ Re	62.60	5/2	2.07	6.1682	22.751 602	KReO ₄ , in D ₂ O
¹⁹³ Ir	62.7	3/2	0.78	0.5080	1.899	—
¹⁹⁷ Au	100	3/2	0.55	0.4692	1.754	—
²⁰⁹ Bi	100	9/2	-0.37	4.3752	16.069 288	Bi(NO ₃) ₃ , in D ₂ O/conc. HNO ₃ (1:1)

^a Most data are taken from Reference [6] (Vol. 5, p. 3301), and References [7] and [10]; some data are my own unpublished measurements.

^b Many values of Q , in particular for heavy nuclei, may not be accurate owing to experimental problems.

^c Radioactive isotope.

^d (2×10^5 years).

signal to higher frequency (or lower field) with respect to the X-frequency of the reference. A negative sign of δX implies a shift to lower frequency (or higher field): $\delta X = [(\nu_X - \nu_{Ref.})/\nu_{Ref.}]10^6$ (often given in ppm; note that ppm is not a physical unit).

The physical meaning of δX [24] is better described by $\sigma(X)$, the screening constant (note that the sign of σ is opposite to that of δ). The screening (or magnetic shielding) of a particular nucleus in an external magnetic field \mathbf{B}_0 is related to the inner electron shells, the valence electron shell, and the electronic structure (e.g. ground and excited states) of a nucleus or atom being part of a molecule. In the frame of this (non-relativistic) concept [25], it is useful to differentiate between a diamagnetic term σ^d and a paramagnetic term σ^p , as shown in equation (2):

$$\sigma(X) = \sigma^d(X) + \sigma^p(X) \quad (2)$$

Within the simplified ‘atom in a molecule’ approach, local terms are used, and $\sigma^d(X)$ (> 0), the so-called Lamb term [26], is almost a constant for each nucleus X, whereas $\sigma^p(X)$ (< 0) is related to the immediate surroundings of X. The local term $\sigma^p(X)$ takes into account differences (ΔE) between relevant ground and excited states (those mixed by the external field \mathbf{B}_0 , i.e. magnetic-dipole allowed transitions), as well as effects arising from changes in the orbital expansion term $\langle r^{-3} \rangle_{np}$ and the bond order charge density term $Q_{A,X}$. In the independent electron model, the average excitation energy approach is given by equation (3) below [27]. An extremely simplified description is that σ^p represents the imbalance of electron density around the respective nucleus, and that it will become increasingly important with the presence of p and d electrons, with different coordination numbers of a nucleus, and also, most importantly,

with the presence of energetically low-lying unoccupied energy levels (i.e. small ΔE values) close to the nucleus.

$$\sigma^P(X) = -(\mu_0 e^2 h^2)/(8\pi m^2) \langle r^{-3} \rangle_{np} (\Delta E)^{-1} \sum_A Q_{A,X} \quad (3)$$

Although equation (3) can be modified to include transition metal nuclei, this is not advisable, considering the complex electronic structures of transition metal complexes [28–32].

1.3 COUPLING CONSTANTS, ${}^nJ(A,X)$

Indirect, electron-mediated, nuclear spin–spin coupling constants ${}^nJ(A,X)$ (where n stands for the number of bonds between the nuclei A and X) are measured in Hz, and they may have either a positive or a negative sign. Frequently, it is advisable to use the notation of reduced coupling constants K (equation (4)); $\gamma_{(A)}$ and $\gamma_{(X)}$ are the respective gyromagnetic ratios—see Tables 1 and 2) in order to obtain data which are independent of individual nuclear magnetic properties. This is particularly important for the comparison of ${}^nJ(A,X)$ values if the γ values are of different sign (see Tables 1 and 2).

$${}^nK(A,X) = 4\pi^2 {}^nJ(A,X)(\gamma_{(A)} \gamma_{(X)} h)^{-1} (\text{N A}^{-2} \text{m}^{-3}) \quad (4)$$

There are various mechanisms which contribute to indirect nuclear spin–spin coupling [33,34]. The most important one is described by the Fermi contact term, as given by equation (5) below, for the independent electron model [35] (neglecting relativistic effects). The valence s electron densities at the nuclei $\Psi_{(A)}^2(0)$ and $\Psi_{(X)}^2(0)$ increase with the effective nuclear charge, and therefore, one expects that the $K(A,X)$ values will increase if A and/or X are changed from lighter to more heavy nuclei within a given group of the Periodic Table. This expectation is not always fulfilled, and in particular if one is looking at unusual bonding situations. The mutual polarizability term $\Pi_{A,X}$ (equation (6)) is responsible for the sign of K , and takes into account the effects arising from lone pairs of electrons at A and/or X , as well as the energies of the ground and excited states in which mainly electrons with s -character are involved.

$${}^nK(A,X) = -16/9 \pi \mu_0 \mu_B^2 \Psi_{(A)}^2(0) \Psi_{(X)}^2(0) \Pi_{A,X} \quad (5)$$

$$\Pi_{A,X} = 4 \sum_j^{\text{occ}} \sum_k^{\text{unocc}} (\epsilon_k - \epsilon_j)^{-1} C_{jsA} C_{ksA} C_{jsX} C_{ksX} \quad (6)$$

The simple vector model proposed by Dirac predicts a positive K (opposite spin orientations lead to a state of lower energy) for one-bond couplings, negative K (alike spin orientations lead to a state of lower energy) for two-bond (geminal) coupling, positive K for three-bond (vicinal) coupling, and so on. These alternating signs are found frequently if nuclei with a so-called open s -shell configuration

(always for ^1H , and, if mixing of s and p levels is likely, e.g. for ^{11}B , ^{27}Al , ^{13}C , ^{29}Si , etc.) are involved. In contrast, one finds a negative sign of 1K and less predictable signs for nK ($n > 1$) for nuclei with a so-called closed s-shell configuration (this means at least one lone pair of electrons is present which possesses predominantly s-character, e.g. ^{19}F , ^{31}P in phosphanes but not in P(V) or phosphonium compounds, ^{77}Se , ^{125}Te , etc.). In the cases of ^1H and ^{13}C , it was found that the magnitude of the coupling constants $^1J(^{13}\text{C}, ^1\text{H})$ could be correlated with the s-character of the C–H bond hybrid orbital [36]. This apparently simple and useful concept was then extended, more or less successfully, to $^1J(\text{N}, \text{H})$, $^1J(^{11}\text{B}, ^1\text{H})$, $^1J(^{13}\text{C}, ^{13}\text{C})$, $^1J(\text{N}, ^{13}\text{C})$ and other combinations of nuclei. Since this model does not expressly include the mutual polarizability term $\Pi_{A, X}$, it should be applied cautiously, with one being aware of a further gross simplification.

Averaging of scalar spin–spin coupling indicates intramolecular exchange processes, whereas the absence of scalar spin–spin coupling may be traced to intermolecular exchange processes. It is often necessary to find conditions in order to slow down these dynamic processes, usually by low-temperature NMR spectroscopy. Considering the low natural abundance of many NMR-active nuclei, it is often important to look for satellite spectra representing the isotopomer containing the nucleus with low natural abundance. Unfortunately, there are numerous reports in the literature from which it is not clear whether a particular scalar spin–spin coupling is really not present or just had not been measured. Taking into account the labile element–element bonds frequently encountered in organometallic chemistry, crucial information can therefore be lost.

Fast nuclear spin relaxation can also lead to unresolved scalar spin–spin coupling. This is true, in particular, if quadrupolar nuclei are involved which very often have short relaxation times T^Q . However, nuclear spin relaxation via the mechanism of chemical shift anisotropy (T_1^{CSA} , T_2^{CSA}), depending on the \mathbf{B}_0^2 , is becoming increasingly important if high-field spectrometers are used, and these interactions can be very efficient for heavy nuclei in unsymmetrical surroundings.

2 HYDRIDES

Hydrogen compounds are known for all elements. This section will deal only with those molecules in which the hydrogen atoms have some sort of a covalent bond with another element, and the discussion will be restricted to ^1H or ^2H NMR spectroscopy.

2.1 BORON HYDRIDES

The work of A. Stock, starting almost 100 years ago, had produced diborane(6), B_2H_6 , and the first polyhedral boranes, B_4H_{10} , B_5H_9 , B_6H_{10} and

$B_{10}H_{14}$, as the last missing species of main group element hydrides [37]. Most of these boranes had been correctly characterized with respect to their composition. However, an understanding of their structures had started only in the late 1940s and in the 1950s of the last century, mainly due to the pioneering work of W.N. Lipscomb [38] (see also an essay on diborane(6) [39]). By the use of X-ray structural analysis, and increasingly by NMR spectroscopy [40], accompanied by the application of more and more advanced theoretical models, a consistent picture did emerge. In the early days of 1H NMR spectroscopy, unusual δ^1H data of polyboranes, often at rather low frequencies, indicated new structural features. The concept of the electron deficient $3c/2e$ B–H–B bond was already alive, and this type of bonding was reflected by increased magnetic shielding of the bridging hydrogen; at that time this was unprecedented in organic chemistry (see Figure 2).

2.2 UNUSUAL CHEMICAL SHIFTS, δ^1H , OF HYDROCARBONS

The chemical shifts, δ^1H , depending on the position of the hydrogen atom with respect to the B_0 -induced so-called (aromatic) ring current [41], are shown in Figure 3. These are early examples of unusual data which, however, have been convincingly explained by analysing the NMR phenomenon with respect to the electronic structure. Such observations have not lost their fascination, as shown by a recent review on cyclophanes [42] The ring current is regarded as a measure of the cyclic delocalization of the p electrons [43], and theory has made use of this phenomenon by calculation of the Nucleus-Independent Chemical Shift (NICS) as a result of a diatropic (negative NICS value, aromatic system) or a paratropic ring current (positive NICS value) [44].

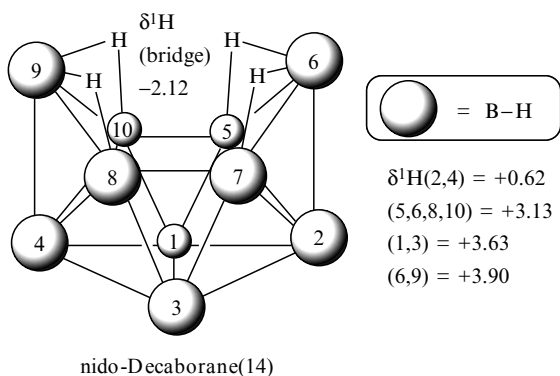


Figure 2 The structure of decaborane(14) and its δ^1H values [40] for bridging and terminal hydrogen atoms

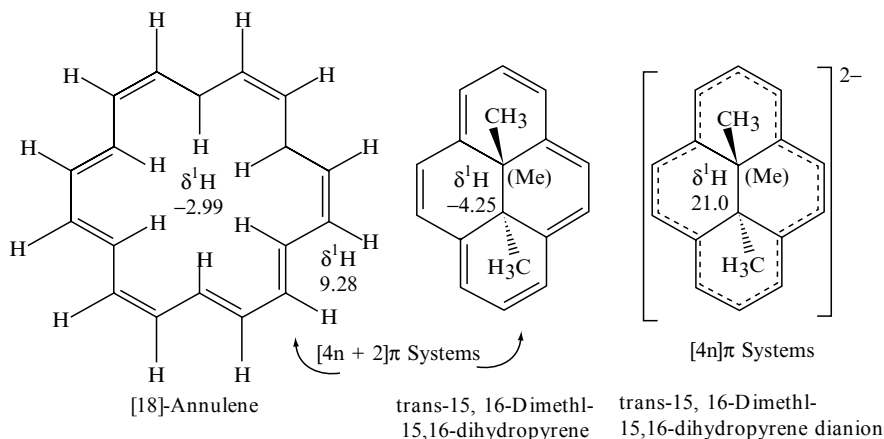


Figure 3 Chemical shifts, $\delta^1\text{H}$, typical of hydrogen atoms in different positions with respect to the B_0 -induced aromatic ring current (data taken from Reference [45])

2.3 CARBOCATIONS

Systematic studies of carbenium ions and carbocations started rather late in organic chemistry, since structural evidence of these frequently elusive species had to be based mainly on NMR spectroscopy. ^1H NMR studies showed that hydrogen atoms directly attached to the carbon atom bearing the positive charge in carbenium ions are strongly deshielded, and that this effect is reduced if the positive charge is delocalized over several carbon atoms. Some representative data are collected together in Figure 4. The μ -hydrido bridging in the cycloalkyl cations is of interest with respect to the low frequency shift of the ^1H resonance of the bridging hydrogen atom (compare with the dimethylcarbenium cation) and the small coupling constants $^1J(^{13}\text{C}, ^1\text{H}_\mu)$ [47–49].

2.4 HYDROGEN BONDING INVOLVING NITROGEN, OXYGEN AND FLUORINE

The important principal concept of the hydrogen bond had already been formulated and widely accepted as early as 1921 [50], a long time before the first successful NMR experiments [1,2]. However, NMR spectroscopy turned out to be an extremely useful tool for studying the hydrogen bond in solution, and later on also in the solid state [51–54]. The $\delta^1\text{H}(\text{bridge})$ values are temperature- and solvent-dependent, and it was possible (by the temperature-dependent changes in $\delta^1\text{H}$ [55]) to distinguish between intra- and intermolecular hydrogen bonds. The $\delta^1\text{H}(\text{bridge})$ values extended the known range of $\delta^1\text{H}$ for organic compounds (about 10 ppm downfield from TMS) to > 20 ppm downfield from TMS, and $\delta^1\text{H}(\text{bridge})$ values in the order of 15–20 are considered to indicate

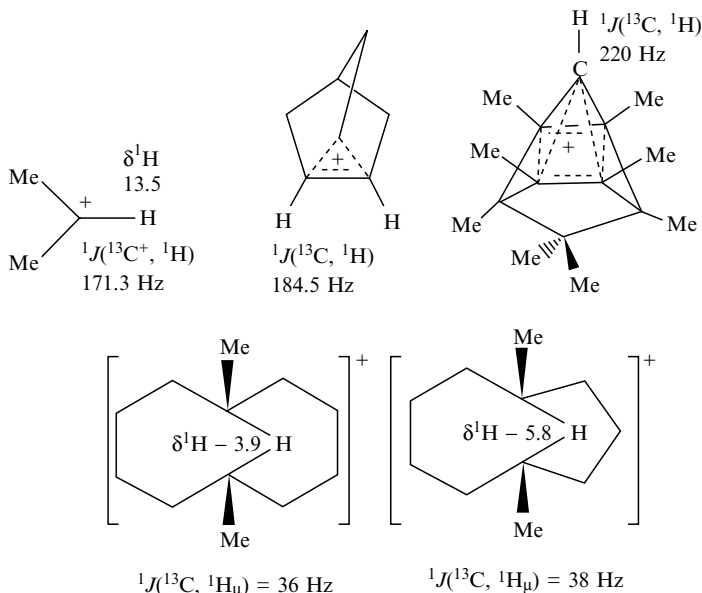


Figure 4 Some $\delta^1\text{H}$ and $^1J(^{13}\text{C}, ^1\text{H})$ values of carbenium ions and carbocations (data taken from References [8b,45–48])

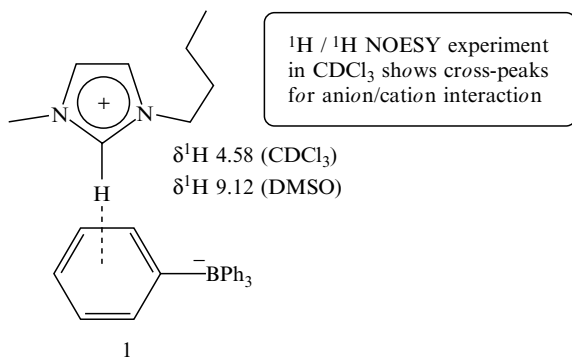
very strong hydrogen bonding. Intramolecular strong hydrogen bonds have also been studied by measuring primary isotope effects, ${}^p\Delta(^1\text{H}, ^2\text{H}) = \delta^1\text{H}(\text{X}) - \delta^2\text{D}(\text{X})$ or ${}^p\Delta(^1\text{H}, ^3\text{H}) = \delta^1\text{H}(\text{X}) - \delta^3\text{T}(\text{X})$ [56]. The concept of resonance-assisted intramolecular N–H...O hydrogen bonding has been discussed by using a comparison of X-ray structural data ($d_{\text{N}\dots\text{O}}$ shortening or lengthening) with information from IR spectra (ν_{NH}) and $\delta\text{H}(\text{NH})$ [57]. In this context, *ab initio* calculations demonstrate that distances, anharmonic proton-stretching frequencies, $\delta^1\text{H}$ values and even coupling between nuclei across the hydrogen bond are related to each other [57,58]. The fact that coupling constants across hydrogen bridges ${}^hJ(\text{X}, \text{Y})$ can be measured (e.g. ${}^hJ(^{31}\text{PO}\dots^1\text{HN})$ in the range of 0.5 to 1.6 Hz, or ${}^hJ(^{31}\text{PO}\dots\text{H}^{15}\text{N}) \approx 1.7$ Hz [59]) is of fundamental importance for structural assignments, in particular in the case of biopolymers [59–61]. This means, experimental evidence is being accumulated, supporting a model of covalent character of the X–H...Y hydrogen bond, alternative to the model of dominantly electrostatic interactions between a proton donor X–H and an acceptor Y. Thus, the hydrogen bond can be described by the valence bond orders $p_{\text{X-H}}$ and $p_{\text{Y-H}}$ as a function of the bond lengths $d_{\text{X-H}}$ and $d_{\text{Y-H}}$, where in the complex X–H...Y the total valency of hydrogen remains unity. An exhaustive description of nuclear spin–spin couplings and geometries by experimental data and *ab initio* MO calculations corroborates the model of covalent bonds X–H and Y–H [62–65]. Another useful approach is to obtain

information on the relaxation time of the acceptor nucleus, which in most cases is ^{14}N or ^{17}O [66], both quadrupolar nuclei.

The role of hydrogen bonding in transition metal chemistry is important considering the function of transition metal complexes in biological processes and in catalysis, e.g. in aqueous systems. Recently, transition metal fluorides have received considerable attention [67–70], and their interaction with hydrogen bond donors (such as HF or H_2O) may modify their reactive properties. Two recent NMR studies [71,72] of well-characterized structurally related bifluoride complexes (Figure 5) demonstrate on the one hand that we are still far from predicting the dynamics and the reactivity of such complexes, while on the other hand it is obvious that NMR spectroscopy is the decisive tool in order to gain further information.

Weak hydrogen bonds [73] are frequently discussed now as attractive forces between electronegative elements and hydrogen atoms linked, e.g. to carbon or transition metals [74], and there is a growing number of examples supplying relevant experimental evidence in solution, for instance, for the ‘dihydrogen bond’ (e.g. the $\text{N}-\text{H}\cdots\text{H}-\text{Ir}$ bridge [75], the $\text{C}-\text{H}\cdots\text{H}-\text{Ru}$ bridge [76], $\text{C}-\text{H}\cdots\text{O}$ [77] or $\text{C}-\text{H}\cdots\text{Se}-\text{C}$ interactions [78]).

$\text{C}-\text{H}\pi$ interaction [79], another sort of weak hydrogen bonding, is shown by significant upfield shifts of the relevant ^1H resonances, as in the example **1** below [79a], where the ions are separated in DMSO and ion pairs are present in CDCl_3 .



2.5 TRANSITION METAL HYDRIDES

In Chapter 3 of this volume, the principal structures of transition metal hydrides are explained. In this context, the most intriguing aspect concerns the dihydrogen complexes in which the H_2 molecule is coordinated side-on to the metal. This causes weakening of the $\text{H}-\text{H}$ bond, a model case of element-hydrogen activation. The presence of such a coordination in solution results from unusually fast nuclear spin relaxation of the ^1H nuclei owing to efficient

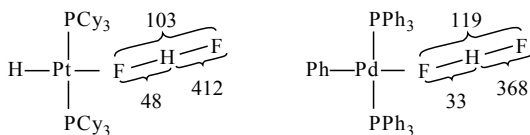


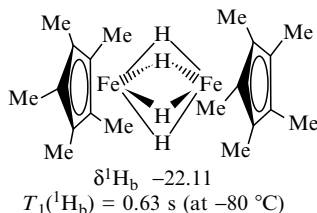
Figure 5 The platinum and the palladium bifluoride complex [71,72] have similar structures, and also similar NMR parameters (coupling constants (shown by braces) $^1J(^{19}\text{F}, ^1\text{H})$ and $^2J(^{19}\text{F}, ^{19}\text{F})$ are given in Hz), as measured from the respective low-temperature NMR spectra. However, the dynamic properties appear to be different: the dynamics of the platinum complex are predominantly caused by intermolecular processes (e.g. by dissociation of HF), whereas the dynamic behaviour of the palladium complex is governed by intramolecular Pd-FHF/Pd-FHF exchange, most likely via an intermediate in which the Pd atom is five-coordinate

dipole-dipole interactions as a result of the short H-H distance (typical $T_1(^1\text{H})$ values are < 30 ms) [80]. Furthermore, the mono- ^2H -labelled complexes enable one to measure the coupling constant $^1J(^2\text{D}, ^1\text{H})$ (typical range 17–34 Hz) for which the magnitude is markedly reduced when compared with the free $^2\text{D}-^1\text{H}$ molecule (43.2 Hz). Transition metal polyhydride complexes are of interest with respect to intramolecular hydrogen exchange, a process associated with a low activation energy as shown, e.g. for $[\text{Ir}(\text{X})(\text{H})_2(\eta^2\text{-H}_2)(\text{P}i\text{Pr}_3)_2]$ ($\text{X} = \text{Cl}, \text{Br}, \text{I}$) in experiments and by DFT calculations [81a]. Dihydrogen/hydride complexes of ruthenium, e.g. $[(\text{Cy}_3\text{P})_2\text{Ru}(\text{bipy})\text{H}(\text{H}_2)]^+$, also show fast intermolecular and intramolecular exchange, as proved by the reaction with D_2 which leads to species containing the combinations H_2D and HD_2 [81b]. The first H_2 -metal cluster interaction was proposed recently for $[\text{H}_6\text{Ru}_4(\text{C}_6\text{H}_6)_4]^{2+}$ on the basis of $T_1(^1\text{H})$ measurements [82].

Unusually large $J(^1\text{H}, ^1\text{H})$ values (up to 1500 Hz), as a result of quantum mechanical exchange [83–85], are measured in some trihydrogen complexes. The magnitude of these coupling constants can be extremely temperature-dependent: in the case of the complex $[(\eta^5\text{-C}_5\text{H}_5)\text{Ir}(\text{H})_3(\text{PPh}_3)]$, the magnitude of $J(^1\text{H}, ^1\text{H})$ increases from 150 to 400 Hz when the temperature is increased from 150 to 200 K.

Another interesting aspect concerns the enormous range of $\delta^1\text{H}$ data (> 50 ppm) of ‘classical’ transition metal hydrides (for a list of $\delta^1\text{H}(\text{MH})$ values of numerous phosphane metal hydride complexes see Reference [86]). The high-field shifts find their explanation in part in the pronounced hydridic character of hydrogen in the M-H terminal bond or in $\mu_2\text{-HM}_2$ and $\mu_3\text{-HM}_3$ units. In addition, there are diatropic (in some cases paratropic) \mathbf{B}_0 -induced currents arising from metal d electrons which in general shield [87] or in some cases deshield (e.g. interstitial hydrogen atoms in $[\text{HRu}_6(\text{CO})_{18}]^-$ and $[\text{HCo}_6(\text{CO})_{15}]^-$ with $\delta^1\text{H} = 16.4$ and 23.2, respectively) the ^1H nuclei. A recent well-characterized example with $\mu_2\text{-H}$ atoms is the very reactive dinuclear iron complex $[(\text{Cp}^*\text{Fe})_2(\mu\text{-H})_4]$ **2** [88], in which four hydrogen atoms are in bridging positions between the two iron atoms. Although the Fe-Fe distance is short

(220.2(2) pm), Fe–Fe bonding interactions (in order to fulfill the 18e rule, an Fe≡Fe bond would be required) are not postulated (*ab initio* MO calculations of the corresponding ruthenium complex [(Cp**Ru*)₂(μ-H)₄] suggest the absence of Ru–Ru bonding [89]).



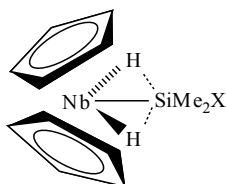
2

In the absence of unbalanced d-orbital contributions, e.g. in the case of Hg–H units, $\delta^1\text{H}$ values are found at rather low field (e.g. Me–Hg–H, $\delta^1\text{H}(\text{Hg–H}) = 16.8$; Ph–Hg–H, $\delta^1\text{H}(\text{Hg–H}) = 13.3$) with large coupling constants $^1J(^{199}\text{Hg}, ^1\text{H})$ in the range of 2300 to 3000 Hz [90].

High-pressure ^1H NMR can be applied to indicate the intermediate formation of transition metal hydrides [91,92]. Another ^1H NMR technique provides attractive potential to study short-lived transition metal hydrides, based on the *para*-hydrogen induced polarization (PHIP) [93–95], as shown, e.g. for rhodium–tin compounds in catalysed hydrogenation [96].

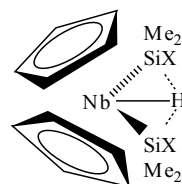
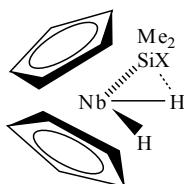
In general, transition metal complexes bearing the $[\text{BH}_4]^-$ ligand [97a] are fluxional with respect to fast exchange of bridging and terminal hydrogen atoms [97b]. In the case of the dinuclear molybdenum complex $[\text{Mo}_2\text{Cp}_2(\mu\text{-SMe})_3(\mu\text{-BH}_4)]$, this exchange is slow, and the ^1H resonances for bridging ($\delta^1\text{H}_b = -15.79$) and terminal hydrogen atoms ($\delta^1\text{H}_t = 2.32, 1.28$; $^2J(^1\text{H}_t, ^1\text{H}_t) = 18 \text{ Hz}$; $^2J(^1\text{H}_t, ^1\text{H}_b) = 3 \text{ Hz}$) can be observed undisturbed under conditions of ^{11}B decoupling ($\delta^{11}\text{B} = -27.0$) [98].

Niobocene silyl hydrides **3** with non-classical interligand interactions have been studied with respect to their NMR properties (^1H , ^{13}C , ^{29}Si , ^{19}F NMR) [99], in particular their ^1H relaxation times [100].



3

X = Ph, Cl, OEt



X = Ph, Cl

3 ALKALI METAL COMPOUNDS

3.1 ALKALIDE ANIONS

With the exception of $[\text{Li}]^-$, the anions of alkali metals, the alkalide anions, have been characterized by their significant low-frequency chemical shifts in ^{23}Na , ^{39}K , ^{87}Rb and ^{131}Cs NMR spectra (Figure 6) [101,102]. The full occupation of the respective *ns* orbital leads to an increase in magnetic shielding which is largest in the case of $[\text{Cs}]^-$, as expected when considering the increasing range of chemical shifts moving down in the group, typical of main group elements.

3.2 ORGANOLITHIUM COMPOUNDS

The successful exploration of solid-state structures of organolithium compounds by X-ray crystallography [103] has called for similarly extensive solution-state studies [104,105]. Structural features can be elucidated by measuring the heteronuclear Overhauser effect (NOE) which reveals the proximity of particular ^1H to $^6/7\text{Li}$ nuclei (HOESY experiments [106–108]).

Since the range of chemical shifts δLi is small, it was hoped that coupling constants $J(\text{Li},\text{X})$ might provide additional information. Thus, numerous $^1J(^{13}\text{C}, ^6/7\text{Li})$ data are available (for a list, see Reference [104]). These measurements are particularly useful and straightforward for the analysis of the aggregation state with ^6Li -enriched derivatives, since the ^6Li nucleus ($I = 1$; see Table 2, also for ^7Li) possesses a very small quadrupole moment and behaves, at least for solution-state NMR measurements, more like a spin-1/2 nucleus as far as nuclear spin relaxation is concerned. Additional ^{13}C -enrichment is another option which is extremely helpful to assess the aggregation of organolithium compounds [109–117]. Figure 7(a) shows a ^{13}C NMR spectrum of *t*BuLi in Et_2O , showing the presence of ^6Li and ^7Li next to ^{13}C , which allows us to assess the association.

The driving force behind the association of organolithium compounds is the coordinatively unsaturated character of the lithium atoms in the absence of suitable donor molecules. This leads to numerous peculiar structures. In the Li-bridged dimer $\{\textit{trans}\text{-}[\text{Pt}(\text{PEt}_3)(\text{Bu})(\text{C}\equiv\text{CPh})_2]\text{Li}\}_2$ the broadened $^{13}\text{C}(\text{Pt})$ -alkynyl signals testify to carbon–lithium bonding. However, here and in general,

$\delta^{23}\text{Na}$	$\delta^{39}\text{K}$	$\delta^{87}\text{Rb}$	$\delta^{133}\text{Cs}$
$[\text{Na}]^-$	$[\text{K}]^-$	$[\text{Rb}]^-$	$[\text{Cs}]^-$
-62	-105	-185	-280

Figure 6 Chemical shifts of the alkalide anions [101,102] with respect to M^+ in aqueous solutions of the respective chlorides

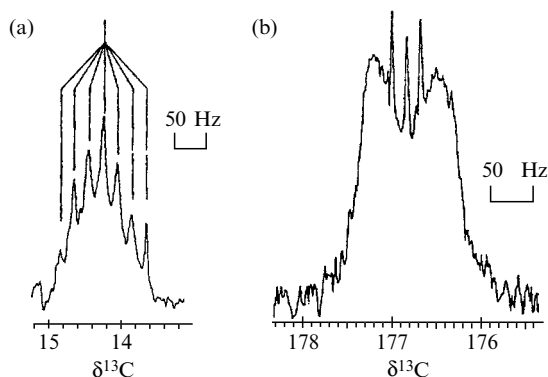


Figure 7 ^{13}C NMR spectra (natural abundance of ^{13}C and $^6/^7\text{Li}$) of two organolithium compounds. (a) The ^{13}C resonance of the quaternary carbon of $t\text{BuLi}$ in Et_2O (1.4 M, -64°C); according to the splitting due to coupling of ^{13}C with two equivalent ^7Li nuclei ($^1J(^{13}\text{C}, ^7\text{Li}) = 20.0$ Hz, a seven-line pattern) a dimer is present. (b) The ^{13}C NMR signal of the lithiated carbon of $2,4,6\text{-}t\text{Bu}_3\text{C}_6\text{H}_2\text{Li}$ (in $\text{D}_8\text{-THF}$ at -79°C) shows the splitting due to partially relaxed $^{13}\text{C}\text{-}^7\text{Li}$ ($^1J(^{13}\text{C}, ^7\text{Li}) = 42.5$ Hz; the two central lines of the 1:1:1:1 pattern are left), and the well resolved 1:1:1 triplet due to $^1J(^{13}\text{C}, ^6\text{Li}) = 16.1$ Hz, which prove the presence of a monomer (adapted from Reference [114])

a multinuclear approach is rewarding: in both ^{195}Pt and ^7Li NMR spectra (Figure 8), the respective pattern due to $^{195}\text{Pt}\text{-}^7\text{Li}$ spin-spin coupling is observed. The fairly large value of the coupling constant ($J(^{195}\text{Pt}, ^7\text{Li}) = 78$ Hz) is suggestive of direct Pt-Li interactions. The main features of the solution-state structure of the dimer are retained in the solid state, as shown by X-ray structural analysis [118].

4 ^{11}B AND ^{27}Al NMR SPECTROSCOPY

4.1 THE STRUCTURES OF BORON COMPOUNDS

Together with ^1H NMR, ^{11}B NMR has been from the beginning of modern boron chemistry an immensely important tool for the structural elucidation of boranes, polyboranes, carboranes, other heteroboranes and metallaboranes. Although ^{11}B is a quadrupolar nucleus ($I = 3/2$; see Table 2 also for ^{10}B), the line widths of the ^{11}B resonance signals are reasonably small in many cases, thus allowing us to distinguish between boron atoms in different surroundings. Early compilations of $\delta^{11}\text{B}$ data [40] were followed by reviews focusing mainly on $\delta^{11}\text{B}$ data of three- and four-coordinate boron compounds [119–121], and of polyhedral boranes [122,123]. Figure 9 presents some $\delta^{11}\text{B}$ data of boranes, borane adducts and borates.

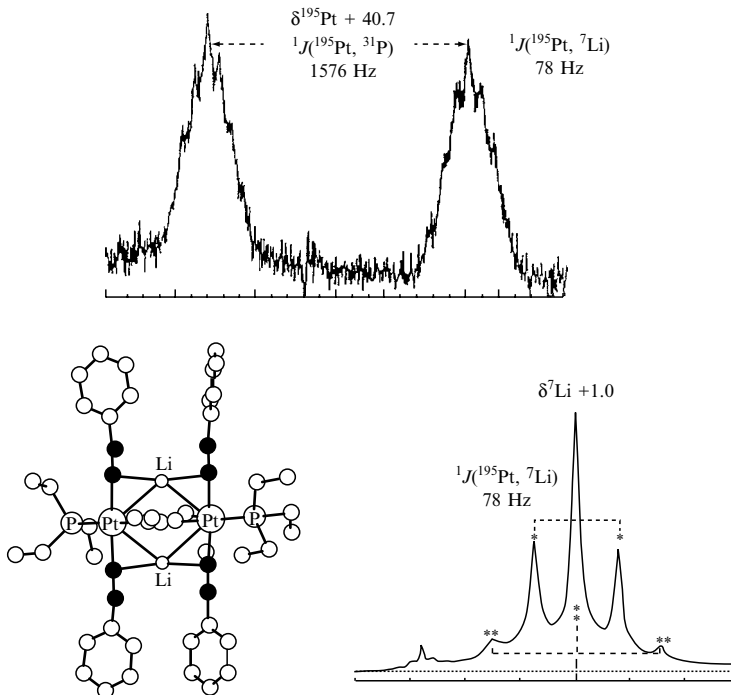


Figure 8 42.8 MHz ^{195}Pt and 77.7 MHz ^7Li NMR spectra of $[\text{Pt}(\text{PEt}_3)(\text{Bu})(\text{C}\equiv\text{CPh})\text{Li}]_2$ (the molecular structure is shown) [118]. Each of the doublet lines in the ^{195}Pt NMR spectrum is broadened and split into a multiplet owing to coupling of ^{195}Pt with two equivalent ^7Li nuclei. The ^7Li NMR signal is accompanied by ^{195}Pt satellites for the isotopomer containing one ^{195}Pt (*) and for the isotopomer containing two ^{195}Pt nuclei (**)

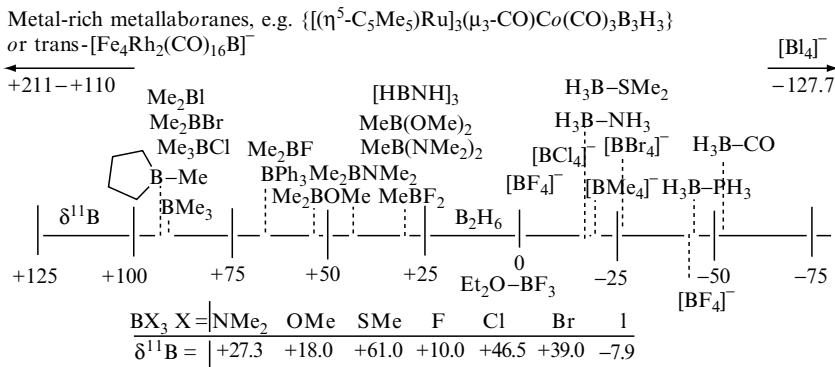
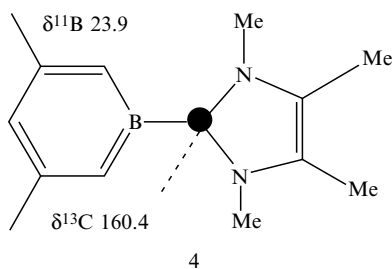
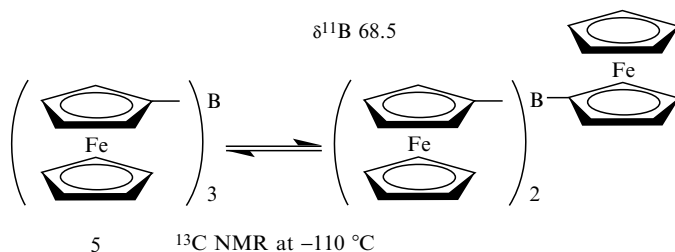


Figure 9 Chemical shifts, $\delta^{11}\text{B}$, of some boranes, borane adducts and borates

The lowest ^{11}B nuclear shielding in conventional trigonal boranes is observed in trialkylboranes ($\delta^{11}\text{B}(\text{Me}_3\text{B}) = 86.0$), and if the ^{11}B nucleus is part of a five-membered ring (as shown in Figure 9) ^{11}B shielding is even slightly more reduced ($\delta^{11}\text{B}[(\text{CH}_2)_4\text{BMe}] = 92.5$). Successive substitution of the alkyl groups by substituents capable of (pp) π interactions (potential π donors and σ acceptors) gives rise to an increase in ^{11}B nuclear shielding (see also $\delta^{13}\text{C}^+$ of isoelectronic carbenium ions, Section 5.1 below). The stabilization of three-coordinate boron in borabenzene as a carbene adduct (**4**) is a recent addition in this context [124]. The relatively high ^{11}B nuclear shielding in the carbene adduct is unprecedented for the trigonal planar surroundings of a boron atom with three B–C bonds.



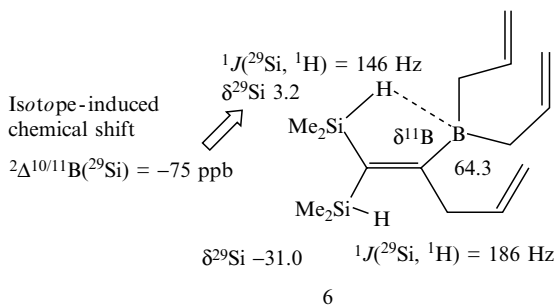
Attempts to crystallize triferrocenylborane (**5**) have led to a single diastereomer in which all three ferrocenyl groups are on one side, as shown by single crystal X-ray analysis and by powder diffractograms of a bulk sample [125]. However, in solution rotation about the B–C bonds is fast, and only at -110°C does ^{13}C NMR reveals the presence of the expected two diastereomers [125].



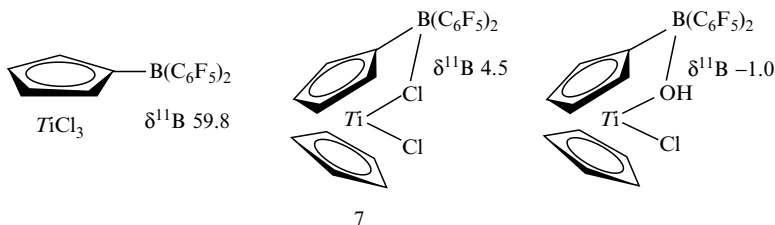
If an alkyl group is replaced by an electropositive substituent such as a silyl group [126] or a dialkylboryl group, leading to tetraalkyldiboranes(4) [127–129], ^{11}B nuclear shielding decreases. This supports the importance of the ΔE model, that the relative energy of both the σ bonds and the unoccupied boron p_z orbital have to be considered. The bonding of trigonal boron to silicon or to

an another trigonal boron atom is expected to increase the energy of σ bonds, and thus, ΔE will decrease.

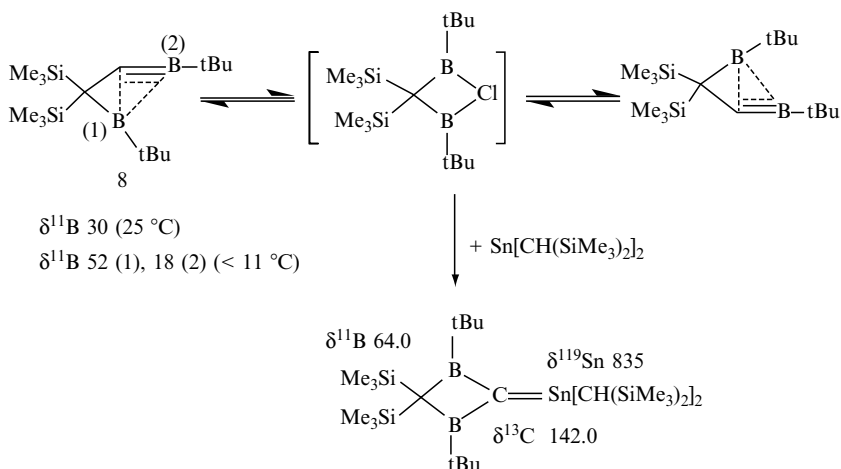
When the the boron atoms become tetracoordinate, the ^{11}B nuclear shielding increases markedly, and therefore, the change in boron coordination number is always indicated by typical $\delta^{11}\text{B}$ values (e.g. $\delta^{11}\text{B}([\text{BMe}_4]^-) = -20.7$, as compared to $\delta^{11}\text{B}(\text{Me}_3\text{B}) = 86.0$). In this context, some rare cases of bridging should be noted. The first Si–H–B bridge (Si–H activation) was identified in 1-silyl-2-boryl-alkenes (**6**) by the increase in ^{11}B nuclear shielding, the decrease in ^{29}Si nuclear shielding, the decrease in the magnitude of $^1J(^{29}\text{Si}, ^1\text{H})$, and by the substantial isotope-induced chemical shift $^2\Delta^{10/11}\text{B}(^{29}\text{Si})$ [130].



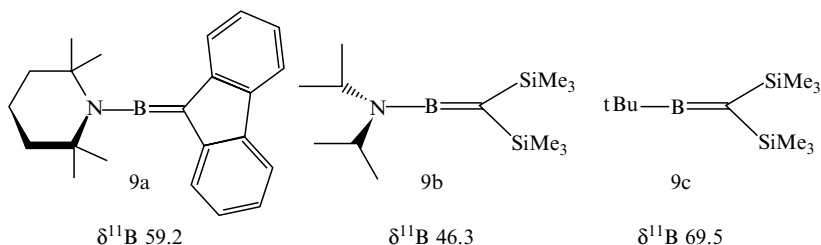
Another, and so far rare case of bridging of the type M–Cl–B in compound **7** was firmly established for M = Ti by $\delta^{11}\text{B}$ values typical of four-coordinate boron (*vide infra*) and also by X-ray structural analysis [131]. Interestingly, this bridging is absent in the TiCl_3 derivative.



Hyperconjugation (σ - π electron delocalization) is an important concept [132] in order to explain certain structural features of carbocations and also of organoboranes. This has been demonstrated in the case of numerous methyleneboranes [133]. The first example, **8**, was shown to possess a fluxional non-classical structure as evidenced by the different ^{11}B resonance signals at low temperature [134]. The rearrangement is believed to take place via a carbene-like species which could be trapped in the reaction with a stannylene [135].



Examples of stable classical methyleneboranes such as **9** are known [136,137], in which the electron deficiency of the boron atom is either compensated by BN(pp) p bonding or where bulky groups contribute to kinetical stabilization.



Extremely rewarding applications of ^{11}B NMR are directed towards the structural elucidation and general characterization of polyhedral boranes. A number of empirical rules has been developed to help with the prediction of structures of these compounds [138] and to classify the $\delta^{11}\text{B}$ data according to prominent structural features [139]. The assignment of the sometimes complex ^{11}B NMR spectra of polyhedral boranes is greatly aided by 2D- $^{11}\text{B}/^{11}\text{B}$ COSY experiments [140–142] which in general show off-diagonal cross-peaks for B–B connectivity in the absence of B–H–B bridging (Figure 10). Careful analysis of these spectra, 2D- $^{11}\text{B}/^1\text{H}$ heteronuclear shift correlations, and if necessary, ^{11}B decoupled 2D $^1\text{H}/^1\text{H}$ COSY experiments, lead to correct structural assignments.

More recently, high-level quantum chemical calculations have been shown to be reliable for optimizing the geometry of polyhedral boranes [143], and the calculation of ^{11}B chemical shifts by either the IGLO approach [144–146] or by

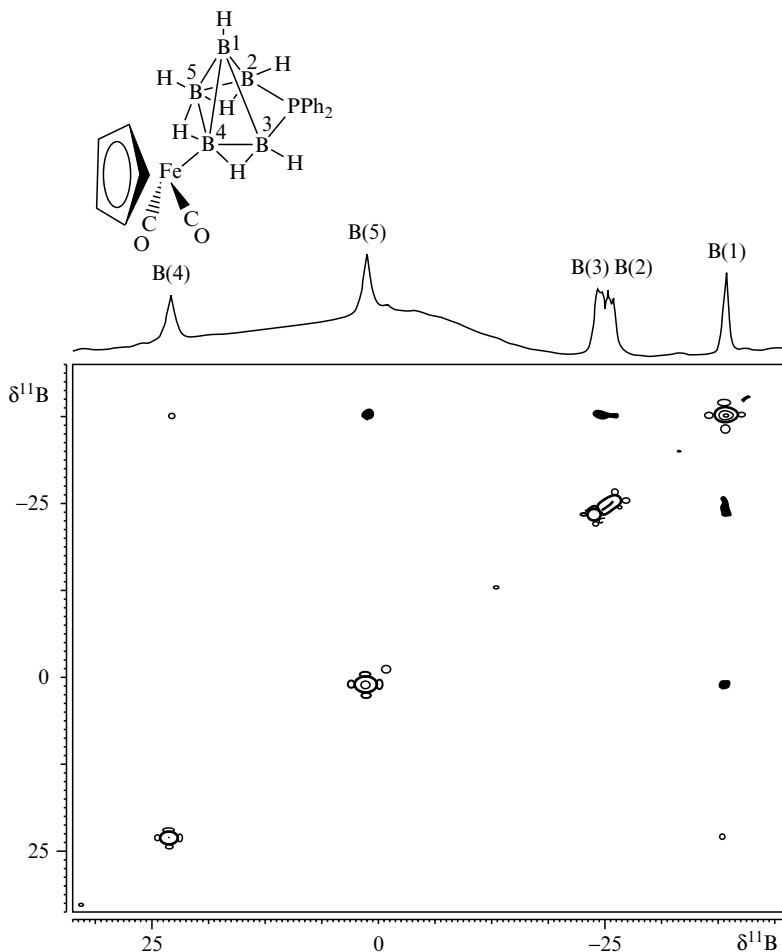
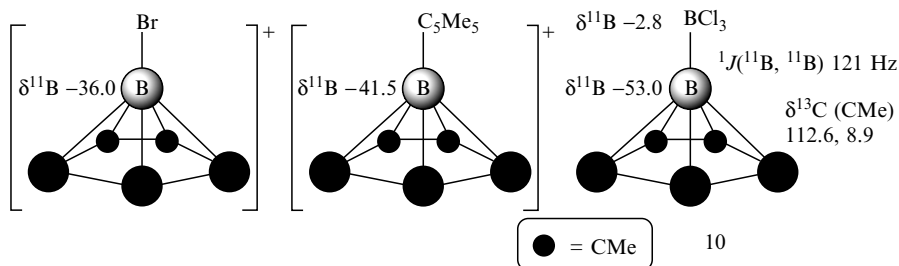


Figure 10 Contour plot of the 160.45 MHz ^1H decoupled $^{11}\text{B}/^{11}\text{B}$ COSY NMR spectrum (25 °C, CDCl_3) for 4- $[\text{Fe}(\eta^5\text{-Cp})(\text{CO})_2]\text{B}_5\text{H}_7\text{-}\mu\text{-}2,3\text{-PPh}_2$ (adapted from Reference. [142]). The signal for the apical boron atom B(1) shows off-diagonal cross-peaks to all basal boron atoms B(2,3,4,5), whereas there are no off-diagonal cross-peaks for the basal boron atoms which are linked either by hydrogen bridges or by the μ -phosphido bridge. The assignment of the basal boron atoms is based on $^{31}\text{P}\text{-}^{11}\text{B}$ coupling (resolved in the projection) and by the 1 H coupled 1D- ^{11}B NMR spectrum (not shown)

the GIAO method [147] enables one to correlate the experimental and calculated $\delta^{11}\text{B}$ data with the experimentally determined structure or with the geometry optimized by *ab initio* MO calculations [148].

The cations $[\text{Cp}^*\text{B-Br}]^+$ and $[\text{Cp}^*_2\text{B}]^+$ have been already reported in 1978 [149–151] and the η^5/η^1 -structure of $[\text{Cp}^*_2\text{B}]^+$ has been correctly predicted on

the basis NMR data, including the highly shielded apical ^{11}B nucleus ($\delta^{11}\text{B}$, -41.5); now this structure has been confirmed by X-ray analysis, showing a short B-ring centroid distance (126.9(5) pm) [152]. Interestingly, the beryllocenes $(\text{C}_5\text{H}_5)_2\text{Be}$ and $(\text{C}_5\text{Me}_4\text{H})_2\text{Be}$ also possess an η^5/η^1 -structure, whereas the pentamethylcyclopentadienyl rings in Cp^*_2Be are reported to be linked η^5/η^5 to the beryllium atom [153]. The boron-ring centroid distance is also short (126.0(3) pm) in the neutral species **10**, in which the apical boron atom is linked to BCl_3 [154]. The $\delta^{11}\text{B}$ values and the coupling constant $^1J(^{11}\text{B}, ^{11}\text{B})$ prove that the *nido*-structure is retained in solution.

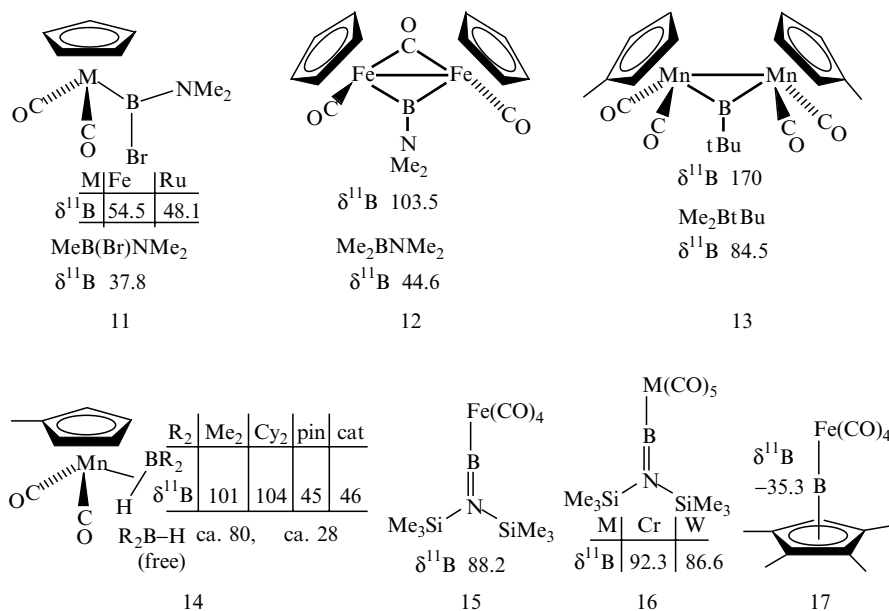


According to electron counting rules [155–158], one bonding pair of electrons is missing in *closo*-tetraboranes of the type B_4X_4 (e.g. $\text{X} = \text{Cl}$) [159] or B_4R_4 ($\text{R} = t\text{Bu}$) [160,161]. Therefore, an energetically low-lying unoccupied orbital is present, available for paramagnetic \mathbf{B}_0 -induced charge circulations. Indeed, the ^{11}B nuclear magnetic shielding is very low ($\delta^{11}\text{B}(\text{B}_4\text{Cl}_4) = 85.0$ [159]; this also holds for other compounds in the series B_nCl_n or B_nBr_n ; $\delta^{11}\text{B}(\text{B}_4t\text{Bu}_4) = 135.4$ [160]) when compared with other polyhedral boranes (e.g. ($\delta^{11}\text{B}(\textit{closo}\text{-B}_4\text{H}_2t\text{Bu}_4) = 14.8$ [162]) with *closo*-, *nido*-, or *arachno*-cage structures. The coupling constant $^1J(^{11}\text{B}, ^{10}\text{B})$ in B_4Cl_4 is small (< 2.5 Hz) which indicates that the tetrahedral arrangement of the boron atoms, typical of $2e$ -multi-center bonds, is retained in solution [163].

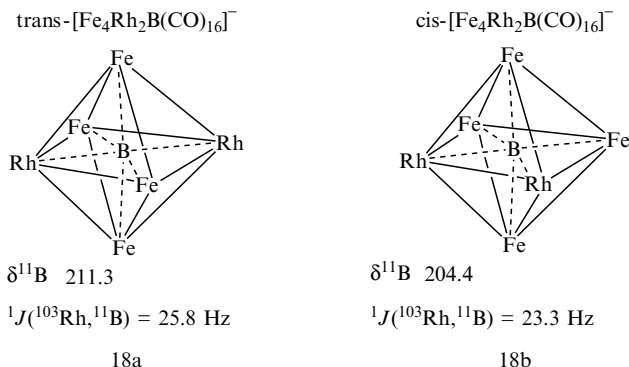
4.2 COMPLEXES WITH TRANSITION METAL–BORON BONDS

In the last decade, numerous transition metal boryl complexes ($\text{M}-\text{BR}_2$) (e.g. **11**) have been prepared and structurally characterized [164–166]. More recently, the first examples of terminal borylene complexes ($\text{M}-\text{BR}$) (15–17) have been reported [167,168], while base-stabilized terminal borylene complexes of osmium [169], and complexes with bridging borylene units ($\text{M}-\text{BR}-\text{M}$) (**12**, **13**) [170–173] are known. There are well characterized complexes in which a borane $\text{R}_2\text{B}-\text{H}$ is coordinated side-on with the $\text{B}-\text{H}$ bond to titanium in $\text{Cp}_2\text{Ti}(\text{HBcat})_2$ [174] (active catalyst in hydroboration reactions [175]), as

well as to manganese (**14**) or rhenium complex fragments [176]. The ^{11}B NMR data of complexes with metal–boron bonds differ significantly from ‘normal’ boranes: the ^{11}B nuclear shielding is reduced (see below, and compare ^{13}C nuclear shielding in carbene and carbyne complexes), and coupling constants $^1J(^{11}\text{B},^1\text{H})$ become small, if the B–H bond is coordinated to the metal center (e.g. in $[(\eta^5\text{C}_5\text{H}_4\text{Me})\text{Mn}((\text{CO})_2(\eta^2\text{-H-Bcat}))]$ with $^1J(^{11}\text{B},^1\text{H}) = 95$ Hz as compared to ca. 180 Hz in the free borane [176]). There are various types of complexes containing four-coordinate boron atoms with M–B bonds [177,178], or in which borane adducts are linked to the metal in an $\text{M}(\eta^1\text{-BH}_3\text{-L})$ fashion ($\text{M} = \text{Cr}, \text{Mo}, \text{W}$; $\text{L} = \text{NMe}_3, \text{PMe}_3, \text{PPh}_3$) [179].



The vast area of polyhedral metallaboranes and metallacarboranes [180,181] cannot be discussed here. A review on systematic metallaborane chemistry, starting from simple boron compounds cites much of the relevant literature [182]. A recent report describes the metallaborane, $[(\text{Cp}^*\text{Ru})_3\text{Co}(\text{CO})_2(\mu_3\text{CO})\text{B}_3\text{H}_3]$ ($\delta^{11}\text{B} = 134.5$), which possesses a cubane cluster structure [183]. Boron can be part of a gold cluster, as shown in the cation $[\text{Cy}_3\text{P-B}(\text{AuPPh}_3)_4]^+$ ($\delta^{11}\text{B} = 12.2$) [184]. Extremely deshielded ^{11}B nuclei are typical of interstitial boron atoms (see data for **18**) [185].



4.3 PENTAMETHYLCYCLOPENTADIENYL (Cp*) ALUMINUM COMPOUNDS

The long history of Al(t) chemistry [186] is being continued at present in particular by the investigation of Cp*Al compounds. ²⁷Al NMR is used in these studies since the ²⁷Al NMR signals are reasonably sharp in spite of the sizable quadrupole moment of the spin-5/2 nucleus (see Table 2). Thus, $\delta^{27}\text{Al} = -80.7$ for the tetramer [Cp*Al]₄ [187a], and $\delta^{27}\text{Al} = -149$ for the monomeric species [187b] have been reported. In Cp*Al–Al(C₆F₅)₃, the high-field ²⁷Al NMR signal at $\delta - 115.7$ is assigned to the Cp*Al, whereas a very broad ²⁷Al signal ($\delta + 107$) belongs to the Al(C₆F₅)₃ fragment [188]. Transition metal complexes of Cp*Al have been characterized with Cr(CO)₅ ($\delta^{27}\text{Al} = -26.1$ [189]), Fe(CO)₄ fragments ($\delta^{27}\text{Al} = +0.4$ [190]), and recently the tetrahedrally coordinated platinum(0) complex (dcpe)Pt(AlCp*)₂ (dcpe = bis(dicyclohexylphosphanyl)ethane; $\delta^{27}\text{Al} = -114.5$ (broad)) have been obtained [191].

Various routes lead to the cation [(η^5 -Cp*)₂Al]⁺ which has parallel cyclopentadienyl rings in a staggered conformation in the solid state (in contrast to [Cp*₂B]⁺ [152]; for a review on main group metallocenes see Reference [192]) and a $\delta^{27}\text{Al}$ value of $\delta - 114.5$ [193] or $\delta - 115.2$ (sharp signal) has been measured by several groups [194,195a]. For the parent cation [(η^5 -Cp)₂Al]⁺, a sharp ($h_{1/2} = 30$ Hz) ²⁷Al NMR signal has been measured [195b].

5 GROUP 14 ELEMENT CHEMISTRY IN THE LIGHT OF NMR

5.1 CARBON ATOMS IN UNUSUAL SURROUNDINGS

Ever since fullerenes, C₆₀, C₇₀ and others, had been established as novel modifications of the element carbon [196], one is tempted to cite these molecules as examples of carbon atoms in unusual surroundings. However, the carbon atoms in fullerenes are three-coordinate and the $\delta^{13}\text{C}$ values are found

exactly in the range typical of olefinic carbon atoms: $\delta^{13}\text{C}(\text{C}_{60}) = 143.2$, and $\delta^{13}\text{C}(\text{C}_{70}) = 130.9, 145.4, 147.4, 148.1$ and 150.7 (in a ratio of 10:20:10:20:10) [197]. This is also true for anions, if they are diamagnetic and their solutions can be studied by ^{13}C NMR, as has been shown recently for C_{70}^{6-} [198a] or the endohedral metallofullerene anion $[\text{La}@\text{C}_{82}]^-$, for which the solid-state structure is unknown. In solutions of $[\text{La}@\text{C}_{82}]^-$, the number of ^{13}C NMR signals indicate a structure with C_{2v} symmetry [198b]. Fascinating endohedral compounds of noble gases such as $\text{He}@\text{C}_{60}$ and $\text{He}@\text{C}_{70}$ have been prepared and studied by ^3He NMR [199,200]: the increase in magnetic shielding of the ^3He nuclei ($\delta^3\text{He} = -6.3$ for $\text{He}@\text{C}_{60}$ and -28.8 for $\text{He}@\text{C}_{70}$ with respect to free dissolved ^3He) indicate the effect of \mathbf{B}_0 -induced ring currents inside of the fullerenes. Similar to C_{60} , transition metal complexes containing fullerenes as π -coordinate ligands do not exhibit unusual $\delta^{13}\text{C}$ values [201].

In carbenium ions, the deshielding of the carbon atom which formally carries the positive charge is remarkable [202–204] (Figure 11). However, the deshielding is a consequence of small energy differences of σ - π transitions involving the formally empty p_z orbital at C^+ . There is a roughly linear relationship between $\delta^{13}\text{C}(\text{C}^+)$ of carbenium ions and $\delta^{11}\text{B}$ of isoelectronic and isostructural boranes [205–207]. Marked deviations from this relationship can be traced either to more significant (pp) π bonding in the case of the carbenium ions or to significantly different structures, e.g. in α -ferrocenylcarbenium ions (fairly strong $\text{Fe}-\text{C}^+$ interaction [208]) and ferrocenylboranes (weak $\text{Fe}-\text{B}$ interaction [209,210]).

	$\delta^{13}\text{C}^+$		$\delta^{13}\text{C}^+$		$\delta^{13}\text{C}^+$
Me_3C^+	335.7	Ph_3C^+	211.8	$\text{Ph}(\text{N}_3)(\text{HO})\text{C}^+$	184.7
$\text{Me}_2(\text{H})\text{C}^+$	320.6	$(2\text{-thienyl})_3\text{C}^+$	153.3	$\text{Et}(\text{EtO})_2\text{C}^+$	191.6
$\text{Me}_2(\text{Ph})\text{C}^+$	254.1	$(\text{cyclopropyl})_3\text{C}^+$	272.0	$\text{Et}(\text{MeS})_2\text{C}^+$	246.9
$\text{Me}_2(\text{MeCC})\text{C}^+$	269.0	$(\text{cyclohexyl})\text{C}^+\text{-Me}$	329.6	$\text{Et}(\text{MeSe})_2\text{C}^+$	265.3
$\text{Me}_2(2\text{-furyl})\text{C}^+$	193.1	$(\text{cyclopentyl})\text{C}^+\text{-Me}$	337.3	$\text{Me}(\text{MeO})(\text{Me}_2\text{N})\text{C}^+$	176.3
$\text{Me}_2(\text{Cl})\text{C}^+$	312.8	$(\text{cyclopropyl})\text{C}^+$	177.0	$\text{Me}(\text{MeS})(\text{Me}_2\text{N})\text{C}^+$	191.6
$\text{Me}_2(\text{F})\text{C}^+$	282.9	$(\text{cyclohexadienyl})\text{C}^+$	209.7	$\text{F}(\text{HO})_2\text{C}^+$	157.8
$\text{Me}_2(\text{HO})\text{C}^+$	250.3	$(\text{cycloheptatrienyl})\text{C}^+$	156.2	$(\text{HO})_3\text{C}^+$	166.3
$\text{Me}_2(\text{Me}_2\text{N})\text{C}^+$	189.5	$(\text{cyclooctatrienyl})\text{C}^+$	126.6	$(\text{cyclopentadienyl})\text{S}^+\text{-SMe}$	190.4
$(\text{bicyclo[2.2.1]hept-2-yl})\text{C}^+$	300.6	$(\text{cyclohexadienyl})\text{C}^+\text{-Me}$	126.6	$(\text{H}_2\text{N})_3\text{C}^+$	160.0
$(\text{cyclopropyl})\text{C}^+=\text{C}(\text{cyclopropyl})$	234.2	$(\text{cycloheptatrienyl})\text{C}^+\text{-Me}$	126.6	$\text{Me}-\text{C}^+=\text{O}$	150.3
$(\text{cyclohexadienyl})\text{C}^+(\text{H})\text{Me}$	117.9	$(\text{cyclooctatrienyl})\text{C}^+\text{-Me}$	126.6	$\text{HCC}-\text{C}^+=\text{O}$	124.1
$(\text{ferrocenyl})\text{C}^+(\text{H})\text{Me}$	117.9	$(\text{cycloheptatrienyl})\text{C}^+(\text{H})\text{Me}$	126.6	$\text{F}-\text{C}^+=\text{O}$	117.5
		$(\text{cycloheptatrienyl})\text{C}^+(\text{H})\text{Me}$	126.6	$(\text{cycloheptatrienyl})\text{C}^+$	139.3
		$(\text{cycloheptatrienyl})\text{C}^+(\text{H})\text{Me}$	126.6	$(\text{cycloheptatrienyl})\text{C}^+(\text{H})\text{Me}$	$^1J(^{13}\text{C}, ^1\text{H})$ 47 Hz

Figure 11 Chemical shifts $\delta^{13}\text{C}$ of some carbenium ions (data taken from References [8b,202–204,207,208])

In carbocations, non-classical structural features are present, reminding us of the bonding in polyhedral boranes and carboranes [211]. Thus, the dication $[\text{C}_6\text{Me}_6]^{2+}$ [212,213] shows two ^{13}C resonances in a 5:1 ratio for the quaternary carbon atoms, one at low field ($\delta^{13}\text{C}$ 126.3), in the typical region for coordinated $[\text{Cp}^*]^-$, and one at rather high field ($\delta^{13}\text{C}$ -2.0), in spite of the twofold positive charge. This leaves only the structure shown in Figure 12. The dication $[\text{C}_6\text{Me}_6]^{2+}$ is a member of a series of polyhedral molecules with *nido*-structures, in which mutual isolobal replacement of boron and carbon atoms is realized.

Unusual surroundings of carbon atoms are frequently found in transition metal complexes. Some fascinating examples are the recently studied mononuclear homoleptic cationic square-planar rhodium, palladium and platinum carbonyls $[\text{Rh}(\text{CO})_4]^+$ ($\delta^{13}\text{C}$ = 173.0; $^1J(^{103}\text{Rh}, ^{13}\text{C})$ = 61.1 Hz), $[\text{Pd}(\text{CO})_4]^{2+}$ ($\delta^{13}\text{C}$ = 144.0) and $[\text{Pt}(\text{CO})_4]^{2+}$ ($\delta^{13}\text{C}$ = 137.0; $^1J(^{195}\text{Pt}, ^{13}\text{C})$ = 1550 ± 10 Hz) [214a], as well as the high-nuclear transition metal carbonyl clusters [214b] (see

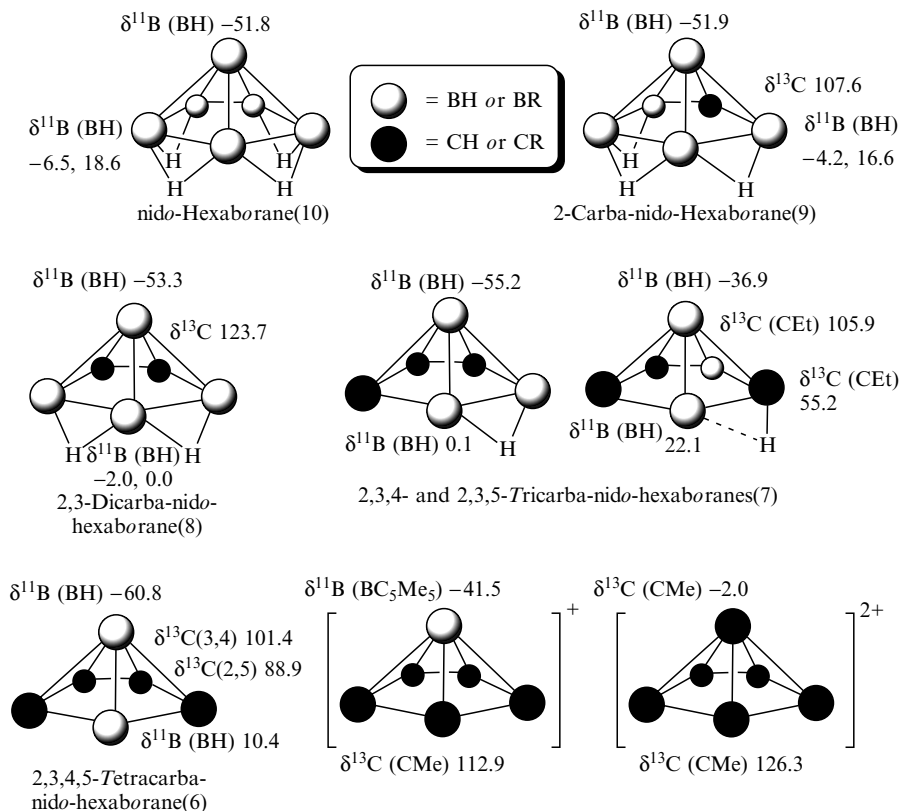
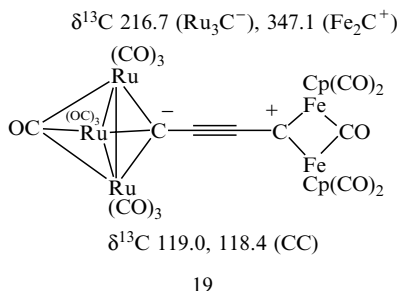
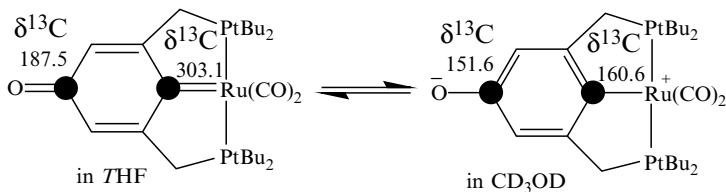


Figure 12 Chemical shifts $\delta^{11}\text{B}$ and $\delta^{13}\text{C}$ of the isoelectronic series of compounds with a *nido*-cage structure from B_6H_{10} to $[\text{C}_6\text{Me}_6]^{2+}$ by isolobal substitution

Reference [587] for a theoretical treatment of ^{13}C nuclear shielding in simple metal carbonyl complexes, carbyne complexes [215–217], carbene complexes [218–220], *N*-heterocyclic carbenes and their complexes [221–223] (see also stable carbenes [224]), vinylidene [225–227], and related complexes with more unsaturated carbon atoms attached in a chain to the metal [228–234]. Many of these compounds are catalytically active. One of numerous fascinating applications concerns olefin metathesis [235]. The deshielding of the ^{13}C nuclei linked to the metal is characteristic for these complexes. In the polynuclear Fe–Ru complex **19** (see below), the metals are linked by a C_4 -unit; although the $\delta^{13}\text{C}$ data do not rule out the structure with a $\text{C}=\text{C}=\text{C}=\text{C}$ unit, the X-ray structural data are more consistent with a $\text{C}-\text{C}\equiv\text{C}-\text{C}$ chain. Both terminal carbon atoms are strongly deshielded, with the one which carries the formal positive charge being extremely deshielded [236].



The $\text{M}=\text{C}$ bond can be envisaged to be comparable to the $\text{O}=\text{C}$ bond, e.g. in quinones. The first metallaquinone ($\text{M} = \text{Rh}$) (**20**) exists either in a structure with the $\text{M}=\text{C}$ bond (in less polar solvents and, according to MO calculations in the gas phase) or as a zwitterion (in polar solvents and in the solid state) [237]. As in carbene complexes, the $^{13}\text{C}(\text{C}=\text{M})$ nucleus is significantly deshielded in the metallaquinone.



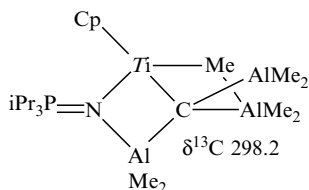
20

Again, the \mathbf{B}_0 -induced circulation of charge, involving energetically low-lying states at this particular carbon atom as well as on the adjacent metal atom, is

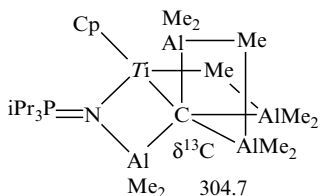
responsible for the strong deshielding (see also $\delta^{11}\text{B}$ data of transition metal boron compounds in Section 4.2 above).

Agostic interactions play an important role in organotransition metal compounds [238]. One of the most characteristic feature is the reduced magnitude of $^1J(^{13}\text{C}, ^1\text{H})$ as the result of M–H bonding which weakens the C–H bond. A recent example is shown in the tantalum complex $[(\eta^5\text{-C}_5\text{H}_5)_2\text{Ta}(\text{CH}_3)\text{-CH}_2\text{-B}(\text{C}_6\text{F}_5)_3]$ (formed by addition of $\text{B}(\text{C}_6\text{F}_5)_3$ to the respective nucleophilic carbene complex) with $\delta^{13}\text{C}(\text{TaCH}_2) = 150.3$ and $^1J(^{13}\text{C}, ^1\text{H}) = 98.7$ Hz (averaged value) [239]. In the case of another tantalum complex, it is shown that α -agostic interactions arising in the Ta–Et fragment are much stronger than in the Ta–Me fragment in the same molecule $[\text{Tp}^{\text{Me}_2}\text{Ta}(\eta^2\text{-PhCCMe})(\text{Me})(\text{Et})]$ (Tp^{Me_2} = hydrotris(3,5-dimethylpyrazolyl)borate), as shown by the $^{13}\text{C}(\text{TaCH}_2)$ resonance at $\delta^{13}\text{C} = 78.4$ with $^1J(^{13}\text{C}, ^1\text{H}) = 102$ Hz for the agostic hydrogen and 122 Hz for the non-agostic hydrogen [240].

Various types of titanium and zirconium complexes with cyclopentadienyl-, indenyl- or fluorenyl-derived ligands are intensively studied in order to explore their potential catalytic activity in olefin polymerization [241,242]. The rotation about the metal–ring centroid axis can be slowed down at low temperature as shown by dynamic ^{13}C NMR of η^5 -*tert*-alkylcyclopentadienyl zirconium complexes [243]. If in dicyclopentadienyltitanium or -zirconium complexes, one or both cyclopentadienyl groups are substituted by indenyl or fluorenyl groups, another type of fluxionality frequently arises, namely a change in the hapticity of the fluorenyl or indenyl ligands, again shown by dynamic ^{13}C NMR of zirconium-ansa-fluorenyl complexes [244]. The analysis of ^{13}C chemical shifts of similar compounds points towards the same direction [245]. In this context, the fluxional behaviour of indenyl-derived ytterbocene(II) complexes is noteworthy, studied by using the $\text{Si}(\text{H})\text{Me}_2$ substituent as an NMR spectroscopic sensor [246]. In addition, in the field of catalytic studies, the presence of five-coordinate carbon atoms in Ti–Al–C systems has recently been revealed by ^{13}C NMR in solution and X-ray analysis in the solid state [247]. Both of the complexes **21** and **22**, in equilibrium via AlMe_3 , show ^{13}C resonances for the carbide carbon atoms at very high frequencies.



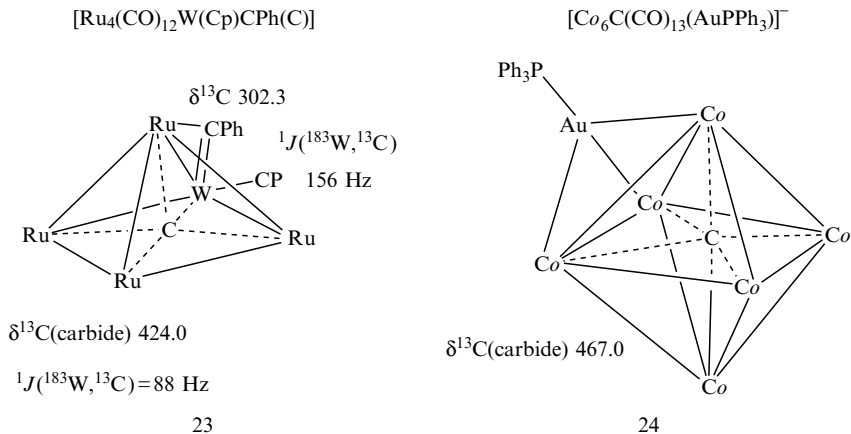
21



22

In titanium or zirconium complexes containing four-coordinate carbon atoms with planar surroundings, the $\delta^{13}\text{C}$ values are found in the range of aromatic systems [248].

The ^{13}C nuclear shielding of carbide carbons (e.g. **23**, **24**) is generally low (see below for a recent example [249]). There are several examples of interstitial carbon atoms surrounded by metal atoms in octahedral geometry [250a] or in prismatic geometry [250b]. In the former, the ^{13}C nuclear shielding is lower ($\delta^{13}\text{C}$ in the range of 460—see below for **24**) than in the latter cases ($\delta^{13}\text{C}$ in the range 330–360). In this context, the hexa-coordinate carbon atoms in gold complexes also deserve a mention [251].



5.2 ORGANOSILICON, -GERMANIUM, -TIN AND -LEAD COMPOUNDS: AN ALMOST PERFECT PLAYING FIELD FOR NMR SPECTROSCOPY

Except for germanium (^{73}Ge , $I = 9/2$; see Table 2), there is at least one spin-1/2 nucleus (Table 1) for each of the elements silicon (^{29}Si), tin (^{119}Sn , ^{117}Sn and ^{115}Sn) and lead (^{207}Pb). The development of the chemistry of these elements, and the continued search for unusual structures, either analogous to that found in carbon chemistry or those which are not readily, if at all, realized with carbon, called for the extensive application of ^{29}Si [252,253], ^{119}Sn [254–256] and ^{207}Pb NMR spectroscopy [257].

Looking for derivatives in which Si, Sn or Pb are two-coordinate, the only examples for silicon are bis(amino)silylenes [258,259], homologues of bis(amino)carbenes [260]. Similar compounds are also known for tin and lead [261–263]. Other two-coordinate derivatives such as silynes (and related compounds with M–element triple bonds) are still a major synthetic challenge,

and stable examples have not been prepared as yet [264]. Monomeric carbene homologues (in solution) with two tin–carbon or lead–carbon bonds had been described for the first time as early as 1973 [265]. The solution-state NMR data indicate a monomer–dimer (as in the solid state) equilibrium in the case of $\text{Sn}[\text{CH}(\text{SiMe}_3)_2]_2$ [266–268]. Cyclic tin(II) [269,270a] and a lead(II) derivative [270b] have been prepared [269,270] (Figure 13) which were found to be monomers both in the solid state and in solution. The lead compound $\text{Pb}[\text{CH}(\text{SiMe}_3)_2]_2$ is strictly monomeric in solution, and recently monomeric derivatives $\text{R}(\text{R}')\text{Pb}$ [$\text{R} = \text{Me}, t\text{Bu}, \text{Ph}$, and the terphenyl ligand

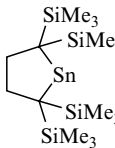
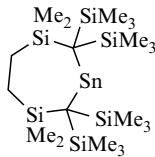
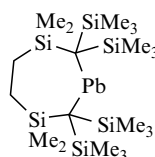
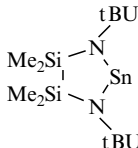
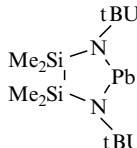
	$\delta^{119}\text{Sn}$	$\delta^{207}\text{Pb}$	
$\text{Sn}[\text{CH}(\text{SiMe}_3)_2]_2$	+ 2315	+ 9112	$\text{Pb}[\text{CH}(\text{SiMe}_3)_2]_2$
	+ 2323		
	+ 2299	+ 10050	
$\text{Sn}[\text{C}_6\text{H}_2(\text{CF}_3)_3\text{-}2,4,6]_2$	+ 723	+ 4878	$\text{Pb}[\text{C}_6\text{H}_2(\text{CF}_3)_3\text{-}2,4,6]_2$
$\text{Sn}\{\text{C}_6\text{H}_2[\text{CH}(\text{SiMe}_3)_2\text{-}2,4,6]\}_2$	+ 2208	+ 8888	$\text{Pb-C}_6\text{H}_2[\text{CH}(\text{SiMe}_3)_2\text{-}2,4,6]$ $\text{C}_6\text{H}_2i\text{Pr}_3\text{-}2,4,6$
$\text{Sn}[\text{N}(\text{SiMe}_3)_2]_2$	+ 776	+ 4916	$\text{Pb}[\text{N}(\text{SiMe}_3)_2]_2$
	+ 759	+ 4900	

Figure 13 ^{119}Sn and ^{207}Pb chemical shifts of some stannylenes and plumbylenes (data taken from References [254,257,270,588,589]). The increased shielding in the derivatives with the $\text{C}_6\text{H}_2(\text{CF}_3)_3\text{-}2,4,6$ ligand can be ascribed to weak Sn–F or Pb–F interactions. For the plumbylene $\text{Pb}[\text{C}_6\text{H}_3(\text{C}_6\text{H}_2\text{Me}_3\text{-}2,4,6)_2\text{-}2,6]_2$ a value of $\delta^{207}\text{Pb} = 3870$ has been reported [590] which does not fit into the pattern (should be remeasured)

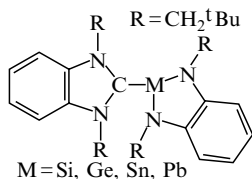
$R' = C_6H_3(C_6H_2iPr_{3-2,4,6})_{2-2,6}$ have been fully characterized by ^{207}Pb NMR in solution [$\delta^{207}Pb = +7420$ ($R = Me$) and $+7853$ ($R = tBu$)] and by X-ray crystallography in the solid state [271]. The fairly extreme $\delta^{119}Sn$ and $\delta^{207}Pb$ values for such compounds indicate the unusual electronic structures. The deshielding of the ^{119}Sn or ^{207}Pb nuclei is due to the presence of a lone pair of electrons at the site of the respective nucleus, the energetically high-lying Sn–C or Pb–C σ orbitals and the energetically low-lying formally unoccupied Sn- or Pb- p_z orbital. For both nuclei, relativistic effects may contribute considerably to the deshielding [272]. The bulky terphenyl substituent, $R = C_6H_3(C_6H_2iPr_{3-2,4,6})_{2-2,6}$, has been used to stabilize a tin(II) hydride $RSnH$ which exists as a H-bridged dimer in the solid state, and for which a monomer structure has been proposed in solution ($\delta^1H(SnH) = 7.87$ (broad); $^1J(^{117/119}Sn, ^1H) = 592$ Hz; $\delta^{119}Sn$ 698.7) [273].

Turning to three-coordinate organosilicon-, -tin and -lead compounds, there are numerous examples for silicon and tin, but next to nothing in the case of lead. Some examples for neutral organosilicon compounds are those in which there is a silicon–element double bond [274–277], while base-free transition metal silylene complexes [278–283] also belong into this category. The availability of stable neutral silylenes [259] has led to a large number of silylene complexes [259,284–287]. The deshielding of ^{29}Si in the complexes ($\delta^{29}Si$ values range from ca. 95 to 150) derived from the stable silylene is less pronounced than in complexes ($\delta^{29}Si$ values range from 250 to 350 in most cases) derived from silylenes which are not stable as free ligands. However, the ^{29}Si magnetic shielding is relatively high in the complex $[Cp_2W-\eta^2-Si_2Me_4]$ ($\delta^{29}Si = -48.1$, $^1J(^{183}W, ^{29}Si) = 50.7$ Hz), in which the ligand can be assumed to be the unstable tetramethyldisilene [287b]. Dynamic ^{29}Si NMR studies have shown that the Si = Si bonds in tetrasilyl-substituted disilenes (see Reference [288] for a review on persilyldisilenes containing information on their ^{29}Si nuclear shielding) are rather weak (barrier to rotation about the Si = Si bond, 15 kcal/mol) [289]. Although there are not so many examples, some derivatives with tin–element double bonds are known [290–292], and there are numerous stannylene complexes [293–296]. Stannylenes and plumblylenes can be readily stabilized as complexes with Lewis bases. These are attractive ligands in transition metal complexes [297,298].

Adduct formation (**25**) between a bis(amino)carbene and bis(amino)silylene, -stannylene and -plumbylene has been studied by ^{13}C , ^{29}Si , ^{119}Sn and ^{207}Pb NMR [299], and changes in the chemical shifts as well as their temperature-dependence suggest rather weak C–M ($M = Si, Sn, Pb$) bonds.

A three-coordinate lead(II) compound (**26**), containing a Pb–Pb bond, has been characterized in the solid state by X-ray analysis and also in solution by NMR. In order to determine the coupling constant $^1J(^{207}Pb, ^{207}Pb)$, the ^{207}Pb labeled compound had to be prepared [300].

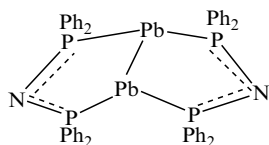
The reactivity of bisaminostannylenes opens the way to many attractive types of structures such as tin–nitrogen heterocubanes. Figure 14 shows the



25

$\delta^{13}\text{C}$ (carbene)	δM
216.5	77.1 (^{29}Si)
200.8	10.5 (^{119}Sn)
211.5	2250 (^{207}Pb)

(All chemical shifts are markedly temperature-dependent)



26

$$\delta^{207}\text{Pb} \quad -608.8$$

$$^1J(^{207}\text{Pb}, ^{207}\text{Pb}) = 7708 \text{ Hz}$$

$$^1J(^{207}\text{Pb}, ^{31}\text{P}) = 2660 \text{ Hz}$$

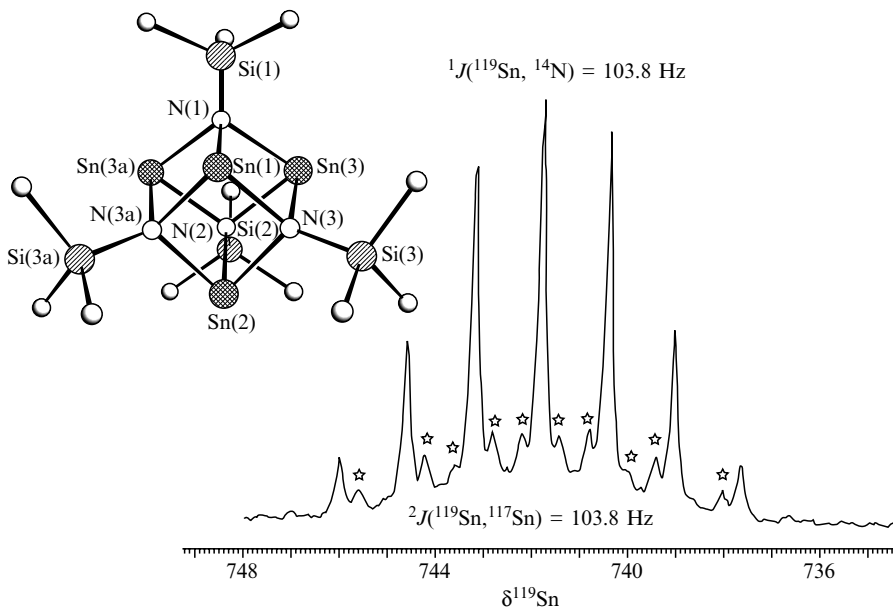
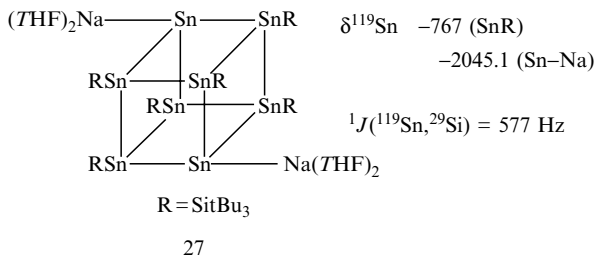


Figure 14 The molecular structure and the 74.6 MHz ^{119}Sn NMR spectrum of the tin–nitrogen heterocubane $[\text{SnNSiMe}_3]_4$ [301]; the ^{119}Sn NMR spectrum shows resolved $^{119}\text{Sn} - ^{14}\text{N}$ coupling (1:3:6:7:6:3:1 pattern) and ^{117}Sn satellites (marked by stars) according to $^2J(^{119}\text{Sn}, ^{117}\text{Sn})$

results of the X-ray structural analysis and the ^{119}Sn NMR spectrum, a rare example of well-resolved ^{119}Sn - ^{14}N coupling [301].

A novel anionic tin cluster (27), containing low-valent tin, stabilized by supersilyl groups ($\text{Si}t\text{Bu}_3$), shows an extreme ^{119}Sn nuclear shielding for the tin atoms which formally bear the negative charges [302].

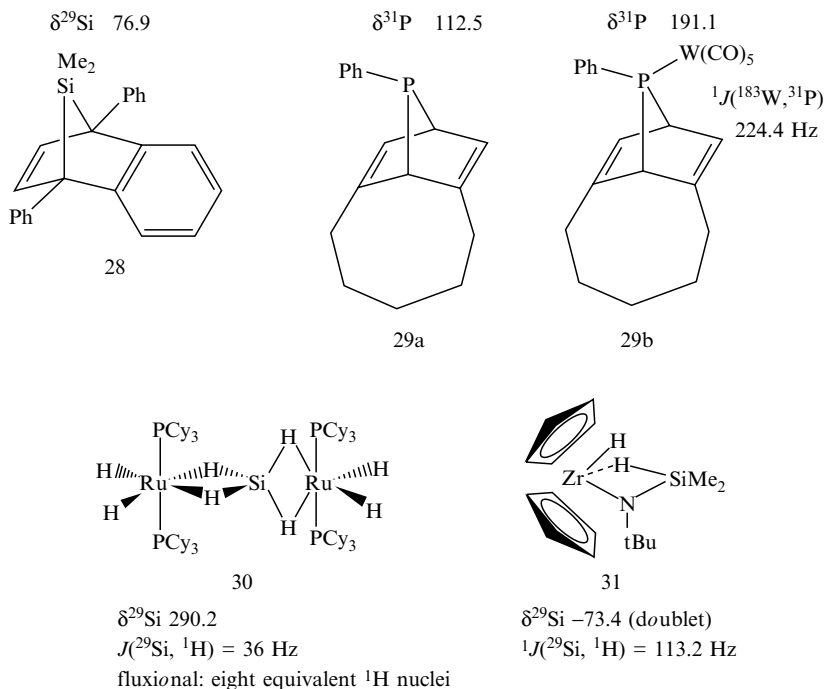


There is a long-lasting and continuing search for cations containing three-coordinate silicon [303,304] or tin atoms, the homologues of carbenium cations. Similarly to the latter which can be handled in super acids (in contrast to the silicon and tin species), both the silicon and tin cations appear to be extremely electrophilic, and it seems almost impossible to find suitable conditions (counterions and/or a solvent) to study these cations free of association with other species. However, $\delta^{29}\text{Si}$ and $\delta^{119}\text{Sn}$ for trimesitylsilyl and -stannyl cations with the $[\text{B}(\text{C}_6\text{F}_5)_4]^-$ counterion [305], or for a silatropylium cation derivative ($\delta^{29}\text{Si} = 142.9$) [306], for $[(\eta^2, \eta^3\text{-Cp}^*)_2\text{SiH}]^+$ [307a], $[(\eta\text{-Cp})\text{Fe}(\eta\text{-C}_5\text{H}_4)\text{-SiMe}_2\text{-THF}]^+$ [307b], and $\delta^{119}\text{Sn}$ data of a tributyltin cation with the 'non-coordinating' anion $[\text{CB}_{11}\text{Me}_{12}]^-$ [308] show that in some cases the situation comes close to free cations (Figure 15). Another approach towards this direction reveals that in certain zwitterionic compounds the positive charge on tin or lead can be delocalized and the coordinatively unsaturated tin [309,310] or lead atoms [311] can be stabilized by weak intramolecular coordination of R_3Sn^+ or R_3Pb^+ to a $\text{C}\equiv\text{C}$ bond. As in the almost free cations, the ^{119}Sn nuclei, as well as the ^{207}Pb nuclei, become strongly deshielded. (Figure 15).

7-Silanorbornadienes (e.g. 28) are examples for extreme deshielding of ^{29}Si nuclei [312] in tetraorganosilanes. Similar deshielding effects are observed for ^{31}P nuclei in 7-phosphanorbornadiene derivatives (29) [313,314].

Si-H activation [99,315-318] normally leads to ^{29}Si deshielding, as shown below for an extreme example (30) with SiH_4 (free silane: $\delta^{29}\text{Si} = -92.0$) [319]; however, in the case of a Si-H-Zr complex (31), the ^{29}Si nuclear shielding increases (free aminosilane $\text{NH}(t\text{Bu})\text{SiMe}_2\text{H}$: $\delta^{29}\text{Si} = -18.3$ with $^1J(^{29}\text{Si}, ^1\text{H}) = 192.6$ Hz) [320].

The ^{29}Si nuclei in silyl lithium compounds, which are monomeric in THF solution, become deshielded when compared with the starting materials (usually the corresponding silicon chlorides). This has been shown in an extensive



NMR study focusing on [(amino)phenylsilyl]lithiums [321] (e.g. $\delta^{29}\text{Si}$ [(Et₂N)₂PhSiLi] = 27.9 and $\delta^{29}\text{Si}$ [(Et₂N)₂PhSiCl] = -18.8). The ²⁹Si-⁷Li coupling can be observed at low temperature (e.g. in (Et₂N)₂PhSiLi: $^1J(^{29}\text{Si}, ^7\text{Li}) = 57$ Hz at 173 K), and in the case of ¹⁵N-enriched compounds the ²⁹Si-¹⁵N couplings have been measured [321] (e.g. for (Et₂N)₂PhSiLi: $^1J(^{29}\text{Si}, ^{15}\text{N}) = 13$ Hz; the magnitude is markedly reduced when compared with the starting chloride (Et₂N)₂PhSiCl: $^1J(^{29}\text{Si}, ^{15}\text{N}) = 31$ Hz; or with the hydride (Et₂N)₂PhSiH: $^1J(^{29}\text{Si}, ^{15}\text{N}) = 24$ Hz).

In general, one finds that tetra-coordinate ¹¹⁹Sn or ²⁰⁷Pb nuclei become deshielded when they are attached to transition metals by forming metal-Sn or metal-Pb σ bonds. This trend is much enhanced if multi-center bonding is involved at the same time [322], as shown for the examples given in Figure 16. The coupling constants $^1J(^{119}\text{Sn}, ^{57}\text{Fe})$ (e.g. 42.7 Hz in [CpFe(CO)₂-SnMe₃]) and $^1J(^{207}\text{Pb}, ^{57}\text{Fe})$ (e.g. 89.1 Hz in [(CpFe(CO)₂-PbMe₃]) have been measured from ⁵⁷Fe satellites in the ¹¹⁹Sn and ²⁰⁷Pb NMR spectra, respectively [321,322]. The most deshielded tin nuclei found so far are observed in planar complex anions which contain low-valent tin ([Cr(CO)₅Cr]₃Sn)²⁻ with $\delta^{119}\text{Sn} = +3924$ [323a]. Similarly, the ²⁰⁷Pb nucleus in the corresponding dianion ([Cr(CO)₅Cr]₃Pb)²⁻ is much deshielded ($\delta^{207}\text{Pb} = +7885$) [324].

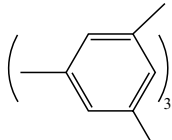
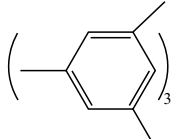
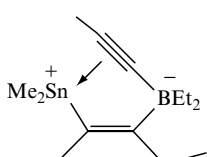
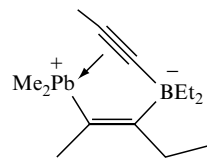
	δM
 $\text{Si}^+ [\text{B}(\text{C}_6\text{F}_5)_4]^-$	225.5 (^{29}Si)
 $\text{Sn}^+ [\text{B}(\text{C}_6\text{F}_5)_4]^-$	806.0 (^{119}Sn)
$\text{Bu}_3\text{Sn}^+ [\text{CB}_{11}\text{Me}_{12}]^-$	454.3 (^{119}Sn)
 $\text{Me}_2\text{Sn}^+ \text{---} \text{C} \text{---} \text{BEt}_2^-$	189.1 (^{119}Sn)
 $\text{Me}_2\text{Pb}^+ \text{---} \text{C} \text{---} \text{BEt}_2^-$	722.7 (^{207}Pb)

Figure 15 ^{29}Si , ^{119}Sn and ^{207}Pb chemical shifts of cationic [305,308] and zwitterionic species [309–311] with weak or stronger intermolecular or intramolecular association. The δM values indicate some cationic character but are still far, in particular for $\delta^{119}\text{Sn}$, from the values expected for ‘free’ cationic species

The extreme end, at low frequency, of ^{29}Si , ^{119}Sn and ^{207}Pb resonances is reserved for the respective metallocene derivatives. In the case of silicocene, the decamethyl derivative Cp^*_2Si is stable, and in the crystalline state two isomers have been found, one with parallel Cp^* rings, and the other with the expected bent arrangement of the Cp^* rings [325]. These isomers have also been detected by solid-state ^{29}Si NMR [$\delta^{29}\text{Si}$ -423.4 (parallel) and -403.2 (bent); not shown by solid-state ^{13}C CP MAS NMR] [326]. The solution-state $\delta^{29}\text{Si}$ value ($\delta = -398.0$) is close to that for the bent arrangement in the solid. Therefore, it is likely that the bent arrangement dominates in solution, in agreement with the results of the gas-phase electron diffraction study [325b]. Figure 17 lists some $\delta^{29}\text{Si}$, $\delta^{119}\text{Sn}$ and $\delta^{207}\text{Pb}$ data of metallocenes. The high shielding of the metal nuclei in metallocenes correlates with the electronic structure. The lone pair of electrons at the metal nuclei is low in energy and there is a large energy gap between the occupied and unoccupied energy levels [327].

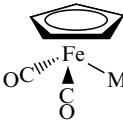
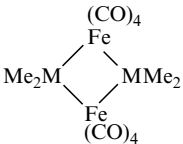
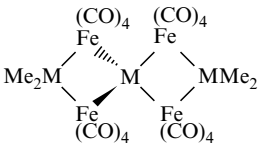
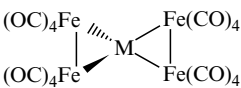
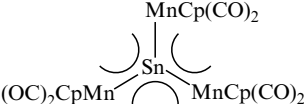
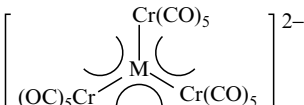
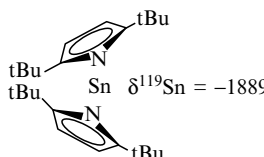
	$\delta^{119}\text{Sn}$	$\delta^{207}\text{Pb}$
	$[^2J(^{119}\text{Sn}, ^{119}\text{Sn})]$	$\{^2J(^{207}\text{Pb}, ^{207}\text{Pb})\}$
 M = Sn, Pb	144.1	243.1
	87.8 [1798.0]	293.4
	123.8 (SnMe ₂) 287.7 (Sn) [1580.0]	344.8 (PbMe ₂) 745.3 (Pb) {1090.0}
	1532.0	3586.6
	3301.0	
	3924.0	7885.0

Figure 16 ^{119}Sn and ^{207}Pb chemical shifts of some iron–tin [320] and iron–lead compounds [321], and of low-valent tin–manganese [322b] and anionic tin– [322a] and lead–chromium complexes [323]

The positive sign of the coupling constant $^1J(^{119}\text{Sn}, ^{73}\text{Ge}) = +37.0$ Hz (also the reduced coupling constant $^1K(^{119}\text{Sn}, ^{73}\text{Ge}) > 0$!) has been determined for $\text{Ge}(\text{SnMe}_3)_4$ by a 2D $^{73}\text{Ge}/^1\text{H}$ HETCOR experiment (Figure 18), a rare example of ^1H polarization transfer, using the long-range scalar coupling, $^3J(^{73}\text{Ge}, \text{Sn}, \text{C}, ^1\text{H})$, to the quadrupolar ^{73}Ge nucleus [328a]. Analogous experiments for $\text{Si}(\text{SnMe}_3)_4$ and $\text{Sn}(\text{SnMe}_3)_4$ also revealed positive signs of $^1J(^{119}\text{Sn}, ^{29}\text{Si}) = +227.1$ Hz and $^1J(^{119}\text{Sn}, ^{119}\text{Sn}) = +873.3$ (both $^1K > 0$!). Interestingly, $^1K(^{119}\text{Sn}, ^{73}\text{Ge}) = +23.39$ is even slightly smaller than $^1K(^{119}\text{Sn}, ^{29}\text{Si}) = +24.58$, although the valence s electron density $|\Psi_{\text{Ge}}(0)|^2$ (9.5433) is larger by

	$(\eta^5\text{-C}_5\text{H}_5)_2\text{Sn}$	$(\eta^5\text{-C}_5\text{H}_5)_2\text{Pb}$
	$\delta^{119}\text{Sn} = -2199$	$\delta^{207}\text{Pb} = -5030$
	-2162.8, -2224.4 (solid)	
$(\eta^5\text{-C}_5\text{Me}_5)_2\text{Si}$	$(\eta^5\text{-C}_5\text{Me}_5)_2\text{Sn}$	$(\eta^5\text{-C}_5\text{Me}_5)_2\text{Pb}$
$\delta^{29}\text{Si} = -398$	$\delta^{119}\text{Sn} = -2129$	$\delta^{207}\text{Pb} = -4390$
-402.3, -423.4 (solid)	-2136.6, -2140.2 (solid)	-4474 (solid)
	$(\eta^5\text{-C}_5\text{Ph}_5)_2\text{Sn}$	$(\eta^5\text{-C}_5\text{Ph}_5)_2\text{Pb}$
	$\delta^{119}\text{Sn} -2215$ (solid)	$\delta^{207}\text{Pb} -6150$ (solid)



$\delta^{119}\text{Sn} = -1889$

Figure 17 Liquid-state and solid-state ^{29}Si , ^{119}Sn and ^{207}Pb chemical shifts of a silicocene [325,326], and several stannocenes and plumbocenes (taken from References. [254b,257])

a factor of ca. 2.5 than $|\Psi_{\text{Si}}(0)|^2$ (3.8105). On the other hand, the increase in $^1K(^{119}\text{Sn}, ^{119}\text{Sn})$ (+52.08) with respect to $^1K(^{119}\text{Sn}, ^{73}\text{Ge})$ is larger than expected on the basis of $|\Psi_{\text{Sn}}(0)|^2$ (12.6795). This indicates that the electronic structure of $\text{Ge}(\text{SnMe}_3)_4$ differs considerably from that of the corresponding silicon and tin derivative, most likely due to electronic low-lying unoccupied levels involving the Ge–Sn bonds. However, it should be noted that one-bond coupling constants involving tetra-coordinate heavy nuclei of group 14 elements in their formal +4 oxidation state can be of either sign. This has been found for $^1J(^{207}\text{Pb}, ^{13}\text{C})$ in alkynyllead compounds [329], and also in the case of some Me_2Pb derivatives [330] and $t\text{Bu}_3\text{Pb}$ -phosphanes [331]. Sign inversion of $^1J(^{207}\text{Pb}, ^{119}\text{Sn})$ has been found in some stannylplumbanes where the lead atom bears three $t\text{Bu}$ groups. [332]. $^1K(^{207}\text{Pb}, ^{119}\text{Sn})$ has a positive sign in $\text{Me}_3\text{Pb-SnMe}_3$ [333] and a negative sign in $t\text{Bu}_3\text{Pb-SnMe}_3$ [332].

6 NITROGEN COMPOUNDS. WHAT CAN WE LEARN FROM NITROGEN NMR?

There are two naturally abundant isotopes, ^{14}N and ^{15}N (see Tables 1 and 2), both suitable for NMR studies. The quadrupolar nucleus ^{14}N ($I = 1$) gives rise to more or less broad lines, depending on the quadrupole coupling constant and the experimental conditions (see the attempts to measure ^{14}N NMR spectra in supercritical solvents or low-viscosity liquefied gases [334,335]). The spin-1/2

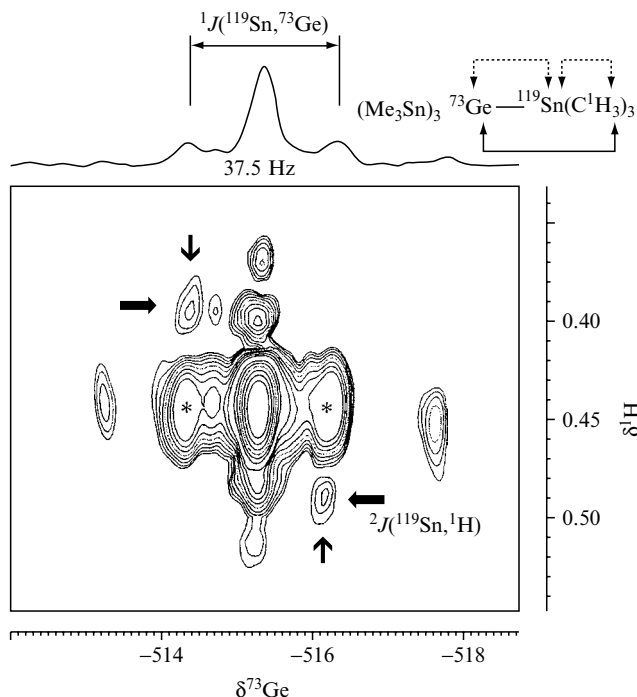


Figure 18 Contour plot of the 17.5 MHz $^{73}\text{Ge}/^1\text{H}$ HETCOR experiment of $\text{Ge}(\text{SnMe}_3)_4$ in C_6D_6 , based on $^3J(^{73}\text{Ge}, ^1\text{H}) \approx 1.5$ Hz; the marked cross-peaks show a negative tilt and by this indicate opposite signs of $^2K(^{117/119}\text{Sn}, ^1\text{H}) (< 0)$ and $^1K(^{117/119}\text{Sn}, ^{73}\text{Ge}) (> 0)$. The cross-peaks without tilt (*) are the result of polarization transfer from ^1H via magnetically non-active tin nuclei to ^{73}Ge

nucleus ^{15}N suffers—from the NMR point of view—from low natural abundance (0.37 %), a fairly small magnetic moment, a negative gyromagnetic ratio ($\gamma(^{15}\text{N}) < 0$), and frequently its direct NMR detection is hampered by long relaxation times, $T_1(^{15}\text{N})$. All of these difficulties can be overcome in various ways (e.g. ^{15}N -labelling, special pulse sequences, etc.) which means that ^{15}N is in general the preferred nucleus, since it gives sharp NMR signals, and coupling constants $J(^{15}\text{N}, \text{X})$ can be accurately determined. However, there are numerous cases (e.g. many small molecules), where ^{14}N resonance signals are also rather sharp and can be acquired in a very short time. Since the line widths of ^{14}N NMR signals contain information on the quadrupolar relaxation rate, in addition to the $\delta^{14}\text{N}$ value (which is of course identical with $\delta^{15}\text{N}$), ^{14}N NMR spectroscopy remains an attractive tool. The range of δN values is large (> 1200 ppm) which means that changes in the electronic structure around the nitrogen atom will be well reflected (see Figure 19 for an overview). Most coupling constants will only be resolved with the ^{15}N nucleus. Both of the

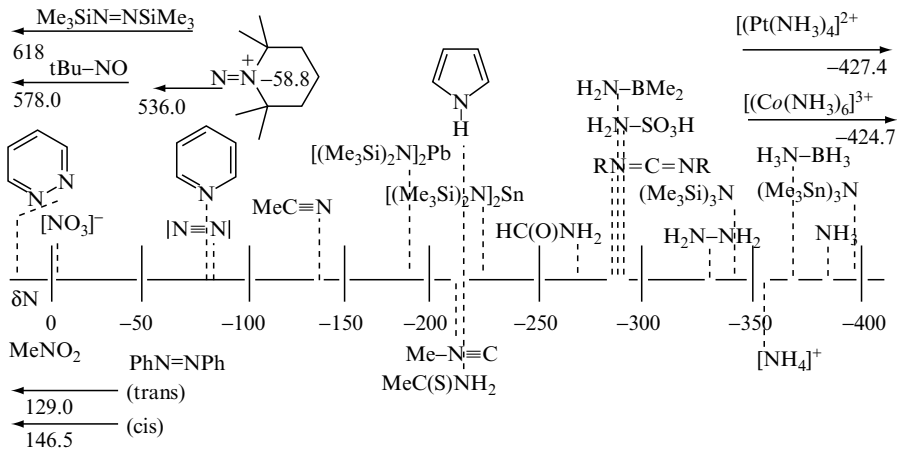


Figure 19 An overview of nitrogen chemical shifts, with some examples

parameters δN and $J(^{15}\text{N}, X)$ are attractive for discussing the multifaceted structural chemistry of nitrogen [336,337]

6.1 SOME SIMPLE NITROGEN COMPOUNDS: N_2 , N_2O , $[\text{N}_3]^-$, $[\text{N}_5]^+$ AND OTHERS

^{14}N or ^{15}N NMR data have been obtained for most of the small neutral, cationic or anionic species containing nitrogen. The deshielding of the nitrogen nuclei in N_2 is related to the presence of two lone pairs of electrons. In N_2O , both of the nitrogen nuclei become shielded ($\delta N(\text{terminal}) = -222$; $\delta N(\text{central}) = -138$) when compared with N_2 ($\delta N = -66$). This is also true for the azide anion $[\text{N}_3]^-$ ($\delta N(\text{terminal}) = -281$; $\delta N(\text{central}) = -130.4$) and azide derivatives (**32**) in general (see below; data taken from Reference [11]; see also Reference [585] for δN of covalent azides).

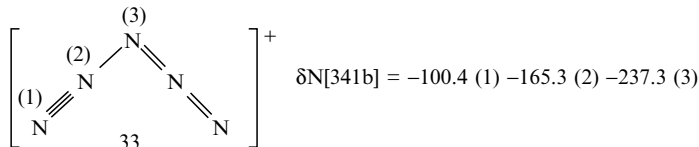
32	α	β	γ	Resonance structures of azide anion				
	$\text{R}-\text{N}=\text{N}=\text{N}$			$\text{R}-\text{N}=\text{N}=\text{N}^-$	\longleftrightarrow	$\text{R}-\text{N}^-=\text{N}=\text{N}^+$		
R	H	Me	Ph	Me_3Si	$\text{Me}_2\text{P}(\text{O})$	Tosyl	Cl	NC
$\delta N(\alpha)$	-324.9	-321.2	-287.9	-324.3	-294.3	-240.4	-273.5	-314.8
$\delta N(\beta)$	-134.5	-129.7	-136.2	-149.7	-146.4	-146.0	-124.1	-114.5
$\delta N(\gamma)$	-179.0	-171.0	-146.9	-213.0	-175.0	-138.3	-114.5	-147.0

In contrast, the nitrogen shielding in $[\text{NO}]^+$ (δN ca. 0), isoelectronic to N_2 , is further slightly reduced when compared with N_2 . The deshielding effect of the

lone pair of electrons on nitrogen in nuclear shielding becomes also evident by comparing the δN values for the linear nitronium cation $[\text{NO}_2]^+$ (-126) and the bent nitrite anion $[\text{NO}_2]^-$ ($+237$). These are examples which demonstrate convincingly that the oversimplified correlation of nuclear shielding with charge leads to completely erroneous results.

The nitrogen chemical shifts of azo compounds ($\text{R}-\text{NN}-\text{R}$) [338], as well as nitroso compounds ($\text{R}-\text{NO}$) [339], can be correlated with the magnetic-dipole allowed (electron-dipole forbidden) long-wave electronic transition assigned to the n and π^* orbitals. Thus, the highly shielded nitrogen nuclei in ammonia or amines can be explained by the nature of the lone pair of electrons which is part of the σ bonding framework, and low-energy electronic transitions are absent. Therefore, the δN values of amines and ammonium salts are similar, and the changes correspond closely to those that are well known for $\delta^{13}\text{C}$ of alkanes. This means that useful correlations can be established for δN and $\delta^{13}\text{C}$ of comparable compounds with the respective coordination numbers 4, 3, 2 and 1 (for linear compounds, see e.g. [340]).

For the cation $[\text{N}_5]^+$ (**33**) three nitrogen NMR signals have been detected and assigned on the basis of ^{15}N labelling experiments, confirmed by the calculated nitrogen chemical shifts. This and other physicochemical evidence suggest a bent structure [341].



6.2 LITHIUM AMIDES

Lithium amides are extremely useful reagents in synthesis and their solid-state structures have been extensively studied [342]. Knowledge about the structures of lithium amides in solution [343,344] can be crucial for optimizing reaction conditions. In the last decade, numerous NMR studies have been carried out, frequently by taking advantage of ^{15}N and ^6Li labelling, in order to determine the nature of bonding and the aggregation in solution (Figure 20) [343–345].

6.3 BORON–NITROGEN COMPOUNDS

The picture of the $\text{B}-\text{N}$ unit being isoelectronic to the $\text{C}-\text{C}$ unit has stimulated boron–nitrogen chemistry for more than 50 years, starting from borazine $(\text{HBNH})_3$, i.e. the inorganic benzene [346]. The nitrogen NMR of $\text{B}-\text{N}$ compounds [347] has revealed much about the electronic structure, and has offered information complementary to that coming from ^{11}B NMR. In this field, ^{14}N

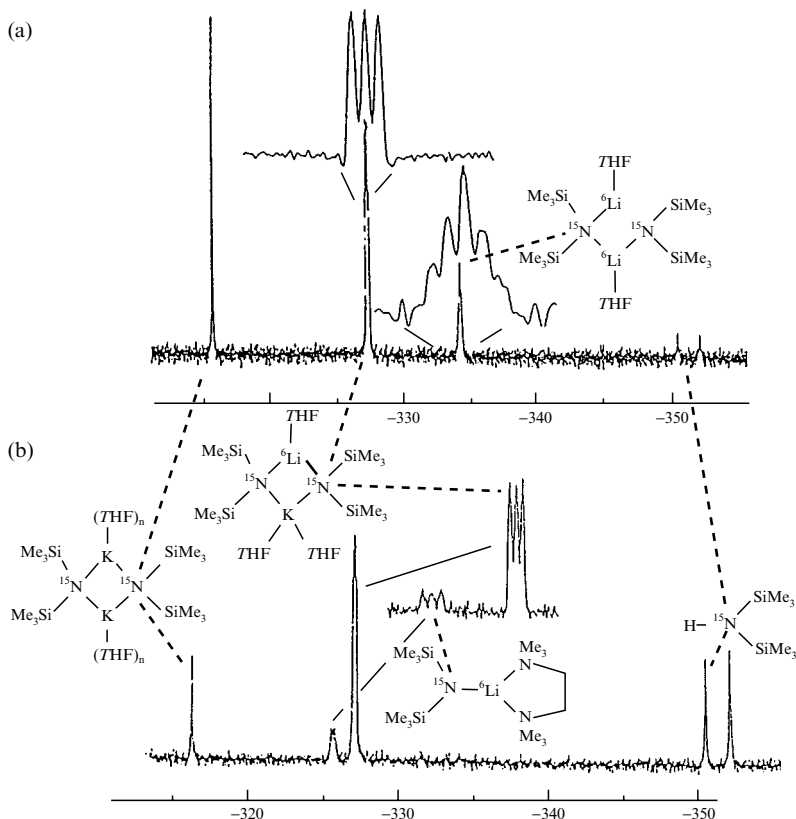


Figure 20 ^{15}N NMR spectra for a mixture of $[\text{}^6\text{Li} - \text{}^{15}\text{N}(\text{SiMe}_3)_2]$ and $[\text{K} - \text{}^{15}\text{N}(\text{SiMe}_3)_2]$ in toluene at -80°C : (A) THF (4 equivalents) was added; (B) TMEDA (4.4 equivalents) and THF (1.1 equivalents) were added. (Adapted from Reference [344].)

NMR measurements are often preferred, since the ^{15}N NMR spectra of the $^{15}\text{N} - \text{}^{11}\text{B}$ isotopomer suffer from extremely low signal-to-noise ratios because of broad ^{15}N NMR signals owing to partially relaxed scalar $^{15}\text{N} - \text{}^{11}\text{B}$ coupling [348,349]. If there are N–H bonds present, inverse $^1\text{H}/^{15}\text{N}$ detection can be carried out in order to observe the broad ^{15}N signals within comparatively short times [350].

In the cases of borane–amine adducts, the δN values correspond to those of $\delta^{13}\text{C}$ of alkanes or δN of ammonium salts [351]. In aminoboranes, borazines and related compounds however, the question of delocalization of the nitrogen lone pair of electrons arises, if one wants to keep up the picture of $\text{B} = \text{N}$ bonds which is suggested by the results of a large number of X-ray structural analyses. As shown by the data presented in Figure 21, the expected deshielding of the nitrogen nuclei is observed, increasingly with the number of potential BN (pp) π interactions per nitrogen atom, which is particularly obvious in the series

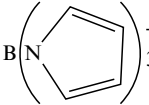
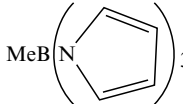
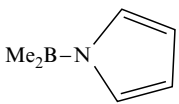
	$\delta^{11}\text{B}$	$\delta^{14}\text{N}$		$\delta^{11}\text{B}$	$\delta^{14}\text{N}$
$\text{B}(\text{NMe}_2)_3$	27.3	-365		27.8	-207
$\text{MeB}(\text{NMe}_2)_2$	33.5	-337			
$(\text{MeBNMe})_3$	35.8	-275		34.8	-203
$\text{Me}_2\text{B-NMe}_2$	44.6	-296			
$(\text{Me}_2\text{B})_2\text{NMe}$	58.5	-253			
$(\text{Me}_2\text{B})_3\text{N}$	61.5	-187		54.2	-182

Figure 21 Nitrogen and boron chemical shifts of aminoboranes and *N*-pyrrolylboranes

Me_2BNMe_2 , $(\text{Me}_2\text{B})_2\text{NMe}$ and $(\text{Me}_2\text{B})_3\text{N}$ [352]. However, in *N*-pyrrolylboranes, $\text{BN}(\text{pp})\pi$ interactions are of minor importance, as shown by the relatively small range of the δN values (Figure 21), by $\delta^{13}\text{C}$ values and by the results of X-ray analyses [353]. This fits to the model of heteroaromaticity, where, in the case of pyrroles, the free pair of electrons at the nitrogen atom is required for aromatic stabilization.

In parallel to aminoborane chemistry, the search for two-coordinate boron compounds has also been continuing [354,355]. Thus, *N,B*-dialkyl-iminoboranes have been prepared and were found to be reasonably stable for bulky alkyl groups (e.g. *t*Bu), and their ^{11}B and nitrogen NMR parameters (e.g. *t*Bu-B-N-*t*Bu: $\delta^{11}\text{B} = 2.4$; $\delta\text{N} = -254$ [356]), as well as the structural parameters (e.g. $d_{\text{B}\equiv\text{N}} = 122$ pm) are indeed comparable to those of isoelectronic alkynes.

A few examples of azapolyboranes are known [158]. The analogues of *ortho*-carborane, $1,2\text{-C}_2\text{B}_{10}\text{H}_{12}$, $\text{HNB}_{11}\text{H}_{11}$, are particularly noteworthy [357]. It is tempting to compare the set of $^{11}\text{B}/^{14}/^{15}\text{N}$ NMR data of the aza derivatives with ^{13}C NMR data of the corresponding carboranes. Although only few data pairs are available so far, the analogous trends of the data seem to be promising [358].

6.4 CARBON-NITROGEN COMPOUNDS

Here, just a few simple compounds, neutral, cationic or anionic, are mentioned, in some of which either nitrogen or carbon may serve to form bonds to transition metal compounds, namely the cyanide anion, nitriles, nitrile oxides [359], isonitriles and complexes [360], nitrilium cations and pyridine (Figure 22).

Blocking the lone pair of electrons at the carbon atom of the cyanide anion leads to $\text{H-C}\equiv\text{N}$ or nitriles, $\text{R-C}\equiv\text{N}$, and the ^{13}C nuclear shielding is increased ($\delta^{13}\text{C}(\text{CN}^-) = 166.1$; $\delta^{13}\text{C}(\text{H-CN}) = 110.9$; $\delta^{13}\text{C}(\text{Me-CN}) = 117.7$). Engaging the lone pair of electrons at the nitrogen atom in $[\text{CN}]^-$ leads to isonitriles, $\text{R-N}\equiv\text{C}$, in which the nitrogen shielding is increased. If a transition metal fragment becomes attached to the carbon atom, as in metal cyanides ($\text{M-C}\equiv\text{N}$)

$\delta N (^1J(^{15}N, ^{13}C))$		$\delta N (^1J(^{15}N, ^{13}C))$	
$[C\equiv N]^-$	-96 (-5.4)	Me-C \equiv N	-137.1 (-17.5)
		Me ₃ Si-C \equiv N	-130.5 (-11.8)
		C \equiv N-Me	-218 (5.8) (-10.7 Me)
		[Me-C \equiv N-Me] ⁺	-248.2
		(OC) ₅ Cr-N \equiv C-Me	-144
$[C\equiv N-O]^-$	-176	Me ₃ Si-C \equiv N-O	-164.6 (-51.2)
$[N=C=O]^-$	-300	Me ₃ Si-N=C=O	-346.4 (-42.75)
$[N=C=S]^-$	-166	Me ₃ Si-N=C=S	-264.4 (-35.95)
$[N=C=Se]^-$	-136		
		Me ₃ Si-N=C=N-SiMe ₃	-329.1 (-37.4)
		Me ₃ Si-N=C=C(SiMe ₃) ₂	-245.2 (-25.77)
		H ₂ C=N ¹ =N ²	-96 (N ¹) (-20.2) 7.8 (N ²)

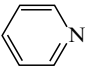
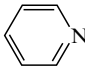
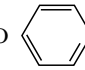
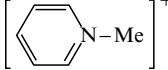
			trans-[Rh(Cl) ₂ (py) ₄]Cl	
δN -60.6	-87.5	-136	-161.9	-175

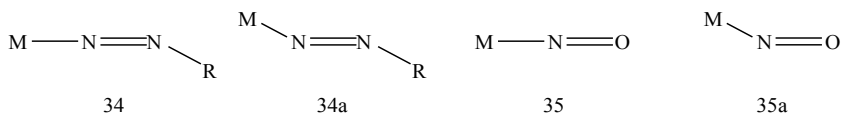
Figure 22 Chemical shifts δN and coupling constants $^1J(^{15}N, ^{13}C)$ of nitriles, isonitriles, the cyanide anion, related compounds and of some pyridine derivatives (data taken from References [11,336,337,361-364], showing the effect of the lone pair of electrons on nitrogen NMR parameters

(e.g. $\delta^{13}C$ ([Ni(CN)₄]) = 136.5) or in isonitrile metal complexes (M-C \equiv N-R), similar shifts of the ¹³C resonances are observed, although the magnitudes can be much smaller. Similarly, metal coordination to the nitrogen atom in nitriles (M-N \equiv C-R) leads to increased nitrogen nuclear shielding [361], although less so than in nitrilium cations. This shows that, in addition to the unsaturated nature of these compounds, again the presence of lone pairs of electrons has to be considered in order to account for changes in nuclear shielding.

6.5 COMPLEXES WITH TRANSITION METAL-NITROGEN BONDS

The ligand properties of the N₂ molecule in transition metal complexes lead to end-on [365-368], side-on [369,370], and bridging bonding modes [371], all of which can be conveniently studied by nitrogen NMR (preferably by ¹⁵N NMR of ¹⁵N-labelled complexes). Furthermore, there are nitrido complexes in which the nitrogen atom can bridge two metal complex fragments (M = N = M) [372], or in which the M \equiv N bond is present and nitrogen possesses the coordination number 1 [372].

In diazenido complexes, M-N=N-R, (34), two arrangements of the diazenido ligands have been detected. In the doubly bent arrangement, nitrogen nuclear shielding is significantly reduced [373]. The analogous result is true for nitroso complexes (35) with a linear (NO functions as a 3e donor) or a bent (NO acts as a 1e donor) arrangement [374,375].



Interstitial nitrogen nuclei in metal carbonyl clusters can be shielded, e.g. in the anions $[\text{Co}_6(\text{CO})_{15}\text{N}]^-$ ($\delta\text{N} = -184$) or $[\text{Rh}_6(\text{CO})_{15}\text{N}]^-$ ($\delta\text{N} = -273$) [376] (in contrast with the corresponding carbide dianions where the ^{13}C (carbide) nuclei are deshielded: $\delta^{13}\text{C} = 330$ and 265), or deshielded as in $[\text{Ru}_6(\text{CO})_{16}\text{N}]^{3-}$ ($\delta\text{N} = 179$) [377a]. Other nitrido clusters have been studied by ^{15}N NMR, showing markedly deshielded nitrogen nuclei (e.g. $\delta^{15}\text{N} [\text{Ph}_3\text{PAuFe}_4\text{N}(\text{CO})_{12}] = 592.9$ [377b]).

7 PHOSPHORUS, AN ELEMENT MADE FOR NMR STUDIES

The advent of modern pulse Fourier-transform techniques in ^{31}P NMR spectroscopy [11,378–382] has changed the world of phosphorus chemistry into an ‘adventure land’, so fascinating and exciting that it is difficult to select just a few examples in order to illustrate the development. Even the attempt to cover the chemistry of a single class of compound, such as phosphalkynes, $\text{R}-\text{C}\equiv\text{P}$, in the light of ^{31}P NMR, would be a formidable task. The chemistry of phosphalkynes (**36**) started almost unnoticed with $\text{R} = \text{H}$ [383], and ‘exploded’ into a vast research area [384,385] after the finding that these compounds are fairly stable with bulky groups R (e.g. $\text{R} = t\text{Bu}$ [386]; see, e.g. two recent reports on cyclo-dimerization [387], and cyclo-oligomerization reactions of phosphalkynes [388]). Similar, although perhaps less spectacular, jumps are evident for the development of the chemistry of other low-coordinated phosphorus compounds [389], and transition metal phosphorus compounds in general, all aided greatly by application of ^{31}P NMR spectroscopy.

$\text{R}-\text{C}\equiv\text{P}$	R	H	Me	iPr	tBu	Ph	SiMe ₃
36	$\delta^{31}\text{P}$	-32.0	-60.0	-64.3	-69.0	-32.0	96.0

The chemical shifts $\delta^{31}\text{P}$ cover a large range of about 2000 ppm, from $\delta^{31}\text{P} = -488$ for P_4 in CS_2 [390] ($\delta^{31}\text{P} = -533.1$, extrapolated to zero pressure in the gas phase [391]), or exactly from -554.7 for the unique phosphorus atom in the phosphorus-tin-cage molecule $\text{P}(\text{SnPh}_2)_3\text{P}_3$ [392] to $+1362$ in $\{t\text{BuP}[\text{Cr}(\text{CO})_5]_2\}$ for transition metal phosphinidene complexes [393]. At both ends of the range of $\delta^{31}\text{P}$ data, three-coordinate phosphorus atoms are involved. This shows that it is not a particularly helpful approach to search for a general relationship between $\delta^{31}\text{P}$ and the coordination number of phos-

phorus. It is again more useful to look for structural features which suggest that energetically low-lying unoccupied levels are available for \mathbf{B}_0 -induced rotation of charge increasing the paramagnetic term of nuclear shielding [394]. The absence of such conditions explains the highly shielded phosphorus atoms in P_4 , in many phosphanes, phosphoranes and in hexa-coordinated phosphorus compounds. The presence of energetically low-lying unoccupied levels certainly explains the enormous deshielding of phosphorus in the majority phosphinidene complexes [395,396], also evident from the observed relationship between $\delta^{31}\text{P}$ and UV absorptions [393] for these complexes, and the low nuclear shielding in neutral or cationic two-coordinate phosphorus compounds. Useful relationships emerge by comparing $\delta^{31}\text{P}$ and δN of two-coordinate phosphorus and nitrogen compounds ($\delta(-\text{N} =) = 0.75 \delta^{31}\text{P}(-\text{P} =) - 209$) [397] as well as $\delta^{31}\text{P}$ of phosphalkynes and δN of nitriles and coupling constants $^1J(^{31}\text{P} \equiv ^{13}\text{C})$ and $^1J(^{15}\text{N} \equiv ^{13}\text{C})$ (δN (nitrile) = $0.37\delta^{31}\text{P}(\text{phosphaalkyne}) - 111.9$; $^1J(^{15}\text{N} \equiv ^{13}\text{C}) = -0.17^1J(^{31}\text{P} \equiv ^{13}\text{C}) - 9.0$) [398]. Although, in nitriles and phosphalkynes the principal electronic structures are different (the HOMO in the phosphalkynes represents the triple bond, whereas in the nitriles the HOMO consists mainly of the lone pair of electrons at nitrogen), the influence of substituents and the dependence of nuclear shielding or coupling constants on the structural geometry are analogous. On the basis of the linear correlations, the $\delta^{31}\text{P}$ values for monomeric $\text{P} \equiv \text{N}$ (ca. 150) and for the $\text{P} \equiv \text{P}$ molecule (ca. 860) have been evaluated [398].

Some intriguing examples of transition metal phosphorus compounds (see Figure 23) are complexes in which elemental phosphorus serves as a ligand. There are complexes with naked phosphorus [399–401], and adducts of these [402] which show rather deshielded ^{31}P nuclei. The small value of the coupling constant, $^1J(^{183}\text{W}, ^{31}\text{P}) = 138 \text{ Hz}$ [399b], across the $\text{W} \equiv \text{P}$ bond can be explained by the presence of the lone pair of electrons at the phosphorus atom [403]. In the adduct, this pair of electrons is engaged, and the magnitude of the coupling constant (562.5 Hz [402]) is more in the range expected for a $\text{W} \equiv \text{P}$ bond. The P_4 molecule serves as a ligand in various ways [404–406], and many examples known are based on P_2 [407]. Furthermore, P_5 [408], $[\text{P}_5]^-$ [409,410] or P_6 [411–413] are coordinated to the metal.

The isolobal [414,415] relationship between P and a CH fragment has stimulated numerous further studies in which ^{31}P NMR has played an important role [416]. Examples include the η^5 -phospholy complexes, **37–39**, which have become increasingly available for main group metals as well as transition metals [417–419].

At a first glance, it seems that nothing unusual is to be expected for derivatives of the phosphonium cation $[\text{PH}_4]^+$. However, the discovery of such a cation (**40**) (see below), in which the surroundings of the four-coordinate phosphorus atom are planar (low ^{31}P nuclear shielding) corrects this view [420].

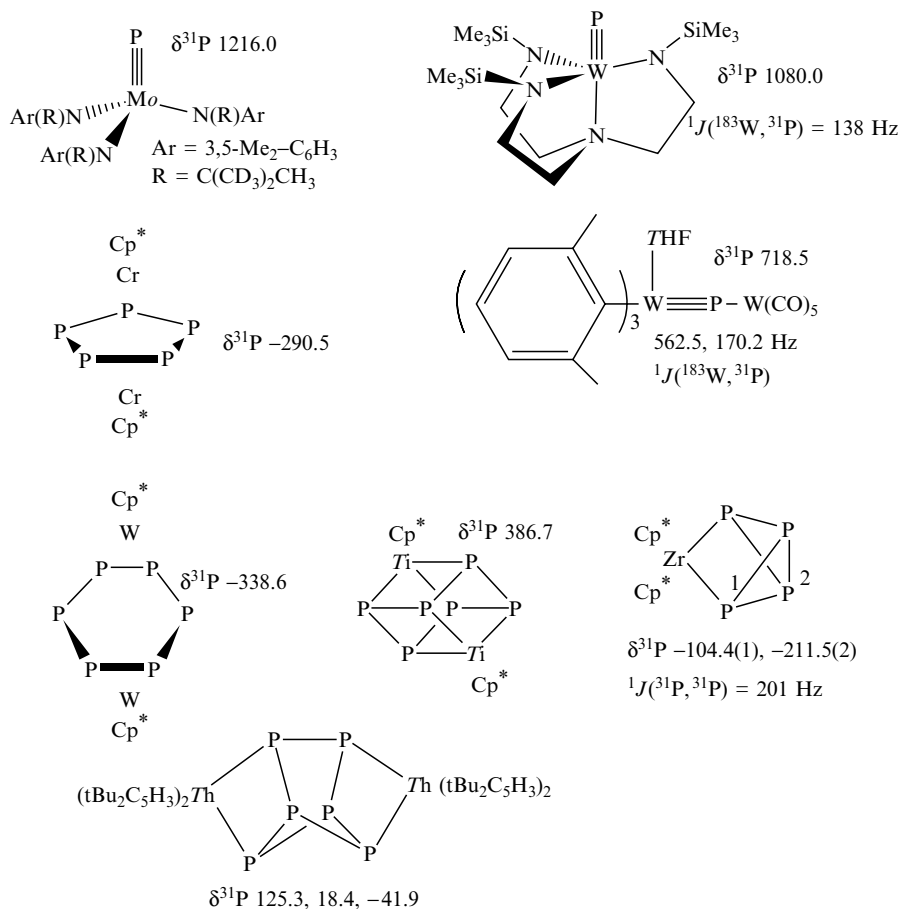
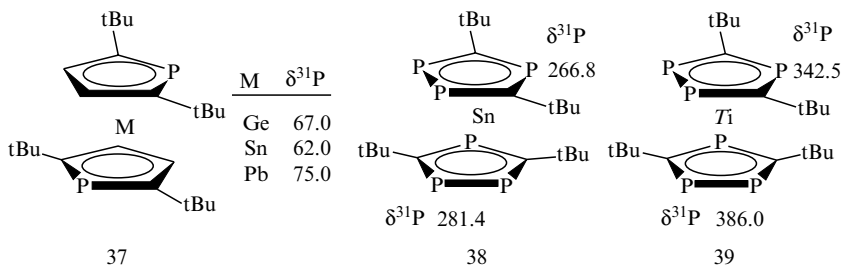
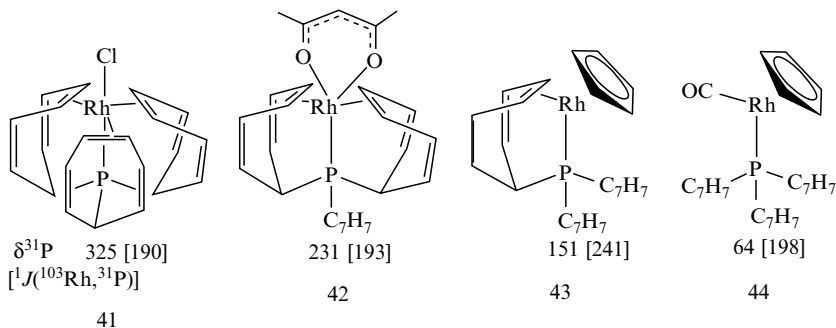
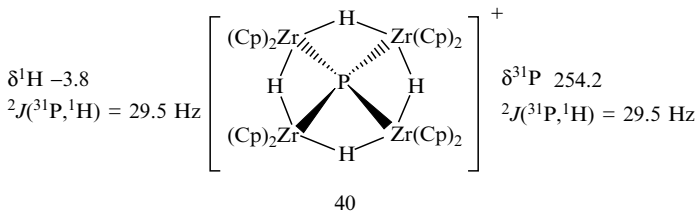


Figure 23 ^{31}P chemical shifts of transition metal complexes with elemental phosphorus as the ligand



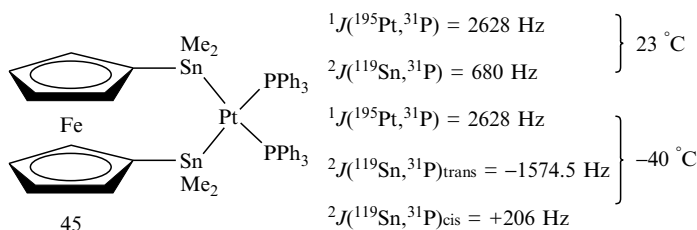


${}^{31}\text{P}$ chemical shifts allow us to distinguish between phosphido and phosphonium ligands in transition metal complexes. ${}^{31}\text{P}$ nuclear magnetic shielding in phosphonium complexes is about 100 ppm lower, and if coupling constants to the metal nuclei can be measured (e.g. ${}^1J({}^{183}\text{W}, {}^{31}\text{P})$), they are substantially larger in magnitude [421].

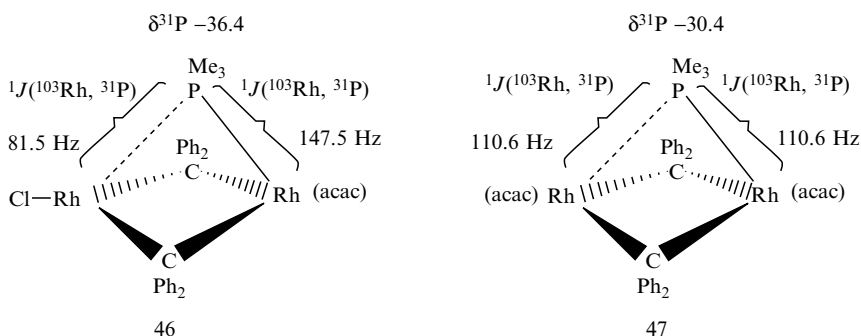
The loss of aromaticity of a 2,2'-diphosphinine becomes apparent by $\delta^{31}\text{P}$ data when coordination to the trinuclear osmium cluster $\text{Os}_3(\text{CO})_{12}$ takes place. If the aromaticity is retained, the $\delta^{31}\text{P}$ values are expected to lie in the range 178–220, whereas $\delta^{31}\text{P} = 26.2$ and -146.2 ($J({}^{31}\text{P}, {}^{31}\text{P}) = 108 \text{ Hz}$) are observed [422].

There are still numerous open problems in apparently simple transition metal phosphane complexes which can be solved by ${}^{31}\text{P}$ NMR. The coordination shifts for phosphane ligands have been interpreted by using a DFT/*ab initio* approach [423]. A practical example concerns *mer*- $[\text{Mo}(\text{CO})_3(\text{PF}_3)_3]$ which was originally proposed to have been formed as a single isomer, whereas a careful ${}^{19}\text{F}$ and ${}^{31}\text{P}$ NMR analysis (including a gas-phase ${}^{19}\text{F}$ NMR spectrum at 600°C !) has now proved that an approximately 1:1 mixture of *mer*- $[\text{Mo}(\text{CO})_3(\text{PF}_3)_3]$ and *fac*- $[\text{Mo}(\text{CO})_3(\text{PF}_3)_3]$ is present [424]. Further instructive examples can be found in the coordination chemistry of tris(1-cyclohepta-2,4,6-trienyl)phosphane [425]. The $\delta^{31}\text{P}$ values provide straightforward information as to whether the phosphane uses none, one, two or three olefinic double bonds for coordination to a metal centre in addition to the metal–P bond (e.g. 41–44) [426].

For many years, distortion of the square-planar surroundings of Pt(II) complexes were believed to be weak. Now evidence is growing that there are many examples of bis(phosphane)platinum(II) complexes in which significant deviations from square-planar geometry are observed, leading even to fluxional structures [427–430]. This is shown by averaged ^{31}P -X couplings if another NMR-active nucleus X is present (e.g. X = ^{199}Hg , ^{29}Si or ^{119}Sn). NMR spectra at low temperatures reveal the expected pattern of coupling constants. In the case of the type of complex **45**, even the information on the opposite signs of the coupling constants $^2J(^{119}\text{Sn}, ^{31}\text{P})$ becomes available [428,429].



A final example concerns the end of the long lasting search for triorganophosphanes as truly bridging ligands in coordination chemistry. In dinuclear rhodium complexes, trimethylphosphane can act as a semi-bridging or symmetrically bridging ligand, as follows from X-ray structural analysis in the solid state and by the coupling constants $^1J(^{103}\text{Rh}, ^{31}\text{P})$ in solution for the complexes **46** and **47** [431].



8 OXYGEN COMPOUNDS: ^{17}O NMR

8.1 SOME SIMPLE OXYGEN COMPOUNDS: WATER, OZONE, SULFUR DIOXIDE AND OTHERS

Unfortunately, nature has denied us a spin-1/2 nucleus for the element oxygen. There is just the quadrupolar nucleus ^{17}O (see Table 2) with $I = 5/2$ and an

extremely low natural abundance (0.037 %). The latter problem can be solved by ^{17}O -labelling; however, efficient quadrupolar relaxation sometimes prevents the accurate measurement of $\delta^{17}\text{O}$, and in general the straightforward observation of spin–spin coupling to other nuclei. Therefore, spin–spin ^{17}O –X coupling values as desirable parameters for structural assignments are hardly available. Nevertheless, ^{17}O NMR is attractive [11,432–434], considering the amount and variety of oxygen compounds. Furthermore, oxygen is part of many small, apparently simple molecules present in our daily life.

The dioxygen diradical, O_2 , is not accessible by NMR spectroscopy; however, its allotrope ozone, O_3 , is diamagnetic. The ^{17}O NMR spectrum of ozone shows two signals in a 2:1 ratio ($\delta^{17}\text{O} = 1032$ (terminal), 1598 (central)) at rather low field, with the one for the central ^{17}O nucleus being at very low field [435]. This deshielding is in agreement with the UV spectral properties of ozone. A comparison with the $\delta^{17}\text{O}$ value of the valence-isoelectronic sulfur dioxide, SO_2 ($\delta^{17}\text{O} = 513$ [436]), points towards the different electronic structure of these molecules, which is also apparent, of course, from the application of other physical methods (e.g. UV or photoelectron spectroscopy).

Carbon monoxide, CO (gaseous, 2 atm., $\delta^{17}\text{O} = 350.2$), and carbon dioxide, CO_2 (gaseous, 7 atm., $\delta^{17}\text{O} = 64.5$) form another prominent pair of oxides [437] with completely different electronic structures. Whereas CO is isoelectronic with N_2 , and the ^{17}O nucleus is deshielded as has been found for the nitrogen nuclei in N_2 (see Section 6.1 above), CO_2 is a member of the class of linear 16-valence electron molecules or ions, in which the terminal nuclei usually possess high magnetic shielding (see δN of the azide anion (Section 6.1 above), or $\delta^{17}\text{O}$ (N_2O) = 114.9 [437]). The $\delta^{17}\text{O}$ values of Me_2SO (δ 20) or Me_2SO_2 (δ 163) [438] (see also Reference [439] for sulfolenes and sultines), and also of phosphorus(v) compounds, e.g. $(\text{MeO})_3\text{PO}$ ($\delta^{17}\text{O} = 19$ (PO), 68 (MeO) [440]) show that there are no element–oxygen double bonds in the sense of the $\text{C}=\text{O}$ bond in aldehydes or ketones (e.g. $\delta^{17}\text{O}$ ($\text{MeC}(\text{H})=\text{O}$) = 592 or $\delta^{17}\text{O}$ ($\text{Me}_2\text{C}=\text{O}$) = 569 [441]).

The marked difference in the $\delta^{17}\text{O}$ values for H_2O as a liquid (0.0) and as a gas (–36.1) indicates the influence of hydrogen bridging [437].

Transition metal carbonyls (Figure 24) show reasonably sharp ^{17}O NMR signals which can be useful for studying the dynamic behaviour if the ^{13}C (carbonyl) resonances are too close. This has been demonstrated in the case of *cis*- $[\text{Fe}(\text{SnMe}_3)_2(\text{CO})_4]$ [442]. In carbene complexes, the ^{17}O resonance of the carbonyl group in the *trans*-position with respect to the carbene ligand is shifted markedly to low field [443]. The ^{17}O nuclear shielding in the carbonyl complexes (see Reference [587] for a theoretical analysis of ^{17}O nuclear shielding in CO and metal carbonyls) is similar to that in acyl cations (Figure 24) [444], which can be explained by the comparable local symmetry around the oxygen atoms in both classes of compounds.

^{17}O NMR studies of trigonal boranes with $\text{B}–\text{O}$ bonds [448,449] reveal trends in $\delta^{17}\text{O}$ similar to those of δN for aminoboranes (see Section 6.3, Figure 21 above). Thus, ^{17}O nuclear shielding decreases in going from $\text{B}(\text{OMe})_3$

$\delta^{17}\text{O}$				$\delta^{17}\text{O}$	
	M = Cr	Mo	W		
$\text{M}(\text{CO})_6$	382.2	373.1	363.7	$\text{W}(\text{CPh}_2)(\text{CO})_5$	364.7 (<i>cis</i>) 452.6 (<i>trans</i>)
$\text{CpM}(\text{CO})_3$	366.3	353.0	339.9	$\text{W}(\text{CN}t\text{Bu})(\text{CO})_5$	350 (<i>cis</i>) 348 (<i>trans</i>)
$\text{Mn}_2(\text{CO})_{10}$	392.6 (<i>eq</i>)	374.1 (<i>ax</i>)		$\text{Me}_2\text{Sn}[\text{Re}(\text{CO})_5]_2$	365.9 (<i>eq</i>) 350.8 (<i>ax</i>)
$\text{Fe}(\text{CO})_5$	391.3			$\text{Me}_2\text{Sn}[\text{Co}(\text{CO})_4]_2$	359.7
$\text{Ni}(\text{CO})_4$	362			<i>cis</i> - $\text{Fe}(\text{SnMe}_3)_2(\text{CO})_4$	360.4 (<i>eq</i>) 350.6 (<i>ax</i>)
		R	$\delta^{17}\text{O}$		
$\text{R}-\text{C}^+=\text{O}$		Me	299.5		
		Ph	318.0		

Figure 24 ^{17}O chemical shifts of transition metal carbonyls and of acyl cations (data taken from References [360,442–447])

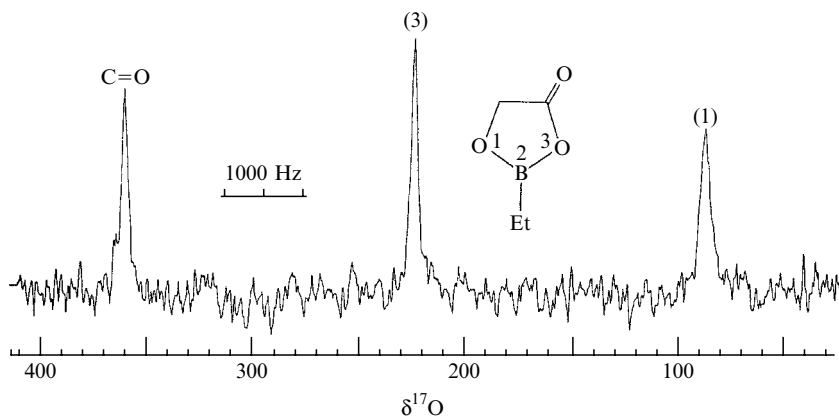


Figure 25 ^{17}O NMR spectrum of a boron–oxygen heterocycle [449]. The two different signals for the ester group at 80 °C in toluene prove that exchange of B–O bonds must be slow on the NMR time-scale

($\delta^{17}\text{O} = 11.0$) to $\text{MeB}(\text{OMe})_2$ ($\delta^{17}\text{O} = 51.0$), Me_2BOMe ($\delta^{17}\text{O} = 95.0$), $(\text{MeBO})_3$ ($\delta^{17}\text{O} = 152.0$), and $(\text{Et}_2\text{B})_2\text{O}$ ($\delta^{17}\text{O} = 223.0$). Furthermore, important structural information becomes available. The ^{17}O NMR spectrum of 2-ethyl-1,3,2-dioxaborolane-4-one [449] (Figure 25) shows three ^{17}O NMR signals, indicating that opening and closure of the B–O(4) bond must be slow on the NMR time-scale. Other physical methods do not provide this information unambiguously. The $\delta^{17}\text{O}$ values of various siloxanes [450] cover a much smaller range than that observed for the B–O compounds, in agreement with a smaller degree of Si–O multiple-bond character.

8.2 COMPLEXES WITH TRANSITION METAL–OXYGEN BONDS

The ^{17}O nuclear magnetic shielding is reduced, with few exceptions, if a transition metal is linked to oxygen. The exceptions concern oxygen which bridge three, four, five or six metal atoms (e.g. $\delta^{17}\text{O}$ ($[\text{Mo}_6\text{O}_{19}]^{2-}$) = -32 (bridging six Mo sites), 559 (bridging two Mo sites), and 927 (terminal oxygen, $\text{M} = \text{O}$) [451]. Typically, terminal ^{17}O nuclei are markedly deshielded (see $\delta^{17}\text{O}$ (CrO_2Cl_2) 1460 , $\delta^{17}\text{O}$ (RuO_4) 1119 ; and $\delta^{17}\text{O}$ (OsO_4) 796 [452]). The comparison of $\delta^{17}\text{O}$ values of simple oxoanions (**48**) (see below) of main group (S, Se, Cl) and transition metal elements (V, Cr, Mo, W, Mn, Tc, Re) clearly shows the deshielding effect (most pronounced for the first-row transition metal elements) exerted by transition metals as a result of \mathbf{B}_0 -induced charge circulation involving metal d orbitals.

48	$[\text{SO}_4]^{2-}$	$[\text{SeO}_4]^{2-}$	$[\text{ClO}_4]^-$	$[\text{VO}_4]^{3-}$	$[\text{CrO}_4]^{2-}$	$[\text{MoO}_4]^{2-}$	$[\text{WO}_4]^{2-}$	$[\text{MnO}_4]^-$	$[\text{TcO}_4]^-$	$[\text{ReO}_4]^-$
$\delta^{17}\text{O}$	167	204	290	568	835	530	420	1230	749	569

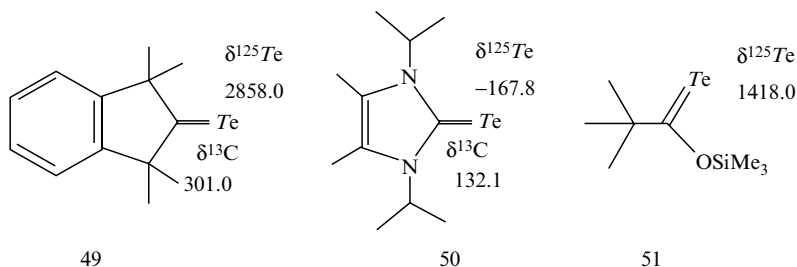
In $\text{Cp}^*\text{Re}(\text{O})\text{X}_2$ ($\text{X} = \text{F}, \text{Cl}, \text{Br}, \text{I}$), the range of the $\delta^{17}\text{O}$ values is small ($\delta^{17}\text{O} = 854, 865, 868$ for $\text{X} = \text{Cl}, \text{Br}, \text{I}$, respectively) except for $\text{X} = \text{F}$ ($\delta^{17}\text{O} = 619$) [453]. In the dimer $[\text{Cp}^*\text{Re}(\text{O})\text{O}]_2$, the bridging and terminal oxygen atoms are clearly distinguished by their $\delta^{17}\text{O}$ values ($\delta^{17}\text{O}(\text{bridge}) = 104$ and $\delta^{17}\text{O}(\text{terminal}) = 747$) [453]. It was shown, in the case of oxo(cyano)rhenate(v) complexes, that ^{17}O NMR can be used to monitor the degree of condensation from monomers to dimers since the $\delta^{17}\text{O}$ value of the bridging oxygen atom in the dimer is significantly different to that in a terminal OH group [454].

Labelling with ^{17}O has finally enabled us to detect the broad ^{17}O NMR signal of peroxydic oxygen atoms in molybdenum(vi) complexes. In the dianion $[\text{Mo}(\text{CN})_4(\text{O})(\text{O}_2)]$, the $^{17}\text{O}(\text{O}_2)$ NMR signal has $\delta^{17}\text{O} = 487$ ($h_{1/2} = 1800$ Hz), whereas for the terminal oxygen the a rather sharp ^{17}O NMR signal at $\delta^{17}\text{O} = 705$ ($h_{1/2} = 80$ Hz) has been found [455].

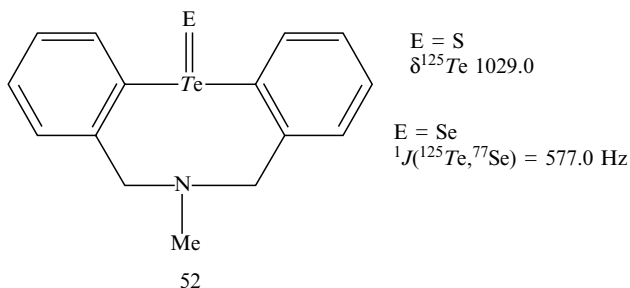
9 SELENIUM AND TELLURIUM COMPOUNDS: ^{77}Se AND ^{125}Te NMR

Although there is already a wealth of NMR data for both of the nuclei ^{77}Se [452, 456–458] and ^{125}Te [452, 458] (there is also ^{123}Te as a less abundant spin-1/2 nucleus (see Table 1) which can be used to determine $J(\text{Te}, \text{Te})$ [459]), the development of organometallic chemistry of Se and Te is still at its beginning. ^{77}Se and ^{125}Te NMR measurements are not always applied routinely, and therefore numerous interesting compounds have been reported without the information on $\delta^{77}\text{Se}$ or $\delta^{125}\text{Te}$, or without coupling constants involving these nuclei. Sometimes, this is also due to low solubility of these compounds.

The changes in shielding are large for both nuclei, even if the structures are apparently similar. This is shown below for the two types of telluroketones **49**, the telluro urea derivative **50** [460,461] and a telluro ester [462]. The low ^{125}Te nuclear shielding in the telluroketones is parallel to $\delta^{77}\text{Se} = 2131$ for $t\text{Bu}_2\text{C}=\text{Se}$ [463]. Even these extreme chemical shifts are close to the linear correlation $\delta^{125}\text{Te} = a\delta^{77}\text{Se}$ (with a ca. 1.8 or 1.6) [464]. The other telluro urea derivative **50** with highly shielded ^{125}Te is a carbene adduct. This ^{125}Te shielding reminds us of phosphane tellurides (e.g. $\delta^{125}\text{Te}$ ($t\text{Bu}_3\text{P}=\text{Te}$) = -80.0 [465]).

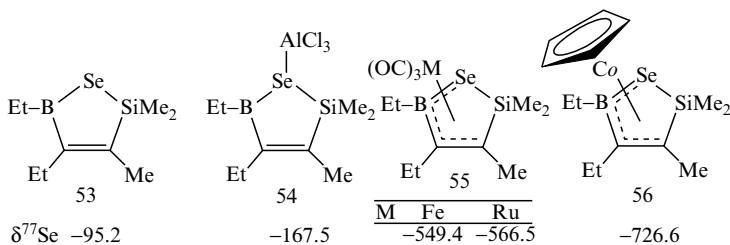


A rare example of Te–Group 16 element compounds with partial double bond character is shown below **52** [466]. The magnitude of the coupling constant $^1J(^{125}\text{Te}, ^{77}\text{Se})$ is much larger than, e.g. in $\text{MeTe}=\text{SeMe}$ ($^1J(^{125}\text{Te}, ^{77}\text{Se}) = -169$ Hz [467]); however, it is in the same range (if the sign is the same!) as in the dications $\text{cis}[\text{Te}_2\text{Se}_2]^{2+}$ ($^1J(^{125}\text{Te}, ^{77}\text{Se}) = 470$ Hz) or $\text{trans}[\text{Te}_2\text{Se}_2]^{2+}$ ($^1J(^{125}\text{Te}, ^{77}\text{Se}) = 550$ Hz) [468]. Recently, selenotelluronium ($[\text{C}_6\text{F}_5\text{SeTe}(\text{mes})_2]^+$, mes = mesityl) and tellorotelluronium cations ($[\text{mesTeTe}(\text{mes})_2]^+$) have been studied by ^{77}Se and ^{125}Te NMR [469].

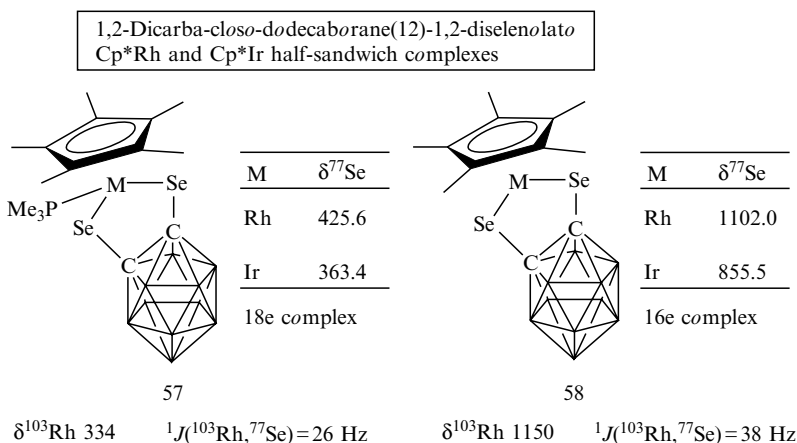


Both selenium and tellurium compounds possess great potential as ligands in transition metal chemistry [470–472]. Many heteroboranes are useful π donor ligands in transition metal complexes. Thus, 2,5-dihydro-1,2,5-heterosilaboroles

(see below) function as heterodienes, and if selenium is the heteroatom (**53**), application of ^{77}Se NMR is indicated [472]. The shielding of ^{77}Se increases dramatically in the transition metal complexes **55** and **56**. The line width of the ^{77}Se NMR signals and the relaxation time T^{O} of the ^{11}B nuclei have served for the calculation of $^1J(^{77}\text{Se},^{11}\text{B}) = 60 \pm 10$ Hz in the free borane, as well as in the tricarbonyliron and -ruthenium complexes [472].



The chemical shifts $\delta^{77}\text{Se}$ can be used to differentiate 18e **57** and 16e **58** rhodium- and iridium selenolate complexes, where significant deshielding of the ^{77}Se nuclei is associated with the 16e complexes [473,474]. The patterns due to the coupling constants $^1J(^{103}\text{Rh},^{77}\text{Se})$ can also be helpful in assessing the molecular structures in solution [475,476] (Figure 26).



In contrast with $[\text{Pt}(\text{Se}_4)_2]^{2-}$ ($\delta^{77}\text{Se} = 680, 790$ [477a]), the ^{77}Se NMR spectrum of $[\text{Pt}(\text{Se}_4)\text{dppe}]$ shows only one broad ^{77}Se NMR signal [477b]. In the complex $\text{Ph}_4\text{P}[\text{Cp}^*\text{W}(-=\text{Se})_3]$, the terminal selenide atoms are readily characterized by the typical [478b,c] value $\delta^{77}\text{Se} = +1437$ [478a].

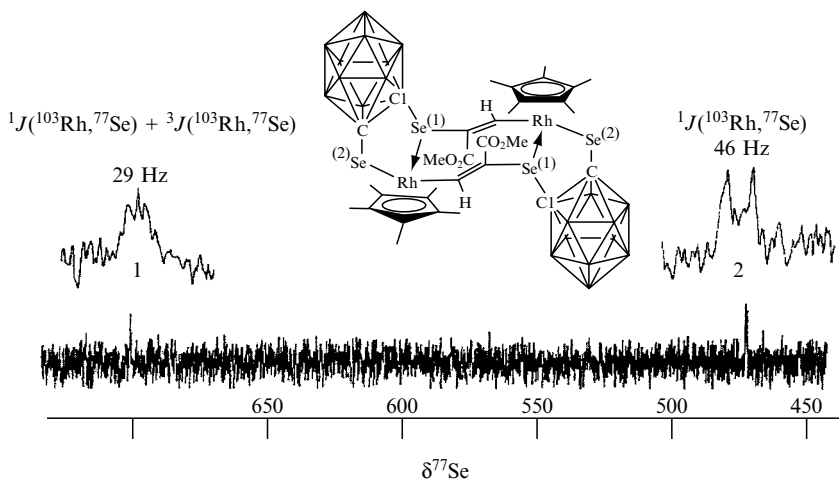


Figure 26 ^{77}Se NMR spectrum of a dimeric rhodium complex [476]. The dimeric structure was established by X-ray crystallography for the solid state. In solution, the appearance of the ^{77}Se resonances as a pseudo-triplet and a pseudo-doublet because of AA'X spin-systems (neglecting isotope effects) prove that the dimeric structure is retained in solution

10 FLUORINE COMPOUNDS: ^{19}F , A NUCLEUS WITH EXCELLENT NMR PROPERTIES

10.1 SOME SIMPLE MOLECULES: F_2 , Cl-F , OF_2 , XeF_2 , NF_3 AND OTHERS

The high NMR receptivity of ^{19}F and the frequently rather extreme chemistry of fluorine and its compounds have led to an enormously large data set of $\delta^{19}\text{F}$ values and coupling constants $J(^{19}\text{F}, \text{X})$ [11,479–481]. Clearly, ^{19}F NMR can be used in the same way as ^1H NMR of organic ligands to establish the framework of fluorinated ligands (e.g. for CF_3 or C_6F_5 groups which are frequently used). An overview of the $\delta^{19}\text{F}$ values of some simple fluorine compounds is given in Figure 27. The enormous change in ^{19}F nuclear shielding, by 842.3 ppm, in going from F_2 ($\delta^{19}\text{F} = 422.9$) to F-Cl ($\delta^{19}\text{F} = -419.4$) is unexpected at a first glance. The analysis of the tensor components shows that the strongly deshielding contribution from $\sigma_{xx} = \sigma_{yy}$ in F_2 become shielding for the ^{19}F nucleus in F-Cl (and deshielding for ^{35}Cl or ^{37}Cl), whereas the shielding σ_{zz} component is hardly affected.

Most reduced coupling constants $^1K(^{19}\text{F}, \text{X})$ possess a negative sign. However, in the case of boron fluorides, further experimental evidence is necessary for four-coordinate boron fluorides. In the case of transition metal fluorides, there is also ambiguity about the signs (see below), and a meaningful discussion requires further experimentally determined coupling signs.

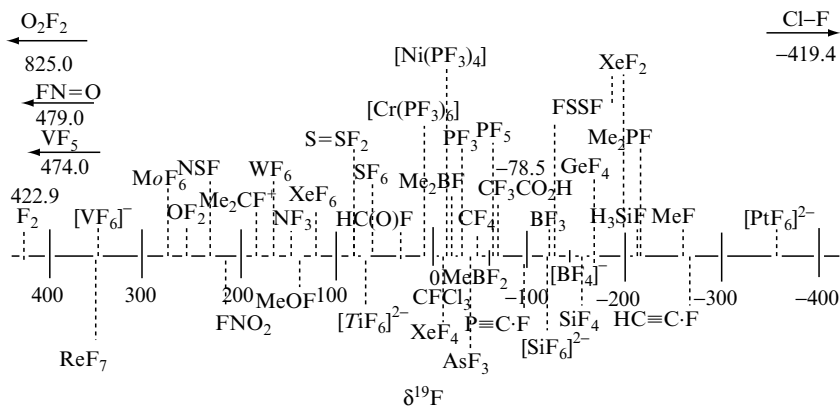


Figure 27 Overview of the $\delta^{19}\text{F}$ values of some simple fluorine compounds

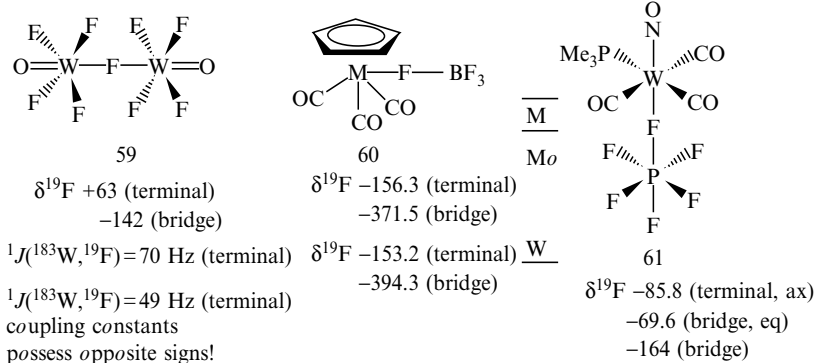
In fluorides of three-coordinate boron, the $\delta^{19}\text{F}$ values [479] follow the trend of the $\delta^{11}\text{B}$ values [119]. An increase in ^{11}B nuclear shielding is also reflected by an increase in ^{19}F nuclear shielding. This trend continues for four-coordinate boron compounds. Similarly, the magnitude of the coupling constants $^1J(^{19}\text{F}, ^{11}\text{B})$ changes from -122 Hz in Me_2BF , and -77 Hz in MeBF_2 , to ca. 15 Hz (either sign, most likely negative) in BF_3 , and to 1.1 Hz (either sign) in $[\text{BF}_4]^-$ [480]. The small magnitude of $^1J(^{19}\text{F}, ^{11}\text{B})$ in $[\text{BF}_4]^-$ should be compared with the large and negative coupling constant $^1J(^{19}\text{F}, ^{13}\text{C})$ in CF_4 (-257 Hz) [480]. Therefore, it is to be expected, in contrast to $^1J(^{19}\text{F}, ^{13}\text{C})$ in all fluorinated hydrocarbons, that the sign of $^1J(^{19}\text{F}, ^{11}\text{B})$ can change from negative to positive in four-coordinate boron–fluorine compounds.

10.2 TRANSITION METAL FLUORIDES

One of the most exciting new aspects in the chemistry of transition metal fluorides concerns their application in catalysis, in particular in asymmetric catalysis [482,483]. In most cases, the $\delta^{19}\text{F}$ values allow us to distinguish between terminal and bridging fluorine atoms, with the latter ^{19}F nuclei being markedly better shielded [484–487] (e.g. **59–61**; see also Reference [586] for C–F–Zr or C–F–Ti bridges, where the C–F function is part of a $\text{B}(\text{C}_6\text{F}_5)_3$ unit). Recent literature gives ^{19}F NMR data for technetium fluorides [488], osmium fluorides (e.g. $[\text{OsO}_4\text{F}]^-$ [489]), or tantalum fluorides [490].

11 CHEMISTRY OF XENON: ^{129}Xe NMR

^{129}Xe NMR is an important tool for studying the growing family of xenon compounds [491]. A recent addition to this family is the first organoxenon(IV)



compound, $[\text{C}_6\text{F}_5\text{XeF}_2]^+ [\text{BF}_4]^-$, in which the ^{129}Xe magnetic shielding is significantly increased with respect to $[\text{C}_6\text{F}_5\text{Xe}]^+$ [492].

Gaseous xenon remains attractive for NMR studies. Laser-polarized ^{129}Xe has been used frequently in order to study solids [493], e.g., carbon nanotubes [494]. The endohedral complex xenon@cryptophane-A has now been investigated by ^{129}Xe NMR, and it has been shown that the $\delta^{129}\text{Xe}$ data are sensitive to deuteration of the cryptophane-A [495].

12 ORGANOTRANSITION METAL COMPLEXES—A WIDE FIELD OF NMR

There are several transition elements with spin-1/2 nuclei (Table 1), although the majority possesses quadrupolar nuclei (Table 2) with rather large quadrupole moments. Much of the NMR work in this area has been reviewed [496,497]. Useful transition metal spin-1/2 nuclei for solution-state NMR spectroscopy [498,499] are ^{57}Fe , ^{103}Rh , $^{107/109}\text{Ag}$, $^{111/113}\text{Cd}$, ^{183}W , ^{187}Os , ^{195}Pt and ^{199}Hg , of which ^{57}Fe , and even more so, ^{187}Os , are extremely difficult to detect directly. The most useful quadrupolar transition metal nuclei for solution-state NMR are ^{51}V , ^{55}Mn , ^{59}Co , $^{63/65}\text{Cu}$, ^{95}Mo , ^{99}Tc (in spite of being a radioactive nucleus) and ^{99}Ru . All of the other quadrupolar nuclei are almost unsuitable for solution-state NMR studies owing to their large quadrupole moments, which lead to exceedingly broad NMR signals. However, in some cases, when the electric field gradient at the site of the nucleus is small, NMR signals can be detected. This is easy to predict for perfect tetrahedral or octahedral symmetry (e.g. $^{47/49}\text{Ti}$ NMR of TiCl_4 or $[\text{TiF}_6]^{2-}$, and others [500]). However, in most cases (some examples are given in the following), experiments are required in order to search for more or less broad signals. Thus, $\delta^{49}\text{Ti} = +1258$ has been determined for MeTiCl_3 [501], while ^{53}Cr NMR (e.g. of numerous pentacarbonylchromium carbene complexes with line widths in the range of 1–3 kHz [502])

has been carried out. Occasionally, measurements of ^{59}Ni NMR of some Ni(0) complexes [503], ^{91}Zr NMR of $\text{Zr}(\text{BH}_4)_4$ ($\delta^{91}\text{Zr} + 40.7$ relative to Cp_2ZrBr_2 ; $^1J(^{91}\text{Zr}, ^1\text{H}) = 28$ Hz, and $^2J(^{91}\text{Zr}, ^{11}\text{B}) = 18$ Hz) [504] or $t\text{Bu}_4\text{Zr}$ ($\delta^{91}\text{Zr} + 799$ relative to Cp_2ZrBr_2) [505], and some dicyclopentadienylzirconium complexes [506] or ^{93}Nb NMR of cyclopentadienylniobium borohydrides [507] have been successful. When transition metal compounds had been dissolved in supercritical solvents or low-viscosity liquefied gases (the solubility may be enhanced by adding THF or CH_2Cl_2), a considerable reduction in the line widths, e.g. of ^{53}Cr , ^{59}Co , ^{91}Zr or ^{95}Mo NMR signals, has been reported [335b]. So far, NMR signals of nuclei such as $^{177/179}\text{Hf}$, $^{191/193}\text{Ir}$, and ^{197}Au have not been detected in solutions.

12.1 VANADIUM COMPLEXES: ^{51}V NMR

Because of the high NMR receptivity of ^{51}V , its relatively small quadrupole moment (Table 2), and the numerous diamagnetic vanadium complexes, a large set of ^{51}V NMR data is available (see Reference [508] for a recent review on organovanadium complexes). The chemistry of CpV or Cp^*V and $(\eta^7\text{-C}_7\text{H}_7)\text{V}$ compounds is particularly well developed, and Figure 28 shows the chemical shift ranges of some types of complexes with vanadium in different formal oxidation states [509–512]. Considering the large ranges of $\delta^{51}\text{V}$ values for each class of compounds, the idea of a correlation between oxidation state and ^{51}V nuclear shielding should not be pursued.

The quadrupolar relaxation rate of the ^{51}V nucleus can be slowed down at elevated temperatures in order to observe scalar $^{51}\text{V}\text{-X}$ coupling which otherwise would be hidden in the broad ^{51}V NMR signal. This is shown in Figure 29 for a rare case of resolved $^{51}\text{V}\text{-}^{14}\text{N}$ coupling (both are quadrupolar nuclei!) together with $^{51}\text{V}\text{-}^{31}\text{P}$ coupling [513].

12.2 ^{95}Mo AND ^{183}W NMR

The quadrupolar ^{95}Mo nucleus [514] and the spin-1/2 nucleus ^{183}W [515] are both suitable for solution-state NMR studies, and NMR parameters have been reviewed.

Although, in general, ^{95}Mo NMR signals are broad (up to 3 kHz), there are numerous examples of sharp ^{95}Mo NMR signals. Then it is even possible to observe scalar coupling to other nuclei. Thus, scalar $^{95}\text{Mo}\text{-}^{14}\text{N}$ coupling is resolved in nitrosyl and thionitrosyl complexes (**62–64**). At the same time, the $\delta^{95}\text{Mo}$, as well as the δN values, indicate the different electronic structures of the NO and NS ligands [516]. There are also 16e complexes of this type with an NO ligand [517]. A marked deshielding of ^{95}Mo is observed when compared with the 18e complexes (**62**), and furthermore the ^{95}Mo becomes deshielded in the order $\text{F} < \text{Cl} < \text{I}$ —known as an inverse halogen dependence (usually observed for the early transition metal elements such as Ti or V).

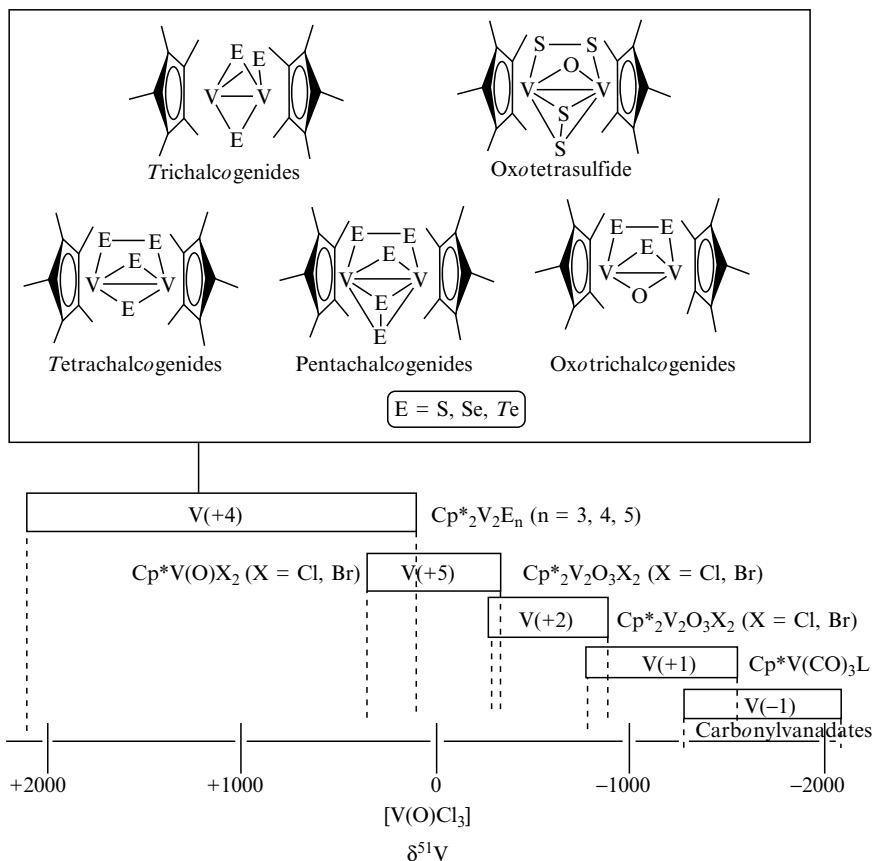


Figure 28 Chemical shifts $\delta^{51}\text{V}$ of cyclopentadienylvanadium complexes containing vanadium in different formal oxidation states

18e complexes		16e complexes		
$\text{H-B}(3,5\text{-Me}_2\text{pz})_3\text{Mo}(\text{CO})_2\text{NO}$	$\text{H-B}(3,5\text{-Me}_2\text{pz})_3\text{Mo}(\text{CO})_2\text{NS}$	$\text{H-B}(3,5\text{-Me}_2\text{pz})_3\text{MoX}_2\text{NO}$		
62	63	64		
$\delta^{95}\text{Mo}$	-743	X	F	Cl
$\delta^{14}\text{N}$	17	64	1274	1811
$^1J(^{95}\text{Mo}, ^{14}\text{N})$	60 Hz	64	2272	2272
		$\delta^{14}\text{N}$	14	26
			46	46

Most of the recent work on solution-state ^{183}W deals with various polyoxo-oxungstates [518–522], and organometallic chemistry is less well represented. This shows that the measurement of ^{183}W is not trivial, and indeed most data

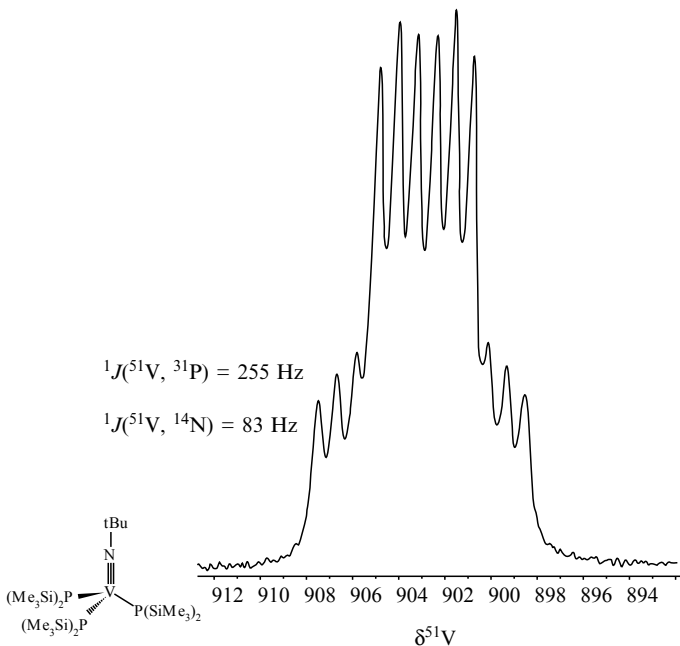


Figure 29 ^{51}V NMR spectrum of $t\text{BuN-V[P(SiMe}_3)_2]_3$ ($\delta^{31}\text{P} = 197:8$) in toluene at 373 K [513]; $\delta^{51}\text{V} = 903$

on organometallic compounds have been obtained by indirect methods, e.g. by $^1\text{H}\{^{183}\text{W}\}$, $^{19}\text{F}\{^{183}\text{W}\}$ or $^{31}\text{P}\{^{183}\text{W}\}$ selective heteronuclear double resonance experiments [523], or by inverse detection via (Figure 30) 2D $^1\text{H}/^{183}\text{W}$ [524,525], $^{31}\text{P}/^{183}\text{W}$ [524] or $^{19}\text{F}/^{183}\text{W}$ [526] HMQC experiments.

There is a huge range (> 6000 ppm) of $\delta^{183}\text{W}$ values; as for ^{95}Mo , the ^{183}W nuclei become strongly deshielded in complexes with M–M double and triple bonds. Since there are already many organometallic tungsten complexes with unusual bonding situations (e.g. as exemplified by ^{13}C or ^{31}P NMR studies) which are still waiting to be studied by ^{183}W NMR, it can be hoped that the known range of $\delta^{183}\text{W}$ values will be further expanded in the future.

12.3 ^{55}Mn AND ^{99}Tc NMR

All magnetically active isotopes of Mn, Tc and Re possess relatively large quadrupole moments (Table 2), giving rise to rather broad NMR signals, except when in highly symmetric surroundings. However, in the cases of ^{55}Mn and ^{99}Tc , the line widths are still small with respect to the range of chemical shifts, and therefore meaningful spectra can be obtained within a

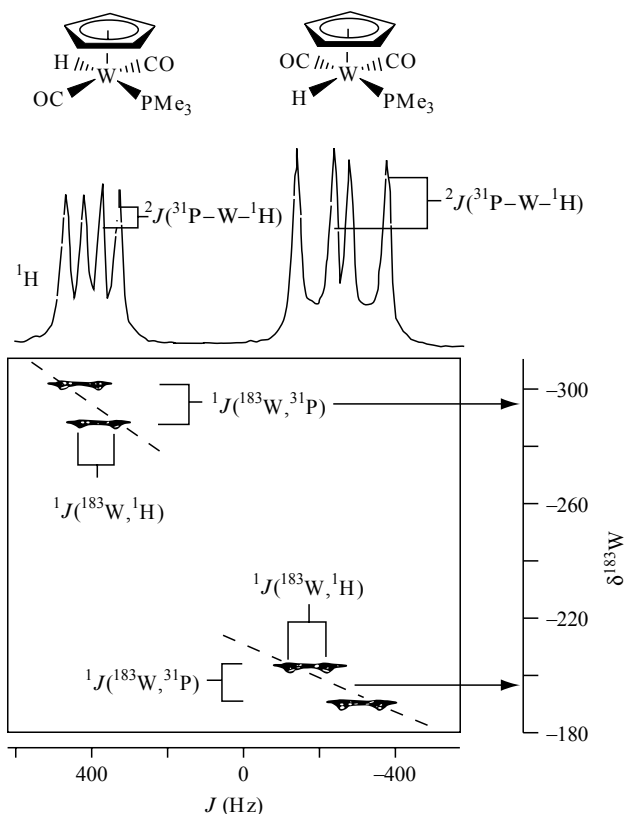


Figure 30 Contour plot of the 2D $^{183}\text{W}/^1\text{H}$ HMQC shift correlation of a *cis/trans* mixture of hydride complexes with ‘piano-stool’ structure [525]. The $\delta^{183}\text{W}$ data can be measured, and the relative signs of the coupling constants $^1J(^{183}\text{W}, ^{31}\text{P})$ and $^2J(^{31}\text{P}, \text{W}, ^1\text{H})$ can be compared (the negative tilt of the cross-peaks indicate opposite signs). Since it is known that $^1J(^{183}\text{W}, ^{31}\text{P}) > 0$ it follows that $^2J(^{31}\text{P}, \text{W}, ^1\text{H}) < 0$; this explains why the value of $^2J(^{31}\text{P}, \text{W}, ^1\text{H})$ is smaller (less negative!) in the *trans*-isomer

short time, whereas applications of solution-state $^{185/187}\text{Re}$ NMR is not helpful because of the exceedingly broad resonance signals.

Most ^{55}Mn NMR data have been reviewed [496], and there are very few more recent results. The application of ^{55}Mn NMR to manganese sandwich complexes, derived from $[(\eta^5\text{-C}_5\text{H}_5)\text{Mn}(\eta^6\text{-C}_6\text{H}_6)]$, has been demonstrated [527] (Figure 31), showing that fairly broad lines can be tolerated because of the large range of $\delta^{55}\text{Mn}$ chemical shifts, in particular, if a high-field spectrometer is used.

It should be noted that those sandwich complexes derived from $[(\eta^5\text{-C}_5\text{H}_5)\text{Mn}(\eta^6\text{-C}_6\text{H}_6)]$ (**65**) contain Mn in the formal oxidation state +1, and

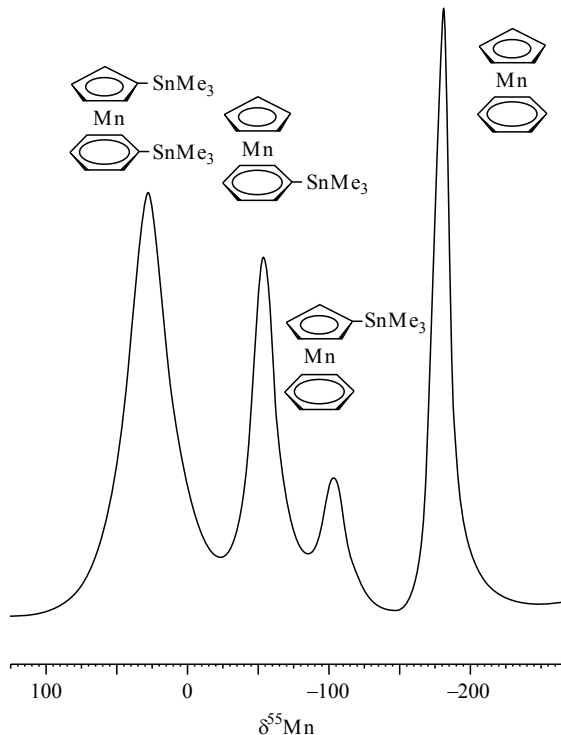
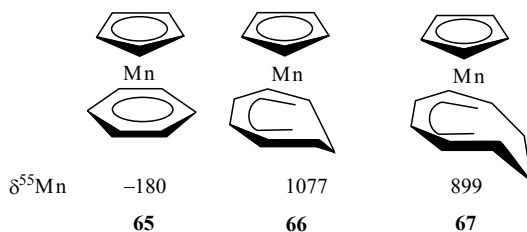


Figure 31 123.5 MHz ^{55}Mn NMR spectrum [514a] of a mixture containing $[(\eta^5\text{-Cp})\text{Mn}(\eta^6\text{-C}_6\text{H}_6)]$ and its Me_3Sn^- substituted derivatives (the assignment follows from relative signal intensities in ^1H , ^{13}C and ^{119}Sn NMR spectra)

that the $\delta^{55}\text{Mn}$ values are in the vicinity of the reference, $\delta^{55}\text{Mn}([\text{MnO}_4]^-) = 0$, in which Mn possesses formally the oxidation state +7. Clearly, any attempt to relate transition metal nuclear shielding with oxidation states will lead to erroneous results. The range of $\delta^{55}\text{Mn}$ values is further extended to higher frequencies by the $\delta^{55}\text{Mn}$ values of the half-open sandwich complexes **66** and **67**. The nuclear shielding of ^{55}Mn in the sandwich complexes depends on the HOMO–LUMO difference of the filled and empty d orbitals centred mainly at the manganese nucleus. Three of these orbitals are occupied and two are empty. Apparently, the electronic structure of the half-open sandwich complexes differs significantly from that of the sandwich complexes. The analogous behaviour is revealed by ^{57}Fe nuclear shielding of comparable complexes (see Section 12.4 below).

^{99}Tc NMR spectra are easy to obtain; however, owing to the limited number of compounds available, in particular of organometallic derivatives, only a small set of ^{99}Tc NMR data has been collected [528–530].



12.4 ^{57}Fe , ^{99}Ru AND ^{187}Os NMR

The most 'difficult' spin-1/2 nuclei, ^{57}Fe and ^{187}Os (Table 1) and a quadrupolar nucleus, ^{99}Ru , form this group from the NMR point of view. The relevant NMR parameters of these nuclei have been reviewed [531]. The important role that iron complexes are playing in numerous biological processes have stimulated the use of ^{57}Fe NMR for studying ^{57}Fe labelled samples. In particular, porphyrin complexes, myoglobin derivatives [532] and heme proteins [533] are frequently studied, and they exhibit extremely deshielded ^{57}Fe nuclei, extending the range of $\delta^{57}\text{Fe}$ up to about 10 000 ppm.

In early ^{57}Fe NMR studies of ferrocene and ferrocene derivatives, in particular of α -ferrocenyl carbocations (**68**), ^{57}Fe labeling has also been used, and the $\delta^{57}\text{Fe}$ values have been determined indirectly by selective $^{13}\text{C}\{^1\text{H}, ^{57}\text{Fe}\}$ heteronuclear triple resonance experiments, taking advantage of the small coupling constants $J(^{57}\text{Fe}, ^{13}\text{C})$ (≈ 4.8 Hz) [208,534]. Depending on the substituents at the carbon atom which bear the positive charge, the cyclopentadienyl ring is distorted towards a fulvene-like structure, especially in the case of $[\text{Fc}-\text{CH}_2]^+$ ($\text{Fc} = (\eta^5\text{-C}_5\text{H}_5)\text{Fe}(\text{C}_5\text{H}_4)$, ferrocenyl), where rehybridization of the iron d orbitals occurs, thus leading to significant shielding of the ^{57}Fe nucleus. If, however, the electron-withdrawing effect of the positively charged carbon dominates, deshielding of ^{57}Fe is observed. Of course, these are counteracting influences of $\delta^{57}\text{Fe}$, and the extreme cases show a shift difference $\Delta^{57}\text{Fe}$ of > 1000 ppm.

In natural abundance of iron, the indirect detection via ^1H or ^{31}P nuclei is the method of choice if Fe-H or Fe-P bonds are present which give rise to substantial scalar $^{57}\text{Fe}-^1\text{H}$ or $^{57}\text{Fe}-^{31}\text{P}$ coupling [535]. In the majority of

$\delta^{57}\text{Fe}$	R^1	R^2
-523.6	H	H
-219.3	H	Me
221.0	H	Ph
368.7	H	$\text{C}_5\text{H}_4\text{Mn}(\text{CO})_3$
699.0	H	$\text{C}_5\text{H}_4\text{Fe}(\text{Cp})$
405.0	H	$\text{C}_5\text{H}_4\text{Ru}(\text{Cp})$
288.5	Me	Me
σ, σ		

68

(Cp)Fe(Cp)

known iron compounds, these conditions are not fulfilled, and therefore ^{57}Fe NMR has not found widespread application. The amount of sample (1g or more) and the required spectrometer time (12 to 24 h or more) appears to be prohibitive [536–538].

The advent of high-field spectrometers with $B_0 \geq 11.5$ T has improved the situation considerably, at least for such compounds where the relaxation of the ^{57}Fe nuclei takes place via the chemical shift anisotropy (CSA) relaxation mechanism, as is true for ferrocene derivatives [539]. It has been shown that the ^{57}Fe NMR signal of ferrocene (0.8 M in CDCl_3 ; ca. 70 mg of ferrocene in 0.5 ml) could be detected after about 30 min of spectrometer time, using optimized conditions for a 5 mm low-frequency probehead at $B_0 = 11.5$ T (16.1 MHz ^{57}Fe NMR) [540]. An example of a ^{57}Fe NMR spectrum of a mixture of *N*-ferrocenyl-*N*-boryl amines is shown in Figure 32 [541]. The comparison of $\delta^{57}\text{Fe}$ and $\delta^{55}\text{Mn}$ values for analogous heteroelement-substituted sandwich complexes (see Section 12.2 above) reveals strikingly similar trends, indicating analogous electronic structures [540].

Very few organometallic ruthenium compounds have been studied by ^{99}Ru NMR [531,543]. However, it appears that it is possible to calculate ^{99}Ru shielding constants, and this may stimulate researchers to determine more experimental data [544]. The comparison of the differences in chemical shifts $\Delta^{57}\text{Fe}(\text{ferrocene} - [\text{Fe}(\text{CN})_6]^{4-}) = -913.6$ [545] and $\Delta^{99}\text{Ru}(\text{ruthenocene} - [\text{Ru}(\text{CN})_6]^{4-}) = -1270$ [543] suggests that the range of ^{99}Ru chemical shifts may be slightly larger than that for $\delta^{57}\text{Fe}$.

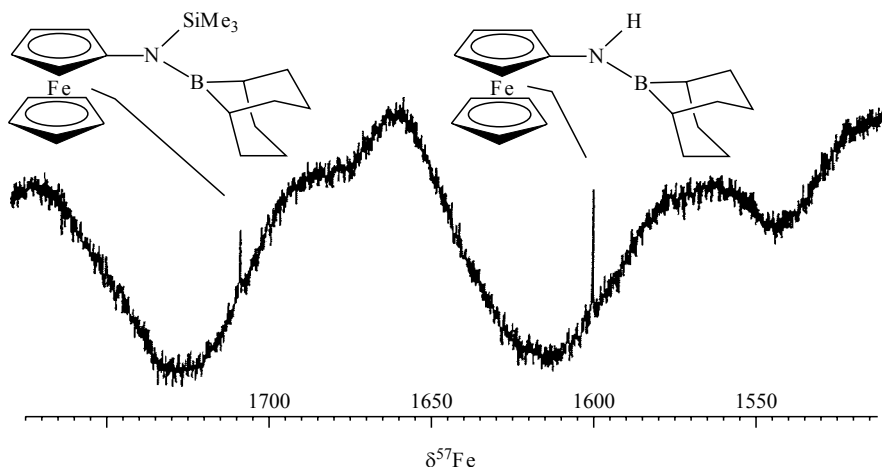


Figure 32 16.2 MHz ^{57}Fe NMR spectrum of a mixture containing two *N*-ferrocenylaminoboranes [541] (the rolling baseline owing to acoustic ringing is a typical feature of NMR spectra if low-frequency nuclei are measured without using special pulse sequences [542])

The few $\delta^{187}\text{Os}$ data available [531] are insufficient for establishing relationships of $\delta^{187}\text{Os}$ to nuclear shielding of ^{57}Fe or ^{99}Ru . The majority of $\delta^{187}\text{Os}$ values have been obtained by inverse detection using compounds with Os–H or Os–P bonds [546].

12.5 ^{59}Co AND ^{103}Rh NMR

The quadrupolar ^{59}Co nucleus (Table 2) has been at the centre of numerous NMR studies, and the extremely large range of $\delta^{59}\text{Co}$ values had already been discovered shortly after the first successful NMR experiments. Although direct NMR measurements can be used to detect NMR signals of the spin-1/2 nucleus ^{103}Rh (Table 1) in solution, most $\delta^{103}\text{Rh}$ data have been determined by selective double-resonance techniques, e.g. $^1\text{H}\{^{103}\text{Rh}\}$ or $^{31}\text{P}\{^{103}\text{Rh}\}$, or by 2D inverse $^1\text{H}/^{103}\text{Rh}$ correlations (see Figure 33). Polarization transfer techniques such as INEPT or DEPT are also useful for measuring ^{103}Rh NMR signals, provided that scalar $^{103}\text{Rh}\text{--}^1\text{H}$ or $^{103}\text{Rh}\text{--}^{31}\text{P}$ coupling is sufficiently large. Reviews cover most important development in the field of ^{59}Co [497,547,548] and ^{103}Rh NMR [497,548].

The sensitivity of $\delta^{59}\text{Co}$ to very small changes in the surroundings is best demonstrated by isotope-induced chemical shifts $^2\Delta^{1/2}\text{H}(\text{}^{59}\text{Co})$, e.g. by deuteration of amine ligands, as has been shown again in a recent study [549]. Another ‘old’ candidate for NMR studies is the cluster $\text{Co}_4(\text{CO})_{12}$, which has been the subject of ^{59}Co relaxation measurements and of 2D EXSY ^{59}Co NMR spectroscopy [550] (see also Reference [335b] for line width measurement in supercritical solvents).

^{103}Rh NMR can contribute to the study of rhodium hydride complexes, in which the hydrogen atoms can be bonded as hydride and/or as the dihydrogen ligand (see Section 2.5 above). The 2D inverse $^1\text{H}/^{103}\text{Rh}$ shift correlation of such a complex containing H_2 and two hydrides (fast intramolecular exchange) [551] is shown in Figure 33.

When a complex has been well characterized in the solid state, there is always the question as to whether the main structural features are retained in solution. The rare $\kappa^2(\text{N},\text{B}\text{--}\text{H})$ coordination mode of the $[\text{HB}(2,5\text{-Me}_2\text{pz})_3]^-$ ligand is clearly shown in the crystal structure (Figure 34) [552]. In solution, the evidence for this particular type of bonding is based on the coupling constant $^1J(^{103}\text{Rh},^1\text{H})$ and the reduced magnitude of $^1J(^{11}\text{B},^1\text{H})$, typical of a bridging hydrogen atom.

A large number of Rh complexes has been studied by ^{103}Rh and ^{119}Sn NMR in order to describe the assumed Rh–H–Sn three-centre bond [553]; however, there are still numerous open questions. Experimental and calculated ^{103}Rh chemical shifts show good agreement for a number of rhodium–olefin complexes [554].

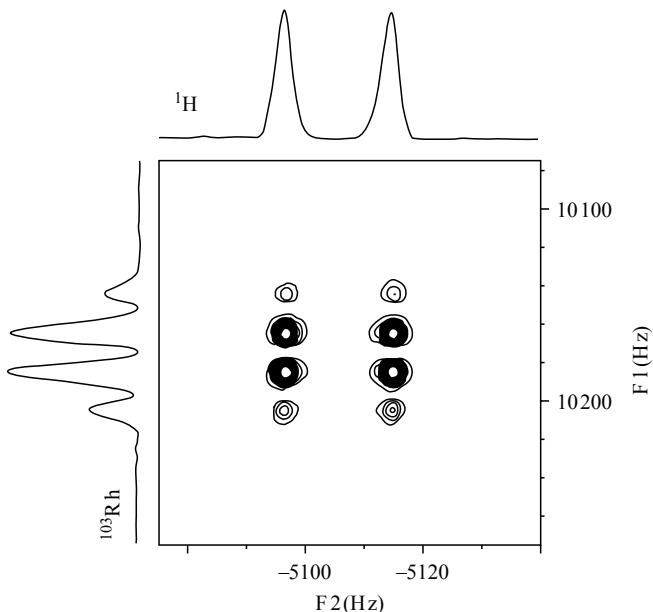


Figure 33 Contour plot of the 2D $^{103}\text{Rh}/^1\text{H}$ HMQC shift correlation of $[\text{HB}(3,5\text{Me}_2\text{pz})_3\text{Rh}(\text{H}_2)\text{H}_2]$ in CD_2Cl_2 at 253 K [551]. The ^1H NMR spectrum (F_2 projection) of the hydride region ($\delta^1\text{H} = -12.76$) shows the doublet due to averaged (fast exchange between $\eta^2\text{-H}_2$ and hydride hydrogen atoms) $^1J(^{103}\text{Rh}, ^1\text{H}) = 18.1$ Hz, and the ^{103}Rh NMR spectrum (F_1 projection) shows four lines ($\delta^{103}\text{Rh} = 805$) corresponding to the number of ^1H nuclei coupled to ^{103}Rh . In contrast to ‘normal’ 1D ^1H coupled ^{103}Rh NMR spectrum (multiplicity, $n + 1$), the multiplicity is n , corresponding directly to the number of the ^1H nuclei coupled to ^{103}Rh

12.6 ^{195}Pt NMR

Owing to the favourable nuclear properties of ^{195}Pt , the NMR spectroscopy of platinum compounds, especially ^{195}Pt NMR has become a powerful tool in the characterization of Pt complexes. Since platinum chemistry is very well developed, including aspects of biochemistry (e.g. anti-tumor properties of ‘cis-platinum’ and related compounds [555]), there is a wealth of data available, and ^{195}Pt NMR has been reviewed several times [556–558].

The first homoleptic, dinuclear Pt(II) carbonyl cation $\{[\text{Pt}(\text{CO}_3)_2]_2\}^{2+}$ has been characterized by ^{195}Pt [559]. The experimental and simulated ^{195}Pt NMR spectrum of the 99% ^{13}C enriched complex is shown in Figure 35. The magnitude of $^1J(^{195}\text{Pt}, ^{195}\text{Pt}) = 550.9$ Hz [559] is surprisingly small when compared with dinuclear dianions of the type $\{[\text{PtX}_2(\text{CO})]_2\}^{2-}$ ($\text{X} = \text{Cl}$ and Br , with $^1J(^{195}\text{Pt}, ^{195}\text{Pt}) = 5250$ and 4770 Hz, respectively [560]), whereas the magnitude of the coupling constants $^1J(^{195}\text{Pt}, ^{13}\text{C})$ in $\{[\text{Pt}(\text{CO}_3)_2]_2\}^{2+}$ is only slightly smaller than in the anions $\{[\text{PtX}_2(\text{CO})]_2\}^{2-}$. However, in other related

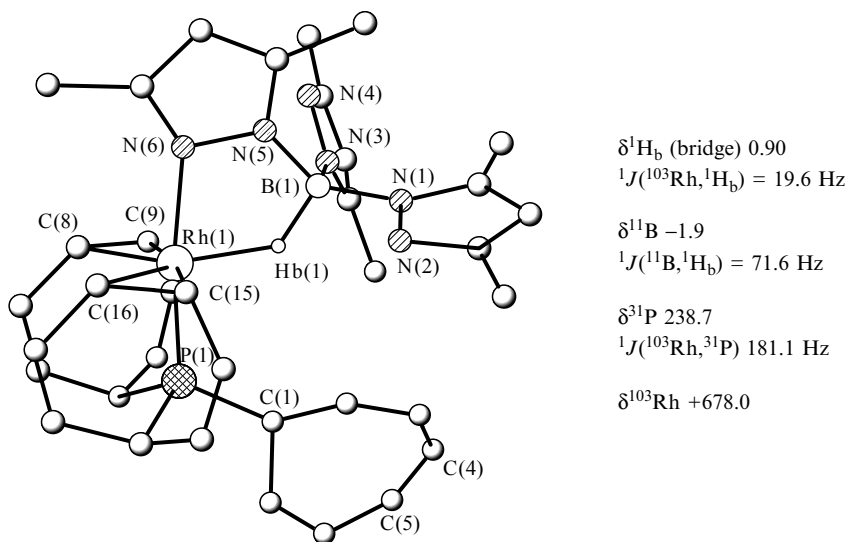


Figure 34 Molecular structure of $\{\text{HB}(3,5\text{-Me}_2\text{pz})_3\text{Rh}[\text{P}(\text{C}_7\text{H}_7)_3]\}$, with the tris(3,5-dimethyl-1-pyrazolyl)borate in $\kappa^2(\text{N}, \text{B}-\text{H})$ coordination mode, and solution-state NMR data, showing that the most prominent feature of the solid-state structure, the bridged Rh-H-B unit, is retained in solution [552]

dinuclear complexes [561], such as $\{[\text{PtCl}(\text{CO})(\text{PPh}_3)_2]_2\}$ ($^1J(^{195}\text{Pt}, ^{195}\text{Pt}) = 760$ Hz) or $\{[\text{Pt}(\text{CNMe}_3)_3]_2\}^{2+}$ ($^1J(^{195}\text{Pt}, ^{195}\text{Pt}) = 507$ Hz), the coupling constants $^1J(^{195}\text{Pt}, ^{195}\text{Pt})$ have been found to lie in the similar range of magnitude as in $\{[\text{Pt}(\text{CO})_3]_2\}^{2+}$.

Phosphido-bridged dinuclear platinum complexes (for examples, see **69–72** [561]) are the source of a multitude of NMR data [562–564], and these are all reactive species. Again, the magnitude of $^1J(^{195}\text{Pt}, ^{195}\text{Pt})$ is small, except for the di-insertion product **72** [562].

	69	70	71	72
$\delta^{195}\text{Pt}$	-5483 (A) -5220 (B)	-5549 (A) -5162 (B)	-4928.5 -4523.3	-4364.4 -4364.4
$^1J(^{195}\text{Pt}, ^{195}\text{Pt})$	185 Hz	178 Hz	293 Hz	2100 Hz

The enantiomeric composition of mixtures can be determined by using chiral derivatization agents (CDAs) which, in the case of platinum-containing CDAs,

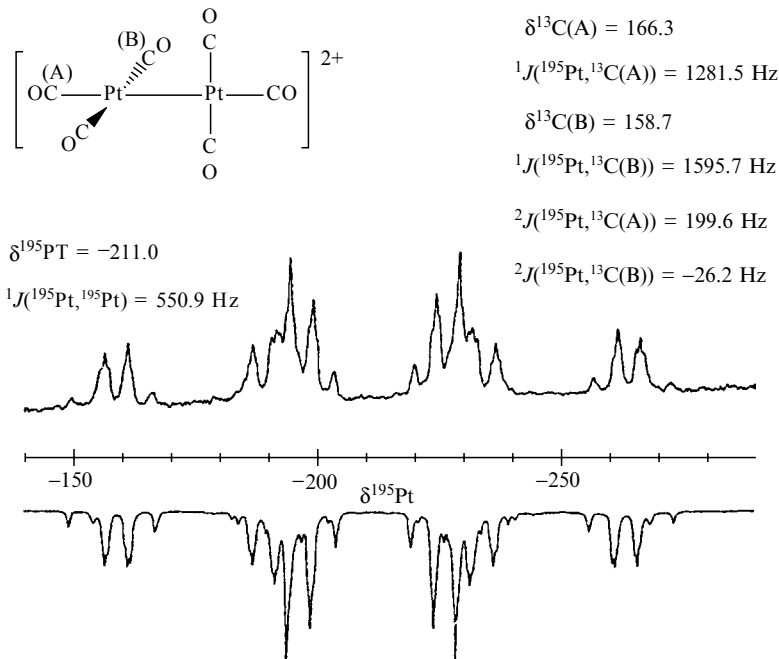
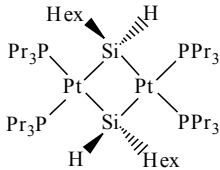
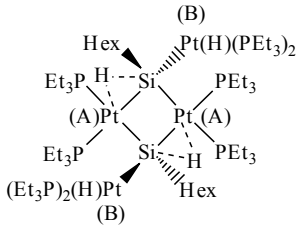


Figure 35 42.8 MHz ^{195}Pt NMR spectrum (observed (top) and simulated (bottom)) of 99 % ^{13}C -enriched $[\text{Pt}(\text{CO}_3)_2]^{2+}$ in concentrated D_2SO_4 (adapted from Reference [558])

make use of the sensitivity of ^{195}Pt nuclear shielding to small changes in the surroundings of the platinum atom. Thus, chiral complexes of the type $\text{cis-}[\text{PtCl}_2(\eta^2\text{-H}_2\text{C}=\text{CH}_2)\text{amine}^*]$, where amine* is a chiral amine such as (*S*)- α -methylbenzylamine, can be used for olefinic substrates. If the olefin contains a substituent with a chiral centre, the diastereomeric mixtures are then formed by elimination of ethene from the coordination sphere of Pt [565].

Platinum–silicon four-membered rings (**73** and **74**) have been prepared from the reaction of $[\text{Pt}(\text{PR}_3)_3]$ ($\text{R} = \text{Et}, \text{Pr}$) with hexylsilane, $\text{Si}(\text{Hex})\text{H}_3$, and ^{195}Pt NMR (also ^{29}Si and ^{31}P NMR) has been used extensively (in 1D and 2D experiments) in order to characterize the reaction and decomposition products. Many useful experiments have been carried out, and the solution-state NMR data for the rings have been discussed with respect to the results of the X-ray analyses [566].

In the chemistry of the dianion $[\text{Pt}(\text{CN})_4]^{2-}$ the reactions with $\text{Tl}(\text{CN})_3$ are of considerable interest, since they lead, depending on the cyanide concentration, to species **75–78**, which according to the large magnitude of the coupling constants $^1J(^{203/205}\text{Tl}, ^{195}\text{Pt})$ (these are the largest one-bond heteronuclear coupling constants known so far) possess Pt–Tl bonds [567].

		
	73	74
$\delta^{195}\text{Pt}$	-244	-411 (A) -970 to -1120 (B)
$\delta^{29}\text{Si}$	-94	194
$^1J(^{195}\text{Pt}, ^{29}\text{Si})$	600 Hz	1080 Hz Pt(A)

	$[(\text{NC})_5\text{Pt}-\text{TI}]$ 75	$[(\text{NC})_5\text{Pt}-\text{TI}-\text{CN}]^-$ 76	$[(\text{NC})_5\text{Pt}-\text{TI}(\text{CN})_2]^{2-}$ 77	$[(\text{NC})_5\text{Pt}-\text{TI}(\text{CN})_3]^{3-}$ 78
$^1J(^{205}\text{Tl}, ^{195}\text{Pt}) =$	71 000	57 000	47 000	38 000 Hz
$\delta^{195}\text{Pt}$	+473	+383	+184	+68
(relative to aq. $[\text{Na}_2\text{PtCl}_6]$)				

A final example is given for Pt(IV) chemistry, concerning the dynamic behaviour of trimethylplatinum dithiocarbamate complexes. These are dimers, and, depending upon the substituents at the nitrogen atom, various rotamers can exist in solution. ^{195}Pt NMR spectroscopy (Figure 36) has been used to show that the dimeric structure is retained in solution, and that the rearrangement of the rotamers is slow on the NMR time-scale [568].

12.7 $^{63/65}\text{Cu}$ AND $^{107/109}\text{Ag}$ NMR

Applications of $^{63/65}\text{Cu}$ NMR (see Table 2 for the nuclear properties) have been reviewed [569]. Although copper compounds (not always well-defined) play an important role in organic synthesis, $^{63/65}\text{Cu}$ NMR is not very helpful in this context owing to the extremely broad NMR signals. A single organocopper compound, the tetrameric carbonylcopper complex $\{[\text{Cu}(\text{CO})(\text{OtBu})_4]_4\}$, ^{13}C labelled, has been studied, and $^1J(\text{Cu}, ^{13}\text{C}) = \approx 600\text{--}800$ Hz has been measured [570].

There are two spin-1/2 Ag nuclei (Table 1), both suitable for NMR studies. Because of the intrinsic instability of most organometallic silver compounds, $^{107/109}\text{Ag}$ NMR has received scant attention. In organosilver compounds, there is frequently scalar $\text{Ag}-^1\text{H}$ coupling, and therefore, the δAg data can be obtained conveniently by $^1\text{H}\{\text{Ag}\}$ selective double-resonance experiments [571] or by polarization transfer (see Figure 37) [572].

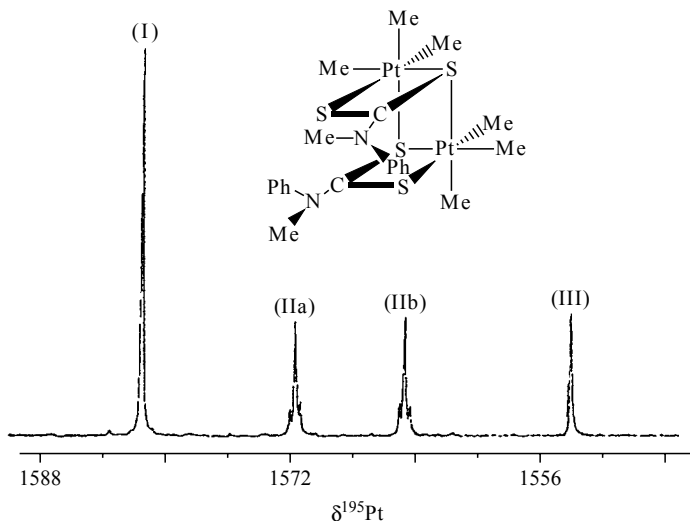


Figure 36 128 MHz ^{195}Pt NMR spectrum of a dimeric trimethylplatinum dithiocarbamate complex (as shown) in CDCl_3 at 298 K [566]. Owing to hindered rotation about the C–N bond of the dithiocarbamate ligands ($\Delta G^\ddagger = 86.45, 87.24$ and $87.15 \text{ kJ mol}^{-1}$) three rotamers (I), (II) and (III) are present in solution. In both (I) and (III), the surroundings of the two respective platinum atoms are identical, whereas in (II) the surroundings are different, thus leading to two ^{195}Pt NMR signals in a 1:1 ratio. These signals are accompanied by ^{195}Pt satellites corresponding to $^2J(^{195}\text{Pt}, ^{195}\text{Pt}) = 87 \text{ Hz}$ for the isotopomer containing two non-equivalent ^{195}Pt nuclei

The Organometallic chemistry of silver is not well developed as yet, and it is expected that future work will make more use of the powerful modern NMR methods, since δAg values appear to be extremely sensitive to the surroundings of the silver atoms [573].

12.8 $^{111/113}\text{Cd}$ AND ^{199}Hg NMR

In this group, ^{67}Zn NMR (see Table 2) is not well developed and probably not very helpful either, in strong contrast with the situation for the other elements which possess one or two spin-1/2 nuclei, i.e. ^{199}Hg and $^{111/113}\text{Cd}$, all with favourable NMR properties (Table 1). Cd NMR has found important application in biochemical science, and there are also many organometallic cadmium compounds. Mercury chemistry has a very long tradition; many organomercury compounds are known, and in the last two decades it has been found that mercury can be implemented in numerous transition metal clusters [573]. Consequently, Cd NMR [574] and ^{199}Hg NMR spectroscopy has been repeatedly reviewed [574,575].

In recent work, using ^{113}Cd NMR, (^{113}Cd data for CdX_2 adducts ($\text{X} = \text{Cl}, \text{Br}, \text{I}$) have been reported without a reference compound or frequency (!) [576].

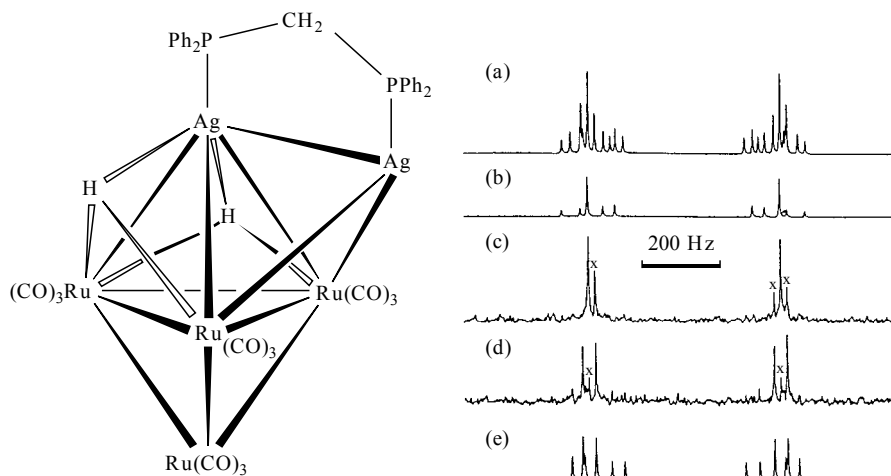
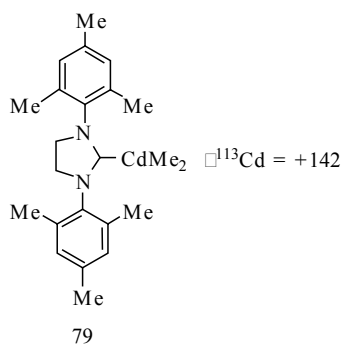


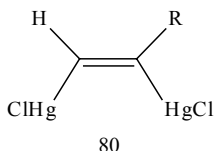
Figure 37 $^{109}\text{Ag}\{^1\text{H}\}$ NMR spectra (observed and simulated) for the ruthenium–silver cluster compound (as shown): (a) simulated total spectrum; (b) simulated sub-spectrum for the ^{109}Ag ^{109}Ag isotopomer; (c) observed spectrum with the INEPT delays optimized for the ^{109}Ag ^{109}Ag isotopomer; (d) observed spectrum with the INEPT delays optimized for the ^{107}Ag ^{109}Ag isotopomer; (e) simulated sub-spectrum for the ^{107}Ag ^{109}Ag isotopomer. The marked signals in the experimental spectra arise from non-suppressed magnetization of the other respective isotopomer

Dimethylcadmium forms a weak complex (**79**) with a bis(amino)carbene, as shown by the decrease in ^{113}Cd nuclear magnetic shielding [577].



The formerly largest magnitude of one-bond homo- and heteronuclear coupling constants, $^1J(^{199}\text{Hg}, ^{199}\text{Hg}) = 139\,700 \pm 300$ Hz in the cation $[\text{Hg}-\text{Hg}-\text{Hg}]^{2+}$ [578], ranks now in second place. When the two mercury atoms in $[\text{Hg}-\text{Hg}]^{2+}$ are complexed by different crown ethers, the ^{199}Hg NMR spectra shows the AB spin system (only the inner lines were observable) of the ^{199}Hg - ^{199}Hg satellites with $^1J(^{199}\text{Hg}, ^{199}\text{Hg}) = 284\,100 \pm 860$ Hz [579].

The ^{199}Hg NMR data of a series of chloromercury and bis(chloromercury)alkenes (**80**) [580] may serve as a typical application of ^{199}Hg NMR for NMR spectroscopic characterization of new organomercury compounds. Particularly remarkable are the large values of $^3J(^{199}\text{Hg}, ^{199}\text{Hg})$ across the C=C bond.



R	CH ₂ OMe	CM _e ₂ OMe
$\delta^{199}\text{Hg}(1)$	-1212	-1205
$\delta^{199}\text{Hg}(2)$	-1317	-1318
$^3J(^{199}\text{Hg}, ^{199}\text{Hg})$ (Hz)	8628	8820

13 LANTHANIDES AND ACTINIDES

Unfortunately, the exciting organometallic chemistry of the lanthanides and of some actinides is hardly reflected by NMR measurements. Most of the compounds are paramagnetic, and if they are diamagnetic, the respective lanthanide or actinide nuclei, in general, have unfavourable nuclear properties (see, e.g. Table 2 for ^{139}La , and Reference [581] for ^{139}La NMR of some allyllanthanum complexes). Exceptions to this are the spin-1/2 nuclei ^{89}Y (not really a lanthanide) and ^{171}Yb (Table 1). However, the organometallic chemistry of yttrium is not well developed as yet. ^{171}Yb NMR of Yb(II) complexes has been reviewed recently [582].

14 CONCLUSIONS

The elements throughout the Periodic Table provide a large number of nuclei suitable for solution-state NMR measurements, and extensive data sets for chemical shifts δX and coupling constants $J(A,X)$ have become available. By analysing the physical picture behind these data, their relationship to structure and bonding has become increasingly apparent. In the last two decades it was found that tailored ligands can be used in order to stabilize metal nuclei in unusual surroundings. Thus, it is hard to understand that sometimes brilliant work on fascinating organometallic compounds is frequently not accompanied by a more complete multinuclear NMR analysis; instead just the routine NMR data (^1H or ^{13}C , and ^{19}F or ^{31}P , when appropriate) have been acquired. There is necessarily a strong emphasis on the results of X-ray structural analyses in order to obtain information on the solid-state structures. However, a missing or incomplete multinuclear magnetic resonance data set for the solution-state leads to a somewhat unbalanced situation, considering that

most of the chemistry of organometallic compounds takes place in solution. Therefore, the search for structure/reactivity principles may sometimes end up the wrong way by focusing solely on the solid state. An important message from this present chapter is to collect and to analyse carefully the solution-state multinuclear magnetic resonance data, in spite of the seemingly conclusive direct structural evidence coming from diffraction methods applied to solids. Appropriate solid-state NMR measurements which have also become feasible in the last two decades have been demonstrated to be extremely useful tools to link solid- and liquid-state structures.

In the case of chemical shifts (or nuclear magnetic shielding) of nuclei other than ^1H , the existence of energetically low-lying levels, close to the nucleus in question, and their \mathbf{B}_0 -induced mixing with occupied ground states, appears to be the most important factor contributing to deshielding, whereas the absence of such conditions often leads to highly shielded nuclei. Obviously, both conditions in their extremes are related to unusual bonding situations.

The magnitude and the sign of coupling constants $J(\text{A},\text{X})$ reveal important information on the structure and the bonding situation in general. Frequently, the magnitude of $J(\text{A},\text{X})$ can be obtained from routine NMR spectra, in contrast to the sign of J . The sign, however, is required in order to classify the data either as 'normal', 'expected', or to note an unusual behaviour which may (in most cases) point towards unusual properties of the bond(s) connecting A and X. In general, the unusual behaviour is found if nuclei are involved possessing one or more lone pairs of electrons, or if heavy nuclei are involved, such as ^{119}Sn , ^{207}Pb , ^{195}Pt or ^{199}Hg , to name just a few examples of main group elements and transition metals.

The recent literature on organometallic compounds is almost saturated with DFT calculations applied mainly to mechanistic problems. The calculation of NMR parameters of the lighter nuclei, including ^{29}Si and ^{31}P , has made great progress in the last few years, and it is hoped that an analogous treatment of the more heavy nuclei, in particular of transition metal nuclei, will come into the reach of chemists [583]. There are some bright, promising views, e.g. for calculating $\delta^{99}\text{Ru}$ [544] or $\delta^{103}\text{Rh}$ data [554], while a more gloomy picture has been drawn in some cases, e.g. for the calculation of $\delta^{57}\text{Fe}$ in ferrocene [584], where it is pointed out that better exchange correlation functions are required. Clearly, a successful quantum chemical treatment of nuclear shielding and coupling constants involving heavy nuclei will be a great stimulant for collecting more experimental data in the future.

15 ACKNOWLEDGEMENTS

I am grateful to the Deutsche Forschungsgemeinschaft (DFG) and the Fonds der Chemischen Industrie for continuous support. I also wish to thank Cinvestav (Mexico

City) and the people there for their support and hospitality which helped me a great deal in the writing of this review.

16 REFERENCES

1. F. Bloch, W. Hansen and M. Packard, *Phys. Rev.*, **69**, 127 (1946).
2. E. M. Purcell, H. C. Torrey and R. V. Pound, *Phys. Rev.*, **69**, 37 (1946).
3. H. S. Gutowsky and D. W. McCall, *Phys. Rev.*, **82**, 748 (1951).
4. (a) G. Wilkinson, M. Rosenblum, M. C. Whiting and R. B. Woodward, *J. Am. Chem. Soc.*, **74**, 2125 (1952). (b) E. O. Fischer and W. Pfab, *Z. Naturforsch.*, **B**, **7**, 377 (1952). (c) G. Wilkinson, *J. Organomet. Chem.*, **100**, 273 (1975).
5. (a) T. J. Kealy and P. L. Pauson, *Nature*, **168**, 1039 (1951). (b) S. A. Miller, J. A. Tebboth and J. F. Tremaine, *J. Chem. Soc.*, 632 (1952).
6. D. M. Grant and R. K. Harris (Eds), *Encyclopedia of NMR*, Wiley, Chichester, 1996 (see vol. 1 for the history and development of NMR spectroscopy).
7. (a) R. K. Harris and B. E. Mann (Eds), *NMR and the Periodic Table*, Academic Press, London, 1978. (b) R. K. Harris, F. D. Becker, S. M. C. de Menezes, R. Goodfellow, P. Granger, *Pure Appl. Chem.*, **73**, 1795 (2001).
8. (a) B. E. Mann and B. F. Taylor, *¹³C NMR Data for Organometallic Compounds*, Academic Press, London, 1981. (b) S. Berger, S. Braun and H.-O. Kalinowski, *¹³C NMR Spektroskopie*, Thieme, Stuttgart, 1984.
9. P. Laszlo (Ed.) *NMR of Newly Accessible Nuclei: Chemical and Biological Applications*, vols 1 and 2, Academic Press, New York, 1983.
10. J. Mason (Ed.), *Multinuclear NMR*, Plenum Press, New York, 1987.
11. S. Berger and S. Braun and H.-O. Kalinowski, *NMR Spectroscopy of the Non-Metallic Elements*, Wiley, Chichester, 1997.
12. K. G. Orrell, *Annu. Rep. NMR Spectrosc.*, **37**, 1–74 (1999).
13. S. Beyreuther, A. Frick, J. Hunger, G. Huttner, B. Antelmann and P. Schober and R. Söltek, *Eur. J. Inorg. Chem.*, 597 (2000).
14. R. Rupp, A. Frick, G. Huttner, P. Rutsch, U. Winterhalter, A. Barth, P. Kircher and L. Zsolnai, *Eur. J. Inorg. Chem.*, 523 (2000).
15. (a) C. L. Perrin and T. J. Dwyer, *Chem. Rev.*, **90**, 935 (1990). (b) R. Willem, *Progr. NMR Spectrosc.*, **20**, 1 (1987).
16. I. D. Gridnev, P. R. Schreiner, O. Tok and Yu. N. Bubnov, *Chem. Eur. J.*, **5**, 2828 (1999).
17. D. Neuhaus and M. Williamson, *The Nuclear Overhauser Effect in Structural and Conformational Analysis*, VCH, Weinheim, 1989.
18. P. Stilbs, *Progr. NMR Spectrosc.* **19**, 1 (1987).
19. C. Zuccaccia, G. Bellachioma, G. Cardaci and A. Macchioni, *Organometallics*, **10**, 4663 (2000).
20. M. Valentini, P. S. Pregosin and H. Rügger, *Organometallics*, **19**, 2551 (2000).
21. H. Fukui, *Progr. NMR Spectrosc.*, **31**, 317–342 (1997).
22. R. H. Contreras, J. E. Peralto, C. G. Giribet, M. C. Ruiz de Azua and J. C. Facelli, *Annu. Rep. NMR Spectrosc.*, **41**, 55 (2000).
23. H. Fukui, *Progr. NMR Spectrosc.*, **35**, 267 (1999).
24. (a) J. Mason, *Adv. Inorg. Chem. Radiochem.*, **18**, 197 (1976). (b) J. Mason, *Adv. Inorg. Chem. Radiochem.*, **22**, 199 (1979). (c) J. Mason, *Chem. Rev.*, **87**, 1299 (1987). (d) A. C. de Dios and C. J. Jameson, *Annu. Rep. NMR Spectrosc.*, **29**, 1 (1994).

25. (a) N. F. Ramsey, *Phys. Rev.*, **77**, 567 (1950). (b) N. F. Ramsey, *Phys. Rev.*, **78**, 699 (1950). (c) N. F. Ramsey, *Phys. Rev.*, **83**, 540 (1951). (d) N. F. Ramsey, *Phys. Rev.*, **86**, 243 (1952).
26. W. E. Lamb, Jr, *Phys. Rev.*, **60**, 817 (1941).
27. (a) J. A. Pople, *Discuss. Faraday Soc.*, **34**, 7 (1962). (b) J. A. Pople, *J. Chem. Phys.*, **37**, 53 (1962). (c) J. A. Pople, *J. Chem. Phys.*, **37**, 60 (1962). (d) J. A. Pople, *Mol. Phys.*, **7**, 301 (1964).
28. R. Freeman, G. R. Murray and R. E. Richards, *Proc. R. Soc. London, A*, **242**, 495 (1957).
29. J. S. Griffith and L. E. Orgel, *Trans. Faraday Soc.*, **53**, 601 (1957).
30. N. Juranic, *Inorg. Chem.*, **19**, 1093 (1980).
31. N. Juranic, *J. Am. Chem. Soc.*, **110**, 8341 (1988).
32. R. Bramley, M. Brorson, A. M. Sargeson and C. E. Schaffer, Jr, *J. Am. Chem. Soc.*, **107**, 280 (1985).
33. N. F. Ramsey and E. M. Purcell, *Phys. Rev.*, **85**, 143 (1952).
34. N. F. Ramsey, *Phys. Rev.*, **91**, 303 (1953).
35. J. A. Pople and D. P. Santry, *Mol. Phys.*, **8**, 1 (1964).
36. (a) J. N. Shoolery, *J. Chem. Phys.*, **31**, 1427 (1959). (b) N. Muller and D. E. Pritchard, *J. Chem. Phys.*, **31**, 768 (1959). (c) N. Muller and D. E. Pritchard, *J. Chem. Phys.*, **31**, 1471 (1959).
37. A. Stock, *Hydrides of Boron and Silicon*, Cornell University Press, Ithaca, NY, 1933.
38. W. N. Lipscomb, *Angew. Chem.*, **89**, 685 (1977).
39. P. Laszlo, *Angew. Chem.*, **112**, 2151 (2000); *Angew. Chem. Int. Ed. Engl.*, **39**, 2071 (2000).
40. G. R. Eaton and W. N. Lipscomb, *NMR Studies of Boron Hydrides and Related Compounds*, W. A. Benjamin Inc., New York, 1969, and references cited therein.
41. (a) H. J. Bernstein, W. G. Schneider and J. A. Pople, *Proc. R. Soc. London, A*, **236**, 515 (1956). (b) J. A. Pople, *J. Chem. Phys.*, **24**, 1111 (1956). (c) J. A. Pople, *Mol. Phys.*, **1**, 175 (1958). (d) C. E. Johnson and F. A. Bovey, *J. Chem. Phys.*, **29**, 1012 (1958).
42. L. Ernst, *Progr. NMR Spectrosc.*, **37**, 47 (2000).
43. P. Lazzaretti, *Progr. NMR Spectrosc.*, **36**, 1 (2000).
44. P. v. R. Schleyer, C. Maercker, A. Dransfeld, H. Jiao and N. J. R. v. E. Hommes, *J. Am. Chem. Soc.*, **118**, 6317 (1996).
45. H. Günther, *NMR-Spektroskopie*, Thieme, Stuttgart, 1992, pp. 86, 88.
46. R. N. Young, *Progr. NMR Spectrosc.*, **12**, 261 (1979).
47. R. P. Kirchen, K. Ranganayakulu, A. Rauk, B. P. Singh and T. S. Sorensen, *J. Am. Chem. Soc.*, **103**, 588 (1981).
48. R. P. Kirchen, K. Ranganayakulu, B. P. Singh and T. S. Sorensen, *Can. J. Chem.*, **59**, 2173 (1981).
49. R. P. Kirchen, N. Okazawa, K. Ranganayakulu, A. Rauk and T. S. Sorensen, *J. Am. Chem. Soc.*, **103**, 597 (1981).
50. (a) M. L. Huggins, *Angew. Chem.*, **83**, 163 (1971); *Angew. Chem. Int. Ed. Engl.*, **10**, 147 (1971). (b) For a unified H-bonding theory see, e.g. G. Gilli and P. Gilli, *J. Mol. Struct. (THEOCHEM)*, **552**, 1 (2000).
51. F. Hibbert and J. Emsley, *Adv. Phys. Org. Chem.*, **26**, 255 (1990).
52. G. A. Jeffrey, *Introduction to Hydrogen Bonding*, Oxford University Press, Oxford, UK, 1997.
53. G. A. Kumar and M. A. McAllister, *J. Org. Chem.*, **63**, 6968 (1988).
54. H. Benedict, H.-H. Limbach, M. Wehlan, W. P. Fehlhammer, N. S. Golubev and R. Janoschek, *J. Am. Chem. Soc.*, **120**, 2939 (1998).
55. M. Garcia-Viloca, R. Gilabert, A. Gonzalez-Lafont, M. Moreno and J. M. Lluch, *J. Am. Chem. Soc.*, **120**, 10203 (1998).

56. S. Bolvig, P. E. Hansen, H. Morimoto, D. Wemmer and P. Williams, *Magn. Reson. Chem.*, **38**, 525 (2000).
57. P. Gilli, V. Bertolasi, V. Ferretti and G. Gilli, *J. Am. Chem. Soc.*, **122**, 10405 (2000).
58. J. E. Del Bene and M. J. T. Jordan, *J. Am. Chem. Soc.*, **122**, 4794 (2000).
59. F. Löhr, S. G. Mayhew and H. Rüterjans, *J. Am. Chem. Soc.*, **122**, 9289 (2000).
60. G. Gemmecker, *Angew. Chem.*, **112**, 1276 (2000); *Angew. Chem. Int. Engl.*, **39**, 1224 (2000).
61. (a) A. Liu, A. Majumdar, W. Hu, A. Kettani, E. Skripkin and D. J. Patel, *J. Am. Chem. Soc.*, **122**, 3206 (2000). (b) A. Meissner and O. W. Sørensen, *J. Magn. Reson.*, **143**, 387 (2000). (c) X. Yan, X. Kong, Y. Xia, K. H. Sze and G. Zhu, *J. Magn. Reson.*, **147**, 357 (2000).
62. S. A. Perera and R. J. Bartlett, *J. Am. Chem. Soc.*, **122**, 1231 (2000).
63. (a) H. Benedict, I. G. Shenderovich, O. L. Malkina, V. G. Malkin, G. S. Denisov, N. S. Golubev and H.-H. Limbach, *J. Am. Chem. Soc.*, **122**, 1979 (2000). (b) R. M. Claramunt, D. Sanz, S. H. Alarcon, M. P. Toralba, J. Elguero, C. Foces-Foces, M. Pietrzak, U. Langer and H.-H. Limbach, *Angew. Chem.*, **113**, 434 (2001); *Angew. Chem. Int. Ed. Engl.*, **40**, 420 (2001).
64. J. E. Del Bene, S. A. Perera and R. J. Bartlett, *J. Am. Chem. Soc.*, **122**, 3560 (2000).
65. J. E. Del Bene and R. J. Bartlett, *J. Am. Chem. Soc.*, **122**, 10480 (2000).
66. A. Bagno, S. Gerard, J. Kevelam, E. Menna and G. Scorrano, *Chem. Eur. J.*, **6**, 2915 (2000).
67. N. M. Doherty and N. W. Hoffmann, *Chem. Rev.*, **91**, 553 (1991).
68. E. F. Murphy, R. Murugavel and H. W. Roesky, *Chem. Rev.*, **97**, 3425 (1997).
69. H. Plenio, *Chem. Rev.*, **97**, 3363 (1997).
70. V. V. Grushin, *Angew. Chem.*, **110**, 1042 (1998); *Angew. Chem. Int. Ed. Engl.*, **37**, 994 (1998).
71. N. A. Jasim and R. N. Perutz, *J. Am. Chem. Soc.*, **122**, 8685 (2000).
72. D. C. Roe, W. J. Marshall, F. Davidson, P. D. Soper and V. V. Grushin, *Organometallics*, **19**, 4575 (2000).
73. (a) M. J. Calhorda, *J. Chem. Soc., Chem. Commun.*, 801 (2000). (b) G. R. Desiraju and T. Steiner, *The Weak Hydrogen Bond in Structural Chemistry and Biology*, Oxford University Press, Oxford, UK, 1999. (c) J. A. Cowan, J. A. C. Clyburne, M. G. Davidson, R. L. W. Harris, J. A. K. Howard, P. Küpper, M. A. Leech, S. P. Richards, *Angew. Chem. Int. Ed. Engl.*, **41**, 1432 (2002).
74. D. Braga, F. Grepioni and E. Tedesco, in *Solid State Organometallic Chemistry: Methods and Applications*, M. Gielen, R. Willem and B. Wrackmeyer (Eds), Physical Organometallic Chemistry, Vol. 2, Wiley, Chichester, UK, 1999, pp. 91-111.
75. S. H. Park, A. J. Lough, G. P. A. Yap and R. H. Morris, *J. Organomet. Chem.*, **609**, 110 (2000).
76. D. G. Gusev, M. Madott, F. M. Dolgushin, K. A. Lyssenko and M. Yu. Antipin, *Organometallics*, **19**, 1734 (2000).
77. M.-H. Chao, S. Kumaresan, Y.-S. Wen, S.-C. Lin, J. R. Hwu and K.-L. Lu, *Organometallics*, **19**, 714 (2000).
78. R. Michalczyk, J. G. Schmidt, E. Moody, Z. Li, R. Wu, B. Dunlap, J. D. Odom and L. A. Silks, III, *Angew. Chem.*, **112**, 3200 (2000); *Angew. Chem. Int. Ed. Engl.*, **39**, 3067 (2000).
79. (a) J. Dupont, P. A. Z. Suarez, R. F. De Souza, R. A. Burrow and J. P. Kintzinger, *Chem. Eur. J.*, **6**, 2377 (2000). (b) C. D. Abernethy, C. L. B. Macdonald, J. A. C. Clyburne and A. H. Cowley, *J. Chem. Soc., Chem. Commun.*, 61 (2001).

80. (a) R. H. Crabtree, *Angew. Chem.*, **105**, 828 (1993); *Angew. Chem. Int. Ed. Engl.*, **32**, 789 (1993). (b) G. J. Kubas, *Metal Dihydrogen and G-Bond Complexes*, Kluwer Academic/ Plenum Publ., New York, 2001.
81. (a) S. Li, M. B. Hall, J. Eckert, C. M. Jensen and A. Albinati, *J. Am. Chem. Soc.*, **122**, 2903 (2000). (b) D. M. Heinekey, H. Mellows and T. Pratum, *J. Am. Chem. Soc.*, **122**, 6498 (2000).
82. G. Suess-Fink, L. Plasserand, A. Maise-Francoir, H. Stoeckli-Evans, H. Berke, T. Fox, R. Gautier and J.-Y. Saillard, *J. Organomet. Chem.*, **609**, 196 (2000).
83. K. W. Zilm, D. M. Heinekey, J. M. Millar, N. G. Payne and P. Demou, *J. Am. Chem. Soc.*, **111**, 3088 (1989).
84. K. W. Zilm and J. M. Millar, *Adv. Magn. Opt. Reson.*, **15**, 163 (1990).
85. D. H. Jones, J. A. Labinger and D. P. Weitekamp, *J. Am. Chem. Soc.*, **111**, 3087 (1989).
86. K. Abdur-Rashid, T. P. Fong, B. Greaves, D. G. Gusev, J. G. Hinman, S. E. Landau, A. J. Lough and R. H. Morris, *J. Am. Chem. Soc.*, **122**, 9155 (2000).
87. A. D. Buckingham and P. J. Stephens, *J. Chem. Soc.*, 2747, 4583 (1964).
88. Y. Ohki and H. Suzuki, *Angew. Chem.*, **112**, 3250 (2000); *Angew. Chem. Int. Ed. Engl.*, **39**, 3120 (2000).
89. N. Koga and K. Morokuma, *J. Mol. Struct. (THEOCHEM)*, **300**, 181 (1993).
90. K. Kwetkat and W. Kitching, *J. Chem. Soc., Chem. Commun.*, 345 (1994).
91. D. C. Roe, *J. Magn. Res.*, **63**, 388 (1985).
92. R. Churland, U. Frey, F. Metz and A. E. Merbach, *Inorg. Chem.*, **39**, 4137 (2000).
93. R. Eisenberg, T. C. Eisenschmid, M. S. Chinn and R. W. Kiss, *Adv. Chem. Ser.*, **230**, 47 (1992).
94. J. Natterer and J. Bargon, *Progr. NMR Spectrosc.*, **31**, 293 (1997).
95. C. B. Duckett and C. J. Sleigh, *Progr. NMR Spectrosc.*, **34**, 71 (1999).
96. C. Ulrich, A. Permin, V. Petrosyan and J. Bargon, *Eur. J. Inorg. Chem.*, 889 (2000).
97. (a) Z. Xu and Z. Lin, *Coord. Chem. Rev.*, **156**, 139 (1996), and references cited therein. (b) S. L. J. Conway, L. H. Doerrer and M. L. H. Green, *Organometallics*, **19**, 630 (2000), and references cited therein.
98. P. Schollhammer, N. Cabon, F. Y. Petillon, J. Talarmin and K. W. Muir, *J. Chem. Soc., Chem. Commun.*, 2137 (2000).
99. G. I. Nikonov, L. G. Kuzima, S. F. Vyboishchikov, D. A. Lemenovskii and J. A. K. Howard, *Chem. Eur. J.*, **5**, 2947 (1999).
100. V. I. Bakhmutov, J. A. K. Howard, D. A. Keen, L. G. Kuzmina, M. A. Leech, G. I. Nikonov, E. V. Vorontsov and C. C. Wilson, *J. Chem. Soc., Dalton Trans.*, 1631 (2000).
101. D. M. Holton, P. P. Edwards, D. C. Johnson, C. J. Page, W. McFarlane and B. Wood, *J. Chem. Soc., Chem. Commun.*, 740 (1984).
102. M. L. Tinkham and J. L. Dye, *J. Am. Chem. Soc.*, **107**, 6129 (1985).
103. A.-M. Sapse and P. v. R. Schleyer (Eds), *Lithium Chemistry, a Theoretical and Experimental Overview*, Wiley, New York, 1995.
104. H. Günther, in *Advanced Applications of NMR to Organometallic Chemistry*, M. Gielen, R. Willem and B. Wrackmeyer (Eds), Physical Organometallic Chemistry, Vol. 1, Wiley, Chichester, UK, 1996, pp. 247–285.
105. W. Bauer, in *Lithium Chemistry, a Theoretical and Experimental Overview*, A.-M. Sapse and P. v. R. Schleyer (Eds), Wiley, New York, 1995, pp. 125–172.
106. W. Bauer and P. v. R. Schleyer, *Magn. Reson. Chem.*, **26**, 827 (1988).
107. H. Balzer and S. Berger, *Chem. Ber.*, **125**, 733 (1992).
108. A. Fuerstner, G. Seidel, H.-E. Mons and R. Mynott, *Eur. J. Inorg. Chem.*, 1771 (1998), and references cited therein.
109. G. Fraenkel, M. Henrichs, J. M. Hewitt, B. M. Su and M. J. Geckle, *J. Am. Chem. Soc.*, **102**, 3345 (1980).

110. D. Seebach, H. Siegel, J. Gabriel and R. Hässig, *Helv. Chim. Acta*, **63**, 2046 (1980).
111. (a) G. Fraenkel and P. Pramanik, *J. Chem. Soc., Chem. Commun.*, 1527 (1983). (b) R. D. Thomas, R. M. Jensen, T. C. Young, *Organometallics*, **6**, 565 (1987).
112. R. Hässig and D. Seebach, *Helv. Chim. Acta*, **66**, 2269 (1983).
113. D. Seebach, R. Hässig and J. Gabriel, *Helv. Chim. Acta*, **66**, 308 (1983).
114. W. Bauer, W. R. Winchester and P. v. R. Schleyer, *Organometallics*, **6**, 2371 (1987).
115. O. Eppers and H. Günther, *Tetrahedron Lett.*, **30**, 6155 (1989).
116. W. Bauer and C. Griesinger, *J. Am. Chem. Soc.*, **115**, 10871 (1993).
117. T. Rüffer, C. Bruhn, A. H. Maulitz, D. Ströhl and D. Steinborn, *Organometallics*, **19**, 2829 (2000).
118. A. Sebal, B. Wrackmeyer, C. R. Theocharis and W. Jones, *J. Chem. Soc., Dalton Trans.*, 747 (1984).
119. H. Nöth and B. Wrackmeyer, in *Nuclear Magnetic Resonance Spectroscopy of Boron Compounds*, P. Diehl, E. Fluck and R. Kosfeld (Eds), NMR—Basic Principles and Progress, Vol. 14, Springer-Verlag, Berlin, 1978.
120. B. Wrackmeyer and R. Köster, in *Analytik der Organobor-Verbindungen*, in R. Köster (Ed.), Houben-Weyl, Methoden der Organischen Chemie, Vol. XIII/3c, Thieme, Stuttgart, 1984, pp. 377–611.
121. B. Wrackmeyer, *Annu. Rep. NMR Spectrosc.*, **20**, 61 (1988).
122. J. D. Kennedy, in *Multinuclear NMR*, J. Mason (Ed.), Plenum Press, New York, 1987, pp. 221–258.
123. L. J. Todd and A. R. Siedle, *Progr. NMR Spectrosc.*, **13**, 87 (1979). (b) A. R. Siedle, *Annu. Rep. NMR Spectrosc.*, **20**, 205 (1988).
124. G. E. Herberich and X. Zheng, *Organometallics*, **19**, 3751 (2000).
125. B. Wrackmeyer, U. Dörfler, W. Milius and M. Herberhold, *Z. Naturforsch., B*, **50**, 201 (1995).
126. (a) W. Biffar, H. Nöth, *Z. Naturforsch., B*, **36**, 1509 (1981) (b) W. Biffar, H. Nöth, *Liebigs Ann. Chem.* 2067 (1981).
127. H. Noeth and H. Pommerening, *Chem. Ber.*, **114**, 3044 (1981).
128. W. Biffar and H. Nöth, H. Pommerening, *Angew. Chem.*, **92**, 63 (1980); *Angew. Chem. Int. Ed. Engl.*, **19**, 56 (1980).
129. K. Schlüter and A. Berndt, *Angew. Chem.*, **92**, 64 (1980); *Angew. Chem. Int. Ed. Engl.*, **19**, 57 (1980).
130. B. Wrackmeyer, O. L. Tok and Yu. N. Bubnov, *Angew. Chem.*, 1999 **111**, 214 (1999); *Angew. Chem. Int. Ed. Engl.*, **38**, 124 (1999).
131. S. J. Lancaster, S. Al-Benna, M. Thornton-Pett and M. Bochmann, *Organometallics*, **19**, 1599 (2000).
132. S. Sieber, P. Buzek, P. v. R. Schleyer, W. Koch and J. W. de M. Carneiro, *J. Am. Chem. Soc.*, **115**, 259 (1993), and literature cited therein.
133. A. Berndt, *Angew. Chem.*, **105**, 1034 (1993); *Angew. Chem. Int. Ed. Engl.*, **32**, 985 (1993).
134. H. Klusik and A. Berndt, *Angew. Chem.*, **95**, 895 (1983); *Angew. Chem. Int. Ed. Engl.*, **22**, 877 (1983).
135. H. Meyer, G. Baum, W. Massa, S. Berger and A. Berndt, *Angew. Chem.*, **99**, 559 (1987); *Angew. Chem. Int. Ed. Engl.*, **26**, 546 (1987).
136. B. Glaser and H. Nöth, *Angew. Chem.*, **97**, 424 (1985); *Angew. Chem. Int. Ed. Engl.*, **24**, 416 (1985).
137. (a) R. Boese, P. Paetzold and A. Tapper, *Chem. Ber.*, **120**, 1069 (1987). (b) R. Boese, P. Paetzold, A. Tapper and R. Ziembinski, *Chem. Ber.*, **122**, 1057. (c) A. Ziegler, H. Pritzkow and W. Siebert, *Eur. J. Inorg. Chem.*, 387 (2001).
138. R. E. Williams, *Chem. Rev.*, **92**, 177 (1992).
139. S. Hermanek, *Chem. Rev.*, **92**, 325 (1992).

140. T. L. Venable, T. L. Hutton and R. N. Grimes, *J. Am. Chem. Soc.*, **104**, 4716 (1982).
141. D. Reed, in *Encyclopedia of NMR*, Vol. 2, D. M. Grant and R. K. Harris (Eds), Wiley, Chichester, 1996, pp. 1002–1015.
142. B. H. Goodreau and J. T. Spencer, *Inorg. Chem.*, **31**, 2612 (1992).
143. M. Bühl, in *Encyclopedia of Computational Chemistry*, Vol. 3, P. v. R. Schleyer (Ed.), Wiley, Chichester, 1999, pp. 1835–1845.
144. W. Kutzelnigg, *Isr. J. Chem.*, **19**, 193 (1980).
145. M. Schindler and W. Kutzelnigg, *J. Chem. Phys.*, **76**, 1919 (1982).
146. W. Schindler and W. Kutzelnigg, *J. Am. Chem. Soc.*, **105**, 1360 (1983).
147. K. Wolinski, J. F. Hilton and P. Pulay, *J. Am. Chem. Soc.*, **112**, 8251 (1990).
148. M. Diaz, J. Jaballas, D. Tran, H. Lee, J. Arias and T. Onak, *Inorg. Chem.*, **35**, 4536 (1996); and references cited therein.
149. P. Jutzi and A. Seufert, *J. Organomet. Chem.*, **161**, 5 (1978).
150. P. Jutzi, A. Seufert and W. Buchner, *Chem. Ber.*, **112**, 2488 (1979).
151. C. Dohmeier, R. Köppe, Ch. Robl and H. Schnöckel, *J. Organomet. Chem.*, **487**, 127 (1995).
152. A. Voigt, S. Fillipponi, C. L. B. MacDonald, J. D. Gorden and A. H. Cowley, *J. Chem. Soc., Chem. Commun.*, 911 (2000).
153. M. M. Coneja, R. Fernández, E. Gutierrez-Puebla, A. Monge, C. Ruiz and E. Carmona, *Angew. Chem.*, **112**, 2025 (2000); *Angew. Chem. Int. Ed. Engl.*, **39**, 1949 (2000).
154. P. Greiwe, A. Bethäuser, H. Pritzkow, T. Kühler, P. Jutzi and W. Siebert, *Eur. J. Inorg. Chem.*, 1927 (2000).
155. K. Wade, *J. Chem. Soc., Chem. Commun.*, 792 (1971).
156. K. Wade, *Adv. Inorg. Chem. Radiochem.*, **18**, 1 (1976).
157. R. E. Williams, *Adv. Inorg. Chem. Radiochem.*, **18**, 67 (1976).
158. P. Paetzold, *Eur. J. Inorg. Chem.*, 143 (1998).
159. T. Davan and J. A. Morrison, *Inorg. Chem.*, **18**, 3194 (1979).
160. T. Mennekes, P. Paetzold, R. Boese and D. Bläser, *Angew. Chem.*, **103**, 199 (1991); *Angew. Chem. Int. Ed. Engl.*, **30**, 173 (1991).
161. T. Davan and J. A. Morrison, *J. Chem. Soc., Chem. Commun.*, 250 (1981).
162. P. Paetzold, *Angew. Chem.*, **109**, 2211 (1997); *Angew. Chem. Int. Ed. Engl.*, **36**, 2117 (1997).
163. W. Keller, W. Haubold and B. Wrackmeyer, *Magn. Reson. Chem.*, **37**, 545 (1999).
164. H. Wadepohl, U. Arnold and H. Pritzkow, *Angew. Chem.*, **109**, 1009 (1997); *Angew. Chem. Int. Ed. Engl.*, **36**, 974 (1997).
165. (a) H. Braunschweig, *Angew. Chem.*, **110**, 1882 (1998); *Angew. Chem. Int. Ed. Engl.*, **37**, 1787 (1998). (b) H. Braunschweig, M. Colling, C. Hu, K. Radacki, *Angew. Chem. Int. Ed. Engl.*, **41**, 1359 (2002).
166. G. J. Irvine, G. Lesley, T. B. Marder, N. C. Norman, R. C. Rice, E. G. Robins, W. R. Roper, G. R. Whitell and L. J. Wright, *Chem. Rev.*, **98**, 2685 (1998).
167. H. Braunschweig, *Angew. Chem.*, **110**, 3355 (1998); *Angew. Chem. Int. Ed. Engl.*, **37**, 3179 (1998).
168. A. H. Cowley, V. Lomeli and A. Voigt, *J. Am. Chem. Soc.*, **120**, 6491 (1998).
169. G. J. Irvine, C. E. F. Rickard, W. R. Roper, A. Williamson and L. J. Wright, *Angew. Chem.*, **112**, 978 (2000); *Angew. Chem. Int. Ed. Engl.*, **39**, 948 (2000).
170. H. Braunschweig and T. Wagner, *Angew. Chem.*, **107**, 904 (1995); *Angew. Chem. Int. Ed. Engl.*, **34**, 825 (1995).
171. H. Braunschweig and B. Ganter, *J. Organomet. Chem.*, **545**, 163 (1997).
172. H. Braunschweig and M. Müller, *Chem. Ber.*, **130**, 1295 (1997).

173. H. Braunschweig, C. Kollmann and K. W. Klinkhammer, *Eur. J. Inorg. Chem.*, 1523 (1999).
174. J. F. Hartwig, C. N. Mugoro, X. He, O. Eisenstein and R. Bosque and F. Maseras, *J. Am. Chem. Soc.*, **118**, 10936 (1996).
175. J. F. Hartwig and C. N. Muhoro, *Organometallics*, **19**, 30 (2000).
176. S. Schlecht and J. F. Hartwig, *J. Am. Chem. Soc.*, **122**, 9435 (2000).
177. M. Shimoi, S. Ikubo Y. Kawano, *J. Am. Chem. Soc.*, **120**, 4223 (1998).
178. Y. Kawano, T. Yasue and M. Shimoi, *J. Am. Chem. Soc.*, **121**, 11744 (1999).
179. M. Shimoi, S. Nagai, M. Ichikawa, Y. Kawano, K. Katoh, M. Uruichi and H. Ogino, *J. Am. Chem. Soc.*, **121**, 11704 (1999).
180. N. N. Greenwood, *Chem. Soc. Rev.*, **21**, 49 (1992).
181. A. K. Saxena, J. A. Maguire and N. S. Hosmane, *Chem. Rev.*, **97**, 2421 (1997), and references cited therein.
182. T. P. Fehlner, *Organometallics*, **19**, 2643 (2000).
183. X. Lei, M. Shang and T. P. Fehlner, *Organometallics*, **19**, 4429 (2000).
184. A. Blumenthal, H. Beruda and H. Schmidbaur, *J. Chem. Soc., Chem. Commun.*, 1005 (1993).
185. (a) R. Khattar, J. Puga, T. P. Fehlner and A. L. Rheingold, *J. Am. Chem. Soc.*, **111**, 1877 (1989). (b) K. S. Harpp, C. E. Housecroft, A. L. Rheingold and M. S. Shongwe, *J. Chem. Soc., Chem. Commun.*, 965 (1988). (c) F. E. Hong, T. J. Coffy, D. A. McCarthy and S. G. Shore, *Inorg. Chem.*, **28**, 3284 (1989). (d) For the interpretation of the ^{11}B nuclear deshielding, see R. Khattar, T. P. Fehlner and P. T. Czech, *New J. Chem.*, **15**, 705 (1991).
186. C. Dohmeier and D. Loos and H. Schnöckel, *Angew. Chem.*, **108**, 141 (1996); *Angew. Chem. Int. Ed. Engl.*, **35**, 129 (1996).
187. (a) D. Loos, E. Baum, A. Ecker, H.-G. Schnöckel and A. J. Downs, *Angew. Chem.*, **108**, 894 (1997); *Angew. Chem. Int. Ed. Engl.*, **36**, 860 (1997). (b) A. Haaland, K.-G. Martinsen, S. A. Shlykov, H. V. Volden, C. Dohmeier and H. Schnöckel, *Organometallics*, **14**, 3116 (1995).
188. J. D. Gorden, C. L. B. Macdonald and A. H. Cowley, *J. Chem. Soc., Chem. Commun.*, 75 (2001).
189. Q. Yu, A. Purath, A. Donchev and H.-G. Schnöckel, *J. Organomet. Chem.*, **584**, 94 (1999).
190. J. Weiss, D. Setzkamp, B. Nuber, R. A. Fischer, C. Boehme and G. Frenking, *Angew. Chem.*, **109**, 95 (1997); *Angew. Chem. Int. Ed. Engl.*, **36**, 70 (1997).
191. D. Weiss, T. Steinke, M. Winter, R. A. Fischer, N. Fröhlich, J. Uddin and G. Frenking, *Organometallics*, **19**, 4583 (2000).
192. P. Jutzi and N. Burford, *Chem. Rev.*, **99**, 969 (1999).
193. C. Dohmeier, H. Schnöckel, C. Robl, U. Schneider and R. Ahlrichs, *Angew. Chem.*, **105**, 1714 (1993); *Angew. Chem. Int. Ed. Engl.*, **32**, 1655 (1993).
194. U. Holtmann, P. Jutzi, T. Kühler, B. Neumann and H.-G. Stammer, *Organometallics*, **18**, 5531 (1999).
195. (a) C. T. Burns, D. S. Stelck, P. J. Shapiro, A. Vij, G. Kunz, G. Kehr, T. Concolino and A. L. Rheingold, *Organometallics*, **18**, 5432 (1999). (b) M. Bochmann and D. M. Dawson, *Angew. Chem.*, **108**, 2371 (1996); *Angew. Chem. Int. Ed. Engl.*, **35**, 2226 (1996).
196. (a) H. W. Kroto, J. R. Heath, S. C. O'Brien, R. F. Curl and R. E. Smalley, *Nature*, **318**, 162 (1985). (b) W. Krätschmer, L. D. Lamb, K. Fostiropoulos and D. R. Huffman, *Nature*, **347**, 354 (1990).
197. H. Ajie, M. A. Alvarez, S. J. Anz, F. Diederich, K. Fostiropoulos, D. R. Huffman, W. Krätschmer, Y. Rubin, K. E. Schriver, D. Sensharma and R. J. Whetton, *J. Phys. Chem.*, **94**, 8630 (1990).

198. (a) T. Sternfeld, R. E. Hoffman, I. Aprahamian and M. Rabinovitz, *Angew. Chem.*, **113**, 469 (2001); *Angew. Chem. Int. Ed. Engl.*, **40**, 455 (2001). (b) T. Akasaka, T. Wakahara, S. Nagese, K. Kobayashi, M. Waelchli, K. Yamamoto, M. Mondo, S. Shirakura, S. Okubo, Y. Maedo, T. Kato, M. Kako, Y. Nakadaira, R. Nagahato, X. Gao, E. Van Caemelbecke and K. M. Kadish, *J. Am. Chem. Soc.*, **122**, 9316 (2000), and references cited therein.
199. M. Saunders, H. A. Jimenez-Vazquez, R. J. Cross, S. Mroczkowski, D. I. Freedberg and F. A. L. Anet, *Nature*, **367**, 256 (1994).
200. (a) M. Saunders, H. A. Jimenez-Vazquez, B. W. Bangerter, R. J. Cross, S. Mroczkowski, D. I. Freedberg and F. A. L. Anet, *J. Am. Chem. Soc.*, **116**, 3621 (1994). (b) G.-W. Wang, M. Saunders and R. J. Cross, *J. Am. Chem. Soc.*, **123**, 256 (2001).
201. (a) R. E. Douthwaite, M. L. H. Green, A. H. H. Stephens and J. F. C. Turner, *J. Chem. Soc., Chem. Commun.*, 1522 (1993). (b) M. L. H. Green and A. H. H. Stephens, *J. Chem. Soc., Chem. Commun.*, 793 (1997). (c) L.-C. Song, J.-T. Liu, Q.-M. Hu and L.-H. Weng, *Organometallics*, **19**, 1643 (2000). (d) L.-C. Song, J. T. Liu, Q.-M. Hu, G.-F. Wang, P. Zanello and M. Fontani, *Organometallics*, **19**, 5342 (2000).
202. (a) G. A. Olah, P. W. Westerman and D. A. Forsyth, *J. Am. Chem. Soc.*, **97**, 3419 (1975). (b) G. A. Olah, A. L. Berrier and G. K. S. Prakash, *J. Org. Chem.*, **47**, 3903 (1982). (c) A. Mertens, M. Arvanaghi and G. A. Olah, *Chem. Ber.*, **116**, 3926 (1983). (d) G. A. Olah, A. Burrichter, T. Mathew, Y. D. Vankar, G. Rasul and G. K. S. Prakash, *Angew. Chem.*, **109**, 1958 (1997); *Angew. Chem. Int. Ed. Engl.*, **36**, 1875 (1997).
203. (a) B. Abarca, G. Asensio, R. Ballesteros and C. Luna, *Tetrahedron Lett.*, **27**, 5657 (1986). (b) L. Hevesi, S. Desauvage, B. Georges, G. Evard, P. Blaupain, A. Michel, S. Harkema and G. J. van Hummel, *J. Am. Chem. Soc.*, **106**, 3784 (1984). (c) J. E. McMurry, T. Lectka and C. N. Hodge, *J. Am. Chem. Soc.*, **111**, 8867 (1989).
204. H.-U. Siehl, T. Müller, J. Gauss, P. Buzek and P. v. R. Schleyer, *J. Am. Chem. Soc.*, **116**, 6384 (1994).
205. B. Spielvogel and J. M. Pursor, *J. Am. Chem. Soc.*, **93**, 4418 (1971).
206. H. Nöth and B. Wrackmeyer, *Chem. Ber.*, **107**, 3089 (1974).
207. B. Wrackmeyer and *Z. Naturforsch., B*, **25**, 430 (1980).
208. (a) A. A. Koridze, N. M. Astakhova and P. V. Petrovskii, *J. Organomet. Chem.*, **254**, 345 (1983). (b) M. A. Z. Kreindlin, F. M. Dolgushin, A. I. Yanovsky, Z. A. Kerzina, P. V. Petrovskii and M. I. Rybinskaya, *J. Organomet. Chem.*, **616**, 106 (2000), and references cited therein. (c) For similar interaction of Cr-C⁺, see M. Acompara, A. Ceccon, M. Dal Farra, G. Giacometti and G. Rigatti, *J. Chem. Soc., Perkin Trans 2*, 483 (1977). (d) For Co-C⁺ interactions, see R. Gleiter, H. Schimanne, S. J. Silverio, M. Büchner and G. Huttner, *Organometallics*, **15**, 5635 (1996). (e) For Mn-C⁺ interactions, see M. A. O. Volland, S. Kudis, G. Helmchen, I. Hyla-Kryspin, F. Rominger and R. Gleiter, *Organometallics*, **20**, 227 (2001).
209. B. Wrackmeyer, U. Dörfler, W. Milius and M. Herberhold, *Polyhedron*, **14**, 1425 (1995).
210. A. Appel, H. Nöth and M. Schmidt, *Chem. Ber.*, **128**, 621 (1995).
211. J. Casanova (Ed.), *The Borane, Carborane, Carbocation Continuum*, Wiley, New York, 1999.
212. H. Hogeveen and P. W. Quant, *Acc. Chem. Res.*, **8**, 413 (1975).
213. H. Hogeveen and E. M. G. A. van Kruchten, *J. Org. Chem.*, **46**, 1350 (1981).
214. (a) H. Willner, M. Bodenbinder, R. Bröchler, G. Hwang, S. J. Rettich, J. Trotter, B. von Ahsen, U. Westphal, V. Jonas, W. Thiel and F. Aubcke, *J. Am. Chem. Soc.*, **123**, 588 (2001). (b) T. Eguchi and B. T. Heaton, *J. Chem. Soc. Dalton Trans.*, 3523 (1999).
215. E. O. Fischer, G. Kreis, C. G. Kreiter, G. Huttner and H. Lorenz, *Angew. Chem.*, **85**, 618 (1973); *Angew. Chem. Int. Ed. Engl.*, **12**, 564 (1973).

216. M. A. Gallop and W. R. Roper, *Adv. Organomet. Chem.*, **25**, 121 (1986).
217. (a) F. Furno, T. Fox, H. W. Schmalke and H. Berke, *Organometallics*, **19**, 3620 (2000). (b) T. B. Wen, S.-Y. Yang, Z. Y. Zhou, Z. Lin, C.-P. Lau and G. Jia, *Organometallics*, **19**, 3757 (2000). (c) T. B. Wen, Y. K. Cheung, J. Yao, W.-T. Wong, Z. Y. Zhou and G. Jia, *Organometallics*, **19**, 3803 (2000). (d) R. Dembinski, S. Szafert, P. Haquette, T. Lis and J. A. Gladysz, *Organometallics*, **18**, 5438 (1999). (e) L. Zhang, M. P. Gamasa, J. Gimeno, M. F. C. Guedes da Silva, A. J. L. Pombeiro, C. Graiff, M. Lanfranchi and A. Tiripicchio, *Eur. J. Inorg. Chem.*, 1707 (2000). (f) J. N. Coalter, III, J. C. Bollinger, O. Eisenstein and K. G. Caulton, *New. J. Chem.*, **24**, 925 (2000). (g) T. B. Wen, Z. Y. Zhou and G. Jia, *Angew. Chem.*, **113**, 2005 (2001); *Angew. Chem. Int. Ed. Engl.*, **40**, 1951 (2001).
218. (a) U. Schubert (Ed.), *Advances in Metal Carbene Chemistry*, Kluwer Academic Publishers, Dordrecht, The Netherlands, 1989. (b) M. Schwarz, G. Kickelbick and U. Schubert, *Eur. J. Inorg. Chem.*, 1811 (2000).
219. L. S. Hegedus, in *Comprehensive Organometallic Chemistry II*, Vol. 12, E. W. Abel, G. Wilkinson and F. G. A. Stone (Eds), Pergamon Press, Oxford, UK, 1995, p. 549.
220. (a) M. A. Sierra, *Chem. Rev.*, **100**, 3591 (2000). (b) G. Bertrand (Ed.), *Transition Metal Complexes of Carbenes and Related Species in 2000*, *J. Organomet. Chem.*, **617-618**, 1-771 (2001).
221. T. Weskamp, V. P. W. Boehm and W. A. Herrmann, *J. Organomet. Chem.*, **600**, 12 (2000).
222. O. Guerret, S. Sole, H. Gornitzka, G. Trinquier and G. Bertrand, *J. Organomet. Chem.*, **600**, 112 (2000).
223. L. Xu, W. Chen, J. F. Bickley, A. Steiner and J. Xiao, *J. Organomet. Chem.*, **598**, 409 (2000).
224. D. Bourissou, O. Guerret, F. P. Gabbai and G. Bertrand, *Chem. Rev.*, **100**, 39 (2000).
225. M. I. Bruce, *Chem. Rev.*, **98**, 2797 (1998).
226. (a) H. Werner, K. Ilg and B. Weberndörfer, *Organometallics*, **19**, 3145 (2000). (b) K. Urtel, A. Frick, G. Huttner, L. Zsolnai, P. Kircher, P. Rutsch, E. Kaifer and A. Jacobi, *Eur. J. Inorg. Chem.*, 33 (2000). (c) G. Albertin, S. Antoniutti, E. Bordignon and D. Bresolin, *J. Organomet. Chem.*, **609**, 10 (2000).
227. D. Huang, W. E. Streib, O. Eisenstein and K. G. Caulton, *Organometallics*, **19**, 1967 (2000).
228. B. Bildstein, M. Schweiger, H. Angleitner, H. Kopacka, K. Wurst, K.-H. Ongania, M. Fontani and P. Zanello, *Organometallics*, **18**, 4286 (1999).
229. B. Bildstein, M. Schweiger, H. Angleitner, H. Kopacka, K.-H. Ongania and K. Wurst, *Organometallics*, **17**, 2414 (1998).
230. (a) S. Szafert, P. Haquette, S. B. Falloon and J. A. Gladysz, *J. Organomet. Chem.*, **604**, 52 (2000). (b) T. Bartik, B. Bartik, M. Brady, P. Dembinsky and J. A. Gladysz, *Angew. Chem.*, **108**, 467 (1996); *Angew. Chem. Int. Ed. Engl.*, **35**, 414 (1996).
231. K. Ilg and H. Werner, *Angew. Chem.*, **112**, 1691 (2000); *Angew. Chem. Int. Ed. Engl.*, **39**, 1632 (2000).
232. R. F. Winter, *Eur. J. Inorg. Chem.*, 2121 (1999).
233. M. Saoud, A. Romerosa and M. Peruzzini, *Organometallics*, **19**, 4005 (2000).
234. M.-C. Chung, A. Sakurai, M. Akita and Y. Moro-oka, *Organometallics*, **18**, 4684 (1999).
235. (a) A. Fuerstner, *Angew. Chem.*, **112**, 3140 (2000); *Angew. Chem. Int. Ed. Engl.*, **39**, 3012 (2000). (b) T. M. Trnka and R. H. Grubbs, *Acc. Chem. Res.*, **34**, 18 (2001).
236. M. Akita, M.-C. Chung, A. Sakurai and Y. Moro-oka, *J. Chem. Soc., Chem. Commun.*, 1285 (2000).

237. J. M. L. Martin and D. Milstein, *J. Am. Chem. Soc.*, **122**, 8797 (2000).
238. (a) M. Brookhart, M. L. H. Green and L.-L. Wong, *Progr. Inorg. Chem.*, **36**, 1 (1988). (b) S. A. Svejda, L. K. Johnson and M. Brookhart, *T. Am. Chem. Soc.*, **121**, 10634 (1999). (c) J. Gao, M.C. Jennings and R. J. Puddephat, *Organometallics*, **20**, 1882 (2001).
239. K. S. Cook, W. E. Piers, S. J. Rettig and R. McDonald, *Organometallics*, **19**, 2243 (2000).
240. J.-C. Hierso and M. Etienne, *Eur. J. Inorg. Chem.*, 839 (2000).
241. G. J. P. Britovesek, V. C. Gibson and D. F. Wass, *Angew. Chem.*, **111**, 448 (1999); *Angew. Chem. Int. Ed. Engl.*, **38**, 422 (1999).
242. H. G. Alt and A. Koepl, *Chem. Rev.*, **100**, 1205 (2000).
243. (a) G. Erker, T. Mühlenbrand, R. Benn, A. Rufinska, Y.-H. Tsay and C. Krüger, *Angew. Chem.*, **97**, 330 (1985); *Angew. Chem. Int. Ed. Engl.*, **24**, 330 (1985). (b) G. Erker, R. Nolte, C. Krueger, R. Schlund, R. Benn, H. Grondey and R. Mynott, *J. Organomet. Chem.*, **364**, 119 (1989).
244. D. Draga P. S. Pregosin and A. Razzavi, *Organometallics*, **19**, 1802 (2000).
245. H. G. Alt, M. Jung and G. Kehr, *J. Organomet. Chem.*, **562**, 153 (1998).
246. M. G. Klimpfel, W. A. Herrmann and R. Anwander, *Organometallics*, **19**, 4666 (2000).
247. J. E. Kickham, F. Guerin, J. C. Stewart and D. W. Stephan, *Angew. Chem.*, **112**, 3406 (2000); *Angew. Chem. Int. Ed. Engl.*, **39**, 3263 (2000).
248. (a) G. Erker, *Comments Inorg. Chem.*, **13**, 111 (1992). (b) P. Binger, F. Sandmeyer, C. Krüger, J. Kuhnigk, R. Goddard and G. Erker, *Angew. Chem.*, **106**, 213 (1994); *Angew. Chem. Int. Ed. Engl.*, **33**, 197 (1994).
249. S.-F. Hwang, Y. Chi, S.-J. Chiang, S.-M. Peng and G.-H. Lee, *Organometallics*, **20**, 215 (2001).
250. (a) R. Reina, O. Riba, O. Rossell, M. Seco, D. de Montanzon, M. A. Bellinghelli, A. Tripicchio, M. Font-Bordia and X. Solans, *J. Chem. Soc., Dalton Trans.*, 4464 (2000). (b) S. Martinuengo, D. Stramulo, P. Chini, V. G. Albano and D. Braga, *J. Chem. Soc., Dalton Trans.*, 35 (1985).
251. H. Schmidbaur, *Chem. Soc. Rev.*, 391 (1995).
252. E. Kupce and E. Lukevics, in *Isotopes in the Physical and Biomedical Sciences*, Vol. 2, E. Buncl and J. R. Jones (Eds), Elsevier, Amsterdam, 1991, pp. 213–295.
253. M. A. Brook, *Silicon in Organic, Organometallic and Polymer Chemistry*, Wiley, Chichester, 2000.
254. (a) B. Wrackmeyer, *Annu. Rep. NMR Spectrosc.*, **16**, 73 (1985). (b) B. Wrackmeyer, *Annu. Rep. NMR Spectrosc.*, **38**, 203 (1999).
255. J. D. Kennedy and W. McFarlane, in *Multinuclear NMR*, J. Mason (Ed.), Plenum Press, New York, 1987, pp. 305–333.
256. J. C. Martins, M. Biesemans and R. Willem, *Progr. NMR Spectrosc.*, **36**, 271 (2000).
257. (a) B. Wrackmeyer and K. Horchler, *Annu. Rep. NMR Spectrosc.*, **22**, 249 (1990). (b) B. Wrackmeyer, *Annu. Rep. NMR Spectrosc.*, 0000, 000 (2002).
258. B. Gehrhus, P. B. Hitchcock, M. F. Lappert, J. Heinicke, R. Boese and D. Blaeser, *J. Organomet. Chem.*, **521**, 211 (1996).
259. R. West and M. Denk, *Pure Appl. Chem.*, **68**, 785 (1996).
260. A. J. Arduengo III, H. V. Rasika Dias, R. L. Harlow and M. Kline, *J. Am. Chem. Soc.*, **114**, 5330 (1992).
261. (a) D. H. Harris and M. F. Lappert, *J. Chem. Soc., Chem. Commun.*, 895 (1974). (b) M. S. J. Gynane, D. H. Harris, M. F. Lappert, P. P. Power, P. Riviere and M. Riviere-Baudet, *J. Chem. Soc., Dalton Trans.*, 2004 (1977).

262. M. Veith, *Angew. Chem.*, **87**, 287 (1975); *Angew. Chem. Int. Ed. Engl.*, **14**, 263 (1975).
263. K. Horchler, C. Stader and B. Wrackmeyer, *Inorg. Chim. Acta*, **117**, L39 (1986).
264. (a) P. Jutzi, *Angew. Chem.*, **112**, 3953 (2000); *Angew. Chem. Int. Ed. Engl.*, **39**, 3797 (2000). (b) L. Pu, B. Twamley, S. T. Haubrich, M. M. Olstead, B. V. Mork, R. S. Simons and P. P. Power, *J. Am. Chem. Soc.*, **122**, 650 (2000). (c) U. Kobayashi, N. Tagaki and S. Nagase, *Organometallics*, **20**, 234 (2001).
265. P. J. Davidson and M. F. Lappert, *J. Chem. Soc., Chem. Commun.*, 317 (1973).
266. K. W. Zilm, G. A. Lawless, R. M. Merrill, J. M. Miller and G. G. Webb, *J. Am. Chem. Soc.*, **109**, 7236 (1987).
267. S. Masamune, Y. Eriyama and T. Kawase, *Angew. Chem.*, **99**, 601 (1987); *Angew. Chem. Int. Ed. Engl.*, **26**, 584 (1987).
268. C. Stader and B. Wrackmeyer, *Z. Naturforsch., B*, **42**, 1515 (1987).
269. M. Kira, R. Yauchibara, R. Hirano, C. Kabuto and H. Sakurai, *J. Am. Chem. Soc.*, **113**, 7785 (1991).
270. (a) C. Eaborn, M. S. Hill, P. B. Hitchcock, D. Patel, J. D. Smith and S. Zhang, *Organometallics*, **19**, 49 (2000). (b) C. Eaborn, T. Ganicz, P. B. Hitchcock, J. D. Smith and S. E. Sözerli, *Organometallics*, **16**, 5621 (1997).
271. L. Pu, P. Twamley and P. P. Power, *Organometallics*, **19**, 2874 (2000).
272. B. Wrackmeyer, C. Stader and K. Horchler, *J. Magn. Reson.*, **83**, 601 (1989).
273. B. E. Eichler and P. P. Power, *J. Am. Chem. Soc.*, **122**, 8785 (2000).
274. J. Escudie, H. Ranaivonjatovo and L. Rigon, *Chem. Rev.*, **100**, 3639 (2000), and references cited therein.
275. P. P. Power, *Chem. Rev.*, **99**, 3463 (1999), and references cited therein.
276. A. G. Brook and M. A. Brook, *Adv. Organomet. Chem.*, **39**, 71 (1996).
277. M. A. Chaubon, H. Ranaivonjatovo, J. Escudie and J. Satge, *Main Group Met. Chem.*, **19**, 145 (1996).
278. D. A. Strauss, S. D. Grumbine and T. D. Tilley, *J. Am. Chem. Soc.*, **112**, 7801 (1990).
279. S. D. Grumbine, T. D. Tilley and A. L. Rheingold, *J. Am. Chem. Soc.*, **115**, 358 (1993).
280. S. D. Grumbine, T. D. Tilley, F. P. Arnold and A. L. Rheingold, *J. Am. Chem. Soc.*, **115**, 7884 (1993).
281. S. K. Grumbine, T. D. Tilley, F. P. Arnold and A. L. Rheingold, *J. Am. Chem. Soc.*, **116**, 5495 (1994).
282. J. C. Peters, J. D. Feldman and T. D. Tilley, *J. Am. Chem. Soc.*, **121**, 9871 (1999).
283. P. W. Wanadi, P. B. Glaser and T. D. Tilley, *J. Am. Chem. Soc.*, **122**, 972 (2000).
284. M. Denk, R. K. Hayashi and R. West, *J. Chem. Soc., Chem. Commun.*, 33 (1994).
285. N. Metzler and M. Denk, *J. Chem. Soc., Chem. Commun.*, 23 (1996).
286. N. Metzler and M. Denk, *J. Chem. Soc., Chem. Commun.*, 2657 (1996).
287. (a) J. M. Dysard and T. D. Tilley, *Organometallics*, **19**, 4726 (2000). (b) D. H. Berry, J. H. Chey, H. S. Zipin and P. J. Carroll, *J. Am. Chem. Soc.*, **112**, 452 (1990).
288. M. Kira and T. Iwamoto, *J. Organomet. Chem.*, **611**, 236 (2000).
289. M. Kira, S. Ohya, T. Iwamoto and C. Kabuto, *Organometallics*, **19**, 1817 (2000).
290. H. Schumann, M. Glanz, F. Girgsdies, E. F. Hahn, M. Tamm and A. Grzegorski, *Angew. Chem.*, **109**, 2328 (1997); *Angew. Chem. Int. Ed. Engl.*, **36**, 2232 (1997).
291. A. Schäfer, M. Weidenbruch, W. Saak and S. Pohl, *J. Chem. Soc., Chem. Commun.*, 1157 (1995). (b) M. Weidenbruch, H. Kilian, M. Stürmann, S. Pohl, W. Saak, H. Marsmann, D. Steiner and A. Berndt, *J. Organomet. Chem.*, **530**, 255 (1997).

292. J. Escudie, C. Couret and H. Ranaivonjatovo, *Coord. Chem. Rev.*, **178–180**, 565 (1998).
293. M. F. Lappert and R. S. Rowe, *Coord. Chem. Rev.*, **100**, 267 (1990).
294. M. Veith and O. Recktenwald, *Topics Curr. Chem.*, **104**, 1 (1982).
295. W. Petz, *Chem. Rev.*, **86**, 1019 (1986).
296. J. J. Schneider, N. Czap, D. Bläser and R. Boese, *J. Am. Chem. Soc.*, **121**, 1409 (1999).
297. K. Angermund, K. Jones, C. Krüger, J. L. Latten and Y.-H. Tsay, *J. Organomet. Chem.*, **353**, 17 (1989).
298. D. Agustin, G. Rima, H. Gornitzka and J. Barrau, *Eur. J. Inorg. Chem.*, 693 (2000).
299. B. Gehrhus, P. B. Hitchcock and M. F. Lappert, *J. Chem. Soc., Dalton Trans.*, 3094 (2000).
300. A. Winkler, W. Bauer, F. W. Heinemann, V. Garcia-Montalvo, M. Moll and J. Ellermann, *Eur. J. Inorg. Chem.*, 437 (1998).
301. M. Veith, M. Opsölder, M. Zimmer and V. Huch, *Eur. J. Inorg. Chem.*, 1143 (2000).
302. N. Wiberg, H.-W. Lerner, S. Wagner, H. Nöth and T. Seifert, *Z. Naturforsch., B*, **54**, 877 (1999).
303. J. B. Lambert, L. Kania and S. Zhang, *Chem. Rev.*, **95**, 1191 (1995).
304. (a) C. A. Reed, *Acc. Chem. Res.*, **31**, 325 (1998). (b) G. A. Olah, G. Rasul and G. K. S. Prakash, *J. Am. Chem. Soc.*, **121**, 9615 (1999).
305. J. B. Lambert, Y. Zhao, H. Wu, C. Tse and B. Kuhlmann, *J. Am. Chem. Soc.*, **121**, 5001 (1999).
306. T. Nishinaga, Y. Izukawa and K. Komatsu, *J. Am. Chem. Soc.*, **122**, 9312 (2000).
307. (a) P. Jutzi and E.-A. Bunte, *Angew. Chem.*, **104**, 1636 (1992); *Angew. Chem. Int. Ed. Engl.*, **31**, 1605 (1992). (b) M. J. MacLachlan, S. C. Bourke, A. J. Lough and I. Manners, *J. Am. Chem. Soc.*, **122**, 2126 (2000).
308. I. Zharov, B. T. King, Z. Havlas, A. Pardi and J. Michel, *J. Am. Chem. Soc.*, **122**, 10253 (2000).
309. B. Wrackmeyer, G. Kehr and R. Boese, *Angew. Chem.*, **103**, 1374 (1991); *Angew. Chem. Int. Ed. Engl.*, **30**, 1370 (1991).
310. B. Wrackmeyer, S. Kundler and R. Boese, *Chem. Ber.*, **126**, 1361 (1993).
311. B. Wrackmeyer, K. Horchler and R. Boese, *Angew. Chem.*, **101**, 1563 (1989); *Angew. Chem. Int. Ed. Engl.*, **28**, 1500 (1989).
312. (a) H. Sakurai, H. Sakabo and Y. Nakadaira, *J. Am. Chem. Soc.*, **104**, 6156 (1982). (b) H. Sakurai, Y. Nakadaira, T. Koyama and H. Sakaba, *Chem. Lett*, 213 (1983).
313. M. J. van Eis, H. Zappey, F. J. J. de Kanter, W. H. de Wolf, K. Lammertsma and F. Bickelhaupt, *J. Am. Chem. Soc.*, **122**, 3386 (2000).
314. M. J. van Eis, C. M. D. Komen, F. J. J. de Kanter, W. H. de Wolf, K. Lammertsma, F. Bickelhaupt, M. Lutz and A. L. Spek, *Angew. Chem.*, **110**, 1656 (1998); *Angew. Chem. Int. Ed. Engl.*, **37**, 1547 (1998).
315. J. J. Schneider, *Angew. Chem.*, **108**, 1132 (1996); *Angew. Chem. Int. Ed. Engl.*, **35**, 1068 (1996).
316. U. Schubert, *Adv. Organomet. Chem.*, **30**, 151 (1990).
317. W. A. Herrmann, N. W. Huber and J. Behm, *Chem. Ber.*, **125**, 1405 (1992).
318. (a) X.-L. Luo, G. J. Kubas, C. J. Burns, J. C. Bryan and C. J. Unkefer, *J. Am. Chem. Soc.*, **117**, 1159 (1995). (b) Y.-J. Kim, S.-C. Lee, K. Osakada, J.-C. Choi and T. Yamamoto, *J. Chem. Soc., Dalton Trans.*, 417 (2000).
319. I. Atheaux, B. Donnadieux, V. Rodriguez, S. Sabo-Etienne, B. Chaudret, K. Hussein and J.-C. Barthelot, *J. Am. Chem. Soc.*, **122**, 5664 (2000).
320. L. Procopio, P. J. Carroll and D. H. Berry, *J. Am. Chem. Soc.*, **116**, 177 (1994).

321. A. Kawachi and K. Tamao, *J. Am. Chem. Soc.*, **122**, 1919 (2000).
322. (a) B. Wrackmeyer, B. Distler and M. Herberhold, *Z. Naturforsch., B*, **47**, 1749 (1992). (b) M. Herberhold, V. Tröbs, W. Milius and B. Wrackmeyer, *Z. Naturforsch., B*, **49** 1781 (1994).
323. (a) P. Kircher, G. Huttner and K. Heinze, *J. Organomet. Chem.*, **562**, 217 (1998). (b) B. Schiemenz, G. Huttner, L. Zsolnai, P. Kircher and T. Diercks, *Chem. Ber.*, **128**, 187 (1995).
324. P. Rutsch and G. Huttner, *Angew. Chem.*, **112**, 2187 (2000); *Angew. Chem. Int. Ed. Engl.*, **39**, 2118 (2000).
325. (a) P. Jutzi, D. Kanne and C. Krüger, *Angew. Chem.*, **98**, 163 (1986); *Angew. Chem. Int. Ed. Engl.*, **25**, 164 (1986). (b) P. Jutzi, U. Holtmann, D. Kanne, C. Krüger, R. Blom, R. Gleiter and I. Hyla-Kryspin, *Chem. Ber.*, **122**, 1629 (1989).
326. B. Wrackmeyer, A. Sebald and L. H. Merwin, *Magn. Reson. Chem.*, **29**, 260 (1991).
327. P. Jutzi, F. Kohl, P. Hofmann, C. Krüger and Y.-H. Tsay, *Chem. Ber.*, **113**, 757 (1980).
328. (a) B. Wrackmeyer and P. Bernatowicz, *Magn. Reson. Chem.*, **37**, 418 (1999). (b) B. Wrackmeyer and P. Bernatowicz, *J. Organomet. Chem.*, **579**, 133 (1999).
329. (a) B. Wrackmeyer, *J. Magn. Reson.*, **42**, 287 (1981). (b) B. Wrackmeyer and K. Horchler, *J. Magn. Reson.*, **90**, 569 (1990).
330. B. Wrackmeyer and K. Horchler, *Magn. Reson. Chem.*, **28**, 56 (1990).
331. M. Herberhold, C. Köhler, V. Tröbs and B. Wrackmeyer, *Z. Naturforsch., B*, **55**, 939 (2000).
332. M. Herberhold, V. Tröbs and B. Wrackmeyer, *J. Organomet. Chem.*, **541**, 391 (1997).
333. J. D., Kennedy, W. McFarlane and B. Wrackmeyer, *Inorg. Chem.*, **15**, 1299 (1976).
334. M. P. Waugh and G. A. Lawless, in *Advanced Applications of NMR to Organometallic Chemistry*, M. Gielen, R. Willem and B. Wrackmeyer (Eds), Physical Organometallic Chemistry, Vol. 1, Wiley, Chichester, 1996, pp. 227–245.
335. (a) S. Gaemers and C. J. Elsevier, *Magn. Reson. Chem.*, **38**, 650 (2000). (b) S. Gaemers, J. Groeneveld and C. J. Elsevier, *Eur. J. Inorg. Chem.*, 829 (2001).
336. G. J. Martin, M. L. Martin and J.-P. Gouesnard, *¹⁵N-NMR Spectroscopy, NMR—Basic Principles and Progress*, P. Diehl, E. Fluck and R. Kosfeld (Eds), Vol. 18, Springer, Berlin, 1981.
337. (a) M. Witanowski and G. A. Webb, *Nitrogen NMR*, Plenum Press, London, 1973. (b) M. Witanowski, L. Stefaniak and G. A. Webb, *Annu. Rep. NMR Spectrosc.*, **25**, 1 (1993).
338. J. Kroner, W. Schneid, N. Wiberg, B. Wrackmeyer and G. Ziegler, *J. Chem. Soc., Faraday Trans. 2*, **74**, 1909 (1978).
339. L.-O. Andersson, J. Mason and W. van Bronswijk, *J. Chem. Soc. (A)*, **296** (1970).
340. B. Wrackmeyer, K. Horchler, A. Sebald, L. H. Merwin and C. Ross, II, *Angew. Chem.*, **102**, 821 (1990); *Angew. Chem. Int. Ed. Engl.*, **29**, 807 (1990).
341. (a) K. O. Christe, W. W. Wilson, J. A. Sheehy and J. A. Boatz, *Angew. Chem.*, **111**, 2112 (1999); *Angew. Chem. Int. Ed. Engl.*, **38**, 2004 (1999). (b) K. O. Christe, W. W. Wilson, J. A. Sheehy, J. A. Boatz, *Angew. Chem.*, **113**, 3034 (2001).
342. (a) R. E. Mulvey, *Chem. Soc. Rev.*, **20**, 167 (1991). (b) R. E. Mulvey, *Chem. Soc. Rev.*, **27**, 339 (1998). (c) K. Gregory, P. v. R. Schleyer and R. Snaith, *Adv. Inorg. Chem.*, **37**, 47 (1991).
343. P. C. Andrews, P. J. Duggan, G. D. Fallon, T. D. McCarthy and A. C. Peatt, *J. Chem. Soc., Dalton Trans.*, 1937 (2000), and references cited therein.
344. (a) K. B. Aubrecht, B. J. Licht and D. B. Collum, *Organometallics*, **18**, 2981 (1999). (b) J. L. Rutherford and D. B. Collum, *J. Am. Chem. Soc.*, **123**, 199 (2001).
345. M. A. Nichols, D. Waldmüller and P. G. Williard, *J. Am. Chem. Soc.*, **116**, 1153 (1994).

346. E. Wiberg and A. Bolz, *Chem. Ber.*, **73**, 209 (1940). (b) E. Wiberg, *Naturwissenschaften*, **35**, 184 (1948).
347. H. Nöth, in *¹¹B- und ¹⁴N-NMR-Spektren von Bor-Stickstoff-Verbindungen mit freifach koordiniertem Bor*, K. Niedenzu (Ed.), Gmelin, 8. Auflage, Vol. 23/5, Springer, Berlin, 1975, pp. 197–277.
348. B. Wrackmeyer, *J. Magn. Reson.*, **54**, 174 (1983).
349. B. Wrackmeyer, *Z. Naturforsch., B*, **41**, 59 (1986).
350. B. Wrackmeyer, E. Kupce, R. Köster and G. Seidel, *Magn. Reson. Chem.*, **30**, 393 (1992).
351. H. Nöth and B. Wrackmeyer, *Chem. Ber.*, **107**, 3070 (1974).
352. W. Storch and H. Nöth, *Chem. Ber.*, **110**, 1636 (1977).
353. (a) B. Wrackmeyer, B. Schwarze and W. Milius, *Inorg. Chim. Acta*, **241**, 87 (1996). (b) B. Wrackmeyer, B. Schwarze, W. Milius, R. Boese, O. Parchment and G. A. Webb, *J. Organomet. Chem.*, **552**, 247 (1998).
354. P. Paetzold and C. von Plotho, *Chem. Ber.*, **115**, 2819 (1982).
355. H. Nöth, *Angew. Chem.*, **100**, 1664 (1988); *Angew. Chem. Int. Ed. Engl.*, **27**, 1603 (1988).
356. P. Paetzold, C. von Plotho, G. Schmid, R. Boese, B. Schrader, D. Bougeard, U. Pfeiffer, R. Gleiter and W. Schäfer, *Chem. Ber.*, **117**, 1089 (1984).
357. L. Schneider, U. Englert and P. Paetzold, *Chem. Ber.*, **127**, 87 (1994).
358. J. Müller, P. Paetzold, B. Steuer, W. Preetz and B. Wrackmeyer, *Z. Anorg. Allg. Chem.*, **625**, 2003 (1999).
359. F. De Sarlo, A. Brandi, A. Guarna and N. Niccolai, *J. Magn. Reson.*, **50**, 64 (1982).
360. M. P. Guy, J. L. Coffey, J. S. Rommel and D. W. Bennett, *Inorg. Chem.*, **27**, 2942 (1988).
361. W. Becker, W. Beck and R. Rieck, *Z. Naturforsch., B*, **25**, 1332 (1970).
362. B. Wrackmeyer and E. Kupce, *Z. Naturforsch., B*, **53**, 411 (1998).
363. E. Kupce and B. Wrackmeyer, *J. Magn. Reson.*, **97**, 568 (1992).
364. N. Logan, in *Nitrogen NMR*, M. Witanowski and G. A. Webb (Eds), Plenum Press, London, 1973, pp. 319–366.
365. N. J. Lazarowych, R. H. Morris and J. M. Ressler, *Inorg. Chem.*, **25**, 3926 (1986).
366. S. Donovan-Mtunzi, R. L. Richards and J. Mason, *J. Chem. Soc., Dalton Trans.*, 469 (1984).
367. D. T. Thorn, T. H. Tulip and J. A. Ibers, *J. Chem. Soc., Dalton Trans.*, 2022 (1979).
368. J. R. Dilworth, S. D. Donovan-Mtunzi, C. T. Kann, R. L. Richards and J. Mason, *Inorg. Chim. Acta*, **53**, L161 (1981).
369. S. Donovan-Mtunzi, R. L. Richards and J. Mason, *J. Chem. Soc., Dalton Trans.*, 2429 (1984).
370. S. N. Anderson, D. L. Hughes and R. L. Richards, *J. Chem. Soc., Chem. Commun.*, 1291 (1982).
371. (a) J. M. Manriquez, D. R. McAlister, E. Rosenberg, A. M. Shiller, K. L. Williamson, S. I. Chan and J. E. Bercaw, *J. Am. Chem. Soc.*, **100**, 3078 (1978). (b) S. Nielsen-Marsh, R. J. Crowte and P. G. Edwards, *J. Chem. Soc., Chem. Commun.*, **699** (1992).
372. T. Godemeyer, K. Dehnicke and E. Fluck, *Z. Anorg. Allg. Chem.*, **565**, 41 (1988).
373. B. L. Haymore, M. Hughes, J. Mason and R. L. Richards, *J. Chem. Soc., Dalton Trans.*, 2935 (1988).
374. (a) D. H. Evans, D. M. P. Mingos, J. Mason and A. Richards, *J. Organomet. Chem.*, **249**, 293 (1983). (b) L. K. Bell, J. Mason, D. M. P. Mingos and D. G. Tew, *Inorg. Chem.*, **22**, 3497 (1983). (c) R. E. Botto, B. W. S. Kolthammer, P. Legzdins and J. D. Roberts, *Inorg. Chem.*, **18**, 2049 (1979).

375. P. A. Duffin, L. F. Larkworthy, J. Maon, A. N. Stephens and R. M. Thompson, *Inorg. Chem.*, **26**, 2034 (1987).
376. S. Martinengo, G. Ciani, W. Sironi, B. Heaton and J. Mason, *J. Am. Chem. Soc.*, **101**, 7095 (1979).
377. (a) W. L. Gladfelter, *Adv. Organomet. Chem.*, **24**, 41 (1985). (b) M. L. Blohm and W. L. Gladfelter, *Inorg. Chem.*, **26**, 459 (1987).
378. M. M. Crutchfield, C. H. Dungan, L. H. Letcher, V. Mark and J. R. van Wazer, *Topics Phosphorus. Chem.*, **5**, 1 (1967).
379. G. D. Gorenstein, *Phosphorus-31 NMR: Principles and Applications*, Academic Press, New York, 1983.
380. J. C. Tebby (Ed.), *CRC Handbook of Phosphorus-31 Nuclear Magnetic Resonance Data*, CRC Press, Boca Raton, FL, 1991.
381. J. G. Verkade and L. D. Quin (Eds), *Phosphorus-31 NMR Spectroscopy in Stereochemical Analysis*, VCH, Weinheim, 1987.
382. L. D. Quin and J. G. Verkade (Eds), *Phosphorus 31 NMR Spectral Properties in Compound Characterization and Structural Analysis*, VCH, New York, 1994.
383. T. E. Gier, *J. Am. Chem. Soc.*, **83**, 1769 (1961).
384. M. Regitz, *Chem. Rev.*, **90**, 191 (1990).
385. M. Regitz, B. Breit and H. Memmesheimer, in *Phosphorus-31 NMR Spectral Properties in Compound Characterization and Structural Analysis*, L. D. Quin and J. G. Verkade (Eds), VCH, New York, 1994, pp. 147–158.
386. G. Becker, G. Gresser and W. Uhl, *Z. Naturforsch., B*, **36**, 16 (1981).
387. M. F. Meidine, A. J. L. Pombeiro and J. F. Nixon, *J. Chem. Soc., Dalton Trans.*, 3041 (1999).
388. P. Kramkowski and M. Scheer, *Eur. J. Inorg. Chem.*, 1869 (2000).
389. M. Regitz and O. J. Scherer, (eds), *Multiple Bonding and Low Coordination in Phosphorus Chemistry*, Thieme, Stuttgart, 1990.
390. H. S. Gutowsky and D. S. McCall, *J. Chem. Phys.*, **22**, 162 (1954).
391. G. Heckmann and E. Fluck, *Mol. Phys.*, **23**, 75 (1972).
392. G. Heckmann, H. Binder and D. Bongert, *Magn. Reson. Chem.*, **36**, 250 (1998).
393. G. Huttner, *J. Organomet. Chem.*, **308**, C11 (1986).
394. K. Eichele, R. E. Wasylshen, J. F. Corrigan, N. J. Taylor and A. J. Carty, *J. Am. Chem. Soc.*, **117**, 6961 (1995).
395. J. H. Yamamoto, L. Scoles, K. A. Udachin, G. D. Enright and A. J. Carty, *J. Organomet. Chem.*, **600**, 84 (2000).
396. G. Huttner, J. Borm and L. Zolnai, *J. Organomet. Chem.*, **263**, C33 (1984).
397. A. Schmidpeter and B. Wrackmeyer, *Z. Naturforsch., B*, **41** 553 (1986).
398. B. Wrackmeyer, *Z. Naturforsch., B*, **43**, 923 (1988).
399. (a) C. E. Laplaza, W. M. Davis and C. C. Cummins, *Angew. Chem.*, **107**, 2181 (1995); *Angew. Chem. Int. Ed. Engl.*, **34**, 2042 (1995). (b) N. C. Zanetti, R. R. Schrock and W. M. Davis, *Angew. Chem.*, **107**, 2182 (1995); *Angew. Chem. Int. Ed. Engl.*, **34**, 2044 (1995).
400. M. Scheer, *Coord. Chem. Rev.*, **163**, 271 (1997).
401. K. H. Whitmire, *Adv. Organomet. Chem.*, **42**, 2 (1998).
402. P. Kramkowski, G. Baum, U. Radius1 and M. Kaupp and M. Scheer, *Chem. Eur. J.*, **5**, 2890 (1999).
403. V. M. S. Gil and W. von Philipsborn, *Magn. Reson. Chem.*, **27**, 409 (1989).
404. (a) O. J. Scherer, *Acc. Chem. Res.*, **32**, 751 (1999). (b) J. Wachter, *Angew. Chem.*, **110**, 782 (1998); *Angew. Chem. Int. Ed. Engl.*, **37**, 750 (1998).
405. M. Di Vaira, M. P. Ehses, M. Peruzzini and P. Stoppioni, *Eur. J. Inorg. Chem.*, 2193 (2000).
406. H. C. Aspinall and D. C. Bradley, *J. Chem. Soc., Dalton Trans.*, 2211 (1988).

407. (a) J. E. Davies, M. J. Mays, P. R. Raithby, G. D. Shields, P. K. Tompkin and A. D. Woods, *J. Chem. Soc., Dalton Trans.*, 1925 (2000), and literature cited therein. (b) J. E. Davies, N. Feeder, M. J. Mays, P. K. Tompkin and A. D. Woods, *Organometallics*, **19**, 984 (2000).
408. O. J. Scherer, J. Schwalb, G. Wolmershäuser, W. Kaim and R. Groß *Angew. Chem.*, **98**, 349 (1986); *Angew. Chem. Int. Ed. Engl.*, **25**, 363 (1986).
409. O. J. Scherer, T. Brueck and G. Wolmershaeuser, *Chem. Ber.*, **121**, 935 (1988).
410. (a) M. Baudler, *Angew. Chem.*, **99**, 429 (1987); *Angew. Chem. Int. Ed. Engl.*, **26**, 419 (1987). (b) M. Baudler, D. Düster and D. Ouzoumis, *Z. Anorg. Allg. Chem.*, **544**, 87 (1987).
411. O. J. Scherer, *Angew. Chem.*, **97**, 358 (1985); *Angew. Chem. Int. Ed. Engl.*, **23**, 351 (1985).
412. O. J. Scherer, *Angew. Chem.*, **103**, 562 (1991); *Angew. Chem. Int. Ed. Engl.*, **30**, 553 (1991).
413. H. Schumann and G. M. Fritsch, *Z. Naturforsch., B*, **36**, 1244 (1981).
414. R. Hoffmann, *Angew. Chem.*, **94**, 725 (1982); *Angew. Chem. Int. Ed. Engl.*, **21**, 711 (1982).
415. F. G. A. Stone, *Angew. Chem.*, **96**, 85 (1984); *Angew. Chem. Int. Ed. Engl.*, **23**, 85 (1984).
416. K. B. Dillon, F. Mathey and J. F. Nixon, *Phosphorus, The Carbon Copy*, Wiley, Chichester, 1998.
417. K. Forissier, L. Ricard, D. Carmihael and F. Mathey, *J. Chem. Soc., Chem. Commun.*, 1273 (1999).
418. (a) F. G. N. Cloke, J. R. Hanks, P. B. Hitchcock and J. F. Nixon, *J. Chem. Soc., Chem. Commun.*, 1731 (1999). (b) J. J. Durkin, M. D. Francis, P. B. Hitchcock, C. Jones and J. F. Nixon, *J. Chem. Soc., Dalton Trans.*, 4057 (1999).
419. A. Elvers, F. W. Heinemann, B. Wrackmeyer and U. Zenneck, *Chem. Eur. J.*, **5**, 3143 (1999).
420. M. Driess, J. Aust, K. Merz and C. van Wüllen, *Angew. Chem.*, **111**, 3967 (1999); *Angew. Chem. Int. Ed. Engl.*, **38**, 3677 (1999).
421. H. Nakazawa, *J. Organomet. Chem.*, **611**, 349 (2000).
422. M. J. Bakker, F. W. Vergeer, F. Hartl, K. Goubitz, J. Fraanje, P. Rosa and P. L. Floch, *Eur. J. Inorg. Chem.*, 843 (2000).
423. M. Kaupp, *Chem. Ber.*, **129**, 535 (1996).
424. C. G. Barlow, D. L. Miller and R. A. Newmark, *Magn. Reson. Chem.*, **38**, 38 (2000).
425. M. Herberhold, K. Bauer and W. Milius, *Z. Anorg. Allg. Chem.*, **620**, 2198 (1994).
426. M. Herberhold, W. Milius and S. Eibl, *Z. Anorg. Allg. Chem.*, **625**, 341 (1999).
427. Yu. K. Grishin, V. A. Rozniatowsky, Yu. A. Ustyniuk, S. N. Tutova, G. A. Domrachev and G. A. Razuvaev, *Polyhedron*, **2**, 895 (1983).
428. M. Herberhold, U. Steffl, W. Milius and B. Wrackmeyer, *Angew. Chem.*, **109**, 1545 (1997); *Angew. Chem. Int. Ed. Engl.*, **36**, 1510 (1997).
429. M. Herberhold, U. Steffl, W. Milius and B. Wrackmeyer, *Chem. Eur. J.*, **4**, 1027 (1988).
430. Y. Tsuji and Y. Obora, *J. Organomet. Chem.*, **611**, 343 (2000).
431. T. Pechmann, C. D. Brandt and H. Werner, *Angew. Chem.*, **112**, 4069 (2000); *Angew. Chem. Int. Ed. Engl.*, **39**, 3909 (2000).
432. D. W. Boykin, (Ed.), *¹⁷O NMR Spectroscopy in Organic Chemistry*, CRC Press Uniscience, Boca Raton, FL, 1991.
433. W. McFarlane and H. C. E. McFarlane, in *Multinuclear NMR*, J. Mason (Ed.), Plenum Press, New York, 1987, pp. 403–416.
434. J. P. Kintzinger, in *NMR—Basic Principles and Progress*, Vol. 17, P. Diehl, E. Fluck and R. Kosfeld (Eds), Springer, Berlin, 1981, pp. 1–64.

435. T. J. Solomon, J. Kieth, A. J. Kacmarek and J. K. Ranay, *J. Am. Chem. Soc.*, **90**, 5408 (1968).
436. B. N. Figgis, R. S. Kidd and R. S. Nyholm, *Proc. R. Soc. London, A*, **269**, 469 (1962).
437. R. E. Wasylshen, S. Mooibroek and J. B. MacDonald, *J. Chem. Phys.*, **81**, 1057 (1984).
438. E. Block, A. A. Bazzi, J. B. Lambert, S. M. Wharry, K. K. Anderson, D. C. Dittmer, H. P. Bhalchandra and D. J. H. Smith, *J. Org. Chem.*, **45**, 4807 (1980).
439. E. Roversi, F. Monnat, K. Schenk, P. Vogel, P. Brana and J. A. Sordo, *Chem. Eur. J.*, **6**, 1858 (2000).
440. H. A. Christ and P. Diehl, *Helv. Phys. Acta*, **36**, 170 (1963).
441. (a) C. Delseith and J. P. Kintzinger, *Helv. Chim. Acta*, **59**, 466 (1976). (b) C. Delseith and J. P. Kintzinger, *Helv. Chim. Acta*, **59**, 1411 (1976).
442. W. Petz, B. Wrackmeyer and W. Storch, *Chem. Ber.*, **122**, 2261 (1989).
443. S. Onaka, T. Sugawara, Y. Kawada and H. Iwamura, *J. Chem. Soc., Dalton Trans.*, 257 (1982).
444. G. A. Olah, P. S. Iyer, G. K. S. Prakash and V. V. Krishnamurthy, *J. Org. Chem.*, **49**, 4317 (1984).
445. S. Aime, L. Milone, D. Osella, G. E. Hawkes and E. W. Randall, *J. Organomet. Chem.*, **178**, 171 (1979).
446. I. R. Lyatifov, T. K. Gasanov, P. V. Petrovski and A. I. Lutsenko, *J. Organomet. Chem.*, **361**, 181 (1989).
447. S. Onaka, S. Takagi, H. Furuta, Y. Kato and A. Mizuno, *Bull. Chem. Soc. Jpn*, **63**, 42 (1990).
448. W. Biffar, H. Nöth, H. Pommerening and B. Wrackmeyer, *Chem. Ber.*, **113**, 333 (1980).
449. B. Wrackmeyer and R. Köster, *Chem. Ber.*, **115**, 2022 (1982).
450. U. Scheim, K. Rühlmann, J. W. Kelly and S. A. Evans, *J. Organomet. Chem.*, **375**, 33 (1989).
451. M. Filowitz, W. G. Klemperer, L. Messerle and W. Shum, *J. Am. Chem. Soc.*, **98**, 2345 (1976). (b) M. Filowitz, R. K. C. Ho, W. G. Klemperer and W. Shum, *Inorg. Chem.*, **18**, 93 (1979).
452. C. Rodger, N. Sheppard, H. C. E. McFarlane and W. McFarlane, in *NMR and the Periodic Table*, R. K. Harris and B. E. Mann (Eds), Academic Press, London, 1978, pp. 383–419.
453. H. J. Kneuper, P. Härter and W. A. Herrmann, *J. Organomet. Chem.*, **340**, 353 (1988).
454. A. Roodt, J. G. Leipoldt, L. Helm and A. E. Merbach, *Inorg. Chem.*, **31**, 2864 (1992).
455. M. Postel, C. Brevard, H. Arzoumanian and J. G. Riess, *J. Am. Chem. Soc.*, **105**, 4922 (1983).
456. T. M. Klapötke and M. Broschag, *Compilation of Reported ⁷⁷Se NMR Chemical Shifts*, Wiley, Chichester, UK, 1996.
457. H. Dudgeck, *Progr. NMR Spectrosc.*, **27**, 1 (1995).
458. H. C. E. McFarlane and W. McFarlane, in *Multinuclear NMR*, J. Mason (Ed.), Plenum Press, New York, 1987, pp. 417–435.
459. C. R. Lassigne and E. J. Wells, *J. Chem. Soc., Chem. Commun.*, 956 (1978).
460. M. Mihoura, T. Kawashima and E. Okazaki, *J. Am. Chem. Soc.*, **115**, 7019 (1993).
461. N. Kuhn, G. Henkel and T. Kratz, *Chem. Ber.*, **126**, 2047 (1993).
462. T. Severengiz and W. W. du Mont, *J. Chem. Soc., Chem. Commun.*, 820 (1987).
463. F. R. Cullen, F. S. Guzic, C. J. Murphy, T. C. Wong and K. K. Anderson, *J. Am. Chem. Soc.*, **103**, 7055 (1981).

464. (a) H.C.E. McFarlane and W. McFarlane, *J. Chem. Soc., Dalton Trans.*, 2416 (1973). (b) G. A. Kalabin, R. B. Valeev and D. F. Kushnarev, *Zh. Org. Khim.*, **17**, 947 (1981).
465. W. W. Du Mont and H. J. Kroth, *Z. Naturforsch., B*, **36**, 332 (1981).
466. N. Fujihara, T. Uehara and N. Furukawa, *J. Am. Chem. Soc.*, **117**, 6388 (1995).
467. G. Pfisterer and H. Dreeskamp, *Ber. Bunsenges. Phys. Chem.*, **73**, 654 (1969).
468. G. J. Schrobilgen, R. C. Burns and P. Granger, *J. Chem. Soc., Chem. Commun.*, 957 (1978).
469. J. Jeske, W.-W. du Mont, F. Ruthe, P. G. Jones, L. M. Mercuri and P. Deplano, *Eur. J. Inorg. Chem.*, 1591 (2000).
470. (a) E. W. Abel, K. G. Orrell and A.W.G. Platt, *J. Chem. Soc., Dalton Trans.*, 2345 (1983). (b) E. W. Abel, K. G. Orrell, S. P. Scanlan, D. Stevenson, T. Kemmitt and W. Levason, *J. Chem. Soc., Dalton Trans.*, 591 (1991).
471. (a) W. Levason, S. D. Orchard and G. Reid, *J. Chem. Soc., Dalton Trans.*, 2537 (2000). (b) W. Levason, S. D. Orchard and G. Reid, *Inorg. Chem.*, **39**, 3853 (2000). (c) A. J. Barton, W. Levason, G. Reid, and V.-A. Tolhurst, *Polyhedron*, **19**, 235 (2000). (d) A. J. Barton, J. Conolly, W. Levason, A. Mendia-Jalon, S. D. Orchard and G. Reid, *Polyhedron*, **19**, 1373 (2000). (e) W. Levason, B. Patel, G. Reid and A. J. Ward, *J. Organomet. Chem.*, **619**, 218 (2001).
472. R. Koester, G. Seidel and B. Wrackmeyer, *Chem. Ber.*, **121**, 1955 (1988).
473. M. Herberhold, G.-X. Jin, H. Yan, W. Milius and B. Wrackmeyer, *J. Organomet. Chem.*, **587**, 252 (1999).
474. M. Herberhold, G.-X. Jin, H. Yan, W. Milius and B. Wrackmeyer, *Eur. J. Inorg. Chem.*, 873 (1999).
475. M. Herberhold, M. Keller, W. Kremnitz, T. Daniel, W. Milius, B. Wrackmeyer and H. Nöth, *Z. Anorg. Allg. Chem.*, **624**, 1324 (1998).
476. M. Herberhold, H. Yan, W. Milius and B. Wrackmeyer, *Organometallics*, **19** 4289 (2000).
477. (a) J. A. Connachie, M. A. Ansari and J. A. Ibers, *Inorg. Chem.*, **32**, 3250 (1993). (b) M. R. Lewtas, C. P. Morley and M. Di Vaira, *Polyhedron*, **19**, 751 (2000). (c) S. Nagao, H. Seino, T. Okada, Y. Mizobe and M. Hidai, *J. Chem. Soc., Dalton Trans.*, 3546 (2000).
478. (a) H. Kawaguchi and K. Tatsumi, *J. Chem. Soc., Chem. Commun.*, 1299 (2000). (b) R.W.M. Wardle, S. Bhaduri, C.-N. Chau and J. A. Ibers, *Inorg. Chem.*, **27**, 1747 (1988). (c) J. H. Shin and G. Parkin, *Organometallics*, **14**, 1104 (1995).
479. J. W. Emsley and L. Phillips, *Progr. NMR Spectrosc.*, **7**, 1 (1971).
480. J. W. Emsley, L. Phillips and V. Wray, *Progr. NMR Spectrosc.*, **10**, 85 (1977).
481. (a) V. Wray, *Annu. Rep. NMR Spectrosc.*, **10B**, 1 (1980). (b) V. Wray, *Annu. Rep. NMR Spectrosc.*, **14**, 1 (1983).
482. B. L. Pagenkopf and E. M. Carreira, *Chem. Eur. J.*, **5**, 3437 (1999).
483. R. O. Duthaler and A. Hafner, *Angew. Chem.*, **109**, 43 (1997); *Angew. Chem. Int. Ed. Engl.*, **36**, 43 (1997).
484. W. McFarlane, A. M. Noble and J. M. Winfield, *J. Chem. Soc. (A)*, 948 (1970).
485. J. Fawcett, G. A. Griffith, R. D. Peacock and D. R. Russell, *Polyhedron*, **7**, 2015 (1988).
486. (a) K. Sünkel, G. Urban and W. Beck, *J. Organomet. Chem.*, **252**, 187 (1983). (b) M. Appel and W. Beck, *J. Organomet. Chem.*, **319**, C1 (1987).
487. (a) R. V. Honeychuck and H. W. Hersh, *Inorg. Chem.*, **28**, 2869 (1989). (b) R. V. Honeychuck and H. W. Hersh, *J. Am. Chem. Soc.*, **111**, 6056 (1989).
488. N. LeBlond, H. P. A. Mercier, D. A. Dixon and G. J. Schrobilgen, *Inorg. Chem.*, **39**, 4449 (2000).
489. M. Gerken, D. A. Dixon and G. J. Schrobilgen, *Inorg. Chem.*, **39**, 4244 (2000).

490. S. M. Mullins, J. R. Hagadorn, R. G. Bergman and J. Arnold, *J. Organomet. Chem.*, **607**, 227 (2000).
491. C. I. Ratcliffe, *Annu. Rep. NMR Spectrosc.*, **36**, 124 (1998).
492. H.-J. Frohn, N. LeBlond, K. Lutar and B. Zemva, *Angew. Chem.*, **112**, 405 (2000); *Angew. Chem. Int. Ed. Engl.*, **39**, 391 (2000).
493. T. Pietrass, *Magn. Reson. Rev.*, **17**, 263 (2000).
494. J. M. Kneller, R. J. Solo, S. E. Surber, J.-F. Colomer, A. Fonseca, J. B. Nagy, G. Van Tenedlo and T. Pietrass, *J. Am. Chem. Soc.*, **122**, 10591 (2000).
495. T. Brotin, A. Lesage, L. Emsley and A. Collet, *J. Am. Chem. Soc.*, **122**, 1171 (2000).
496. P. S. Pregosin (Ed.), *Transition Metal Nuclear Magnetic Resonance*, Elsevier, Amsterdam, 1991.
497. D. Rehder, *Coord. Chem. Rev.*, **110**, 161 (1991).
498. R. Benn and A. Rufinska, *Angew. Chem.*, **25**, 861 (1986); *Angew. Chem. Int. Ed. Engl.*, **25**, 851 (1986).
499. W. von Philipsborn, *Chem. Soc. Rev.*, **28**, 95 (1999).
500. A. Foris, *Magn. Reson. Chem.*, **38**, 1044 (2000).
501. S. Kleinhenz and K. Sepelt, *Chem. Eur. J.*, **5**, 3573 (1999).
502. A. Hafner, L. S. Hegedus, G. deWeck, B. Hawkins and K. H. Dötz, *J. Am. Chem. Soc.*, **110**, 8413 (1988).
503. K. D. Behringer and J. Bluemel, *Magn. Reson. Chem.*, **33**, 729 (1995).
504. B. G. Sayer, J. I. A. Thompson, H. Nguyen, T. Birchall, D. R. Eaton and M. J. McGlinchey, *Inorg. Chem.*, **20**, 3748 (1981).
505. P. Bougeard, J. J. McCullough, B. G. Sayer and M. J. McGlinchey, *Inorg. Chim. Acta*, **89**, 133 (1984).
506. R. Benn and A. Rufinska, *J. Organomet. Chem.*, **273**, C51 (1984).
507. H. Brunner, G. Gehart, W. Meier, J. Wachter, B. Wrackmeyer, B. Nuber and M. L. Ziegler, *J. Organomet. Chem.*, **436**, 313 (1992).
508. D. Rehder and D. Rodewald, in *Advanced Applications of NMR to Organometallic Chemistry*, M. Gielen, R. Willem and B. Wrackmeyer (Eds), Physical Organometallic Chemistry, Vol. 1, Wiley, Chichester, 1996, pp. 291–311.
509. M. Herberhold, W. Kremnitz and M. Kuhnlein, *Z. Naturforsch., B*, **42**, 1520 (1987).
510. M. Herberhold, M. Kuhnlein, M. L. Ziegler and B. Nuber, *J. Organomet. Chem.*, **349**, 131 (1988). (b) M. Herberhold, M. Kuhnlein, M. Schrepfermann, M. L. Ziegler and B. Nuber, *J. Organomet. Chem.*, **398**, 259 (1990). (c) M. Herberhold and M. Schrepfermann, *J. Organomet. Chem.*, **419**, 85 (1991).
511. M. Herberhold and M. Schrepfermann, *J. Organomet. Chem.*, **458**, 19 (1993).
512. M. Herberhold, G. Frohmader and W. Milius, *J. Organomet. Chem.*, **522**, 185 (1996).
513. F. Preuss and F. Tabellion, *Z. Naturforsch., B*, **55**, 735 (2000).
514. (a) M. Minelli, J. H. Enemark, R. C. Brownlee, M. J. O'Connor and A. G. Wedd, *Coord. Chem. Rev.*, **68**, 169 (1985). (b) J. Malito, *Annu. Rep. NMR Spectrosc.*, **33**, 151 (1997).
515. C. Brevard and R. Thouvenot, in *Transition Metal Nuclear Magnetic Resonance*, P. S. Pregosin (Ed.), Elsevier, Amsterdam, 1991, pp. 82–89.
516. M. Minelli, J. L. Hubbard, D. L. Lichtenberger and J. H. Enemark, *Inorg. Chem.*, **23**, 2721 (1984).
517. C. G. Young, M. Minelli, J. H. Enemark, W. Hussain, C. J. Jones and J. A. McCleverty, *J. Chem. Soc., Dalton Trans.*, 619 (1987).
518. O. A. Kholdeeva, G. M. Maksimov, R. I. Maksimovskaya, L. A. Kovaleva, M. A. Fedotov, V. A. Grigoriev and C. L. Hill, *Inorg. Chem.*, **39**, 3828 (2000).
519. Z.-G. Sun, Q. Liu and J.-F. Liu, *Polyhedron*, **19**, 125 (2000).

520. (a) M. M. Caldeira, M. L. Ramos, G. G. Pereire and V. M. S. Gil, *Polyhedron*, **19**, 193 (2000).
521. R. J. Errington, R. L. Wingad, W. Clegg and M. R. J. Elsegood, *Angew. Chem.*, **112**, 4042 (2000); *Angew. Chem. Int. Ed. Engl.*, **39**, 3884 (2000).
522. X.-H. Wang, J.-F. Liu, Y.-G. Chen, Q. Liu, J.-T. Liu and M. T. Pope, *J. Chem. Soc., Dalton Trans.*, 1139 (2000).
523. (a) H. C. E. McFarlane, W. McFarlane and D. S. Rycroft, *J. Chem. Soc., Dalton Trans.*, 1616 (1976). (b) W. McFarlane, A. M. Noble and J. M. Winfield, *J. Chem. Soc. (A)*, 948 (1971).
524. (a) R. Benn, H. Brennecke, J. Heck and A. Rufinska, *Inorg. Chem.*, **26**, 2826 (1987). (b) R. Benn and A. Rufinska, *Magn. Reson. Chem.*, **26**, 895 (1988).
525. B. Wrackmeyer, H. G. Alt and H. E. Maisel, *J. Organomet. Chem.*, **399**, 125 (1990).
526. R. Benn, A. Rufinska, M. A. King, C. E. Osterberg and T. G. Richmond, *J. Organomet. Chem.*, **376**, 359 (1989).
527. (a) B. Wrackmeyer, T. Hofmann and M. Herberhold, *J. Organomet. Chem.*, **486**, 255 (1995). (b) M. Herberhold, T. Hofmann, S. Weinberger and B. Wrackmeyer, *Z. Naturforsch., B*, **52**, 1037 (1997).
528. (a) M. Findeisen, L. Kaden, B. Lorenz and M. Wahren, *Inorg. Chim. Acta*, **142**, L15 (1987). (b) M. Findeisen, L. Kaden, B. Lorenz and M. Wahren, *Inorg. Chim. Acta*, **142**, 3 (1987).
529. (a) M. J. Buckingham, G. E. Hawkes and J. R. Thornback, *Inorg. Chim. Acta*, **56**, L41 (1981). (b) J. Vanderheyden, A. R. Ketring, K. Libson, M. J. Heeg, L. Roecker, P. Motz, R. Whittle, R. C. Elder and D. Deutsch, *Inorg. Chem.*, **23**, 3184 (1984).
530. N. Aebischer, R. Schibli, R. Alberto and A. E. Merbach, *Angew. Chem.*, **112**, 260 (2000); *Angew. Chem. Int. Ed. Engl.*, **39**, 250 (2000).
531. R. Benn, in *Transition Metal Nuclear Magnetic Resonance*, P. S. Pregosin (Ed.), Elsevier, Amsterdam, 1991, pp. 103–142.
532. (a) T. Nozawa, M. Sato, M. Hatano, N. Kobayashi and T. Osa, *Chem. Lett.*, 1289 (1983). (b) H. C. Lee, J. K. Gard, T. L. Brown and E. Oldfield, *J. Am. Chem. Soc.*, **107**, 4087 (1985).
533. (a) C. G. Kalodimos, I. P. Gerothanassis, R. Pieratelli and A. Troganis, *J. Inorg. Biochem.*, **38**, 520 (2000). (b) C. G. Kalodimos, I. P. Gerothanassis, E. Rose, G. E. Hawkes and R. Pieratelli, *J. Am. Chem. Soc.*, **121**, 2903 (1999).
534. A. A. Koridze, P. V. Petrovskii, S. P. Gubin and E. I. Fedin, *J. Organomet. Chem.*, **93**, C26 (1975).
535. R. Benn, H. Brennecke, A. Frings, H. Lehmkuhl, G. Mehler, A. Rufinska and T. Wildt, *J. Am. Chem. Soc.*, **110**, 5661 (1988).
536. (a) W. von Philipsborn, *Pure Appl. Chem.*, **58**, 513 (1986). (b) T. Jenny, W. von Philipsborn, J. Kronenbitter and A. Schwenk, *J. Organomet. Chem.*, **205**, 211 (1981). (c) E. J. M. Meier, W. Kozmiński, A. Linden, P. Lustenberger and W. von Philipsborn, *Organometallics*, **15**, 2469 (1996).
537. (a) E. Haslinger, W. Robien, K. Schlögl and W. Weissensteiner, *J. Organomet. Chem.*, **218**, C11 (1981). (b) E. Haslinger, K. Koci, W. Robien and K. Schlögl, *Monatsh. Chem.*, **114**, 495 (1983).
538. R. Benn, A. Rufinska, M. S. Kralik and R. D. Ernst, *J. Organomet. Chem.*, **375**, 115 (1989).
539. L. Baltzer, E. D. Becker, B. A. Averill, J. M. Hutchinson and O. A. Gansow, *J. Am. Chem. Soc.*, **106**, 2444 (1984).
540. B. Wrackmeyer, A. Ayazi, H. E. Maisel and M. Herberhold, *J. Organomet. Chem.*, **630**, 263 (2001).
541. B. Wrackmeyer, H. E. Maisel, M. Herberhold, *Z. Naturforsch., B.*, **56**, 1373 (2001).

542. W. Kozminski and K. Jackowski, *Magn. Reson. Chem.*, **38**, 459 (2000), and references cited therein.
543. (a) C. Brevard and P. Granger, *J. Chem. Phys.*, **75**, 4175 (1981). (b) C. Brevard and P. Granger, *Inorg. Chem.*, **22**, 532 (1983).
544. M. Buehl, S. Gaemers and C. J. Elsevier, *Chem. Eur. J.*, **6**, 3272 (2000).
545. C. Janiak, T. Dorn, H. Paulsen and B. Wrackmeyer, *Z. Anorg. Allg. Chem.*, **627**, 1663 (2001).
546. (a) R. Benn, H. Brenneke, E. Jousen, H. Lehmkuhl and F. Lopez Ortiz, *Organometallics*, **9**, 756 (1990). (b) R. Benn, E. Jousen, H. Lehmkuhl, F. Lopez Ortiz and A. Rufinska, *J. Am. Chem. Soc.*, **111**, 8754 (1989).
547. J. C. C. Chan and S. C. F. Au-Yeung, *Annu. Rep. NMR Spectrosc.*, **41**, 1 (2000).
548. B. Mann and P. S. Pregosin, in *Transition Metal Nuclear Magnetic Resonance*, P. S. Pregosin (Ed.), Elsevier, Amsterdam, 1991, pp. 143–215. (b) P. Granger, in *Advanced Applications of NMR to Organometallic Chemistry*, M. Gielen, R. Willem and B. Wrackmeyer (Eds), Physical Organometallic Chemistry, Vol. 1, Wiley, Chichester, UK, 1996, pp. 313–356.
549. F. Asaro, L. Liguori and G. Pellizer, *Angew. Chem.*, **112**, 2068 (2000); *Angew. Chem. Int. Ed. Engl.*, **39**, 1932 (2000).
550. C. Sizum, P. Kempgens, J. Raya, K. Elbayed, P. Granger and J. Rose, *J. Organomet. Chem.*, **604**, 27 (2000).
551. U. E. Bucher, T. Lengweiler, D. Nanz, W. von Philipsborn and L. M. Venanzi, *Angew. Chem.*, **102**, 573 (1990); *Angew. Chem. Int. Ed. Engl.*, **29**, 548 (1990).
552. M. Herberhold, St. Eibl, W. Milius and B. Wrackmeyer, *Z. Anorg. Allg. Chem.*, **626**, 552 (2000).
553. L. Carlton, *Inorg. Chem.*, **39**, 4510 (2000).
554. M. Bühl, M. Hakansson, A. H. Mahmoudkhani and L. Öström, *Organometallics*, **19**, 5589 (2000).
555. S. Kameda, M. Lutz, A. L. Spek, M. Chikuma and J. Reedijk, *Inorg. Chem.*, **39**, 4230 (2000).
556. P. S. Pregosin, in *Transition Metal Nuclear Magnetic Resonance*, P. S. Pregosin (Ed.), Elsevier, Amsterdam, 1991, pp. 217–263.
557. P. S. Pregosin, *Coord. Chem. Rev.*, **44**, 247 (1982).
558. P. S. Pregosin, *Annu. Rep. NMR Spectrosc.*, **17**, 285 (1986).
559. Q. Xu, B. T. Heaton, C. Jacob, K. Mogi, Y. Ichibashi, Y. Souma, K. Kanamori and T. Eguchi, *J. Am. Chem. Soc.*, **122**, 6862 (2000).
560. N. M. Boag, P. L. Goggin, R. J. Goodfellow and J. R. Herbert, *J. Chem. Soc., Dalton Trans.*, 1101 (1983).
561. N. M. Boag, J. Browning, C. Crocker, P. L. Goggin, R. J. Goodfellow, M. Murray and J. L. Spencer, *J. Chem. Res. (M)*, 2962 (1978).
562. (a) S. Cristofani, P. Leoni, M. Pasquali, F. Eisentraeger and A. Albinati, *Organometallics*, **19**, 4589 (2000). (b) P. Mastroilli, M. Palma, F. P. Fanizzi and C. F. Nobile, *J. Chem. Soc., Dalton Trans.*, 4272 (2000).
563. (a) J. Jans, R. Naegeli, L. M. Venanzi and A. Albinati, *J. Organomet. Chem.*, **247**, C37 (1983). (b) A. R. Siedle, R. A. Newmark and W. B. Gleason, *J. Am. Chem. Soc.*, **108**, 767 (1986).
564. A. L. Bandini, G. Banditelli and G. Minghetti, *J. Organomet. Chem.*, **595**, 224 (2000).
565. (a) G. Uccello-Barretta, R. Bernardini, R. Lazzaroni and P. Salvadori, *J. Organomet. Chem.*, **598**, 174 (2000). (b) G. Uccello-Barretta, R. Bernardini, F. Balzano, R. Lazzaroni and P. Salvadori, *J. Organomet. Chem.*, **605**, 68 (2000).
566. L. M. Sanow, M. Chai, D. B. McConnville, K. J. Galat, R. S. Simons, P. L. Rinaldi, W. J. Youngs and C. A. Tessier, *Organometallics*, **19**, 192 (2000).

567. P. J. Heard, K. Kite, J. S. Nielson and D. A. Tocher, *J. Chem. Soc., Dalton Trans.*, 1349 (2000).
568. M. Maliarik, K. Berg, J. Glaser, M. Sandström and I. Toth, *Inorg. Chem.*, **37**, 2910 (1998).
569. J. Malito, *Annu. Rep. NMR Spectrosc.*, **38**, 265 (1999).
570. S. Kitigawa and M. Munakata, *Inorg. Chem.*, **23**, 4388 (1984).
571. H. Brunner, D. Mijolovic, B. Wrackmeyer and B. Nuber, *J. Organomet. Chem.*, **579**, 298 (1999).
572. S. S. D. Brown, I. J. Colquhoun, W. McFarlane, M. Murray, I. D. Salter and V. Sik, *J. Chem. Soc., Chem. Commun.*, 53 (1986).
573. (a) L. J. Farrugia, *J. Chem. Soc., Chem. Commun.*, 147 (1987).
574. P. Granger, in *Transition Metal Nuclear Magnetic Resonance*, P. S. Pregosin (Ed.), Elsevier, Amsterdam, 1991, pp. 264–346.
575. B. Wrackmeyer and R. Contreras, *Annu. Rep. NMR Spectrosc.*, **24**, 267 (1992).
576. A. Castineiras, I. Garcia, E. Bermejo and D. X. West, *Polyhedron*, **19**, 873 (2000).
577. A. J. Arduengo, III, J. R. Goerlich, F. Davidson and W. J. Marshall, *Z. Naturforsch., B*, **54**, 1350 (1999).
578. R. J. Gillespie, P. Granger, K. R. Morgan and G. J. Schrobilgen, *Inorg. Chem.*, **23**, 887 (1984).
579. R. Malleier, H. Kopacka, W. Schuh, K. Wurst and P. Peringer, *J. Chem. Soc., Chem. Commun.*, 51 (2001).
580. T. N. Mitchell, *J. Organomet. Chem.*, **471**, 39 (1994).
581. H. Windisch, J. Scholz, R. Taube and B. Wrackmeyer, *J. Organomet. Chem.*, **520**, 23 (1996).
582. J. M. Keates and G. A. Lawless, in *Advanced Applications of NMR to Organometallic Chemistry*, M. Gielen, R. Willem and B. Wrackmeyer (Eds), Physical Organometallic Chemistry, Vol. 1, Wiley, Chichester, UK, 1996, pp. 357–370.
583. M. Kaupp, V. G. Malkin and O. L. Malkina, in *Encyclopedia of Computational Chemistry*, Vol. 3, P.v.R. Schleyer (Ed.), Wiley, Chichester, UK, 1999, pp. 1857–1865.
584. G. Schreckenbach, *J. Chem. Phys.*, **110**, 11936 (1999).
585. (a) P. Geissler, T. M. Klapötke and H. J. Kroth, *Spectrochim. Acta, A*, **51**, 1075 (1995). (b) A. E. Ayers, T. M. Klapötke and H.V.R. Dias, *Inorg. Chem.*, **40**, 1000 (2001).
586. (a) G. J. Pindado, M. Thornton-Pett and M. Bochmann, *J. Chem. Soc., Dalton Trans.*, 3115 (1997). (b) T. J. Woodman, M. Thornton-Pett and M. Bochmann, *J. Chem. Soc., Chem. Commun.*, 329 (2001).
587. Y. Ruiz, G. Schreckenbach and T. Ziegler, *J. Phys. Chem.*, **100**, 3359 (1996).
588. S. Brooker, J. K. Buijink and F. T. Edelmann, *Organometallics*, **10**, 25 (1991).
589. N. Tokitoh, N. Kano, K. Shibata and R. Okazaki, *Organometallics*, **14**, 3121 (1995).
590. R. S. Simons, L. Pu, M. M. Olmstead and P. P. Power, *Organometallics*, **16**, 1920 (1997).

3 Deuterium Spin–Lattice Relaxation and Deuterium Quadrupole Coupling Constants. A Novel Strategy for Characterization of Transition Metal Hydrides and Dihydrogen Complexes in Solution

VLADIMIR I. BAKHMUTOV†

Institute of Organo-Element Compounds of Russian Academy of Sciences, 28 Vavilova, Moscow 117813, Russia, and Departamento de Química, Centro de Investigación y de Estudios Avanzados del IPN, AP 14-740 Mexico, DF 07000 Mexico

1 INTRODUCTION. HYDRIDE LIGANDS FROM A CONCEPT OF PROTONS BURIED IN METAL ORBITALS TO HYDRIDES SHOWING QUANTUM MECHANICAL BEHAVIOUR

Transition metal hydride complexes represent one of the most important classes of organometallic compounds which play a great role in modern fundamental and practical chemistry [1,2]. This circumstance is explained by the high reactivity of the M–H bonds. In addition, metal hydrides often possess catalytic activity in homogeneous hydrogenations. Since the discovery of dihydrogen complexes [3–5] with H₂, binding to a metal atom in the η^2 -fashion, the chemistry of transition metal hydrides has undergone a renaissance due to the emergence of new ideas about the nature of the metal–hydride bonding. In this context, it is of great interest to review briefly the historic development of structural hydride chemistry [1].

One of most important aspects in structural formulations of transition metal hydride complexes is the correct localization of the hydride ligands. This well-known problem of determination of coordinates for a small hydride atom, binding to a heavy metal center, has played a dramatic role in the development of theoretical concepts and representations about the nature of M–H bonds.

†Present address: Department of Chemistry, Texas A & M University, PO Box 30012, College Station, TX 77842-3012, USA.

These concepts have changed dramatically due to the accumulation of new experimental data and the appearance of new experimental techniques.

Among the transition metal hydrides, the first molecular structure was reported by Ewens and Lister for the gaseous hydride complex $\text{CoH}(\text{CO})_4$ in 1939 [6]. According to electron diffraction experiments, the metal center was surrounded by a tetrahedron of carbons and thus the non-located hydrogen atom *exerted no stereochemical perturbation*. Nevertheless numerous studies in hydride chemistry had already revealed the presence of hydrogen binding to metals. In this connection, Hieber suggested the idea that H atoms in metal hydrides act *as protons buried in the metal orbitals* [7]. This idea was supported experimentally, for example, by ^1H NMR of the complex ReHCp_2 . The latter showed a hydride signal in an unusual high field [8]. In addition, LCAO calculations of $\text{CoH}(\text{CO})_4$ led to an unusually short Co–H distance of 1.2 Å [9].

It seems surprising now that Hieber's idea (about the presence of some H-delocalization) had been exploited by chemists over the period of the next 20 years. It was only in 1963 that the hydride atom was truly located in the X-ray structure of the complex $\text{RhH}(\text{CO})[\text{P}(\text{C}_6\text{H}_5)_3]_3$, showing a normal covalent Rh–H bond of 1.72 Å [10]. This study demonstrated clearly that the hydride atom (in spite of its small size) participates in the creation of a coordination sphere of the metal.

Later, numerous spectroscopic data, obtained for transition metal hydrides, were re-interpreted on the basis of the concept of a covalent M–H bond. The modern theory of hydride chemical shifts in ^1H NMR spectra operates under a paramagnetic current, localized in an adjacent metal fragment, which is responsible for *large negative chemical shifts* of hydride resonances [11]. For example, theoretical calculations of the high-field hydride chemical shifts in complexes of Cr, Mn, Re and Fe, based on the paramagnetic current, reproduce well the experimental values [11]. It is interesting to add that, in contrast to transition metals, hydride ligands, binding to non-transition metals, for example, in the complexes HHgR , show hydride resonances in extremely *low* fields up to +18 ppm [12]. Thus, the hydride chemical shift, being a function of the metal nature, covers a range between +18 and –50 ppm.

The concept of a normal (covalent) M–H bond was the theoretical basis in studies of chemical and physical properties of transition metal hydrides up to 1989. However, in 1989 it was unexpectedly established that transition metal hydride ligands can show quantum mechanical behaviour [13,14]. This behaviour appears as an extremely large and temperature-dependent splitting, ($J^{\text{exch}}(\text{H}-\text{H})$), observed for hydride resonances in low-temperature ^1H NMR spectra. Such $J^{\text{exch}}(\text{H}-\text{H})$ constants, being very sensitive to the formation of hydrogen bonds and weak solvent coordinations [15], disappear due to displacement of H by deuterium or tritium. This intriguing phenomenon, recognized on the basis of tunnelling models [16,17] as quantum mechanical exchange in a pair of H-ligands, renews, in a sense, the idea about *delocalization* of the hydride ligands, binding to a heavy metal [18].

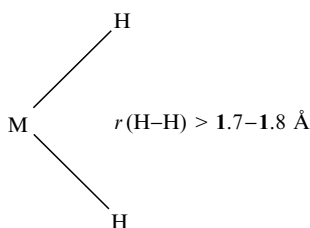
The short historical review illustrates a pronounced dependence of theoretical representations in the chemistry of transition metal hydride on the level of experimental techniques and strongly stimulates searches for new experimental approaches to these interesting compounds.

This present chapter focuses on the deuterium quadrupole coupling constants (DQCCs), determined by deuterium spin-lattice relaxation experiments in solutions of transition metal hydrides [19], and shows how the DQCC values can be used in a novel strategy for their characterization. One can also hope that the new approach will be interesting for chemists working in other fields of modern chemistry and actively using NMR spectroscopy.

2 APPLICATIONS OF ^1H NMR IN THE CHEMISTRY OF TRANSITION METAL HYDRIDE COMPLEXES

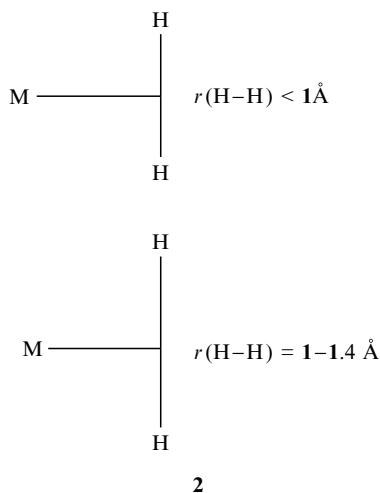
Among the different physical methods applied in hydride chemistry, ^1H NMR spectroscopy occupies a central place. Actually, this method provides rapid and reliable information about the structure and features of transition metal hydride complexes in solution. Therefore, a short review of the main methodical ^1H NMR approaches seems to be appropriate here.

Transition metal hydrides can be structurally formulated as normal classical hydrides with a H...H separation of $> 1.7\text{--}1.8 \text{ \AA}$ (**1**), dihydrogen complexes with a short hydride-hydride distance ($< 1 \text{ \AA}$) (**2**) [4,5] and dihydrogen complexes with a long H-H bond ($r(\text{H-H}) = 1.0\text{--}1.4 \text{ \AA}$) [20-23]. Hydride ligands in complexes showing quantum exchanges (or so-called exchange couplings in the ^1H NMR spectra), are usually separated by $1.6\text{--}1.7 \text{ \AA}$. Hence, such systems lie close to the borderline between dihydrogen complexes and normal classical hydrides.



1

It is obvious that the presence (or absence) of H-H bonding interactions between hydride ligands represents a key question in the structural formulations of hydride systems. This problem can be resolved in the framework of quantum-chemical calculations of transition metal hydrides on the basis of an analysis of the topological properties of the electronic density, $\rho(r)$, in terms of its critical points (cp), where $\nabla\rho(r_{\text{cp}}) = 0$ [20,24].



On an experimental level, this problem can be resolved by observation of the spin-spin coupling constants $J(\text{H-D})$ for hydride resonances in the ^1H NMR spectra of partially deuterated complexes. The coupling constants are caused by the Fermi-contact interactions [25] with s electrons, and, therefore, for example, the $J(\text{H-D})$ constant of 43.2 Hz in a free HD molecule corresponds to the spin-spin coupling through a strong chemical bond with a H-H separation of 0.74 Å.

It has recently been found that the $J(\text{H-D})$ values correlate well with the $r(\text{H-H})$ distances [26], as follows:

$$r(\text{H-H}) = -0.0167J(\text{H-D}) + 1.42 \quad (1)$$

determined from neutron diffraction studies of solid dihydrogen complexes. This correlation was rationalized theoretically and thus the $J(\text{H-D})$ constants of 20–34 Hz show the strong H-H bonding interactions in dihydrogen ligands. In contrast, the direct H-H bonding is absent in classical hydrides and therefore their *magnetic* H-D spin-spin couplings, transmitted only by a metal atom, take the small $J(\text{H-D})$ values of < 2–3 Hz.

The objective difficulties in applications of the X-ray or neutron diffraction methods for studies of dihydrogen complexes are well known. The IR spectral identification of these compounds is often also problematic because the ν_{HH} bands of dihydrogen ligands are usually very weak and broadened [4,5]. All of these circumstances explain why ^1H NMR spectroscopy has become a most important physical method in hydride chemistry.

Applications of the ^1H spin-lattice (T_1) NMR relaxation approaches [27] allow us to distinguish classical and non-classical transition metal hydrides in solution. In practice, short H-H distances in dihydrogen ligands cause unusually short T_1 times (< 30 ms at 250 MHz) of the hydride lines. In addition, the solution T_1 relaxation technique provides a determination of the hydride-

hydride distances or even the M–H bond lengths for such metals as Mn, Co, Re, Nb, Ta and V [28]. Thus, the NMR relaxation is actually a reliable tool for hydride localization in solution. This is the second important reason for intensive applications of NMR in this field.

Important information about the structural and dynamic features of transition metal hydrides can be obtained from studies of isotopic perturbations in ^1H NMR spectra. Isotope shifts upon partial D-substitution of the hydride positions in dihydrogen or polyhydride complexes are usually small (0–70 ppb), up-field and temperature-independent [29]. However, in the case of the fluxional (H_2)/H systems they become large, down-field and temperature-dependent. For example, such behaviour was detected in the VT ^1H NMR spectra of the complex $[\text{TpIr}(\text{PMe}_3)(\text{H}_2)\text{H}]^+$, where the difference, $\Delta = \delta(\text{IrH}_2\text{D}) - \delta(\text{IrH}_3)$, reaches 228 ppb at 215 K. This phenomenon was explained in terms of an isotope perturbation of a fast hydride/dihydrogen exchange equilibrium when the heavy isotope prefers to occupy the terminal hydride position [29].

The VT ^1H NMR spectra reflect dynamic features of complexes such as hydride/hydride or hydride/dihydrogen exchanges. When the exchanges operate on the NMR time-scale, they can be studied quantitatively [4,5,30]. Note, however, that sometimes the processes cannot be stopped on the NMR time-scale, even in the solid state [31]. Finally, hydride systems showing the quantum hydride/hydride exchange were also found on the basis of their ^1H NMR spectra.

3 DEUTERIUM NMR APPROACH TO STUDIES OF TRANSITION METAL HYDRIDE COMPLEXES

In contrast to ^1H NMR, deuterium NMR spectra have been used less often, with their applications being limited only by the magnetic properties of ^2H . For example, the traditional recording of VT NMR spectra or even a line-shape analysis of the ^2H resonances have been applied in studies and measurements of the isotopic effects in classical [32] or quantum [33] hydride–hydride exchanges. Deuterium NMR spectra have also been used for spectral identifications of dihydrogen ligands. In fact, sometimes dihydrogen complexes do not show the (H_2) resonances in ^1H NMR spectra for relaxation reasons [21].

However, besides its magnetic properties, the deuteron possesses the nuclear quadrupole moment (Q) behaviour, which is described in the framework of quadrupolar interactions. This situation can be used for the characterization of transition metal hydrides and should reveal principally new information about M–H bonds.

3.1 DEUTERIUM AS A QUADRUPOLE NUCLEUS

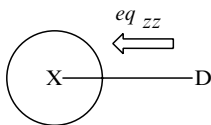
The appearance of the quadrupole moment, Q , on a deuterium nucleus is caused by a non-spherical distribution of the nuclear charge. The parameter

Q is a fundamental property of numerous nuclei having a spin angular momentum $> 1/2$. These quadrupole nuclei can be recorded by NQR or NMR experiments based on quantized energy levels corresponding to different orientations of Q with respect to the electric field gradient at a quadrupole nucleus [34].

The electric field gradient, $q_{zz} = \partial^2 V / \partial z^2$, where V is the electrostatic potential at a D nucleus [35], is a parameter of a strong non-homogeneous electric field changing along a chemical bond between atoms X and D (3). In contrast to the electrostatic potential, described mathematically as a scalar, the electric field gradient represents a tensor magnitude, as follows:

$$\begin{vmatrix} q_{xx} & 0 & 0 \\ 0 & q_{yy} & 0 \\ 0 & 0 & q_{zz} \end{vmatrix} \quad (2)$$

with all of the off-diagonal elements equal to zero. According to the theory of electrostatic interactions, a plot of the tensor, $q_{zz} + q_{yy} + q_{xx}$, is always equal to zero.



3

By convention, the largest element of the tensor, q_{zz} , is oriented along the X–D bond (the z -axis). This major component of the electric field gradient tensor is expressed through a fundamental parameter of D, the deuterium quadrupole coupling constant (DQCC), as follows:

$$\text{DQCC} = e^2 q_{zz} Q / h \quad (3)$$

The electric field gradient, being the tensor, can be characterized by a space shape. This shape is described by the asymmetry parameter η , according to the following:

$$\eta = |q_{xx} - q_{yy}| / q_{zz} \quad (4)$$

as a ratio between the corresponding diagonal elements. It follows from equation (4) that the electric field gradient can be axially symmetric ($q_{xx} = q_{yy}$, $\eta = 0$), or it may have a non-axial symmetry ($q_{xx} \neq q_{yy}$, $\eta \neq 0$). It is important that in practice the axial symmetry of the tensor is often realized, for example, in simple chemical bonds X–D ($X = \text{C, O, B and N}$) [35]. Here, the asymmetry parameter, $\eta(\text{D})$, takes values ≤ 0.2 [36] and hence the eq tensors appear to be practically axially symmetric.

As follows from the definitions, the electric field gradient and its shape are dictated by the symmetry of a charge distribution at D. This is absolutely valid for a deuterium atom binding to a metal atom. Even on a qualitative level, it is obvious that an octahedral symmetry of the charge distribution around a deuterium ligand, for example, in solid PdD [35], gives zero values of DQCC and η . Such a situation can also be expected for free D^- or D^+ ions.

On a quantitative level, the electric field gradient at any quadrupolar nucleus can be expressed as the sum of nuclear and electronic contributions, as follows:

$$eq_{zz} = +\sum_n K_n(3z_n^2 - r_n^2)/r_n^5 - e \langle \psi^* | \sum_i (3z_i^2 - r_i^2)/r_i^5 | \psi \rangle \quad (5)$$

where K and e are the charges of the neighbouring nuclei and electrons, respectively, and r represents the corresponding distances [35]. Note that the q_{xx} and q_{yy} elements are described by similar equations. Thus, the electric field gradient at a deuterium ligand (and hence DQCC) should be a function of the metal charge as well as the M–D bond length. In other words, the DQCC value can be used as a parameter for characterizing the metal–hydride bonding mode.

3.2 METHODS FOR DQCC DETERMINATION

Nuclear quadrupole coupling constants and their variations are usually investigated by using the nuclear quadrupole resonance method in the solid state [34]. Application of this technique for D is problematic because of its small quadrupole moment. However, it is namely this circumstance which allows us to apply NMR spectroscopy.

3.2.1 ^2H Solid-State NMR Spectroscopy

In the most common case, the DQCC values can be determined by the solid-state NMR technique [37]. A typical powder ^2H NMR spectrum, presented schematically in Figure 1, shows the so-called quadrupolar splitting, $\Delta\nu$, (the

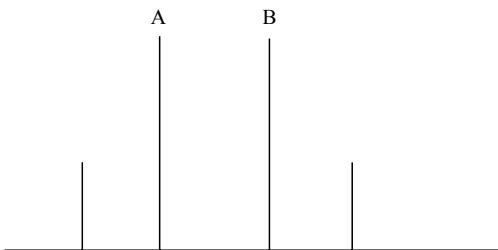


Figure 1 Schematic representation of a typical powder ^2H NMR spectrum

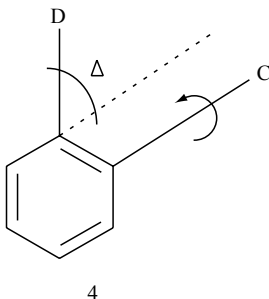
distance between lines A and B) which gives directly a static DQCC value from the following relationship:

$$\Delta\nu = 3/4(e^2qQ/h) \quad (6)$$

The equation is valid only in the absence of intensive molecular motions. Fast molecular motions [38], leading to re-orientations of the eq_{zz} vectors, complicate the situation, modifying strongly the line-shape of an ^2H resonance. For example, fast diffusion around the C–C bond (4) reduces the $\Delta\nu$ splitting, observed in a solid-state ^2H NMR spectrum, and in this case the DQCC value is calculated from the following:

$$\Delta\nu = 3/4(e^2qQ/h)[(3 \cos^2 \Delta - 1)/2] \quad (7)$$

where Δ is the angle between the rotational axis and the major axis of the electric field gradient at D.



The effects of fast solid-state motions of hydride ligands on the line-shapes of solid-state ^2H resonances in transition metal complexes have been recently studied by Limbach and co-workers [39]. They have considered theoretically the coherent quantum and incoherent mutual exchanges between two deuterium ligands and formulated the spectral ^2H NMR features distinguishing the processes. For single crystals, the effects of both exchanges are strongly different, especially when the process rates are of the order of the quadrupole splitting. Powder spectra are less sensitive to the exchange character.

The strong influence of fast motions on the line-shape of ^2H resonances in solid-state studies shows that the quadrupole splitting provides a correct DQCC determination when the types of molecular motions and orientations of the major axes of the electric field gradient are known from independent data. Therefore, in practice, ^2H solid-state NMR spectra are often applied in order to resolve the opposite task—the study of molecular (or intramolecular) motions and their frequencies on the basis of the already known DQCC values [37,38].

Numerous VT ^2H NMR studies of solid organic compounds have revealed remarkable effects of the η values on the line-shapes of deuterium resonances

[37,38]. Hence, the spatial extension of the electric field gradient at D can be determined by solid-state NMR. An application of this technique for transition metal hydrides can be found, for example, in Reference [40].

Finally, it should be noted that the DQCC values and frequency characteristics of molecular motions can be obtained by solid-state ^2H NMR using a combination of the full line-shape analysis and spin-lattice relaxation experiments. This approach was recently applied for the solid BD_3NH_3 and BH_3ND_3 molecules [41]. However, an important feature is that the final results of such experiments and their treatment depend strongly on the signal-to-noise ratios reached in the ^2H NMR spectra. Commonly, achievement of good signal-to-noise ratios in solid-state ^2H NMR spectra remain problematic even in the cases of the D-derivatives of transition metal hydrides because of the long relaxation times and a relatively low content of D.

3.2.2 Molecular Orbital Calculations

Any molecular orbital calculation results in an electric charge density distribution. In turn, wave functions and nuclear positions give elements of the electric field gradient at D. Then, the calculated q_{zz} values, expressed in atomic units, can be converted into DQCC values through ratio (8) [35]. Thus, MO calculations of transition metal hydride complexes:

$$\text{DQCC} = q_{zz}(\text{au}) 672 (\text{kHz au}^{-1}) \quad (8)$$

can also be applied in DQCC studies [19]. These theoretical studies play an important role for three reasons. They give (i) the values of the eq_{xx} , eq_{yy} , eq_{zz} components of the electric field gradient at a D ligand, (ii) the shapes of the electric field gradient, and (iii) the eq_{zz} orientations in the molecular coordinate system. This is especially important in the case of dihydrogen complexes where experimental determinations of all of the parameters are quite difficult [19,42]. However, note that MO calculations of even simple molecules can give DQCC values which are considerably larger than those found experimentally. This situation takes place, for example, in the case of ND_3BD_3 , studied both theoretically and by solid state ^2H NMR [41], or even in the case of the H_2 molecule [43]. Actually, a high-level calculation of H_2 gives a DQCC value of 267 kHz versus a value of 227 kHz measured experimentally [35].

3.2.3 ^2H Spin-Lattice Relaxation (T_1) in Solution

The solution ^2H T_1 technique can also be applied for determining DQCC [19]. The T_1 relaxation represents the process of the return of nuclear spins to an equilibrium state after their excitation by radiofrequency pulses. In turn, the T_1 constants are calculated by applying standard fitting procedures to the collected inversion-recovery data. These procedures are simple and absolutely valid for mono-exponential NMR decays. In such cases they provide good accuracy in the

T_1 calculations [28]. Note that a non-exponential deuterium relaxation is often detected only in the solid-state or glassy state. For example, non-exponential relaxation processes have been reported for both solid D-benzene [44] and super-cooled D-toluene systems [45]. It is interesting that D_2 in aqueous solutions also shows an unusual bi-exponential behaviour, with two quite long T_1 components of 2.0 and 39.1 s (at room temperature). This phenomenon was attributed to the presence of *ortho*- and *para*-forms of hydrogen [46]. However, the relaxation process again becomes rapid and mono-exponential when the D_2 molecule is binding to a metal centre in dihydrogen complexes [43].

The solution 2H T_1 relaxation is completely governed by quadrupole interactions [47]. When the T_1 time, measured, for example, for D-ligands in transition metal hydrides, reaches a minimum in the variable-temperature NMR experiments, a DQCC value can be calculated by using the following relationship:

$$\text{DQCC (kHz)} = 1.220 (1 + \eta^{2/3})^{-1/2} (\nu (\text{MHz}) / T_{1(\text{min})} (\text{s}))^{1/2} \quad (9)$$

where ν is the Larmor frequency of D [19,43,48]. This equation shows that DQCC determinations can be simple and convenient when the electric field gradient at D is axially symmetric ($\eta = 0$). As mentioned above, it is also true for D in numerous chemical X–D bonds with $\eta(\text{D}) \leq 0.2$ [36]. It is obvious that the effects of such η magnitudes on the DQCC values, determined from $T_{1\text{min}}$, are negligible. Actually, the $(1 + \eta^{2/3})^{1/2}$ factor in equation (9) is calculated as ≤ 1.006 . According to MO calculations, tensors of the electric field gradient at D-ligands in terminal transition metal hydrides are also axially symmetric ($\eta(\text{D}) \leq 0.085$) [43]. Hence, the 2H $T_{1\text{min}}$ approach can be successfully used for DQCC determinations in solutions of such hydride systems. In addition, even a η value of 0.8, reported for the solid dihydrogen complex $\text{Os}(\text{D}_2)\text{Cl}_2(\text{CO})(\text{PPr}_3)_2$ (from 2H MAS NMR spectra) [40], also looks insignificant in terms of DQCC determinations from the solution $T_{1\text{min}}$ times.

Finally, it should be noted that solutions of the D-derivatives of transition metal hydride complexes allow us to obtain good quality 2H NMR spectra and hence, good accuracy in the $T_{1\text{min}}$ (and DQCC) measurements.

3.3 DEUTERIUM QUADRUPOLE COUPLING CONSTANTS IN TERMINAL TRANSITION METAL HYDRIDES: RESULTS AND INTERPRETATION

Theoretical and experimental studies of X–D bonds in organic compounds (X = C, N, B and O) have revealed that the DQCC values are strongly affected by the X–D bonding mode [35]. The DQCC values are also sensitive to the formation of hydrogen bonds. This fact explains why the DQCC values in liquid hydrogen-bonded systems are bracketed by solid and gas values and increase with temperature [49]. For example, the DQCCs of two amide deuterons in liquid formamide- D_3 are temperature-dependent, varying from 230 to

290 kHz, while the formyl deuteron exhibits a similar DQCC value (170 kHz) at different temperatures [50].

The first experimental DQCC determinations were carried out for terminal transition metal hydrides by using the solid-state NMR technique. The solid complexes $\text{MnD}(\text{CO})_5$ [51], Cp_2MoD_2 [52], Cp_2WD_2 and Cp_2ZrD_2 [53] showed DQCC values of 68.1, 52, 54 and 46.7 kHz, respectively, thus demonstrating the influence of the metal atoms. These values are quite characteristic and significantly less than those measured for the X–D bonds in C_6D_6 (185 kHz) [35], ND_3BH_3 (200 kHz) [41], and HD (227 kHz) [35]. Nevertheless, the tensors of the electric field gradients on the D ligands remain axial-symmetric, as in the case of the X–D bonds.

The DQCC disparison for hydride systems was later expanded from 33 kHz in LiD [35] to 90 KHz (at 140 K) in the binuclear complex $[\text{Et}_4\text{N}][\text{DCr}_2(\text{CO})_{10}]$ [54]. Currently, the largest DQCC value lies close to 105 kHz, measured for the solid borohydride NH_3BD_3 [41].

The appearance of a minimal ^2H T_1 time on the VT relaxation curves is a characteristic behaviour of compounds investigated in the solid state. Actually, solid-state experiments provide a very large temperature range. In work carried out for solutions, which strongly limit temperature studies, the observation of ^2H $T_{1\text{min}}$ was surprising [48]. However, this phenomenon is well established now for numerous D-derivatives of transition metal hydrides [42,55].

The solution VT studies show that the ^2H $T_{1\text{min}}$ times of D-ligands in terminal transition metal hydrides cover a range between 11 and 30 ms at 61.402 MHz (Table 1). The DQCC values, reported for solid LiD, Cp_2ZrD_2 and HD, provide an increase in this range from 84 to 1.8 ms (see equation (9) at $\eta = 0$). Thus, the experimentally measured parameter ($T_{1\text{min}}$) changes significantly and hence its variation can actually be used for interpretations. It should be additionally emphasized that some specific methodical aspects of the solution ^2H $T_{1\text{min}}$ measurements are discussed in detail in Reference [19].

Table 2 lists all of the known DQCC values reported for terminal hydrides. Among these, the largest value is observed in the unsaturated rhodium

Table 1 ^2H $T_{1\text{min}}$ times, determined for terminal hydride ligands at 61.402 MHz in toluene- H_6 solutions [28,48]

Complex	$T_{1\text{min}}$ (ms)
HD	1.8 ^a
$\text{OsD}_4(\text{PTol}_3)_3$	11.1
$\text{OsD}(\text{D}_2)\text{Cl}(\text{CO})(\text{PPr}_3^i)_2$	12.0
<i>cis</i> - $\text{ReD}(\text{CO})(\text{PMe}_3)_4$	16.5
$\text{MnD}(\text{CO})_3(\text{PEt}_3)_2$	20.5
$\text{WD}(\text{CO})_2(\text{NO})(\text{PPh}_3)_2$	30.0
Cp_2ZrD_2	41.9 ^a
LiD	84 ^a

^a Calculated from the solid-state DQCC values via equation (10) at $\eta = 0$.

Table 2 Deuterium quadrupole coupling constants (DQCCs) and the ionic character of M–D bonds (*i*) in terminal hydrides [42,43,48,55–58]

Complex	DQCC (kHz)	<i>i</i>
LiD	33	0.855
<i>trans</i> -W(CMes)(dmpe) ₂ D	35	0.846
Cp ₂ ZrD ₂	46.7	0.794
Cp ₂ MoD ₂	52 ± 3	0.771
Cp ₂ WD ₂	54 ± 4	0.762
WD(CO) ₂ (NO)(PPh ₃) ₂	55.2 ± 0.6	0.757
WD(CO) ₂ (NO)(PMe ₃) ₂	55.0 ± 0.6	0.758
MnD(NO) ₂ (PET ₃) ₂	56.4 ± 0.6	0.751
MnD(CO) ₃ (PEt ₃) ₂	66.7 ± 1.0	0.706
MnD(CO) ₅	68.1	0.700
ReD(NO) ₂ (PPr ⁱ) ₂	68 ^a	0.700
ReD(NO) ₂ (PCy ₃) ₂	63–64 ^a	0.720
ReD ₂ (CO)(NO)(POPr ⁱ) ₂	66.3 ± 1.0, 68.8 ± 1.0	0.708, 0.697
ReD ₂ (CO)(NO)(PMe ₃) ₂	65.3 ± 1.0, 70.0 ± 1.0	0.712, 0.692
ReD ₂ (CO)(NO)(PCy ₃) ₂	66.7 ± 1.0, 69.5 ± 1.0	0.706, 0.694
ReD ₂ (CO)(NO)(PPr ⁱ) ₂	68.8 ± 1.0, 71.0 ± 1.0	0.697, 0.687
<i>cis, mer</i> -ReD(CO) ₂ (PMe ₃) ₃	63.5 ± 1.0	0.720
<i>trans, mer</i> -ReD(CO) ₃ (PMe ₃) ₂	64.7 ± 1.0	0.715
<i>fac</i> -ReD(CO) ₃ (PMe ₃) ₂	66.1 ± 1.0	0.709
<i>trans</i> -ReD(CO)(PMe ₃) ₄	66.8 ± 1.0	0.706
<i>cis</i> -ReD(CO)(PMe ₃) ₄	74.4 ± 1.0	0.672
[ReD ₂ (CO)(PMe ₃) ₄] ⁺	74.9 ± 1.0	0.670
PP ₃ RuD ₂	73.3 ± 1.0, 76.1 ± 1.0	0.677, 0.665
(triphos)(CO)RuD ₂	78.2 ± 1.0	0.655
Cp*(dppm)RuDMe	81.3 ± 1.0	0.642
[Cp*RuD ₂ (dppm)] ⁺	71.0	0.687
[RuD(D ₂)(dppe) ₂] ⁺	79.0	0.652
PP ₃ OsD ₂	79.7 ± 1.0	0.649
OsD(D ₂)(CO)Cl(PPr ⁱ) ₂	87.3 ± 1.0	0.615
[OsD(D ₂)(dppe) ₂] ⁺	81.0	0.643
OsD ₄ (PTol ₃) ₃	91.0 ± 1.0	0.599
(triphos)RhD ₃	83.2 ± 1.0	0.633
(triphos)IrD ₃	95.0 ± 1.0	0.581
RhDCl ₂ (PPr ⁱ) ₂	136 ± 2.0	0.401
BD ₃ NH ₃	105	0.537
(CD ₂)-group	167	0.264
HD	227	0

^a Calculated via equation (11) because only the ionic character was reported in Reference [58].

dihydride RhD₂Cl(PPrⁱ)₂. At the same time, the 18-electron rhodium complex, (triphos)RhD₃, shows a moderate DQCC value (83 kHz) [57]. These two results illustrate a quite complicated dependence of DQCC on the nature of the M–H bonds.

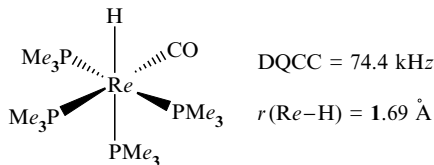
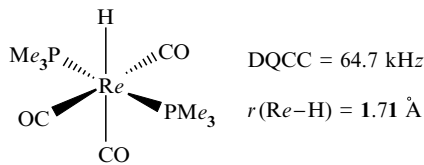
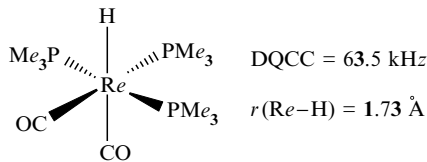
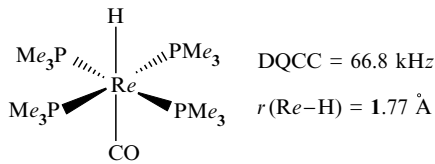
To rationalize DQCC variations in M–D bonds, Butler and co-workers have suggested a point-charge model, where DQCC is strongly affected by the

metal-hydride bond length (r_{M-H}) and an effective charge (K) on the metal center [54], as follows:

$$DQCC \sim Kr_{M-H}^{-3} \quad (10)$$

Note that this model was successfully applied for the solid binuclear complexes $[\text{Ph}_4\text{P}][\text{DM}_2(\text{CO})_{10}]$ and $[\text{Et}_4\text{N}][\text{DM}_2(\text{CO})_{10}]$ ($M = \text{Cr}$ and W) in order to establish relationships such as $DQCC/r_{M-H}$ and $\eta/M-H-M$ geometry.

In the framework of the Butler model, the large DQCC value in the dihydride $\text{RhD}_2\text{Cl}(\text{PPr}_3)_2$ could reasonably be explained by the extremely short rhodium-hydride distance of 1.43 Å [48]. Among four rhenium hydride complexes (**5**), the maximum DQCC value of 74.4 kHz is observed again for the shortest rhenium-hydride bond of 1.69 Å. Note that all of the distances have been determined from the solution-state ^1H NMR relaxation studies [48].



According to equation (10), an increase in charge on a metal center causes an additional electric field gradient along the metal–D bond. The terminal hydride ligands in the complexes PP_3RuD_2 and $[\text{PP}_3\text{Ru}(\text{D}_2)\text{D}]^+$ (Table 3) could represent a good illustration of the validity of the point-charge model. Actually, the appearance of a positive charge in $[\text{PP}_3\text{Ru}(\text{D}_2)\text{D}]^+$ is accompanied by a significant increase of DQCC from 73 to 88 kHz [43]. At the same time, the DQCC values in *cis*- $\text{DRe}(\text{PMe}_3)_4\text{CO}$ and $[\text{D}_2\text{Re}(\text{PMe}_3)_4\text{CO}]^+$ are practically identical. The similarity of the DQCC values in the complexes $\text{Cp}^*(\text{dppm})\text{RuDMe}$ (81 kHz) and $[\text{Cp}^*\text{RuD}_2(\text{dppm})]^+$ (82 kHz) seems also to be unreasonable in the framework of the simple point-charge model. In addition, MO calculations of alkali metal hydrides have revealed a weak variation in DQCC between 33 and 19.7 kHz, whereas the M–H distance changed strongly from 1.595 (LiD) to 2.494 Å (CsD) [35].

In common cases, the nuclear and electronic terms contribute to the electric field gradient (or DQCC) at the deuterium atom (see equation (5)). Table 4 shows the DQCC values, DQCC^{TOT} , determined experimentally for some X–D bonds, and also their expressions obtained from nuclear (DQCC^{NT}) and electron (DQCC^{ET}) terms. Note that these nuclear terms were estimated as described in References [35,54] on the basis of the X–D bond lengths, with the latter taken

Table 3 DQCC values measured for terminal hydride ligands of some neutral and positively charged hydride complexes [42,43,48]

Complex	DQCC (kHz)
PP_3RuD_2	73.3, 76.1 ^a
$[\text{PP}_3\text{Ru}(\text{D}_2)\text{D}]^+$	88.0
<i>cis</i> - $\text{ReD}(\text{PMe}_3)_4\text{CO}$	74.4
$[\text{ReD}_2(\text{PMe}_3)_4\text{CO}]^+$	74.9
$[\text{Cp}^*\text{RuD}_2(\text{dppm})]^+$	82.0
$\text{Cp}^*(\text{dppm})\text{RuDMe}$	81.3

^a Measured for two different D ligands.

Table 4 Experimental DQCC values (DQCC^{TOT}) for D in X–D bonds, plus the corresponding nuclear (DQCC^{NT}) and electronic (DQCC^{ET}) contributions (see text for details)

X–D	DQCC (kHz)		
	DQCC^{TOT}	DQCC^{NT}	DQCC^{ET}
H–D	227	404	177
C–D	175	910	735
Mn–D	68	1171	1116
Re–D	67	2693	2627
Mo–D	52	1748	1696

from the literature. Then, the electron terms can be obtained as a difference, i.e. $DQCC^{TOT} - DQCC^{NT}$, under the proposition that all of the quadrupole constants are positive [35]. It is seen that the electron terms increase significantly on going from covalent H–D or C–D bonds to M–D bonds in transition metal hydrides. This effect reduces the $DQCC^{TOT}$ values. In addition, the DQCC values shown in Table 2 change dramatically along the row of the Periodic Table of elements on going from Rb to Rh, namely RbD (19.7 kHz), Cp_2ZrD_2 (46.7 kHz), Cp_2MoD_2 (52 kHz), PP_3RuD_2 (73 or 76 kHz) and $RhDCl_2(PPr_3)_2$ (136 kHz).

Such a variation can be rationalized in terms of an ionicity of the metal–hydride bonds. Alkali metals give ionic M^+D^- bonds with a spherical negative charge distribution around D. In accord, their DQCC values are small and vary between 33 and 19.7 kHz [35], in spite of the strong elongation of the M–H bonds (see above).

Recent valence bond calculations showed the metal–hydride bonds to be extremely covalent in transition metal hydride cations [59]. Hence, under the limits of the above concept, their DQCC values should be larger with respect to alkali metals (see Table 2). On the other hand, the chemical properties of the H-ligands in the complexes Cp_2ZrH_2 and Cp_2MoH_2 reveal their high hydride character [60–62]. The kinetic hydricity [60] decreases from Cp_2ZrD_2 to Cp_2MoD_2 , which corresponds well with the increase of DQCC from 46.7 to 52.0 kHz. Finally, a maximum DQCC value can be expected for the HD molecule with the pure covalent H–D bond. In fact, this value was measured as 227 kHz [35].

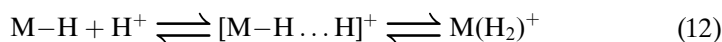
All of the above qualitative considerations can be expressed (using an analogy with interpretations of ^{35}Cl quadrupole constants [63]) by the following relationship [48]:

$$i = 1 - DQCC/227 \quad (11)$$

where i represents the ionic character of the M–D bonds, DQCC (kHz) is a measured magnitude, and the coefficient of 227 is equal to the DQCC value in ‘pure’ HD.

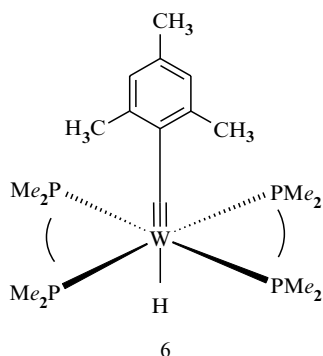
Trends in the variation of DQCC, expressed in terms of the ionic character (see Table 2), seem to be constructive from the chemical point of view. The hydride LiD show a high i value of 0.85. Less ionicity is estimated for all of the transition metal hydrides. In addition, the M–H ionic character, as expressed by DQCC in Table 2, correlates with the ionic characters derived from Sanderson’s electronegativities of the elements [48]. The ionicity of the B–D bonds in the borohydride NH_3BD_3 is significantly lower ($i = 0.54$, because $DQCC = 105$ kHz [41]). These bonds show practically an upper limit of the covalent character among the hydride molecules presented in Table 2. Nevertheless, the B–D ionicity is quite high in order to form intermolecular dihydrogen B–H...H bonds where the borohydride atoms act as proton acceptors [64]. Finally, the C–D bonds in CD_2 groups appear once more to be reasonably covalent ($i = 0.26$).

The relationship shown above in equation (11) is very simple and therefore seems to be quite convenient. However, for this very reason, such an expression requires additional experimental evidence. Some chemical support for such DQCC interpretations is provided by the behaviour of transition metal hydride systems in the presence of acids. Recent studies have revealed that hydride ligands, binding to transition metals, act in many cases as proton acceptors in proton-transfer reactions [62,65–68]. These relatively fast and reversible reactions lead to the formation of intermolecular $M-H^{\delta+} \dots \delta^-H$ hydrogen bonds to finally yield the dihydrogen complexes, as follows:



It should be noted that this phenomenon has been observed for practically all of the transition metal hydrides with $i \geq 0.58$ on the ionic scale (11).

Among the hydrides presented in Table 2, the complex *trans*-W(CMes)(dmpe)₂D (**6**), recently reported by Berke and co-workers [56], is of the greatest interest. The DQCC value for this complex was measured by two independent methods via solution VT ²H T₁ measurements (34.1 kHz) and from quadrupole splitting in the ²H solid-state NMR spectra (34.8 kHz). Note that the values obtained by both methods are in excellent agreement. Equation (11) gives, for this W–D bond, a surprising high ionicity ($i = 0.84-0.85$) which is close to that of the LiD molecule. It is interesting to note that the X-ray structure of the complex showed an extremely long W–H bond of 2.001 Å. All of the physical data are in good agreement with a high potential of the complex in different hydrogen-transfer reactions. For example, this complex even allows a facile insertion of the C–O moiety of CO₂ into the W–H bond.



A pronounced hydridic reactivity has been established for anionic transition metal hydride species [69] which also show strong proton–hydride interactions [70]. Unfortunately, up until now, the DQCC values in such systems have not yet been measured.

The DQCC data and their interpretation provide good evidence that the metal-hydride bonds in transition metal hydride complexes are polarized in the ground state. For example, Os-H bonds appear to be ionic to the order of 60–65 % (see Table 2). According to quantum-chemical calculations for the complex $\text{OsH}_4(\text{PH}_3)_3$, its hydride ligands actually bear negative charges of $-0.16 e$ [20]. On the other hand, numerous transition metal hydrides show acidic properties and even dissociate in solution to give H^+ [2]. This situation has already been discussed in the literature and, for example, a quite high energy barrier for the deprotonation reaction of $\text{HCo}(\text{CO})_4$ was attributed to the necessity of a repolarization of the Co-H bond [71].

4 CONCLUDING REMARKS

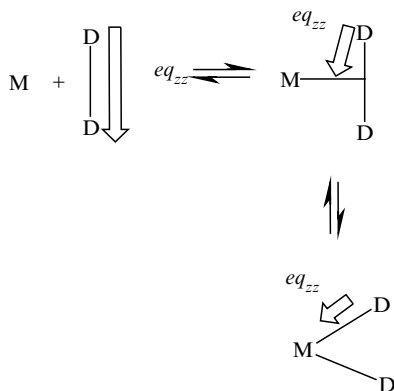
This chapter summarizes the DQCC values which have been experimentally measured in terminal hydrides. Most of these have been obtained by the $^2\text{H } T_1$ relaxation technique in solution. A chemical interpretation of the DQCC variation between 35 and 136 kHz has been recognized in terms of the ionic character of the metal-hydride bonds. DQCC studies of transition metal hydride complexes with systematic variations in the ligand environment could give important practical information about the metal-hydride bond ionicity. Thus, such studies can be used as a novel strategy for the characterization of transition metal hydride systems in solution.

Measurements of the electric field gradient at the D-ligands which form $\text{M-H}^{\delta+} \dots \delta^- \text{H}$ dihydrogen bonds also seems to be the next important task. Actually, the DQCC values in organic compounds are sensitive to the formation of hydrogen bonds and these can become temperature-dependent. Recent studies of ethanol binary solutions have revealed a linear correlation between the DQCCs in the OD group and the proton chemical shifts δ_{OH} [72]. On the other hand, it is known that the concentration (and temperature)-dependencies of δ_{OH} reflect the hydrogen bonding. Similar studies of transition metal hydrides in the presence of proton donors could give new information about hydride ligands acting as proton acceptors.

The above protonation reactions, starting from the formation of $\text{M-H}^{\delta+} \dots \delta^- \text{H}$ dihydrogen bonds, finally give dihydrogen complexes as the products of full proton-transfer mechanisms. A study of variations in the electric field gradient at the D-ligands along the reaction coordinates could represent a description of the processes in new terms. In addition, the field of DQCC and η measurements in dihydrogen complexes is absolutely open for further studies and will require applications of both theoretical and experimental approaches.

The first quantum-chemical [35,43] and experimental studies in solution [43], as well as in the solid state [42], have revealed the following features when D_2 is binding to a metal center: the DQCC value of 227 kHz decreases significantly, the electric field gradient becomes non-axially symmetric ($\eta \neq 0$), and the eq_{zz}

vector moves from the D–D bond towards the M–D direction (7). The gradient is again axially symmetric in a classical dihydride structure and the eq_{zz} vector is lying now along an M–D bond. The question regarding DQCC changes during the last transformation is still open because of objective difficulties in the correct DQCC measurements in dihydrogen complexes. Such difficulties are caused by fast dihydrogen ligand motions [19,42,43]. However in spite of this, such studies provide a very intriguing perspective, as well as giving a new physical description of the M–(H₂) bonding mode.



7

5 ACKNOWLEDGEMENTS

Thanks are given to NATO for financial support through the contract ‘²H-Relaxation as a Tool to Study Hydrogen-Transfer Reactions’ (Grant No. HTECH-CRG 972135). Thanks are also expressed to Professor R. H. Morris for help in presentation of the original results.

6 REFERENCES

1. E. I. Muetterties, *Transition Metal Hydrides*, Marcel Dekker, New York, 1971.
2. A. Dedieu, *Transition Metal Hydrides*, VCH, Weinheim, 1991.
3. G. J. Kubas, R. R. Ryan, B. I. Swanson, P. J. Vergamini and H. Wasserman, *J. Am. Chem. Soc.*, **106**, 451 (1984).
4. D. M. Heinekey and W. J. Oldham, *Chem. Rev.*, **93**, 913 (1993).
5. P. G. Jessop and R. H. Morris, *Coord. Chem. Rev.*, **121**, 155 (1992).
6. R. V. G. Ewens and M. W. Lister, *Trans. Faraday Soc.*, **35**, 681 (1939).
7. H. Hieber, *Die Chemie.*, **55**, 24 (1942).
8. F. A. Cotton and G. Wilkinson, *Chem. Ind. (London)*, 1305 (1956).

9. F. A. Cotton, *J. Am. Chem. Soc.*, **80**, 4425 (1958).
10. G. J. La Placa and J. A. Ibers, *J. Am. Chem. Soc.*, **85**, 3501 (1963).
11. Y. Ruiz-Morales, G. Schreckenbach and T. Ziegler, *Organometallics*, **15**, 3920 (1996).
12. P. J. Craig, M. I. Needham, N. Ostah, G. H. Stojak, M. Symons and P. Teesdale-Splitte, *J. Chem. Soc., Dalton Trans.*, 153 (1996).
13. D. H. Jones, J. A. Labinger and D. P. Weitekamp, *J. Am. Chem. Soc.*, **111**, 3087 (1989).
14. K. W. Zilm, D. M. Heinekey, J. M. Millar, N. G. Payne and P. Demou, *J. Am. Chem. Soc.*, **111**, 3088 (1989).
15. R. Kuhlman, E. Clot, C. Leforestier, W. E. Streib, O. Eisenstein and K. G. Caulton, *J. Am. Chem. Soc.*, **119**, 10153 (1997).
16. H. H. Limbach, G. Scherer, M. Maurer and B. Chaudret, *Angew. Chem. Int. Ed. Engl.*, **31**, 1369 (1992).
17. E. Clot, C. Leforestier, O. Eisenstein and M. Pelissier, *J. Am. Chem. Soc.*, **117**, 1797 (1995).
18. A. Lledos, *Euro-Hydrides—2000 Conference*, Dijon, France, Abstract PL2 (2000).
19. V. I. Bakhmutov, in *Recent Advances in Hydride Chemistry*, R. Poli (Ed.), Elsevier, Amsterdam, 2000, pp. 375–391.
20. F. Maseras, A. Lledos, M. Costas and J. M. Poblet, *Organometallics*, **15**, 2947 (1996).
21. A. Albinati, V. I. Bakhmutov, K. G. Caulton, E. Clot, J. Eckert, O. Eisenstein, D. G. Gusev, V. V. Grushin, B. E. Hauger, W. Klooster, T. F. Koetzle, R. K. McMullan, T. J. O'Loughlin, M. Pelissier, J. S. Ricci, M. P. Sigalas and A. E. Vymenits, *J. Am. Chem. Soc.*, **115**, 7300 (1993).
22. W. T. Klooster, T. F. Koetzle, G. Jia, T. P. Fong, R. H. Morris and A. Albinati, *J. Am. Chem. Soc.*, **116**, 7677 (1994).
23. P. A. Maltby, M. Schlaf, M. Steinbeck, A. J. Lough, R. H. Morris, W. T. Klooster, T. F. Koetzle and R. C. Srivastava, *J. Am. Chem. Soc.*, **118**, 5396 (1996).
24. A. Castillo, G. Barea, M. A. Esteruelas, F. J. Lahoz, A. Lledos, F. Maseras, J. Modrego, E. Onate, L. A. Oro, N. Ruiz and E. Sola, *Inorg. Chem.*, **38**, 1814 (1999).
25. J. W. Emsley, J. Feeney and L. H. Sutcliffe, *High Resolution Nuclear Magnetic Resonance Spectroscopy*, Pergamon Press, Oxford, UK, 1965, pp. 151–153.
26. R. H. Morris, *Can. J. Chem.*, **74**, 1907 (1996).
27. D. G. Hamilton and R. H. Crabtree, *J. Am. Chem. Soc.*, **110**, 4126 (1988).
28. V. I. Bakhmutov and E. V. Vorontsov, *Rev. Inorg. Chem.*, **18**, 183 (1998).
29. W. J. Oldham, A. S. Hinkle and D. M. Heinekey, *J. Am. Chem. Soc.*, **119**, 11028 (1997).
30. D. G. Gusev and H. Berke, *Chem. Ber.*, **129**, 1143 (1996).
31. L. L. Wisniewski, M. Mediatl, C. M. Jensen and K. W. Zilm, *J. Am. Chem. Soc.*, **115**, 7533 (1993).
32. S. Feracin, T. Burgi, V. I. Bakhmutov, I. L. Eremenko, E. V. Vorontsov, A. B. Vimenits and H. Berke, *Organometallics*, **13**, 4194 (1994).
33. K. W. Zilm and J. M. Millar, *Adv. Magn. Opt. Reson.*, **15**, 163 (1990).
34. T. P. Das and E. L. Hahn, *Nuclear Quadrupole Resonance Spectroscopy*, Academic Press, New York, 1958.
35. L. G. Butler and E. A. Keiter, *J. Coord. Chem.*, **32**, 121 (1994).
36. M. J. Hansen, M. A. Wendt and T. C. Farrar, *J. Phys. Chem., A*, **104**, 5328 (2000).
37. J. B. Lambert and F. G. Riddell, *The Multinuclear Approach to NMR Spectroscopy*, D. Reidel Publishing Company, Boston, MA, 1982, pp. 151–167.
38. E. C. Reynhardt and L. Latanowicz, *J. Magn. Reson.*, **130**, 195 (1998).
39. G. Buntkowsky, H. H. Limbach, F. Wehrmann, I. Sack, H. M. Vieth and R. H. Morris, *J. Phys. Chem., A*, **101**, 4679 (1997).

40. G. A. Facey, D. G. Gusev, R. H. Morris, S. Macholl and G. Buntkowsky, *Phys. Chem., Chem. Phys.*, **2**, 935 (2000).
41. G. H. Penner, Y. C. Chang and J. Hutzal, *Inorg. Chem.*, **38**, 2868 (1999).
42. G. A. Facey, T. P. Fong, D. Gusev, P. M. Macdonalds, R. H. Morris, M. Schlaf and W. Xu, *Can. J. Chem.*, **77**, 1899 (1999).
43. V. I. Bakhmutov, C. Bianchini, F. Maseras, A. Lledos, M. Peruzzini and E. V. Vorontsov, *Eur. J. Chem.*, **5**, 3318 (1999).
44. I. Roggatz, E. Rossler, M. Taupitz and R. Richert, *J. Phys. Chem.*, **100**, 12193 (1996).
45. E. Rossler and H. Sillescu, *Chem. Phys. Lett.*, **112**, 941 (1984).
46. H. Gilboa, B. E. Chapman and P. W. Kuchel, *J. Magn. Reson.*, **119**, 1 (1996).
47. A. Abragam, *The Principles of Nuclear Magnetism*, Oxford University Press, New York, 1971.
48. D. Nietlispach, V. I. Bakhmutov and H. Berke, *J. Am. Chem. Soc.*, **115**, 9191 (1993).
49. E. H. Hardy, R. Witt, A. Dolle and M. D. Zeidler, *J. Magn. Reson.*, **134**, 300 (1998).
50. R. Ludwig, J. Bohmann and T. C. Farrar, *J. Phys. Chem.*, **99**, 9681 (1995).
51. P. S. Ireland, L. W. Olson and T. L. Brown, *J. Am. Chem. Soc.*, **97**, 3548 (1975).
52. I. Y. Wei and B. M. Fung, *J. Chem. Phys.*, **55**, 1486 (1971).
53. W. L. Jarrett, R. D. Farlee and L. G. Butler, *Inorg. Chem.*, **26**, 1381 (1987).
54. A. J. Kim, F. R. Fronczek, L. G. Butler, S. Chen and E. A. Keitler, *J. Am. Chem. Soc.*, **113**, 9090 (1991).
55. V. I. Bakhmutov, J. Bertran, M. Esteruelas, A. Lledos, F. Maseras, J. Modrego, L. A. Oro and E. Sola, *Chem. Eur. J.*, **2**, 815 (1996).
56. F. Furno, T. Fox, H. W. Schmalte and H. Berke, *Organometallics*, **19**, 3620 (2000).
57. V. I. Bakhmutov, C. Bianchini, M. Peruzzini, F. Vizza and E. V. Vorontsov, *Inorg. Chem.*, **39**, 1655 (2000).
58. D. G. Gusev, A. Llamazares, G. Artus, H. Jacobsen and H. Berke, *Organometallics*, **18**, 75 (1999).
59. J. Galbraith, M. A. Shurki and S. Shaik, *J. Phys. Chem., A*, **104**, 1262 (2000).
60. J. A. Labinger, in *Transition Metal Hydrides*, A. Dedieu, (Ed.), VCH, New York, 1992, Ch. 10, pp. 361-379.
61. N. Sarker and J. W. Bruno, *J. Am. Chem. Soc.*, **121**, 2174 (1999).
62. T. Y. Cheng, B. S. Brunschwig and R. M. Bullock, *J. Am. Chem. Soc.*, **120**, 13121 (1998).
63. L. Ramakrishnan, S. Soundararajan, V. S. S. Sastry and J. Ramakishna, *Coord. Chem. Rev.*, **22**, 123 (1977).
64. W. T. Klooster, T. F. Koetzle, P. E. M. Seigbahn, T. B. Richardson and R. H. Crabtree, *J. Am. Chem. Soc.*, **121**, 6337 (1999).
65. R. A. Henderson and K. E. Oglieve, *J. Chem. Soc. Dalton Trans.*, 3431 (1993).
66. E. S. Shubina, N. V. Belkova, A. N. Krylov, E. V. Vorontsov, L. M. Epstein, D. G. Gusev, M. Niedermann and H. Berke, *J. Am. Chem. Soc.*, **118**, 1105 (1996).
67. E. S. Shubina, N. V. Belkova, E. V. Bakhmutova, E. V. Vorontsov, V. I. Bakhmutov, A. V. Ionidis, C. Bianchini, L. Marvelli, M. Peruzzini and L. M. Epstein, *Inorg. Chim. Acta*, **280**, 302 (1998).
68. J. A. Ayllon, C. Gervaux, S. Sabo-Etienne and B. Chaudret, *Organometallics*, **16**, 2000 (1997).
69. M. Y. Darensbourg and C. E. Ash, *Adv. Organomet. Chem.*, **27**, 1 (1987).
70. K. Addur-Rashid, D. G. Gusev, S. E. Landau, A. J. Lough and R. H. Morris, *J. Am. Chem. Soc.*, **120**, 11826 (1998).
71. S. S. Kristjansdottir, J. R. Norton, A. Moroz, R. L. Sweany and S. L. Whittenburg, *Organometallics*, **10**, 2357 (1991).
72. T. D. Ferris, M. D. Zeidler and T. C. Farrar, *Mol. Phys.*, **98**, 737 (2000).

4 NMR Studies of Ligand Nuclei in Organometallic Compounds—New Information from Solid-State NMR Techniques

GUY M. BERNARD and RODERICK E. WASYLISHEN

*Department of Chemistry, University of Alberta, Edmonton, Alberta, Canada,
T6G 2G2*

1 INTRODUCTION

Virtually every tool available to chemists has been used to characterize organometallic compounds [1]. Since pulse Fourier-transform multinuclear magnetic resonance spectrometers became commercially available in the early 1970s, NMR spectroscopy has been particularly important, and is regarded as indispensable by most researchers. Although many NMR studies of organometallic compounds have focused on the metal nuclei [2], there is also considerable interest in the NMR properties of unsaturated-carbon moieties in organometallic complexes [3]. The goals of this review are threefold, i.e. (i) to provide an overview of the solid-state NMR literature on this important class of compounds, (ii) to summarize the data in a consistent format (see Section 2.3 below), and (iii) to encourage other researchers to explore the potential of solid-state NMR techniques in their own research. Studies of η -coordinated unsaturated-carbon ligands have been grouped into four sections, i.e. the carbides, the metal–olefins and acetylenes, the metallocenes, and adsorbed olefins and acetylenes. Most NMR literature reviewed here involves ^{13}C NMR investigations of diamagnetic systems, and in particular those that have reported the chemical shift tensors. However, the results of ^1H and ^2H NMR studies, and of a few studies involving the metal nuclei, are also included.

Organometallic complexes have been studied extensively by solution ^{13}C NMR [3]. In general, the isotropic shielding of η^2 -coordinated olefinic [4] carbon nuclei increases significantly as a result of coordination with metals. In contrast, the isotropic shielding of the acetylenic [4] carbon nuclei of

η^2 -coordinated metal–acetylene complexes often decreases when compared to the values for the corresponding uncoordinated ligands [3].

There are numerous benefits to studying organometallic compounds in the solid state. Such compounds may be insoluble or unstable in solution, thus precluding solution NMR studies. If soluble, the presence of solvent molecules will affect the observed NMR data; inter- or intramolecular exchange processes which often influence spectra acquired from solution NMR studies are greatly reduced or eliminated in the solid state. Solid-state NMR data may be interpreted in terms of the crystal structure, when available, and in the absence of diffraction data, often offers the most reliable structural information on these compounds. Perhaps the greatest advantage of solid-state NMR is that orientation-dependent chemical shift (CS) tensors can be characterized. In addition to the isotropic chemical shift, δ_{iso} , the only nuclear magnetic shielding parameter readily available from solution NMR studies, the principal components of the CS tensor and some details about its orientation in the molecular framework are available from solid-state NMR experiments. Such data are essential in developing a better understanding of chemical shifts.

The increasing capacity of computers has enabled reliable *ab initio* calculations of NMR shielding parameters for the ligand nuclei of organometallic compounds. Progress in this area has been discussed in several recent reviews [5]. Combined with experimental results, these techniques allow one to gain a better understanding of the relationship between nuclear magnetic shielding and molecular structure in this important class of compounds [6].

2 THEORETICAL BACKGROUND

2.1 LIGAND–METAL BONDING

The bonding of olefins and acetylenes to metals is usually discussed either in terms of a model developed in the 1950s by Dewar, and Chatt and Duncanson [7], or in terms of a metallocyclopropane structure [8]. In the former, a σ bond is formed between the occupied π molecular orbital (MO) of the olefin and unoccupied d orbitals of the metal (Figure 1(a), left). In addition, there is some π back donation (or π back bonding) arising from the donation of charge to the unoccupied π^* MO of ethylene from the occupied d orbital of the metal (Figure 1(a), right). The extent of π back bonding depends on the metal, the other ligands coordinated to the metal and on the ligand [1]. This, in turn, affects the structure of the complexes. The metallocyclopropane model [8] (Figure 1(b)) considers the structure as arising from the formation of two σ bonds, leading to a three-membered ring. Both models account for the C–C bond lengthening and the bending back of the ligand substituents that has been observed experimentally. Numerous theoretical studies have been carried out to identify the bonding scheme for several metal–olefin and metal–acetylene

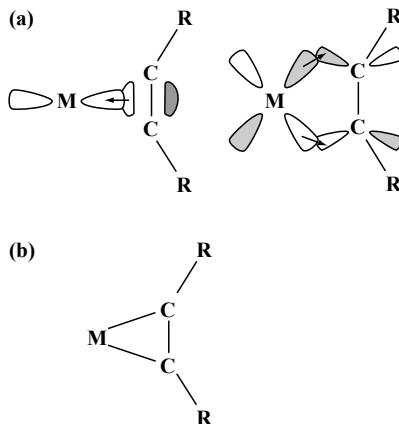


Figure 1 Models for the coordination of olefins or acetylenes with metals: (a) the σ -bonding and π -back bonding model proposed by Dewar, and Chatt and Duncanson [7]; (b) the metalloacyclopropane structure

complexes [9]. In the ensuing discussion, specific molecular structures will be discussed as the NMR data are presented.

2.2 THE CHEMICAL SHIFT TENSOR

2.2.1 Nuclear Magnetic Shielding and Chemical Shift

In general, a second-rank tensor is required to fully describe the nuclear magnetic shielding at a particular nucleus. To a good approximation, the line shapes observed in the NMR spectra of solids are only dependent on the symmetric portion of the magnetic shielding tensor [10–12]; this may be described by three principal components σ_{ii} ($i = 1, 2, 3$) and three Euler angles, α , β and γ , which describe the orientation of the principal axis system (PAS) of the magnetic shielding tensor relative to the molecular framework [10,12,13]. The σ_{ii} parameters denote the nuclear magnetic *shielding* relative to the bare nucleus with the convention $\sigma_{33} \geq \sigma_{22} \geq \sigma_{11}$. While *ab initio* methods calculate magnetic shielding tensors, experimentally one measures a chemical *shift* tensor, δ_{ii} relative to a chosen reference with the convention $\delta_{11} \geq \delta_{22} \geq \delta_{33}$. The two sets of components are related by the following:

$$\delta_{ii} = \frac{\nu_{ii} - \nu_{\text{ref}}}{\nu_{\text{ref}}} \times 10^6 = \frac{\sigma_{\text{ref}} - \sigma_{ii}}{1 - \sigma_{\text{ref}}} \quad (1)$$

where ν_{ii} and ν_{ref} are the resonance frequencies of the ii^{th} tensor component and of the reference, respectively. For carbon, $\sigma_{\text{ref}} \ll 1$, and so $\delta_{ii} \approx \sigma_{\text{ref}} - \sigma_{ii}$. To relate experimental data to those calculated by *ab initio* methods requires the establishment of an absolute shielding scale for the nucleus of interest [14]; for

carbon the scale was established by Jameson and Jameson [15], as well as by Raynes and co-workers [16].

2.2.2 Ramsey's Theory

It has been traditional to discuss magnetic shielding in terms of the model proposed by Ramsey [17] in which the shielding is partitioned into diamagnetic, σ^d , and paramagnetic, σ^p , terms:

$$\sigma_{ii} = \sigma_{ii}^d + \sigma_{ii}^p \quad (2)$$

The contribution to shielding from σ^d is always positive, leading to increased shielding, while σ^p is usually negative. Since σ^d and σ^p show weak and strong orientation dependence, respectively, significant deshielding of a tensor component is usually a consequence of σ^p .

The diamagnetic term is a first-order property which can be calculated accurately by either *ab initio* or semi-empirical methods. As well, Gierke and Flygare [18] have shown that σ^d may be approximated if the molecular structure is known. For example, the shielding for nucleus *A* when the *x*-axis is along the applied magnetic field is given by:

$$\sigma_{xx}^d \approx \sigma_{av}^d(\text{free atom}) + \frac{\mu_0}{4\pi} \frac{e^2}{2m} \sum_{B \neq A} \frac{Z_B}{r_{AB}^3} (y_B^2 + z_B^2) \quad (3)$$

where $\sigma_{av}^d(\text{free atom})$ is the shielding for the 'free' atom. For carbon, $\sigma_{av}^d(\text{free atom}) = 260.7$ ppm [19]. The summation in equation (3) is carried out over all other nuclei in the molecule, Z_B is the atomic number of nucleus *B* with Cartesian coordinates y_B and z_B , and r_{AB} is the distance from this nucleus to *A*, the nucleus of interest. The remaining components of σ^d may be approximated by cyclic permutations of equation (3). Relatively small higher-order corrections to equation (3) have also been described by Flygare and co-workers [18].

The paramagnetic term is affected by those excited related states which are singlet to the ground state by magnetic-dipole allowed transitions. The application of Ramsey's theory to nuclear magnetic shielding has been discussed in several texts [20]. Nuclear magnetic shielding may also be discussed in terms of electronic current density, thus leading to an equivalent partitioning of the shielding into diamagnetic and paramagnetic terms [21].

2.3 NOTATION

The solid-state NMR literature can be confusing since a universally accepted consensus on notation has not been reached [22]. As well, chemical shift data are not necessarily referenced to the same compound. Further confusion arises from the fact that some authors apparently are unaware of the important

distinction between chemical shift and nuclear magnetic shielding discussed in the preceding section.

In this review, the ‘Maryland’ convention described by Mason will be used to describe the NMR data [23]. The nuclear magnetic shielding and chemical shift tensors will be described in terms of their span, Ω , and skew, κ , where:

$$\Omega = \sigma_{33} - \sigma_{11} = \delta_{11} - \delta_{33} \quad (4)$$

and

$$\kappa = \frac{3(\sigma_{\text{iso}} - \sigma_{22})}{\Omega} = \frac{3(\delta_{22} - \delta_{\text{iso}})}{\Omega} \quad (5)$$

Although the principal components of a CS tensor can be described by three parameters (either δ_{iso} , Ω and κ , or δ_{11} , δ_{22} and δ_{33}), we will report all six parameters. Literature data reported using other conventions or references will be converted to the above convention, with ^{13}C chemical shifts relative to TMS ($\delta_{\text{iso}} = 0.00$ ppm). Although chemical shifts are measured experimentally, it is convenient when comparing data to speak of increased or decreased shielding. The reader is reminded that increased shielding implies a decrease in both the chemical shift and of the resonance frequency.

2.4 AB INITIO CALCULATIONS OF MAGNETIC SHIELDING TENSORS

Because paramagnetic contributions to nuclear magnetic shielding arise from a summation of energy differences between the ground and all excited singlet electronic states of the molecule, accurate *ab initio* calculation of magnetic shielding is very challenging [24], and in fact is one of the most rigorous tests of computational techniques [5]. Current computational programs do not calculate magnetic shielding according to equation (2); some provide a breakdown of the magnetic shielding into diamagnetic and paramagnetic shielding, but these values should be regarded as approximate, since the breakdown is arbitrary [25]. The principal components of the nuclear magnetic shielding tensor are calculated according to the following [5a]:

$$\sigma_{\alpha, \beta} = \left(\frac{\partial^2 E}{\partial \mu_{\alpha} \partial \mathbf{B}_{\beta}} \right)_{\mu, \mathbf{B}=0} \quad (6)$$

where α , β are the Cartesian coordinate components (i.e. $\alpha, \beta = x, y, z$), E is the total electronic energy, μ is the nuclear magnetic moment and \mathbf{B} is the applied magnetic field.

First principle calculations of CS tensors are particularly daunting in the case of organometallic complexes, since all-electron calculations on molecules with heavy nuclei are computationally demanding [26]. As well, the effects of relativity [27], which may be significant even for the shielding of the ligand nuclei

[28], should in principle be considered. The development of pseudopotentials, also known as effective core potentials (ECPs), has greatly reduced the computational time by replacing the core electrons of heavy nuclei with parameterized functions which account for relativistic effects [29]. While their use is not recommended for the calculation of the magnetic properties of the metal [30], accurate magnetic shielding parameters for organometallic ligand atoms have been achieved using ECPs for the heavy nuclei [31]. The inclusion of electron correlation effects is also important [32] but is usually not practical for *ab initio* calculations on organometallic compounds. Density functional theory (DFT) has been developed to efficiently include electron correlation effects [20b]. Application of existing DFT methods to the calculation of magnetic shielding properties is very challenging [30], but several groups have reported promising results [33].

Accurate calculation of magnetic resonance properties requires large basis sets on the nuclei of interest. However, Chesnut and co-workers have shown that calculated magnetic shielding using locally dense basis sets is virtually identical to that obtained using large basis sets for the complete molecule [34]. The technique entails placing a large basis set on the nuclei of interest and perhaps on the neighbouring nuclei, but placing a much smaller basis set on all other nuclei.

3 EXPERIMENTAL TECHNIQUES

Virtually all ^{13}C NMR spectra of solids are acquired with high-power proton decoupling and cross-polarization (CP) [35]. Most spectra are also obtained under the condition of magic-angle spinning (MAS). Spectra acquired with MAS are generally well resolved, but with the exceptions discussed below, do not yield information about the CS tensor components. Such experiments will not be considered in detail here since the focus of this review is on experiments which provide information on anisotropic shielding [36]. A detailed discussion of experimental techniques for solid-state NMR experiments is beyond the scope of this review, but the basic concepts describing the experiments used in the cited literature are presented in the following sections. Readers are referred to several excellent articles for detailed discussions of these and other solid-state NMR techniques [12,37].

The symmetric portion of a CS tensor can often be determined unambiguously by acquiring NMR spectra of single crystals as a function of the crystal orientation with respect to \mathbf{B}_0 [38]. It should be noted that if the system under investigation contains crystallographically equivalent but magnetically distinct nuclei, it may not be possible to assign a CS tensor to a particular nucleus [39]. In addition, single crystals of sufficient size and quality are not always available, and the experiments can be time-consuming, particularly when dilute spins such as ^{13}C are considered. Isotopic labelling increases the signal inten-

sity, but may introduce complications, such as intra- and intermolecular dipolar coupling. The carbon CS tensors discussed in this review have been characterized by one (or more) of three methods, i.e. (i) analysis of spectra of an isolated spin of a stationary powder sample, (ii) analysis of spectra of a stationary powder sample containing an isolated spin pair, using the dipolar-chemical shift method, or (iii) analysis of the spinning sideband patterns of spectra of slow MAS samples.

3.1 THE PRINCIPAL COMPONENTS OF A CS TENSOR FOR AN ISOLATED SPIN- $1/2$ NUCLEUS

In a stationary powder sample, crystallites are oriented randomly in the applied magnetic field, giving rise to a so-called powder pattern. In the absence of interactions with other magnetic nuclei (i.e. an isolated spin), the NMR line shape of a stationary powder will reflect the orientation dependence of the magnetic shielding. The ^{13}C NMR spectrum expected for a stationary powder sample of ethylene (natural-abundance ^{13}C) is shown in Figure 2(a) [40,41]. The magnitudes of the principal components of the CS tensor can be determined from the discontinuity and shoulders of the spectrum, but information about the tensor orientation in the molecular framework is usually unavailable—the orientation illustrated here was determined from a different experiment [40,41]. Information about the CS tensor orientation may sometimes be surmised from molecular symmetry. For example, Figure 2(b) illustrates the ^{13}C NMR spectrum expected for a stationary sample of acetylene at natural abundance, based on the parameters reported for $^{13}\text{C}_2\text{H}_2$ by Zilm and Grant [40]. The NMR spectrum of the axially symmetric CS tensor arises from the symmetry of the molecule: the chemical shift when \mathbf{B}_0 is perpendicular to the molecular axis, usually referred to as δ_{\perp} , corresponds to the discontinuity in the spectrum, while the shoulder corresponds to the chemical shift when \mathbf{B}_0 is parallel to the molecular axis, usually referred to as δ_{\parallel} .

3.2 THE DIPOLAR CHEMICAL SHIFT METHOD

Two spins which are close to one another but separated or decoupled from other spins are referred to as an isolated spin pair. In the ensuing discussion, the case of an isolated homonuclear spin pair, which is most frequently encountered for ^{13}C NMR of labelled samples, is presented. However, readers should be aware that the same general concept may be applied to an isolated heteronuclear spin pair and that the spins are not required to be adjacent to one another if the dipolar interaction between them is sufficiently large. In addition to the anisotropy in the magnetic shielding, the ^{13}C NMR spectra of an isolated spin pair will be affected by the direct dipolar interaction between the adjacent carbon nuclei [42]. This interaction is described by the dipolar coupling constant, R_{DD} , as follows:

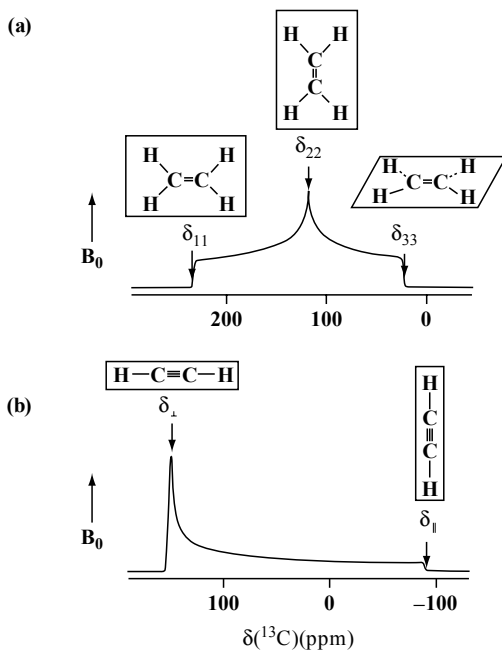


Figure 2 (a) Simulation of the ^{13}C NMR spectrum expected for a stationary sample of ethylene at natural abundance (a), and (b) the spectrum expected for acetylene. The shoulders and discontinuities in the spectra arise from the molecules oriented as shown, for an applied magnetic field in the vertical direction. Note that the horizontal scales in (a) and (b) differ

$$R_{\text{DD}} = \left[\frac{\mu_0}{4\pi} \right] \left[\frac{\hbar}{2\pi} \right] \gamma_{\text{C}}^2 \langle r_{\text{CC}}^{-3} \rangle \quad (7)$$

In this equation, μ_0 is the permeability of free space, γ_{C} is the magnetogyric ratio for ^{13}C , and $\langle r_{\text{CC}}^{-3} \rangle$ is the motionally averaged inverse cube of the internuclear separation. Each homonuclear spin pair gives rise to two or four transitions for magnetically equivalent and nonequivalent nuclei, respectively. The relative frequencies of these transitions depend on the orientation of the internuclear vector, \mathbf{r}_{CC} , relative to \mathbf{B}_0 and on the magnitude of R_{DD} [42,43]. By considering the contribution to the NMR powder pattern from crystallites oriented such that \mathbf{B}_0 is parallel to a given CS tensor component, it is possible to gain information about the orientation of that component relative to \mathbf{r}_{CC} . However, since the direct dipolar coupling tensor is axially symmetric, the calculated spectrum is invariant to simultaneous rotation of the two CS tensors about \mathbf{r}_{CC} . In addition, the supplement of the angle which defines the orientation of the CS tensor component relative to \mathbf{r}_{CC} also yields the same calculated spectrum, and hence in general the dipolar-chemical shift method yields an infinite set of solutions, with the given tensor components oriented about two

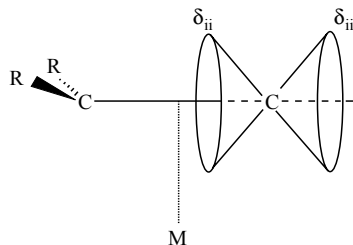


Figure 3 Possible orientations of a tensor component about a dipolar vector, as determined by the dipolar-chemical shift method

cones, as shown in Figure 3. The span of the CS tensor (in frequency units) is proportional to the applied magnetic field, unlike R_{DD} . Hence, it is advisable to conduct experiments at two or more applied magnetic field strengths to ensure that features of a powder NMR pattern have not been improperly assigned. Accurate CS tensor parameters will reproduce the powder NMR spectrum regardless of applied field strength.

As discussed above, the CS tensor orientation may sometimes be inferred from the local molecular symmetry. For example, nuclei in a mirror symmetry plane have two CS tensor principal components in and one component perpendicular to this plane. Orientations for CS tensors may be predicted on the basis of known CS tensor orientations in closely related compounds. There is growing evidence that the results of *ab initio* calculations [5,6,44] accurately calculate carbon CS tensor orientations.

3.3 CS TENSORS FROM SPECTRA OF MAS SAMPLES

The spinning-sideband pattern in the NMR spectrum of an isolated spin can be used to determine the principal components of the carbon CS tensors. The method of Herzfeld and Berger [45] is used extensively to determine the magnitudes of the principal components of the carbon CS tensor, from the relative intensities of the spinning sidebands. This method is particularly useful for the analysis of spectra with several carbon sites where isotopic labelling is not feasible. However, the standard Herzfeld–Berger method cannot readily be applied to a spin pair. Alternatively, the tensor components may, in principle, be determined from an analysis of the second moments [46].

Two-dimensional techniques, magic-angle hopping (MAH) and magic-angle turning (MAT), have been developed to obtain CS tensor information [47]. The MAH technique [48] entails rapidly reorienting (or hopping) the sample about the magic angle between three positions that are 120° apart from one another; acquisition occurs while the sample is stationary between hopping steps. In the MAT technique, spectra are acquired with very slow MAS [49]. As with other MAS techniques, these methods do not provide information about the CS tensor orientation.

3.4 SAMPLE SIZE

An important consideration in all experiments is the amount of sample required to obtain spectra with acceptable signal-to-noise ratios in a reasonable amount of time. In the case of ^{13}C NMR, techniques that allow analysis of samples at natural abundance, such as those outlined above in Sections 3.1 and 3.3, are appealing because the synthesis of the samples is less expensive and requires less time. However, these benefits may be more than offset by the time required to acquire suitable spectra, particularly if two-dimensional techniques are used. Our experience has been that as little as 10 mg of a $^{13}\text{C}_2$ -labelled sample is sufficient for the acquisition of suitable NMR spectra, although 50 to 100 mg is desirable. In contrast, acquiring spectra of samples at natural abundance in less than 24 h may require samples of several hundred mg.

4 EXPERIMENTAL RESULTS

4.1 METAL CARBIDES

The metal carbides are ionic solids which generally have the NaCl structure [50]. Those that have been investigated by solid-state NMR consist of alkali-metal and alkaline-earth metal (group 1 and 2) carbides of the type M_2C_2 and MC_2 , respectively, as well as a recent study of alkali metal transition metal acetylides. The results of these studies are summarized in Table 1 and discussed below.

4.1.1 Carbon CS Tensors for the Alkali-Metal Carbides

The carbon CS tensors of the alkali-metal carbides have been determined through the analysis of ^{13}C NMR spectra of stationary powder (Li_2C_2 and Na_2C_2) [51] and MAS (Na_2C_2 and K_2C_2) [52] samples. The CS tensors for the alkali-metal complexes are close to axially symmetric with spans of 300–400 ppm. Since the quasi-unique component is in the direction of greatest shielding (i.e. the value of κ is close to 1.0), it has been assumed that δ_{33} is approximately along the C–C bond, as for acetylene [40].

In a related study, Ruschewitz and co-workers investigated a series of ternary metal transition metal acetylides of the type A_2MC_2 ($\text{A} = \text{Na}, \text{K}; \text{M} = \text{Pd}, \text{Pt}$) [53]. These compounds consist of chains of C_2^{2-} anions separated by the transition metal; the alkali-metal atoms are between the chains [54]. ^{13}C NMR spectra of MAS samples of the Pd compounds were analysed by using the method of Herzfeld and Berger [45]; the spinning sidebands of the Pt compounds were not of sufficient intensity, and hence only isotropic values are reported for these [53]. Slightly non-axially symmetric CS tensors were reported for the two Pd-containing compounds, suggesting that the alkali metal atoms are a factor in the magnetic shielding.

Table 1 Principal components of the carbon chemical shift tensors for some metal carbides^a

Carbide	δ_{iso}	δ_{11}	δ_{22}	δ_{33}	Ω	κ	Ref.
Li ₂ C ₂	195(10)	343(15)	297(15)	-55(25)	398	0.77	51
Na ₂ C ₂	172	305	267	-56	361	0.79	52
Na ₂ C ₂	170(3)	308(5)	274(5)	-67(5)	375	0.83	51
K ₂ C ₂	186	295	267	-4	299	0.81	52
CaC ₂	200(5)	315(7)	315(7)	-30(5)	345	1.00	51
CaC ₂	206.2	350	283	-14	364	0.63	56
CaC ₂ (technical)	206	347	283	-10	357	0.66	57
CaC ₂ (pure)	196	343	271	-18	361	0.60	
Ca ₅ Cl ₃ (C ₂)(CBC)	198	318	282	-3	321	0.78	57
SrC ₂	212(3)	318(5)	318(5)	-1(5)	319	1.00	51
SrC ₂	213	323	317	-2	325	0.96	57
BaC ₂	229(2)	320(3)	320(3)	50(3)	270	1.00	51
BaC ₂	232.1	354	288	55	299	0.56	56
BaC ₂	230	326	313	54	272	0.98	57
Na ₂ PdC ₂	157(1)	301	253	-82	383	0.75	53
K ₂ PdC ₂	162(1)	284	252	-49	333	0.81	53
Na ₂ PtC ₂ ^b	156(1)	—	—	—	—	—	53
K ₂ PtC ₂ ^b	162(1)	—	—	—	—	—	53

^a Chemical shifts are relative to TMS; all data except κ are in ppm. Uncertainties in the last digits, where reported, are given in parentheses.

^b The principal components of the chemical shift tensor were not determined for these complexes.

4.1.2 Carbon CS Tensors for the Alkaline-Earth Metal Carbides

In an early NMR investigation, Haworth and Wilkie [55] reported the isotropic chemical shift of CaC₂, based on the analysis of a stationary powder sample. Two isotropic peaks were observed, at 167 and -72 ppm. The authors assumed that the high-frequency peak arose from a graphite impurity, but, subsequent studies suggest this is the C₂²⁻ peak (Table 1); principal components of the CS tensor were not reported. Several groups have reported values for the principal components of the carbon CS tensors for CaC₂ and BaC₂ through the analysis of ¹³C NMR spectra of stationary powder [51] or MAS samples [56,57]. While all groups report similar isotropic shifts, there are significant discrepancies in the values reported for the principal components of the CS tensor, particularly in the direction of greatest shielding. Duncan reported axially symmetric CS tensors for these two compounds, and also for SrC₂ [51], while those determined from the analysis of spectra of MAS samples were reported to be non-axially symmetric [56,57]. Clayden *et al.* have shown that CS tensor components determined through the analysis of spectra of slow MAS samples are subject to significant error if these tensors are close to being axially symmetric [58]. Based on the symmetry of these acetylides, Duncan concluded that the direction of greatest shielding is along the C-C bond [51]. The only

reported carbon CS tensor for a more complex metal carbide is that of $\text{Ca}_5\text{Cl}_3(\text{C}_2)(\text{CBC})$ [57,59]. The structure of this compound consists of C_2^{2-} and CBC^{5-} anions sandwiched between layers of Ca^{2+} cations. The C_2^{2-} anions are coordinated by a distorted octahedron of Ca^{2+} cations [59].

4.1.3 Comparison of CS Tensors for Metal Carbides

The chemical shift for the 'free' C_2^{2-} anion has not been determined, but Wrackmeyer and co-workers have predicted that this value is 140 ppm, based on the shielding of the nitrogen nucleus for CN^- , which is isoelectronic with C_2^{2-} [56]. The isotropic ^{13}C chemical shifts of the metal carbides are significantly greater than this value, implying a significant electronic effect on the shielding from the metal centres. The different CS tensors for the barium and calcium carbides are interpreted as an indication of some covalent interactions between C_2^{2-} and the cations [56]. The variation of the δ_{33} components with the metal centre (Table 1) implies a significant paramagnetic term in the total shielding (equation (2)), consistent with the argument that covalent bonding is affecting the shielding. The carbon CS tensors of the transition metal carbides [53] are not very different from those of the corresponding alkali-metal carbides [51,52], thus suggesting that the transition-metal atoms have a negligible effect on the magnetic shielding.

4.1.4 Solid-State NMR Studies of Fullerides

Although not strictly within the definition of this section, a few representative papers on solid-state NMR investigations of fullerides are discussed here in order to draw attention to this emerging field of study. The preparation of alkali-metal doped C_{60} and C_{70} films [60] has prompted some solid-state NMR studies to investigate the properties of these materials. These compounds are of the type A_xC_{60} , where $\text{A} = \text{Na}, \text{K}, \text{Rb}$ or Cs , and $x = 1, 3, 4$ or 6 . Those with $x = 1$ have been the subject of numerous recent studies because of their unusual properties [61].

The phase transitions of CsC_{60} and RbC_{60} were investigated with ^{13}C , ^{87}Rb and ^{133}Cs NMR [61]. By measuring the temperature-dependence of the NMR transitions and of the nuclear spin-lattice relaxation rates, it was shown that a phase transition occurs at 300 K for both compounds. From the large temperature-dependent chemical shifts in the ^{87}Rb and ^{133}Cs NMR spectra, the authors conclude that the compounds in the high-temperature phase are paramagnets. Although the spectra of the low-temperature phases are not well understood, the authors suggest that the greatly reduced ^{13}C spin-lattice relaxation times observed for these phases may be a consequence of the formation of a metallic state [61].

An important preliminary task in determining the nuclear magnetic properties of CsC_{60} is to assign the 16 non-equivalent ^{13}C nuclei. This was recently

investigated by de Swiet and co-workers [62]. This work entailed the analysis of high-speed 1D MAS NMR, 2D ^{13}C – ^{13}C correlation NMR and $^{13}\text{C}\{^{133}\text{Cs}\}$ REDOR [63] spectra. The assignment is further complicated by the fact that some resonances depend on the MAS frequency; this is attributed to temperature-dependent Knight shifts. The analyses led to two possible sets of assignments; DFT calculations were undertaken to distinguish between these. The orthorhombic phase ($T < 350$ K) of CsC_{60} has been investigated by ^{13}C and ^{133}Cs NMR [64]. Spectra of MAS samples were acquired to provide insight into the electronic structure of this phase. Recently, the low-temperature behaviour of CsC_{60} was investigated by ^{13}C and ^{133}Cs NMR [65]. The authors report a structural phase transition at 13.8 K.

4.2 METAL–OLEFIN AND METAL–ACETYLENE COMPLEXES

Interest in unsaturated-carbon organometallic compounds dates back to the report of the first metal–olefin complex, $\text{K}[\text{Pt}(\text{C}_2\text{H}_4)\text{Cl}_3]$, commonly known as Zeise's salt, by William Christoffer Zeise in 1827 [66,67]. The electronic structure for this compound, based on the models of Dewar, and Chatt and Duncan [7], was not proposed until the 1950s.

The structure of Zeise's anion (Figure 4(a)) and of $\text{Pt}(\text{C}_2\text{H}_4)(\text{PPh}_3)_2$ (Figure 4(b)) illustrate the differences between Pt(II) and Pt(0) complexes. In the former, an example of a weak coordination complex, the ethylene ligand is perpendicular to the plane defined by the PtCl_3 moiety and the C–C bond length, 1.37 Å [68], is only slightly longer than that of uncoordinated ethylene, i.e. 1.338 Å [69]. In a strong coordination complex such as $\text{Pt}(\text{C}_2\text{H}_4)(\text{PPh}_3)_2$, the ethylene ligand is in the plane defined by the platinum and phosphorus atoms and the C–C bond length, 1.434 Å [70], is intermediate between those of ethylene [69] and ethane [71], 1.338 and 1.535 Å, respectively. The nature of the metal–ligand coordination in platinum–olefin complexes has recently been studied by high-level *ab initio* calculations [72].

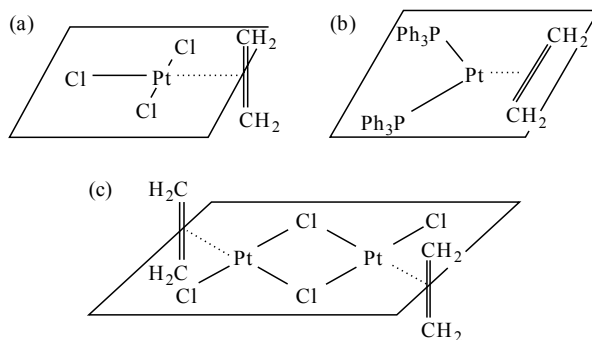


Figure 4 Structures of (a) Zeise's anion, (b) $\text{Pt}(\text{C}_2\text{H}_4)(\text{PPh}_3)_2$ and (c) Zeise's dimer

4.2.1 Carbon-13 NMR Studies

The results of ^{13}C NMR studies on metal–olefin complexes have been discussed in terms of the ligand and of the metal centre. The data are summarized in four tables, namely η^2 -coordinated platinum complexes (Table 2), η^2 -coordinated copper complexes (Table 3), η^4 -coordinated cyclooctadiene complexes (Table 4) and the remaining η^4 -coordinated olefin–metal complexes (Table 5). The results of solid-state NMR studies of platinum–acetylene complexes are summarized in Table 6.

Table 2 Principal components of the carbon chemical shift tensors for some platinum–olefin complexes^a

Compound	δ_{iso}	δ_{11}	δ_{22}	δ_{33}	Ω	κ	Ref.
C_2H_4^b	126	234.0(25)	120.0(25)	24.0(25)	210	−0.09	41
$\text{K}[\text{Pt}(\text{C}_2\text{H}_4)\text{Cl}_3]^c$	63(10)	135(10)	67(10)	−10(10)	145	0.08	73
	61(10)	133(10)	64(10)	−12(10)	145	0.06	
$\text{K}[\text{Pt}(\text{C}_2\text{H}_4)\text{Cl}_3]$	75.9	160	68	0	160	−0.15	75
$\text{K}[\text{Pt}(\text{C}_2\text{H}_4)\text{Cl}_3]$	76.0(5)	150(5)	79(5)	0(5)	150	0.06	76
$[\text{Pt}(\text{C}_2\text{H}_4)\text{Cl}_2]_2$	77(10)	157(10)	84(10)	−14(10)	171	0.12	73
$\text{Pt}(\text{C}_2\text{H}_4)(\text{PPh}_3)_2^c$	39.7(5)	65(5)	44(5)	10(5)	55	0.23	76
	38.7(5)	61(5)	42(5)	13(5)	48	0.21	
tsb^d	128	215(2)	120(2)	49(2)	166	−0.15	77
$\text{Pt}(\text{tsb})(\text{PPh}_3)_2$	68	92(2)	71(2)	41(2)	51	0.18	77

^a Data for the uncoordinated ligand are included for comparison, with all measurements carried out at room temperature, unless otherwise specified. Chemical shifts are relative to TMS; all data except κ are in ppm. Uncertainties in the last digits, where reported, are given in parentheses.

^b Measured at 30 K.

^c The CS tensors for non-equivalent olefinic carbon sites were reported.

^d *tsb*, *trans*-stilbene.

Table 3 Principal components of the carbon chemical shift tensors for some η^2 -coordinated copper–olefin complexes^a

Compound	δ_{iso}	δ_{11}	δ_{22}	δ_{33}	Ω	κ	Ref.
C_2H_4^b	126	234.0(25)	120.0(25)	24.0(25)	210	−0.09	41
$\text{Cu}(\text{C}_2\text{H}_4)(\text{OTf})^c$	90	218	82	−32	250	−0.1	79
<i>cis</i> -2-butene	124	232.0(25)	119.0(25)	22.0(25)	210	−0.07	41
$\text{Cu}(\textit{cis}\text{-butene})(\text{OTf})^c$	98	172	116	5.4	166.6	0.32	79
<i>dmb</i> ^d	123	217	126	35	182	0.05	79
$\text{Cu}(\textit{dmb})(\text{OTf})^c$	110	158	127	45	113	0.45	79
<i>cis</i> -cycloheptene	133	245.0(5)	126.0(5)	27.0(5)	218	−0.09	41
$\text{Cu}(\textit{cycloheptene})(\text{OTf})^c$	109	161	112	54	107	0.08	79

(continued)

Table 3 (continued)

Compound	δ_{iso}	δ_{11}	δ_{22}	δ_{33}	Ω	κ	Ref.
cyclohexene	127	—	—	—	—	—	79
Cu(cyclohexene)(OTf) ^c	105	—	—	—	—	—	79
cis-cyclooctene	131	—	—	—	—	—	79
Cu(cyclooctene)(OTf) ^c	106	—	—	—	—	—	79

^a For a discussion of uncertainties, see text. See also footnote *a* of Table 2.

^b Measured at 30 K.

^c OTf, trifluoromethane sulfonate.

^d dmb, 2,3-dimethyl-2-butene.

Table 4 Principal components of the carbon chemical shift tensors for some η^4 -coordinated metal–cod^a complexes^b

Compound	δ_{iso}	δ_{11}	δ_{22}	δ_{33}	Ω	κ	Ref.
cod	128	238	126	21	217	−0.03	79
[Rh(cod)Cl] ₂	80.5	161.7	76.7	20.5	141.2	−0.08	75
[Rh(cod)Cl] ₂	80	140	79	14.5	125.5	−0.02	79
[Ir(cod)Cl] ₂	62	122	67	−1	123	0.12	79
Pt(cod)Cl ₂	117	225	125	1	224	0.11	79
Pt(cod)Cl ₂ ^c	103.0	182.3	104.0	18.0	164.3	0.02	75
Pt(cod)Cl ₂ ^c	101	185	112	3	182	0.18	79
Pt(cod)Me ₂	98.0	179(1)	99(1)	15(1)	164	0.02	84
	101.7	185(3)	103(3)	17(2)	168	0.02	
Pt(cod)(Me)Cl ^d	86.1	159(3)	88(2)	10(2)	149	0.04	84
	114.0	203(2)	115(1)	22(2)	181	0.02	
	117.2	208(2)	122(2)	22(2)	186	0.08	
Pt(cod)[CH ₂ SiMe ₃] ₂ ^d	95.4	170(3)	107(2)	9(4)	161	0.22	84
	100.7	188(4)	108(3)	7(5)	181	0.12	
	102.8	187(5)	106(3)	15(5)	172	0.06	
Pt(cod)(C ₂ - ^t Bu) ₂ ^d	103.5	192(4)	102(5)	15(4)	177	−0.03	84
	106.6	196(4)	113(5)	15(5)	181	0.11	
[Cu(cod)Cl] ₂ ^e	118.8	203.5	116.0	36.5	167.0	−0.05	75
[Ag(cod) ₂]BF ₄ ^f	124.8	225.0	115.0	34.0	191.0	−0.15	75

^a cod, 1,5-cyclooctadiene.

^b See footnote *a* of Table 2.

^c See Figure 7(a) for the molecular structure.

^d Non-equivalent sites were reported.

^e See Figure 7(c) for the molecular structure.

^f See Figure 7(b) for the molecular structure.

Table 5 Principal components of the olefinic carbon CS tensors for some η^4 -coordinated metal–olefin complexes^a

Compound	δ_{iso}	δ_{11}	δ_{22}	δ_{33}	Ω	κ	Ref.
nbd ^b	143	259	130	40	219	−0.18	79
[Rh(nbd)Cl] ₂	52	120	66	−31	151	0.28	79
Pt(nbd)Me ₂	89.0	179.2(10)	77.0(7)	10.7(9)	168.5	−0.21	84

(continued)

Table 5 (continued)

Compound	δ_{iso}	δ_{11}	δ_{22}	δ_{33}	Ω	κ	Ref.
Pt(nbd)[CH ₂ SiMe ₃] ₂	83.3	171.8(12)	70.7(11)	7.4(11)	164.4	-0.23	84
	85.0	178(3)	73(2)	4(2)	174	-0.21	
	88.1	182(6)	76(5)	7(5)	175	-0.21	
	91.7	181.1(8)	81.6(7)	12.4(7)	168.7	-0.18	
Pt(nbd)(4- <i>t</i> -Bu-phenyl) ₂	93.3	195(12)	73(18)	10(10)	185	-0.33	84
	100.5	189(7)	102(6)	9(4)	180	0.03	
cot ^c	133	234	127	43	191	-0.09	79
[Rh(cot)Cl] ₂ ^d	81	142	80	12	130	-0.01	79
hmdb ^e	149	244(6)	149(6)	55(22)	189	0.00	85
[Rh(hmdb)Cl] ₂ ^d	68	138	60	10.7	127.3	-0.19	79

^a See footnote *a* of Table 2.^b nbd, norbornadiene.^c cot, 1,3,5,7-cyclooctatetraene.^d The CS tensor components for the coordinated olefinic carbons are given here.^e hmdb, hexamethyl dewar benzene, measured at 87 K. Values for the olefinic carbon nuclei are given here.**Table 6** Principal components of the carbon CS tensors for some metal-acetylene complexes^a

Compound	δ_{iso}	δ_{11}	δ_{22}	δ_{33}	Ω	κ	Ref.
dpa ^b	89.8(2)	165(2)	147(2)	-42(2)	207	0.85	86
Pt(dpa)(PPh ₃) ₂ ^c	135(1)	230(5)	145(5)	30(5)	200	0.15	86
	133(1)	232(5)	141(5)	27(5)	205	0.12	
	128(1)	216(5)	140(5)	26(5)	190	0.19	
	127(1)	207(5)	141(5)	32(5)	175	0.24	
Cu(dpa)(OTf) ^d	93	—	—	—	—	—	79
dma ^e	91	158(6)	158(6)	-44(17)	202	1.00	85
Cu(dma)(OTf) ^d	81	—	—	—	—	—	79
acetylene ^f	70	150.0(25)	150.0(25)	-90.0(25)	240.0(25)	1.00	40
Cu(acetylene)(OTf) ^d	77	—	—	—	—	—	79
btsa ^g	114	—	—	—	—	—	79
Cu(btsa)(OTf)	114	—	—	—	—	—	79

^a See footnote *a* of Table 2.^b dpa, diphenylacetylene.^c Non-equivalent acetylenic carbon nuclei were observed for this complex.^d OTf, trifluoromethane sulfonate.^e dma, dimethylacetylene, measured at 87 K.^f Measured at 15 K.^g btsa, *bis*-(trimethylsilyl) acetylene.

4.2.1.1 Platinum-olefin complexes

The reported carbon CS tensors for platinum-olefin complexes are summarized in Table 2. As fundamental metal-olefin complexes, the Pt-ethylene complexes

Zeise's salt and $\text{Pt}(\text{C}_2\text{H}_4)(\text{PPh}_3)_2$ are of ongoing interest [1]. Since the carbon CS tensor of uncoordinated ethylene has been determined [40,41] and the structures of the complexes are known [68,70], solid-state NMR studies of these complexes provide fundamental insight into the effects of metal coordination on nuclear magnetic shielding.

Several groups have reported the carbon CS tensors of Zeise's salt through the analysis of the ^{13}C NMR spectra of slow MAS samples [73–75]. The carbon CS tensors were also determined by Bernard *et al.* [76], who analysed the ^{13}C NMR spectra of ^{13}C -labelled stationary samples (Figure 5) by using the dipolar-chemical shift method. CS tensor orientations have been proposed, based on a combination of theoretical and experimental results [76]. The carbon CS tensors of a closely related compound, $[\text{Pt}(\text{C}_2\text{H}_4)\text{Cl}_2]_2$, commonly known as Zeise's dimer (Figure 4(c)), have been reported by Huang *et al.* [73].

The olefinic carbon CS tensors for $\text{Pt}(\text{C}_2\text{H}_4)(\text{PPh}_3)_2$ were determined from the analysis of stationary $^{13}\text{C}_2$ -labelled powder samples [76]. Orientations for the carbon CS tensors were proposed on the basis of experimental results and *ab initio* calculations. This investigation demonstrated that coordination of ethylene with platinum greatly reduces the span of the CS tensor, a consequence of the increased shielding in the direction of the δ_{11} components. Compared to the orientation of the carbon CS tensor for ethylene (Figure 2(a)), the orientations of the δ_{11} and δ_{22} components are rotated by approximately 45° about δ_{33} , which is virtually unaffected by coordination. In a related study, the olefinic carbon CS tensors of $\text{Pt}(\eta^2\text{-trans-stilbene})(\text{PPh}_3)_2$ were determined by using the dipolar-chemical shift method combined with *ab initio* calculations [77]. The reported carbon CS tensors are comparable in magnitude and orientation to those of $\text{Pt}(\text{C}_2\text{H}_4)(\text{PPh}_3)_2$, as expected from the similar orientation of the olefins relative to the $\text{Pt}(\text{PPh}_3)_2$ moiety.

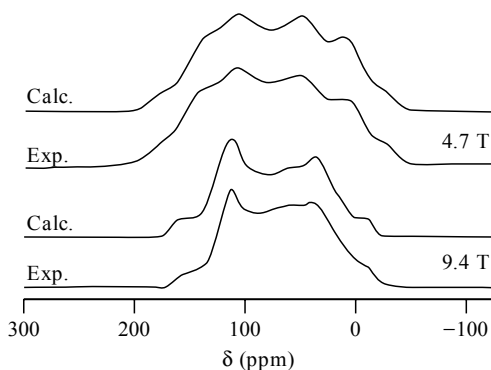


Figure 5 Calculated and experimental ^{13}C NMR spectra of a stationary ^{13}C -labelled sample of Zeise's salt, acquired at 4.7 and 9.4 T (Reprinted with permission from *J. Phys. Chem., A*, **104**, 8131 (2000), Copyright 2000 American Chemical Society)

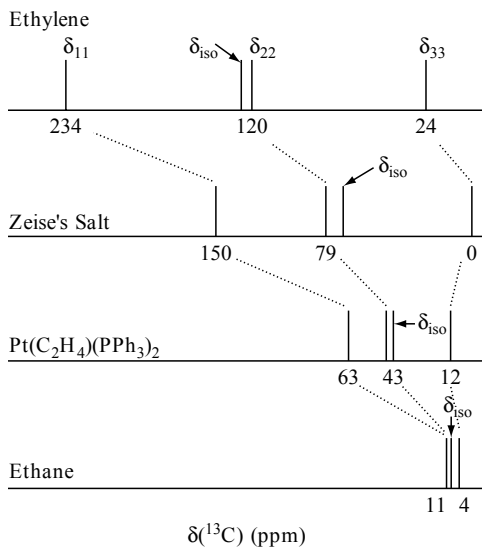


Figure 6 Comparison of the principal components of the carbon CS tensors for ethylene [40,41], ethane [78] and two platinum–ethylene complexes [76]. Note that the average values for the non-equivalent olefinic carbon sites of Pt(C₂H₄)(PPh₃)₂ are illustrated here

The effect of coordination of ethylene with platinum on the magnitudes of the principal components of the CS tensor is shown graphically in Figure 6. This figure illustrates that the large changes in shielding are primarily due to increased shielding in the directions of the δ_{11} and δ_{22} components; the shielding in the direction of δ_{33} is relatively insensitive to coordination. This observation is consistent with the structural changes to ethylene upon coordination. An ethylene ligand coordinated to a metal centre is expected to have properties intermediate between those of ethylene and ethane [1], consistent with the CS tensors for the Pt–ethylene complexes. In particular, the CS tensors for Pt(C₂H₄)(PPh₃)₂ are intermediate between those for ethylene and for ethane, $\delta_{11} = \delta_{22} = 11$ ppm and $\delta_{33} = 4$ ppm [78]. The greater sensitivity to coordination of the CS tensor for Pt(C₂H₄)(PPh₃)₂, compared to that for Zeise's salt, is also consistent with this model, since the structure of the ethylene ligand is significantly modified in this strong coordination complex.

4.2.1.2 Carbon chemical shift tensors of some copper–olefin complexes

Walraff [79] undertook a study of the olefinic carbon CS tensors for several olefins coordinated with Cu(I)–OTf complexes (OTf, trifluoromethane sulfonate); the results obtained are summarized in Table 3. The principal components of the carbon CS tensors were assigned from the analysis of ¹³C NMR spectra of natural-abundance stationary powder samples. The reported values have

significant uncertainties associated with them, a consequence of the broad ^{13}C NMR spectra complicated by contributions from the methyl ^{13}C nuclei. The line broadening is attributed primarily to the dipolar coupling with the $^{63/65}\text{Cu}$ nuclei. For example, the dipolar coupling to ^{63}Cu ($I = 3/2$, natural abundance = 69.09%) and ^{65}Cu ($I = 3/2$, natural abundance = 30.91%) is predicted to be 905 and 969 Hz, respectively, for the olefinic carbon nuclei of the cyclohexene–Cu complex, based on the reported Cu–C bond lengths of 2.07 Å [80]. Dipolar coupling to the ^{19}F nuclei of the triflate ion are also expected to contribute to the line broadening. In addition, the author suggests that motion of the olefin ligands may contribute to the line broadening and hence to significant uncertainty in the reported NMR parameters. However, spectra of the cyclooctadiene complex acquired at 77 K are not different from those obtained at room temperature. In addition to the CS tensor data summarized in Table 3, the author also reported the isotropic carbon chemical shift of the cyclohexene– and *cis*-cyclooctadiene–copper complexes [79]. Although the isotropic carbon chemical shift decreases for all ligands upon coordination to copper, it is not possible to ascribe the changes to specific tensor components, a consequence of the approximate nature of the data.

4.2.1.3 Carbon chemical shift tensors for η^4 -coordinated transition-metal–olefin complexes

The extensive studies of solid metal–cod (cod, 1,5-cyclooctadiene) complexes allow a comparison of the effect of the metal centre on the shielding of the carbon nuclei. The data are summarized in Table 4; Figure 7 illustrates the structures of some Pt– [81], Ag– [82] and Cu–cod [83] complexes investigated by solid-state NMR. The data have been reported by three groups: Oldfield and co-workers [75], as well as Gay and Young [84], analysed the ^{13}C NMR spectra of MAS samples, whereas Walraff [79] analysed spectra of stationary powder samples. The CS tensors are affected to varying degrees by coordination with the metal centre, but qualitatively the effects are the same as those discussed above for the Pt–olefin complexes (see Section 4.2.1.1). The δ_{33} components

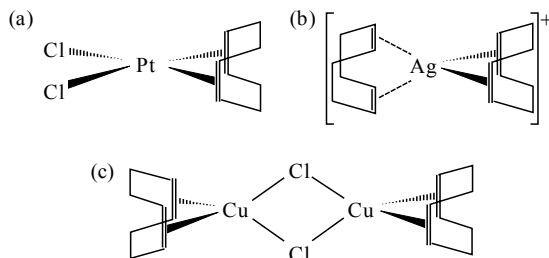


Figure 7 Structures of (a) $\text{Pt}(\text{cod})\text{Cl}_2$ [81], (b) the $\text{Ag}[(\text{cod})_2]^+$ cation (B) [82] and (c) $[\text{Cu}(\text{cod})\text{Cl}]_2$ [83]

are essentially invariant to coordination while the shielding in the directions of δ_{11} and δ_{22} increases. Walraff has attempted to rationalize the results on the basis of the Dewar, and Chatt and Duncanson model [7]. However some discrepancies are unexplained [79], illustrating that nuclear magnetic shielding cannot always be explained by simple models. Likewise, Oldfield and co-workers ‘found no striking correlations’ [75] between the observed CS tensor parameters and various molecular properties. These experiments did not yield the CS tensor orientations, although Oldfield and coworkers [75] reported orientations obtained from DFT calculations. These authors report that the orientations of the CS tensors are, in general, sensitive to the degree of back bonding—increased back bonding leads to a tilting of the CS tensor. For the most affected compound, $[\text{RhCl}(\text{cod})]_2$ the δ_{22} and δ_{33} components form angles of 37.5 and 107.3°, respectively, with the olefinic C–C bond.

The olefinic carbon CS tensors for several other η^4 -coordinated metal complexes have been determined by the analysis of NMR spectra of stationary powder [79] or of MAS samples [84]; the results are summarized in Table 5. The unsaturated ligands investigated include norbornadiene (nbd) [79], 1,3,5,7-cyclooctatetraene (cot) [79], and hexamethyl dewar benzene (hmdb) [85]. In general, the effect of metal coordination on the olefinic carbon CS tensors of η^4 -coordinated ligands is comparable to that observed for the η^2 -coordinated ligands.

4.2.1.4 Carbon chemical shift tensors for some transition-metal–acetylene complexes

The only reported carbon CS tensor for a metal–acetylene complex is that obtained for $\text{Pt}(\eta^2\text{-diphenylacetylene})(\text{PPh}_3)_2$ (Table 6) [86]. Using the dipolar-chemical shift method, the principal components of the carbon CS tensors were determined, as well as their orientations relative to \mathbf{r}_{cc} . The results demonstrate that the magnitudes and orientations of the carbon CS tensors of the coordinated diphenylacetylene are comparable to those of an uncoordinated ethylene. These changes are consistent with the C–C bond lengthening that occurs upon coordination with platinum, as well as the change in the ‘coordination number’ of the carbon nuclei (2 for uncoordinated diphenylacetylene and 3 for the metal complex).

Wallraff reported the isotropic chemical shifts for some copper–acetylene complexes [79], determined by ^{13}C NMR studies of solid MAS samples. The results, summarized in Table 6, show that coordination of acetylenes with copper has a negligible effect on δ_{iso} . This does not prove that the magnetic shielding is unaffected by metal coordination, since the invariance of δ_{iso} probably is a consequence of opposing changes to the CS tensor components—see the results for $\text{Pt}(\eta^2\text{-diphenylacetylene})(\text{PPh}_3)_2$ discussed above. In addition, consider the carbon CS tensor for acetylene. Since it is a linear molecule, $\sigma_{\parallel}^p = 0$. However, if the linear symmetry is broken by coordination

to a metal, the magnetic shielding in the direction of the C–C bond is expected to be reduced when compared to its value for the uncoordinated ligand; this may not be apparent from δ_{iso} since the shielding in the other directions may increase.

4.2.2 Solid-State NMR Studies of Internal Dynamics

The sensitivity of ^2H NMR spectra to molecular motion has been exploited in order to gain insight into the dynamics of ethylene coordinated with metal centres. By analysing the ^2H NMR spectra of deuterated-ethylene analogues of Zeise's salt and $\text{Pt}(\text{C}_2\text{H}_4)(\text{PPh}_3)_2$, Bernard and co-workers showed that the ethylene ligand in these complexes is subject to little or no motion in the solid state [76]. In contrast, for solid $\text{Rh}(\text{acac})(\text{C}_2\text{H}_4)_2$, variable-temperature NMR experiments indicate that the ethylene ligand undergoes rapid 180° jumps at 298 K [87]. The free energy of activation for this process, determined by variable-temperature ^{13}C MAS NMR, is $56.5 \pm 3 \text{ kJ mol}^{-1}$. Conclusions about the rotation of the ethylene ligand were corroborated with ^2H NMR experiments and through the measurement of $T_{1\rho}(^1\text{H})$. In their ^{13}C NMR investigation of solid osmium–ethylene complexes, Lewis and co-workers concluded that at temperatures above 250 K the ethylene ligand undergoes rotation about the axis perpendicular to the C–C bond with a barrier to internal rotation that is comparable to that measured for the sample in solution [88]. The free energy of activation for this process, determined by variable-temperature ^{13}C NMR, is 50.5 kJ mol^{-1} .

The dynamics of 1-butene and 1-pentene adsorbed in zeolites were investigated through the analysis of the ^1H NMR spectra of MAS samples, as well as with 2-dimensional (NOESY) spectra [89]. The authors obtained ^1H NMR spectra which are sensitive to the loading level of the molecules in the zeolite cages, thus allowing an investigation of the interaction of the olefins with the zeolite. They conclude that the molecules within the zeolite cages are subject to fast librational motion, as well as reorientation and translation.

Fyfe and co-workers have investigated the dynamics of the cyclooctatetraene (cot) ligand in solid iron [90,91] and ruthenium [91,92] carbonyl complexes. By observing the temperature-dependence of the ^1H NMR line width, these authors concluded that the cot ligands of $\text{Fe}(\text{cot})(\text{CO})_3$ and $\text{Fe}_2(\text{cot})(\text{CO})_5$ are fluxional (Figure 8) at temperatures above 298 K, but is rigid in $\text{Fe}_2(\text{cot})(\text{CO})_6$ [90]; these conclusions were corroborated by measurement of the ^1H relaxation times T_1 and $T_{1\rho}$ [91]. Similar experiments indicate that the cot ligand of $\text{Ru}_3(\text{cot})_2(\text{CO})_4$ is fluxional above 150 K [91,92a].

4.3 METALLOCENES

The unique molecular properties of the metallocenes have led to numerous solid-state NMR studies of these compounds. In addition, solid-state NMR has been

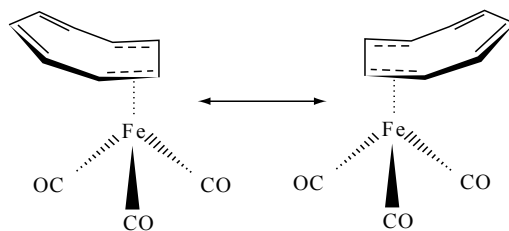


Figure 8 The fluxional character of $\text{Fe}(\text{cot})(\text{CO})_3$

used extensively to study the dynamics of these molecules as guests trapped in channels of various inclusion compounds. Some representative papers are discussed below.

4.3.1 Carbon CS Tensors

Reported carbon CS tensor data derived from ^{13}C NMR studies of solid metallocene complexes are summarized in Tables 7 (cyclopentadienyl–iron complexes), 8 (other cyclopentadienyl–metal complexes) and 9 (η^6 -coordinated complexes). These studies considered internal motion in the analysis of the data. In Section 4.3.2 below, the solid-state NMR literature which considered

Table 7 Principal components of the cyclopentadienyl carbon CS tensors for some iron–cyclopentadiene complexes^a

Compound	T (K) ^b	δ_{iso}	δ_{11}	δ_{22}	δ_{33}	Ω	κ	Ref.
$[\text{Cp}]^c$	20	106	182(3)	114(3)	21(3)	161	0.15	94
FeCp_2^d	9–25	68(2)	121(3)	71(2)	13(2)	108	0.08	97
FeCp_2	RT	70	96	96	18	78	1.00	97
FeCp_2	RT	68	94	94	17	77	1.00	96
FeCp_2	77	70	95	95	19	76	1.00	95
FeCp_2	RT	69.3	95.0(5)	95.0(5)	17.8(5)	77.2	1.00	98
$2\text{FeCp}_2/\text{Na}_{55}\text{Y}^e$	300	69.7	94.7	94.7	19.7	75	1.00	100
$\text{FeCp}_2/\text{thiourea}$	125	71.3	96.5(16)	96.5(16)	21.0(27)	75.5	1.00	111
$\text{FeCp}(\text{CO})_2\text{Me}$	200	87.2	116(1)	116(1)	29(2)	87	1.00	84
$\text{FeCp}(\text{CO})_2\text{Me}$	150	87.4	124(2)	112(2)	26(2)	98	0.75	84
$[\text{FeCpPh}][\text{AsF}_6]^f$	< 270	68	101	101	2	99	1.00	101
$\text{Fe}(\text{C}_5\text{Me}_5)_2$	77	79.2	127.7(10)	86.2(10)	23.6(10)	104.1	0.20	95,99

^a See footnote *a* of Table 2.

^b RT, room temperature.

^c Cp, cyclopentadienyl.

^d Spectra were acquired at 9, 15 and 25 K. The average values of the CS tensor components, which did not deviate by more than 3 ppm, are listed here.

^e Ferrocene adsorbed in faujasite-type zeolites. The principal components of the CS tensor have been calculated from the reported values of δ_{iso} and Ω according to $\delta_{11} = \delta_{22} = \delta_{\text{iso}} + (1/3)\Omega$ and $\delta_{33} = \delta_{\text{iso}} - (2/3)\Omega$.

^f See Table 9 for the carbon CS tensors of the phenyl ring. Comparable values were reported for temperatures between 270 and 310 K.

Table 8 Principal components of the ring carbon CS tensors for some η^5 -coordinated cyclopentadienyl–metal complexes^a

Compound	<i>T</i> (K) ^b	δ_{iso}	δ_{11}	δ_{22}	δ_{33}	Ω	κ	Ref.
[Cp] ^c	20	106	182(3)	114(3)	21(3)	161	0.15	94
MgCp ₂	77	109	153	153	21	132	1.00	95
MgCp ₂	RT	108.3	152.0(5)	152.0(5)	21.0(5)	131.0	1.00	98
RuCp ₂	77	74	100	100	21	79	1.00	95
RuCp ₂	RT	72.3	99.0(5)	99.0(5)	19.0(5)	80.0	1.00	98
TiCp ₂ Cl ₂	77	116	168	168	13	155	1.00	95
MoCp(CO) ₃ Me	296	94.3	137(7)	122(7)	22(3)	115	0.72	84
MoCp(CO) ₃ Me	170	94.8	139.5(9)	121.5(11)	23.5(12)	116.0	0.69	84
MoCp(CO) ₃ Et	RT	94.5	139.6(10)	122.7(13)	22.2(14)	117.4	0.72	84
CoCp(CO) ₂ ^d	183	86.5	117.3	117.3	25	92.3	1.00	100
Ti(η -Cp)(σ -Cp) ^e	182	117.3	158(1)	158(2)	36(2)	122	1.00	102
Co(C ₅ Me ₅) ₂ Cl ^f	77	114	180(5)	124(5)	39(10)	141	0.21	95
		107	172(5)	111(5)	39(10)	133	0.09	

^a See footnote *a* of Table 2.^b RT, room temperature.^c Cp, cyclopentadienyl.^d Adsorbed in zeolite Na₅₅Y. The principal components of the CS tensor have been calculated from the reported values of δ_{iso} and Ω according to $\delta_{11} = \delta_{22} = \delta_{\text{iso}} + (1/3)\Omega$ and $\delta_{33} = \delta_{\text{iso}} - (2/3)\Omega$.^e The carbon CS tensors for the η^5 -coordinated ring are given here.^f Non-equivalent sites were reported.**Table 9** Principal components of the ring carbon CS tensors for some η^6 -coordinated complexes^a

Compound	<i>T</i> (K) ^b	δ_{iso}	δ_{11}	δ_{22}	δ_{33}	Ω	κ	Ref.
C ₆ H ₆	14	119.8	216.9(32)	140.7(20)	1.0(30)	215.9	0.29	104
Cr(C ₆ H ₆) ₂	77	77	115	115	1	114	1.00	95
Cr(C ₆ H ₆)(CO) ₃	—	99	152(5)	138(5)	7(5)	145	0.81	106
Cr(C ₆ H ₆)(CO) ₃	129	96	158	126	3	155	0.58	107
[FeCpPh] [AsF ₆] ^c	< 270	95	129	129	28	101	1.00	101
C ₆ Me ₆	87	133	227(4)	155(4)	19(4)	208	0.32	105
Cr(C ₆ Me ₆)(CO) ₃	—	111	170(5)	138(5)	25(5)	145	0.56	106
C ₆ Et ₆ ^d	RT	135.3	220.4(7)	163.7(7)	21.7(7)	198.7	0.43	105
	—	135.0	219.4(11)	165.1(11)	20.6(11)	198.8	0.45	
	—	135.4	220.5(7)	163.8(7)	21.8(7)	198.7	0.43	
Cr(C ₆ Et ₆)(CO) ₃ ^e	—	120	170(5)	161(5)	29(5)	141	0.87	106
	—	112	168(5)	146(5)	22(5)	146	0.70	

^a See footnote *a* of Table 2.^b RT, room temperature; note that temperatures have not specified in some cases.^c See Table 7 for the carbon CS tensors of the cyclopentadienyl ring. Comparable values were reported for temperatures between 270 and 310 K.^d Et, ethyl.^e Non-equivalent carbon sites were reported.

only the internal dynamics of the ligands is discussed. A recent review has summarized the data on cyclopentadienyl–metal complexes [93].

4.3.1.1 Carbon-13 NMR studies of cyclopentadienyl–metal complexes

There have been numerous ^{13}C NMR studies of cyclopentadienyl–metal complexes. These studies provide information about the internal dynamics of the cyclopentadienyl rings, and since the carbon CS tensor for the uncoordinated cyclopentadienyl anion has been reported [94], ^{13}C NMR studies also provide insight into the effect of coordination on nuclear magnetic shielding.

Ferrocene was one of the earliest metallocene compounds to be studied by solid-state NMR [95]. The fact that the carbon CS tensor appears axially symmetric, even at 77 K, suggests that in-plane rotation of the cyclopentadienyl rings is rapid. The principal components, measured at 77 K (Table 7), are comparable to those obtained from spectra of powder samples acquired at room temperature [96–98]. The unique CS tensor component is assumed to be perpendicular to the cyclopentadienyl ring while in-plane components are averaged by rotation of the ring [96,97]. Hallock *et al.* reached the same conclusion, based on the results of ^{13}C two-dimensional chemical shift correlation spectroscopy [98].

Orendt and co-workers [97] determined the principal components of the carbon CS tensor for ferrocene from spectra of stationary powder samples acquired at temperatures of 9 ± 1 K and higher (Table 7 and Figure 9). As expected, the two ‘in-plane’ components, $\delta_{11} = 121$ ppm and $\delta_{22} = 71$ ppm, have an average value corresponding to δ_{\perp} observed for spectra acquired at room temperature. By obtaining ^{13}C NMR spectra as a function of temperature, these authors determined that motion of the ring about the C_5 symmetry axis is not significant below 45 K. Comparison of the magnitudes of the δ_{33} components obtained in the absence of motional averaging, $\delta_{33} = 13$ ppm, with those obtained at room temperature, allowed a determination of the orientation of this component relative to the C_5 rotation axis of the ligand, $\pm(12.4 \pm 0.7^\circ)$; as for the dipolar chemical shift method, the supplement of an angle determined experimentally is also a possible orientation for a given CS tensor component. Nuclear magnetic shielding calculations using DFT were undertaken on optimized structures and on the three known structures of ferrocene, as determined from diffraction studies [97]. These calculations accurately predict the CS tensor components, and hence the orientation of the δ_{33} component was assigned based on the calculated results (Figure 10). The proposed orientation for the carbon CS tensor is comparable to that found for permethyl ferrocene [95,99]. In the latter case, two possible orientations were also determined; these authors assumed that the direction of greatest shielding is in the direction of the iron atom.

In addition to the studies of crystalline ferrocene samples discussed above, Overweg and co-workers have reported the carbon CS tensors of ferrocene

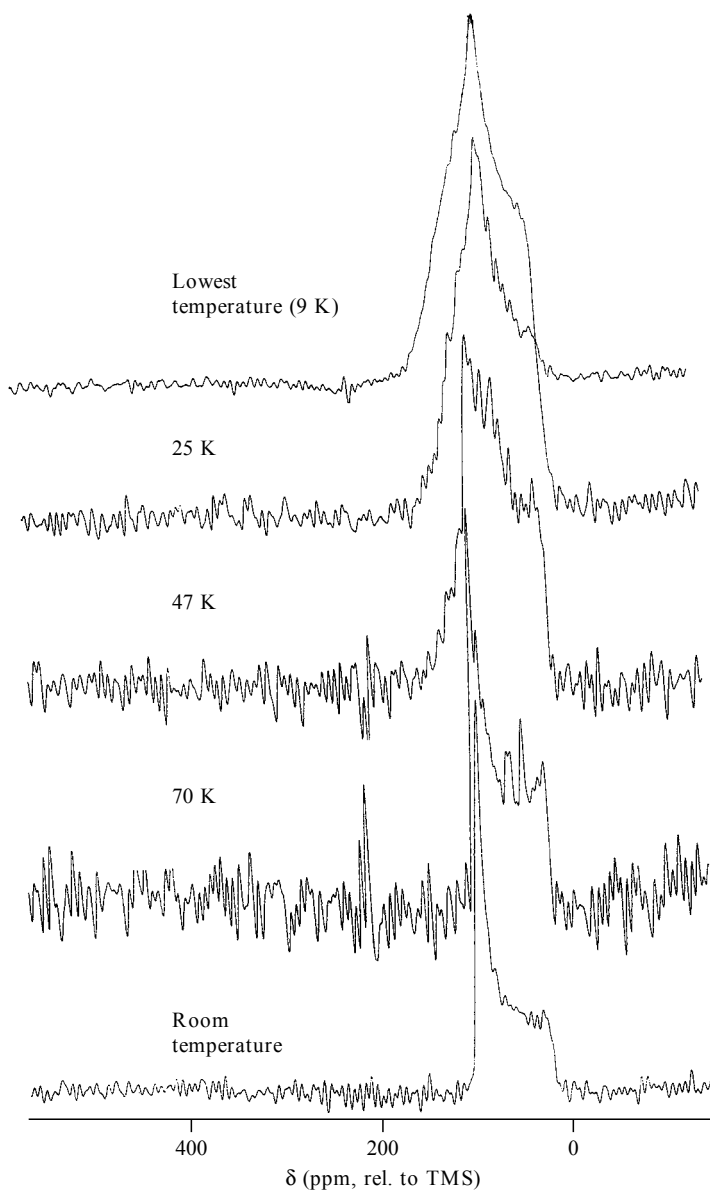


Figure 9 Carbon-13 NMR spectra of a stationary sample of ferrocene acquired at temperatures from 9 K (upper trace) to room temperature (lower trace). (Reprinted with permission from *J. Phys. Chem., A*, **102**, 7692 (1998), Copyright 1998 American Chemical Society)

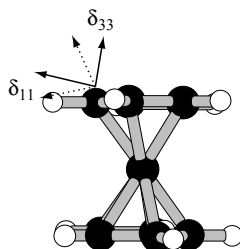


Figure 10 Orientation of the carbon CS tensor for ferrocene [97]. The solid arrows indicate the orientation proposed on the basis of combined experimental and theoretical results, while the dotted arrows represent an alternate solution, based on the experimental results. The δ_{22} component is approximately tangential to the cyclopentadienyl ring, perpendicular to the plane of the page

adsorbed in a zeolite [100]. The axially symmetric carbon CS tensors observed for this compound show that, while the cyclopentadienyl ligand is rotating rapidly at or close to room temperature, the molecule itself does not undergo rapid translational or rotational motion.

There have also been ^{13}C NMR studies on magnesium [95,98], ruthenium [95,98] and titanium [95] sandwich complexes (Table 8). These room-temperature studies all yielded axially symmetric carbon CS tensors due to motional averaging of the in-plane components of the tensor. The δ_{33} component is oriented perpendicular to the ring with a comparable magnitude to that obtained for the uncoordinated cyclopentadienyl anion [94]. We note that motional averaging will also affect the δ_{33} component unless it is exactly in the direction of rotation axis of the ligand, as has been demonstrated for ferrocene [97]. The relative insensitivity to metal coordination of the shielding in the direction of the δ_{33} components for these compounds is reminiscent of a similar observation for the olefinic carbon CS tensors of the metal–olefin complexes (Section 4.2 above). The carbon CS tensors for the mixed sandwich complex $[\text{FeCpPh}][\text{AsF}_6]$ have also been reported [101].

Gay and Young [84] reported the results of a ^{13}C NMR study of some iron and molybdenum ‘piano-stool’ complexes (Tables 7 and 8). The principal components of the carbon CS tensors were obtained by using the Herzfeld–Berger method [45]. Non-axially symmetric CS tensors were observed for the Mo complex at temperatures up to 296 K, suggesting that in-plane rotation of the ring is restricted in these compounds compared to the sandwich complexes. However, these authors note that the large uncertainties in the data make this conclusion tentative.

The carbon CS tensors of $\text{Ti}(\eta\text{-Cp})_2(\sigma\text{-Cp})_2$ were reported by Heyes and Dobson [102]. At 182 K, the η -coordinated cyclopentadienyl ligand is rotating rapidly (i.e. the rotation frequency is greater than the span, in frequency units, of the CS tensor). Isotropic values for some solid cobaltocenium salts of the type $[\text{CoCp}_2]^+$ were reported [103]. Although the CS tensor components are not

reported, the direct and indirect ^{13}C – ^{59}Co coupling, as well as the anisotropy in the indirect coupling tensor (ΔJ), were reported. In a complementary study to their investigation of ferrocene, Overweg and co-workers determined the principal components of the carbon CS tensors for $\text{CoCp}(\text{CO})_2$ adsorbed in faujasite-type zeolites [100]. The authors found that rapid motion of the molecule within the zeolite leads to averaging of the CS tensor components at room temperature. On cooling to 183 K, the only motion is the rotation of the Cp ligands about their approximate C_5 symmetry axes.

4.3.1.2 Carbon-13 NMR Studies of η^6 -coordinated complexes

The ^{13}C NMR data for the η^6 -coordinated complexes are summarized in Table 9. Since the carbon CS tensor for benzene [104], as well as those for hexamethylbenzene [105] and hexaethylbenzene [105], are known, this class of compounds can also offer information about the effect of metal coordination on carbon magnetic shielding. Wemmer and Pines [95] determined the principal components of the carbon CS tensor of bis(benzene)chromium. From the axially symmetric CS tensor, these authors concluded that the rings are rotating rapidly at 77 K. Maricq *et al.* [106] determined the carbon CS tensors for the ring carbons of the corresponding arene chromium tricarbonyl complexes by using the method of moments [46]. Their study showed that the increased isotropic shielding of 15 to 20 ppm arose almost entirely from the increased shielding in the direction of δ_{11} . Assuming that the orientations of the carbon CS tensors are unchanged by coordination with chromium (Figure 11), the authors suggested that the affected component is the one in the ring plane perpendicular to the C–H bond. In a later ^{13}C NMR study, the aromatic carbon CS tensors of this compound were reported to be non-axially symmetric at 129 K, based on an analysis of the spectra of MAS samples [107].

4.3.2 Other Solid-State NMR Studies

The hydrogen CS tensor of ferrocene was determined by Spiess *et al.* through the investigation of single crystals of ferrocene with multiple-pulse techniques [108]. Spherical samples were used to minimize bulk susceptibility effects. As for

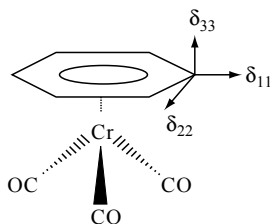


Figure 11 Orientation of the aromatic carbon CS tensor for $\text{Cr}(\text{C}_6\text{H}_6)(\text{CO})_3$ [106]

the carbon CS tensors of ferrocene discussed above, rapid rotation of the cyclopentadienyl ligands results in averaging of the in-plane components of the hydrogen CS tensor. However, in contrast to the ^{13}C NMR studies, the unique CS tensor component is in the direction of least shielding, $\delta_{\parallel} = 8.6 \pm 0.2$ ppm; the averaged in-plane components are $\delta_{\perp} = 2.0 \pm 0.2$ ppm.

Rotary resonance recoupling of the heteronuclear $^{13}\text{C}-^1\text{H}$ dipolar interaction in MAS samples of solid ferrocene was used to determine the magnitude of this interaction, and hence the C-H bond length [109]. The technique entails acquiring spectra at the rotary resonance condition (i.e. the proton decoupling field is an integer multiple of the MAS frequency). Under such conditions, a 'Pake-like' pattern is observed. A C-H bond length of 1.15 ± 0.04 Å is predicted using this technique, slightly longer than the 1.08 Å predicted from neutron diffraction studies of similar compounds [110].

In their study of ferrocene adsorbed in zeolites, Overweg *et al.* used ^2H NMR to gain insight into the motion of the molecule within the zeolite cages [100]. These authors found that, below 225 K, the only significant motion of ferrocene in Na_{55}Y is rapid rotation of the cyclopentadienyl ring, confirming the conclusions reached from a ^{13}C NMR study [100].

Nakai *et al.* investigated the dynamics of ferrocene included in thiourea [111] through ^{13}C NMR of oriented and powder samples. At 125 K, axially symmetric powder patterns are observed, suggesting that the only motion at this temperature is rapid rotation of the cyclopentadienyl ligands. From the two peaks observed in the low-temperature ^{13}C NMR spectra of a sample oriented such that the thiourea channels are parallel to \mathbf{B}_0 , it was concluded that the ferrocene is frozen such that the C_5 axes are oriented either along or perpendicular to the thiourea channels, but not at intermediate orientations. As the temperature is increased, the lines narrow for both the oriented and powder samples, although the onset of narrowing is different for the two samples. At room temperature, isotropic peaks are observed for both samples. Rather than isotropic tumbling of the ferrocene guest, the authors suggest that the guest reorients rapidly such that the C_5 axes reorient rapidly about four directions, namely in the channel direction and perpendicular to this direction, along the threefold channel axes (the thiourea is in a rhombohedral phase at room temperature). These conclusions were supported by a ^2H NMR study of perdeuterated ferrocene guests in thiourea [112]. The authors reported activation energies of 6.4 ± 0.5 kJ mol $^{-1}$ for reorientations in directions perpendicular to the channel direction, and 10.1 ± 1.0 kJ mol $^{-1}$ for reorientation from the perpendicular to the parallel directions [112].

Heyes and Dobson investigated the fluxional behaviour of $\text{Ti}(\eta^5\text{-Cp})_2(\sigma\text{-Cp})_2$ with variable-temperature solid-state ^{13}C NMR [102]. Broadened peaks in the spectra of MAS samples obtained at 369 K suggest that interchange between η - and σ -bonding may be occurring at this temperature (i.e. the cyclopentadienyl ligands are rapidly exchanging between η^5 -coordination and a single σ bond with the metal).

Benn and co-workers [113] investigated the dynamic behaviour of substituted cyclopentadienyl ligands coordinated with zirconium and hafnium. Through the acquisition of two-dimensional ^{13}C MAS exchange spectra [114] at various temperatures, the authors found that at 300 K the unsubstituted cyclopentadienyl ligands rotate rapidly about the C_5 symmetry axis of the ring. The barriers to internal rotation were determined for several substituted ligands.

Wagner and Hanson [115] investigated the internal dynamics of $\text{Mo}(\eta^6\text{-C}_6\text{H}_5\text{CH}_3)(\text{CO})_3$ and $\text{Cr}(\eta^6\text{-C}_6\text{H}_5\text{CH}_3)(\text{CO})_3$. From the observation that the line widths of the aromatic ^{13}C NMR peaks of MAS samples of these compounds are invariant to temperature between 196 and 333 K, these authors concluded that the arene group is not subject to significant motion in the solid state. This must be a consequence of the methyl substituent on the phenyl ring since wide-line ^1H NMR experiments with the $\eta^6\text{-C}_6\text{H}_6$ analogue shows that the unsubstituted benzene ligand undergoes rapid rotation at temperatures above 108 K [116].

Shabanova and co-workers have analysed the ^{13}C NMR spectra of MAS samples of $\text{C}_{60}(\text{FeCp}_2)_2$ (Figure 12) [117]. The possibility that this compound is a charge-transfer complex [118] was investigated. If such a complex were created, the ferrocene, which is the electron donor, would become positively charged and Fe^{3+} would be paramagnetic. The ^{13}C NMR spectra are comparable to those of the separate molecules, thus leading to the conclusion that charge transfer does not occur [117].

4.4 ADSORBED OLEFINS AND ACETYLENES

There has been much interest in surface-adsorbed molecules because of the catalytic activity at the surface. Many texts have discussed surface science and

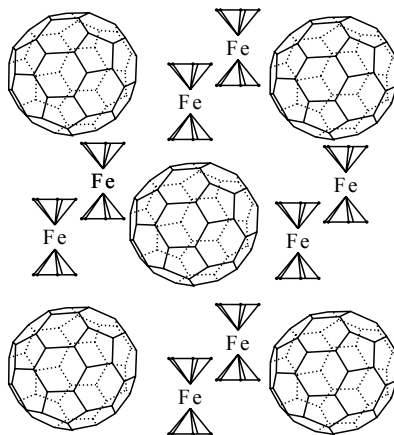


Figure 12 Crystal packing of $\text{C}_{60}(\text{FeCp}_2)_2$

some representative examples will be given here [119]. Solid-state NMR can offer a wealth of information about surface-supported organic molecules [120], such as structure, surface dynamics or the nature of the interaction with the surface, but its use has been restricted because it is inherently an insensitive technique [121]. The samples investigated are usually adsorbed on surfaces of small particles which are themselves held on a support such as silica or alumina, thus resulting in small sample sizes when compared to those available for most solid-state NMR experiments. Recently, Maciel and co-workers have demonstrated a technique for acquiring ^{13}C NMR spectra of samples adsorbed on metal foils [122].

The solid-state NMR literature on olefins and acetylenes adsorbed on metal surfaces is considered here; many of these are actually investigations of the products of the adsorption process rather than of the ligands themselves. A review of the literature to 1994 on surface-supported organometallics, including olefins, has been given by Reven [123]. Earlier reviews by Slichter [124] and co-workers [125] and by Duncan and Dybowski [126] have also discussed applications of solid-state NMR to the elucidation of the structures of olefins and acetylenes adsorbed on metal surfaces. The structures and energetics of organic ligands adsorbed on platinum have been investigated by using *ab initio* methods [127]. The extensive literature on NMR studies of organic ligands adsorbed in zeolites has been reviewed by Pfeifer and Ernst [128] and by Reven [123]; these will not be discussed here.

4.4.1 Solid-State NMR Studies of Adsorbed Olefins

Table 10 summarizes the solid-state NMR investigations of surface-supported olefins. The structure of ethylene adsorbed on platinum was investigated by Slichter and co-workers [129,130]. Based on the ^{13}C – ^{13}C dipolar coupling of the ^{13}C -labelled samples, these authors found that most of the carbon atoms are comprised of C–C pairs with a bond length of 1.49 ± 0.02 Å, which compares with the C–C bond lengths of 1.338 and 1.54 Å for uncoordinated ethylene [69] and ethane [71], respectively. The authors thus concluded that the ethylidene ($\equiv\text{C}-\text{CH}_3$) species is adsorbed on platinum. This conclusion is reinforced by a ^2H NMR investigation of deuterated ethylene adsorbed on platinum [131], which indicates that the deuterons are separated by 1.673 ± 0.004 Å, comparable to the value expected for methyl groups. However, Shibnuma and Matsui [132], as well as Gay [133], reached different conclusions about the nature of the adsorbed species at room temperature. From the ^1H NMR line shapes of stationary powder samples, Shibnuma and Matsui suggested that the major species is $=\text{CH}-\text{CH}_2-$ [132]. Gay [133] undertook dipolar-dephasing experiments [134], which only detect NMR signals from quaternary or methyl carbon nuclei. From the absence of NMR signals in these experiments, the author concluded that the ethylidene species is not present at room temperature, suggesting that the major species is π -bonded ethylene. Similar observations were reported by Chin and Ellis [135], but these authors suggest that the

Table 10 Solid-state NMR experiments on surface-supported ethylene complexes

Complex ^a	Observed nucleus	Information gained	Ref.
C ₂ H ₄ on Pt ^b	¹ H	Structure	132
C ₂ H ₄ on Pt ^b	² H	Structure, dynamics	131
C ₂ H ₄ on Pt/Al ₂ O ₃	² H, ¹³ C	Structure, dynamics	135,136
C ₂ H ₄ on Pt/Al ₂ O ₃	² H	Kinetics	137
C ₂ H ₄ on Pt/Al ₂ O ₃	¹³ C	Structure, temperature effects	129,130 ^c
C ₂ H ₄ on Pt/Al ₂ O ₃ or SiO ₂	¹³ C	Structure	133
C ₂ H ₄ on Pt or Ir/η-Al ₂ O ₃	¹³ C	Reaction path and activation energy	138
C ₂ H ₄ on Ag/SiO ₂	¹³ C	Structure, carbon CS tensor ^d	140
C ₂ H ₄ on Ag/Al ₂ O ₃	¹³ C	Structure, dynamics, carbon CS tensor ^e	135,139,141
C ₂ H ₄ /Cs on Ag/Al ₂ O ₃	¹³ C	Structure with Cs ⁺ , carbon CS tensor ^f	143,144
C ₂ H ₄ /Cs on Ag/Al ₂ O ₃	¹³³ Cs	Cs atom location	144
[RhClL] ₂ on Al ₂ O ₃ ^g	¹³ C	Structure	146
C ₂ H ₄ on Ru/SiO ₂	¹³ C	Structure, reaction products	147

^a Alumina (Al₂O₃) exists in various phases, but this is not always specified. Because of the greater surface area of γ -alumina (see Reference [141]), it is the most common support. Where reported, samples prepared with a different form of alumina are specified.

^b The support was not specified.

^c The platinum was supported on η -alumina.

^d The carbon CS tensor components determined at 190 K are $\delta_{11} = 180(5)$ ppm, $\delta_{22} = 112(5)$ ppm, $\delta_{33} = 37(5)$ ppm and $\delta_{\text{iso}} = 109.6(5)$ ppm.

^e The carbon CS tensor components are $\delta_{11} = 193.6(5)$ ppm, $\delta_{22} = 115.6(7)$ ppm, $\delta_{33} = 11.8(5)$ ppm and $\delta_{\text{iso}} = 107.0$ ppm (Reference [139]). Similar values were reported in Reference [135].

^f The carbon CS tensor components for the sample in the absence of Cs⁺, determined at 77 K, are $\delta_{11} = 191.5(3)$ ppm, $\delta_{22} = 117.7(15)$ ppm, $\delta_{33} = 11.8(3)$ ppm and $\delta_{\text{iso}} = 107.0(2)$ ppm (Reference [144]). Slightly different values were reported for adsorbed ethylene in the presence of Cs⁺.

^g L, (C₂H₄)₂, cyclooctadiene.

absence of NMR signals is a consequence of the reduced efficiency of the CP experiment, attributed to the near-ferromagnetic nature of the platinum surface. Combined with some ²H NMR experiments, the authors concluded that π -bonded, σ -bonded and ethylidene species are all present at room temperature [135]; the different experimental observations reported by various groups is attributed to the sensitivity of the Pt/alumina catalyst to experimental conditions. A similar study by Reimer and co-workers also concluded that the ethylidene and π -bonded species are present at room temperature [136].

The thermodynamic properties of ethylene adsorbed on platinum have been investigated by Slichter and co-workers [129,130]. By heating samples to 690 K, and then cooling and acquiring NMR spectra at 77 K, it was found that the major high-temperature species is isolated carbon atoms, separated from neighbouring carbon atoms by at least 3 Å. The reaction kinetics of ethylene at various temperatures were investigated by ²H NMR [137]. From the analysis of ¹³C NMR spectra, Slichter *et al.* [138] determined that the C–C bond scission

energy of adsorbed ethylene is comparable for ethylene supported on platinum or iridium, i.e. 151 kJ mol^{-1} .

The nature of ethylene on the surface of silver supported on alumina [135,139] or silica [140] has been investigated by ^{13}C NMR. A donor-acceptor complex [139,140], based on the Dewar, and Chatt and Duncanson model [7], was proposed. The C–C bond length determined from the ^{13}C – ^{13}C dipolar coupling observed for a sample prepared from ethylene- $^{13}\text{C}_2$, $1.34 \pm 0.004 \text{ \AA}$ [135], is equivalent to that of ethylene [69], suggesting that the coordination of ethylene with silver is weak. This is consistent with the observation of isotropic ^{13}C NMR signals at room temperature, since weakly coordinated ligands are expected to reorient rapidly on the surface, averaging the observed NMR signal. From spectra acquired at low temperatures, the principal components of the carbon CS tensors were determined (Table 10) [135,139,140]. Chin and Ellis [135] analysed the spectrum of a $^{13}\text{C}_2$ -labelled sample, determining that the carbon CS tensor is oriented as for ethylene (see Figure 2). In a later ^{13}C NMR study, Wang and Ellis characterized the motion of ethylene on alumina-supported silver [141]. The authors conclude that molecular reorientation at lower temperatures may be described by a 4- and 6-site jump model. The oxidation of ethylene adsorbed on alumina and silica-supported silver has been studied by ^{13}C NMR [142]. The species present were identified on the basis of the isotropic chemical shifts observed for spectra of MAS samples.

The effect of Cs promoters on the structure of ethylene adsorbed on $\text{Ag}/\text{Al}_2\text{O}_3$ has been investigated with ^{13}C NMR [143,144] and with $^{133}\text{Cs}\{^1\text{H}\}$ spin-echo double resonance (SEDOR) experiments [144,145]. Although ^{133}Cs is a spin-7/2 nucleus, it has a very small nuclear quadrupole moment. The ^{13}C NMR experiments indicate that the δ_{22} and δ_{33} components of the CS tensor are affected by the presence of the cesium cations, which are close to the ethylene ligands. The authors report that the C–C bond length increases with the amount of Cs^+ present in the sample, with a corresponding decrease in the isotropic shielding of the carbon nuclei. Particularly sensitive to the presence of Cs^+ is the δ_{22} component [144]; at 26% incorporation of Cs relative to Ag, $\delta_{22} = 105.4 \text{ ppm}$, compared to 117.7 ppm in the absence of Cs^+ and 120 ppm for uncoordinated ethylene [41]. The δ_{11} component, although less sensitive to the presence of Cs^+ , is affected more by coordination with Ag: $\delta_{11} = 191 \text{ ppm}$ for the support in the absence of Cs^+ , compared to 234 ppm for uncoordinated ethylene [41]. Similar data were reported by Wang and Ellis, who found that the direction of greatest shielding is relatively unaffected by the presence of Cs^+ [143].

Vierkötter and co-workers undertook a detailed ^{13}C NMR study of rhodium–ethylene and rhodium–cyclooctadiene complexes adsorbed on alumina [146]. These authors found that the spectra of the chemisorbed complexes are essentially unchanged from those of the complexes obtained before chemisorption but are distinct from those of the corresponding physisorbed olefin (i.e. the olefin is coordinated directly to the support). Hence, the authors

concluded that the olefins remain bound to the rhodium centres following chemisorption of the complexes.

The products present following adsorption of ethylene on ruthenium supported on silica were investigated by Pruski *et al.* [147]. Numerous species, including *cis*- and *trans*-butene, were identified. By acquiring ^{13}C NMR spectra of the silica under identical conditions to that of the supported-ruthenium sample, the authors demonstrated that, with the exception of a narrow peak, signals observed in the subsequent experiments were due to the adsorption of ethylene on ruthenium and not on the silica support.

4.4.2 Carbon-13 NMR Studies of Adsorbed Acetylene

The literature on solid-state NMR investigations of surface-supported acetylenes is summarized in Table 11. The structure of acetylene adsorbed on platinum was investigated by Slichter and co-workers [130,148]. The experiment was conducted in the same manner as the authors' investigation of ethylene adsorbed on platinum [130], discussed above, and similar conclusions were reached. The structure of the adsorbed species depends on the temperature: at room temperature, the major species is vinylidene ($> \text{C}=\text{CH}_2$), while at high temperatures (to 690 K) the carbon atoms are isolated. Chin and Ellis showed that acetylene adsorbed on the alumina support makes a significant contribution to the observed spectra [149]. In a ^2H NMR study, Klug *et al.* studied the kinetics of the conversion of vinylidene to ethylidene [150]. By measuring the ^{13}C - ^{13}C dipolar interaction, Wang and co-workers [138] determined that the C-C scission energy for acetylene adsorbed on Ir and Pt is 155 and 222 kJ mol^{-1} , respectively. The adsorption of acetylene on ruthenium was reported in an early ^{13}C NMR study [151]. Spectra of MAS and stationary samples suggest the presence of two species, with NMR signals appearing in the acetylenic and olefinic regions of the ^{13}C NMR spectra [151].

The presence of vinylidenes on palladium surfaces was surmised from the analysis of ^{13}C NMR spectra of MAS samples of adsorbed acetylene [152,153].

Table 11 Solid-state NMR experiments on surface-supported acetylene complexes

Complex	Observed nucleus	Information gained	Ref.
C_2H_2 on Pt/ η - Al_2O_3	^2H	Structure, kinetics	150
C_2H_2 on Pt/ η - Al_2O_3	^{13}C	Structure, temperature effects	130
C_2H_2 on Pt/ η - Al_2O_3	^{13}C	Structure, temperature effects	148
C_2H_2 on Pt, Ir or Os on η - Al_2O_3	^{13}C	Reaction path and activation energy	138
C_2H_2 on Pd/ Al_2O_3^a	^{13}C	Surface reactions, structure	152
C_2H_2 on Ru/ SiO_2	^{13}C	Surface reactions	151
C_6H_6 on Pt/ η - Al_2O_3	^1H	Surface dynamics	154

^a The phase of the alumina support was not specified.

Combined with other experiments, the formation of benzene due to acetylene cyclotrimerization was monitored.

4.4.3 Solid-State NMR Studies of Other Adsorbed η -Coordinated Organometallics

Dybowski and co-workers have investigated benzene adsorbed on both Pt/Al₂O₃ and on Al₂O₃ by using ¹H NMR [154]. Comparison of spectra acquired with a single pulse with those acquired with a multiple-pulse line-narrowing technique (REV-8) [155] indicated that the ¹H nuclei of benzene experience a static homonuclear dipolar coupling of 50–80 Hz. Hence, the authors concluded that, although benzene is not held rigidly, the motion is slightly anisotropic and is on the time-scale of the experiment, i.e. 5–10 ms.

5 CONCLUSIONS

An overview of the literature on applications of solid-state NMR to the investigation of η -coordinated unsaturated-carbon ligands of organometallic complexes has been presented. A wide diversity of solid-state NMR experiments have been used to investigate these compounds, attesting to the versatility of the technique. The work surveyed here demonstrates that solid-state NMR provides structural information about compounds that do not readily lend themselves to analysis by diffraction techniques, such as surface-supported species and amorphous materials. Furthermore, the practicality of solid-state NMR in the investigation of molecular dynamics has been demonstrated. In addition to these studies, the determination of magnetic shielding tensors for these compounds has been summarized. With ongoing improvements, such as better instrumentation, more powerful computers and higher applied magnetic fields, solid-state NMR will continue to provide fundamental information about the molecular properties of these important compounds. The role of computational NMR as a complement to experimental results has also been discussed. The increasing capacity of computers, combined with ongoing research into computational techniques, ensures that such approaches will continue to be an important part of a detailed investigation of nuclear magnetic shielding. It is hoped that this survey of the solid-state NMR literature of η -coordinated complexes will encourage researchers to consider these and other solid-state NMR techniques in their own work.

6 ACKNOWLEDGMENTS

We are grateful to members of the solid-state NMR group at the University of Alberta for critiquing this manuscript, and to Dr Roland Rösler for translating the German-

language papers reviewed herein. We thank Professors Orendt and Grant for providing a copy of a figure used herein, and Professor Ruschewitz for providing a preprint of his paper. Work in our laboratory is made possible through the generous financial support of the Natural Sciences and Engineering Research Council (NSERC) of Canada. GMB thanks NSERC, the Izaak Walton Killam Trust and the Walter C. Sumner Foundation for postgraduate scholarships. REW thanks the Government of Canada for the Canada Research Chair at the University of Alberta.

7 REFERENCES AND NOTES

1. (a) F. R. Hartley, in *Comprehensive Organometallic Chemistry*, G. Wilkinson (Ed.), Vol. 6, Pergamon Press, Oxford, UK, 1982, p. 471. (b) G. B. Young, in *Comprehensive Organometallic Chemistry II*, E. W. Abel, F. G. A. Stone, G. Wilkinson and R. J. Puddephatt (Eds), Vol. 9, Pergamon Press, New York, 1995, p. 533.
2. (a) R. K. Harris and B. E. Mann (Eds), *NMR and the Periodic Table*, Academic Press, London, 1978. (b) J. B. Lambert and F. G. Riddell (Eds), *The Multinuclear Approach to NMR Spectroscopy*, NATO ASI Series, D. Reidel Publishing Co., Dordrecht, The Netherlands, 1983. (c) P. Laszlo (Ed.), *NMR of Newly Accessible Nuclei*, Vols 1 and 2, Academic Press, New York, 1983. (d) J. Mason (Ed.), *Multinuclear NMR*, Plenum Press, New York, 1987. (e) P. S. Pregosin (Ed.), *Transition Metal Nuclear Magnetic Resonance*, Elsevier, Amsterdam, 1991. (f) M. Gielen, R. Willem and B. Wrackmeyer (Eds), *Advanced Applications of NMR to Organometallic Chemistry*, Physical Organometallic Chemistry, Vol. 1, Wiley, Chichester, UK, 1996.
3. (a) O. A. Gansow and W. D. Vernon, in *Topics in Carbon-13 NMR Spectroscopy*, edited G. C. Levy (Ed.), Vol. 2, Wiley, New York, 1976, Ch. 5 pp. 269–341. (b) G. C. Levy, R. L. Lichter and G. L. Nelson, *Carbon-13 Nuclear Magnetic Resonance Spectroscopy*, 2nd Edn, Wiley, New York, 1980, p. 182. (c) B. E. Mann and B. F. Taylor, *¹³C NMR Data for Organometallic Compounds*, Academic Press, London, 1981. (d) P. W. Jolly and R. Mynott, *Adv. Organomet. Chem.*, **19**, 257 (1981).
4. For continuity, terms such as ‘olefinic’ or ‘acetylenic’ will be used to describe the carbon atoms of the uncoordinated ligand as well as the corresponding atoms of the complex, although in the latter case this does not correspond to a strict definition of the term.
5. (a) G. A. Webb, in *Nuclear Magnetic Shieldings and Molecular Structure*, J. A. Tossell (Ed.), Kluwer Academic Publishers, Dordrecht, The Netherlands, 1993, p. 1. (b) D. B. Chesnut, *Ann. Rep. Nucl. Magn. Reson. Spectrosc.*, **29**, 71 (1994). (c) J. Gauss, *Ber. Bunsenges. Phys. Chem.*, **99**, 1001 (1995). (d) A. C. de Dios, *Prog. Nucl. Magn. Reson. Spectrosc.*, **29**, 229 (1996). (e) C. J. Jameson and A. C. de Dios in *Nuclear Magnetic Resonance—A Specialist Periodical Report*, Vol. 29, G. A. Webb (Ed.), The Royal Society of Chemistry, Cambridge, UK, 2000, Ch. 2, pp. 41–84, and previous volumes in this annual series.
6. J. C. Facelli, in *Encyclopedia of Nuclear Magnetic Resonance*, D. M. Grant and R. K. Harris (Eds), Wiley, Chichester, UK, 1996, p. 4327.
7. (a) M. J. S. Dewar, *Bull. Soc. Chim. Fr.*, **18**, C71 (1951). (b) J. Chatt and L. A. Duncanson, *J. Chem. Soc.*, 2939 (1953).
8. F. A. Cotton and G. Wilkinson, *Advanced Organometallic Chemistry*, 5th Edn, Wiley, New York, 1988, Ch. 2.12, pp. 71–76.
9. For a recent review of computational studies, see G. Frenking and N. Fröhlich, *Chem. Rev.*, **100**, 717 (2000).

10. U. Haeberlen, in *Advances in Magnetic Resonance*, Supplement 1, J. S. Waugh (Ed.), Academic Press, New York, 1976.
11. (a) F. A. L. Anet and D. J. O'Leary, *Concepts Magn. Reson.*, **3**, 193 (1991). (b) F. A. L. Anet and D. J. O'Leary, *Concepts Magn. Reson.*, **4**, 35 (1992).
12. K. Schmidt-Rohr and H. W. Spiess, *Multidimensional Solid-State NMR and Polymers*, Academic Press, London, 1994.
13. M. Mehring, *NMR Basic Princ. Prog.*, **11**, 1 (1976).
14. C. J. Jameson, in *Encyclopedia of Nuclear Magnetic Resonance*, D. M. Grant and R. K. Harris (Eds), Wiley, Chichester, UK, 1996, p. 1273.
15. A. K. Jameson and C. J. Jameson, *Chem. Phys. Lett.*, **134**, 461 (1987).
16. W. T. Raynes, R. McVay and S. J. Wright, *J. Chem. Soc., Faraday Trans.*, **2**, **85**, 759 (1989).
17. (a) N. F. Ramsey, *Phys. Rev.*, **77**, 567 (1950). (b) N. F. Ramsey, *Phys. Rev.*, **78**, 699 (1950). (c) For a recent discussion of Ramsey's theories of NMR shielding, see P. Pyykkö, *Theor. Chem. Acc.*, **103**, 214 (2000).
18. (a) T. D. Gierke and W. H. Flygare, *J. Am. Chem. Soc.*, **94**, 7277 (1972). (b) W. H. Flygare, *Molecular Structure and Dynamics*, Prentice-Hall, Englewood, New Jersey, 1978, Ch. 6, pp. 331–422.
19. G. Malli and C. Froese, *Int. J. Quantum Chem.*, **IS**, 95 (1967).
20. (a) C. J. Jameson and J. Mason, in *Multinuclear NMR*, J. Mason (Ed.), Plenum Press, New York, 1987, Ch. 3 pp. 51–88. (b) G. Schreckenbach, R. M. Dickson, Y. Ruiz-Morales and T. Ziegler, in *Chemical Applications of Density-Functional Theory*, B. B. Laird, R. B. Ross and T. Ziegler (Eds), ACS Symposium Series 629, American Chemical Society, Washington, DC, 1996, Ch. 23 pp. 1–17. (c) J. B. Grutzner, in *Recent Advances in Organic NMR Spectroscopy*, J. B. Lambert and R. Rittner (Eds), Norell Press, Landisville, NJ, 1987, Ch. 2, pp. 17–42.
21. K. B. Wiberg, J. D. Hammer, K. W. Zilm, J. R. Cheeseman and T. A. Keith, *J. Phys. Chem. A*, **102**, 8766 (1998).
22. For a recent example of the controversy over notation, see (a) R. K. Harris, *Solid State Nucl. Magn. Reson.*, **10**, 177 (1998), and (b) C. J. Jameson, *Solid State Nucl. Magn. Reson.*, **11**, 265 (1998). (c) See also a summary of the recent IUPAC recommendations: R. K. Harris, E. D. Becker, S. M. C. De Menezes, R. Goodfellow and P. Granger, *Pure App. Chem.* **73**, 1795 (2001).
23. J. Mason, *Solid State Nucl. Magn. Reson.*, **2**, 285 (1993).
24. For a general discussion of theoretical methods, see G. A. Webb, in *Encyclopedia of Nuclear Magnetic Resonance*, D. M. Grant and R. K. Harris (Eds), Wiley, Chichester, UK, 1996, p. 4307.
25. W. Kutzelnigg, U. Fleischer and M. Schindler, *NMR Basic Princ. Prog.*, **23**, 165 (1991).
26. For a discussion of *ab initio* calculations in organometallic complexes, see G. Frenking and U. Pidun, *J. Chem. Soc., Dalton Trans.*, 1653 (1997).
27. (a) P. Pyykkö, *Chem. Rev.*, **88**, 563 (1988). (b) J. Li, G. Schreckenbach and T. Ziegler, *Inorg. Chem.*, **34**, 3245 (1995).
28. (a) M. Kaupp, V. G. Malkin, O. L. Malkina and D. R. Salahub, *J. Am. Chem. Soc.*, **117**, 1851 (1995). (b) M. Kaupp, O. L. Malkina and V. G. Malkin, *J. Chem. Phys.*, **106**, 9201 (1997).
29. For a discussion of effective core potentials, see K. Balasubramanian, in *Encyclopedia of Computational Chemistry*, P. v. R. Schleyer (Ed.), Wiley, New York, 1998, p. 2471.
30. M. Kaupp, V. G. Malkin and O. L. Malkina, in *Encyclopedia of Computational Chemistry*, P. v. R. Schleyer (Ed.), Wiley, New York, 1998, p. 1857.

31. (a) M. Kaupp, V. G. Malkin, O. L. Malkina and D. R. Salahub, *Chem. Phys. Lett.*, **235**, 382 (1995). (b) M. Kaupp, V. G. Malkin, O. L. Malkina and D. R. Salahub, *Chem. Eur. J.*, **2**, 24 (1996). (c) M. Kaupp, *Chem. Ber.*, **129**, 527 (1996). (d) M. Kaupp, *Chem. Ber.*, **129**, 535 (1996). (e) G. Schreckenbach, Ph.D. Thesis, University of Calgary, Canada, 1996.
32. M. Kaupp, O. L. Malkina and V. G. Malkin, *Chem. Phys. Lett.*, **265**, 55 (1997).
33. For a recent review, see M. Bühl, M. Kaupp, O. L. Malkina, V. G. Malkin, *J. Comput. Chem.*, **20**, 91 (1999).
34. (a) D. B. Chesnut and K. D. Moore, *J. Comput. Chem.*, **10**, 648 (1989). (b) D. B. Chesnut, B. E. Rusiloski, K. D. Moore and D. A. Egolf, *J. Comput. Chem.*, **14**, 1364 (1993).
35. (a) A. Pines, M. G. Gibby and J. S. Waugh, *J. Chem. Phys.*, **56**, 1776 (1972). (b) A. Pines, M. G. Gibby and J. S. Waugh, *J. Chem. Phys.*, **59**, 569 (1973).
36. J. C. Facelli, D. M. Grant and J. Michl, *Acc. Chem. Res.*, **20**, 152 (1987).
37. (a) C. A. Fyfe, *Solid State NMR for Chemists*, CFC Press, Guelph, Canada, 1983. (b) M. Mehring, *Principles of High Resolution NMR in Solids*, 2nd Edn, Springer-Verlag, Berlin, 1983. (c) J. C. Facelli and D. M. Grant, in *Topics in Stereochemistry*, Vol. 19, E. L. Eliel and S. H. Wilen (Eds), Wiley, New York, 1989, p. 1. (d) E. O. Stejskal and J. D. Memory, *High Resolution NMR in the Solid State*, Oxford University Press, New York, 1994. (e) L. W. Jelinski and M. T. Melchior, in *NMR Spectroscopy Techniques*, M. D. Bruch (Ed.), Marcel Dekker, New York, 1996, p. 417. (f) B. E. Mann, in *Encyclopedia of Nuclear Magnetic Resonance*, D. M. Grant and R. K. Harris (Eds), Wiley, Chichester, UK, 1996, p. 3400. (g) D. L. Bryce, G. M. Bernard, M. Gee, M. D. Lumsden, K. Eichele and R. E. Wasylishen, *Can. J. Analyt. Sci. Spectrosc.* **46**, 46 (2001). (h) M. J. Duer, *Solid-State NMR Spectroscopy Principles and Applications*, Blackwell Science, Oxford, UK, 2002.
38. (a) M. A. Kennedy and P. D. Ellis, *Concepts Magn. Reson.*, **1**, 35 (1989). (b) M. A. Kennedy and P. D. Ellis, *Concepts Magn. Reson.*, **1**, 109 (1989). (c) R. J. Iuliucci, C. G. Phung, J. C. Facelli and D. M. Grant, *J. Am. Chem. Soc.*, **118**, 4880 (1996). (d) R. J. Iuliucci, C. G. Phung, J. C. Facelli and D. M. Grant, *J. Am. Chem. Soc.*, **120**, 9305 (1998). (e) K. Eichele, G. C. Ossenkamp, R. E. Wasylishen and T. S. Cameron, *Inorg. Chem.*, **38**, 639 (1999). (f) M. Gee, R. E. Wasylishen and K. Eichele, *J. Phys. Chem. A*, **104**, 4598 (2000).
39. S. Kroeker, K. Eichele, R. E. Wasylishen and J. F. Britten, *J. Phys. Chem. B*, **101**, 3727 (1997).
40. K. W. Zilm and D. M. Grant, *J. Am. Chem. Soc.*, **103**, 2913 (1981).
41. K. W. Zilm, R. T. Conlin, D. M. Grant and J. Michl, *J. Am. Chem. Soc.*, **102**, 6672 (1980).
42. R. E. Wasylishen, in *Encyclopedia of Nuclear Magnetic Resonance*, D. M. Grant and R. K. Harris (Eds), Wiley, Chichester, UK, 1996, p. 1685.
43. K. Eichele and R. E. Wasylishen, *J. Magn. Reson., A*, **106**, 46 (1994).
44. A. C. de Dios, J. L. Roach and A. E. Walling, in *Modeling NMR Chemical Shifts*, J. C. Facelli and A. C. de Dios (Eds), American Chemical Society, Washington, DC, 1999, Ch. 16, pp. 220–239.
45. J. Herzfeld and A. E. Berger, *J. Chem. Phys.*, **73**, 6021 (1980).
46. M. M. Maricq and J. S. Waugh, *J. Chem. Phys.*, **70**, 3300 (1979).
47. J. Z. Hu, W. Wang and R. J. Pugmire, in *Encyclopedia of Nuclear Magnetic Resonance*, D. M. Grant and R. K. Harris (Eds), Wiley, Chichester, UK, 1996, p. 2914.
48. (a) A. Bax, N. M. Szevereniy and G. E. Maciel, *J. Magn. Reson.*, **52**, 147 (1983). (b) J. Z. Hu, A. M. Orendt, D. W. Alderman, C. Ye, R. J. Pugmire and D. M. Grant, *Solid State Nucl. Magn. Reson.*, **2**, 235 (1993).

49. (a) Z. Gan, *J. Am. Chem. Soc.*, **114**, 8307 (1992). (b) J. Z. Hu, A. M. Orendt, D. W. Alderman, R. J. Pugmire, C. Ye and D. M. Grant, *Solid State Nucl. Magn. Reson.*, **3**, 181 (1994).
50. See reference [8], Chapter 8.3.
51. T. M. Duncan, *Inorg. Chem.*, **28**, 2663 (1989).
52. S. Hemmersbach, B. Zibrowius and U. Ruschewitz, *Z. Anorg. Allg. Chem.*, **625**, 1440 (1999).
53. S. Hemmersbach, B. Zibrowius, W. Kockelmann and U. Ruschewitz, *Chem. Eur. J.*, **7**, 1952 (2001).
54. M. Weiß and U. Ruschewitz, *Z. Anorg. Chem.*, **623**, 1208 (1997).
55. D. T. Haworth and C. A. Wilkie, *J. Inorg. Nucl. Chem.*, **40**, 1689 (1978).
56. B. Wrackmeyer, K. Horchler, A. Sebald, L. H. Merwin and C. Ross II, *Angew. Chem.*, **102**, 821 (1990); B. Wrackmeyer, K. Horchler, A. Sebald, L. H. Merwin and C. Ross II, *Angew. Chem. Int. Ed. Eng.*, **29**, 807 (1990).
57. O. Reckeweg, A. Baumann, H. A. Mayer, J. Glaser and H.-J. Meyer, *Z. Anorg. Allg. Chem.*, **625**, 1686 (1999).
58. N. J. Clayden, C. M. Dobson, L.-Y. Lian and D. J. Smith, *J. Magn. Reson.*, **69**, 476 (1986).
59. O. Reckeweg and H.-J. Meyer, *Angew. Chem.*, **110**, 3619 (1998); O. Reckeweg and H.-J. Meyer, *Angew. Chem. Int. Ed. Eng.*, **37**, 3407 (1998).
60. R. C. Haddon, A. F. Hebard, M. J. Rosseinsky, D. W. Murphy, S. J. Duclos, K. B. Lyons, B. Miller, J. M. Rosamilia, R. M. Fleming, A. R. Kortan, S. H. Glarum, A. V. Makhija, A. J. Muller, R. H. Eick, S. M. Zahurak, R. Tycko, G. Dabbagh and F. A. Thiel, *Nature*, **350**, 320 (1991).
61. R. Tycko, G. Dabbagh, D. W. Murphy, Q. Zhu and J. E. Fischer, *Phys. Rev. B*, **48**, 9097 (1993).
62. T. M. de Swiet, J. L. Yarger, T. Wagberg, J. Hone, B. J. Gross, M. Tomaselli, J. J. Titman, A. Zettl and M. Mehring, *Phys. Rev. Lett.*, **84**, 717 (2000).
63. T. Gullion and J. Schaefer, *J. Magn. Reson.*, **81**, 196 (1989).
64. V. Brouet, H. Alloul, E. Lafontaine, L. Malier and L. Forro, *Appl. Phys., A*, **64**, 289 (1997).
65. B. Simovic, D. Jérôme, F. Rachdi, G. Baumgartner and L. Forró, *Phys. Rev. Lett.*, **82**, 2298 (1999).
66. (a) W. C. Zeise, *Pogg. Ann. Phys.*, **9**, 632 (1827). (b) W. C. Zeise, *Pogg. Ann. Phys.*, **21**, 497 (1831) (cited from Reference [67a]).
67. (a) For a discussion of the work of W. C. Zeise, including an English-language translation of Reference [66b], see G. B. Kaufman, *Classics in Coordination Chemistry*, Part 2, Selected Papers, Dover Publications Inc., New York, 1976, p. 17. (b) See also J. S. Thayer, *J. Chem. Edu.*, **46**, 442 (1969).
68. (a) P. G. Eller, R. R. Ryan and R. O. Schaeffer, *Cryst. Struct. Comm.*, **6**, 163 (1977). (b) R. A. Love, T. F. Koetzle, G. J. B. Williams, L. C. Andrews and R. Bau, *Inorg. Chem.*, **14**, 2653 (1975). (c) J. A. J. Jarvis, B. T. Kilbourn and P. G. Owston, *Acta Crystallogr., B*, **27**, 366 (1971).
69. J. L. Duncan, *Mol. Phys.*, **28**, 1177 (1974).
70. P.-T. Cheng and S. C. Nyburg, *Can. J. Chem.*, **50**, 912 (1972).
71. E. Hirota, Y. Endo, S. Saito and J. L. Duncan, *J. Mol. Spectrosc.*, **89**, 285 (1981).
72. J. Uddin, S. Dapprich, G. Frenking and B. F. Yates, *Organometallics*, **18**, 457 (1999).
73. Y. Huang, D. F. R. Gilson and I. S. Butler, *J. Chem. Soc., Dalton Trans.*, 2881 (1992).
74. S. Ding and C. A. McDowell, *Chem. Phys. Lett.*, **268**, 194 (1997).

75. R. Havlin, M. McMahon, R. Srinivasan, H. Le and E. Oldfield, *J. Phys. Chem., A*, **101**, 8908 (1997).
76. G. M. Bernard, R. E. Wasylishen and A. D. Phillips, *J. Phys. Chem., A*, **104**, 8131 (2000).
77. G. M. Bernard, G. Wu and R. E. Wasylishen, *J. Phys. Chem., A*, **102**, 3184 (1998).
78. M. S. Solum, J. C. Facelli, J. Michl and D. M. Grant, *J. Am. Chem. Soc.*, **108**, 6464 (1986).
79. G. M. Wallraff, PhD Thesis, University of Utah, Salt Lake City, UT, 1985.
80. P. J. J. A. Timmermans, A. Mackor, A. L. Spek and B. Kojić-Prodić, *J. Organomet. Chem.*, **276**, 287 (1984).
81. A. Syed, E. D. Stevens and S. G. Cruz, *Inorg. Chem.*, **23**, 3673 (1984).
82. A. Albinati, S. V. Meille and G. Carturan, *J. Organomet. Chem.*, **182**, 269 (1979).
83. J. H. van den Hende and W. C. Baird, Jr. *J. Am. Chem. Soc.*, **85**, 1009 (1963).
84. I. D. Gay and G. B. Young, *Organometallics*, **15**, 2264 (1996).
85. A. Pines, M. G. Gibby and J. S. Waugh, *Chem. Phys. Lett.*, **15**, 373 (1972).
86. G. M. Bernard, PhD Thesis, Dalhousie University, Halifax, Nova Scotia, Canada, 2000.
87. S. A. Vierkötter, C. E. Barnes, G. L. Garner and L. G. Butler, *J. Am. Chem. Soc.*, **116**, 7445 (1994).
88. M. A. Gallop, B. F. G. Johnson, J. Keeler, J. Lewis, S. J. Heyes and C. M. Dobson, *J. Am. Chem. Soc.*, **114**, 2510 (1992).
89. W. Böhlmann, D. Michel and J. Roland, *Magn. Reson. Chem.*, **37**, S126 (1999).
90. A. J. Cambell, C. A. Fyfe and E. Maslowski, Jr, *J. Am. Chem. Soc.*, **94**, 2690 (1972).
91. A. J. Cambell, C. E. Cottrell, C. A. Fyfe and K. R. Jeffrey, *Inorg. Chem.*, **15**, 1321 (1976).
92. (a) C. E. Cottrell, C. A. Fyfe and C. V. Senoff, *J. Organomet. Chem.*, **43**, 203 (1972).
(b) J. R. Lyerla, C. A. Fyfe and C. S. Yannoni, *J. Am. Chem. Soc.*, **101**, 1351 (1979).
93. P. Jutzi and N. Burford, *Chem. Rev.*, **99**, 969 (1999).
94. H. Strub, A. J. Beeler, D. M. Grant, J. Michl, P. W. Cutts and K. W. Zilm, *J. Am. Chem. Soc.*, **105**, 3333 (1983).
95. D. E. Wemmer and A. Pines, *J. Am. Chem. Soc.*, **103**, 34 (1981).
96. C. D. Hughes, M. H. Sherwood, D. W. Alderman and D. M. Grant, *J. Magn. Reson., A*, **102**, 58 (1993).
97. A. M. Orendt, J. C. Facelli, Y. J. Jiang and D. M. Grant, *J. Phys. Chem., A*, **102**, 7692 (1998).
98. K. J. Hallock, D. K. Lee and A. Ramamoorthy, *Chem. Phys. Lett.*, **302**, 175 (1999).
99. D. E. Wemmer, D. J. Ruben and A. Pines, *J. Am. Chem. Soc.*, **103**, 28, (1981).
100. A. R. Overweg, H. Koller, J. W. de Haan, L. J. M. van de Ven, A. M. van der Kraan and R. A. van Santen, *J. Phys. Chem., B*, **103**, 4298 (1999).
101. I. Sayer, *J. Chem. Soc., Chem. Commun.*, 227 (1988).
102. S. J. Heyes and C. M. Dobson, *J. Am. Chem. Soc.*, **113**, 463 (1991).
103. H. Heise, F. H. Köhler, E. B. Brouwer, R. K. Harris and S. Steuernagel, *Magn. Reson. Chem.*, **37**, 573 (1999).
104. M. Linder, A. Höhener and R. R. Ernst *J. Magn. Reson.*, **35**, 379 (1979).
105. S. Pausak, J. Tegenfeldt and J. S. Waugh, *J. Chem. Phys.*, **61**, 1338 (1974).
106. M. M. Maricq, J. S. Waugh, J. L. Fletcher and M. J. McGlinchey *J. Am. Chem. Soc.*, **100**, 6902 (1978).
107. A. E. Aliev, K. D. M. Harris, F. Guillaume and P. J. Barrie, *J. Chem. Soc., Dalton Trans.*, 3193 (1994).
108. H. W. Spiess, H. Zimmermann and U. Haeberlen, *Chem. Phys.*, **12**, 123 (1976).

109. S. J. Kitchin, K. D. M. Harris, A. E. Aliev and D. C. Apperley, *Chem. Phys. Lett.*, **323**, 490 (2000).
110. F. H. Allen, O. Kennard, D. G. Watson, L. Brammer, A. G. Opren and R. Taylor, *J. Chem. Soc., Perkin Trans. II*, S1 (1987).
111. T. Nakai, T. Terao, F. Imashiro and A. Saika, *Chem. Phys. Lett.*, **132**, 554 (1986).
112. S. J. Heyes, N. J. Clayden and C. M. Dobson, *J. Phys. Chem.*, **95**, 1547 (1991).
113. R. Benn, H. Grondey, R. Nolte and G. Erker, *Organometallics*, **7**, 777 (1988).
114. (a) N. M. Szeverenyi, M. J. Sullivan and G. E. Maciel, *J. Magn. Reson.*, **47**, 462 (1982). (b) D. Suter and R. R. Ernst, *Phys. Rev.*, *B*, **25**, 6038 (1982).
115. G. W. Wagner and B. E. Hanson, *Inorg. Chem.*, **26**, 2019 (1987).
116. P. Delise, G. Allegra, E. R. Mognaschi and A. Chierico, *J. Chem. Soc., Faraday Trans. II*, **71**, 207 (1975).
117. E. Shabanova, K. Schaumburg and F. S. Kamounah, *Can. J. Analyt. Sci. Spectrosc.*, **43**, 53 (1998).
118. For a discussion of fullerene charge-transfer complexes, see (a) R. Taylor, *Lecture Notes on Fullerene Chemistry: a Handbook for Chemists*, Imperial College Press, London, 1999, p. 217, and (b) D. V. Konarev, R. N. Lyubovskaya, N. V. Drichko, E. I. Yudanova, Y. M. Shul'ga, A. L. Litvinov, V. N. Semkin and B. P. Tarasov, *J. Mater. Chem.*, **10**, 803 (2000).
119. (a) M. A. White, *Properties of Materials*, Oxford University Press, New York, 1999. Ch. 10, pp. 204–209. (b) J. T. Yates, Jr, *Experimental Innovations in Surface Science*, Springer-Verlag, New York, 1998. (c) V. E. Henrich and P. A. Cox, *The Surface Science of Metal Oxides*, Cambridge University Press, Cambridge, UK, 1994, Ch. 6 pp. 247–377. (d) J. B. Hudson, *Surface Science. An Introduction*. Butterworth-Heinemann, Boston, MA, 1992. (e) A. Zangwill, *Physics at Surfaces*, Cambridge University Press, Cambridge, UK, 1988. (f) *Lectures on Surface Science*, G. R. Castro and M. Cardona (Eds), Springer-Verlag, Berlin, 1987.
120. *NMR Techniques in Catalysis*, A. T. Bell and A. Pines (Eds), Marcel Dekker, New York, 1994.
121. D. I. Hoult, in *Encyclopedia of Nuclear Magnetic Resonance*, D. M. Grant and R. K. Harris (Eds), Wiley, Chichester, UK, 1996, p. 4256.
122. J. Xiong, H. Lock, T. Tao, C. Keeler and G. E. Maciel, *Solid State Nucl. Magn. Reson.*, **14**, 95 (1999).
123. L. Reven, *J. Mol. Catal.*, **86**, 447 (1994).
124. C. P. Slichter, *Annu. Rev. Phys. Chem.*, **37**, 25 (1986).
125. P.-K. Wang, J.-P. Ansermet, S. L. Rudaz, Z. Wang, S. Shore, C. P. Slichter and J. H. Sinfelt, *Science*, **234**, 35 (1986).
126. T. M. Duncan and C. Dybowski, *Surf. Sci. Rep.*, **1**, 157 (1981).
127. J. Kua and W. A. Goddard III, *J. Phys. Chem.*, *B*, **102**, 9492 (1998).
128. H. Pfeifer and H. Ernst, *Annu. Rev. Nucl. Magn. Reson. Spectrosc.*, **28**, 91 (1994).
129. P.-K. Wang, C. P. Slichter and J. H. Sinfelt, *J. Phys. Chem.*, **89**, 3606 (1985).
130. P.-K. Wang, J.-P. Ansermet, C. P. Slichter and J. H. Sinfelt, *Phys. Rev. Lett.*, **55**, 2731 (1985).
131. K. Sakaie, C. P. Slichter and J. H. Sinfelt, *J. Magn. Reson. A*, **119**, 235 (1996).
132. T. Shibanuma and T. Matsui, *Surf. Sci.*, **154**, L215 (1985).
133. I. D. Gay, *J. Catalysis*, **108**, 15 (1987).
134. S. J. Opella and M. H. Frey, *J. Am. Chem. Soc.*, **101**, 5854 (1979).
135. Y.-H. Chin and P. D. Ellis, *J. Am. Chem. Soc.*, **115**, 204 (1993).
136. J. M. Griffiths, A. T. Bell and J. A. Reimer, *J. Phys. Chem.*, **97**, 9161 (1993).
137. D. B. Zax, C. A. Klug, C. P. Slichter and J. H. Sinfelt, *J. Phys. Chem.*, **93**, 5009 (1989).
138. P.-K. Wang, C. P. Slichter and J. H. Sinfelt, *J. Phys. Chem.*, **94**, 1154 (1990).

139. J. M. Koons, E. Hughes and P. D. Ellis, *Anal. Chim. Acta*, **283**, 1045 (1993).
140. I. L. Mudrakovskii, V. M. Mastikhin, N. E. Bogdanchikova and A. V. Khasin, *React. Kinet. Catal. Lett.*, **34**, 185 (1987).
141. J. Wang and P. D. Ellis, *J. Am. Chem. Soc.*, **115**, 212 (1993).
142. E. F. Fernandes, A. J. Benesi and M. A. Vannice, *J. Phys. Chem.*, **98**, 8498 (1994).
143. J. Wang and P. D. Ellis, *J. Am. Chem. Soc.*, **113**, 9675 (1991).
144. E. Hughes, J. M. Koons, J. Wang and P. D. Ellis, *J. Catalysis*, **183**, 182 (1999).
145. For a discussion of the SEDOR experiment, see M. Emshwiller, E. L. Hahn and D. Kaplan, *Phys. Rev.*, **118**, 414 (1960).
146. S. A. Vierkötter, C. E. Barnes, T. L. Hatmaker, J. E. Penner-Hahn, C. M. Stinson, B. A. Huggins, A. Benesi and P. D. Ellis, *Organometallics*, **10**, 3803 (1991).
147. M. Pruski, J. C. Kelzenberg, B. C. Gerstein and T. S. King, *J. Am. Chem. Soc.*, **112**, 4232 (1990).
148. P.-K. Wang, C. P. Slichter and J. H. Sinfelt, *Phys. Rev. Lett.*, **53**, 82 (1984).
149. Y.-H. Chin and P. D. Ellis, *J. Am. Chem. Soc.*, **111**, 7653 (1989).
150. C. A. Klug, C. P. Slichter and J. H. Sinfelt, *J. Phys. Chem.*, **95**, 2119 (1991).
151. I. D. Gay, *J. Magn. Reson.*, **58**, 413 (1984).
152. W. T. Tysoc, *Isr. J. Chem.*, **38**, 313 (1998).
153. M. Kaltchev, D. Stacchiola, M. Molero, G. Wu, A. Blumenfeld and W. T. Tysoc, *Catalysis Lett.*, **60**, 11 (1999).
154. C. F. Tirendi, G. A. Mills and C. Dybowski, *J. Phys. Chem.*, **88**, 5765 (1984).
155. W.-K. Rhim, D. D. Elleman and R. W. Vaughan, *J. Chem. Phys.*, **58**, 1772 (1973).

5 Metal Atom Motion in Some Iron Organometallics

ROLFE H. HERBER

*Racah Institute of Physics, The Hebrew University of Jerusalem,
91904 Jerusalem, Israel*

1 INTRODUCTION

Mössbauer effect spectroscopy has proven itself to be of considerable utility in the study of organometallics, especially those of iron and tin, and a large literature in this field has been accumulated since the early 1960s [1]. In particular, the 14.4 keV gamma resonance in ^{57}Fe has been used to elucidate the structure and bonding in a wide variety of iron organometallics, especially those related to ferrocene, which was the first molecule with Fe–C bonding to be subjected to such studies [2]. However, much of the focus of the work reported in the literature has concerned itself with the hyperfine interaction parameters, i.e. the isomer shift (IS), related to the electron density at the metal atom nucleus, and the quadrupole splitting (QS), related to the symmetry of the charge distribution. The major bonding interaction between the metal atom and the Cp moiety occurs through the overlap between the metal d-orbitals and the π cloud of the ring. Thus, changes in the electronegativity of the ring substituents, which are held by bonds having largely σ -character, have a relatively small effect on the IS and QS parameters. Because of this observed insensitivity of these parameters to changes in ring substituents, relatively few studies have focused on their variation with the detailed molecular-level architecture of such complexes, and the information which can be extracted from the temperature-dependencies of these parameters has been rather modest.

Even less attention has been paid to the temperature-dependence of the recoil-free fraction, f , which is related to the mean-square-amplitude of vibration (MSAV) $\langle x^2 \rangle$, of the metal atom by the relationship $f \propto e^{-\kappa^2 \langle x^2 \rangle}$, where κ is the γ -ray wave vector, $\lambda/2\pi$. The parameter $f(T)$ can be readily extracted from the temperature-dependence of the area under the resonance curve, $A(T)$, for an optically 'thin' absorber. In addition, the anisotropy of the mean-square-amplitude of vibration, known as the Gol'danskii–Karyagin effect (GKE) [3],

has been reported for only a very small number of iron organometallics. In several recent studies [4], however, it has been shown that the temperature-dependence of the MSAV can serve to elucidate a number of interesting properties of such complexes, and the present study was designed to examine these parameters in greater detail.

Simple theoretical considerations lead to the conclusion that in the high-temperature limit, that is, at temperatures equal to or larger than approximately half the lattice temperature (comparable to the Debye temperature of a monatomic cubic solid), the dependence of $\ln A$ on temperature should be linear. Moreover, this behavior should persist to temperatures very close to the melting point (T_{mp}) of the matrix under study. While this prediction has been borne out for a number of atomic solids for which $\ln A$ is a linear function of T to temperatures within half a degree of T_{mp} , several research groups have examined the region just below this temperature. In a pioneering 1961 Mössbauer study of metallic (β)Sn, using the 23.87 keV γ -radiation of ^{119}Sn over the temperature range from 120 K to the melting point, Boyle *et al.* [5] observed that the resonance absorption shows a rapid drop at temperatures close to T_{mp} , accompanied by a marked increase in the resonance line width. The origin of this effect was ascribed to self-diffusion, and the diffusion coefficient was estimated to be $\sim 10^{-8} \text{ cm}^2 \text{ s}^{-1}$ at about 0.6° below T_{mp} . In a subsequent re-investigation of the (β)Sn system by Longworth and Packwood [6], it was shown, however, that the effects observed by Boyle *et al.* [5] were due to the presence of (low-level) impurities in the metallic matrix, and that by use of 5N β -Sn, they were able to show that $d \ln A/dT$ is, in fact, linear to within 0.25° of T_{mp} .

As noted above, the behavior of $\ln A$ as a function of T close to T_{mp} in a number of iron organometallics shows evidence for an unexpected deviation from simple theoretical predictions, and this present study was undertaken in order to examine this behavior in some detail for ferrocene-related organometallics.

2 BASELINE STUDIES

In order to examine $\ln A(T)$ in molecular compounds of iron, it is necessary to study this detailed behavior in matrices in which T_{mp} , while above room temperature, is sufficiently low so that the MSAV of the metal atom still permits the experimental observation of a resonance effect. An examination of appropriate compounds for such a study showed that 1,1-dimethylferrocene ($T_{\text{mp}} = 310\text{--}313 \text{ K}$, ferrocenylacetonitrile ($T_{\text{mp}} = 354\text{--}356 \text{ K}$) and hydroxymethylferrocene (commercial product, $T_{\text{mp}} = 352\text{--}355 \text{ K}$) (**1**) are suitable candidates, and the latter was chosen to provide a baseline for evaluating $\ln A(T)$ over the temperature range, $90 \leq T \leq 350 \text{ K}$.

2.1 HYDROXYMETHYLFERROCENE

A commercial sample of hydroxymethylferrocene (**1**) [1273-86-5][†] was recrystallized several times from deionized water and dried under vacuum. The purified product showed a narrow melting point of 351.5 ± 0.3 K, in agreement with values reported in the literature [7], although the latter range from 351 to 355 K. The crystal structure of **1** has apparently not yet been reported. The Mössbauer parameters at 90 K, and parameters derived therefrom, are summarized in Table 1, and are in reasonable agreement with the values reported in the literature [8]. The isomer shift (*IS*) values from 298 K to temperatures just below the T_{mp} show a linear dependence (see Table 1), with a negative slope. The variation of the quadrupole splitting with temperature $QS(T)$ is also reasonably well fitted by a negative linear correlation over the whole temperature range, as expected from thermal expansion considerations. A plot of $\ln A(T)$ is shown in Figure 1, from which it can be seen that $\ln A$ is a linear function in the range $90 \leq T \leq 350$ K with a correlation coefficient (CC) of 0.997 for 18 data points. The inset in this figure shows the behavior at temperatures near T_{mp} , from which it can be seen that the recoil-free fraction decreases dramatically at the reduced temperature ($T_{\text{R}} = T/T_{\text{mp}}$) of about 0.975, and becomes unobservable at ~ 348 K, i.e. about 3° below T_{mp} . Qualitatively, this behavior parallels that of Sn containing impurities, as reported by Boyle *et al.* [5], but this is unlikely to be the correct explanation here since the experimental sample has been rigorously purified by multiple recrystallizations. A more plausible explanation for this pre-melting phenomenon may be found in a softening of the lattice due to the onset of rotation of one or both of the Cp rings prior to melting.

Table 1 Mössbauer data obtained for the various compounds discussed in the text

Compound	1	2	3	4	5	6
<i>IS</i> (90) (mm s ⁻¹)	0.528(5)	0.492(3)	0.498(2)	0.492(7)	0.507(2)	0.496(1)
<i>QS</i> (90) (mm s ⁻¹)	2.409(1)	2.473(2)	2.460(1) ^a	0.082(42)	2.411	0.154(1)
-d <i>IS</i> /dT (mm s ⁻¹ K ⁻¹ × 10 ⁻⁴)	5.51(10) ^b	3.17(13)	2.63(19)	4.13(68)	3.16(16)	3.68(27)
-d <i>QS</i> /dT (mm s ⁻¹ K ⁻¹ × 10 ⁻⁴)	1.48(7)	— ^c	— ^d	—	— ^e	1.44(15)
-d ln <i>A</i> /dT (K ⁻¹ × 10 ⁻³)	7.72(16) ^f	7.97(40)	9.81(61)	13.50(41)	8.73(35)	9.18(88) ^g
<i>M</i> _{eff} (Da)	75.5	131	—	100	132	119
<i>t</i> _M (K)	115	86	—	76	82	84

^a $85 \leq T \leq 210$ K.^b $T \geq 298$ K.^c Small maximum at ~ 200 K.^d \sim Temperature-independent.^e Small minimum at ~ 200 K.^f $90 \leq T \leq 335$ K.^g $230 \leq T \leq 320$ K.

[†] Represent American Chemical Society Chemical Abstracts Service (CAS) Registry Number for this and for subsequent materials discussed in this chapter.

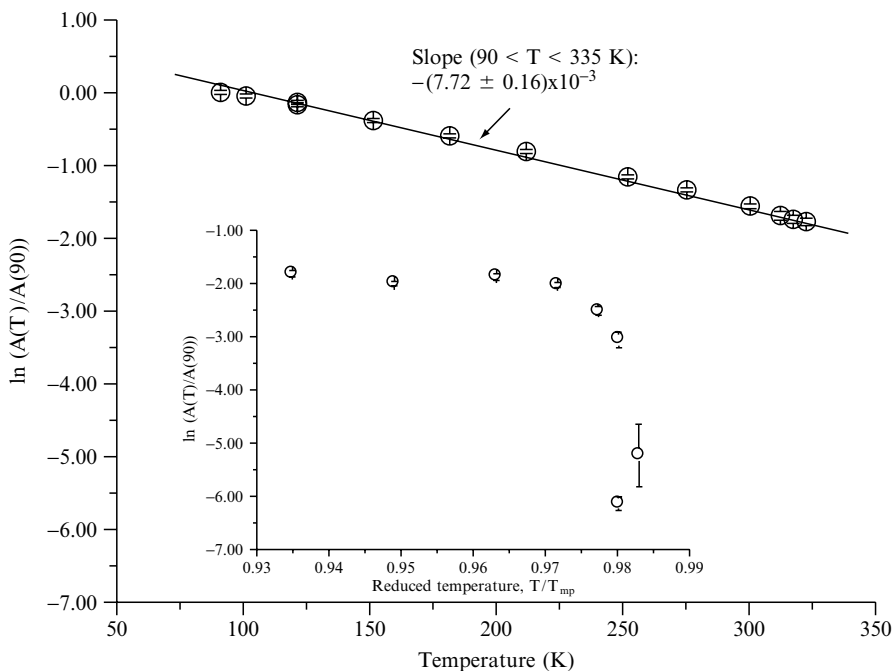


Figure 1 Temperature-dependence of $\ln A$ for ferrocenylmethanol (**1**). The inset shows the high-temperature data with the abscissa expressed in terms of the reduced temperature, T_R . The resonance effect is readily measurable to within about 3° of T_{MP}

Finally, in this context, it is worthwhile noting that the ‘effective mass’ (M_{eff}), calculated from $IS(T)$ in the high-temperature limit [9] is 75 ± 1 Da, comparable to that reported [10] for other ferrocenyl compounds, and that the Mössbauer lattice temperature (Θ_M), calculated from $IS(T)$ and $\ln A(T)$ in the high-temperature limit is 115 K, validating the lattice dynamical assumptions underlying the application of a modified Debye model to such solids.

2.2 DECAMETHYLFERROCENE

To explore the effect of the onset of ring rotation on the $\ln A$ behavior, and therefore the implied msav behavior, of the metal atom in ferrocene-related solids, a comparable study was undertaken of decamethylferrocene (**2**) [12126-50-0] (commercial product, $T_{\text{mp}} = 550$ K; recrystallized material $T_{\text{mp}} = 551\text{--}552$ K). The X-ray crystal structure of **2** was reported by Struchkov *et al.* [11], and in a revised form by Raymond and co-workers [12]. The structure at room temperature has a crystallographic site symmetry of C_{2h} , and consists of staggered rings with the methyl groups located ~ 0.06 Å above the rings, and an Fe–Cp distance of 1.657 Å. A ^1H solid-state NMR study has been

reported by Kobayashi *et al.* [13], and has shown two solid-state phase transitions at 397 ± 1 and 501 ± 2 K. In the low-temperature regime, there is a methyl group displacement with a uniaxial reorientation of the whole molecule about its C_5 axis. These authors have characterized these phases as ‘plastic’. A sample of **2** was repeatedly recrystallized from absolute alcohol and then vacuum-dried for 48 h at room temperature. The Mössbauer parameters at 90 K, and the appropriate derived parameters, are presented in Table 1 and are in (modestly) good agreement with the 80 K data reported by Silver and co-workers [14] and those of Vertes *et al.* [15], but with the additional observation that the QS is, in fact, not temperature-independent, but shows a positive dependence in the range $90 \leq T \leq 200$ K, with a negative temperature coefficient at higher temperatures. While the former is somewhat unusual, the latter is a direct consequence of the thermal expansion of molecular solids. In this context, it is again worth noting that although the electron-donating effects of the methyl groups have a significant effect on the electron density of the ferrocene core, this is not markedly observable in the hyperfine parameters, as reflected in the Mössbauer data on the iron atom. Similar comments also apply to the octamethyl- and nonamethyl-compounds, which will be discussed below.

In $\ln A(T)$ behavior of **2** is summarized in Figure 2, from which it can be seen that over the whole range of temperatures, $\ln A$ is not well represented by a linear regression. Especially at $T \geq 325$ K ($T_R = 0.59$), there is a marked decrease in the recoil-free fraction, even though this regime is some 225° below T_{mp} . That this marked decrease in $\ln A/dT$ does not arise from sample impurity, but rather is due to an intrinsic molecular property, can be concluded from the facts that the data points for the commercial sample (open circles and arrows) and those for a rigorously recrystallized sample (filled circles) are essentially superimposable. Again, it is plausible to infer that this decrease in $\ln A$ with increasing temperature is associated with the effects of ring rotation which, in turn, influence the MSAV of the metal atom, and hence the recoil-free fraction. It should be noted here that the decrease in $\ln A$ above ~ 325 K is relatively gradual, in contrast to the more sudden behavior observed for **1** near T_{mp} , but is still consistent with the characterization of these phases as ‘plastic’ [13]. Moreover, as is obvious, ring rotation in dexamethylferrocene can occur without necessitating strong librational motion of the rings. Thus, the pseudo-planarity of the rings relative to each other can be maintained, even above the onset of the ring rotation in the solid state.

2.3 NONAMETHYLFERROCENE AND NONAMETHYLFERROCENIUM HEXAFLUOROPHOSPHATE

A more dramatic variation of $\ln A$ —and thus of the MSAV of the metal atom—is observed in nonamethylferrocene (**3**) [41311-84-6]. The T_{mp} of this solid is 481 ± 1 K. The IS and QS values at 90 K, and the derived parameters,

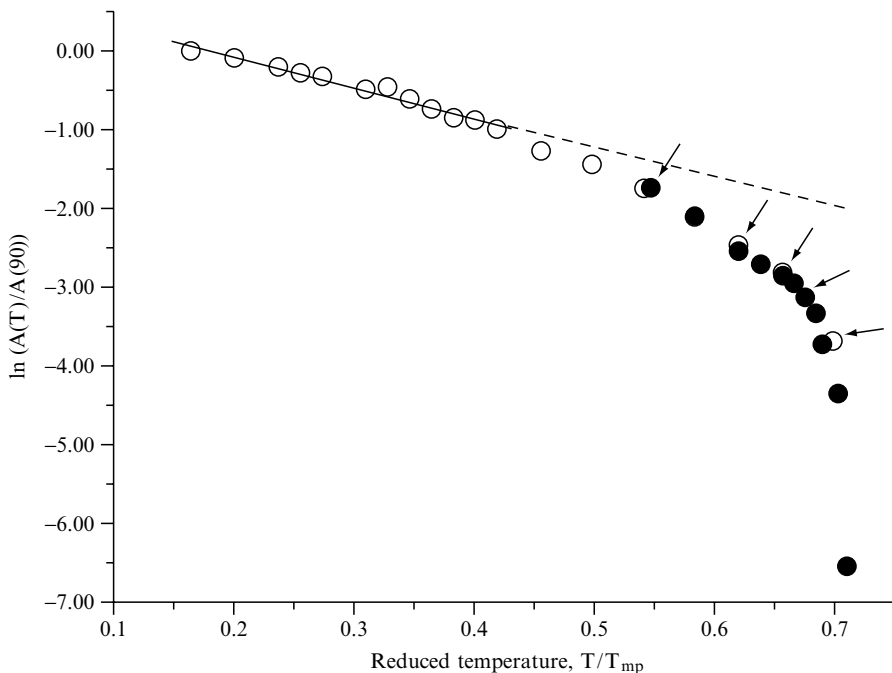


Figure 2 Temperature-dependence of $\ln A$ for decamethylferrocene (**2**), where the dashed line is an extension of the data between 90 and 230 K. The open circles (and the data points flagged with an arrow) represent the data accumulated for a commercial sample of $\sim 97\%$ purity, while the filled circles represent the corresponding data obtained for a rigorously recrystallized sample, showing that the departure from linearity has its origin in an *intramolecular* characteristic of this solid

are presented in Table 1, and are otherwise unremarkable. The $\ln A(T)$ behavior of **3**—for which preliminary data have been reported earlier [16]—is shown in Figure 3 (lower curve, open circles), in which the abscissa is expressed in terms of T_R . From this figure, it can be seen that the recoil-free fraction drops significantly at $T \sim 225$ K, and becomes essentially unobservable at $T > \sim 255$ K, i.e. some 225° below T_{mp} ! As reported in two recent studies [17,18], similar behaviors have been observed in octamethylferrocene (OMF) [4], ethynyloctamethylferrocene [4], and ethynyloctamethylferrocene; in all cases, $\ln A$ decreases sharply far below T_{mp} . The common molecular architectural feature of these complexes is that they have one fully substituted ring and a second ring in which one of the carbon atoms is bonded only to hydrogen. With the onset of ring rotation, it is thus expected that one or more librational modes of the rings will become activated, and that this libration—in turn—is reflected in a large increase in the MSAV of the metal atom. It is interesting to observe in this context that crystal structure data acquired at room temperature have been reported [11,19] for OMF ($T_{mp} = 431.5 \pm 0.5$ K) in which $\ln A$

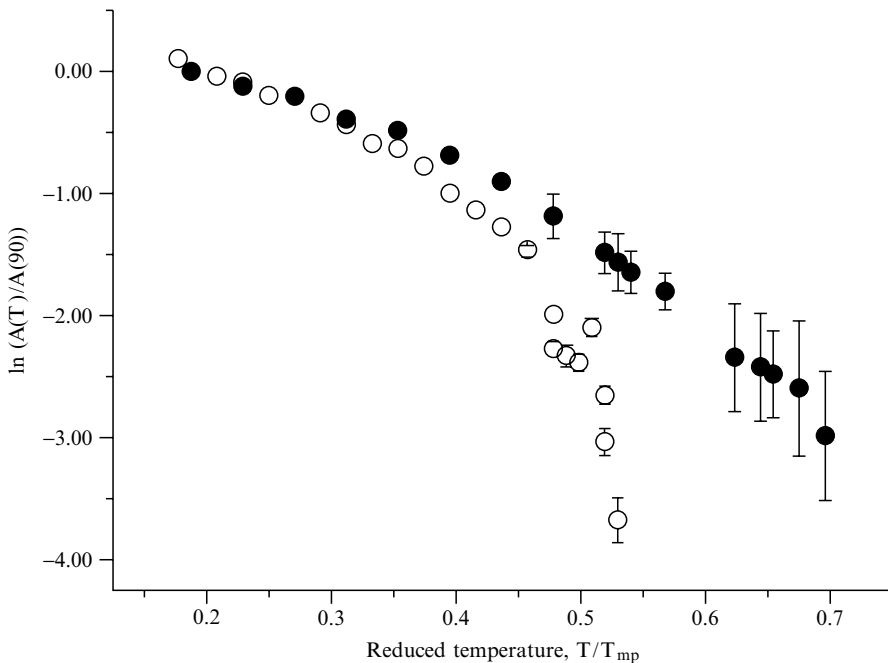


Figure 3 Temperature-dependence of $\ln A$ for nonamethylferrocene (open circles) and its hexafluorophosphate salt (filled circles), where the abscissa is expressed in terms of the reduced temperature, T_R . These data suggest that the strong departure from linearity can be associated with the librational-rotational motion of the five-membered rings

becomes vanishingly small at $T > 348$ K, but not—as concluded from a careful examination of both *Chemical Abstracts* and the *Cambridge X-ray Crystallographic Database*—for those compounds, including **3**, in which this phenomenon occurs below room temperature. It must be assumed in the latter case that the onset of ring rotation and libration below 300 K precludes the existence of the long-range order necessary for X-ray diffraction structural observations.

In contrast to the neutral iron organometallics, which give rise to Mössbauer spectra consisting of well-resolved doublets, one-electron oxidation products, such as nonamethylferrocenium hexafluorophosphate (**4**), frequently give spin-lattice relaxation spectra consisting of a broadened resonance line or of doublet spectra with very small QS parameters. In the case of **4**, the QS is essentially temperature-independent, with an average value of 0.082 ± 0.042 mm s⁻¹ over the range $90 \leq T \leq 335$ K. The IS and QS values at 90 K are presented above in Table 1.

The $\ln A(T)$ data for **4** are shown in the upper plot of Figure 3 (filled circles). It can be seen from these data that at $T < \sim 170$ K, the $\ln A(T)$ data for **3** and **4** are essentially superimposable. Above this temperature, $\ln A(T)$ for **4** drops significantly more slowly than is true for **3**, and this observation is consistent

with the above ring-rotation hypothesis. The presence of the bulky, charged PF_6^- anions appears to inhibit to some extent the ring rotation seen in the neutral **3** complex, and the resonance effect in **4** is still clearly observable at $T_{\text{R}} > \sim 0.7$. The MSAV of the metal atom in **4** at $T_{\text{R}} > \sim 0.5$ is significantly smaller than that in **3**, in consonance with the assumed model.

2.4 ETHYNYLOCTAMETHYLFERROCENE AND ETHYNYLOCTAMETHYLFERROCENIUM HEXAFLUOROPHOSPHATE

A one-pot synthesis of ethynyloctamethylferrocene (**5**) [201472-67-5] was reported by Jutzi and Kleinebeckel [20], who obtained the yellow-brown, air- and moisture-stable solid in 68 % overall yield. The reported melting point is 424 K. This material has been used in a number of syntheses, but only the crystal structure of adducts—for example, those of terpyridine, by Siemling *et al.* [21]—have been reported. In this context, attempts to grow diffractable single crystals of **5** at room temperature have—so far—failed [22]. The neutral compound can only be obtained as a glassy matrix at room temperature. On the other hand, the crystal structure of the one-electron hexafluorophosphate oxidation product (**6**) has been refined to an R_1 factor of 0.0389, and has recently been discussed by Schottenberger and co-workers [23].

The Mössbauer hyperfine parameters of **5** at 90 K are included in the data provided above in Table 1, and are otherwise unremarkable. The $\ln A(T)$ data are summarized in the lower curve of Figure 4 (open circles), and again show the sudden decrease of the recoil-free fraction at $T > \sim 248$ K, i.e. some 176° below T_{mp} . The DSC scan of the neutral compound has been reported in a preliminary publication [18], and displays a sharp endotherm (on heating) with a mid-point at ~ 250 K, as well as the endotherm expected at T_{mp} . These data have been accounted for on the basis of an *intramolecular* effect, again presumably due to the onset of ring-rotation in the solid, at temperatures well below T_{mp} . Moreover, the sharpness of the $\text{dln} A/\text{d}T$ discontinuity, in contrast to the data reported for complex **2** above, strongly suggests that the librational contribution in **5** is significantly greater than in **2**, due to the presence of the ethynyl group on one ring, and the H-atom substituent on the other, thus giving rise to a ‘gear-wheel’ effect, with its concomitant influence on the metal atom motion.

The significance of the presence of a hydrogen atom on one of the Cp rings (in place of a methyl group) is emphasized by the recoil-free fraction observations made on ethynylferrocene [1271-58-8]. This compound was first prepared by Benkeser and Fitzgerald [24], and further numerous improvements in the synthetic procedure have been reported in the literature [25]. The T_{mp} of this complex is 328 K, although its crystal structure has (apparently) not been reported. The synthesis of $\text{Fc}-\text{C}\equiv\text{C}-\text{Fc}$ has been reported by Rosenblum *et al.* [25] and by Pauson and Watts [26], and here too no crystal structures

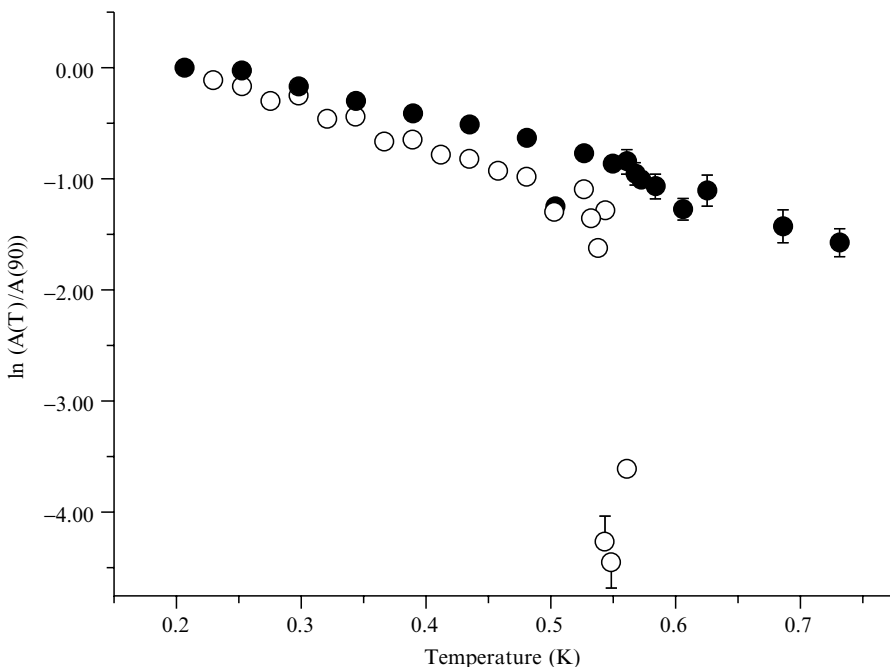


Figure 4 Temperature-dependence of $\ln A$ for **5** (open circles) and **6** (filled circles) as a function of the reduced temperature, T_R , illustrating the ‘gear-wheel’ effect discussed in the text

appear to have been carried out. On the other hand, the crystal structure of $\text{Fc-C}\equiv\text{C-C}\equiv\text{C-Fc}$ has been determined by Rodriguez *et al.* [27]. In this structure, the Cp rings are eclipsed and planar with a dihedral angle of $3.1(1)^\circ$, and a similar structure is reasonable for the mono-iron precursor. Thus, no particular librational motion is expected in the latter, and indeed the Mössbauer data which have been reported previously [17] show that the resonance effect is readily observable to within 3° of T_{mp} . Hence, it is inferred that the presence of eight methyl groups, as well as a single C–H ring position, in **5** play a major role in the magnitude of the MSAV of the metal atom, as noted above.

As referred to above, the resonance spectra of the PF_6^- salt of the one-electron oxidation product of **5** consist of typical spin–lattice relaxation spectra, with relaxation times (τ) at $T > 90$ K, which are fast on the Mössbauer time-scale. Typical values of τ are $7.2(3) \times 10^{-10}$ and $1.5(2) \times 10^{-11}$ s at 85 and 298 K, respectively. The $\ln A(T)$ data are summarized in the upper curve of Figure 4 (filled circles) and clearly show that the recoil-free fraction behavior noted for **5** at $T \sim 245$ K is absent in **6**. Data for the temperature-dependence of $\ln A$ for these two compounds are also included above in Table 1. The ratio of the linear regression slopes is ~ 1.37 , i.e. $\ln A$ decreases more slowly for **6** than for **5**. Here again, the presence of the PF_6^- anion appears to inhibit the onset of

ring rotation, and is reflected in the absence of the librational motion at $T > 248$ K observed for **5**, and hence (presumably) the absence of the ‘gear-wheel’ effect referred to above. The crystal structure of **6** [24] was determined at 218 K, and provides evidence that the two half counter-ions in the asymmetric unit are disordered. One, with P(1) in an inversion center has an occupancy factor of 0.6:0.4, while the other, with P(2) on a two-fold axis, has an occupancy factor of 0.8:0.2.

3 EXPERIMENTAL

The details of the procedures used to carry out temperature-dependent Mössbauer spectroscopy have been given in previous publications from these laboratories [18]. Spectrometer calibration was effected by the use of a α -Fe reference foil at room temperature, and all isomer shifts are reported with respect to the centroid of such spectra. A source of ^{57}Co in Rh (~ 100 mCi) was used in these measurements, in conjunction with a fast proportional counter, and—as needed—up to 4×10^7 counts per channel were acquired at each temperature. The temperature control was estimated to be constant to ± 0.2 K over the data acquisition time-interval.

Because sample loss, by evaporation or sublimation, could mimic a decrease in spectral area (especially in a sequential warming regime), the plastic sample holders were hermetically sealed with Perspex glue to provide unambiguous sample confinement. The efficacy of this technique was validated by observing that the spectral area at ~ 300 K was reproducible to better than 98% after data accumulation at 370 K for 24 h.

With the exception of nonamethylferrocene, ethynyloctamethylferrocene, and its PF_6^- salt, all samples were obtained commercially and examined both with and without further purification. Hydroxymethylferrocene (**1**) was repeatedly recrystallized from deionized water, and then vacuum-dried at room temperature. Decamethylferrocene (**2**) was repeatedly re-crystallized from absolute alcohol and again vacuum-dried at room temperature. Samples of the complexes **3–6** were generously made available by Professor H. Schottenberger of the University of Innsbruck, and were used without further purification. Melting points were determined by using a Thomas-Hoover Unimelt total-immersion apparatus, and are otherwise uncorrected.

4 ACKNOWLEDGEMENTS

The author is especially indebted to Professor H. Schottenberger for providing some of the samples used in this study, as well as contributing a number of constructive comments and suggestions. A similar debt is owed to Professor I. Nowik for his help in the analysis of the data reported herein.

5 REFERENCES

1. (a) J. G. Stevens (Ed.), *Mössbauer Effect Reference and Data Journal*, Vol. 24, Mössbauer Effect Data Center, Asheville, NC, 2001, pp. 229–232, and similar listings in earlier volumes. (b) A review of the early literature can be found in N. N. Greenwood and T. C. Gibb, *Mössbauer Spectroscopy*, Chapman & Hall, London, 1971, and references therein. (c) See also J. Silver, *Solid State Organometallic Chemistry. Methods and Applications*, Physical Organometallic Chemistry, Vol. 2, M. Gielen, R. Willem and B. Wrackmeyer (Eds), Wiley, Chichester, UK, 1999, Ch. 7, pp. 279–396.
2. (a) G. K. Wertheim and R. H. Herber, in *Proceedings of the 2nd international Conference on the Mössbauer Effect*, Saclay, France, 1961, D. M. J. Compton and A. H. Schoen (Eds), Wiley, New York, 1962, pp. 105–111. (b) U. Zahn, P. Kienle and H. Eicher, in *Proceedings of the 2nd International Conference on the Mössbauer Effect*, Saclay, France, 1961, D. M. J. Compton and A. H. Schoen (Eds), Wiley, New York, 1962, pp. 271–273. (c) U. Zahn, P. Kienle and H. Eicher, *Z. Physik.*, **166**, 220 (1962). (d) G. K. Wertheim and R. H. Herber, *J. Chem. Phys.*, **38**, 2106 (1963).
3. (a) V. I. Gol'danskii, G. M. Gorodinskii, S. V. Karyagin, L. A. Korytko, L. M. Krizhanskii, E. F. Makarov, I. P. Suzdalev, V. V. Khrapov, *Dokl. Akad. Nauk., SSSR*, **117**, 127 (1962). (b) S. V. Karyagin, *Dokl. Akad. Nauk., SSSR*, **148**, 1102 (1963).
4. R. H. Herber and I. Nowik, *Hyperfine Interactions*, **126**, 127 (2000).
5. A. J. F. Boyle, D. St. P. Bunbury, C. Edwards and H. E. Hall, *Proc. Phys. Soc.*, **77**, 129 (1961).
6. G. Longworth and R. H. Packwood, *Phys. Lett.*, **14**, 75 (1965).
7. (a) G. D. Broadhead, J. M. Osgerby and P. L. Pauson, *J. Chem. Soc.*, 650 (1958) [77–78 °C]. (b) S. I. Goldberg and W. D. Loebel, *J. Org. Chem.*, **33**, 2971 (1968) [78–79 °C]. (c) R. F. Kovar and M. D. Rausch, *Macromolecules*, **3**, 746 (1970) [79–81 °C]. (d) M. Hisatome and K. Yamakawa, *Tetrahedron*, **27**, 2101 (1971) [80–82 °C]. (e) C. V. Pittman, Jr, J. C. Lai, D. P. Vanderpool, M. Good and R. Prado, *J. Organomet. Chem.*, **35**, 361 (1972) [81–82 °C].
8. (a) A. V. Lesikar, *J. Chem. Phys.*, **40**, 2746 (1964). (b) L. Korecz, H. Abou, G. Ortaggi, M. Graziani, U. Belluco and K. Burger, *Inorg. Chim. Acta*, **9**, 209 (1974).
9. R. H. Herber, *Chemical Mössbauer Spectroscopy*, R. H. Herber, (Ed.), Plenum Press, New York, 1984, pp. 199–216.
10. R. H. Herber, I. Nowik and M. Rosenblum, *Organometallics*, **21**, 846 (2000).
11. Yu. T. Struchkov, V. G. Adrianov, T. N. Salnikova, I. R. Lyatifov and R. B. Materiakova, *J. Organomet. Chem.*, **145**, 213 (1978).
12. D. P. Freyberg, J. L. Robbins, K. N. Raymond and J. C. Smart, *J. Amer. Chem. Soc.*, **101**, 892 (1979).
13. T. Kobayashi, H. Ohki and R. Ikeda, *Mol. Cryst., Liq. Cryst. Sci. Technol.*, **A**, **257**, 279 (1994).
14. A. Houlton, J. R. Miller, R. M. G. Roberts and J. Silver, *J. Chem. Soc., Dalton Trans.*, 2181 (1990).
15. A. Vertes, Z. Klencsar, M. Gal and E. Kuzmann, *Fullerene Sci. Technol.*, **5**, 97 (1997).
16. R. H. Herber, *Inorg. Chim. Acta*, **291**, 74 (1999).
17. H. Schottenberger, M. R. Buchmeiser and R. H. Herber, *J. Organomet. Chem.*, **612**, 1 (2000).
18. I. Nowik and R. H. Herber, *Inorg. Chim. Acta*, **310**, 191 (2000), and references therein.

19. D. Schmitz, J. Fleischhauer, U. Meier, W. Scleker and G. Schmitt, *J. Organomet. Chem.*, **205**, 381 (1981).
20. P. Jutzi and B. Kleinebckel, *J. Organomet. Chem.*, **545/546**, 573 (1997).
21. U. Siemling, U. Vorfeld, B. Neumann, H.-G. Stammler, P. Zanello and F. F. Biani, *Eur. J. Inorg. Chem.*, 1 (1999).
22. K. Wurst and H. Schottenberger, Personal communication.
23. R. H. Herber, H. Schottenberger and K. Wurst, *J. Organomet. Chem.*, **625**, 200 (2000).
24. R. A. Benkeser and W. P. Fitzgerald, *J. Org. Chem.*, **26**, 4179 (1961).
25. (a) M. Rosenblum, N. Brawn, J. Papenmeyer and M. Applebaum, *J. Organomet. Chem.*, **6**, 173 (1966). (b) K. Schloegl and W. Steyrer, *Monatsh. Chemie.*, **96**, 1520 (1965). (c) K. Schloegl and H. Egger, *Monatsh. Chemie*, **94**, 376 (1993).
26. P. L. Pauson and W. E. Watts, *J. Chem. Soc.*, 2990 (1963).
27. J.-G. Rodriguez, A. Onate, R. M. Martin-Villamil and I. Fonseca, *J. Organomet. Chem.*, **513**, 71 (1996).

6 Magnetic Communication in Binuclear Organometallic Complexes Mediated by Carbon-Rich Bridges

FRÉDÉRIC PAUL and CLAUDE LAPINTE

Institut de Chimie de Rennes, UMR CNRS 6509 Organométalliques et Catalyse, Université de Rennes 1, Campus de Beaulieu, 35402 Rennes, Cedex France

ABBREVIATIONS

Ar	aromatic group
bt	2,2'-bithiazoline
tBu	<i>tert</i> -butyl substituent
bypm	2,2'-bipyrimidine
bzp	bromazepan
Cp	cyclopentadienyl
Cp'	methylcyclopentadienyl
Cp''	ethylcyclopentadienyl
Cp*	pentamethylcyclopentadienyl
Cp [#]	pentaphenylcyclopentadienyl
DFT	density functional theory
dippe	1,2-bis(di- <i>iso</i> -propylphosphino)ethane
dppe	1,2-bis(diphenylphosphino)ethane
e	electron
EHMO	extended Hückel molecular orbital (calculations)
[Et ₈ N ₄]	<i>meso</i> -octaethylporphyrinogen tetra-anion
Fc	ferrocenyl
G	Gauss (units)
GS	ground state
HDvV	Heisenberg–Dirac–van Vleck (Hamiltonian)
IVCT	intervalence charge transfer
<i>J</i> (or <i>J</i> _{AB})	isotropic exchange coupling
<i>J</i> _{AB}	coulomb integral (in electronic correlation energies)

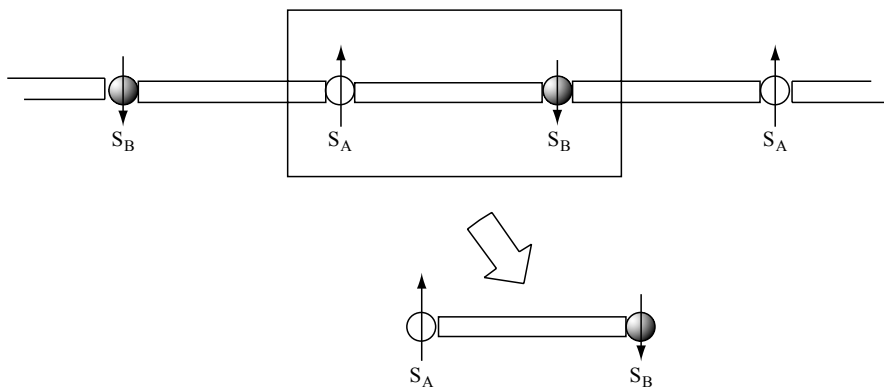
K_{AB}	exchange integral (in electronic correlation energies)
Mes	mesityl (2,4,6-trimethylphenyl) substituent
MO	molecular orbital
MV	mixed-valence (complex)
Ph	phenyl substituent
S	(global) spin
(S)	singlet state
SOMO	singly occupied molecular orbital
S/T	singlet/triplet (gap)
T	temperature
(T)	triplet state
THF	tetrahydrofuran
TIP	temperature-independent paramagnetism
TMP	5,10,15,20-tetramesitylporphyrin
Tpz	hydridotris(3,5-dimethylpyrazolyl) borate
V_{ab}	electronic coupling parameter
Ψ, γ	dihedral angles (see also Tables 6–8)

1 INTRODUCTION

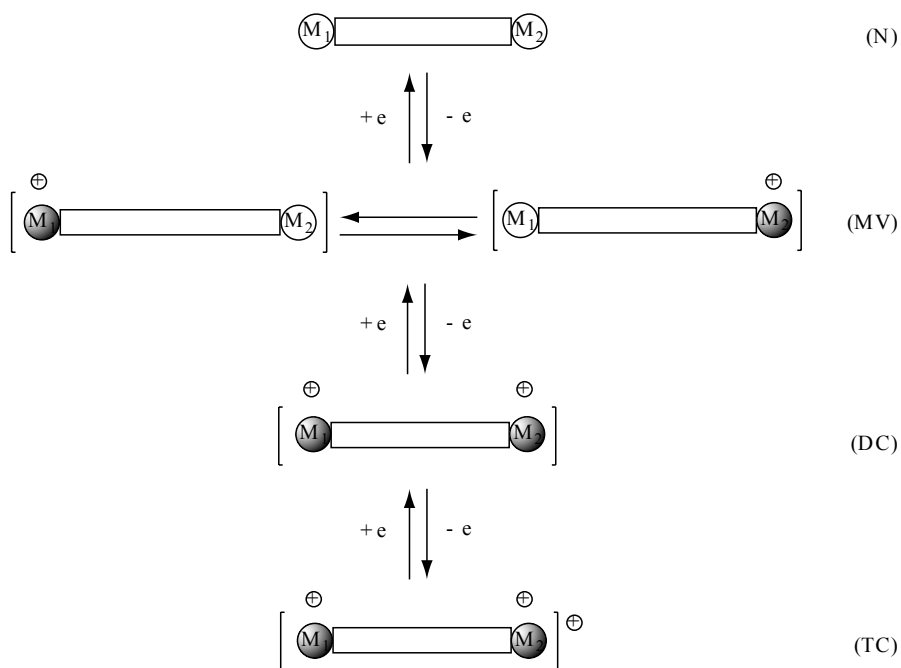
Magnetism is a bulk property and, as a consequence, was traditionally considered as being the field of the physicist or solid-state chemist [1,2]. During the last few decades, however, the quest for new magnetic materials has involved more and more (molecular) synthetic chemists, based on the idea that these materials could be engineered ‘from the bottom’ by an appropriate choice of ‘building blocks’. This has resulted in a growing molecular-based understanding of the magnetic phenomenon [3,4]. Notably, one facet of the challenge was to link paramagnetic units by spacers able to induce a co-operative behavior between the isolated spins [5–8]. Inorganic spin carriers proved to constitute very interesting building blocks in this respect [4,9–17]. As a result, systematic investigations were conducted on several discrete inorganic ditopic polyradicals, used to modelize the repeat unit(s) in a sometime hypothetical solid-state ‘polymer’ (Scheme 1) [10,12,18]. The purpose here is to understand better the intramolecular magnetic interactions taking place between two adjacent spin carriers.

Among the discrete polynuclear metal-centered polyradicals studied so far, most do not possess M–C bonds. These ‘organometallic’ polytopic polyradicals constitute, however, very interesting compounds, especially when unsaturated carbon-rich linkers connect the metallic spin-carriers. With redox-active spin carriers, many representatives of this class of polyradicals belong to redox families. Typically, dicationic ditopic diradicals, bridged by sp- or sp²-carbon atom linkers, result after two-electron oxidation of the corresponding neutral dinuclear precursors (DC in Scheme 2) [19]. Such

compounds have indeed been isolated [20,21]. Higher oxidation states (TC in Scheme 2) could also be characterized or isolated in a few rare instances [22–25]. In these redox families, the structure of the carbon-rich linker appears quite versatile, depending on the redox state. Structural changes take place between the redox parents, and separate spectroscopic studies of the



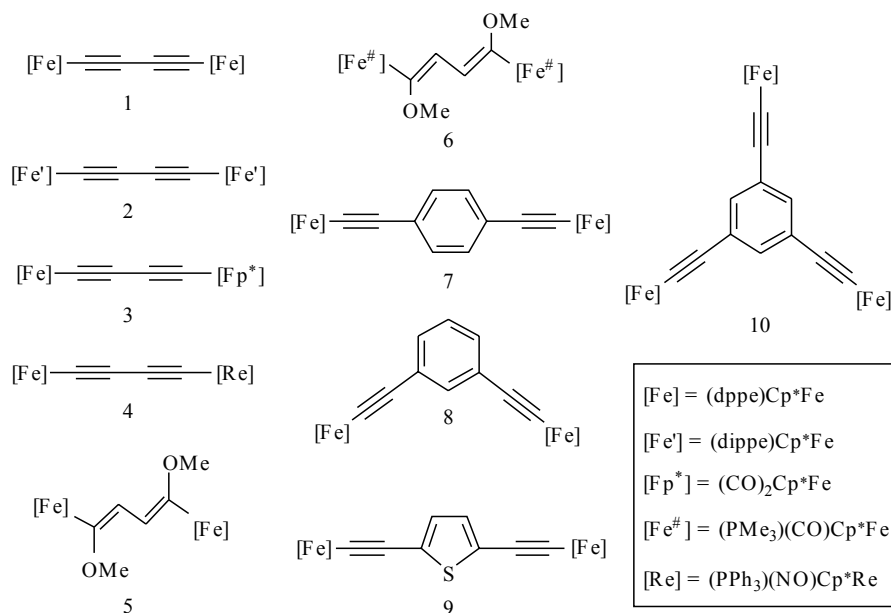
Scheme 1



Scheme 2

various redox congeners have provided decisive information on these electron-transfer-induced changes. As expected, such compounds have attracted considerable attention over the last few years as potential architectures for elaboration of new nanoscale-sized devices in molecular-based electronics [26–45]. Up until now, the mixed-valent (MV) states have been thoroughly studied from the point of view of intramolecular electron transfer. In this respect, polyene- or polyene-based compounds appear to present outstanding properties for the realization of ‘molecular wires’ [19,24,25,46,47]. Far less is known, however, about the higher oxidation states which in principle should exist as polyradicals, especially regarding the intramolecular magnetic interactions.

We have provided this present contribution in order to clarify the role of the magnetic interactions in the polyradical states of such organometallic complexes featuring carbon-rich spacers. The analysis will be largely based on recent results obtained in our research group with organoiron redox congeners (Scheme 3), but will also comprehensively include all of the recent data on related complexes, with respect to molecular magnetism. First, we will briefly recall the theoretical background underlying the intramolecular magnetic interaction between unpaired spins in such polyradicals. Then, after a succinct description of the properties of the prototypical $[(\eta^2\text{-diphos})(\eta^5\text{-C}_5\text{Me}_5)\text{Fe}]^+$ radical cation fragment, we will describe the magnetic properties of organoiron polynuclear complexes featuring this end-group. Next, we will discuss these results in a more general way and review the data reported for related organometallic



Scheme 3

compounds, especially regarding the structural implications of the magnetic interactions. Finally, we would like to stress that this contribution deals with ongoing work and, as a logical consequence, will then present some speculations regarding unanswered questions.

2 GENERAL NOTIONS REGARDING MAGNETIC INTERACTIONS IN POLYRADICALS

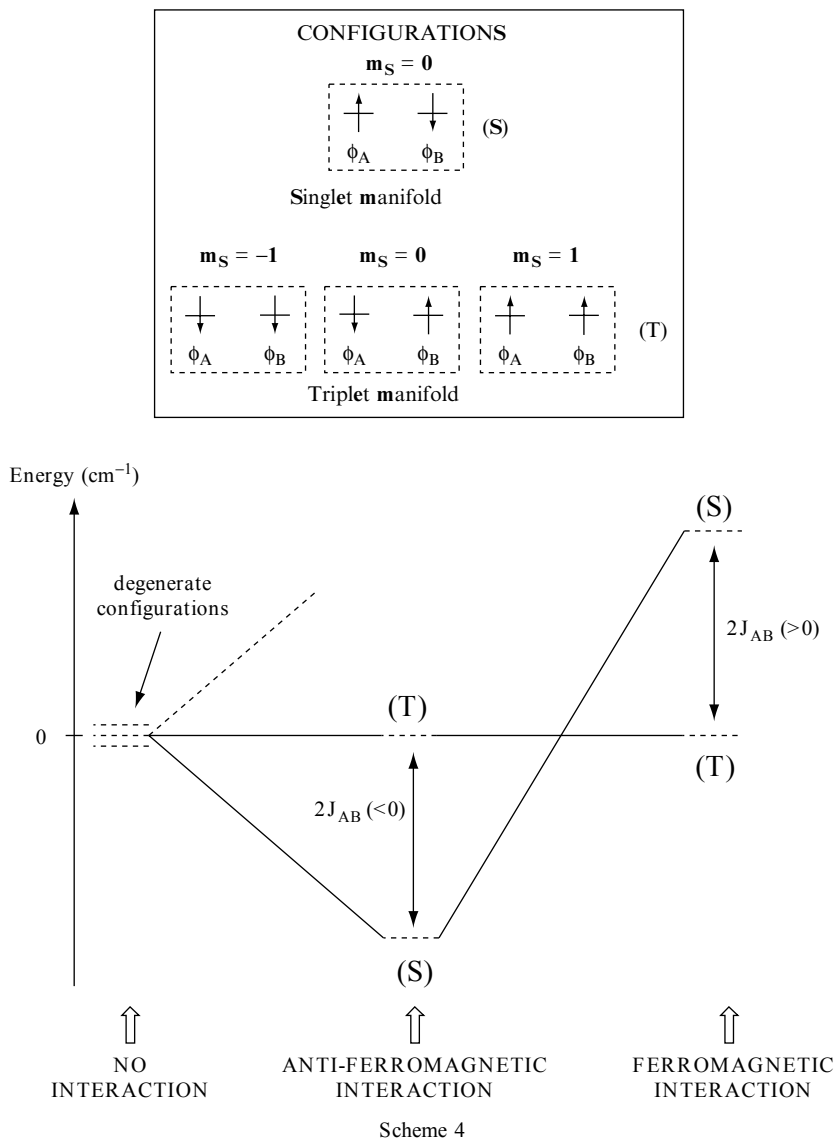
2.1 ANTIFERRO- AND FERROMAGNETIC EXCHANGE INTERACTIONS

Let us consider a symmetric bridged diradical with two sites (noted A and B) carrying each an unpaired electron in nearly degenerate singly occupied molecular orbitals (SOMOs) (ϕ_A and ϕ_B , respectively). If there is no interaction between the unpaired electrons, all electronic configurations (also called microstates or terms for metallic ions) resulting from spin inversions and belonging to the two different spin-configurations (or spin-states) have the same energy and can be considered as energetically degenerate. The sign of the spin quantum number associated with each unpaired electron will therefore be random in the absence of an external magnetic field (Scheme 4). In contrast, if there is a sizeable interaction, the energetic degeneracy of the corresponding terms will be lifted, and one spin-configuration will be more stable than the other. Between the two different spin-configurations which result for a diradical, the more stable spin configuration will constitute the ground state (GS). The triplet configuration presents a magnetic moment and threefold degeneracy, whereas the singlet configuration is diamagnetic and non-degenerate. Depending on the GS (triplet or singlet, respectively), the electronic spins will line up either in the same or in the opposite directions and are respectively said to interact in a ferromagnetic or in an antiferromagnetic fashion (Scheme 4).

2.2 THE HEISENBERG–DIRAC–VAN VLECK HAMILTONIAN

Let us consider such a ditopic A–L–B polyradical, made up of two paramagnetic metal centers, where ‘L’ represents the spacer between the paramagnetic sites. When there is no spin–orbit coupling and when second-order interactions (i.e. dipolar interaction, anisotropic and antisymmetric interactions, etc.) are neglected, the energy of the spin states resulting from the electrostatic interaction between the unpaired electrons on sites A and B, respectively, is given by the Heisenberg–Dirac–van Vleck (HDvV) Hamiltonian (equation (1) below).¹

¹ In the Heisenberg–Dirac–van Vleck Hamiltonian, S_A and S_B are the spin operators associated, respectively, with the two spins A and B and J_{AB} is a constant real number. Alternatively, this Hamiltonian is sometimes expressed without the factor ‘2’ before the J_{AB} , with the consequence



The energy separation between the states is given below by equation (2a). In equation (1), J_{AB} represents the isotropic interaction parameter (or magnetic exchange coupling) between the two spins S_A and S_B . The isotropic constant,

being then to double the J_{AB} value. Care has therefore to be taken when comparing J_{AB} values from different sources in the literature. All of the J_{AB} values given in this present contribution have been corrected by considering the Hamiltonian given in equation (1).

J_{AB} , can be either positive or negative [48].² Thus, for a diradical with $S_A = S_B = 1/2$, when the two unpaired spins line up in the same direction (i.e. ferromagnetic interaction), J_{AB} is positive and the GS is the triplet state ($S = 1$), whereas in the other case (i.e. antiferromagnetic interaction), J_{AB} is negative with a singlet GS (Scheme 4).

$$H = -2J_{AB}S_A S_B \quad (1)$$

$$E(S) - E(S - 1) = -2J_{AB}S \quad (2a)$$

$$S = S_A + S_B \quad (2b)$$

In polyradicals of higher topology, several intramolecular inter-sites interactions take place between the unpaired electrons. Accordingly, the Hamiltonian for the intramolecular magnetic interaction can be expressed as a summation of corresponding di-electronic HDvV spin Hamiltonians for each (A, B) couple of sites, thus generating several energetic non-degenerate spin states. The splitting between the various spin levels depends on the different J_{AB} values (equation (3)), determined by the geometry of the polyradical. Once the respective exchange coupling constants, J_{AB} , have been identified, the spin state of the GS can be unambiguously identified [48].

$$H = -\sum_A \sum_{B \neq A} 2J_{AB}S_A S_B \quad (3)$$

Historically, these ‘phenomenological’ Hamiltonians were initially coined for polynuclear complexes of paramagnetic ions. They are based on the assumption that (i) all ‘unpaired electrons’ can be localized on a given nucleus, and (ii) the electronic interactions between the electrons belonging to different sites (A and B) are weaker than their mutual local interactions, which primarily determines S_A and S_B .

2.3 RULES FOR DERIVING THE GROUND STATE

As a primary consequence of the intramolecular isotropic interaction between unpaired electrons, several non-degenerate electronic configurations (terms) corresponding to different spin states are generated. For strictly monotopic polyradicals, such as ‘naked’ transition metal ions or their complexes, Hund’s rule tells us that the GS will correspond to the spin configuration (or spin-state) exhibiting the higher spin multiplicity ($S = \sum_i S_i = 1/2 \times n$, with ‘ n ’ representing the number of unpaired electrons). The extension of Hund’s principle to polyradicals is, however, not always correct [49]. In the very specific case of alternant hydrocarbons, which bear some analogy with carbon-rich bridged polyradicals, more appropriate guiding principles were subsequently independently devised by Borden *et al.* [50] and Ovchinnikov [51], for deriving the nature of the GS.

² Noted also as J for diradicals in the following text.

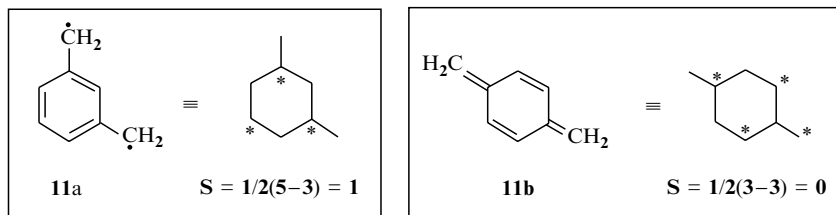
Ovchinnikov took into account the spin polarization effects in a valence bond (VB) formalism and proposed a topological rule allowing us to identify the GS in alternant Hückel hydrocarbons and also to predict its spin state [51,52]. This rule states that in any alternant hydrocarbon, the number of carbon atoms having a π -electron involved in the bonding can be divided into two sets, i.e. a 'starred' set (*) and an 'un-starred' set so that each atom belonging to one of these sets is bounded only to atoms of the second set, as exemplified below for the 1,3- and 1,4-benzoquinodimethanes **11a** and **11b** (Scheme 5). The spin S of the GS can then be derived by using the following equation:

$$S = [(\text{number of } * \text{ atoms}) - (\text{number of non-} * \text{ atoms})]/2 \quad (4)$$

This rule, also known as the 'Ovchinnikov rule', is based on the fact that nearby atoms in a common π -conjugated system tend to polarize their spin density oppositely. Apart from rare exceptions [14,49], the Ovchinnikov rule appears to be correct for most of alternant hydrocarbons experimentally investigated [52], and was successfully extended to alternanting polyradicals featuring carbene sites [53]. When heteroatoms or charged nuclei are present in the carbon skeleton, the rule was shown to fail in several instances [54,55].

Borden, on the other hand, used a MO formalism with SCF-HF methods [56]. He defined another topological criterion which also helps us to understand some of the failures of Ovchinnikov's rule [49,57]. This criterion states that when an alternant diradical has two non-bonding and *orthogonal* SOMOs, the GS will be triplet if these are non-disjoint. On the other hand, if these SOMOs are disjoint, the singlet and triplet state will lie very close in energy. In such a situation, the singlet state can often be slightly more stable owing to electron correlation with closed-shell filled MOs. For alternant hydrocarbon diradicals, the co-extensivity in space (disjoint or non-disjoint nature) of the SOMOs was demonstrated to have a decisive influence on the singlet-triplet gap [7].

The above analyses were restricted to organic polyradicals derived from alternant hydrocarbons. However, they illustrate the fact that Hund's rule cannot be simply extended to polyradicals without precisely considering the



Scheme 5

topology of the magnetic orbitals and the influence of the excited states in the electronic correlation. While Ovchinnikov's rule enables us to predict the nature of the GS, Borden's criterion focuses rather on the energy gap between the GS and the first excited state.

2.4 STRUCTURAL CHANGES BETWEEN SPIN STATES IN DITOPIC DIRADICALS

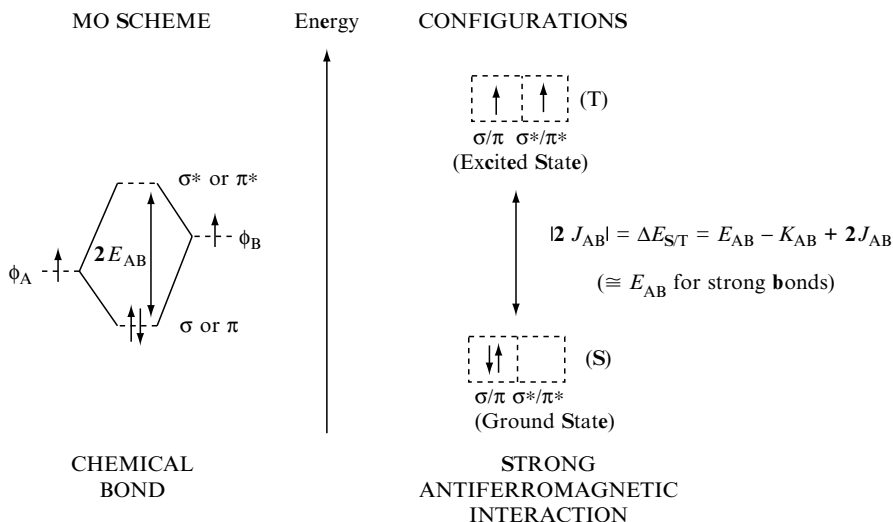
The spin isomers corresponding to various spin states generated by the isotropic intramolecular interaction in ditopic diradicals present different electronic distributions. This means also that sizeable differences in the spatial electron density characterize the two spin isomers. As a result, the geometries of both states, as well as the overall bond order between the spin carrier atoms and the central spacer are different. As we will see, high bond orders are usually favored in the singlet state.

As underlined by many researchers, a chemical bond between two atoms can be considered as an extreme case of antiferromagnetic coupling between the constitutive unpaired electrons on neighboring atoms (Scheme 6) [3,5,7]. The normal state, in which the bonding (σ or π) molecular orbital (MO) is doubly occupied, corresponds to the singlet GS. The excited antibonding configuration with both the bonding (σ or π) and the antibonding (σ^* or π^* , respectively) MOs singly occupied corresponds to the triplet state [58]. This exemplifies that the isotropic interaction is not different from the usual electrostatic interaction leading (or not) to bond formation between atoms. It is, however, much weaker in most stable diradicals, since the unpaired electrons are often 'located' further apart. As a result, the antiferromagnetic coupling does not always induce the formation of an additional chemical bond in the GS. Quite often, the actual structure of a singlet GS exhibits only slight structural changes relative to the corresponding excited triplet state.

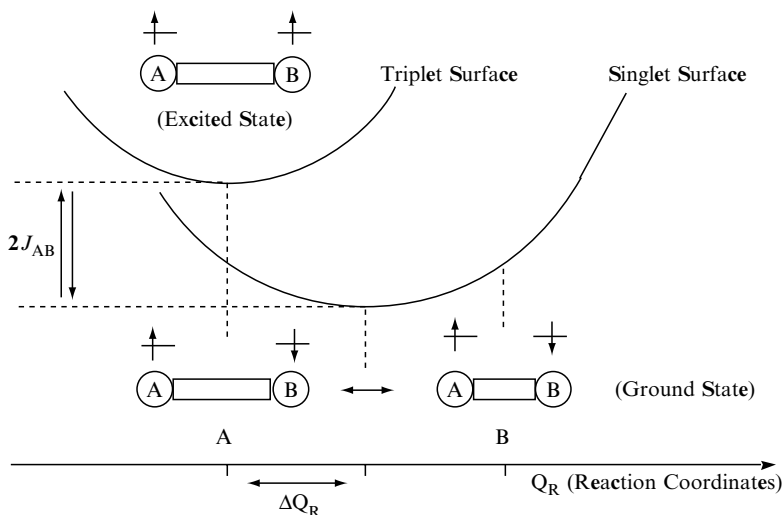
The geometrical changes between spin isomers can be represented by the shift (ΔQ_R) between the corresponding 'wells' in the singlet and triplet Born–Oppenheimer (BO) energy surfaces (Scheme 7). Typically, considering the simple case where just one well is present for each spin isomer, when a singlet GS is stabilized by electronic correlation with closed-shell configurations, the overall geometry is usually driven toward a 'more-bonding' arrangement of the atoms and the structural changes, embodied in the change of reaction coordinates (ΔQ_R), can be pictured by using mesomery³ (Scheme 7). Most often, for antiferromagnetically coupled diradicals, a structural change between spin isomers occurs because the open-shell vertical (i.e. $\Delta Q_R = 0$) singlet VB

³ According to its rules [59], mesomery can only take place between valence bond (VB) structures (i) of the same spin, (ii) of related geometries, and (iii) those close in energy. The electronic spins do not usually show up on Lewis structures and the first of these conditions is then often expressed as 'each mesomer must contain the same number of unpaired electrons' [60] (see Section 4.1.1 below). Importantly, 'unpaired' means, in this instance, 'of opposite spin' and not 'paired'.

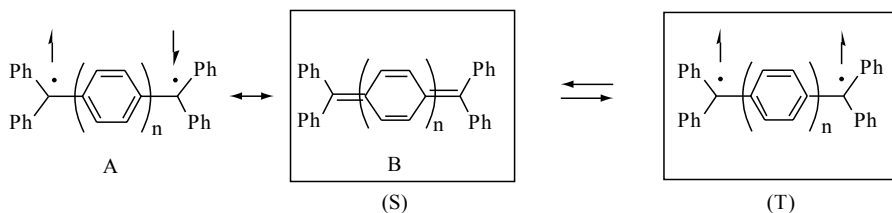
structure of the diradical (**A**) can ‘resonate’ with a closed-shell structure (**B**). In principle, the corresponding excited triplet VB structure may also ‘resonate’ with open-shell triplet structures, thus enlarging the structural change. However, since these correspond usually to excited states much higher in energy, a much smaller structural change is expected for the triplet isomer.



Scheme 6



Scheme 7



Scheme 8

This explains why the GS of alternant hydrocarbon presenting a Kekulé structure are usually singlet states and represented as closed shell structures (such as B in Scheme 8). In fact, structure 'B' is the Lewis structure which possesses the highest weight in the VB description of the GS singlet isomer for these compounds. Thus, Thiele's ($n = 1$) [61] or Tschitschibabin's ($n = 2$) [62] hydrocarbons are often represented with quinone-like structures (i.e. with one more bond) in their singlet GS (Scheme 8). However, in spite of this closed-shell Lewis representation, the GS does not actually correspond to a pure quinoidal structure, but has some (singlet) diradical (open-shell) character, corresponding to the VB structure (A), involved in it [63,64]. Whatever its exact structure, the singlet state of a diradical nevertheless corresponds to a more 'bonding' distribution of the electrons relative to the triplet for this class of diradicals.

2.5 EXPERIMENTAL DETERMINATIONS OF MAGNETIC INTERACTIONS IN DI- OR TRITOPIC POLYRADICALS

Many techniques have been used to obtain information about the spin-spin interactions in polyradicals. We will recall here the basic principles of the most straightforward and widely used techniques, focusing mostly on diradicals. For any polyradical, the situation largely depends on the energy gap separating the GS from the first excited state(s), and the temperature at which the measurement is performed. Typically, for a ditopic diradical, if the spin-orbit coupling and other second-order interactions are neglected (as we did above in Section 2.2.), three limiting cases can be delineated, as follows:

- (i) The two spin states are separated by a large singlet-triplet (S/T) energy gap ($|2J| = \Delta E_{S/T} \gg kT$). In this case, only the GS is populated at all temperatures.
- (ii) The S/T gap is negligible ($|2J| = \Delta E_{S/T} \ll kT$). Both spin states will be statistically populated at all temperatures.
- (iii) The S/T gap is of the same order of magnitude as kT ($|2J| = \Delta E_{S/T} \cong kT$). In this case, the population of each state will be highly temperature-dependent.

Typically, a diradical will behave as a pure diamagnetic (singlet spin isomer) or paramagnetic (triplet spin isomer) compound in case (i), as a 3/1 mixture of paramagnetic ($S = 1$) and diamagnetic ($S = 0$) compounds in case (ii), and will present properties belonging to a changing mixture of each spin isomer in case (iii). Basically, for triradicals, the situation is very similar, except that the spin states are more numerous.

2.5.1 NMR and the Evans Method

The NMR technique is particularly well suited to characterize diamagnetic compounds. It can prove very tedious with paramagnetic samples because the paramagnetic shifts are often large, and because of the well known line-broadening phenomenon, thus complicating the observation of the expected signals. Nevertheless, when satisfactory relaxation conditions are achieved, it constitutes the method of choice for checking the presence of paramagnetic compounds in solution and useful information can be gained from variable temperature studies [5,65,66]. The observed NMR shift of a paramagnetic nuclei (δ_{obs}) is the summation of its normal diamagnetic shift, and a paramagnetic contribution (δ_{iso}), itself composed of a dipolar (δ_{dipolar}) and a contact (δ_{contact}) term, as follows:

$$\delta_{\text{obs}} = \delta_{\text{iso}} + \delta_{\text{dia}} = \delta_{\text{contact}} + \delta_{\text{dipolar}} + \delta_{\text{dia}} \quad (5)$$

While the contact term represents the influence of the unpaired electrons ‘through bonds’, the dipolar term reflects the influence of the unpaired electrons ‘through space’ and is strongly related to the dipolar splitting observed by ESR spectroscopy (see Section 2.5.2 below). For a (poly)radical with a global $S = 1/2$ spin, the paramagnetic contribution will exhibit a linear inverse temperature-dependence, reminiscent of the Curie law (see below). Deviation from this law is usually observed when the global spin of the molecule is larger than $1/2$ ($S > 1/2$). Therefore, study of the NMR shift versus temperature constitutes a simple means to evaluate the magnetic moment of the global spin of a paramagnetic sample. The NMR and ESR techniques compliment each other very well, especially since well-resolved NMR spectra are often obtained when spin-relaxation is too fast to give resolved ESR spectra, and vice-versa [67].

Another simple and attractive approach for determining the global spin value of a paramagnetic compound in solution, is the so-called ‘Evans method’ [65,68,69]. This technique, based on the shift ($\Delta\delta$) displayed by a reference, such as tetramethylsilane (TMS), in the presence of the dissolved paramagnetic substance of interest, allows us to derive specifically the molecular contribution of the latter to the magnetic susceptibility (χ_m in emu/g) as follows:⁴

⁴ Equation (6) is valid only when the (NMR) tube is parallel to the external field [70]; in this relationship, c is the mass concentration of the polyradical (g/mL), χ_0 is the diamagnetic susceptibility of the solvent, and d_0 and d_s are the densities of the pure solvent and solution, respectively.

$$\chi_m = 3\Delta\delta/(4\pi c) + \chi_0 + \chi_0(d_0 - d_S)/c \quad (6)$$

From this value, the global spin value of the compound can, in principle, be derived by using the Curie ($\theta = 0$) or Curie-Weiss law equation (7), when the temperature at which the measurement was performed is accurately known:

$$\chi = C/(T + \theta) \quad (\text{where } C = Ng^2\beta^2S(S + 1)/3kT) \quad (7)$$

We would like to stress here that the Evans method is usually straightforward for polyradicals with a very large energy gap between their first excited state and the GS (case (i)), along with a non-zero spin state for the latter. In the case of diradicals presenting a low energy gap between the various spin states (case (iii)), the singlet state is populated as well at the temperature at which the spectrum is recorded, resulting in the fraction of paramagnetic compound (triplet state) presenting a molecular magnetic moment being lower than 100 %. In order to use equation (6) in this situation, the respective populations of the singlet and triplet states have to be known accurately. Finally, when there is no magnetic interaction (case (ii)), both the triplet and singlet states are statistically populated (75/25 %) in the high-temperature range. In this case, equation (6) is still valid and the term 'C' is corrected accordingly (factor of 0.75).

It is noteworthy that when the S/T gap is of the order of magnitude of kT (case (ii)), the evolution of the paramagnetic NMR shift with temperature (equations (5) or (6)) is related to the spin isomer distribution. In favorable cases, the temperature-dependence can be used to extract the S/T gap by simulation, as carried out for magnetic susceptibility or ESR measurements (see Section 2.5.3 below). Since the NMR spectra must be recorded with homogeneous samples, the temperature range available is, however, often quite restricted.

2.5.2 Electronic Spin Resonance

ESR spectroscopy also constitutes a very powerful technique to determine the energy gap in diradicals when the compounds are sufficiently stable over a wide temperature range. It can be routinely applied with samples in solvent glasses, at low temperatures (anisotropic spectra), or in homogeneous solutions, at higher temperatures (isotropic spectra). Importantly, only the energy states presenting a non-zero spin operator are ESR-active. Therefore, in order to detect a signal, one has to make sure that these states are populated at the temperature of the experiment. Moreover, the presence of several interacting unpaired spins enhances relaxation at the expense of spectral resolution. Therefore, failure to observe an ESR spectrum does not necessarily imply that the sample is diamagnetic (singlet) in the GS.⁵ Conversely, observation of an ESR

⁵ Notably, in many cases, no ESR spectrum can be obtained for otherwise stable and identified triplet diradicals.

spectrum with a given polyradical does not warrant that the resulting signal corresponds to the GS. Typically, when the exchange coupling is weak (case (iii)), both the excited and the ground states can simultaneously be populated, depending on the temperature. Similarly to the temperature-dependent amplitude of the NMR paramagnetic shift (see Section 2.5.1 above), the temperature-dependent intensity of the ESR signal is related to the magnetic susceptibility (χ) and can be used, in favorable cases, to derive the energy gap(s) ($\Delta E_{S/T}$ for diradicals) between spin states by simulation (see Section 2.5.3 below). In this situation, monitoring the intensity of the ESR signals as a function of temperature can reveal the nature of the GS.

For diradicals, when the ESR spectrum is recorded, the sample is subjected to a magnetic field. As a result, the Zeeman effect splits the three m_s sub-levels of the triplet state (Scheme 9A). For a given microwave frequency ($h\nu$), a doubly degenerate transition between the $m_s = -1$ and $m_s = 0$, or $m_s = 0$ and $m_s = 1$, states can be observed, if neither spin-orbit coupling nor zero-field splitting takes place (i.e. no dipolar, anisotropic and antisymmetric interactions) [71]. The isotropic spectrum of such a triplet diradical is characterized by one g -value. The corresponding Hamiltonian is given by equation (8a), where S_1 and S_2 are the respective spin operators of the unpaired electrons in the diradical (S is the global spin operator), H is the field vector and g_1 and g_2 are the local g -tensors:

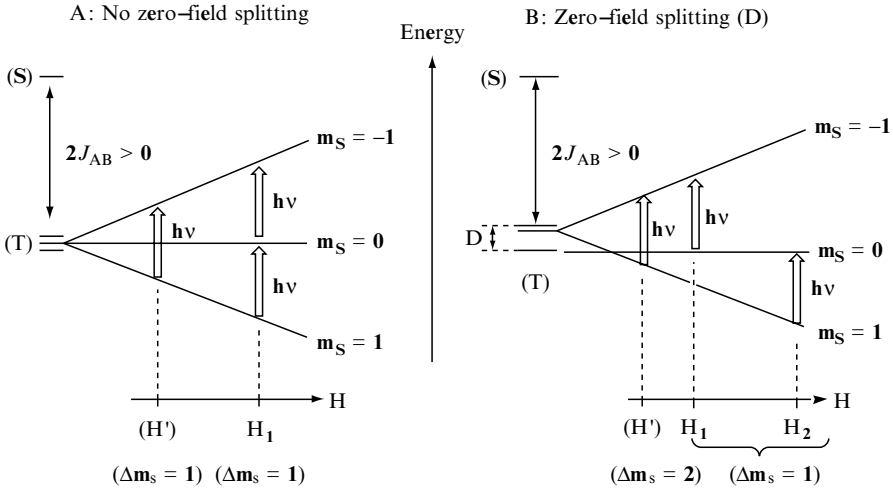
$$H_{\text{ESR}} = \beta H(g_1 S_1 + g_2 S_2) = g\beta H(S_1 + S_2) = g\beta HS \quad (8a)$$

The forbidden ($\Delta m_s = 2$) transition between the $m_s = -1$ and $m_s = 1$ levels may sometimes show up as a very weak signal located at ‘half-field’ in the spectrum. This transition, when observed, yields a half-field g -value which characterizes the triplet state.

$$H_{\text{ESR}} = g\beta H(S_A + S_B) + S_A D S_B \quad (8b)$$

When zero-field splitting takes place, additional terms must be considered in the Hamiltonian and two or more non-degenerate transitions will then occur (Scheme 9B). The zero-field tensor is characterized by axial (D) and rhombic (E) components, depending on the point group symmetry⁶ of the diradical (equation (8b)) [48]. Additional splitting can also be observed in the case of hyperfine coupling (A tensor). This again introduces new terms in equation (8b). Finally, when the spectrum of a given diradical is recorded in a solvent glass (anisotropic ESR spectrum), depending on its symmetry in the solid state, up to three components can be obtained for each transition observed in the corresponding isotropic spectrum. Most often, however, the spectral resolution

⁶ For spherical symmetry, $D = E = 0$, while for rhombic symmetry, $E = 0$. The D and E zero-field tensors contain various contributions, such as the purely dipolar (through-space) interaction, but also (weak) through-bond interactions, such as the spin-orbit, anisotropic and antisymmetric forms. This constitutes second-order contributions in the present case, given the ESR Hamiltonian used (equations (8a) and (8b)).



Scheme 9

is not sufficient to allow the observation of all second-order features, because of line-broadening effects resulting from the fast spin-spin relaxation process taking place in polyradicals.

For triradicals, all non-zero spin states will similarly be split by the Zeeman effect. However, much more complex spectra are often observed, featuring also allowed and forbidden transitions. Interpretation of these spectra is often quite difficult, particularly when some zero-field splitting or hyperfine coupling takes place. Their interpretation will not be discussed further here [48].

2.5.3 Solid-State Magnetic Susceptibility Measurements

With the availability of SQUID (Semiconducting QUantum Interface Device) susceptometers, the bulk magnetic susceptibility can be measured accurately and straightforwardly with solid samples. Solid-state magnetic susceptibility, similarly to the magnetic susceptibility in solution from the Evans method (see Section 2.5.1 above), provides information on the spin states of molecules constituting a given sample [5,72]. In principle, in the absence of strong *inter*-molecular interactions, the temperature-dependence of the molar magnetic susceptibility (χ)⁷ of a polyradical is characteristic of the *intramolecular* magnetic interaction. Thus, proper modelization enables one to determine the energy splitting between the ground and the first excited spin states. The quality of the measurement dramatically depends on the homogeneity and the purity of the sample.

⁷ $\chi = dM/dH$, where M is the induced bulk magnetization and H is the applied static magnetic field.

For a diradical, if the two spins states are separated by a large energetic S/T gap (case (i)) and if the GS is the singlet, the compound is diamagnetic and χ will be roughly constant.⁸ In contrast, if the GS is the triplet ($J > 0$, ferromagnetic coupling), when only the GS is populated the magnetic susceptibility will obey the Curie–Weiss law in the highest temperature range⁹ with $\chi(T - \theta) = 1.0 \text{ emu K mol}^{-1}$ (equation (6)).¹⁰ Now, if the S/T gap is negligible (case (ii)), the diradical will behave as a 3/1 mixture of triplet ($S = 1$) and singlet ($S = 0$) spin isomers in the highest temperature range. The magnetic susceptibility of the sample will also follow the Curie (or Curie–Weiss) law, but with a slope of $0.75 \text{ emu K mol}^{-1}$ in this case.¹¹ Finally, when the S/T gap is small (case (iii)), the resulting susceptibility deviates from the linear laws previously observed, due to the temperature-dependent population change between the spin states. The Bleaney–Bowers law gives the dependence of the molecular magnetic susceptibility on the temperature (equation (9a)) [73]. This expression is often corrected by considering a small molar fraction (ρ) of a related monoradical¹² contaminating the sample (equation (9b)) [48]:

$$\chi = 2Ng^2\beta^2/kT[3 + \exp(-2J/kT)]^{-1} \quad (9a)$$

$$\chi = \{2Ng^2\beta^2/kT[3 + \exp(-2J/kT)]^{-1}\}(1 - \rho) + [Ng^2\beta^2/2kT]\rho \quad (9b)$$

For small S/T gaps (case (iii)), the curvature of the function in a plot of χT versus T characterizes a ferro- ($J > 0$, upward curvature) or antiferromagnetic ($J < 0$, downward curvature) exchange coupling between spins. It gives straightforwardly the nature of the GS (Scheme 10), provided no temperature-independent paramagnetism (TIP)¹³ is present. Notably, TIP or small amounts of paramagnetic impurities can modify significantly the shape of the

⁸ When S is zero, the compound is diamagnetic and χ versus T will be negative and essentially reflect the diamagnetic contribution to the magnetic susceptibility. Since the latter is very weak in comparison with the paramagnetic contribution, we have neglected it in the following expressions for paramagnetic molecules, as well as any temperature-independent paramagnetic contribution (TIP).

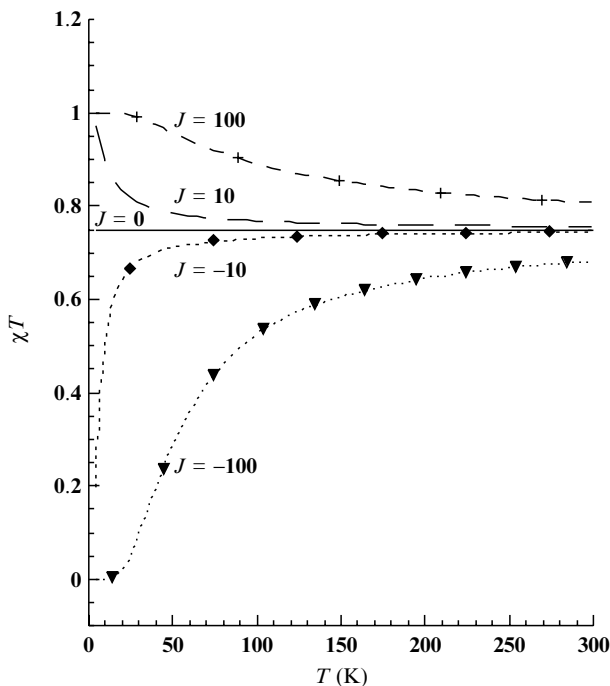
⁹ Importantly, in deriving equation (6), we considered that the intensity of the magnetic field H applied in the susceptometer is much weaker than in ESR and did not consider the Zeeman splitting in the triplet state (i.e. H/T negligible). However, when measuring χ at very low temperatures, H/T is no longer negligible, and the splitting of the m_s sub-levels by H has to be accounted for using Brillouin functions [5]. This results in a loss of linearity at low temperatures for χ .

¹⁰ In these expressions, N is the Avogadro number, g is the isotropic g - (Zeeman) factor, in principle, available from ESR measurements, β is the Bohr magneton and k is the Boltzmann constant. The weak *intermolecular* spin–spin interactions are represented by the constant term θ .

¹¹ This temperature-dependence will be observed regardless of the actual nature of the GS (i.e. regardless of the sign of J). It is noteworthy that it is different from that of independent $S = 1/2$ paramagnetic centers ($\chi T = 0.37 \text{ emu K mol}^{-1}$) and does in principle constitute a means of distinguishing between the two situations.

¹² Importantly, in equation (9b), the contaminant monoradical is assumed to present the same (or a very close) g -factor.

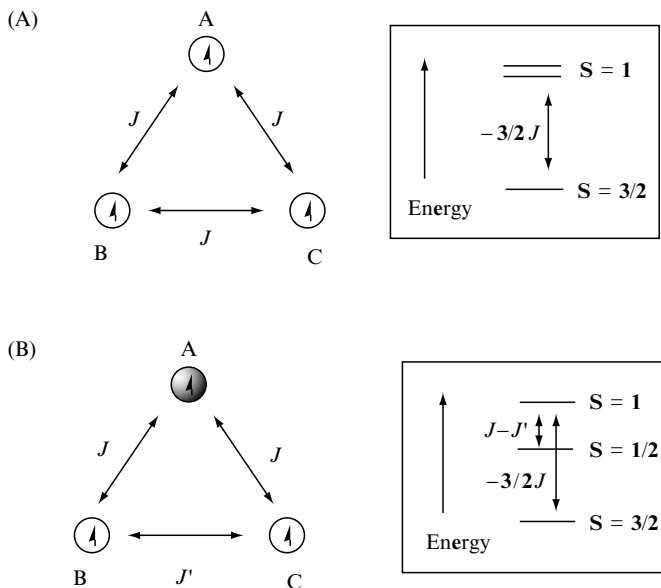
¹³ The presence of TIP results in the appearance of an additional constant term in the χ expression.



Scheme 10

χT curves as a function of T . By fitting the experimental curves with equations (9a) or (9b), the S/T gap ($\Delta_{S/T} = 2J$) of the diradical can be determined. When the isotropic g -constant is known independently from the ESR spectrum, an iteration procedure will be even more reliable, since it is only J - (and possibly ρ -) dependent.

Polytopic triradicals with large or negligible gaps (cases (i) and (ii)), can be treated analogously to diradicals, and will exhibit Curie–Weiss dependences with different slopes [48]. However, when the gap between the GS and the first excited state is moderate, the variation of the magnetic susceptibility with temperature will strongly depend on the topology of the polyradicals. Thus, the temperature-dependence for the magnetic susceptibility of ditopic triradicals resembles that of a diradical, except that the ground and excited spin states are no longer the singlet and triplet states ($S_A = 1$ and $S_B = 1/2$ in the corresponding HDvV Hamiltonian). For tritopic triradicals, however, more complex temperature-dependences of the magnetic susceptibility are possible, depending on the global molecular symmetry of the triradicals. Thus, for triradicals presenting a C_3 symmetry axis, the isotropic coupling between all pairs of unpaired electrons must be identical (Scheme 11A). With a less symmetric triradical, where only two spin carriers remain equivalent (Scheme 11B), two



Scheme 11

different isotropic exchange coupling constants, J and J' , must be considered. These are usually taken as being proportional ($J' = \alpha J$) in the HDvV Hamiltonian (equation (10)) and the temperature-dependence of the magnetic susceptibility is given in equation (11) [74, 103].¹⁴ It is worth noting that putting $\alpha = J' = 0$ in these equations (10 and 11) corresponds to a triradical with no coupling between the two identical sites, as in most symmetric linear triradicals, while putting $\alpha = 1$ gives $J = J'$ and corresponds to the C_3 symmetric triradical (Scheme 11A) [48]:

$$H = -2J(S_{A1}S_B + S_{A2}S_B + \alpha S_{A1}S_{A2}) \quad (10)$$

$$\chi = [(Ng^2\mu_B^2)/4k(T - \theta)][(1 + \exp(2(\alpha - 1)J/kT) + 10 \exp(1 + 2\alpha)J/kT) / (1 + \exp(2(\alpha - 1)J/kT) + 2 \exp(1 + 2\alpha)J/kT)] \quad 7.8(11)$$

For even less symmetric cases, three different isotropic constants must be considered. The magnetic susceptibility dependence becomes then very complex and is out of the scope of this present chapter. As for ESR, we refer the reader to the appropriate monographs [48,75].

Finally, we would like to recall here that equations (9–11) do not account for possible weak *intermolecular* interactions between diradicals (no θ terms). The existence of TIP or the possible influence of minor amounts of paramagnetic

¹⁴ It is worth noting that in equation (11) a unique and mean g -value is used. However, more complete expressions can be found [48].

impurities in a given sample should also not be overlooked. It should be noted that all expressions given in this section are valid only when no spin-orbit or other related strong anisotropic spin-spin interactions take place (dipolar, anisotropic or antisymmetric interactions).

3 MAGNETIC INTERACTIONS IN CATIONIC ORGANOIRON DI- AND TRI-NUCLEAR METAL-CENTERED POLYRADICALS CONTAINING $[(\eta^2\text{-DIPHOS})(\eta^5\text{-C}_5\text{Me}_5)\text{Fe}]^+$ END GROUPS

For several years now, we have been investigating dinuclear and trinuclear organoiron complexes featuring various carbon-rich central spacers or possessing terminal sites of varied electron richness (see Scheme 3 above) [19]. This has allowed us to gain some insight in the structure-property relationships determining the electron-transfer process in these mixed-valence (MV) complexes. We have also accumulated some data on various di- or tricationic species, $\mathbf{1}^{2+}$ – $\mathbf{10}^{2+}$, $\mathbf{3}^{3+}$ and $\mathbf{10}^{3+}$ (see Scheme 3). The detailed synthesis of most compounds has already been presented elsewhere [19].

3.1 THE $[(\eta^2\text{-DIPHOS})(\eta^5\text{-C}_5\text{Me}_5)\text{Fe}]^+$ RADICAL CATION FRAGMENT

3.1.1 The $[(\eta^2\text{-diphos})(\eta^5\text{-C}_5\text{Me}_5)\text{Fe}]^+$ Fragment in Mononuclear Complexes

When appended to unsaturated organic ligands, the $[(\eta^2\text{-diphos})(\eta^5\text{-C}_5\text{Me}_5)\text{Fe}]$ fragment proves usually to be fairly stable under the iron(III) oxidation state, in spite of its radical-cation nature. In fact, most mononuclear complexes presenting such a fragment were usually low-spin 17-electron iron(III) complexes, which can be handled at room temperature under a controlled atmosphere. This stability is most likely of kinetic origin and can be imparted to the fact that the unpaired electron is mainly located at the iron center, strongly sterically shielded by the Cp^* (pentamethylcyclopentadienyl) and the diphosphine ancillary ligands. This can be evidenced by Mössbauer spectroscopy recorded at zero field [76]. The parameters of the iron(III) alkynyl compounds are well differentiated from those of the iron(II) parent compounds [77]. The quadrupole splitting (QS) values (ΔE_Q) are well characteristic of the iron(II) and low-spin iron(III) states. These values are close to 2.0 for the iron(II) complexes with σ -linked R groups and below 1.0 for the related iron(III) derivatives (Table 1). ESR spectroscopy also corroborates this important conclusion. In the spectra recorded at 77 K in solvent glasses ($\text{CH}_2\text{Cl}_2/\text{C}_2\text{H}_4\text{-1,2-Cl}_2$), three well-separated signals were usually observed. These three g -tensor components are characteristic of the low-spin iron(III) complexes in an octahedral symmetry. In some cases, as for the related $[(\eta^2\text{-dppm})(\eta^5\text{-C}_5\text{H}_5)\text{Fe}(\text{C} \equiv \text{CR})]^{*\cdot+}$ complexes,

Table 1 ^{57}Fe Mössbauer parameters for Fe(II) and Fe(III) complexes in the $[(\eta^5\text{-C}_5\text{Me}_5)(\eta^2\text{-dippe})\text{FeL}]^{n+}n[\text{X}^-]$ series at 80 K

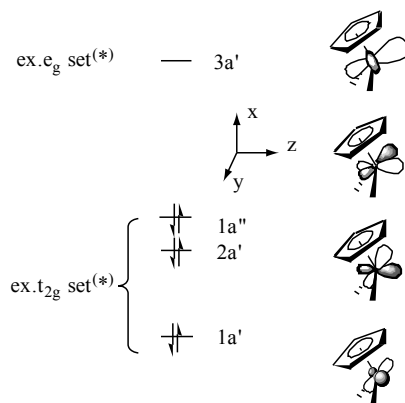
L	<i>n</i>	X	δ (mm s ⁻¹)	ΔE_Q (mm s ⁻¹)	Ref.
CH ₃	0	—	0.15	1.95	88
—C≡C—H	0	—	0.276	1.987	78
—C≡C—(C ₆ H ₅)	0	—	0.27	2.02	78
—C≡C—(C ₆ H ₄)— <i>p</i> -NO ₂	0	—	0.256	2.061	80
—C≡C—C≡C—SiMe ₃	0	—	0.25	1.93	152
—C(=CH ₂)OCH ₃	0	—	0.323	1.904	77
CO	1	PF ₆	0.196	1.842	77
=C(CH ₃)OCH ₃	1	OSO ₂ CF ₃	0.216	1.223	77
=C=CH ₂	1	PF ₆	0.086	1.032	77
=C=C(C ₆ H ₅)H	1	PF ₆	0.116	1.118	77
=C=C=C(CH ₃)OCH ₃	1	BPh ₄	0.160	1.451	77
=C=C=C=C(Fp*)H ^a	1	BF ₄	0.161	1.316	153
=C=C=C=C(Fp*)Me ^a	1	OSO ₂ CF ₃	0.163	1.424	153
CH ₃	1	PF ₆	0.35	0.76	88
—C≡C—(C ₆ H ₅)	1	PF ₆	0.25	0.90	78
—C≡C—(C ₆ H ₄)— <i>p</i> -NO ₂	1	PF ₆	0.120	0.870	80

^a Fp*, (Cp*)Fe(CO)₂.

the two high-field patterns are additionally split into 1:2:1 triplets by hyperfine coupling with the two equivalent ³¹P nuclei [19,78,79].

In mononuclear (η^2 -dippos)(η^5 -C₅Me₅)Fe—R complexes, the Cp* ring occupies three coordination sites, whereas the diphosphine and the 'R' ligand occupy the three remaining sites. The crystal structures solved for different mononuclear iron(II) or iron(III) compounds indicate that the classical pseudo-octahedral geometry invariably observed for iron(II) 'piano-stool' complexes is maintained in the iron(III) oxidation state [80]. The strong ligand field and the asymmetry of the coordination sphere results in a low-spin configuration for the d⁵ manifold of valence electrons.¹⁵ Molecular orbital calculations on the model $[(\eta^2\text{-dpe})(\eta^5\text{-C}_5\text{H}_5)\text{M}]^+$ fragment (M = Fe(II), Ru(II)) with imposed C_s symmetry have shown that three MOs can be identified with the t_{2g} set in O_H symmetry (Scheme 12) [84–87]. Thus, for the 17-electron (17e) fragment, the electronic vacancy is located in the 1a'' orbital of largely d_{yz} character. Typically upon oxidation, for an alkynyl 'C≡C—Ar' ligand, an electron is extracted either from the 1a'' or 2a' level to give the 17e-radical cation, regardless of the nature of the 'Ar' substituent [84]. The unpaired spin density is partly delocalized on the Cp* ligand [88], but also on the R ligand, when sp² or sp carbon atoms are present in α -positions relative to the metal center. Accordingly, with such an

¹⁵ The 'dⁿ' metal configuration is always established by considering the carbon-rich bridge as an anionic ligand. This is an important point since other conventions have been adopted elsewhere [81–83].



Frontier MO scheme for the piano-stool 16e-Fe(II) fragment (*)The symmetry of the parent MOS in (Oh) symmetry are indicated here

Scheme 12

interpretation, the ESR g_1 - and g_2 -values are close to the free-electron g -value ($g = 2.0023$) for mononuclear $[(\eta^2\text{-dppe})(\eta^5\text{-C}_5\text{Me}_5)\text{FeR}]^+$ complexes, whereas the g_3 component is much larger [19]. This is expected for low-spin iron(III) compounds having a singly occupied HOMO with predominant d_{xz} or d_{yz} character [19,78,79,88]. Moreover, an increase in the g_3 -values is observed with decreasing hybridization of the metal-bound carbon center, hence suggesting an active participation of the π -conjugated ligands in the delocalization of the odd electron.

The Cp* and diphosphine units are high-field ligands.¹⁶ In contrast to well-known examples of octahedral mono- or polynuclear d^6 iron(II) complexes [48,91–93], no spin-crossover phenomenon could ever be detected in various monomeric $[(\eta^2\text{-dppe})(\eta^5\text{-C}_5\text{Me}_5)\text{FeR}]^+[\text{PF}_6]^-$ complexes.

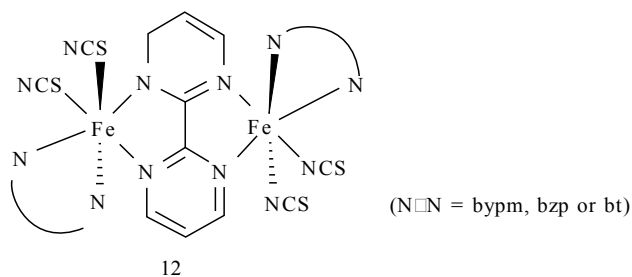
3.1.2 The $[(\eta^2\text{-diphos})(\eta^5\text{-C}_5\text{Me}_5)\text{Fe}]^+$ Fragment(s) in Polynuclear Complexes

Polynuclear complexes featuring $[(\eta^2\text{-dppe})(\eta^5\text{-C}_5\text{Me}_5)\text{FeR}]^+$ units are most usually stable under an inert atmosphere. Various organometallic polynuclear mono- and polyradicals, such as $1^+ - 9^+$, $1^{2+} - 9^{2+}$, and 10^{3+} (see Scheme 3), featuring several such iron(III) sites as end-groups, could be isolated by means of stepwise chemical oxidations starting from the neutral iron(II) precursors (see Scheme 2). All oxidations proceed quantitatively to give the expected

¹⁶ This is especially true when the third 'R' ligand is an unsaturated ligand, such as the butadiynyl ligand. A cumulene R ligand will even induce a stronger crystalline field because of its stronger π -accepting capabilities [89,90], thus also favoring more the low-spin configuration for the $[(\eta^2\text{-diphos})(\eta^5\text{-C}_5\text{Me}_5)\text{Fe}]^+$ end-group.

derivatives as thermally stable dark-green ($1^+ - 9^+$ and 10^{2+}) or deep-blue solids ($1^{2+} - 9^{2+}$, 3^{3+} and 10^{3+}), using ferrocenium hexafluorophosphate. The corresponding cationic mono-, di- and triradicals were then subsequently isolated by precipitation.

The large kinetic stability of these compounds can again be traced to a dominant localization of the electronic vacancies on the iron center(s), as suggested by the ESR and Mössbauer spectra recorded at zero field (see Tables 2, 3 and 4). The $[(\eta^2\text{-diphos})(\eta^5\text{-C}_5\text{Me}_5)\text{Fe}]^+$ units also remain low-spin in the 4–300 K range in these polynuclear assemblies. This is a very important point, since several dinuclear complexes of Fe(II), such as **12**, are known, in which spin-crossover occurs concomitantly with spin transitions [94].¹⁷



3.2 MAGNETIC INTERACTIONS IN POLYNUCLEAR MONO-, DI- AND TRIRADICALS

3.2.1 Magnetic Interactions in Polynuclear Monoradicals

In spite of their polynuclear and MV character, the mono-oxidized complexes $1^+[\text{PF}_6^-] - 10^+[\text{PF}_6^-]$ are monoradicals and present no conceptual difficulty regarding the understanding of their magnetic properties. They behave as mononuclear low-spin paramagnetic compounds possessing one unpaired electron. As a result, their magnetic susceptibility follows the Curie-Weiss law (equation (6)) [48]. This has been verified in several instances, notably with 1^+ and 4^+ (Figure 1) or other $d^6 - d^5$ MV complexes [95,96]. Their ESR spectra resemble those recorded for mononuclear Fe(III) complexes and feature three g_1 , g_2 and g_3 tensors in most cases (Table 2) [19]. Accordingly, with the qualitative observation that the anisotropy of the ESR signal reflects the capability of the 'axial' organic ligand to delocalize the unpaired electron in mononuclear complexes, the 'anisotropy' of the ESR signal in dinuclear MV complexes reflects the metal-metal delocalization, also given by the electronic coupling parameter (V_{ab}) [97].

¹⁷ The spin carriers in these polynuclear compounds are however classic inorganic coordination complexes (like $(\text{N}-\text{N})(\text{NCS})_2$ in **12**) and share little similarity with the $(\eta^2\text{-diphos})(\eta^5\text{-C}_5\text{Me}_5)\text{Fe}$ end-group present in our organometallic assemblies.

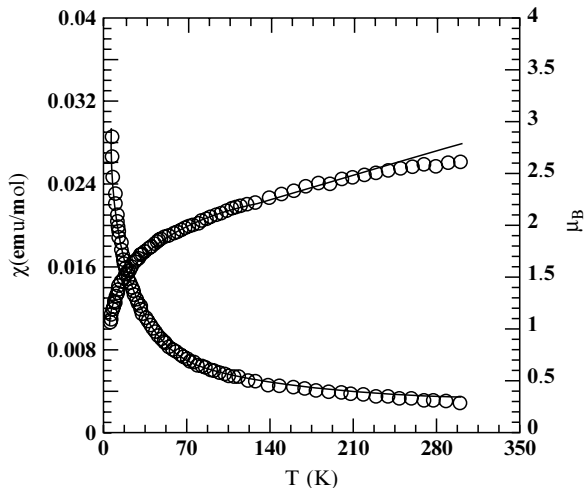


Figure 1 Temperature-dependence of the corrected molar magnetic susceptibility for $2^{2+}[\text{PF}_6^-]$; the solid line represents the best fit

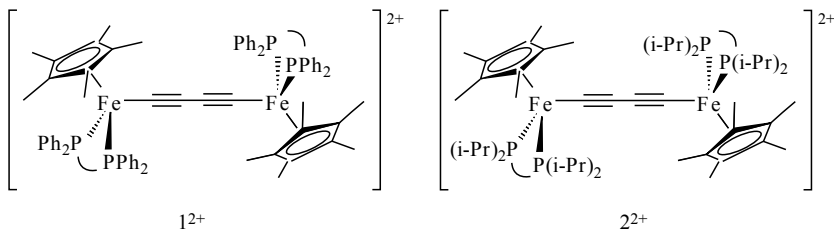
Table 2 ESR data^a and corresponding electronic coupling parameter (V_{ab}) values for selected mixed-valence complexes

X	g_{iso}	g_1	g_2	g_3	Δg	$V_{ab}(\text{cm}^{-1})$	Ref.
$[\text{Fe}]-\text{C}\equiv\text{C}/\text{C}_6\text{H}_5^b$	2.156	1.975	2.033	2.460	0.485		78
1^+	2.102	2.079	2.089	2.139	0.060	3790	20
2^+	2.115	2.015	2.062	2.269	0.254	2480	23
4^+	2.054	1.920	2.008	2.236	0.316	152	25
7^+	2.091	2.031	2.043	2.199	0.168	161	102
8^+	2.170	1.975	2.032	2.505	0.530	2515	103
9^+	2.053	2.006	2.039	2.113	0.107	143	97
10^+	2.155	1.982	2.034	2.450	0.468	117	146
10^{2+}	2.139	1.978	2.030	2.409	0.431	71	146

^a At 77 K in $\text{CH}_2\text{Cl}_2/\text{C}_2\text{H}_4\text{Cl}_2$ (1:1) glass.

^b $[\text{Fe}] = [(\eta^2\text{-diphos})(\eta^5\text{-C}_5\text{Me}_5)\text{Fe}]^+$

3.2.2 Magnetic Interactions in Polynuclear Diradicals



Early investigations on the diradical dication $1^{2+}2[\text{PF}_6^-]$ indicated that the complex was paramagnetic at 25°C , as suggested by the observation of broadened and shifted NMR lines [98]. Unfortunately, no ESR spectrum could be obtained for this complex, presumably owing to fast intramolecular spin–spin relaxation [20]. More recently, very similar observations were made on the related butadiynediyl $2^{2+}2[\text{PF}_6^-]$ complex featuring more electron-rich end-groups [23]. Likewise, Evans measurements for pure $2^{2+}2[\text{PF}_6^-]$ gave a magnetic moment of $0.76 \mu_{\text{B}}$ in dichloromethane solution. Such a value is much too low to make sense if only triplet 2^{2+} is present. Obviously, some diamagnetic singlet 2^{2+} is present in the sample at 20°C . For $1^{2+}2[\text{PF}_6^-]$ and $2^{2+}2[\text{PF}_6^-]$, the magnetic susceptibility measurements in the solid state confirmed that the symmetric dinuclear dicationic complexes present a singlet GS (see Table 5 below) [21,99]. The very small S/T gap found (-18.2 and -1.3 cm^{-1} , respectively) also suggests that the triplet excited state is populated at 20°C . The non-equivalent iron end-groups of each spin isomer are, however, expected to present a distinct Mössbauer signature. Curiously, the Mössbauer spectra recorded at 80 K for both dications exhibit a unique doublet (Table 3). Since the two spin isomers are in equilibrium at 80 K, this observation implies that the exchange between them in the solid state is faster than the Mössbauer time-scale (10^{-7} S).

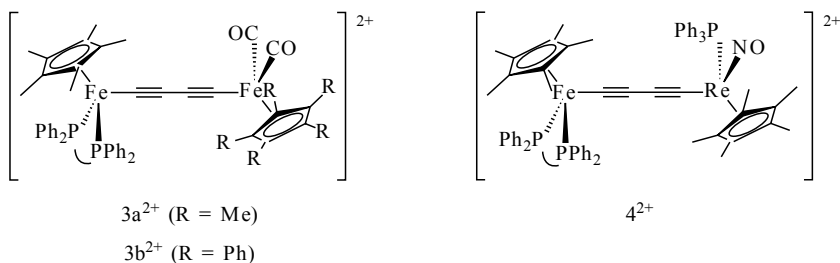


Table 3 ^{57}Fe Mössbauer parameters determined at 77 K for selected dinuclear complexes featuring two or three $[(\eta^2\text{-diphos})(\eta^5\text{-C}_5\text{Me}_5)\text{FeL}]^+$ ([Fe]) units

L/X	δ	QS ($\text{mm}\cdot\text{s}^{-1}$)	Ref.
1^{2+}	0.180	1.050	20
2^{2+}	0.191	1.047	23
4^{2+}	0.138	0.957	25
5^{2+}	0.48	0.83 ^a	100
	0.23	1.06 ^b	
6^{2+}	-0.31	1.93	101
7^{2+}	0.24	0.91	102
8^{2+}	0.28	0.89	103
10^{3+}	0.25	0.88	146

^a $S = 1$.

^b $S = 0$.

Table 4 ESR components of the anisotropic g -tensors for selected organoiron polyradicals at 80 K

X	$T(K)$	g_{iso}	g_1	g_2	g_3	Δg	Ref.
1^{2+}	77			Not ESR-active			20
2^{2+}	77			Not ESR-active			23
2^{3+}	77 ^a	—	2.0308	2.5527		—	23
4^{2+}	45 ^b	—	2.04	2.10	2.15	—	25
5^{2+}	74 ^c		Broad signal at $g = 2.10$ ($\Delta H_{pp} = 530$ G)				100
7^{2+}	77	—	1.9769	2.0356	2.1142	—	102
8^{2+}	77 ^d		Broad signal at $g = 2.10$ ($\Delta H_{pp} = 550$ G)				103
10^{2+}	77	2.139	1.978	2.030	2.409	0.431	146
10^{3+}	77 ^e		Broad signal at $g = 2.13$ ($\Delta H_{pp} = 330$ G)				103

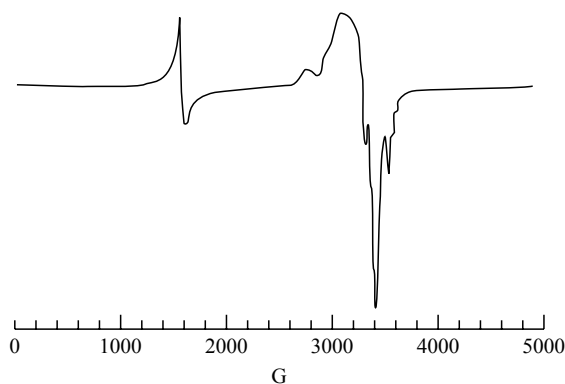
^a At 77 K in $CH_2Cl_2/C_2H_4Cl_2$ (1:1) glass.

^b Transition of $\Delta m_s = 2$ observed at 4.3046.

^c Transition of $\Delta m_s = 2$ observed at 4.31.

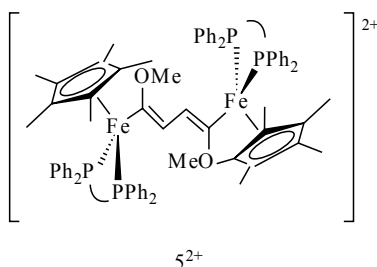
^d Transition of $\Delta m_s = 2$ observed at 4.55.

^e Transitions of $\Delta m_s = 2$ and 3 observed at 4.46 and 7.97, respectively.

**Figure 2** ESR spectrum recorded with a solid sample of $4^{2+}[2PF_6^-]$ at 45 K

We next investigated some non-symmetrical analogs. While the iron(III)/iron(III) dications $3a^{2+}[PF_6^-]$ and $3b^{2+}[PF_6^-]$ decomposed readily upon oxidation of the MV precursors, the blue Fe(III)/Re(II) dication $4^{2+}[PF_6^-]$ proved to be stable at 20°C and could be isolated. The NMR spectrum obtained for the dication $4^{2+}[PF_6^-]$ at 25°C indicates a much weaker paramagnetism than those observed for the complexes $1^{2+}[PF_6^-]$, and $2^{2+}[PF_6^-]$. An ESR spectrum could be obtained from a crude solid sample. This spectrum is quite complex, as expected for such an unsymmetrical diradical presenting two anisotropic metallic sites (Figure 2). It is worth noting that this spectrum is distinct from the spectrum obtained with the MV monocation $4^+[PF_6^-]$ and three different tensors can be extracted from the broad signal by simulation. The forbidden $\Delta m_s = 2$ transition at half-field can be observed in the spectrum and constitutes

the fingerprint of a triplet state (see Table 4). Qualitatively, the temperature-dependence of the spectrum intensity suggests that the observed triplet state is not the GS. The signal intensity increases with temperature, with an optimal spectrum being observed at 45 K. Upon further heating, the signal broadens and disappears, possibly because of an increasingly efficient spin–spin relaxation. Magnetic susceptibility measurements confirm that the GS is the singlet state and reveals a relatively larger S/T gap (175 cm^{-1}), in comparison with the symmetrical dications $1^{2+}2[\text{PF}_6^-]$ or $2^{2+}2[\text{PF}_6^-]$ (Table 5). Again, the Mössbauer spectra exhibit a unique doublet. Thus, in spite of the increased S/T gap, the exchange between the two spin isomers of $4^{2+}2[\text{PF}_6^-]$ remains faster than ca. 10^{-7} s.



With the diradical $5^{2+}2[\text{PF}_6^-]$, having a 1,4-dimethoxy-butadiene-1,4-diyl bridge, the presence of paramagnetism in the sample is suggested by the low resolution of the ^{31}P NMR signal, which appears forty times as broad as the PF_6^- peak [100]. The ESR spectrum at 77 K in a $\text{CH}_2\text{Cl}_2/\text{C}_2\text{H}_4\text{Cl}_2$ glass displays an unresolved signal with a peak-to-peak difference of 530 G at $g = 2.10$, typical for low-spin Fe(III) complexes (Table 4). Again, the broadening of the ESR signal is believed to result from the increased relaxation induced by the spin–spin interactions in this diradical. A weak peak, possibly corresponding to the forbidden $\Delta m_s = 2$ transition, can be detected as well at

Table 5 Exchange coupling parameters (cm^{-1}) derived by fitting the temperature-dependence of the magnetic susceptibility with equation (9b)

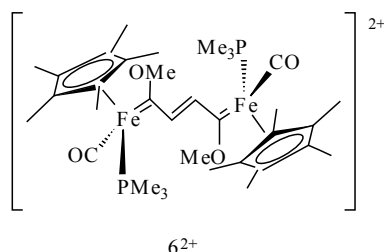
X	$\Delta E_{\text{ST}} = 2J$	g	ρ	Ref.
1^{2+}	-18.2	2.10	0.12	21
2^{2+}	-1.33	2.11	0.018	99
4^{2+a}	-175	2.08	0.04	25
5^{2+}	-27.4	2.10	0.12	100
7^{2+}	-1.0	2.1753	0.16	21
	< -300			
8^{2+}	94.0	2.10	0.0	103
10^{3+b}	18.7–28.8 ^c	2.13	0.0	103

^a Solving equation (9b) gives two sets of parameters.

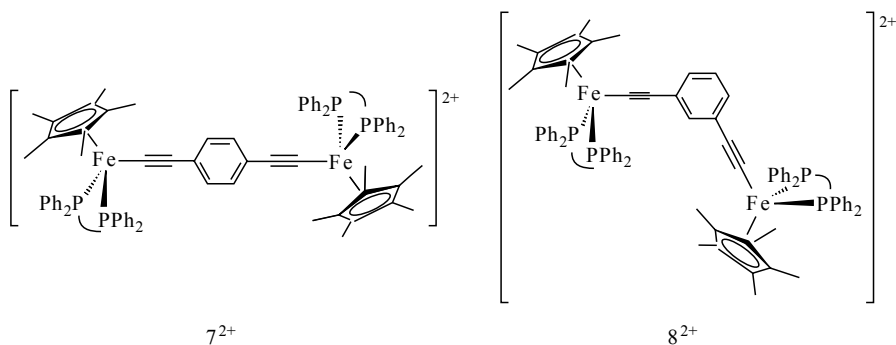
^b Equation (11) was used to fit the temperature-dependence of the magnetic susceptibility.

^c ΔE_{DO} instead of ΔE_{ST} .

$g = 4.31$. Accordingly, with solid-state susceptibility measurements, the intensity of the main signal decreases with the temperature, without variation of g or change in the line broadening. The magnetic susceptibility of $5^{2+}2[\text{PF}_6^-]$ is characteristic of a singlet GS and can be fitted with the Bleaney-Bowers relationship (equation (9b)). An exchange coupling parameter (J) of -27.4 cm^{-1} is extracted (Table 5). In this case, Mössbauer spectroscopy allows the simultaneous observation of two doublets. Their spectroscopic signatures (QS) remain clearly distinct between 4.5 and 293 K (Table 3). The relative amounts of these isomers change reversibly with temperature (Figure 3), suggesting a thermal equilibrium between both species. The ratio of both isomers computed from the Mössbauer spectra, using Boltzmann's law, agree within 10% with the ratio obtained from the magnetic susceptibility measurement. Thus, each doublet corresponds to a distinct spin isomer. Since no averaged doublet is observed, both isomers interconvert more slowly than the time-scale of this spectroscopy. Coalescence is not approached, meaning that the exchange lifetime must be far below 10^{-6} s .



It is noteworthy that the related dinuclear complex $6^{2+}2[\text{PF}_6^-]$ proves to be ESR-inactive at all temperatures and appears as a diamagnetic bis-carbene in the ^1H NMR at 293 K [101].



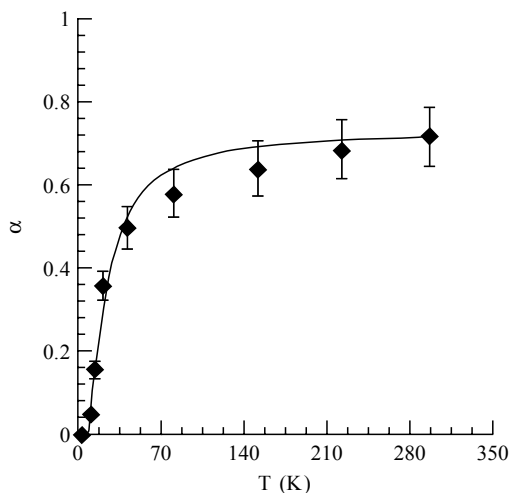


Figure 3 Temperature-dependence of the molar fraction (◆) of the HS isomer of 5^{2+} as determined from the experimental relative absorption areas of the Mössbauer quadrupole doublets. The solid line is the curve calculated for an S/T gap of -27.4 cm^{-1}

Dications incorporating a *para*- or *meta*-substituted aryl group in the bridge, such as 7^{2+} or 8^{2+} , were also examined. With $7^{2+}2[\text{PF}_6^-]$, a weak ESR signal could be recorded at 77 K in a solvent glass (see Table 4). This signal strongly resembles the one obtained for a mononuclear cation but appears much weaker and exhibits three slightly distinct *g*-tensors. Magnetic susceptibility measurements reveal that $7^{2+}2[\text{PF}_6^-]$ has a singlet GS with a value of $1.23 \mu_B$ for its magnetic moment in the solid state [102]. A very small S/T gap of -1.0 cm^{-1} ($= 2J$) can be extracted by simulation (Table 5) [21,103].¹⁸ While the triplet excited state is possibly populated at all temperatures with such a small S/T gap, attempts to fit the experimental data by the Curie–Weiss law proved less accurate than by using a modified Bleaney–Bowers law (equation (8b)) [21]. A single Mössbauer doublet is observed at 77 K for this compound (see Table 3). This value must also be an average between the values of the rapidly interconverting singlet and triplet spin isomers of 7^{2+} .

For the *meta*-substituted analog $8^{2+}2[\text{PF}_6^-]$, the NMR spectrum reveals significant paramagnetism at various temperatures [103]. An intense ESR signal at $g = 2.10$ (Table 4) is also observed at 80 K. The signal is much broader than that usually observed for iron(III) monoradicals ($\Delta H_{pp} = 550 \text{ G}$). Moreover, a second weak transition is observed at half-field ($g = 4.55$), which may

¹⁸ Good fits could also be achieved with this law by using *J* values at around -180 cm^{-1} . Only the smaller value was retained on the basis of the current literature data available.

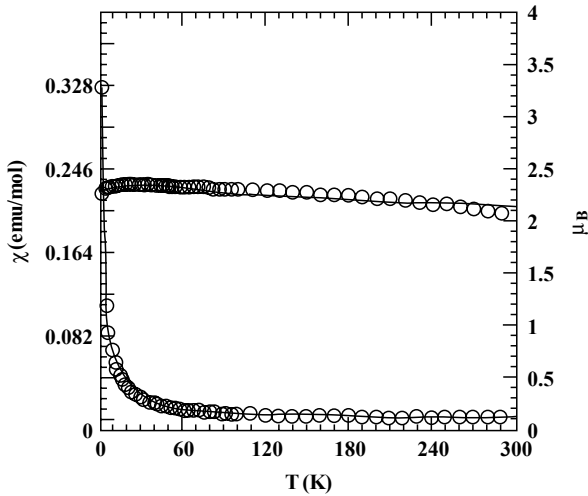
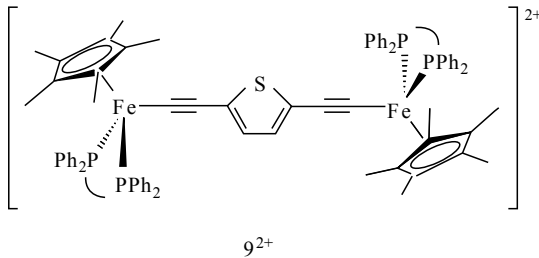


Figure 4 Temperature-dependence of the corrected molar magnetic susceptibility for $8^{2+}[\text{PF}_6^-]_2$. The solid line represents the best fit

constitute the signature of a triplet state ($\Delta m_s = 2$).¹⁹ Magnetic susceptibility measurements provide evidence for a triplet GS (Figure 4), with a T/S gap of ca. 65 cm^{-1} (Table 5). A single doublet is observed in the Mössbauer spectra at 80 K.



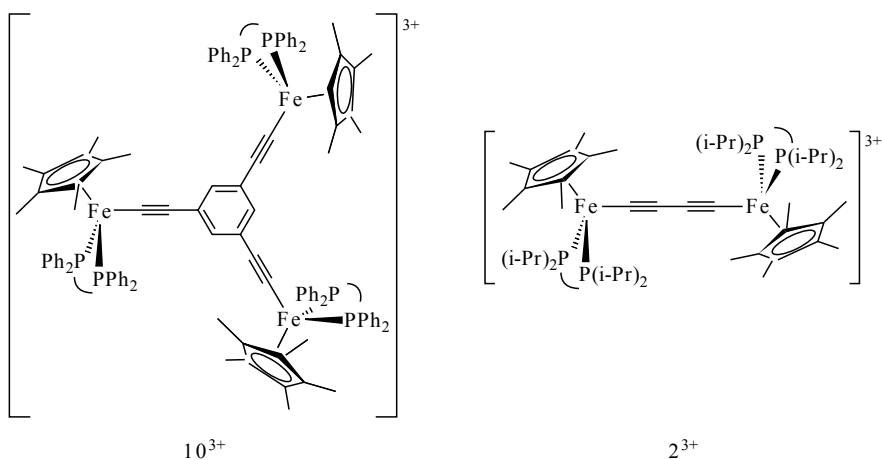
When the phenylene unit is replaced by a 2,5-thienyl unit, as in the dication $9^{2+}2[\text{PF}_6^-]$, the NMR ^{31}P signal, ten times broader than usual, suggests again the presence of paramagnetic species in pure samples of 9^{2+} [104]. This paramagnetic character remains nevertheless weak at 20°C since the signals on the corresponding ^1H NMR spectrum are not shifted very much. The ESR spectrum of the dication obtained at 4 K in the usual solvent glass also displays

¹⁹ The NMR study revealed that the main origin of the paramagnetic shift arises from the contact shift. Accordingly, no dipolar interaction could be evidenced from the analysis of the ESR spectra of this species.

broad signals (Table 4). Two components of the anisotropic g -tensor are observed, suggesting a cylindrical symmetry with $g_{11} = g_1 = g_2 = 2.012$, and $g_{\perp} = g_3 = 2.030$ ($g_{\text{iso}} = 2.018$). A half-field transition, characteristic for the triplet state, is also present at $g = 4.292$. A 'D' value of 51 G can be extracted for the dipolar interaction by simulation. The temperature-dependence of the magnetic susceptibility indicate a singlet GS. The isotropic exchange coupling parameter extracted after fitting the measured values with a Bleaney–Bowers-type law is unfortunately not unique (equation (9b)); the fit converges for $J = -74 \pm 10$ or $J = -89 \pm 10$ (Table 5). Eventhough there is some uncertainty on the value of J , this measurement nevertheless evidences a singlet GS and a much larger S/T splitting than with 7^{2+} . Mössbauer spectroscopy reveals a unique doublet, in accordance with a spin-transition process faster than 10^{-6} s.

3.2.3 Magnetic Interactions in Polynuclear Triradicals

The stable organometallic triradicals $2^{3+}3[\text{PF}_6^-]$ and $10^{3+}3[\text{PF}_6^-]$ could be isolated either by complete oxidation of all iron(II) end-groups present in a trinuclear neutral iron(II) precursor such as **10**, or after additional oxidation of the dinuclear dicationic complex $2^{2+}2[\text{PF}_6^-]$ mentioned above. Trications 1^{3+} and 4^{3+} were also observed by electrochemistry, but proved rather unstable for isolation. The trication 2^{3+} , with the more electron-rich $[(\eta^2\text{-dippe})(\eta^5\text{-C}_5\text{Me}_5)\text{Fe}]$ fragment (dippe = 1,2-di(*iso*-propyl)phosphino ethane), is more stable, and could be isolated and characterized (by X-ray diffraction [23]).



The ^1H NMR behavior of the trinuclear complex $10^{3+}3[\text{PF}_6^-]$ resembles that of the *meta*-substituted dication $8^{2+}2[\text{PF}_6^-]$. A variable-temperature study

reveals that the paramagnetic shift of the signals is mainly due to contact shifts. Clearly, the dipolar coupling in such diradicals must be quite weak. An ESR signal at $g_{\text{iso}} = 2.13$ is also observed at 80 K in a $\text{CH}_2\text{Cl}_2\text{-C}_2\text{H}_4\text{Cl}_2$ solvent glass (Table 4). This signal is much broader than signals usually obtained with iron(III) monoradicals ($\Delta H_{\text{pp}} = 330$ G), but becomes slightly sharper and more intense at 4 K. It is noteworthy that the forbidden transitions ($\Delta m_S = 2$ and 3) at half- and third-field, which constitutes the fingerprint of a quartet state, were identified in the spectra as weak signals located at $g = 4.46$ and 7.97, respectively. In the 90–160 K range, the plot of the intensity of the ESR signal versus $1/T$ deviates upward from a linear relationship. The magnetic susceptibility evolution of $10^{3+3}[\text{PF}_6^-]$ with temperature could be fitted by equation (11), derived from the HDvV Hamiltonian given in equation (10). This corresponds to an isosceles triangular three-spin model triradical (Scheme 11B). The isotropic exchange couplings J and J' are derived by fitting the experimental molar magnetic susceptibility curve against the temperature. The g -value derived from the ESR spectra was used in the fit. Thus, the GS is apparently a quartet state and the value of the isotropic constants extracted are 9.6 cm^{-1} for J and 4.4 cm^{-1} for J' (Table 5), with the two doublet states lying 18.7 ± 0.5 and $28.8 \pm 0.5 \text{ cm}^{-1}$ above, respectively (Figure 5). Similarly to 8^{2+} , the Mössbauer spectra show only a single doublet at 80 K.

The paramagnetic behavior of the linear triradical $2^{3+3}[\text{PF}_6^-]$ is evidenced by Evans measurements. The magnetic moment found at 25°C (equation (7)) corresponds to ca. 2 unpaired electrons, based on the spin only-value [48]. As briefly discussed (above see Section 2.5.1), the evaluation of the global

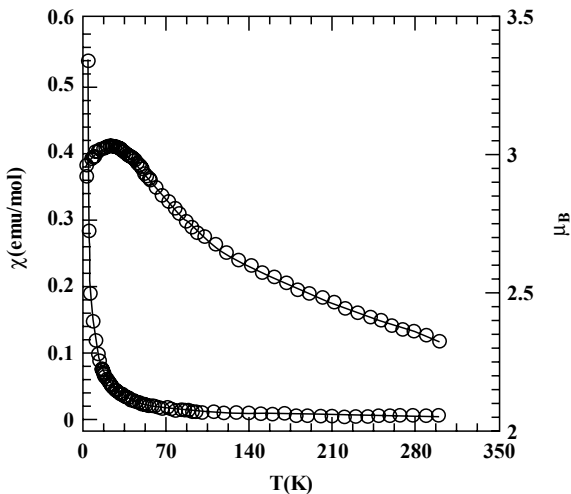


Figure 5 Temperature-dependence of the corrected molar magnetic susceptibility for $10^{3+3}[\text{PF}_6^-]$. The solid line represents the best fit

molecular spin value S using the Evans method might be very approximate for electrons coupled intramolecularly (case (iii)). This approach, nevertheless, indicates that a paramagnetic isomer is present in pure samples of the 2^{3+} compound at 25 °C. The ESR spectrum of a solid sample of $2^{3+}3[\text{PF}_6^-]$ is typical for a fast relaxing paramagnetic species and no signal is obtained at higher temperatures, possibly because of electron–electron interactions. At 4 K, two anisotropic g -components are observed at $g_1 = 2.0308$ and $g_2 = 2.5527$. These are very different from the signal given by the MV complex $2^+[\text{PF}_6^-]$. The large anisotropy detected suggests a strong iron character for the MO containing the flipping electron [99]. Further information on the spin state of the sample is given by the temperature-dependence of the magnetic susceptibility of this species. The latter can be fitted by using the Hamiltonian previously used (equations (10) and (11)), considering $\alpha = 0$ (i.e. the coupling between the extreme spin carriers being negligible)²⁰. A negative value of J is found (-77.2 cm^{-1}), suggesting that a doubly degenerate doublet state constitutes the GS (Table 5). The latter is separated from the excited quartet state by a gap ($= 3J$) of -277.2 cm^{-1} . This also suggests that the observed ESR signal corresponds to the doublet GS isomer ($\Delta m_s = 1$).

3.3 INTRAMOLECULAR MAGNETIC EXCHANGE BETWEEN METAL-CENTERED SPINS IN THE ORGANOIRON POLYNUCLEAR DIRADICALS

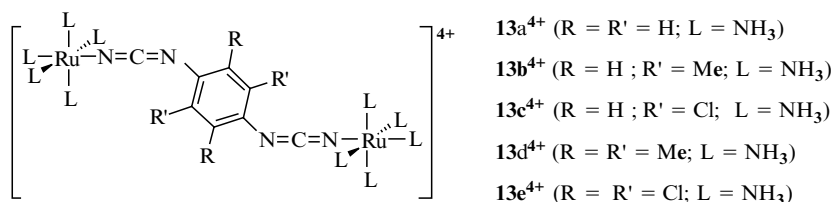
The preceding results demonstrate that for organometallic $[(\eta^2\text{-diphos})(\eta^5\text{-C}_5\text{Me}_5)\text{Fe}]^+$ -based polynuclear, metal-centered polyradicals several spin isomers exist and equilibrate in the 0–293 K range. The energy gaps between the spin isomers were determined by solid-state magnetic measurements. The gaps are sufficiently small for populating the different spin states at 293 K. Remarkably, 8^{2+} and the triradical 10^{3+} exhibit ferromagnetic coupling and constitute the first true organometallic polyradicals where such coupling is evidenced. In all other diradicals, antiferromagnetic coupling between the metal-centered spins takes place. Notably, most experimental antiferromagnetic exchange coupling found deviate from the empirical equation proposed by Coffman and Buettner in 1979 (equation (12)) where $R_{\text{MM}'}$ is the metal–metal distance expressed in angstroms [105]²¹. These $R_{\text{MM}'}$ distances, for species 1^{2+} – 10^{3+} , were derived from solid-state structures or from molecular modelling. Values for 2^{2+} and 7^{2+} appear too low, whereas the values for 4^{2+} and 9^{2+} are much too large.

$$J_{\text{F}} (\text{cm}^{-1}) \leq J_{\text{AF}} (\text{cm}^{-1}) = 1.35 \times 10^7 \exp(-1.80R_{\text{MM}'}) \quad (12)$$

²⁰ The better fit with such an Hamiltonian and not a ‘Bleaney–Bowers’-derived one suggests that we have indeed a tritopic rather than a ditopic triradical here.

²¹ Given the paucity of the experimental data available for such an empiric function could not be proposed ferromagnetic coupling by Coffman and Buettner [105].

Larger values are not unprecedented. For instance, Crutchley and co-workers [106–108] have reported very large deviations from equation (12) for inorganic diradicals featuring metal-centered spins antiferromagnetically coupled like $13a^{4+}-13e^{4+}$. Such deviations were proposed to arise from the fact that the main contribution to superexchange was mediated through π -orbitals, while equation (12) was originally derived for diradicals with interactions through σ -bonds [29,45,106,108].



Regarding the organoiron(III) diradicals, the distribution of J -values does not enable us to draw any firm trend. We nevertheless notice that, depending mostly on the structure of the carbon-rich spacer or of the nature of the end-groups, large differences can be stated between experimental values derived for J at comparable metal–metal distances. Their evolution, for negative values (antiferromagnetic superexchange couplings), parallels roughly the corresponding electronic coupling parameters (V_{ab}), defined for the electron transfer in the corresponding MV complexes (Table 2). Similar observations have also been reported for $13a^{3+}-13e^{3+}/13a^{4+}-13e^{4+}$ [106–108], and were rationalized considering detailed expressions of the isotropic exchange coupling [45,106].²² Since no structural dependence of the isotropic exchange coupling at a fixed metal–metal distance is considered in the empirical relationship (equation (12)) proposed by Coffman and Buettner, following Crutchley, we believe that the latter cannot be a general one as such.²³

4 STRUCTURAL IMPLICATIONS OF THE MAGNETIC EXCHANGE IN POLYTOPIC ORGANOMETALLIC POLYRADICALS FEATURING CARBON-RICH BRIDGES

We have shown that spin equilibrium takes place at 20 °C for various dicationic organoiron complexes (see Section 3 above). Considering the symmetry and the

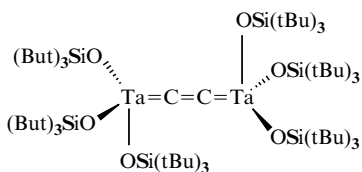
²² Provided that the following conditions are verified: (i) the magnetic orbitals (SOMOs in triplet states) are separated in energy from the other filled and vacant MOs; (ii) the geometry and conformation of the MV complex and dication are similar; (iii) J is dominated by the antiferromagnetic contribution, itself primarily determined by the electron-transfer event.

²³ A more general formulation would result if $R_{MM'}$ becomes the effective spin–spin distance, rather than the metal–metal distance. Such an effective spin–spin distance will evidently depend on structural parameters and many of the reported deviations to equation (12) could then be rationalized by considering that the metal–metal distance is a poor approximation for this distance.

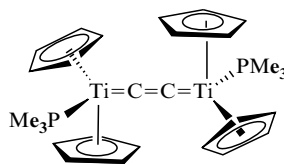
ligand field of the capping metal fragments, many other related d^n-d^n complexes bridged by carbon-rich ligands could similarly be envisaged as metal-centered ditopic diradicals. Two spin states, corresponding to the triplet (T) and singlet (S) states, are then possible, in principle, for their GS. Given the well-known structural flexibility of carbon-rich bridges, the structures of these spin isomers might present noticeable differences (see Section 2.4 above). In the following, we will now analyse the *structural* implications of the magnetic exchange interaction in such polytopic organometallic polyradicals bridged by carbon-rich spacers and discuss these features in a general way, depending on the bridging ligand.

4.1 ALL CARBON(C_{2n})-BRIDGED ORGANOMETALLIC METAL-CENTERED DIRADICALS

4.1.1 Structure of the Spin Isomers in C_{2n} -Bridged Organometallic Diradicals



14



15

If we exclude the mostly synthetic report on the paramagnetic ditopic polyradical $[(\text{Mes}_3\text{V})\text{C}_2(\text{VMes}_3)]^{2-} \cdot 2[\text{Li}(\text{THF})_4]^+$ [109], for which spectroscopic data were hardly provided, the earliest study concerned with all-carbon bridged metal-centered diradicals was possibly the work of Wolcanczki and co-workers on the d^1-d^1 C_2 -bridged complex **14**, in 1986. This paramagnetic tantalum(IV) diradical was structurally characterized in the solid state [110]. However, **14** appears as a paramagnetic substance ($\mu = 3\mu_B$), with magnetic susceptibility measurements revealing a singlet GS with a large antiferromagnetic through-bridge exchange coupling (J) estimated to be larger than 500 cm^{-1} [81].²⁴ Very similar results were obtained a few years later with the related diamagnetic titanium(III) diradical **15**, also structurally characterized in the solid state, by Binger and co-workers [111]. In this case, despite its ‘diradical’ nature, the compound is fully diamagnetic due to the large antiferromagnetic coupling between the two unpaired electrons through the C_2 chain. The S/T gap was

²⁴ The detected paramagnetism is apparently caused by temperature-independent paramagnetism (TIP).

Table 6 Crystallographic reference data for selected $[M]C_{2n}[M]$ compounds

Compound	M	<i>n</i>	M–C _α	C _α –C _β	C _β –C _β	Twist angle ^a	<i>R</i> indices	Ref.
14 ²⁺ 2PF ₆ [−]	Ta(IV)	1	1.96(4)	1.32(4)	—	180.0 ^b	0.107	110
15 ²⁺ 2PF ₆ [−]	Ti(III)	1	2.051(2)	1.25(3)	—	180.0	0.027	111
16 ^{2−} [Li ⁺ (THF) ₄]	Ti(III)	1	2.056(11) 2.051(2)	1.30(1)	—	1.0(2)	0.092	112
17 ²⁺ 2PF ₆ [−]	Re(II)	2	1.909(7) 1.916(7)	1.263(10) 1.260(10)	1.305(10)	23.0 ^c	0.038	95
18a ²⁺ 2PF ₆ [−]	Ru(III)	2	1.858(4) 1.856(5)	1.280(6) 1.269(7)	1.294(7)	39.7	0.057	114
19	Mn(II)	2	1.798(15)	1.263(17)	1.33(3)	90.0 ^d	0.066	46
19 ²⁺ 2BPh ₄ [−]	Mn(III)	2	1.768(4) 1.770(4)	1.289(5) 1.298(5)	1.295(5)	90.0 ^d	0.044	46

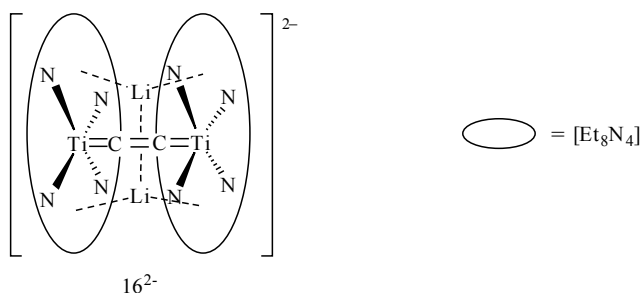
^a (δ)C₅Me₅(centroid)–M(1)–M(2)–C₅Me₅(centroid), or (ψ)L–M(1)–M(2)–L.

^b L = OSi(*t*-Bu)₃.

^c L = NO.

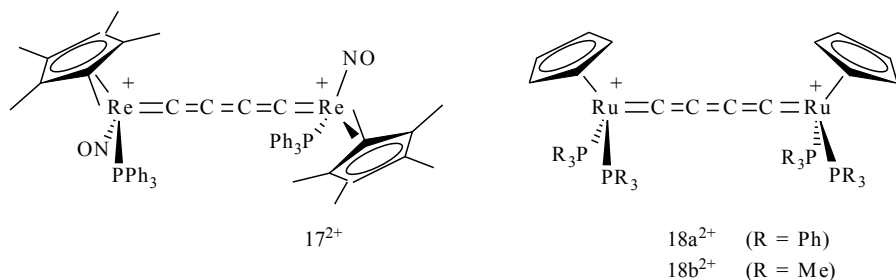
^d L = P_{dppp}.

not estimated here. For the complexes **14** and **15**, the M–C and C–C bond lengths are in accordance with a ‘cumulene-like’ structure (Table 6). In the case of **14**, infrared data ($\nu(\text{Ta}=\text{C})$ at 709 cm^{−1} and $\nu(\text{C}=\text{C})$ at 1617 cm^{−1}) and in the case of **15**, the ¹³C NMR shifts of the bridging carbon atoms ($\delta(\text{C}_\alpha)$ at 258.1 ppm) were also in favor of such a structure.



The paramagnetic titanium(III) diradical **16**^{2−} 2[Li(THF)₄] also presents a cumulene-like bridge, as evidenced by X-ray characterization (Et₈N₄ = *meso*-octaethylporphyrinogen) [112]. In this case, the nature of the GS was not determined, but a magnetic moment of 1.8 μ_B per titanium center at 290 K was reported.

More recently, **1**²⁺, **2**²⁺, and **4**²⁺, plus other stable d⁵–d⁵ metal-centered dications such as **17**²⁺2[PF₆[−]] and **18a**, **b**²⁺2[PF₆[−]] were studied. Similarly to



1^{2+} , 2^{2+} and 4^{2+} , these were obtained by 2-electron oxidation of the corresponding butadiyne-diyl-bridged d^6-d^6 neutral low-spin rhenium(i) (**17**) [95], or ruthenium(ii) complexes (**18a,b**).²⁵ The dications 17^{2+} and **18a,b**²⁺ are diamagnetic at 20 °C and give sharp and unshifted NMR spectra [95].²⁵ Their cumulene-like structure in the solid state is unambiguously evidenced by X-ray data²⁵ available for $17^{2+}2[PF_6^-]$ and $18a^{2+}2[PF_6^-]$ [95,114]. The internal C–C bond lengths are very close to sp^2-sp^2 carbon-carbon double bonds (Table 6) (see p. 61 in Reference [60]). NMR and vibrational spectroscopic data for the bridging carbon atoms are also in favor of such a structure. A typical cumulene stretching was identified, respectively, at 1883 cm^{-1} in the Raman for $17^{2+}2[PF_6^-]$ and at 1767 cm^{-1} in the infrared for **18a,b**²⁺ $2[PF_6^-]$. Thus, when considered as ‘diradicals’, the isolated stable diamagnetic samples indicate a singlet GS for $17^{2+}2[PF_6^-]$ and **18a,b**²⁺ $2[PF_6^-]$ [24,95]. The triplet state is apparently not populated under these conditions, thus suggesting a large intramolecular antiferromagnetic interaction ($J > 500\text{ cm}^{-1}$) between the unpaired spins on the terminal metal atoms. In agreement with such a hypothesis, no ESR spectra could be obtained for 17^{2+} [95].

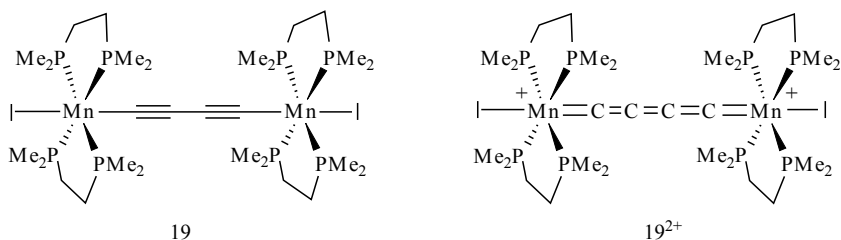
As discussed above (Section 3.2), the symmetric dications 1^{2+} and 2^{2+} , as well as the mixed rhenium(ii)/iron(iii) non-symmetric dication 4^{2+} also present a singlet GS. No typical cumulene absorptions were detected in the infrared for the symmetric dication $1^{2+}2[PF_6^-]$, but an absorption possibly corresponding to such a mode could be located at 1710 cm^{-1} for $2^{2+}2[PF_6^-]$,²⁶ and at 1783 cm^{-1} for $4^{2+}[PF_6^-]_2$ [25]. In this case, however, because of the much smaller S/T gap, both spin isomers are in equilibrium above 20 K. Thus, at 80 K, the observed ⁵⁷Fe Mössbauer *QS* is always larger²⁷ than expected for purely butadiynyl

²⁵ Recently, the significance of crystallographic bond lengths as bond order indicators for metalla-polyyenes has been independently discussed by ourselves, and Gladysz and co-workers [80,113].

²⁶ In symmetric complexes, depending on the pseudo-symmetry around the all-carbon bridging ligand, its stretching mode(s) may selectively show up in Raman spectra, as verified for $17^{2+}[PF_6^-]_2$ [95]. Raman spectra of 1^{2+} and 2^{2+} remain to be recorded.

²⁷ It is noteworthy that no mononuclear and cationic organoiron iron(iii) compound featuring a cumulene ligand is currently available as a model complex for Mössbauer spectroscopy. In this respect, the value obtained at 4 K for $4^{2+}2[PF_6^-]$ (singlet spin isomer) might be closest to the ideal value, because of the large S/T gap for this complex [25].

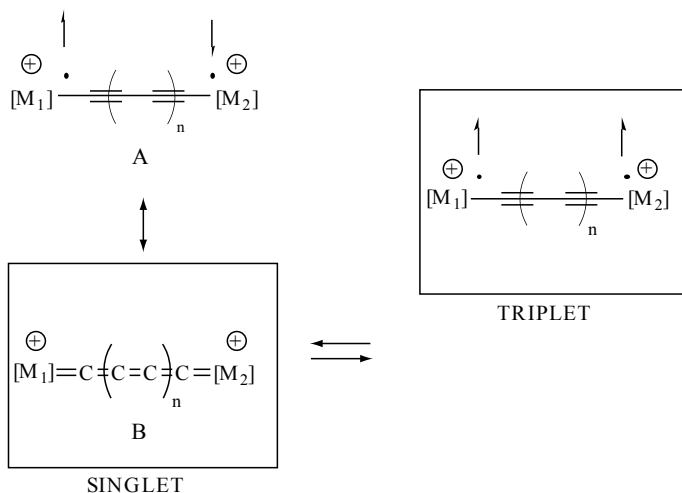
iron(III) end-groups [77]. In fact, the QS increases upon lowering the temperature and translates the change in population of each spin isomer. In agreement with an iron(II) cationic cumulene structure, the QS associated with the structure of the singlet spin isomer (GS) is larger than that of the excited triplet isomer [77]. The triplet spin isomer is believed to present a structure closer to a butadiyne-diyl bridge. Absorptions typical for such a spacer can be detected at 25 °C by infrared spectroscopy, in Nujol suspensions (2160 cm^{-1} and 1950 cm^{-1} for $\mathbf{1}^{2+}2[\text{PF}_6^-]$; 1941 cm^{-1} and cm^{-1} and 1848 cm^{-1} for $\mathbf{4}^{2+}2[\text{PF}_6^-]$) [20].



Recently, the isoelectronic d^5-d^5 neutral manganese(II) diradical **19** and its d^4-d^4 dioxidized congener $\mathbf{19}^{2+}$, were reported by Berke and co-workers [46]. The diradical **19** displays a butadiyne-diyl bridge structure in the GS, whereas a cumulene structure is present in $\mathbf{19}^{2+}$, as clearly evidenced by X-ray studies (Table 6). A typical alkynyl stretching mode is detected at 2127 cm^{-1} for **19**, while a characteristic cumulene absorption shows up at 1607 cm^{-1} for the corresponding dication $\mathbf{19}^{2+}2[\text{BPh}_4^-]$. Magnetic susceptibility measurements suggest a triplet spin isomer for the GS of **19**. In this case, ferromagnetic coupling between the two unpaired electrons located on the low-spin manganese(II) capping groups appears to take place. Accordingly, samples of the complex are paramagnetic. Unfortunately, the magnitude of the S/T gap could not be derived from the magnetic susceptibility measurements, due to the presence of impurities.²⁸ In contrast, the dication $\mathbf{19}^{2+}$ is a fully diamagnetic compound which presents a closed-shell structure resulting from antiferromagnetic coupling between the metal-centered electrons.

The present data suggest that different bridge structures are associated with each spin isomer for these all-carbon-bridged metal-centered diradicals. In each case, compounds characterized in the singlet state appear as closed-shell compounds, with a strong cumulene-like character, whereas the triplet-state isomers have apparently an open-shell structure featuring a polyynes-diyl bridge (see Scheme 13). Similarly to *para*-quinone diradicals (see Scheme 8 above), the actual structure of the singlet isomer can formally be considered to result from

²⁸ In this respect, the infrared absorption reported at 1805 cm^{-1} for the alkynyl bridge could also correspond to the stretching motion of the (cumulene?) bridge of the excited singlet isomer, if the gap is sufficiently small for the later to be populated at 25 °C.



Scheme 13

resonance between the singlet open-shell butadiyne-diyl Lewis structure (A) and the closed shell cumulene-like Lewis structure (B), with the latter structure providing the dominant weight in the VB description. Such a resonance translates the eventual stabilization resulting when the unpaired electrons form an additional bond in the bridging ligand [115]. For the triplet isomer, such resonance is precluded by spin restrictions.

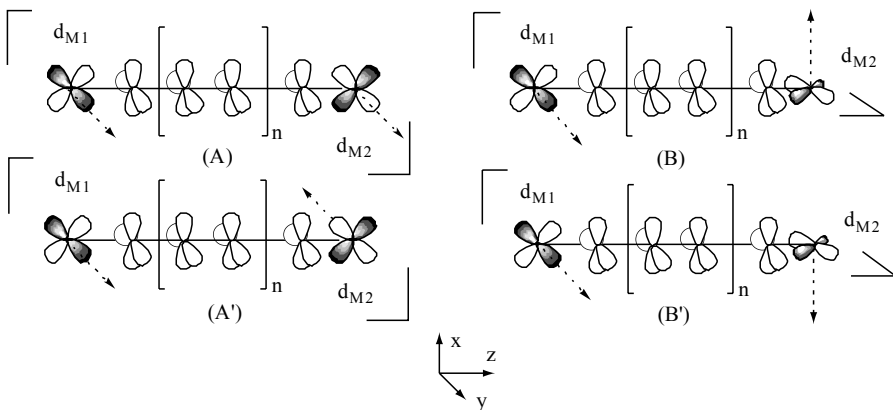
4.1.2 Bonding and Superexchange in C_{2n} -Bridged Organometallic Diradicals

For most of these C_n -bridged organometallic diradicals, the GS is the singlet state and results from the antiferromagnetic coupling of the metal-centered spins. This statement is in opposition to Hund's principle, which would predict a high-spin GS (see Section 2.1.3 above),²⁹ as observed for species **19**. A better understanding can be gained by looking at the orbitals bearing the unpaired electrons on each metal fragment, and the way that these interact with bridge-based frontier orbitals in symmetric compounds.

Let us consider a given capping complex with one unpaired electron located in a *non-degenerate* d_{yz} - or d_{xz} -metal-centered orbital.³⁰ In dinuclear complexes, the metal-based SOMOs will interact mostly with π or π^* ligand-based frontier MOs. Two limiting cases can be delineated depending on the conformations adopted by the all-carbon-bridged diradicals (Scheme 14).

²⁹ Hund's principle was often demonstrated to fail with certain molecules. Its applicability to related organic ditopic cumulene-based diradicals have recently been discussed [116].

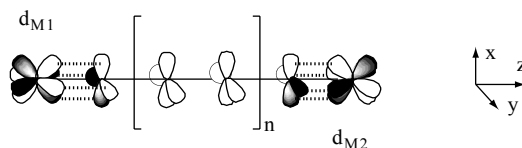
³⁰ Other d metal-based orbitals do not present large interactions with the π manifold of the bridging ligand.



Scheme 14

- (i) In conformations (A) or (A'), corresponding to $\delta = 0$ or 180° (Scheme 14), the singly occupied metal orbitals will overlap with common π or π^* bridge-based orbitals. Considering now the $2(d^1) + 2n(p)$ manifold on the $MC_{2n}M$ core as a linear $(2n + 2)$ -centered pseudo-alternant hydrocarbon (isolobal analogy), Ovchinnikov's rule predicts a singlet GS. The spins should therefore be antiferromagnetically coupled, if a non-negligible interaction takes place.
- (ii) In conformations (B) or (B'), corresponding to $\delta \pm 90^\circ$, the singly occupied metal-based orbital overlaps with perpendicular sets of bridge-based π or π^* orbitals. In such a situation, even if a strong interaction between the metal fragments and the bridge takes place, the single electrons belong to two perpendicular (orthogonal MOs) ' MC_{2n} ' π -manifolds, each with an $S = 1/2$ spin. Depending on the spatial extension of these two new MOs (different electron correlation energies), a triplet or a singlet GS can result and Hund's principle might be verified. Based on Borden's criterion, the triplet GS will be favored by co-extensive (non-disjoint) SOMOs.

Now, if the terminal fragment presents a higher local symmetry and the unpaired electron(s) is/are located in a set of *degenerate* d_{xz} or d_{yz} metal-based orbitals, a different situation results in principle. For each capping fragment, these degenerate orbitals overlap equally with both sets of perpendicular-bridge-based π^* -orbitals, *regardless* of the conformations (A)–(B') considered (Scheme 15). In this case, the triplet configuration, where d_{xz} and d_{yz} metal-based SOMOs formally interact with perpendicular and degenerate π^* bridge-based orbitals, and the singlet configuration, where symmetric (d_{xz} or d_{yz}) metal-based SOMOs overlap with a common π^* bridge-based orbital, have very close energies. In analogy with what happens above with different conformations,



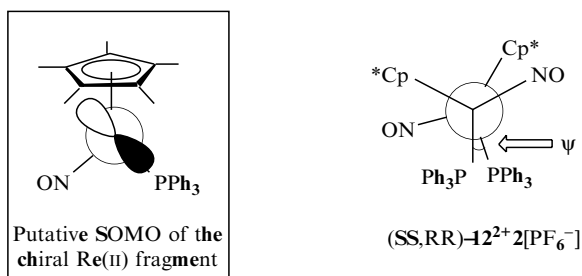
Scheme 15

the triplet configuration is characterized by two perpendicular ‘M–C_{2n}’ SOMOs, whereas the singlet configuration presents one unique and filled ‘M–C_{2n}–M’ HOMO with two paired electrons. Again, depending on the electron correlation energies, one or the other can constitute the GS. Owing to Borden’s criterion, a triplet GS should be favored for non-disjoint SOMOs.

Returning to the examples given in the previous sections, we will now try to analyse the situation in the different cases. In diradicals featuring low-spin d⁵ piano-stool end-groups such as **1**²⁺, **2**²⁺, **4**²⁺, **17**²⁺ or **18a**, **b**²⁺, the unpaired electrons are located in non-degenerate fragment-based orbitals with strong d_{yz} character (for instance, 1a'' in Scheme 12). As indicated by DFT calculations, all of these diradicals should be slightly more stable in conformations (A) or (A') and should therefore exhibit antiferromagnetic superexchange between spins [24,95,117,118]. Moreover, because of the low pseudo-symmetry of piano-stool end groups (C_{2v}), the strict orthogonality between magnetic orbitals can never be realized, even in conformations (B) or (B'). This also disfavors ferromagnetic interactions between spins. In agreement with these calculations, the X-ray data reveal a conformation reasonably close to (A) ($\delta = 39.7^\circ$) for **18a**²⁺2[PF₆⁻] in the solid state [114]. With **17**²⁺2[PF₆⁻], featuring chiral [(Ph₃P)(NO)(η⁵-C₅Me₅)Re]⁺ units with lower pseudo-symmetry (C_s), the bonding interaction between singly occupied metal-based fragment orbitals is also maximized in the solid state. In both cases, the slight differences from the ideal angles are possibly due to packing forces in the solid state. It is noteworthy that with species **17**²⁺ the observed conformation is different from (A) or (A'), since the [(Ph₃P)(NO)(η⁵-C₅Me₅)Re]⁺ fragment of symmetry presents a SOMO differently oriented in space (Scheme 16) [95,119].³¹

The cumulene-like structure in the singlet states for these d⁵–d⁵ complexes originates from the dominant occupancy of MOs with M–C bonding and (CC)_n antibonding character. This compensates for the (CC)_n bonding interaction of lower-lying MOs. As a result, the bond order decreases in the bridge and increases in the M–C bonds. The bond order of the excited triplet isomer will

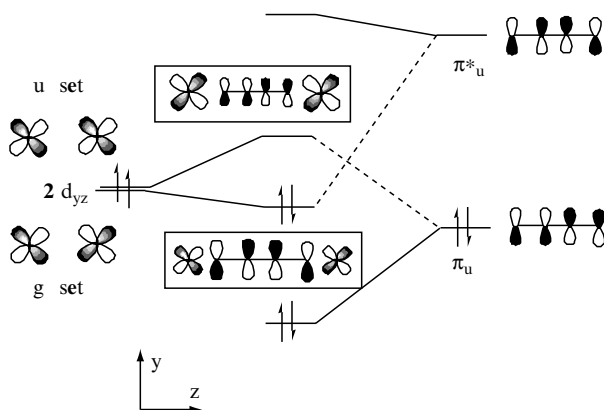
³¹ The HOMO in the [(Ph₃P)(NO)(η⁵-C₅Me₅)Re]⁺ 16e-fragment is a local d_{yz} or d_{yz} oriented along the Re–P axis. Accordingly, the SOMO in the [(Ph₃P)(NO)(η⁵-C₅Me₅)Re]⁺ fragment should have the same orientation. The corresponding dihedral angle Ψ , defined as the P₁–M₁–M₂–P₂ angle, is reported to be 23° in (SS, RR)–**17**²⁺2[PF₆⁻] [95].



Scheme 16

depend on the bonding characteristics of the corresponding SOMOs. In this respect, for symmetric complexes, the thermal promotion of an electron to the LUMO level leads to an excited triplet state with less M–C bonding and more $(\text{CC})_n$ bonding character,³² reinforcing again the bond order within the all-carbon bridge, and decreasing it in the M–C bonds, in accordance with the polyene-diyl structure proposed for the triplet isomers (Scheme 13). However, due to the presence of filled non-bonding and bonding MOs in between these two orbitals, the excited triplet state does relax in a more stable configuration where no marked bonding changes are expected relative to the singlet ground state. Frontier MOs are represented for one of the perpendicular sets of MOs involving the butadiyne-diyl bridge in Scheme 17, but this scheme has a general validity for MC_{2n}M complexes, because of the nodal properties of the $(\text{CC})_n$ fragment [118].

Similar considerations apply to the solid-state structure of the C_2 -bridged complex **15**, where the perfect *anti*-conformations (A') observed in the solid



Scheme 17

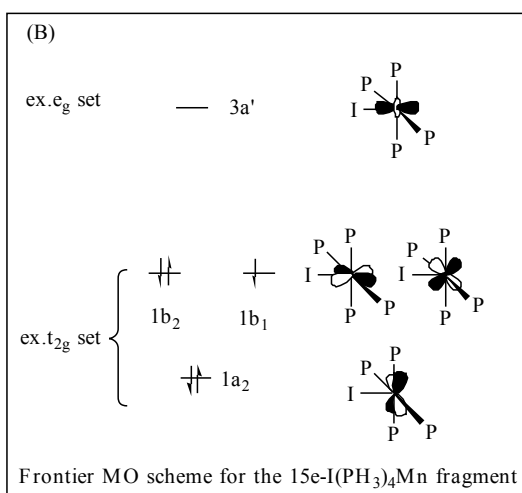
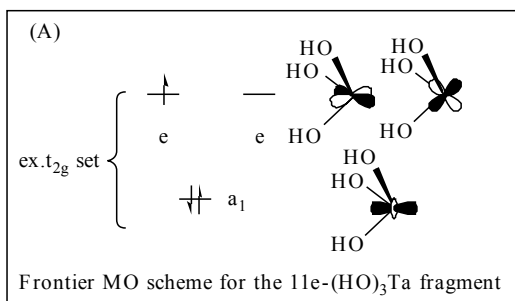
³² It is noteworthy that this result is obtained provided that the spin transition is not accompanied by any conformational change and considering only one set of orthogonal π MOs on the bridging alkynyl (i.e. a “vertical transition”).

state (C_s point group symmetry) between the formally d^1 titanium(III) end-groups allow us to achieve an optimal overlap between the non-degenerated metal fragment-based d_{yz} and d_{xz} orbitals and common empty bridge-based π^* -orbitals [120]. As a result, the unpaired electrons on each titanium fragment remain spin-paired since they belong to the same MO.

As discussed above, the relative rotation of the end-groups at the ends of the all-carbon spacers could have a large influence on the S/T gap for these metal-centered diradicals with non-degenerate SOMOs in the capping fragments. In solution, such a motion is usually easy for alkynyl spacers, as has been experimentally observed with organic molecules for a number of years [121], and also for several of these organometallic diradical representatives, e.g. **17**²⁺ [95]. In fact, the weak rotational barrier computed by DFT analysis for most model complexes suggests that a statistical distribution of conformers will be present in solution at room temperature. For compounds **17**²⁺ and **18a,b**²⁺, the essentially diamagnetic nature of solutions suggests that even strictly perpendicular/twisted conformations such as (B) or (B') do not present markedly reduced S/T gaps.

With diradicals **14**, **16**²⁻ and **19** the S/T gap is not conformation-dependent. Indeed, these organometallic diradicals feature terminal complexes of higher symmetry, where the SOMOs belong to a degenerate set of fragment-based orbitals. The fragment orbitals are shown for the d^1 [^tBu₃SiO)₃Ta] end-groups of C_{3v} local symmetry present in **14** (Scheme 18A) [81], and the d^5 Mn(η^2 -dmpe)₂I end-groups of C_{4v} local symmetry present in **19** (Scheme 18B) (see, for example, Reference [86]). Roughly similar MO diagrams are obtained for **14** and **16**, in spite of the different local symmetries of the d^1 end-groups. A triplet GS is found for both complexes by theoretical (DFT) computations. While the GS of **16** has not been experimentally determined, the high magnetic moment measured at 25 °C would be in accordance with such a GS. Unfortunately, computations fail to predict the correct GS for **14** [81,83]. (This is not surprising, since correlation energies are rather poorly appreciated by simple (EHMO) theoretical treatments.) For compound **19**, the triplet GS is correctly predicted by DFT calculations [46]. Importantly, a triplet GS is also theoretically predicted for the C_{2v} piano-stool (η^5 -C₅H₅)(CO)₂Mn end-group [83]. This suggests that there is no strict symmetry requirement regarding a given capping complex to favor the triplet GS. Apparently, depending on the electronic correlation terms, the near or accidental degeneracy of the d_{xz} and d_{yz} frontier orbitals might be a sufficient condition.

Concerning the all-carbon bridge-structure of the isolated spin isomers **14** and **16**²⁻, the cumulene-like structure is readily explained. Regardless of the term of the (e_g)² configuration considered for the GS (¹E_g, ¹A_{1g} or ³A_{2g}), the unpaired electrons always occupy degenerate MOs with M–C bonding and (CC)_n antibonding character. The occupancy of such MOs decreases the bond order in the bridge and increases it between the M–C bonds. From this



Scheme 18

simple extended-Hückel diagram, the same structure should be observed for the bridge, regardless of the spin isomer being considered. Accordingly a cumulene-like bridge is actually observed for the putative triplet diradicals **16**, **16**⁻², and the singlet isomer **14**. However, in **16**⁻², the two 'Li⁺' cations coordinated to the all-carbon bridge in **16** certainly contribute to the observed decrease in C-C bond order.

Because of d_{yz}/d_{xz} orbital degeneracy, a closely related MO level-ordering occurs in the EHMO diagram of the triplet d^5-d^5 C₄-diradical **19**. However, the fragments are now more electron-rich and the unpaired electrons are located in a higher-lying degenerate set of MOs with M-C antibonding and (CC)_n bonding character. A butadiyne-diyl structure with single M-C bonds is

expected, in accordance with the experimental (X-ray) distances reported [46]. Similar bond distances for the bridge of the corresponding excited singlet isomer are also expected, with a somewhat increased M–C bond order. On the other hand, the cumulene structure of the corresponding dication $\mathbf{19}^{2+}$, formally a ‘tetra-radical’ with two unpaired electrons in the degenerate d_{yz}/d_{xz} orbitals, can now be envisaged to result from a pairwise coupling of each electron with its symmetric counterpart, hence resulting in the formation of two bonding interactions through perpendicular p manifolds of the all-carbon ligand. Depopulation of the two M–C antibonding and $(CC)_2$ bonding SOMOs will result in a more M–C bonding and $(CC)_2$ antibonding arrangement of the all-carbon spacer. Formally, based on bond orders, the bridge of such a d_4/d_4 ‘diradical’ could adopt a bis-carbyne structure [24,82,83]. Only a cumulene-type arrangement results, as evidenced by X-ray analysis and infrared data.

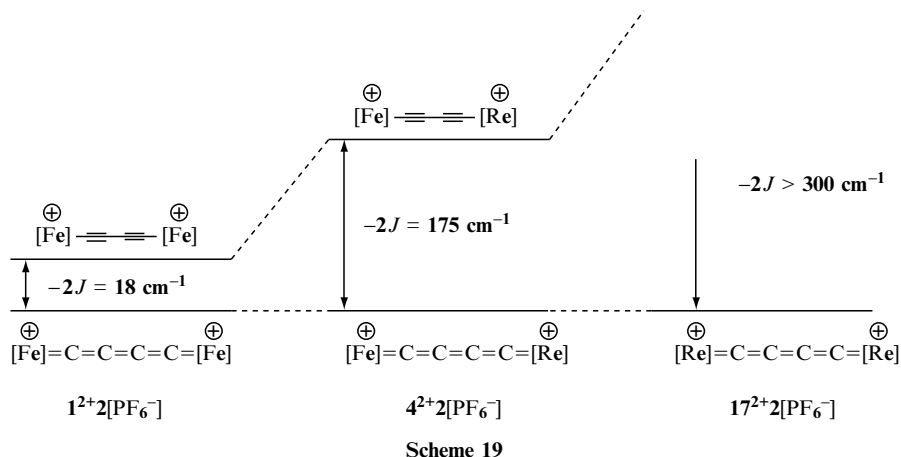
These simple MO-based considerations suggest that for all-carbon bridged organometallic diradicals, different situations arise, depending on the symmetry and degeneracy of the SOMOs of the metal-capping fragment. For fragments with a non-degenerate d_{yz} or d_{xz} SOMO, the conformation adopted does, in principle, influence the nature of magnetic exchange between metal-centered spins. An antiferromagnetic superexchange interaction is usually observed in eclipsed conformations (A) or (A’), thus favoring the bonding, in agreement with predictions based on Ovchinnikov’s rule applied to the $MC_{2n}M$ core. In the twisted conformations (B) or (B’), or when the fragment have degenerate d_{yz}/d_{xz} SOMOs, the nature of the superexchange is more difficult to predict *a priori*.

The structure of the singlet and triplet spin isomers in organometallic diradicals seems to depend equally on the electron ‘richness’ of the metal-capping complexes and also on its symmetry. Diradicals with 17-e piano-stool end-groups, such as $\mathbf{1}^{2+}$, $\mathbf{2}^{2+}$, $\mathbf{4}^{2+}$, $\mathbf{17}^{2+}$ or $\mathbf{18a}, \mathbf{b}^{2+}$, present a singlet GS with a cumulene bridge, while the ‘excited’ triplet isomer is believed to have a ‘less-bonding’ structure, closer to a butadiyne-diyl bridge based on VB schemes. In such a case, the GS can be envisaged as being determined by the need of electron-deficient metal centers to complete their coordination spheres. Thus, the 17-e metal centers in $\mathbf{1}^{2+}$, $\mathbf{2}^{2+}$, $\mathbf{4}^{2+}$, $\mathbf{17}^{2+}$ or $\mathbf{18a}, \mathbf{b}^{2+}$ achieve an 18-e count by sharing the unpaired electrons (Scheme 13). Diradicals with more symmetric end-groups, such as $\mathbf{14}$, $\mathbf{16}^{2-}$ or $\mathbf{19}$, should present less marked structural changes between their spin isomers. Experimental evidence suggests however, that the geometrical changes are not marked between spin isomers in any case.

4.1.3 Magnitude of the S/T Gap in C_{2n} -Bridged Organometallic Diradicals

For antiferromagnetic organometallic diradicals with d^5 low-spin piano-stool end-groups, the S/T gap appears to present large variations. Some indications

regarding the factors which determine its magnitude can be gained from the consistent series of butadiyne-diyl dications 1^{2+} , 4^{2+} and 17^{2+} . Notably, the non-symmetrical complex $4^{2+}2[\text{PF}_6^-]$ has a S/T gap positioned in between that of its symmetrical counterparts, $1^{2+}2[\text{PF}_6^-]$ and $17^{2+}2[\text{PF}_6^-]$ (Scheme 19). This indicates that the global symmetry of the dinuclear compound has an overall smaller influence on the gap than the actual nature of the capping fragments, despite the strong polarization of the bridge taking place in $4^{2+}2[\text{PF}_6^-]$. *A priori*, based on a CI interpretation of the magnetism, the largest S/T gap would be expected for 4^{2+} [4]. Indeed, the MMCT (Fe→Re) excited configuration should stabilize the singlet state relative to the triplet more strongly by virtual coupling (CI) than in the symmetrical homologues 1^{2+} and 17^{2+} . In trying to rationalize the present trend in J -values ($J_{\text{Re-Re}} > J_{\text{Fe-Re}} > J_{\text{Fe-Fe}}$) without considering the influence of any excited configurations (no CI), we propose that the more diffuse nature of the d orbitals on the rhenium induce larger overlap populations. Moreover, the SOMO in the C_s rhenium(II) fragment is apparently energetically more distant from the lower-lying filled orbitals than in the C_{2v} iron(III) piano-stool end-groups. This also will lead to stronger bonding interactions [119]. Thus, a larger antiferromagnetic exchange interaction takes place when rhenium(II) centers are present. Of course, the validity of such a hypothesis should now be assessed by the determination of additional values for S/T gaps in related compounds. If correct, such a statement does, however, open the perspective of being able to tune the S/T gap in this class of organometallic diradicals in a predictable way, by judicious choice of the end-groups.

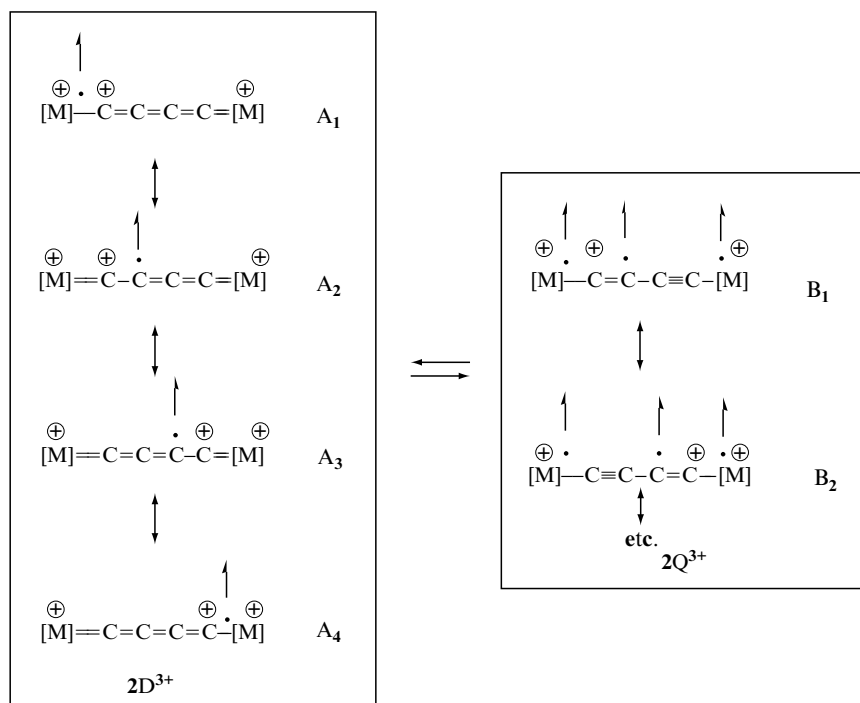


4.1.4 Some Results Regarding the C_{2n} -Bridged Organometallic Ditopic Triradicals

As mentioned earlier, dinuclear trications with all-carbon bridges have been characterized in many instances as having piano-stool end groups [22,25,26], but yet were isolated and structurally characterized by X-rays analysis only in the case of iron ($2^{3+}3[PF_6^-]$) [23]. Regardless of the exact location of the third electronic vacancy, such a triradical can present either a quartet or a doublet GS, depending on the exchange interactions between the electrons (see Scheme 11B above).

The variation of the magnetic susceptibility with the temperature for $2^{3+}3[PF_6^-]$ indicates that a (twofold degenerate) doublet state constitutes the GS in the triradical, and a spin transition takes place with the excited quartet state in the 4–290 K range [99]. The determination of the electronic structure of the bridge for both spin isomers appears not to be trivial. The observation of a single (mean) doublet suggests again a rapid interconversion between them. Moreover, no intervalence (IVCT) band could be detected in the usual near-IR range, despite the odd number of electrons present in $2^{3+}[PF_6^-]$. Thus, a non-symmetric iron(III)/iron(IV) structure, typical for a class-I or a class-II MV complex, is not possible [23]. Accordingly, the magnetic susceptibility temperature-dependence is more accurately fitted by considering a tritopic (equation (11)) rather than a ditopic triradical (equations (9a) and (9b), with $S_A = 1$ and $S_B = 1/2$). From the QS value recorded at 293 K (37 % quartet state) and at 80 K (2 % quartet state; see Table 3), we can derive the hypothetical QS corresponding to the pure quartet (0.879 mm s^{-1}) and doublet spin isomers (0.987 mm s^{-1}). Regarding the structure of the all-carbon bridge, these QS values indicate that the doublet isomer (larger QS) should present a more cumulene-like iron(II) structure ($2D^{3+}$) than the quartet isomer, which is closer to a butadiyne-diyl iron(III) structure ($2Q^{3+}$) (Scheme 20) [77]. It is noteworthy that this interpretation rests on the hypothesis that the odd electron is symmetrically located on the all-carbon chain (i.e. 1 single Mössbauer doublet per spin isomer), and suggests a class-III MV formulation for each spin isomer. Therefore, resonance between the various VB structures A_1/A_4 and B_1/B_2 has to be invoked in order to keep the overall symmetry of the trication. In agreement with such an interpretation, the crystal structure determined for the trication $2^{3+}3[PF_6^-]$ exhibits a clear cumulene-like character when compared with typical butadiyne-diyl structural features, as exhibited by the neutral and diamagnetic complex **1** (Table 7) [23]. It should be noted that typical $C\equiv C$ bond stretches cannot be detected in the $2100\text{--}1700 \text{ cm}^{-1}$ region of the infrared spectra of $2^{3+}3[PF_6^-]$ at 294 K [99].

In the trication $2^{3+}3[PF_6^-]$, as in the dication $2^{2+}2[PF_6^-]$, the all-carbon bridge still behaves as an antiferromagnetic coupler between two metal-centered unpaired electrons, while the third one remains located symmetrically on the spacer and on the iron(III) centers, as indicated by the ESR spectrum recorded at 4 K. Apparently, the all-carbon bridge behaves partly as a spin carrier, as

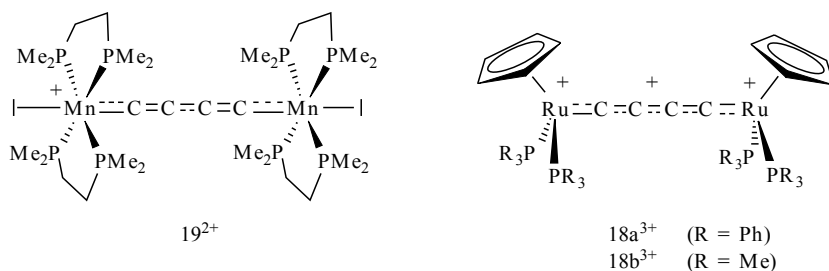
**Table 7** Crystallographic reference data for selected $[M]C_4[M]$ compounds

Compound	M	M–C $_{\alpha}$	C $_{\alpha}$ –C $_{\beta}$	C $_{\beta}$ –C $_{\beta}$	R indices	Ref.
1	Fe(II)	1.884(2) 1.889(2)	1.220(3)	1.374(3)	0.042	117
2³⁺3PF₆⁻	Fe(III/IV)	1.79(1)	1.27(1)	1.33(1)	0.076	23, 117
19⁺PF₆⁻	Mn(II/III)	1.763(3)	1.275(2)	1.313(3)	0.027	46

suggested by the lack of an IVCT band in the NIR region for **2³⁺**. This behavior may be imparted by the presence of the nearby electron-rich metal nuclei, which destabilize the occupied bridge-based MOs. This trication (**2³⁺3[PF₆⁻]**) constitutes an original example of a mixed organic–inorganic triradical.

Two related d^5/d^4 complexes were recently reported. Berke and co-workers isolated and structurally characterized the monocation **19⁺[PF₆^{-]}** after oxidation of the neutral congener **19** [46]. The compound **19⁺[PF₆^{-]}** behaves apparently as a monoradical, as exemplified by its Curie–Weiss paramagnetism reported for the NMR samples between -90 and $+25$ °C, and by its magnetic moment at 200 K ($\mu = 1.99\mu_B$). The isolated compound must therefore also

correspond to the ground doublet spin isomer, resulting from the very strong antiferromagnetic coupling between two of the electrons. The gap for the quartet state was apparently not investigated. Moreover, the electrons appear mostly metal-centered, since this monocation constitute a class-II MV complex, as suggested by ESR studies, with a characteristic IVCT band located at 1610 nm ($V_{ab} = 500 \text{ cm}^{-1} = 0.062 \text{ eV}$). The structure of the bridge is apparently butadiyne-diyl-like, as evidenced by characteristic infrared stretches ($\nu_{C\equiv C} = 2123$ and 1805 cm^{-1}). Nevertheless, in spite of different electron-transfer properties, resulting from different electronic structures for the all-carbon bridge, quite close crystallographic bond lengths for the C_4 spacer are observed in the solid state, for both spin isomers (see Table 7).³³

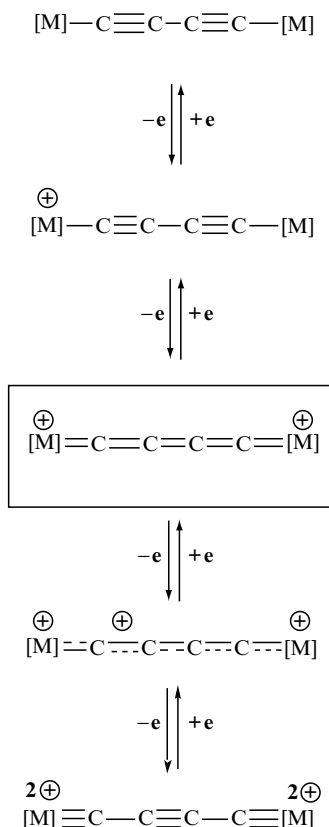


Bruce and co-workers characterized the trications **18a,b**³⁺ in solution after further oxidation of the corresponding dications [24]. These complexes present apparently many more analogies with the organoiron trication **2**³⁺, and correspond also to GS doublet isomers. Likewise, the compounds are believed to be class-III MV complexes, and weak IVCT transitions have been identified near 830 nm ($12\,000 \text{ cm}^{-1}$), hence revealing a strong electronic coupling between the metallic sites ($V_{ab} = 0.76$ and 0.74 , respectively). The structure of the bridge is most likely cumulene-like, since intense and characteristic bands are observed at around 1627 cm^{-1} in the infrared spectra.

4.1.5 Redox Chemistry of the C_{2n} -Bridged Organometallic Diradicals

Several of the organometallic di- and triradicals discussed in this section belong to redox families and therefore give stable parents upon reduction or oxidation. In contrast to spin isomers, the redox parents display significantly different structures. With the question of π -interactions between the alkynyl ligand and

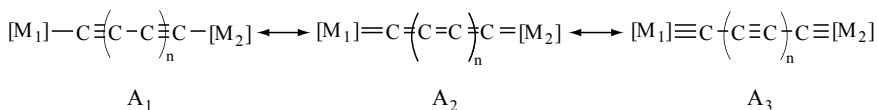
³³ This suggests that different VB formulations do not result in marked geometrical differences in the molecules, as is also shown by the similar bond lengths for the $M-C_n-M$ core computed for different sets of spin states [117]. VB formulation constitutes, however, an interesting and didactic way to show the changes in the electronic interactions.



Scheme 21

the metal atom being central to the chemistry and the physical properties of this fragment [32], the redox-dependent structural changes taking place between redox congeners were therefore thoroughly studied. Typically, the following sequence has been proposed for the d^6-d^6/d^5-d^5 diradicals such as 1^{2+} , 2^{2+} , 4^{2+} , 17^{2+} and **18a**, **b**²⁺ (Scheme 21) [20,23,24,95].

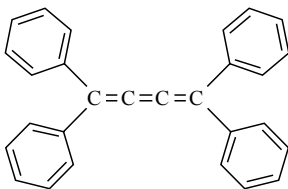
Starting from the corresponding dication, regardless of the conformation adopted, DFT calculations point out that all MOs occupied by the incoming electrons are mostly metal-centered and metal-carbon antibonding in character [24,95,117,118,121]. Thus, the cumulene bridge present in the dication transforms logically into a polyynes-diyl type upon reduction. In this case, reductions do apparently just increase the relative weight of (A_1) relative to (A_2) and (A_3) for polyynes-diyl-bridged d^n-d^n complexes in the VB representation (Scheme 22) (see, for instance, References [82,83,112,122,123]). Alternatively, structural

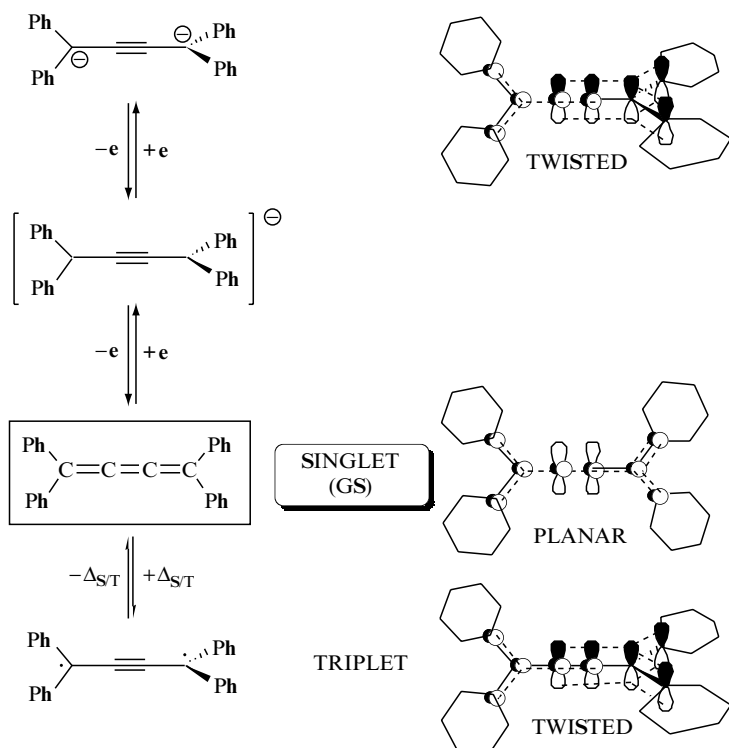


Scheme 22

redox-induced changes involving the (A_2) and (A_3) structures are expected upon 2/6-electron oxidations [24,82,83]. It is noteworthy that the present resonance occurs in the singlet potential surface and such a VB interpretation of the redox-induced structural changes are correct only because $\mathbf{1}^{2+}$, $\mathbf{2}^{2+}$, $\mathbf{4}^{2+}$, $\mathbf{17}^{2+}$ and $\mathbf{18a}$, \mathbf{b}^{2+} are *antiferromagnetically coupled* d^5-d^5 diradicals. In this case, the magnitude of the observed structural change is related to the magnitude of the superexchange which is taking place (i.e. the S/T gap). However, if one of these d^5-d^5 organometallic diradicals would instead have had a triplet GS, such as $\mathbf{19}$, for instance, the redox-dependent structural evolution of the all-carbon spacer upon reduction would have been slightly different. Thus, given a redox family featuring several parents, i.e. $d^{n-1}-d^{n-1}/d^n-d^n/d^{n+1}-d^{n+1}$, structural changes between redox isomers can be expressed by a different balance between (A_1-A_3), only if any diradical of the family has a singlet GS (Scheme 22). Otherwise, structural rearrangements pertaining to triplet spin isomers must be taken into consideration as well.

As discussed above, rotational motions of the end-groups can be very important for organometallic diradicals featuring terminal fragments with a non-degenerate metal-centered HOMO. Such motions influence the relative stability of the singlet cumulene versus triplet polyyne-diyl spin isomers, but also can play a determinant role in their redox chemistry. Typically, when *antiferromagnetically coupled diradicals* are reduced, electrons are injected into the (HOMO + 1) orbital, thus resulting in a net destabilization of the complex in configurations (A) or (A'). Depending on the electronic correlation, rotation of one end-group of 90° might relieve the energetic strain by formation of two degenerate and perpendicular HOMOs in configurations (B) or (B').





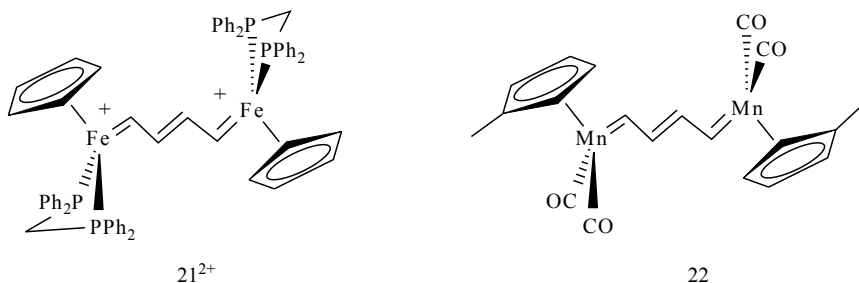
Scheme 23

This is exactly what happens when 1,1,4,4-tetraphenylbutatriene (**20**), isobal to the symmetric dicationic singlet isomers,³⁴ is reduced (Scheme 23) [124]. A twisted conformation of the two Ph_2C end-groups was proposed for the reduced forms (**20⁻** and **20²⁻**), based on Hückel calculations and reactivity studies. Apparently, for the reduced parents **1**, **2** or **4**, the energy differences between the various conformations are far less important, since DFT calculations indicate only very weak rotational barriers [117].

³⁴ Similarly to these dications, **20** can exist in either a paramagnetic polyynelike diradical or a diamagnetic cumulene-like form (**20T** and **20S**, respectively). With **20**, because of the nearly perfect orbital match between the Ph_2C -centered magnetic orbitals, a large S/T gap results. The diamagnetic singlet spin isomer is strongly favored and the triplet diradical is never observed at 25 °C. The interconversion between the most stable forms of these two spin isomers could involve a rotation of 90° of the end-groups.

4.2 END-ON POLYENE-DIYL-BRIDGED ORGANOMETALLIC METAL-CENTERED DIRADICALS

4.2.1 Structure of the Spin Isomers in $(RC=CR')_n$ -Bridged Organometallic Ditopic Polyradicals



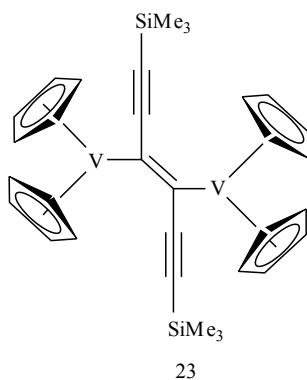
To our knowledge, 21^{2+} , characterized by Sponsler and co-workers in 1994, constituted the first attempt to isolate a d^5-d^5 diradical with a butadiene-diyl bridge [125]. Unexpectedly, the complex was diamagnetic and presented a bis-carbene structure, as demonstrated by X-ray diffraction studies (Table 8). The bond distances are reasonably close to those reported for the isoelectronic dicationic $6^{2+}2[PF_6^-]$ [101], or neutral **22** bis-carbenes [126]. However, the possibility of a spin equilibrium was not discussed for 21^{2+} , although the diamagnetic bis-carbene structure certainly corresponds to the singlet spin isomer in the GS. The absence of paramagnetism suggests, nevertheless, that the S/T gap in 21^{2+} (and also in 6^{2+} or **22**) is sufficiently large for precluding the triplet isomer formation at 20 °C.

With $5^{2+}2[PF_6^-]$, which is closely related to $21^{2+}2[PF_6^-]$, but presents methoxy substituents in positions 1 and 4 on the butadiene linker, the dppe ligand in place of (1,2-diphenylphosphino)methane (dppm) and a permethylated Cp* ligand in place of Cp, we could observe such a spin equilibrium (see Section 3.2 above) [100]. The magnetic susceptibility dependence of $5^{2+}2[PF_6^-]$ clearly shows the antiferromagnetic exchange interaction between the two unpaired electrons on the $[(\eta^2\text{-diphos})(\eta^5\text{-C}_5\text{Me}_5)\text{Fe}]^+$ units through the butadiene-

Table 8 Crystallographic reference data for selected symmetric $[M]_2[(RCCR')_n][M]$ complexes

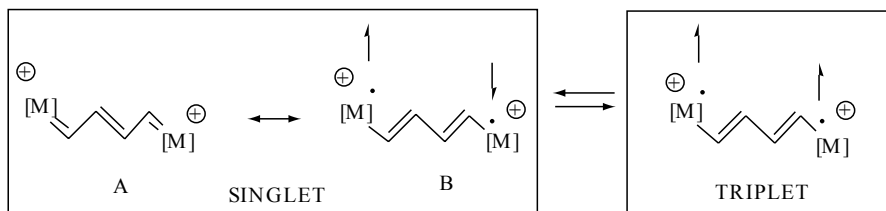
Compound	M	<i>n</i>	R	R'	M-CR-	RC-CR'	R'C-CR'	<i>R</i> indices	Ref.
$21^{2+}2PF_6^-$	Fe(II)	2	H	H	1.841(11)	1.418(14)	1.366(20)	0.069	125
$6^{2+}2PF_6^-$	Fe(II)	2	OMe	H	1.870(7)	1.47(1)	1.31(1)	0.052	101
22	Mn(0)	2	OEt	H	1.893(3)	1.471(4)	1.323(4)	0.032	126
						1.472(4)			
23	V(III)	1	C≡C-TMS		2.165(4)	1.381(9)	—	0.033	127

diyl spacer, so leading to a singlet GS. Here, as well, this singlet state has a bis-carbene structure, while the triplet state appears to display a structure closer to a butadiene-diyl bridge. This is essentially shown by variable-temperature Mössbauer spectroscopy. Comparison with data gathered on model complexes reveals the *QS* of the singlet isomer of $5^{2+}2[\text{PF}_6^-]$, predominant at low temperatures, is typical for an iron(II)-carbene end-group such as $6^{2+}2[\text{PF}_6^-]$, while the *QS* of the second doublet appearing at higher temperature resembles that of an iron(III) alkenyl complex (see Table 3 above) [23]. At 20 °C, the broadness of the Cp* and phosphorous NMR signals suggests that the dinuclear complex is fluxional at room temperature. It is noteworthy that when considering the central double bond in $5\text{S}^{2+}2[\text{PF}_6^-]$, only the *E*-geometric isomer is detected. Thus, a second species, distinct from a bis-carbene complex, is therefore present in solution. Other available spectroscopic data obtained at 20 °C suggest a butadiene-diyl dicationic iron(III) complex.

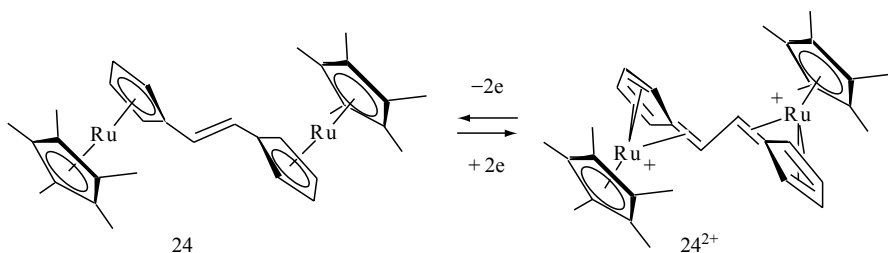


A magnetic susceptibility study has been conducted on the related 1,2-ethene-diyl-bridged ditopic tetradical **23** by Choukroun and co-workers [127]. Similarly to our findings on $5^{2+}2[\text{PF}_6^-]$, these researchers observed anti-ferromagnetic coupling between the four metal-centered spins through the carbon-rich bridge ($\mu = 4.01\mu_B$ at 300 K). Its magnitude was, however, quite weak ($J = -1.9 \text{ cm}^{-1}$). Given the Hamiltonian used to fit the magnetic susceptibility data, no intermolecular contribution was taken in consideration, but a very good fit was achieved (residuals, $R = 2.89 \times 10^{-4}$).³⁵ The solid-state structure of this complex indicates some disorder in the crystallographic cell. The V–C(sp²) bond length (2.16 Å) compares with a typical single V–aryl bond length (2.12–2.15 Å) [128], while the central C=C bond (1.38 Å) is slightly longer than a pure double bond (1.34 Å) (see Ref [60], p. 21). Thus, the bond

³⁵ The authors state that the magnetic susceptibility temperature-dependence could also correspond to independent distorted non-interacting vanadium(II) centers.



Scheme 24



Scheme 25

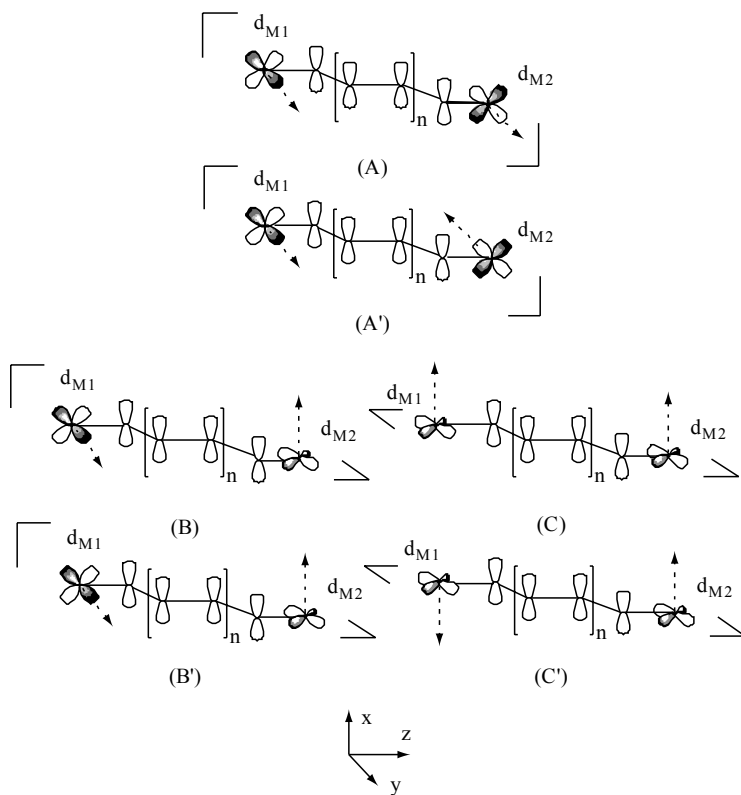
lengths (see Table 8) within the V–C–C–V core of complex **23** are much closer to a 1,2-alkene-diyl structure than to a bis-carbene structure at 180 K. This can be conciliated with a dominant weight of the singlet VB structure B in the GS, which might be traced back to the weak interaction stated.

Thus, here also, different structures are associated with each spin isomer of $(RC=CR')_n$ -bridged organometallic diradicals (Scheme 24). Especially when a sizeable magnetic interaction takes place, the singlet isomer presents a large bis-carbene character (A), while the triplet state appears to have a butadiene-diyl-bridge structure (B). A related, and reversible structural rearrangement was also observed upon the two-electron oxidation of 1,2 ethene-diyl-bridged ruthenocenes such as complex **24** (Scheme 25) [129–131].

4.2.2 Bonding and Superexchange in $(RC=CR^0)_n$ -Bridged Organometallic Diradicals

In the few examples where spin equilibrium could be detected, the singlet spin isomer was always the GS. This is not unusual, since the end-on polyene-diyl linker behaves most often as an antiferromagnetic coupler in organic diradicals, following Ovchinnikov's rule [5,132,133].

This time, in terms of conformations, the situation appears slightly less complex than for the all-carbon bridge (see Section 4.1.2 above). When considering the unpaired electron on the isolated capping fragment in pure d_{xz} - or d_{yz} metal-based magnetic orbitals (Scheme 12 above), only the rotamers (A) or (A') will present appreciable overlap with common π or π^* ligand-based orbitals (Scheme 26). These conformations will give rise to a dominant antiferromagnetic



superexchange interaction between spins, since the metal-centered electrons in the capping fragments should belong to the same MO and are paired. This is shown by the application of Ovchinnikov's rule to this 'new $M(RCCR')_nM''$ π manifold, taken as a pseudo-alternant system. Other conformations, such as, for instance, (B) or (B'), and even more, (C) or (C'), result in two orthogonal frontier MOs, poorly co-extensive in space (or even fully disjoint). Following Borden's criterion, only a weak magnetic interaction should result in comparison to (A) or (A'). Thus, in contrast with the case of polyene-diyl bridges, the existence of a sizeable ferromagnetic coupling between the spin carriers is doubtful in these rotamers.

Semi-empirical Hückel and Fenske-Hall calculations were conducted on model complexes featuring $[\text{Cp}(\text{CO})_2\text{Fe}]$, $[\text{Cp}(\text{PH}_3)_2\text{Fe}]$ (**5'**) or $[\text{Cp}(\text{dppm})\text{Fe}]$ (**21'**) end-groups and $(-\text{XC}=\text{CH}-\text{HC}=\text{CX}-)$ bridges ($\text{X} = \text{OH}, \text{H}$) in the *trans*-arrangement [101,121]. Without any surprise, these confirm the bis-carbene structure of the bridge in the di-oxidized state and suggest, in agreement with the X-ray structure of $\mathbf{21}^{2+}2[\text{PF}_6^-]$, that the SOMOs on the metallic

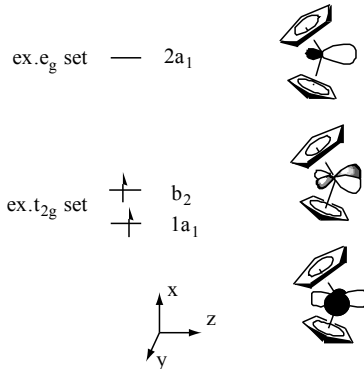
end-group have a strong d_{yz} character. EHMO calculations also revealed that the electronic distribution in these compounds was quite sensitive to bond length changes.³⁶ Thus, regarding the role of the ancillary ligands or substituents on the bridge, trends could be evidenced in the neutral parents **5'** and **21'**, but no firm conclusions could be reached at the EHMO level for the model dications **5'²⁺** and **21'²⁺** because of the very small HOMO–LUMO gap present in these complexes. This is due to the energetical proximity of the set of essentially non-bonding d_{yx} -based MOs (Scheme 12). As stated by Sponsler at that time [121], this was in favor of low-lying open-shell states. It is noteworthy that, at the EHMO level, very similar results are obtained when the bridge is rotated from 90° as in conformations (C)–(C'), due to the presence of the second set of perpendicular d_{xz} metal-based MOs being very close in energy. This also indicates that twisted conformations with the electronic vacancies located in nearly orthogonal (and poorly overlapping) MOs do not present very different stabilities. A consequence of this statement is that the rotation about the bridge axis does present a weak activation energy.

Regarding the ditopic vanadium(III) d^2 – d^2 tetraradical **23**, two unpaired electrons are now present on each [$(\eta^5\text{-C}_5\text{Me}_5)_2\text{V}$] end-group. Only one of these, located in the d_{yz} orbital of the fragment, can interact with the p manifold. The other is located in a ' $d_{y^2-z^2}$ ' orbital, extending mostly along the y-axis, perpendicularly to the bridge, but also in the bridge (z-) direction, and allows only for σ -overlap with the olefin (Scheme 27) [120]. The solid-state conformation adopted by **23** corresponds to conformation (C) or (C') and allows only for a minimal interaction of d_{yz} electrons on the capping fragments with the frontier π bridge-based MOs. Without any surprise, the observed magnetic superexchange is very weak and possibly does result from the interaction between the ' $d_{y^2-z^2}$ ' electrons through the lower-lying σ manifold of ligand-based orbitals. Accordingly, no sizeable change in the distribution of the π -electrons of the bridge takes place and the structural change toward a bis-carbene structure observed in the cases of **5²⁺** and **21²⁺** is not observed.

As predicted by Ovchinnikov's rule, linear alternant hydrocarbons have always a singlet GS. Since the $\text{M}(\text{RCCR}')_n\text{M}$ ($2(d^1) + 2np$) manifold in conformations (A) and (A') might be considered as a linear $2n + 2$ pseudo-alternant hydrocarbon, the coupling between the d_{xz} - or d_{yz} -metal-centered spins in organometallic $\text{M}(\text{CRCR}')_n\text{M}$ diradicals is predicted to be always antiferromagnetic in the GS. A conjugated bis-carbene $\text{M}=(\text{RCCR}')_n=\text{M}$ structure should then result in the GS, when a non-negligible interaction takes place between the metal-based SOMOs and π or π^* frontier orbitals of the bridge. The structural changes in the corresponding excited triplet isomer will depend on the bonding characteristics of the two SOMOs.

From an examination of the symmetry properties of the HOMO and the LUMO in eclipsed conformations (A or A'), analogously to the simple EHMO

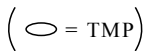
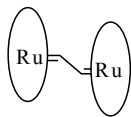
³⁶ This is a common problem with EHMO calculations [81].

Frontier MO scheme for the sandwich 16e- Cp_2V fragment

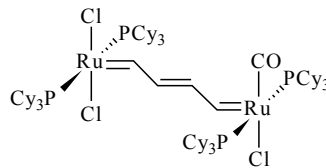
Scheme 27

analysis made previously for antiferromagnetically coupled d_5-d_5 MC_4M dications (Scheme 17), we expect less M-C bonding and more $(CC)_n$ bonding character in the excited triplet isomer structure, provided that no conformational change takes place during the spin transition. This would be in accordance with the proposed polyene-diyl structure (Scheme 24).

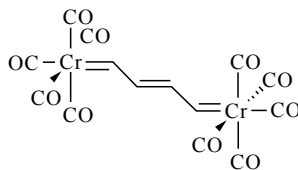
From the present analysis, one may also envisage other known and isolated isoelectronic bis-carbenes, like **25-27** (TMP = 5,10,15,20-tetramesitylphorphyrin), as singlet d^5-d^5 organometallic diradicals. The data published for these compounds suggest large S/T gaps, since no paramagnetism under ambient conditions due to a possible equilibrium between spin isomers was reported.



25



26



27

4.2.3 Considerations on the Spin Transition in (RC=CR')_n-Bridged Organometallic Diradicals

Given the poorness of the data available on such compounds, nothing can be said regarding the electronic factors influencing the magnitude of the S/T gap. Obviously, small changes may have quite a large influence, as observed from the differences between $5^{2+}2[\text{PF}_6^-]$ and $6^{2+}2[\text{PF}_6^-]$ or $21^{2+}2[\text{PF}_6^-]$.

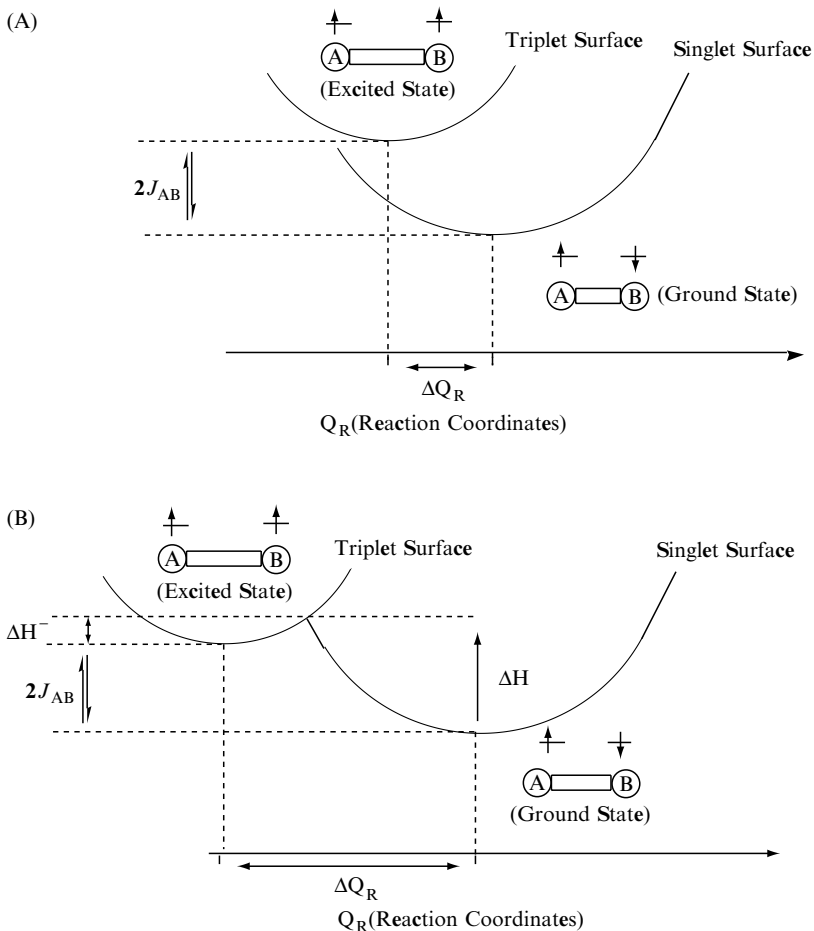
Very interesting is, however, the experimental observation that the spin transition in the solid state for $5^{2+}2[\text{PF}_6^-]$ is much slower than that for the all-carbon (CC)_n bridged analogues. In principle, this kinetic effect has as much to do with the magnitude of the shift between the singlet and triplet state on the reaction coordinate scale (denoted as ΔQ_R in Scheme 7) than with the magnitude of the gap, which reflects largely the thermodynamic effect. Thus, when this shift is not too large, the thermal transition is nearly vertical and its energy ($2J_{AB}$) corresponds to the S/T gap (A, Scheme 28). However, when ΔQ_R becomes large and when the bottom of the well corresponding to the excited surface lies 'outside' of the GS well (B, Scheme 28), this induces a further 'activation barrier' (denoted as ΔH^\ddagger)³⁷ to be added to the S/T gap. As a result, a slower spin transition is expected, and spin isomer trapping phenomena might even be observed at low temperatures, with isomer distribution deviating from the Boltzmann law.

In the case of $5^{2+}2[\text{PF}_6^-]$, interconversion between spin isomers readily takes place, as indicated by the magnetic susceptibility or Mössbauer data, and a satisfactorily modelling using a simple Boltzmann law. This suggests that no large activation barrier exists for the present spin interconversion process, and that the equilibrium situation is always achieved. Thus, in spite of the slower spin-transition, we have apparently not already reached the extreme case B. At least another case of very slow spin transition in the solid state has already been observed. It was attributed to the restricted conformational mobility in the solid state, thus hindering the geometrical changes accompanying the spin transition [134,135]. From the present data, we cannot conclude whether the slower spin transition observed for 5^{2+} is a general feature resulting from the fact that larger structural rearrangements take place for polyene-diyl bridged diradicals than for the corresponding polyynes-diyl bridged diradicals, or whether this is a peculiar feature of $5^{2+}2[\text{PF}_6^-]$ resulting from a non-favorable packing in the solid state.

4.2.4 Redox Chemistry of the d⁵-d⁵ (RC=CR')_n-Bridged Organometallic Diradicals

Analogously to what has been stated for C_{2n}-bridged organometallic diradicals (see Section 4.1.5 above), several of the present (RC=CR')_n-bridged analogues belong to a redox family, and stable redox parents can be generated upon reduction of the diradicals 5^{2+} and 21^{2+} . Here, as well, characteristic structural

³⁷ The term 'activation barrier' is not really well suited since we do not remain on the same spin surface and since the 'crossover' is theoretically forbidden for symmetry reasons.

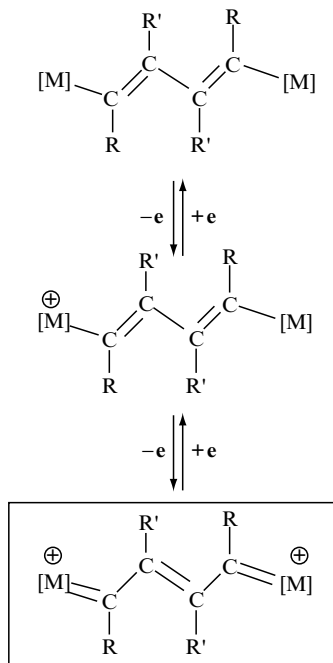


Scheme 28

changes take place upon reduction within each d^6-d^6/d^5-d^5 family (Scheme 29). From what precedes, it appears clearly that the observed structural change of the bridge from the polyene-diyl to the bis-carbene is dictated by the d^5-d^5 electronic configuration, but also by the *singlet* nature of the GS of 5^{2+} and 21^{2+} . This structural change should be increasingly marked with increasingly stronger antiferromagnetic coupling in the d^5-d^5 diradical. With such a bridge, however, the occurrence of a triplet GS appears less probable.

4.3 ORGANOMETALLIC DIRADICALS BRIDGED BY CARBON-RICH SPACERS FEATURING HETERO(ARYL) UNITS

With the exception of our own results with organorion dications (see Section 3.2 above), only scant data are available on this class of organometallic di- or



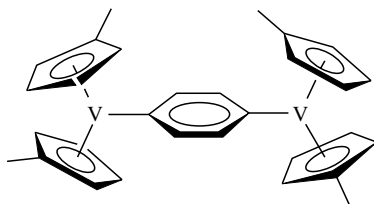
Scheme 29

tritopic polyradicals. We have therefore focused mostly on our own experimental observations in the following and discussed the various bridges together, depending on the central unit which is present.

4.3.1 Simple Aryl-Bridged Ditopic Polyradicals

To our knowledge, the first organometallic ditopic tetradical bridged by a 1,4-phenylene unit was the dinuclear organouranium(IV) complex $[(\eta^5\text{-C}_5\text{Me}_5)_3\text{U}](\text{C}_6\text{H}_4)[(\eta^5\text{-C}_5\text{Me}_5)_3\text{U}]$, synthesized in 1975 by Tsutsui and co-workers [136]. A few years later, a second member of this class of polyradicals was reported with d^2 aryl vanadium(III) end-groups, i.e. $[\text{Mes}_3\text{V}(\text{C}_6\text{H}_4)\text{VMes}_3]^{2-} \cdot 2[\text{Li}(\text{THF})_4]^+$ [109]. Both complexes were paramagnetic at room temperature, as evidenced by paramagnetic ^1H NMR shifts or a by magnetic moment of $2.61 \mu_{\text{B}}$ found in the solid state. Unfortunately, none of these complexes was structurally characterized, and very few spectroscopic data have been reported. As a result, nothing can be said about their GS, or about the 1,4-phenylene spacer structure.

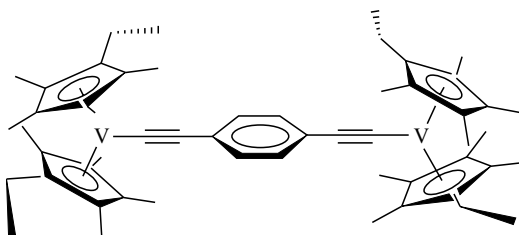
One year later, another d^2 - d^2 1,4-phenylene vanadium(III) tetradical (**28**) was reported by Köhler and co-workers [128]. ^1H NMR spectroscopy indicated a very weak magnetic exchange between the two unpaired spins, the



28

nature of which was not determined. In contrast to the related *para*-quinodimethane organic diradicals (**11a,b**, see Section 2.4 above) [63], the X-ray structure of the compounds showed no distortions of the central aryl ring in **28**. This situation was rationalized by considering that the rotation of the 1,4-phenylene ring in **28** was blocked in solution, for steric reasons, in a conformation parallel to the Cp' ligands. Similarly to what occurs with diradical **21** (see Section 4.2.2 above), this conformation results in a negligible overlap between the d_{yz} vanadium-centered SOMOs and common π orbitals of the aromatic ring. As a result, the superexchange between the spins is very weak.

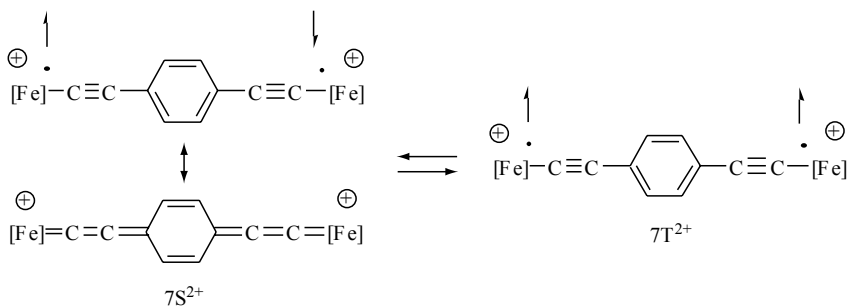
4.3.2 Ditopic Polyradicals Incorporating the 1,4-Diethynylphenyl units



29

The ditopic tetradiradical **29**, closely related to **28**, was apparently the first to be reported for this category and studied for its magnetism [128]. In contrast to **28**, the relative conformation of the two vanadium(III) end-groups is not blocked in the tetradiradical **29**, due to the presence of the ethynyl linkers, which relieve the steric strain imposed by the Cp' ligands in **28**. In spite of this, ^1H NMR of **29** evidenced a very weak superexchange interaction. Its exact nature was, however, not determined.

We are not aware of another example of a potential ditopic polyradical featuring a 1,4-diethynyl aryl bridge, except for the dication $7^{2+}2[\text{PF}_6^-]$ [102]. This dication (7^{2+}) presents a singlet GS [21]. In this case, the situation closely resembles the Thiele ($n = 1$) or Tchitchibabin ($n = 2$) diradical cases (Scheme



Scheme 30

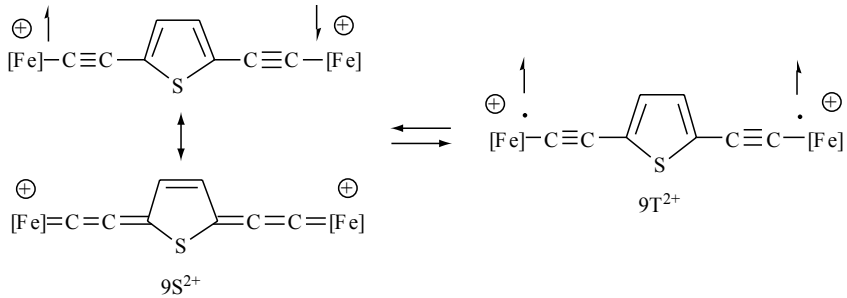
8), where the unpaired electrons are coupled antiferromagnetically (Scheme 30). By analogy, the singlet state is expected to present a certain cumulene/quinone-like character (7S^{2+}), whereas the triplet state should have a diethynyl-1,4-phenylene bridge structure (7T^{2+}). The solid-state infrared spectra exhibits $\nu\text{C}\equiv\text{C}$ bending modes at ca. 1980 cm^{-1} , possibly arising from the triplet (excited) isomer. Given the small S/T gap (ca. 1 cm^{-1}), the latter must be appreciably populated at $20\text{ }^\circ\text{C}$ (see however notes (18) and (38)).

In agreement with a fast spin transition, the spin-dependent structural changes are believed to be quite small. Evidence for this is suggested by Mössbauer spectroscopy, where the average QS (0.911 mm s^{-1}) at 77 K remain close to the one expected for a typical iron(III) phenylalkynyl complex (see Table 3) [80,137]. Noticeably, this value remains on the high side, as expected from the involvement of the cumulene-like structure 7S^{2+} in the equilibrium [77].

4.3.3 Diradicals Incorporating the 2,5-Diethynylthienyl Unit

The dication $9^{2+}2[\text{PF}_6^-]$ featuring a 2,5-thiophene in the bridge behaves very similarly to the dication bearing a *para*-phenylene unit, $7^{2+}2[\text{PF}_6^-]$ [104]. The infrared data reveal a very low $\nu\text{C}\equiv\text{C}$ absorption (1941 cm^{-1}) and the ^{13}C NMR data exhibit characteristic cumulenic resonances at 266.0 and 142.2 ppm, respectively, for the C_α and C_β carbon atoms of the alkynyl linker. These features suggest that the singlet isomer has indeed a dominant cumulene/3-thiacyclopentene-like character (Scheme 31). This is also supported by the Mössbauer data, giving a QS value increasing from 0.96 mm s^{-1} at 300 K to 1.03 mm s^{-1} at 4.5 K where mostly 9^{2+}S is present (see Table 3). Notably, the QS of 1.02 mm s^{-1} at 80 K is rather large for an alkynyl-type bridge. Larger QS values are usually expected for cumulene-iron(II) end-groups relative to alkynyl-iron(III) ones [77].

Interestingly, for $9^{2+}2[\text{PF}_6^-]$ the antiferromagnetic exchange coupling between spins is apparently much stronger for such a bridge than for $7^{2+}2[\text{PF}_6^-]$



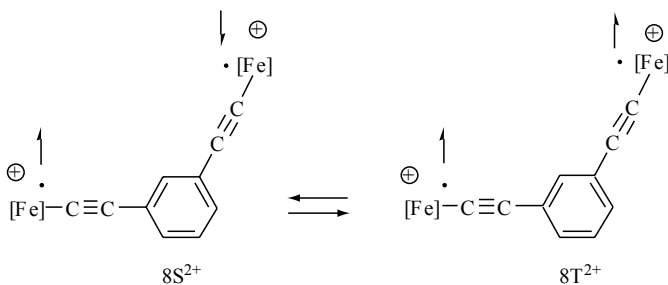
Scheme 31

or for the $1^{2+}2[\text{PF}_6^-]$ species, containing an all-carbon bridge. Here as well, a fast spin-transition takes place between spin isomers (9S^{2+} and 9T^{2+}) relative to the Mössbauer time-scale, in spite of this relatively large *S/T* gap (see Table 5).

4.3.4 Diradicals Incorporating the 1,3-Diethynylphenyl Unit

Finally, with the dication $8^{2+}2[\text{PF}_6^-]$, presenting a 1,3-phenylene unit in the all-carbon bridge, the GS is now the singlet state (Scheme 32), and the *S/T* gap appears larger for $8^{2+}2[\text{PF}_6^-]$ than for $7^{2+}2[\text{PF}_6^-]$ (see Table 5) [103].

In both spin states (8S^{2+} and 8T^{2+}), the bridges must have quite similar structures. This is supported by the infrared data which only display typical alkynyl features, and also by the Mössbauer spectra, where the *QS* value of 0.89 mm s^{-1} , is really diagnostic of an iron(III) phenylalkynyl structure (see Tables 1 and 3 above) [77]. Since markedly different results are obtained for the structurally related 1,4- and 1,3-phenylene-based dications, $7^{2+}2[\text{PF}_6^-]$ and $8^{2+}2[\text{PF}_6^-]$, the magnetic exchange coupling appears to be very topology-sensitive in such diradicals.



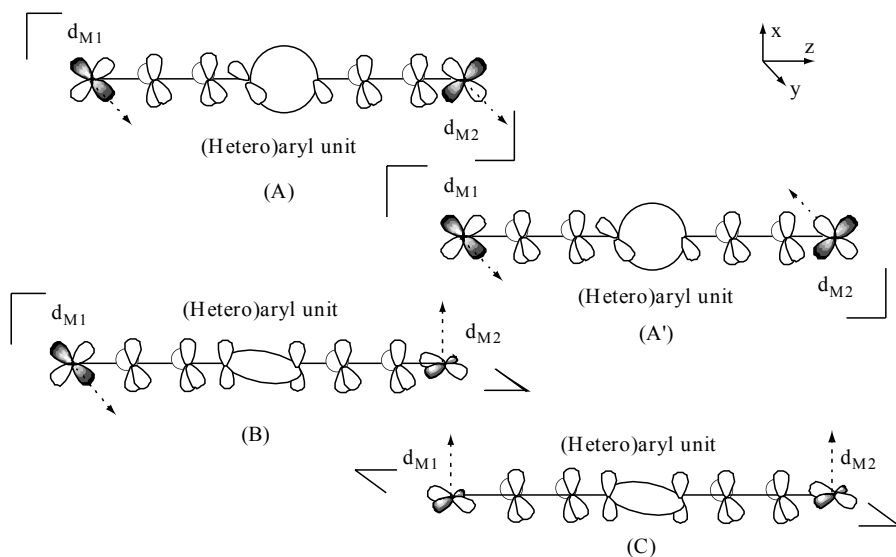
Scheme 32

4.3.5 Bonding and Topology-Dependent Superexchange Interaction in Diethynyl-(Hetero)aryl Diradicals

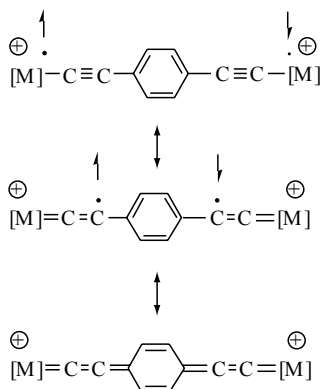
The signs found for the magnetic exchange coupling constants are in full accordance with results gathered on organic diradicals featuring related bridges [5,8]. Typically, *para*-phenylene spacers are well known as antiferromagnetic couplers, as well as 2,5-thienyl units [138], while *meta*-phenylene units were extensively used as ferromagnetic couplers (see, for instance, References [139–141]). Thus, for all these diradicals featuring a unit included in the middle of the alkynyl bridge, the coupling properties of the central unit are apparently preserved.

In terms of conformations, for 7^{2+} and 9^{2+} , the problem is not much different from 5^{2+} featuring a butadiene-diyl bridge (see Section 4.2.2 above). Again, when considering the unpaired electron(s) on the isolated capping fragment in pure d_{xz} - or d_{yz} -metal-based magnetic orbitals (see Scheme 12), only the relative orientations of the capping fragments and the central ring have some importance, due to the presence of the two perpendicular π manifolds on the alkynyl linkers. Thus, only conformations (A) and A' will permit a common interaction of the fragment metal-based SOMOs with one (filled) π or (empty) π^* frontier MOs of the bridging ligand. In conformations (A) or (A'), the alkynyl units act as π -channels and mediate in an optimal way the magnetic superexchange interaction 'through' the central unit. The complete M(CC)[Ar](CC)M unit can then be considered as an alternant manifold. Given the symmetrical disposition, application of Ovchinnikov's rule give a similar result to that for the isolated [Ar] unit. In contrast 'parallel' or 'half-parallel' conformations, such as (C) or (B), respectively, interrupt or reduce drastically the overlap, generating two orthogonal and disjoint SOMOs (Scheme 33). Based on Borden's criterion, the result should be a strongly diminished magnetic exchange. This explains why such a bridge retains the magnetic coupling properties of the isolated central unit.

Thus, understanding the orbital-based origin of the superexchange in such diradicals, invites us to look at the symmetry and spatial arrangement of the frontier orbitals within the central (hetero)aryl unit. The 1,4-connectivity on the phenyl ring, as well as the 2,5-connectivity on the thienyl ring, result in anti-ferromagnetic coupling, due to the strong localization at these positions of common π and π^* frontier orbitals in phase [138,142]. In the case of the *para*-phenylene unit, it has been demonstrated that very strong interactions take place when the energy of the SOMOs correctly matches the energies of the π and π^* frontier MOs on the phenyl ring. Spin pairing and through-ring bonding interactions result and a quinone-like structure is usually adopted by the aryl ring in the singlet GS structure, as show by a classic Lewis VB representation (Scheme 34). Analogous to that which occurs with antiferromagnetically coupled diradicals bridged by 'polyene-type' bridges (see Section 4.2.2 above), the structure of the central spacer in the corresponding excited triplet spin



Scheme 33



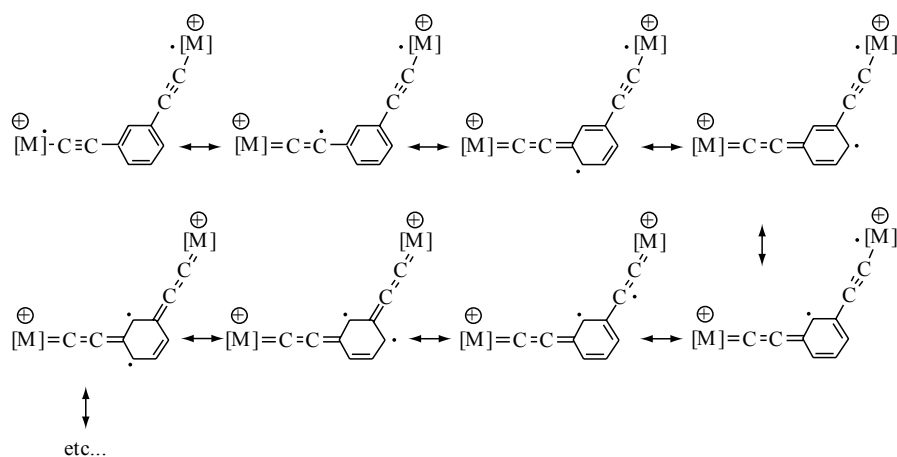
Scheme 34

isomers is closer to a bis-alkynyl-(heteroaryl) form, as proposed on the basis of the spectroscopic data for 9^{2+} (see Scheme 31).

The situation is somewhat different with the 1,3-substituted aryl unit [143,144]. In this case, each (1- and 3-) position features strong weights of different frontier π - and π^* -orbitals of opposite phase (aryl MOs involving *meta*-positions are mutually orthogonal on the ring for symmetry reasons). These nodal properties on the 1- and 3-positions give rise to a negligible

overlap, hence resulting in no electron pairing. They are, however, largely co-extensive in space (non-disjoint) and lead usually to a dominant ferromagnetic interaction between the spins. In a classic VB representation, this situation leads to non-Kekulé VB structures for $\mathbf{8}^{2+}$, typical of a triplet GS (Scheme 35) [145]. Together with the fact that both unpaired electrons belong to topologically orthogonal magnetic orbitals, no new bond can be formed with these electrons in the singlet state. In this case, structural changes between the ground triplet isomer and the excited singlet isomer will be slight, and will essentially originate from electronic correlation effects, as indicated by the spectroscopic data gathered for $\mathbf{8}^{2+}$.

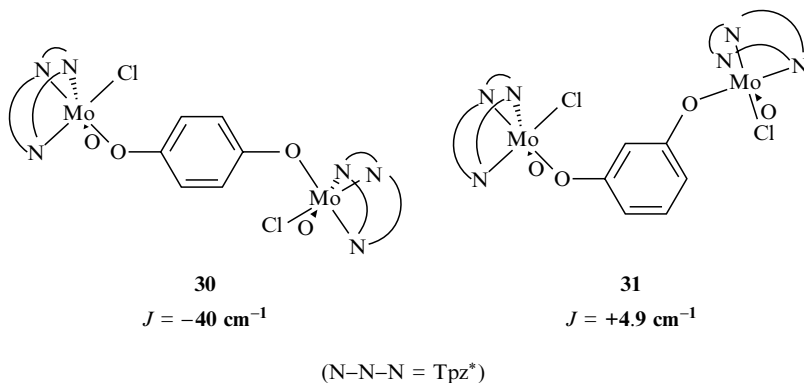
Qualitatively, DFT computations conducted on model complexes bearing $(\text{PH}_3)_2\text{CpFe}$ fragments ($\mathbf{7}^{2+}$ and $\mathbf{8}^{2+}$) with C_{2v} symmetry restrictions are in accordance with these expectations [103].³⁸ First, these calculations confirm that the SOMO has a strong d_{yz} character on each fragment in $\mathbf{7}^{2+}$ and $\mathbf{8}^{2+}$, in accordance with the X-ray data gathered for the monocationic parent $\mathbf{8}^+[\text{PF}_6^-]$ [146]. DFT calculations also confirm that the dication $\mathbf{7}^{2+}$ is diamagnetic and presents a quinoidal-like distortion of the central bridge, with a symmetric HOMO extending onto the complete $\text{Fe}-\text{C}\equiv\text{C}-1,4-(\text{C}_6\text{H}_4)-\text{C}\equiv\text{C}-\text{Fe}$ unit. On the other hand, the dication $\mathbf{8}^{2+}$ is predicted to present a paramagnetic GS with a typical aryl ring geometry in the bridge. Each SOMO of this compound is non-disjoint from the other, but exhibits negligible overlap, mostly because of the different phases of these magnetic orbitals. Thus, for this class of carbon-rich



Scheme 35

³⁸ DFT calculations performed on the $\mathbf{7}^{2+}[\text{PF}_6^-]_2$ dication model complex suggest a larger S/T gap. This appears, however, to be less probable with regard to the literature data, and considering that theoretical computations are often subject to inherent large uncertainties, we have decided to keep the lower J -value as the right one.

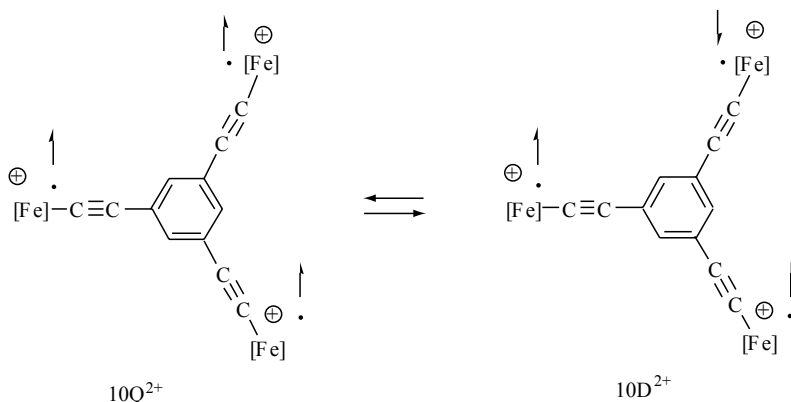
bridged ditopic organometallic diradicals, the GS might appear to be satisfactorily predicted by Ovchinnikov's rule applied to the $M(C_2)[Ar](C_2)M$ core. Taking into account the energetically close (HOMO - 1) perpendicular d_{xz} set of metal-based MOs on each capping fragment, a negligibly small rotation barrier can be computed for both complexes, as in the related case of 1,4-butadiene-diyl-bridged diradicals.



Very similar conclusions regarding the transmission of magnetic interactions through a central aromatic unit were recently reached by MacCleverty and co-workers on ditopic *inorganic* diradicals made from d^1 molybdenum(v) centers with bisphenate spacers [38]. As we can see from the structures of complexes **30** and **31**, the topology of the ligand in these inorganic diradicals influences also the coupling in the way predicted by Ovchinnikov's rule. The *para*-bisphenate bridge behaves as an antiferromagnetic coupler, whereas the *meta*-bisphenate constitutes a ferromagnetic coupler. Likewise, these results have been rationalized on a theoretical basis by a DFT study [147]. Similarly to the organoiron diradicals bridged by carbon-rich spacers presently being discussed, the magnetic interaction appears to mostly result from spin polarization of the π -electronic density on the bridging ligand.

4.3.6 Triradicals Featuring a 1,3,5-Phenylene Unit

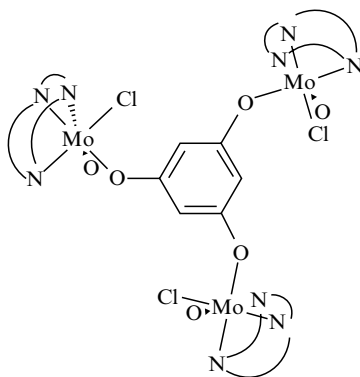
The trinuclear trication $10^{3+3}[PF_6^-]$ constituted the first *organometallic* tritopic triradical studied from the standpoint of magnetic interactions [103]. Its magnetic behavior is not different to that of related organic analogues [74,148]. In terms of magnetic orbitals, this can be rationalized similarly to the *meta*-dication 8^{2+} , extending the argument to the two *meta*-positions [149]. A high-spin quartet $10Q^{3+}$ is the GS in this case, and two degenerate doublet states ($10D^{3+}$) constitute the excited spin isomers (Scheme 36). Similarly to what was observed for the *meta*-dication 8^{2+} , the respective structures of the various spin



Scheme 36

isomers present only minor differences and retain the phenylalkynyl bridge structure present in lower oxidation states. This is supported by infrared spectroscopy, but also by Mössbauer data where the corresponding averaged QS value ($QS = 0.88 \text{ mm s}^{-1}$) matches fairly well that expected for pure iron(III) phenylalkynyls (see Table 3) [77,80].

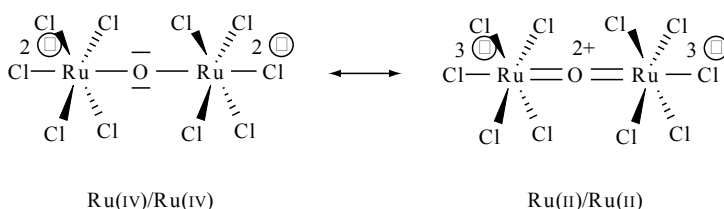
DFT calculations with the model trication bearing $(\text{PH}_3)_2\text{CpFe}$ fragments ($\mathbf{10}^{3+}$) and C_{3v} symmetry restrictions are in accordance with these expectations [103]. It is noteworthy that an overall very similar magnetic behavior is apparent in the related trisphenate–molybdenum(V) *inorganic* triradical **32**, based on EPR measurements [38].

**32**(N–N–N = Tp z^*)

4.4 SPIN-EXCHANGE-INDUCED STRUCTURAL CHANGES OF THE BRIDGING LIGAND

Organometallic architectures featuring metal centers linked by organic π networks currently generate much interest in the emerging field of molecular-scaled electronics [27–45]. It had been realized very early on that the ‘capability’ of a given bridge to convey an electronic interaction was strongly dependent on its actual structure in a given redox state (see Reference [19] and references cited therein). As a logical consequence, the structural changes of the bridging ligand between redox states have attracted considerable attention. Most often, the experimental observations could be rationalized by theoretical studies. However, with the exception of recent (DFT) studies, these investigations were usually semi-empirical approaches and remained confined to singlet (diamagnetic) spin surfaces. In the preceding section, we have indicated the existence of stable high-spin polynuclear open-shell species at room temperature for several representatives of this category of compounds, and discussed the influence of the magnetic exchange interaction on the structure of the carbon-rich spacer.

Considerations regarding the influence of the magnetic exchange on the structure of the bridging ligand in a dinuclear metal-centered polyradical are not recent. As early as 1953, in an attempt to rationalize the unusual linear structure and the diamagnetism of $[(\text{Ru}_2\text{Cl}_{10}\text{O})^{4-} 4\text{K}^+] \cdot \text{H}_2\text{O}$ (**33**⁴⁻), Dunitz and Orgel invoked an antiferromagnetic superexchange coupling between the unpaired spins located on the paramagnetic ruthenium(IV) centers through the oxygen atom [150]. Based on group symmetry and MO considerations, they invoked antiferromagnetic superexchange and proposed that the bridge structure resulted from resonance between the two extremes $(\text{Cl}_5\text{Ru}^{\text{IV}}-\text{O}-\text{Ru}^{\text{IV}}\text{Cl}_5)^{4-}$ and $(\text{Cl}_5\text{Ru}^{\text{II}}=\text{O}^{2+}=\text{Ru}^{\text{II}}\text{Cl}_5)^{4-}$ singlet VB structures.

33⁴⁻

More generally, for a given redox state, this present contribution shows that the redox-induced changes within redox parents (see, for instance, Schemes 21 and 29 above) are in fact largely determined by the nature of the magnetic GS in any (formal) diradical state. Thus, the existence of spin isomers should be systematically taken into consideration when the theoretical rationalization of

experimental data is sought.³⁹ In most cases, the diamagnetic singlet isomer corresponds to the GS and therefore the VB structures derived from MO calculations within the singlet surface for a given polynuclear organometallic complex with carbon-rich spacer(s) are usually correct. We have nevertheless identified several cases, such as species **17**, where the situation is not so simple. In addition, with organometallic complexes featuring $[(\eta^2\text{-diphos})(\eta^5\text{-C}_5\text{Me}_5)\text{Fe}]^+$ end-groups, relatively small S/T gaps have been found in the corresponding organoiron polycations. As a result, several spin states are populated at 20 °C and spin transitions take place between spin-isomers of different structures. Moreover, these spin interconversions can be quite fast ($> 10^{-6}$ s, even in the solid state, as demonstrated by Mössbauer spectroscopy). Thus, any chemist intending to exploit the physico-chemical properties exhibited by such organometallic assemblies has to take account of possible spin equilibria. This becomes particularly true when weak intramolecular magnetic interactions take place. In such a case, for redox states presenting a potential polyradical character, the macroscopic properties measured at a given temperature are in fact a weighted average of those pertaining to each spin-isomer.

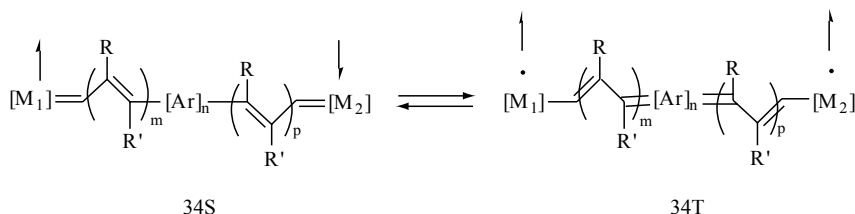
For most organometallic polynuclear d^n-d^n ditopic diradicals bridged by carbon-rich spacers, another interesting issue raised by this contribution is that the nature of the GS (and therefore the structure of the bridge) can be predicted by using a simple topological rule such as the ‘Ovchinnikov rule’. This is particularly true for the organoiron complexes $\mathbf{1}^{2+}-\mathbf{10}^{3+}$, but also for many related organometallic polyradicals characterized to date (see Sections 3 and 4, and also Reference [38]). This statement constitutes an interesting observation since Ovchinnikov’s rule, initially derived for organic alternant hydrocarbon polyradicals [53], proved often of limited validity when heteroatoms were incorporated in alternant hydrocarbon structures [55]. It also confirms that in these complexes, the magnetic interaction is most probably transmitted via spin-polarization of the π -manifold [147]. Accordingly, with $\mathbf{1}^{2+}-\mathbf{10}^{3+}$ and related complexes featuring d^5 piano-stool end-groups, calculations suggest that the frontier metal-based d-orbitals and the π -manifold of the bridging ligand interact strongly and might be envisaged as a new organometallic ‘pseudo’-alternant system incorporating metal centers at its ends [151]. The particular behavior of these carbon-rich ligands relative to more classic inorganic dative ligands can be traced to the low electronegativity of sp- and sp^2 -carbon atoms relative to elements such as oxygen or nitrogen, favoring stronger bonding with the iron metal. More generally, considering the M–(Bridge)–M core as a pseudo-alternant system, it seems that Ovchinnikov’s rule might be applicable for deriving the GS of any related organometallic di- or triradical *provided that the metal-based SOMO of each capping fragment*

³⁹ The observed structural changes, when proceeding from a neutral to a dicationic singlet GS (i.e. antiferromagnetic exchange coupling) can be envisaged to result both from the magnetic superexchange and from the removal of two metal-centered electrons in two antibonding bridge-based electrons.

interacts significantly with the bridge-based π or π^* frontier MOs, and also provided that the interaction takes place with the same π -manifold. In this respect, compound **17** is in opposition with such an approach, essentially because the second condition is not verified (i.e. each unpaired spin can be delocalized in a different π -manifold). Thus, organometallic complexes featuring all-carbon bridges can ‘escape’ the application of Ovchinnikov’s rule in some cases, because of the particular structure of the all-carbon spacers, which present two energetically degenerate and perpendicular π -manifolds [145].

Finally, the dependence of the rate of exchange between spin-isomers, as well as the dependence on the magnetic exchange coupling ($J = 1/2\Delta E_{S/T}$ for diradicals) on structural or electronic factors are presently not well understood and thus justify further investigations. Typically, organometallic dinuclear complexes with unsaturated carbon-rich bridges of increasing length attract more and more attention as potential molecular assemblies for conveying electronic interactions over nano-sized distances [19,45]. For complexes with metal-centered HOMOs, the magnitude of any exchange coupling between electrons residing on terminal sites is expected to decrease upon bridge elongation, as illustrated by the tentative empirical equation (12) [105]. Thus, for longer-chain analogues, even when a diamagnetic GS is expected, the excited spin states will become more and more thermally accessible at 20 °C. This possibility should seriously be taken into consideration when new compounds of this type are being synthesized, with respect to their reactivity (kinetic stability), but also regarding their physico-chemical properties.

In this respect, several d^n-d^n bis-carbene complexes with conjugated bridges presenting structures such as that of species **34** ($[M_1]$, $[M_2]$ = metal complexes; R, R' = substituents; [Ar] = (hetero)aryl group, $n = 0-2$; $m+p = 2-4$) are known. While these complexes usually correspond to stable and diamagnetic molecules for short bridges, they may exhibit more and more diradical (paramagnetic) character upon bridge elongation.



Scheme 37

5 CONCLUSIONS

Organometallic metal-centered polyradicals bridged by carbon-rich ligands constitute a growing class of compounds, for which much still remains to be

learnt, especially regarding the ability of such bridges to convey the magnetic interaction between metal-centered spins. While it might be argued that the metal–carbon bond constitutes just a particular case of the dative bond in coordination complexes, for which the magnetism has been fairly well studied up until now, it is worth recalling that, in contrast with the dative bond, it often possesses significant covalent character, especially with first-row middle-to-late transition metals. This property, associated with the known structural flexibility of metal–carbon bonds, when unsaturated or conjugated ligands are considered, allows for an efficient mediation of the exchange interaction between remote spin carriers. In this respect, polynuclear assemblies of metal-centered radicals connected by carbon-rich bridges are, on their own, certainly worth further detailed investigations. Most of the present magnetic measurements with such polyradicals proved the existence of a singlet GS and low S/T gaps in the case of organoiron derivatives $\mathbf{1}^{2+} - \mathbf{10}^{3+}$. Experimental determination of the gap, when possible, is decisive in obtaining a much better insight regarding the temperature-dependent structural properties of the bridging units. Moreover, precise knowledge of the structural factors influencing the S/T gap in this class of compounds might become crucial when isolation and study of homologues featuring bridges of increasing lengths is being sought.

For many of these organometallic polytopic polyradicals, the GS can be predicted by using rules developed for alternant hydrocarbons, such as Ovchinnikov's rule. In this respect, as a spin carrier, the paramagnetic ($S = 1/2$) fragment $[(\eta^2\text{-dppe})(\eta^5\text{-C}_5\text{Me}_5)\text{Fe}]^+$ appears quite well behaved. The unpaired d-electrons belonging to the metal center in such assemblies might then be considered to present a non-negligible interaction with the π -manifold of the bridging ligand. Alternatively, the $[(\eta^2\text{-dppe})(\eta^5\text{-C}_5\text{Me}_5)\text{Fe}]^+$ end-group constitutes also a good probe for exploring the magnetic properties of a given carbon-rich spacer, in particular because of its Mössbauer activity, which allows us to gather important information on the kinetics of the spin-transition process in the solid state. Much remains to be learnt in this specific domain, as well.

Finally, it is worth recalling that the magnetic exchange interaction in polyradical complexes is not really distinct from the electron-transfer event in the corresponding MV complexes. (Accordingly, it appears as an efficient way to convey information from one site of the molecule to the other.) More generally, intramolecular modulation of the magnetic interaction has given rise to increasing attention at this present time. Envisaged from this standpoint, the bistability or multi-stability phenomena associated with magnetic coupling in organometallic carbon-rich polyradicals make such compounds interesting building blocks. While much remains to be done to approach those far-reaching goals ('dreams'?), like, for example, the realization of nanoscopic devices which allow the processing of information at the molecular level, a necessary prerequisite is nevertheless to improve the understanding of the basic mechanisms underlying the site-to-site electronic communication in simple model compounds, and also to gather more and more data on these compounds.

6 ACKNOWLEDGEMENTS

We are very grateful to Dr J.-F. Halet and Professor M. I. Bruce for helpful comments and fruitful discussions.

7 REFERENCES

1. J. B. Goodenough, *Magnetism and the Chemical Bond*, Wiley, New York, 1963.
2. P. W. Anderson, *Phys. Rev.*, **115**, 2 (1959).
3. C. Kollmar and O. Kahn, *Acc. Chem. Res.*, **26**, 259 (1993).
4. J. S. Miller, A. J. Epstein and W. M. Reiff, *Chem. Rev.*, 201 (1988).
5. A. Rajca, *Chem. Rev.*, 871 (1994).
6. H. Iwamura, *Pure Appl. Chem.*, **65**, 57 (1993).
7. D. A. Dougherty, *Acc. Chem. Res.*, **24**, 88 (1991).
8. H. Iwamura, in *Advances in Physical Organic Chemistry*, Vol. 26, H. Iwamura (Ed.), Academic Press, London, 1990, pp. 179–253.
9. J. S. Miller, *Inorg. Chem.*, **39**, 4392 (2000).
10. O. Kahn, *Acc. Chem. Res.*, **33**, 647 (2000).
11. O. Kahn, *Magnetism, a Supramolecular Function*, Kluwer Academic Publishers, Dordrecht, The Netherlands, 1996.
12. H. Iwamura, K. Inoue and T. Hayamizu, *Pure Appl. Chem.*, **68**, 243 (1996).
13. D. Gatteschi, *Adv. Mater.*, **6**, 635 (1994).
14. J. S. Miller and A. J. Epstein, *Angew. Chem., Int. Ed. Engl.*, **33**, 385 (1994).
15. D. Gatteschi, A. Caneschi, L. Pardi and R. Sessoli, *Science*, **265**, 1054 (1994).
16. O. Kahn, Y. Pei and Y. Journaux (Eds), *Inorganic Materials*, Wiley, Chichester, UK, 1991.
17. O. Kahn, *J. Chim. Phys.*, **85**, 1113 (1988).
18. A. Caneschi, D. Gatteschi and R. Sessoli, *Acc. Chem. Res.*, **22**, 392 (1989).
19. F. Paul and C. Lapinte, *Coord. Chem. Rev.*, **178/180**, 427 (1998).
20. N. Le Narvor, L. Toupet and C. Lapinte, *J. Am. Chem. Soc.*, **117**, 7129 (1995).
21. N. Le Narvor and C. Lapinte, *C. R. Séances Acad. Sci., Tl, Ser. IIC*, 745 (1998).
22. M. I. Bruce, L. I. Denisovich, P. J. Low, S. M. Peregudova and N. A. Ustynyuk, *J. Chem. Soc., Mendeleev Commun.*, 200 (1996).
23. M. Guillemot, L. Toupet and C. Lapinte, *Organometallics*, **17**, 1928 (1998).
24. M. I. Bruce, P. J. Low, K. Costuas, J. F. Halet, S. P. Best and G. H. Heath, *J. Am. Chem. Soc.*, **122**, 1949 (2000).
25. F. Paul, W. Meyer, H. Jiao, L. Toupet, J. A. Gladysz and C. Lapinte, *J. Am. Chem. Soc.*, **122**, 9405 (2000).
26. M. H. Chisholm, *Angew. Chem., Int. Ed. Engl.*, **30**, 673 (1991).
27. W. Beck, B. Niemer and M. Wieser, *Angew. Chem., Int. Ed. Engl.*, **32**, 923 (1993).
28. H. Lang, *Angew. Chem. Int. Ed. Engl.*, **33**, 547 (1994).
29. R. J. Crutchley, *Adv. Inorg. Chem.*, **41**, 273 (1994).
30. M. Akita and Y. Moro-Oka, *Bull. Chem. Soc. Jpn.*, **68**, 420 (1995).
31. N. J. Long, *Angew. Chem., Int. Ed. Engl.*, **34**, 21 (1995).
32. J. Manna, K. D. John and M. D. Hopkins, *Adv. Organomet. Chem.*, **38**, 80 (1995).
33. M. D. Ward, *M. D. Chem. Ind.*, 568 (1996).
34. U. H. F. Bunz, *Angew. Chem., Int. Ed. Engl.*, **35**, 969 (1996).
35. F. Barigelletti, L. Flamigni, J.-P. Collin and J.-P. Sauvage, *J. Chem. Soc., Chem. Commun.*, 333 (1997).
36. M. I. Bruce, *Coord. Chem. Rev.*, **166**, 91 (1997).

37. R. Ziessel, M. Hissler, A. El-gayhoury and A. Harriman, *Coord. Chem. Rev.*, **178–180**, 1251 (1998).
38. J. A. MacCleverty and M. D. Ward, *Acc. Chem. Res.*, **31**, 842 (1998).
39. V. W.-W. Yam, K. K.-W. Lo, and K. M.-C. Wong, *J. Organomet. Chem.*, **578**, 3 (1999).
40. P. F. H. Schwab, M. D. Levin and J. Michl, *Chem. Rev.*, 1863 (1999).
41. R. E. Martin and F. Diederich, *Angew. Chem., Int. Ed. Engl.*, **38**, 1351 (1999).
42. R. Ziessel, *Synthesis*, 1865 (1999).
43. W. Kaim, A. Klein and M. Glöckle, *Acc. Chem. Res.*, **33**, 755 (2000).
44. J. M. Tour, *Acc. Chem. Res.*, **33**, 791 (2000).
45. V. Bazani (Ed), *Electron Transfer in Chemistry*, Vol. 5, Wiley-VCH, Weinheim, 2001, pp. 3–47.
46. S. Kheradmandan, K. Heinze, H. Schmalke and H. Berke, *Angew. Chem., Int. Ed. Engl.*, **38**, 2270 (1999).
47. R. Dembinski, T. Bartik, B. Bartik, M. Jaeger and J. A. Gladysz, *J. Am. Chem. Soc.*, **122**, 810 (2000).
48. O. Kahn, *Molecular Magnetism*, VCH, New York, 1993.
49. W. T. Borden, H. Iwamura and J. A. Berson, *Acc. Chem. Res.*, **27**, 109 (1994).
50. W. T. Borden and E. R. Davidson, *J. Am. Chem. Soc.*, **99**, 4587 (1977).
51. A. O. Ovchinnikov, *Theor. Chim. Acta (Berlin)*, **47**, 297 (1978).
52. D. J. Klein, *J. Chem. Phys.*, **77**, 3098 (1982).
53. D. J. Klein, C. J. Nelin, S. Alexander and F. R. Matsen, *J. Chem. Phys.*, **77**, 3101 (1982).
54. D. E. Seeger, P. M. Lahti, A. R. Rossi and J. A. Berson, *J. Am. Chem. Soc.*, **108**, 1251 (1986).
55. A. P. West, Jr, S. K. Silverman and D. A. Dougherty, *J. Am. Chem. Soc.*, **118**, 1452 (1996).
56. W. T. Borden (Ed.), *Diradicals*, Wiley-Interscience, New York, 1982.
57. W. T. Borden, *Mol. Cryst., Liq. Cryst.*, **232**, 195 (1993).
58. J. Michl, *Acc. Chem. Res.*, **23**, 127 (1990).
59. G. W. Wheland, *Resonance in Organic Chemistry*, Wiley, New York, 1995.
60. J. March, *Advanced Organic Chemistry. Reactions, Mechanisms and Structures*, 4th Edn, Wiley, New York, 1992.
61. J. Thiele and H. Balhorn, *Chem. Ber.*, **37**, 1463 (1904).
62. A. E. Tschitschibabin, *Chem. Ber.*, **40**, 1810 (1907).
63. L. K. Montgomery, J. C. Huffman, E. A. Jurczak and M. P. Grendze, *J. Am. Chem. Soc.*, **108**, 6004 (1986).
64. M. S. Platz, *Diradicals*, Wiley-Interscience, New York, 1982.
65. G. N. La Mar, D. Horrocks and R. Holm, *NMR of Paramagnetic Molecules*, Academic Press, New York, 1973.
66. V. Clementi and C. Luchinat, *Acc. Chem. Res.*, **31**, 351 (1998).
67. I. Bertini, C. Luchinat, F. Mani and A. Scozzafava, *Inorg. Chem.*, **19**, 1333 (1980).
68. D. F. Evans, *J. Chem. Soc.*, 2003 (1959).
69. S. K. Sur, *J. Magn. Res.*, **82**, 169 (1989).
70. E. M. Schubert, *J. Chem. Educ.*, **69**, 62 (1992).
71. R. S. Drago, *Physical Methods in Chemistry*, W. B. Saunders Publishing Company, Philadelphia, PA, 1977.
72. J. S. Miller, *Adv. Mater.*, **6**, 322 (1994).
73. B. Bleaney and K. D. Bowers, *Proc. R. Soc. London, A*, **214**, 451 (1952).
74. F. Kanno, K. Inoue, N. Koga and H. Iwamura, *J. Phys. Chem.*, **97**, 13267 (1993).
75. H. Iwamura and N. Koga, *Acc. Chem. Res.*, **26**, 346 (1993).
76. N. N. Greenwood, *Mössbauer Spectroscopy*, Chapman & Hall, London, 1971.

77. V. Guillaume, P. Thominox, F. Coat, A. Mari and C. Lapinte, *J. Organomet. Chem.*, **565**, 75 (1998).
78. N. G. Connelly, M. P. Gamasa, J. Gimeno, C. Lapinte, E. Lastra, J. P. Maher, N. Le Narvor, A. L. Rieger and P. H. Rieger, *J. Chem. Soc., Dalton Trans.*, 2775 (1993).
79. P. H. Rieger, *Coord. Chem. Rev.*, **135/136**, 203 (1994).
80. R. Denis, L. Toupet, F. Paul and C. Lapinte, *Organometallics*, **19**, 4240 (2000).
81. D. R. Neithamer, R. E. La Pointe, R. A. Wheeler, D. S. Richeson, G. D. Van Duyne and P. T. Wolczanski, *J. Am. Chem. Soc.*, **111**, 9056 (1989).
82. K. G. Caulton, R. H. Cayton, M. H. Chisholm, J. C. Huffman, E. B. Lobkovsky and Z. Xue, *Organometallics*, **11**, 321 (1992).
83. P. Belanzoni, N. Re, M. Rosi, A. Sgamellotti and C. Floriani, *Organometallics*, **15**, 4264 (1996).
84. K. Costuas, F. Paul, J.-F. Halet and C. Lapinte, work in progress.
85. K. Costuas and J.-Y. Saillard, *Organometallics*, **18**, 2505 (1999).
86. J. E. MacGrady, T. Lovell, R. Stranger and M. G. Humphrey, *Organometallics*, **16**, 4004 (1997).
87. B. E. R. Schilling, R. Hoffmann and D. L. Lichtenberger, *J. Am. Chem. Soc.*, **101**, 585 (1979), and references cited therein.
88. C. Roger, P. Hamon, L. Toupet, H. Rabaâ, J.-Y. Saillard, J.-R. Hamon and C. Lapinte, *Organometallics*, **10**, 1045 (1991).
89. M. I. Bruce, *Chem. Rev.*, 2797 (1998).
90. M. I. Bruce, *Chem. Rev.*, 197 (1991).
91. J. Zarembowitch and O. Kahn, *New J. Chem.*, **15**, 181 (1991).
92. J. Kröber, E. Codjovi, O. Kahn, F. Groliere and C. Jay, *J. Am. Chem. Soc.*, **115**, 9810 (1993).
93. S. Hayami, K. Inoue, S. Osaki and Y. Maeda, *Chem. Lett.*, 987 (1998).
94. J.-F. Létard, J. A. Real, N. Moliner, A. B. Gaspar, O. Capes, O. Cador and O. Kahn, *J. Am. Chem. Soc.*, **121**, 10630 (1999).
95. M. Brady, W. Weng, Y. Zhou, J. W. Seyler, A. J. Amoroso, A. M. Arif, M. Böhme and J. A. Gladysz, *J. Am. Chem. Soc.*, **119**, 775 (1997).
96. B. C. Bunker, R. S. Drago, D. N. Hendrickson, R. M. Richman and S. L. Kessel, *J. Am. Chem. Soc.*, **100**, 3805 (1978).
97. S. Le Stang, F. Paul and C. Lapinte, *Organometallics*, **19**, 1035 (2000).
98. N. Le Narvor and C. Lapinte, *J. Chem. Soc., Chem. Commun.*, 357 (1993).
99. M. Guillemot, unpublished results, University of Rennes 1, 1998.
100. V. Guillaume, V. Mahias, A. Mari and C. Lapinte, *Organometallics*, **19**, 1422 (2000).
101. V. Morvan-Mahias, unpublished results, University of Rennes 1, 1997.
102. N. Le Narvor and C. Lapinte, *Organometallics*, **14**, 634 (1995).
103. T. Weyland, K. Costuas, A. Mari, J.-F. Halet and C. Lapinte, *Organometallics*, **17**, 5569 (1998).
104. S. Le Stang, unpublished results, University of Rennes 1, 2000.
105. R. E. Coffman and G. R. Buettner, *J. Phys. Chem.*, **83**, 2387 (1979).
106. M. A. S. Aquino, F. L. Lee, E. J. Gabe, C. Bensimon, J. E. Greedan and R. J. Crutchley, *J. Am. Chem. Soc.*, **114**, 5130 (1992).
107. M. L. Naklicki and R. J. Crutchley, *J. Am. Chem. Soc.*, **116**, 6045 (1994).
108. M. L. Naklicki, C. A. White, L. L. Plante, C. E. B. Evans and R. J. Crutchley, *Inorg. Chem.*, **37**, 1880 (1998).
109. G. Kreisel, P. Scholz and W. Seidel, *Z. Anorg. Allg. Chem.*, **460**, 51 (1980).
110. R. E. La Pointe, P. T. Wolczanski and J. F. Mitchell, *J. Am. Chem. Soc.*, **101**, 6382 (1986).

111. P. Binger, P. Müller, P. Phillips, B. Gabor, R. Minott, A. T. Herrmann, F. Langhauser and C. Krüger, *Chem. Ber.*, **125**, 2209 (1992).
112. F. de Angelis, N. Re, M. Rosi, A. Sgamellotti and C. Floriani, *J. Chem. Soc., Dalton Trans.*, 3841 (1997).
113. T. Bartik, R. Dembinski, B. Bartik, A. M. Arif and J. A. Gladysz, *New J. Chem.*, **21**, 739 (1997).
114. M. Bruce, B. G. Ellis, B. W. Skelton and A. H. White, personal communication, 2000.
115. R. Poli, *Chem. Rev.*, 2135 (1996).
116. N. L. Ma and M. W. Wong, *Angew. Chem. Int. Ed. Engl.*, **37**, 3402 (1998).
117. H. Jiao, K. Costuas, J. A. Gladysz, J. F. Halet, L. Toupet, F. Paul and C. Lapinte, work in progress.
118. P. Belanzoni, N. Re, A. Sgamellotti and C. Floriani, *J. Chem. Soc., Dalton Trans.*, 1825 (1998).
119. B. E. R. Schilling, R. J. Hoffmann and J. W. Faller, *J. Am. Chem. Soc.*, **101**, 592 (1979).
120. J. W. Lauer and R. J. Hoffmann, *J. Am. Chem. Soc.*, **98**, 1729 (1976).
121. M. B. Sponsler, *Organometallics*, **14**, 1920 (1995).
122. N. Re, A. Sgamellotti and C. Floriani, *Organometallics*, **15**, 5330 (1996).
123. N. Re, A. Sgamellotti and C. Floriani, *J. Chem. Soc., Dalton Trans.*, 2521 (1998).
124. A. Zweig and A. K. Hoffmann, *J. Org. Chem.*, **84**, 3278 (1962).
125. B. A. Etzenhouser, Q. Chen and M. B. Sponsler, *Organometallics*, **13**, 4176 (1994).
126. A. Rabier, N. Lugan, R. Mathieu and G. L. Geoffroy, *Organometallics*, **13**, 4676 (1994).
127. R. Choukroun, C. Lorber, B. Donnadiou, B. Henner, R. Frantz and C. Guerin, *J. Chem. Soc. Chem. Commun.*, 1099 (1999).
128. F. H. Köhler, P. Hofmann and W. Prössdorf, *J. Am. Chem. Soc.*, **103**, 6359 (1981).
129. M. Sato, Y. Kawata, A. Kudo, A. Iwai, H. Saitoh and S. Ochai, *J. Chem. Soc., Dalton Trans.*, 2215 (1998).
130. M. Sato, A. Kudo, Y. Kawata and H. Saitoh, *J. Chem. Soc., Chem. Commun.*, 25 (1996).
131. S. Barlow and S. R. Marder, *J. Chem. Soc., Chem. Commun.*, 1555 (2000).
132. P. Karafiloglou, *J. Chem. Phys.*, **82**, 3728 (1984).
133. C. Stroh, P. Turek and R. Ziessel, *J. Chem. Soc., Chem. Commun.*, 2337 (1998).
134. L. C. Bush, R. B. Health and J. A. Berson, *J. Am. Chem. Soc.*, **115**, 9830 (1993).
135. J. A. Berson, *Acc. Chem. Res.*, **30**, 238 (1997).
136. T. Tsutsui, N. Ely and A. Gebala, *Inorg. Chem.*, **14**, 78 (1975).
137. F. Paul and C. Lapinte, work in progress.
138. T. Mitsumori, K. Inoue, N. Koga and H. Iwamura, *J. Am. Chem. Soc.*, **117**, 2467 (1995).
139. A. Rajca, J. Wongsriratanakul and S. Rajca, *J. Am. Chem. Soc.*, **119**, 11674 (1997).
140. A. Rajca, S. Rajca and S. R. Desai, *J. Am. Chem. Soc.*, **117**, 806 (1995).
141. S. Utamapanya, A. Rajca and S. Tayumanavan, *J. Am. Chem. Soc.*, **114**, 1884 (1992).
142. N. A. Richardson and M. B. Hall, *Organometallics*, **12**, 1338 (1993).
143. K. Yoshizawa and R. Hoffmann, *Chem. Eur. J.*, **7**, 403 (1995).
144. K. Yoshizawa and R. Hoffmann, *J. Am. Chem. Soc.*, **117**, 6921 (1995).
145. H. C. Longuet-Higgins, *J. Chem. Phys.*, **18**, 265 (1950).
146. T. Weyland, K. Costuas, L. Toupet, J.-F. Halet and C. Lapinte, *Organometallics*, **19**, 4228 (2000).
147. A. Bencini, D. Gatteschi, F. Totti, D. N. Sanz, J. A. MacClevarty and M. D. Ward, *J. Phys. Chem.*, **A**, **102**, 10545 (1998).

148. H. Tomioka, M. Hattori, K. Hirai, K. Sato, D. Shiomi, T. Takui and K. Itoh, *J. Am. Chem. Soc.*, **120**, 1106 (1998).
149. K. Yoshizawa, M. Hatanaka, Y. Matsuzaki, K. Tanaka and T. Yamabe, *J. Chem. Phys.*, **100**, 4453 (1994).
150. J. D. Dunitz and L. E. Orgel, *J. Chem. Soc.*, 2594 (1953).
151. D. L. Lichtenberger and S. K. Renshaw, *Organometallics*, **12**, 3522 (1993).
152. F. Coat, M.-A. Guillevic, L. Toupet, F. Paul and C. Lapinte, *Organometallics*, **16**, 5988 (1997).
153. F. Coat, M. Guillemot, F. Paul and C. Lapinte, *J. Organomet. Chem.*, **578**, 76 (1999).
154. F. Paul and C. Lapinte, unpublished results.

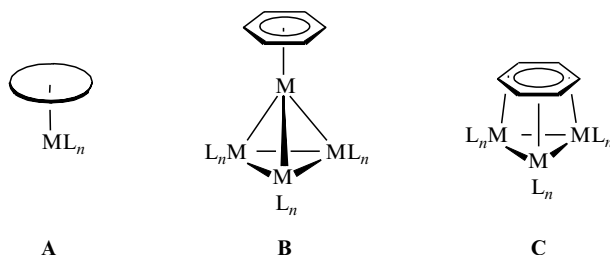
7 Molecular Cluster Complexes with Facial Arene Ligands

HUBERT WADEPOHL

Anorganisch-Chemisches Institut der Ruprecht-Karls-Universität, Im Neuenheimer Feld 270, D-69120 Heidelberg, Germany

1 INTRODUCTION

Metal clusters [1] are the smallest chemical entities which offer a two-dimensional metal 'surface' for the bonding of ligands. This forms the basis of the so-called cluster-surface analogy, which more than 20 years ago was stated as 'a proposition that discrete molecular metal clusters may be reasonable models of metal surfaces in the processes of chemisorption and catalysis' [2]. It is their potential for aromaticity and antiaromaticity which makes the cyclic π -perimeters C_nH_n special in organic chemistry. An important branch of organometallic chemistry has developed based on the sometimes dramatic modification of the properties of a cyclic conjugated π -system upon complexation to a transition metal [3]. Some of the very classic systems in organo-transition metal chemistry, e.g. the sandwich complexes $[(\eta-C_5H_5)_2Fe]$, $[(\eta-C_6H_6)_2Cr]$ and $[(\eta-C_8H_8)_2U]$, indeed result from the central η^n -bonding (A) of C_nH_n to the metal atom. Because of their ubiquity in organic chemistry, the archetypal aromatic molecule, benzene ($n = 6$), and its derivatives are the most important.



In a study of the interaction of organic molecules with metal clusters, the cyclic π -perimeters also deserve special attention. Again, benzene must be the

archetypal molecule. Benzene may be attached in an *apical* fashion to the cluster, via central bonding to one metal atom (an *apex* of the metal cluster, e.g. **B**). Notwithstanding it being potentially somewhat different from that in a mononuclear complex, this type of bonding can qualitatively still be considered a minor modification of bonding type **A**. However, a new quality comes into play with the face-capping (or *facial*) bonding mode **C**, where interaction of the π -system is with a two-dimensional array of (at least three) metal atoms (a *face* of the metal cluster). In terms of the cluster–surface analogy, molecular cluster complexes with facial C_nH_n ligands are a first approximation to the adsorption states of C_nH_n on metal surfaces, which are of considerable scientific and technical interest [4].

Even the essentially flat close-packed surfaces of single metal crystals offer a variety of adsorption sites, which may differ in ‘nuclearity’, i.e. the number of metal atoms simultaneously interacting with the adsorbate, and/or symmetry. For example, benzene has been found in ‘on top’, ‘hollow’ and ‘bridge’ sites (Figure 1) [5]. It has been shown that this molecule is mobile on the surface, and that certain adsorption states are greatly stabilized by the presence of other (co-) adsorbates, e.g. carbon monoxide [6].

In molecular cluster complexes, the number of possible coordination sites is much more limited, due to the small number of metal atoms. In addition, other ligands are invariably present and will have an influence on the coordination mode of the organic substrate.

Although facial benzene was unequivocally established for the first time no more than 15 years ago, a large number of organometallic cluster complexes with facial arenes is now known [7]. In this contribution, we will focus on the

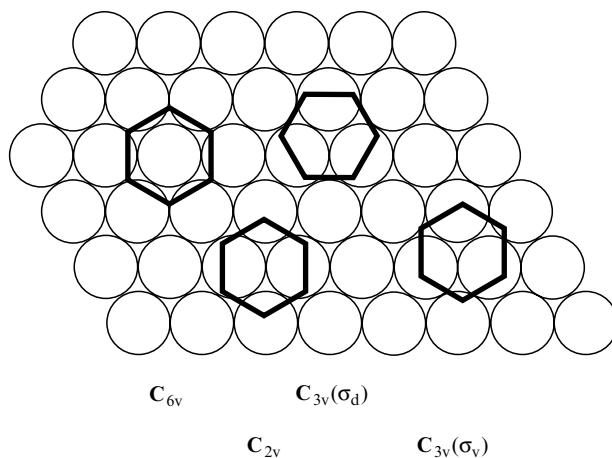


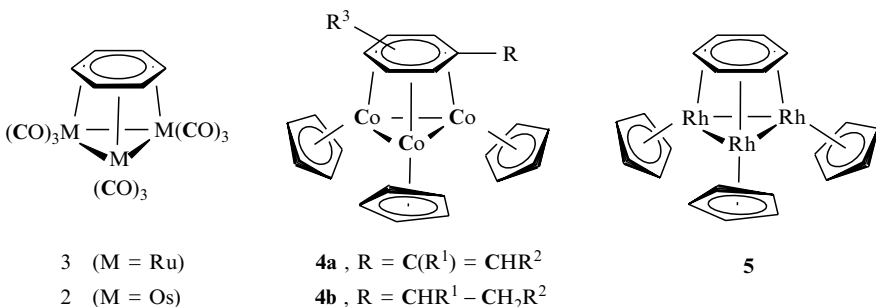
Figure 1 Adsorption sites for benzene on a close-packed metal surface, showing the ‘on top’ (C_{6v}), ‘bridge’ (C_{2v}) and two types of ‘hollow’ (C_{3v}) sites

scope of known systems without attempting any exhaustive coverage. Special emphasis will be placed on the properties of the facial arenes, namely their molecular and electronic structures, dynamic behaviour and chemical reactivity.

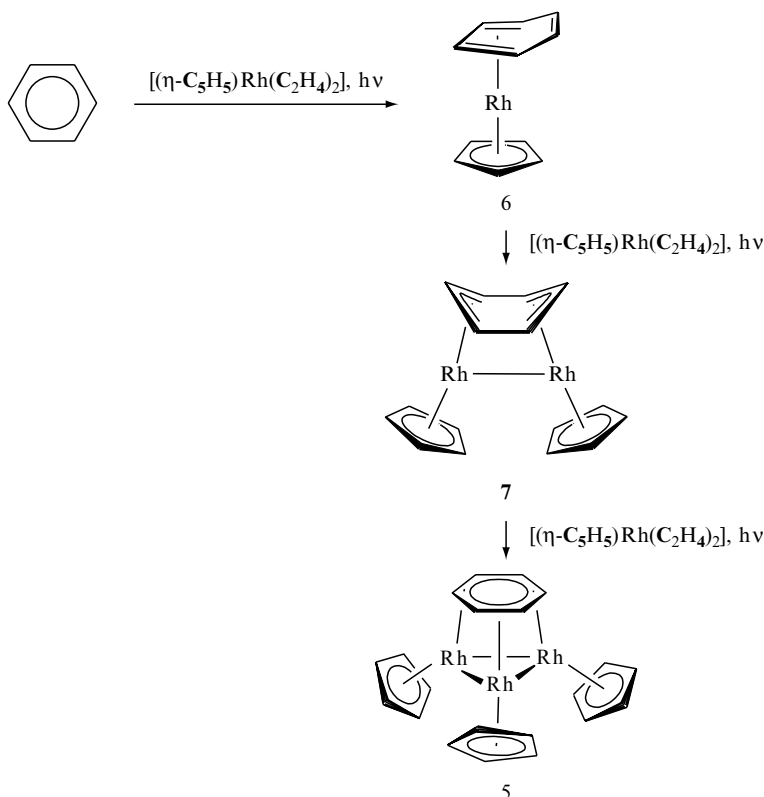
2 SYNTHESSES

Molecular cluster complexes with facial benzene and substituted benzene ligands fall into several types. Here, it will be convenient to distinguish two general classes, based on the type of cluster frame, which may be an oligonuclear carbonyl metal $M_n(\text{CO})_m$ or cyclopentadienyl metal $M_n(\eta\text{-C}_5\text{R}_5)_m$ fragment. In the first group, the nuclearity ranges from 3 up to a maximum of 9, while only trinuclear complexes are known in the second series. This directly reflects the spatial requirements of the 'ancillary' ligands (CO and C_5R_5 , respectively) on the cluster 'surface', and emphasizes the importance of steric factors for facial arene bonding.

A facial benzene ligand was suggested for the first time in the unstable cation $[\text{Os}_3(\text{CO})_9(\text{H})(\text{C}_6\text{H}_6)]^+$ (**1**) [8] and was later proven by an X-ray crystallographic study of its deprotonation product $[\text{Os}_3(\text{CO})_9(\mu_3\text{-C}_6\text{H}_6)]$ (**2**) [9]. The corresponding triruthenium derivative $[\text{Ru}_3(\text{CO})_9(\mu_3\text{-C}_6\text{H}_6)]$ (**3**) has also been prepared [10]. Complexes of the type $[\{(\eta\text{-C}_5\text{R}_5)\text{M}\}_3(\mu_3\text{-arene})]$ e.g. **4** ($\text{M} = \text{Co}$) [11–16], and **5** ($\text{M} = \text{Rh}$) [17] (arene = benzene or substituted-benzene derivative), are close analogues of the Ru_3 and Os_3 complexes, having iso-valence-electronic ($L_n\text{M}$)₃ cluster frames.



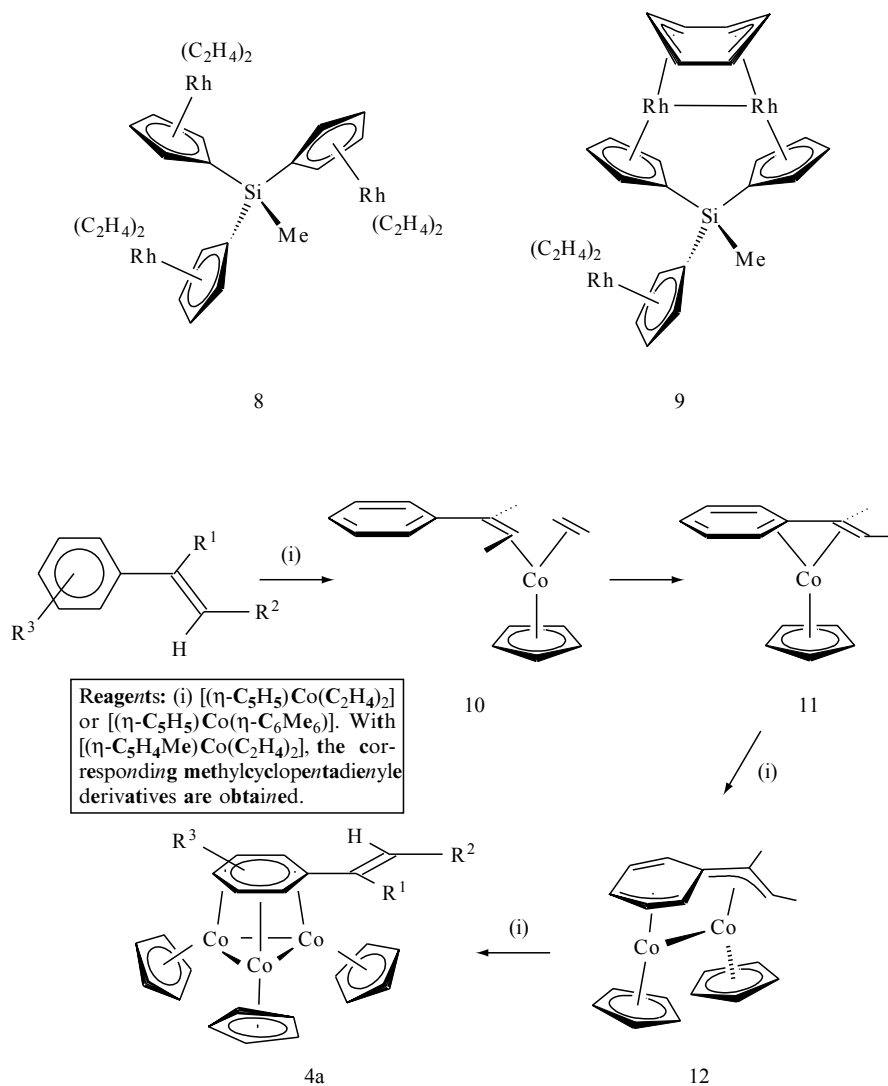
Despite the many similarities of complexes **2–5**, the synthetic routes leading to them are rather different. The perhaps most straightforward pathway, i.e. stepwise addition of three mononuclear metal fragments to the arene, is only feasible for $[\{(\eta\text{-C}_5\text{H}_5)\text{Rh}\}_3(\mu_3\text{-C}_6\text{H}_6)]$ (**5**) (Scheme 1).



Scheme 1

Here, formation of the mononuclear complex **6** is the crucial step, which results in a loss of aromaticity of the η^4 -coordinated benzene. The μ_2 - and μ_3 -benzene complexes **7** and **5**, respectively, are formed in very low yield. The efficiency of the second step of the reaction (formation of the μ_2 -benzene complex **7**) is greatly improved when the 'chelating' trirhodium system $[\text{MeSi}\{(\eta\text{-C}_5\text{H}_4)\text{Rh}(\text{C}_2\text{H}_4)_2\}_3]$ (**8**) is used [18]. Unfortunately, the dinuclear product $[\text{MeSi}\{(\eta\text{-C}_5\text{H}_4)\text{Rh}\}_2(\mu_2\text{-C}_6\text{H}_6)]\{(\eta\text{-C}_5\text{H}_4)\text{Rh}(\text{C}_2\text{H}_4)_2\}$ (**9**) cannot be converted into a μ_3 -benzene cluster [18].

Benzene or alkyl-substituted benzene derivatives do not react with sources of the $(\eta\text{-C}_5\text{H}_5)\text{Co}$ fragment. However, μ_3 -arene cluster complexes $[\{(\eta\text{-C}_5\text{H}_5)\text{Co}\}_3\{\mu_3\text{-R}^3\text{C}_6\text{H}_4(\text{CR}^1=\text{CHR}^2)\}]$ (**4a**) are readily obtained from the Jonas reagent $[(\eta\text{-C}_5\text{H}_5)\text{Co}(\text{C}_2\text{H}_4)_2]$ or $[(\eta\text{-C}_5\text{H}_5)\text{Co}(\eta\text{-C}_6\text{Me}_6)]$ and many alkenylbenzene derivatives. It is assumed that the reaction sequence is initiated by an attack of the metal fragment at the olefinic side-chain, which then guides the metal to the arene ring (Scheme 2) [19]. Assemblage of the tricobalt cluster then proceeds with the assistance of the alkenylbenzene



Scheme 2

template—in several cases with a nearly quantitative overall yield! It is interesting to note that the alkenylbenzene route does not work for the $(\eta\text{-C}_5\text{H}_5)\text{Rh}$ derivatives, where only mono- and dinuclear products are obtained [20].

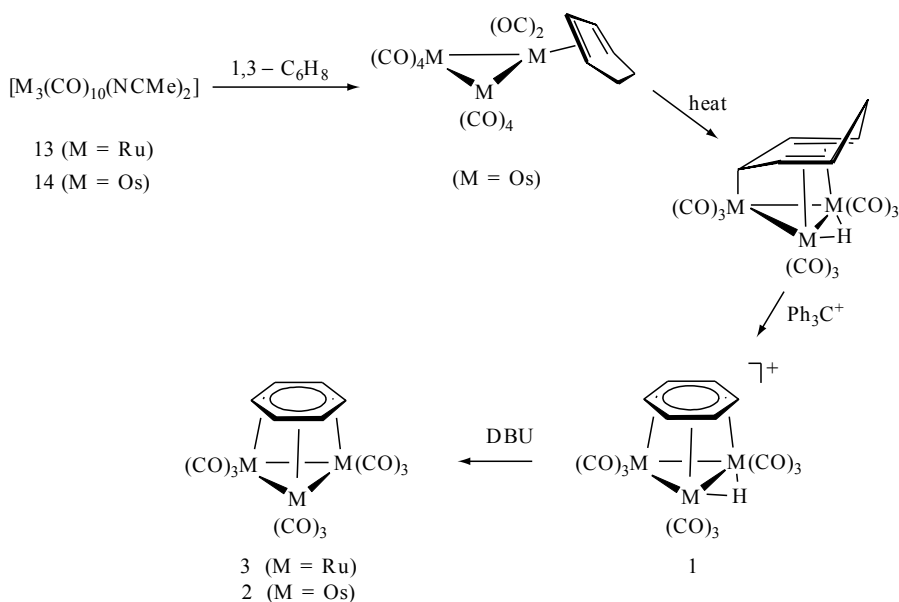
None of the mono- and dinuclear intermediates **10–12** (Scheme 2) have been observed by spectroscopy or even been isolated. The rhodium analogues of **10** and **11** can, however, be isolated [20]. In addition, a number of more stable model systems with cyclopentadienyl and pentamethylcyclopentadienyl

cobalt fragments are available [14,19,21]. Once the cluster complexes **4a** have been formed, the alkene functionality of the side-chain is no longer needed. It can easily be hydrogenated to give the alkylbenzene derivatives $[\{(\eta\text{-C}_5\text{H}_5)\text{Co}\}_3\{\mu_3\text{-R}^3\text{C}_6\text{H}_4(\text{CHR}^1\text{CH}_2\text{R}^2)\}]$ (**4b**), which are not accessible starting from the free alkylbenzene ligands [16].

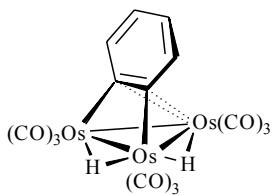
Yet another route has to be taken to synthesize the triruthenium and triosmium μ_3 -benzene cluster complexes **2** and **3**. Starting from the activated trinuclear cluster complexes $[\text{M}_3(\text{CO})_{10}(\text{NCMe})_2]$ **13** ($\text{M} = \text{Ru}$) and **14** ($\text{M} = \text{Os}$), and 1,3-cyclohexadiene, hydrido μ_3 -cyclohexadienyl complexes are prepared first, which are then transformed into the final products **2** and **3**, respectively, by subsequent abstraction of a hydride and a proton (Scheme 3) [22].

Treatment of **14** with benzene does not lead to the formation of the μ_3 -benzene cluster **2**. Instead, CH activation takes place to give the μ_3 -benzynes cluster complex $[\{(\text{CO})_3\text{Os}\}_3(\mu\text{-H})_2(\mu_3\text{-}\eta^1:\eta^2:\eta^1\text{-C}_6\text{H}_4)]$ **15** [23].

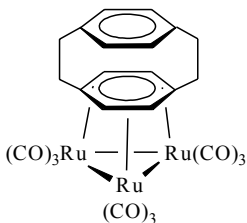
In contrast, strained non-planar arene derivatives appear to be more predisposed towards facial bonding. This is exemplified by the reaction of [2.2]paracyclophane with $[\text{Ru}_3(\text{CO})_{12}]$, which directly gives the μ_3 -arene derivative $[\text{Ru}_3(\text{CO})_9(\mu_3\text{-C}_{16}\text{H}_{16})]$ (**16**), along with the hexanuclear cluster complexes $[\text{Ru}_6\text{C}(\text{CO})_{14-3n}(\eta^6\text{-C}_{16}\text{H}_{16})_n(\mu_3\text{-C}_{16}\text{H}_{16})]$ (**17** ($n = 0$) and **18** ($n = 1$)) [24]. Similarly, cluster complexes with facial fullerenes have been prepared, e.g. $[\{(\text{CO})_3\text{M}\}_3(\mu_3\text{-C}_{60})]$ ($\text{M} = \text{Ru}$ [25], Os [26]), $[\{(\text{CO})_3\text{Ru}\}_3(\mu_3\text{-C}_{70})]$ [27] and



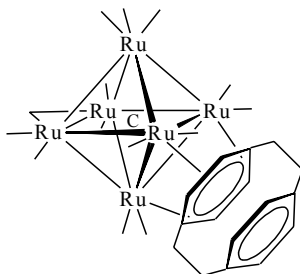
Scheme 3



15



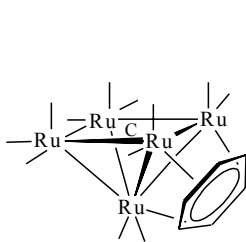
16



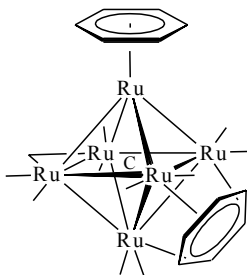
17

$[M_5C(CO)_{11}(PPh_3)(\mu_3-C_{60})]$ ($M = Ru$ [28], Os [29]). Coordination of the fullerene to the metal cluster is always via a six-membered ring of the carbon cage. CH activation is, of course, precluded with the fullerene ligands, due to the lack of carbon hydrogen bonds.

The same general approach as in Scheme 3 has also been used to generate the pentanuclear $[Ru_5C(CO)_{12}(\mu_3-C_6H_6)]$ (**19**) [30] and hexanuclear $[Ru_6C(CO)_{11}(\eta^6-C_6H_6)(\mu_3-C_6H_6)]$ (**20**) [31]. The latter complex is also obtained from a redox reaction between $[Ru_6C(CO)_{13}(\eta-C_6H_6)]^2$ and $[(\eta-C_6H_6)Ru(NCMe)_3]^2+$. In this reaction, one of the two η^6 -coordinated benzene rings is pushed into the facial position [9].



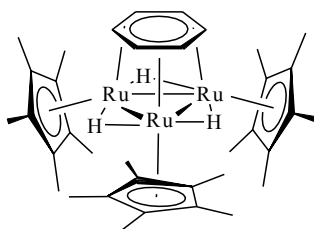
19



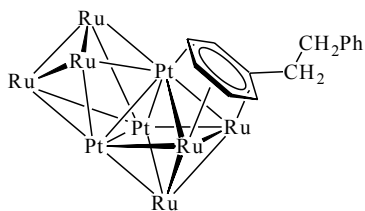
20

The triruthenium complex $[{(\eta-C_5Me_5)Ru}]_3(\mu_2-H)_3(\mu_3-C_6H_6)$ (**21**) has been prepared from $[{(\eta-C_5Me_5)Ru}]_3(\mu_2-H)_3(\mu_3-H)_2$ and cyclohexadiene [32]. Here, CH bond cleavage at the allylic carbon atoms of cyclohexadiene proceeds smoothly at ambient temperature.

A very interesting bimetallic cluster complex, $[Ru_6Pt_3(CO)_{18}(\mu_3-C_6H_5(CH_2)_2Ph)(\mu_3-H)_4]$ (**22**) is isolated in low yield as one of several metal-containing products after hydrogenation of diphenyl acetylene to give stilbene, with $[Ru_6Pt_3(CO)_{20}(\mu_3-PhC_2Ph)(\mu_3-H)(\mu-H)]$ as a catalyst [33]. It is the only known complex with an arene (1,2-diphenylethane) capping a heterotrinnuclear (Ru_2Pt) face.



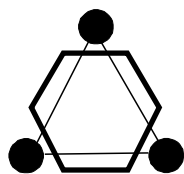
21



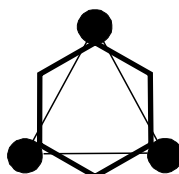
22

3 MOLECULAR STRUCTURE AND DYNAMIC BEHAVIOUR

The molecular structures of many μ_3 -arene clusters have been determined. Here, we shall concentrate only on the salient features of the facial coordination mode. In all structures, the facial arene occupies a trimetal coordination site.



D

 $C_{3v}(\sigma_d)$ 

E

 $C_{3v}(\sigma_v)$

For a six-membered ring there are two highly symmetric ways of capping a trimetal triangle, the staggered ($C_{3v}(\sigma_d)$) (**D**) and eclipsed ($C_{3v}(\sigma_v)$) (**E**) arrangements. In the overwhelming majority of structures, a staggered or nearly staggered arrangement is attained (e.g. see Figures 2–5).

There are some exceptions to this rule, where the μ_3 -arene ligand is rotated within the coordination plane towards the eclipsed arrangement. This is most noticeable with substituted facial benzene ligands and especially with facial [2.2] paracyclophane (e.g. in complexes **17** and **18**) [24]. These distortions most likely arise to avoid excessive intra- and intermolecular steric repulsions. They are also suspected to be the cause of a sometimes occurring twist distortion, which involves each individual ML_n fragment of the arene-capped trimetal cluster face [34].

Interestingly, $[(\eta-C_5Me_5)Ru]_3(\mu_2-H)_3(\mu_3-C_6H_6)$ (**21**) has the staggered structure (**D**, Figure 6), while the eclipsed geometry (**E**) was found for its dication $[21]^{2+}$ (Figure 7). A puckered conformation is adopted by the facial benzene in $[21]^{2+}$ [32].

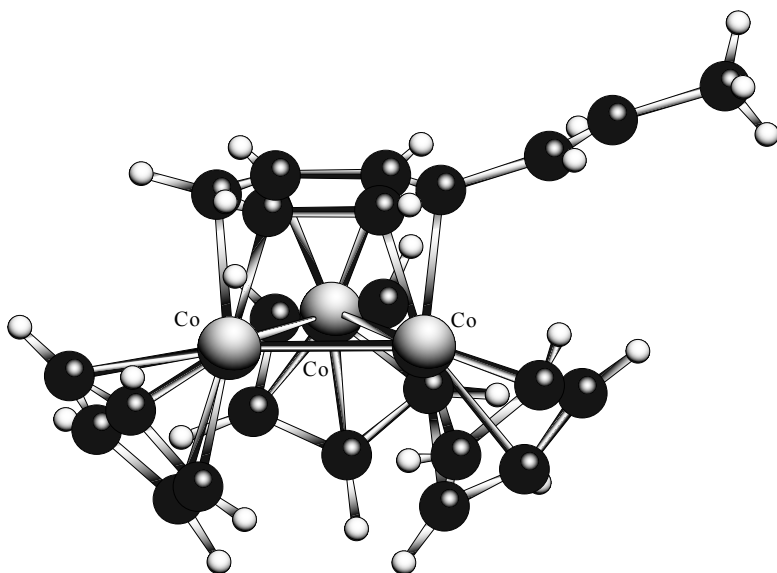


Figure 2 Molecular structure of $[(\eta\text{-C}_5\text{H}_5)\text{Co}]_3(\mu_3\text{-}\beta\text{-methylstyrene})$

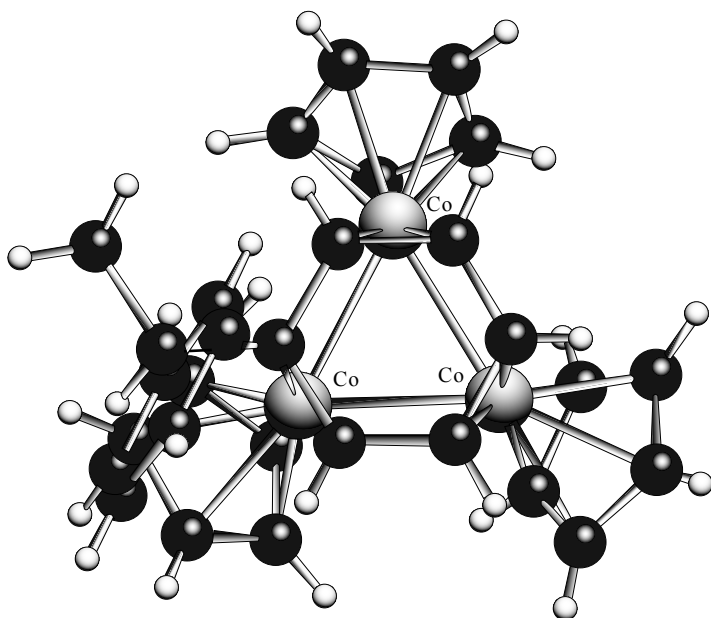


Figure 3 Molecular structure of $[(\eta\text{-C}_5\text{H}_5)\text{Co}]_3(\mu_3\text{-}1,1\text{-diphenylethane})$. Only the diastereoisomer shown here is present in the crystalline solid

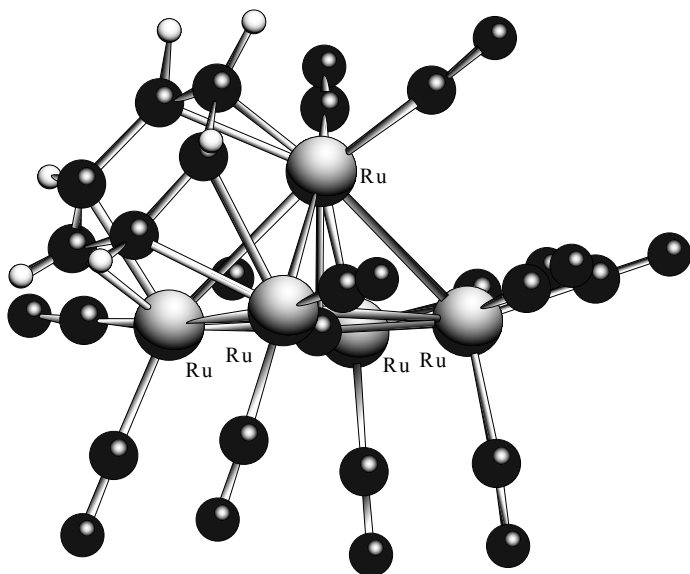


Figure 4 Molecular structure of $[\text{Ru}_5\text{C}(\text{CO})_{12}(\mu_3\text{-C}_6\text{H}_6)]$

The facial arenes are considerably expanded, both with respect to the free hydrocarbons and the ligands in the apical η^6 -coordination mode. Invariably, some alternation of the lengths of the endocyclic carbon carbon bonds is observed. The reported values, ranging between 1.34 and 1.53 Å, have, however, to be taken with some care, due to the widely differing experimental uncertainties. In the many complexes with the staggered arrangement (**D**), the coordinated bonds 'on top' of the metal atoms are generally somewhat shorter than the non-coordinated bonds 'in between' the metals.

A few typical data are collected in Table 1. Complications arise due to the presence of substituents on the facial arene, which themselves have some influence on the ring geometry [35], and can be the cause of steric repulsions with the metal cluster (see, for example, Figure 3). In the vast majority of the structures, the groups of 'longer' and 'shorter' carbon carbon bonds can be identified and analysed separately. Data for complexes of the type $[(\eta\text{-C}_5\text{H}_5)\text{Co}]_3(\mu_3\text{-arene})$ (**4**) are visualized in histogram form in Figure 8.

The bimodal distribution of bond distances is clearly evident. A statistical analysis of the data is presented in Table 2. The difference Δd between the archetypal 'short' and 'long' carbon-carbon bonds in a cluster $[(\eta\text{-C}_5\text{H}_5)\text{Co}]_3(\mu_3\text{-arene})$ is only 0.03 Å. Somewhat larger differences are observed in the ruthenium and osmium μ_3 -arene cluster complexes. However, the larger standard deviations associated with carbon-carbon bonds in molecules containing very heavy atoms render the absolute magnitude of these distortions less significant, especially in the osmium clusters.

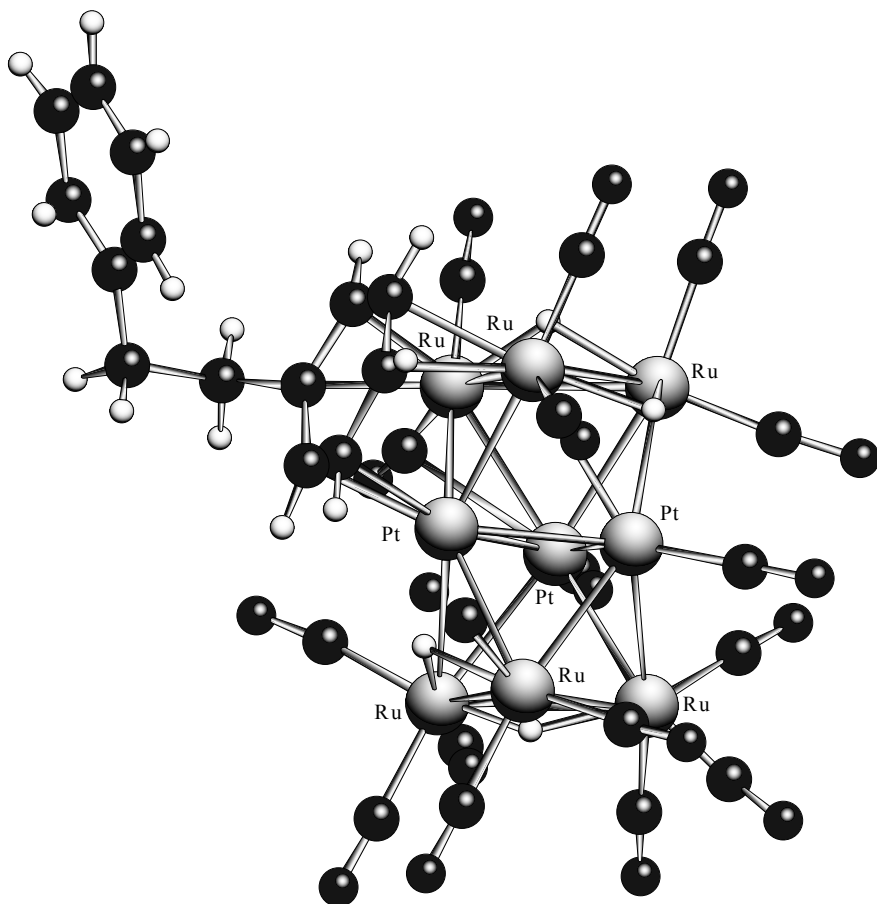
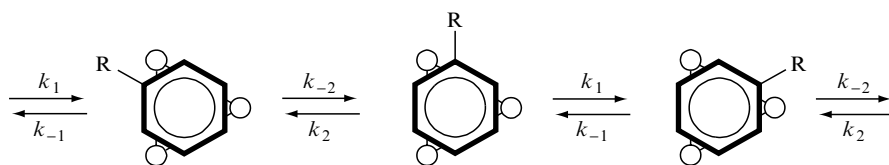


Figure 5 Molecular structure of $[\text{Ru}_6\text{Pt}_3(\text{CO})_{18}(\mu_3\text{-C}_6\text{H}_5(\text{CH}_2)_2\text{Ph})(\mu_3\text{-H})_4]$ (**22**)

Another kind of distortion, namely an out-of-plane bending of the substituents (hydrogen or organic groups) away from the metal cluster, is also prominent in all μ_3 -arene ligands. The bending with respect to the C_6 plane is quite large; in the complexes **4**, typically $16\text{--}24^\circ$ for carbon, $8\text{--}10^\circ$ for fluorine and $13\text{--}20^\circ$ for the less accurately located hydrogens.

The facial arenes are more or less free to rotate within their coordination plane on top of the metal triangles. Using two-dimensional EXSY NMR spectroscopy, the dynamic process could be shown to encompass a sequence of 60° turns of the M_3 and C_6 rings with respect to each other (i.e. [1,2] shifts of the metals around the ring) [7a,36]. Depending on the symmetry of the μ_3 -arene ligand and the metal cluster, different situations can arise. In the most simple case, i.e. benzene capping a cluster with trifold symmetry, a 60° turn of the μ_3 -

ligand generates the same molecule again. For monosubstituted benzene, a mirror image of the original structure is produced (Scheme 4). The actual exchange pathway and energy profile are quite complex, with two different activation barriers.



Scheme 4

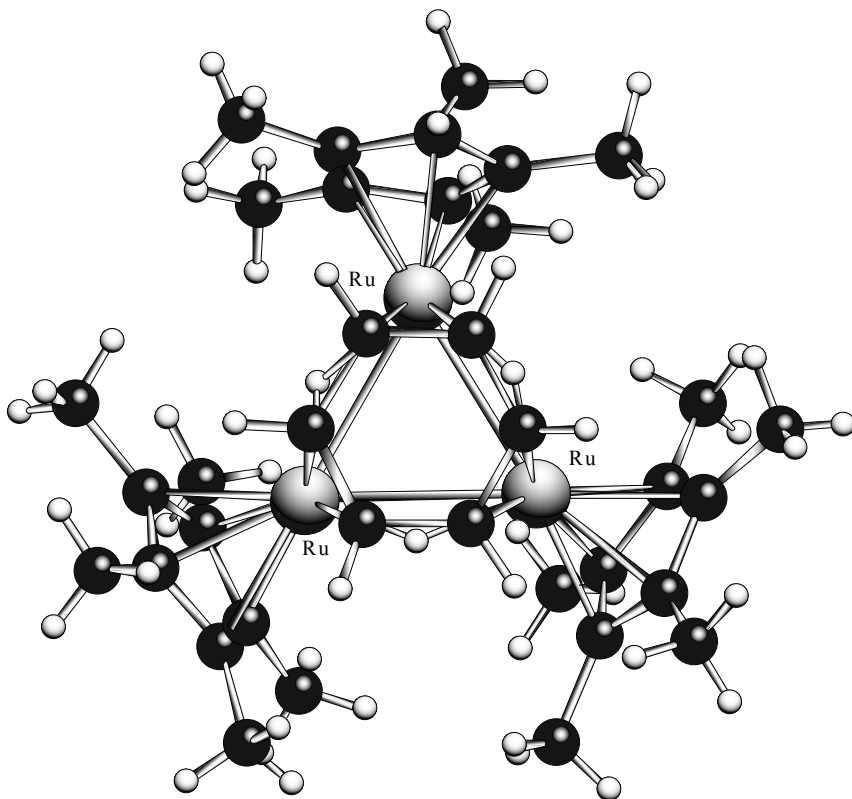


Figure 6 Molecular structure of $[(\eta\text{-C}_5\text{Me}_5)\text{Rh}]_3(\mu_2\text{-H})_3(\mu_3\text{-C}_6\text{H}_6)$ (21)

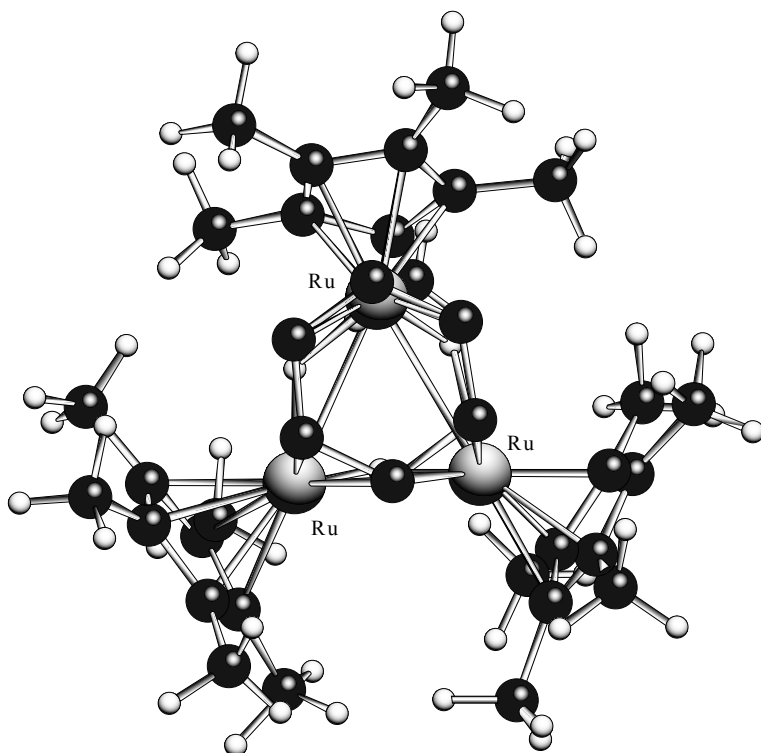


Figure 7 Molecular structure of $[(\eta\text{-C}_5\text{Me}_5)\text{Rh}]_3(\mu_2\text{-H})_3(\mu_3\text{-C}_6\text{H}_5)]^{2+}$ (21^{2+} in crystalline $[21^{2+}][\text{BPh}_4^-]_2$)

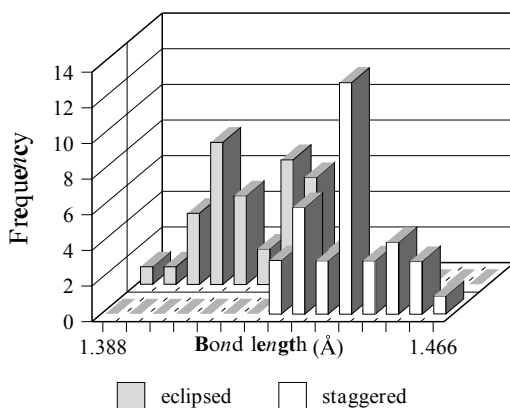


Figure 8 Distribution of the lengths of endocyclic carbon-carbon bonds in the facial arenes in some complexes of the type $[(\eta\text{-C}_5\text{R}_5)\text{Co}]_3(\mu_3\text{-arene})$ (**4**). Data are taken from crystal structure analyses

Table 1 Relevant bond distances (Å) for some cluster complexes with a facial arene

Complex	d (C–C) range ^a d (C–C) mean ^b	d (M–C) range ^a d (M–C) mean ^b	T(K)	Ref.
[[$(\eta\text{-C}_5\text{H}_5)\text{Co}$] ₃ (μ_3 -1,1-diphenylethane)]	1.405–1.443(7) 1.425(14)	2.011–2.069(5) 2.028(19)	Ambient	12
[[$(\eta\text{-C}_5\text{H}_4\text{Me})\text{Co}$] ₃ (μ_3 - β -methylstyrene)]	1.422–1.458(2) 1.439(13)	2.015–2.061(2) 2.028(16)	203	21
[[$(\eta\text{-C}_5\text{H}_5)\text{Rh}$] ₃ (μ_3 -C ₆ H ₆)]	1.40–1.47(1) 1.44(2)	2.144–2.159(1) 2.152(6)	170	18
[[$(\eta\text{-C}_5\text{Me}_5)\text{Ru}$] ₃ (μ_2 -H) ₃ (μ_3 -C ₆ H ₆)]	1.42–1.45(1) 1.43(2)	2.173–2.240(7) 2.197(25)	296	32
[[$(\eta\text{-C}_5\text{Me}_5)\text{Ru}$] ₃ (μ_2 -H) ₃ (μ_3 -C ₆ H ₆) ²⁺]	1.42–1.50(1) 1.46(3)	2.13–2.43(1) 2.26(12)	296	32
[[$(\text{CO})_3\text{Ru}$] ₃ (μ_3 -C ₆ H ₆)]	1.40–1.46(1) 1.43(2)	2.288–2.379(5) 2.332(3)	193	34
[Ru ₅ C(CO) ₁₂ (μ_3 -C ₆ H ₆)]	1.34–1.46(1) 1.40(4)	2.21–2.31(1) 2.26(4)	Ambient	30
[Ru ₆ C(CO) ₁₁ (η -C ₆ H ₆)(μ_3 -C ₆ H ₆)]	1.37–1.50(2) 1.44(5)	2.21–2.35(1) 2.27(5)	Ambient	10
[[$(\text{CO})_3\text{Os}$] ₃ (μ_3 -C ₆ H ₆) ^c]	1.36–1.57(4) 1.46(7)	2.27–2.42(3) 2.33(5)	Ambient	57
[Os ₆ (CO) ₁₁ (μ -H) ₂ (η -C ₆ H ₆)(μ_3 -C ₆ H ₆)]	1.29–1.53(7) 1.40(7)	2.23–2.34(5) 2.28(4)	Ambient	58
[Ru ₆ Pt ₃ (CO) ₁₈ (μ_3 -H) ₄ (μ_3 -C ₆ H ₅ (CH ₂) ₂ Ph)]	1.35–1.48 1.45(6)	2.206, 2.219 ^d 2.213(7) ^d 2.248–2.291 ^e 2.268(17) ^e	293	33

^a The estimated standard deviation of the individual values is given in parentheses.

^b The standard deviation of the mean is given in parentheses.

^c Two independent molecules.

^d Pt–C.

^e Ru–C.

Table 2 Statistical analysis of bond distance data for same cluster complexes [[$(\eta\text{-C}_5\text{H}_5)\text{Co}$]₃ μ_3 -arene]

Bond type	N_{obs}	Median	Mean (Å)	σ (mean) (Å)	σ (sample) (Å)	w -mean ^a (Å)	σ (w -mean) (Å)
$\eta\text{-C-C}^b$	36	1.417	1.418	0.002	0.011	1.422	0.001
C–C ^c	36	1.446	1.447	0.002	0.011	1.449	0.002
All C–C	72	1.432	1.433	0.002	0.018	1.435	0.002

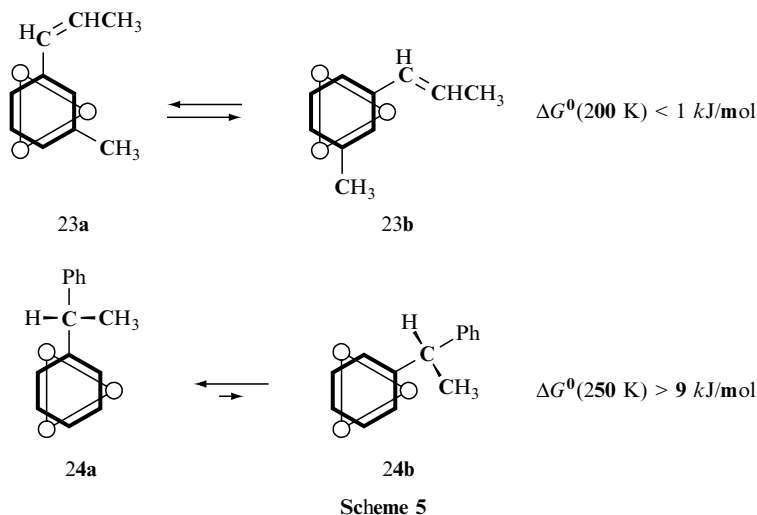
^a Weighted mean.

^b Metal coordinated C–C bonds.

^c Non-coordinated C–C bonds.

In certain cases μ_3 -arene rotation leads to an interconversion of diastereomeric structures. This is shown in Scheme 5 for [[$(\eta\text{-C}_5\text{H}_5)\text{Co}$]₃(μ_3 - m -methylstyrene)] (**23**) and [[$(\eta\text{-C}_5\text{H}_5)\text{Co}$]₃(μ_3 -1,1-diphenylethane)] (**24**), respectively [15,16,37].

At low temperature, both diastereomers of **23** can be observed. In contrast, only one diastereomeric form of **24a** is present in solution below about 250 K, as in the crystalline solid (Figure 3) [16]. From these observations, rough



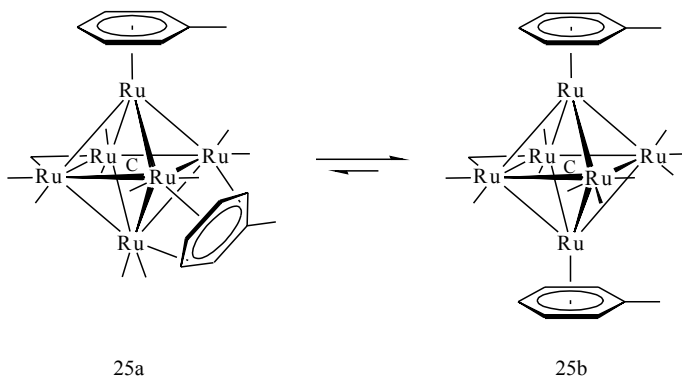
estimations of the upper and lower bounds; respectively, for the standard free enthalpy ΔG^0 of the isomerization equilibrium can be given (see Scheme 5). Activation parameters (ΔG^\ddagger and/or ΔH^\ddagger , ΔS^\ddagger) pertinent to arene rotation in two different types of μ_3 -arene clusters are collected in Table 3. Both thermodynamic (Scheme 5) and kinetic (Table 3) data indicate that the barriers of arene rotation within a particular class of complexes are related to steric hindrance. More bulky substituents decrease the energy barrier for rotation of the μ_3 -arene ring. This observation is in line with theoretical calculations, using molecular mechanics [38] or semiempirical MO methods [39].

In the larger carbonyl metal cluster complexes (nuclearity of five and above), arenes have been shown to be able to move over the cluster surface. Generally, the apical arene coordination is thermodynamically preferred with respect to the facial bonding mode. For example, in solution the facial/apical complex $[\text{Ru}_6\text{C}(\text{CO})_{11}(\eta\text{-C}_6\text{H}_5\text{Me})(\mu_3\text{-C}_6\text{H}_5\text{Me})]$ (**25a**) appears to be in equilibrium with its apical/apical isomer (**25b**). No intermolecular exchange of bound

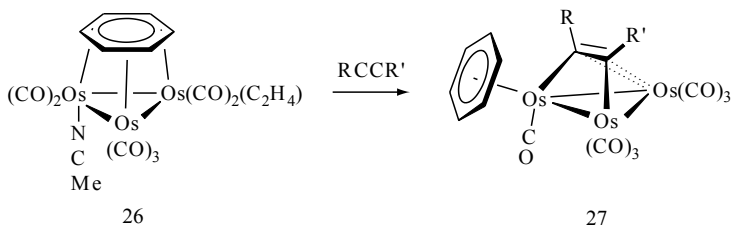
Table 3 Activation parameters for arene rotation in complexes of the type $[(L_nM)_3(\mu_3\text{-arene})]$

$(L_nM)_3$	Arene	ΔH^\ddagger (kJ mol ⁻¹)	ΔS^\ddagger (J mol ⁻¹ K ⁻¹)	ΔG^\ddagger (kJ mol ⁻¹)	T(K)	Ref.
$\{(\eta\text{-C}_5\text{H}_5)\text{Co}\}_3$	$\text{C}_6\text{H}_5^i\text{Pr}$	71(2)	55(7)	—	—	37
$\{[(\eta\text{-C}_5\text{H}_5)\text{Co}]_3(\mu_3\text{-H})\}^+$	$\text{C}_6\text{H}_5^i\text{Pr}$	63(2)	108(8)	—	—	37
$\{(\eta\text{-C}_5\text{H}_5)\text{Co}\}_3$	$\text{C}_6\text{H}_4\text{Et}_2\text{-1,4}$	51(1)	9(5)	—	—	37
$\text{Os}_3(\text{CO})_8(\eta^2\text{-CH}_2\text{CHPh})$	C_6H_6	—	—	48	211	45
$\text{Os}_3(\text{CO})_8(\eta^2\text{-CH}_2\text{CHPh})$	$\text{C}_6\text{H}_5\text{Me}$	—	—	27	177	45

toluene with free toluene- d_8 is observed in this system [40]. The facial arene ligand in $[\text{Ru}_6\text{Pt}_3(\text{CO})_{18}(\mu_3\text{-C}_6\text{H}_5(\text{CH}_2)_2\text{Ph})(\mu_3\text{-H})_4]$ (**22**) also moves to an apical $\eta^6(\text{Ru})$ position on heating [33].



In the trinuclear carbonyl metal based systems, facial to apical arene migration is not a spontaneous process. However, addition of excess alkyne $\text{RC}_2\text{R}'$ to the activated complex $[\text{Os}_3(\text{CO})_7(\text{NCMe})(\text{C}_2\text{H}_4)(\mu_3\text{-C}_6\text{H}_6)]$ (**26**) results in the formation of $[\text{Os}_3(\text{CO})_7(\eta^6\text{-C}_6\text{H}_6)(\mu_3\text{-}\eta^1\text{:}\eta^2\text{:}\eta^1\text{-RC}_2\text{R}')]$ (**27**), due to the strong preference of the alkyne for the face-capping coordination mode [41].



Facial arene exchange in the cluster complexes with a tris (cyclopentadienyl metal) frame, such as **4**, **5** and **21**, has not been observed.

4 ELECTRONIC STRUCTURE

The electronic structure of the cluster complexes $[\{(\eta\text{-C}_5\text{H}_5)\text{M}\}_3(\mu_3\text{-C}_6\text{H}_6)]$ ($\text{M} = \text{Co}, \text{Rh}, \text{Ir}$) and $[\{(\text{CO})_3\text{M}\}_3(\mu_3\text{-C}_6\text{H}_6)]$ ($\text{M} = \text{Fe}, \text{Ru}, \text{Os}$) has been studied by semi-empirical and *ab initio* molecular orbital methods [39,42–47]. The salient structural features of facially bound benzene, i.e. ring expansion, a

certain degree of endocyclic bond length alternation, and the out-of-plane displacement of the hydrogen atoms, are well accounted for already by the simple extended Hückel model. In particular, the Kekulé-type distortion of the facial six-membered ring is traced to a mixing of the benzene e_{1g} (HOMOs) and e_{2u} (LUMOs) orbital sets [43]. Under the threefold symmetry of the complex, this mixing, which is symmetry forbidden in free (D_{6h}) benzene, becomes allowed in phase with metal cluster orbitals. Conceptually, there is only little difference in this respect between the trinuclear μ_3 -arene clusters and mononuclear $[(CO)_3Cr(\eta-C_6H_6)]$ (**28**). In both types of complexes, donation and back-donation from and to the benzene ligand are enhanced by CH bending. The direction of this distortion (away from the metals in the cluster, and towards the metal in the mononuclear complex) is dictated by the geometric requirements of the respective metal frame, which place the metal(s) outside of the ring for $\mu_3\text{-}\eta^2\text{:}\eta^2\text{:}\eta^2$ -benzene, and below the ring centre for η^6 -benzene.

For $[(CO)_3Os]_3(\mu_3-C_6H_6)$ (**2**), the barrier for in-plane rotation of the facial benzene was calculated to 66.6 kJ mol^{-1} on the *ab initio* MP2 level; this was attributed to a decrease in the back-donation and an increase in exchange repulsion due to benzene σ -electrons. In the calculated transition state with $C_{3v}(\sigma_v)$ symmetry (**E**, above) the facial benzene relaxes to a puckered geometry [44].

It is tempting to interpret the ‘staggered’ ($C_{3v}(\sigma_d)$) arrangement of the facial arene with respect to the metal triangle, and its Kekulé-type distortion in terms of the arene ligand ‘being bonded as a triene to the metal cluster’ [9,48]. A regular hexagonal geometry is, however, not required for cyclic electron delocalization (a better descriptive name than aromaticity) in benzene and related molecules. For example, ‘Kekulé benzene’, the strongly bond alternating cyclohexatriene with D_{3h} symmetry, is considered nearly as aromatic as the symmetrical (D_{6h}) structure [49]. Bonded in the η^6 coordination mode under C_{3v} symmetry, benzene undergoes a trigonal (Kekulé-type) distortion, which has a similar magnitude ($\Delta d = 0.02\text{ \AA}$ in $[(CO)_3Cr(\eta-C_6H_6)]$ (**28**) [50]) as in the facial $C_{3v}(\sigma_d)$ coordination. It has been shown that η^6 -benzene in **28** must be considered aromatic [51]. This is illustrated by the nucleus-independent chemical shift NICS(r), based on computed magnetic shieldings, in and $r\text{ \AA}$ above the ring centres. Negative NICSs are indicative of cyclic electron delocalization; effects caused by the π -electrons fade out less rapidly with increasing distance from the ring centre than those due to σ -effects [49]. NICS(1) values of -10.6 and -13.2 have been reported for benzene and **28**, respectively [51]. Very recently, *ab initio* DFT calculations in our laboratory gave strongly negative NICS values for all four compounds in the series benzene, **28**, $[(\eta-C_6H_6)_2Cr]$ and $[(\eta-C_5H_5)Co]_3(\mu_3\text{-}\eta^2\text{:}\eta^2\text{:}\eta^2\text{-}C_6H_6)$, respectively (Figure 9) [42]. Hence, we conclude that facial coordination to a metal cluster does not result in a substantial loss of cyclic electron delocalization and aromaticity of benzene.

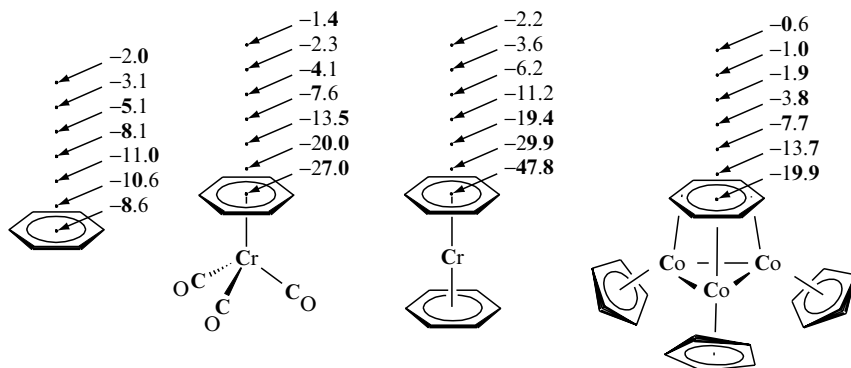


Figure 9 Total NICS values of benzene, $[(\text{CO})_3\text{Cr}(\eta\text{-C}_6\text{H}_6)]$ (**28**), $[\text{Cr}(\eta\text{-C}_6\text{H}_6)_2]$ and $[(\eta\text{-C}_5\text{H}_5)_3\text{Co}]_3(\mu_3\text{-C}_6\text{H}_6)$ calculated at the centres of the rings and at points 0.5 Å apart. Calculations were carried out with Gaussian98 using the B3LYP hybrid functional. For benzene and the mononuclear complexes, the 6-311G* basis set was used for all atoms. Basis sets for the arene cluster were LANL2DZ for Co and 6-31G for C and H

5 REACTIVITY

Surprisingly few studies aimed at the reactivity of facial arenes have appeared in the literature. As already mentioned above, substitution of an μ_3 -arene is not a facile process, especially for the complexes of the type $[\{(\eta\text{-C}_5\text{R}_5)\text{M}\}]_3(\mu_3\text{-arene})$, **4** (M = Co) and **5** (M = Rh).

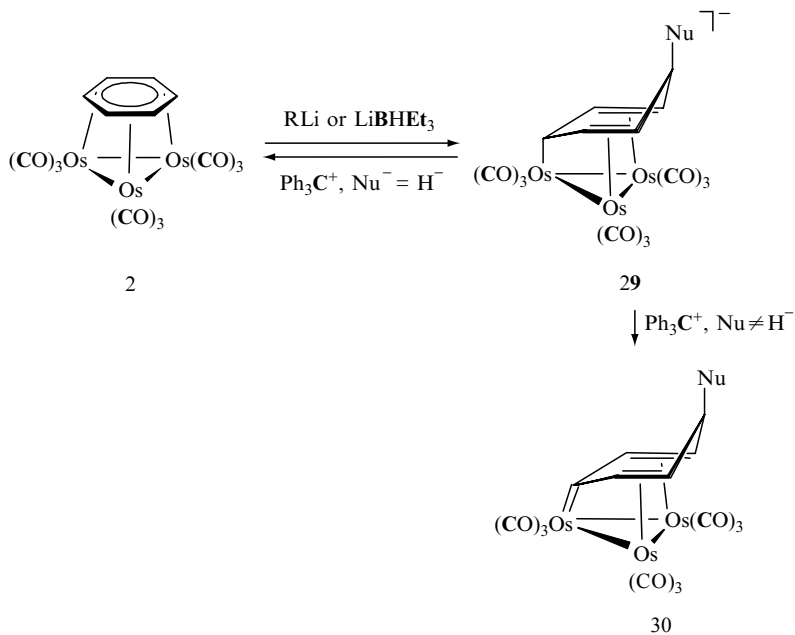
In $[\{(\text{CO})_3\text{Os}\}]_3(\mu_3\text{-C}_6\text{H}_6)$ (**2**), irradiation in the near-UV-visible range initiates photoisomerization, to give the μ_3 -benzynes cluster complex $[\{(\text{CO})_3\text{Os}\}]_3(\mu\text{-H})_2(\mu_3\text{-}\eta^1\text{:}\eta^2\text{:}\eta^1\text{-C}_6\text{H}_4)$ (**15**), probably via a two-stage CH activation process [52].

Electrophilic additions of certain nucleophiles Nu^- (hydride and carbanions) to $[\{(\text{CO})_3\text{Os}\}]_3(\mu_3\text{-arene})$ (**2**) have been reported (Scheme 6) [53].

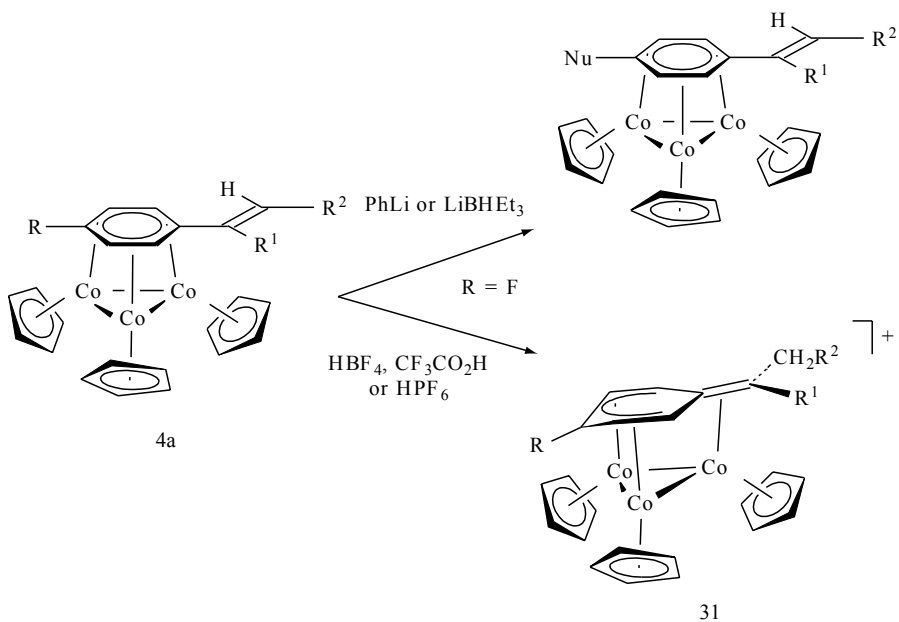
Regio- and stereo-selective *exo*-addition to the face-capping arene takes place, to give anionic μ_3 -cyclohexadienyl complexes $[\{(\text{CO})_3\text{Os}\}]_3(\mu_3\text{-}\eta^2\text{:}\eta^1\text{:}\eta^2\text{-C}_6\text{H}_6\text{Nu})^-$ (**29**). If $\text{Nu}^- = \text{H}^-$, the starting material is regenerated upon treatment with hydride abstraction reagents. In contrast, with $\text{Nu}^- \neq \text{H}^-$, hydride abstraction takes place in the 4-position of the facial cyclohexadienyl ring, to give the novel carbene metal complexes (**30**) (Scheme 6) [54].

In contrast, the complexes $[\{(\eta\text{-C}_5\text{R}_5)\text{Co}\}]_3(\mu_3\text{-arene})$ (**4**) do not add hydride or carbanions. However, when $[\{(\eta\text{-C}_5\text{R}_5)\text{Co}\}]_3(\mu_3\text{-}p\text{-fluoro-}\alpha\text{-methylstyrene})$ is treated with $\text{Li}[\text{HBET}_3]$ or LiPh , regiospecific nucleophilic substitution of fluoride is observed, most likely via an addition/elimination sequence (Scheme 7) [55].

Electrophilic attack of **4a** by protons takes place at the β -carbon atom of the alkenyl substituent, to give the novel cluster stabilized benzyl cations **31** (Scheme 7) [56].



Scheme 6



Scheme 7

6 CONCLUSIONS

Cluster complexes with facial arene ligands are no longer laboratory curiosities. Among the many arene transition metal complexes known they form a large and well-defined subgroup with quite unique structural properties. Large quantities of material can be prepared in a rational way via proven synthetic methods, which are mechanistically well understood. It is somewhat surprising, however, that only complexes with metals from a very small section of the Periodic Table (i.e. the iron and cobalt groups) are known to date. Judging from the range of known mononuclear systems [59] facial arene clusters should be feasible with a much wider selection of metals.

The relationship between molecular cluster complexes with facial arene ligands and metal surface adsorbates of benzene has been looked at mainly from structural and spectroscopic points of view. Now there is no doubt that the structural features of the facial arene ligand in a molecular cluster compound (as described in some detail above) are also present in chemisorbed benzene, at least on an atomically flat metal surface [60].

A nice example is given in a recent NEXAFS spectroscopic study, where a direct comparison has been made between benzene on the Ru(0001) surface and in the trinuclear molecular cluster complex $[\text{Ru}_3(\text{CO})_9(\mu_3\text{-C}_6\text{H}_6)]$ (**3**) [61]. Strong correlations, not only of the structures, but also of the electronic coupling of the ligand with the metal substrate, have been found.

However, the cluster–surface analogy, as cited above, implies two areas, namely structure ('chemisorption') and reactivity ('catalysis'). To a large extent, the interest in the chemisorption of benzene stems from its being involved in many hydrocarbon transformations, which are carried out on a huge scale in the petroleum industry by using metal or metal-modified catalysts [62]. In this respect, it appears that there is not much to be learned from the few reported reactions of facial benzene in molecular cluster complexes. The strength of the molecular cluster complexes appears to lie more in the structural, rather than in functional modelling of metal surface adsorbates.

7 REFERENCES AND NOTES

1. In this paper, the definition of a metal cluster is that given by F. A. Cotton (*Q. Rev. Chem. Soc.*, 416 (1996)): 'A discrete molecule containing at least three metal atoms in which there is a substantial and direct bonding interaction between the metal atoms even though some non-metal atoms may be associated intimately with the cluster'.
2. E. L. Muettterties, T. N. Rhodin, E. Band, C. F. Brucker and W. R. Pretzer, *Chem. Rev.*, **79**, 991 (1979).
3. See, for example: (a) J. B. Collman, L. S. Hegedus, J. R. Norton and R.-G. Finke, *Principles and Applications of Organotransition Metal Chemistry*, University Science Books, Mill Valley, CA, 1987. (b) Ch. Elschenbroich and A. Salzer, *Organometallic chemistry*, 3rd Edn, Teubner, Stuttgart, 1990, Ch. 15.4, pp. 366–438.

4. G. A. Somorjai, *Chemistry in Two Dimensions: Surfaces*, Cornell University Press, Ithaca, NJ, 1981, Ch. 9, pp. 479–515.
5. F. P. Netzer, *Langmuir*, **7**, 2544 (1991), and references cited therein.
6. G. A. Somorjai, *Pure Appl. Chem.*, **60**, 1499 (1988), and references cited therein.
7. Review articles include: (a) H. Wadepohl, *Angew. Chem.*, **104**, 253 (1992). (b) H. Wadepohl, *Comments Inorg. Chem.*, **15**, 369 (1994). (c) D. Braga, P. J. Dyson, F. Grepioni and B. F. G. Johnson, *Chem. Rev.*, **94** 1585 (1994). (d) H. Wadepohl and S. Gebert, *Coord. Chem. Rev.*, **143**, 535 (1995). (e) H. Wadepohl and A. Metz, in *Metal Clusters in Chemistry*, Vol. 1, P. Braunstein, L. A. Oro and P. R. Raithby (Eds), Wiley-VCH, Weinheim, Ch. 1.15, pp. 269–289.
8. E. G. Bryan, B. F. G. Johnson, J. W. Kelland and J. Lewis, *J. Chem. Soc., Chem. Commun.*, 254 (1976).
9. M. P. Gomez-Sal, B. F. G. Johnson, J. Lewis, P. R. Raithby and A. H. Wright, *J. Chem. Soc., Chem. Commun.*, 1682 (1985).
10. B. F. G. Johnson, J. Lewis, M. Martinelli, A. H. Wright, D. Braga and F. Grepioni, *J. Chem. Soc., Chem. Commun.*, 364 (1990).
11. H. Wadepohl, K. Büchner and H. Pritzkow, *Angew. Chem.*, **99**, 1294 (1987).
12. H. Wadepohl, K. Büchner, M. Herrman and H. Pritzkow, *Organometallics*, **10**, 861 (1991).
13. H. Wadepohl, T. Borchert, K. Büchner and H. Pritzkow, *Chem. Ber.*, **126**, 1615 (1993).
14. H. Wadepohl, T. Borchert, K. Büchner, M. Herrmann, F.-J. Paffen and H. Pritzkow, *Organometallics*, **14**, 3817 (1995).
15. H. Wadepohl, K. Büchner, M. Herrmann, A. Metz and H. Pritzkow, *J. Organomet. Chem.*, **571**, 267 (1998).
16. H. Wadepohl, K. Büchner, M. Herrmann and H. Pritzkow, *J. Organomet. Chem.*, **573**, 22 (1998).
17. J. Müller, P. Escarpa Gaede and K. Qiao, *Angew. Chem.*, **105**, 1809 (1993).
18. J. Müller, K. Ha, O. Lettau and R. Schubert, *Z. Anorg. Allg. Chem.*, **624**, 192 (1998).
19. H. Wadepohl, K. Büchner and H. Pritzkow, *Organometallics*, **8**, 2745 (1989).
20. H. Wadepohl, A. Metz and H. Pritzkow, *Chem. Eur. J.*, **8**, 1591, (2002).
21. A. Metz and H. Wadepohl, unpublished results.
22. A. J. Blake, P. J. Dyson, B. F. G. Johnson, C. M. Martin, J. G. M. Nairn, E. Parisini and J. Lewis, *J. Chem. Soc., Dalton Trans.*, 981 (1993).
23. R. J. Goudsmit, B. F. G. Johnson, J. Lewis, P. R. Raithby and M. Rosales, *J. Chem. Soc., Dalton Trans.*, 2257 (1983).
24. P. J. Dyson, B. F. G. Johnson, C. M. Martin, A. J. Blake, D. Braga, F. Grepioni and E. Parisini, *Organometallics*, **13**, 2113 (1994).
25. H. F. Hsu and J. R. Shapley, *J. Am. Chem. Soc.*, **118**, 9192 (1996).
26. J. T. Park, H. Song, J.-J. Cho, M.-K. Chung, J.-H. Lee and I.-H. Suh, *Organometallics*, **17**, 227 (1998).
27. H. F. Hsu, S. R. Wilson and J. R. Shapley, *J. Chem. Soc., Chem. Commun.*, 1125 (1997).
28. K. Lee, H. F. Hsu and J. R. Shapley, *Organometallics*, **16**, 3876 (1997).
29. K. Lee, C. H. Lee, H. Song, J. T. Park, H. Y. Chang and M.-G. Choi, *Angew. Chem.*, **112**, 1871 (2000).
30. P. J. Bailey, D. Braga, P. J. Dyson, F. Grepioni, B. F. G. Johnson, J. Lewis and P. Sabatino, *J. Chem. Soc., Chem. Commun.*, 177 (1992).
31. P. J. Dyson, B. F. G. Johnson, J. Lewis, M. Martinelli, D. Braga and F. Grepioni, *J. Am. Chem. Soc.*, **115**, 9062 (1993).
32. A. Inagaki, Y. Takaya, T. Takemori, H. Suzuki, M. Tanaka and M. Haga, *J. Am. Chem. Soc.*, **119**, 625 (1997).

33. R. D. Adams, T. S. Barnard, Z. Li, W. Wu and J. H. Yamamoto, *J. Am. Chem. Soc.*, **116**, 9103 (1994).
34. D. Braga, F. Grepioni, B. F. G. Johnson, J. Lewis, C. E. Housecroft and M. Martinelli, *Organometallics*, **10**, 1260 (1991).
35. (a) A. Domenicano, A. Vaciano and C. A. Coulson, *Acta Crystallogr., Sect. B*, **31**, 221 (1975). (b) A. Domenicano, in *Accurate Molecular Structures, IUCr Monographs on Crystallography*, Vol. 1, A. Domenicano and I. Hargittai (Eds), International Union of Crystallography and Oxford University Press, Oxford, UK, 1992, Ch. 18, pp. 437–468.
36. H. Wadepohl, in *The Synergy Between Dynamics and Reactivity at Clusters and Surfaces*, L. J. Farrugia (Ed.), NATO ASI Series C: Mathematical and Physical Sciences, Vol. 465, Kluwer Academic Publishers, Dordrecht, The Netherlands, 1995, pp. 175–191.
37. Ch. Jost and H. Wadepohl, unpublished results.
38. P. Mercandelli and A. Sironi, *J. Am. Chem. Soc.*, **118**, 11548 (1996).
39. S. Müller and H. Wadepohl, unpublished results.
40. D. Braga, F. Grepioni, E. Parisini, P. J. Dyson, B. F. G. Johnson, D. Reed, D. Shepherd, P. J. Bailey and J. Lewis, *J. Organomet. Chem.*, **462**, 301 (1993).
41. D. Braga, F. Grepioni, B. F. G. Johnson, J. Lewis, M. Martinelli and M. A. Gallop, *J. Chem. Soc., Chem. Commun.*, 53 (1990).
42. M. Entrialgo Castaño and H. Wadepohl, unpublished results.
43. (a) H. Wadepohl and L. Zhu, *J. Organomet. Chem.*, **376**, 115 (1989). (b) L. Zhu, H. Wadepohl and N. Kostic, *Wuji Huaxue Xuebao*, **8**, 1 (1992).
44. J.-F. Riehl, N. Koga and K. Morokuma, *Organometallics*, **12**, 4788 (1993).
45. M. A. Gallop, B. F. G. Johnson, J. Keeler, J. Lewis, S. J. Heyes and C. M. Dobson, *J. Am. Chem. Soc.*, **114**, 2510 (1992).
46. B. E. R. Schilling and R. Hoffmann, *J. Am. Chem. Soc.*, **101**, 3456 (1979).
47. M. A. Lynn and D. L. Lichtenberger, *J. Cluster Sci.*, **11**, 169 (2000).
48. B. F. G. Johnson, J. Lewis, C. Housecroft, M. Gallup, M. Martinelli and D. Braga, F. Grepioni, *J. Mol. Catal.*, **74**, 61 (1992).
49. P. v. R. Schleyer, C. Maerker, A. Dransfeld, H. Jiao and N. J. R. van Eikema Hommes, *J. Am. Chem. Soc.*, **118**, 6317 (1996).
50. (a) B. Rees and P. Coppens, *Acta Crystallogr., Section B*, **29**, 2516 (1973). (b) See also A. Solladié-Cavallo, *Polyhedron*, **6**, 901 (1985).
51. P. v. R. Schleyer, B. Kiran, D. V. Simion and T. S. Sorensen, *J. Am. Chem. Soc.*, **122**, 510 (2000).
52. M. A. Gallop, B. F. G. Johnson, J. Lewis, A. McCamley and R. N. Perutz, *J. Chem. Soc., Chem. Commun.*, 1071 (1988).
53. M. A. Gallop, B. F. G. Johnson, J. Lewis and A. H. Wright, *J. Chem. Soc., Dalton Trans.*, 481 (1989).
54. A. J. Edwards, M. A. Gallop, B. F. G. Johnson, J. U. Köhler, J. Lewis and P. R. Raithby, *Angew. Chem.*, **106**, 1166 (1994).
55. H. Wadepohl, T. Borchert and H. Pritzkow, *J. Organomet. Chem.*, **516**, 187 (1996).
56. H. Wadepohl, M. J. Calhorda, M. Herrmann, C. Jost, P. E. M. Lopes and H. Pritzkow, *Organometallics*, **15**, 5622 (1996).
57. M. A. Gallop, M. P. Gomez-Sal, C. E. Housecroft, B. F. G. Johnson, J. Lewis, S. M. Owen, P. R. Raithby and A. H. Wright, *J. Am. Chem. Soc.*, **114**, 2502 (1992).
58. J. Lewis, C.-K. Li, P. R. Raithby and W.-T. Wong, *J. Chem. Soc., Dalton Trans.*, 999 (1993).
59. (a) W. E. Silverthorn, *Adv. Organomet. Chem.*, **13**, 47 (1975). (b) R. G. Gastingier and K. J. Klabunde, *Transition Met. Chem.*, **4**, 1 (1979). (c) R. B. King, in *The Organic Chemistry of Iron*, Vol. 2, E. A. Koerner v. Gustorf, F.-W. Grevels and

- I. Fischler (Eds), Academic Press, New York, Vol. 2 1981, pp. 155–187. (d) E. L. Muetterties, J. R. Bleeke, E. J. Wucherer and T. A. Albright, *Chem. Rev.*, 499 (1982).
60. See, for example, G. A. Somorjai, *J. Phys. Chem.*, **94**, 1013 (1990).
61. K. Weiss, S. Gebert, M. Wühh, H. Wadepohl and Ch. Wöll, *J. Vac. Sci. Technol., A*, **16**, 1017 (1998).
62. G. C. Bond, *Heterogeneous Catalysis, Principles and Applications*, 2nd Edn, Oxford Science Publications, Clarendon Press, Oxford, UK, 1987, Ch. 9, pp. 104–130.

8 Cobaltfulvenes and Cobaltapentalenes: Highly Polar Metallacyclic Π -Systems with Unusual Properties

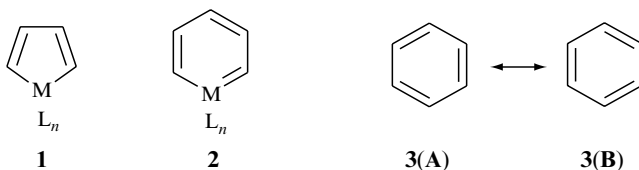
HUBERT WADEPOHL

*Anorganisch-Chemisches Institut der Ruprecht-Karls-Universität,
Im Neuenheimer Feld 270, D-69120 Heidelberg, Germany*

1 INTRODUCTION

To a large part, organo-transition metal chemistry is governed by metal-to-carbon π -bonding, which is, either as a minor or major component of the metal-carbon bond, present in the overwhelming majority of organometallic complexes. The specific properties of the transition metals, which are mainly due to a large number of energetically accessible electrons and/or orbitals are most obviously translated into chemistry when the metal itself forms part of a (sometimes extended) π -system. For example, the chemical properties of transition metal carbene complexes $[L_nM=CR_2]$ have little in common with those of the free carbenes CR_2 , and differ substantially from their all-carbon analogues, the alkenes $R_2C=CR_2$. Carbene metal complexes have been employed in a large variety of chemical transformations which are not possible with all-carbon π -systems, such as the Dötz reaction or olefin metathesis, to name just two.

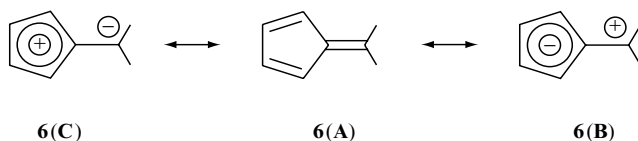
Conjugated metallacyclic π -systems, for example, metallacyclopentadienes (**1**) and metallabenzenes (**2**), play a special role. Such systems are involved in important stoichiometric and catalytic reactions, such as the synthesis of cyclopentadieny complexes [1] and alkyne oligomerization processes [2]. Also of fundamental interest is whether conjugated metallacycles exhibit aromatic or antiaromatic properties [3].



Benzene is the prototype of an aromatic π -system, with a high degree of cyclic electron delocalization, which is commonly expressed by the equal importance of the two resonance structures **3(A)** and **3(B)**.

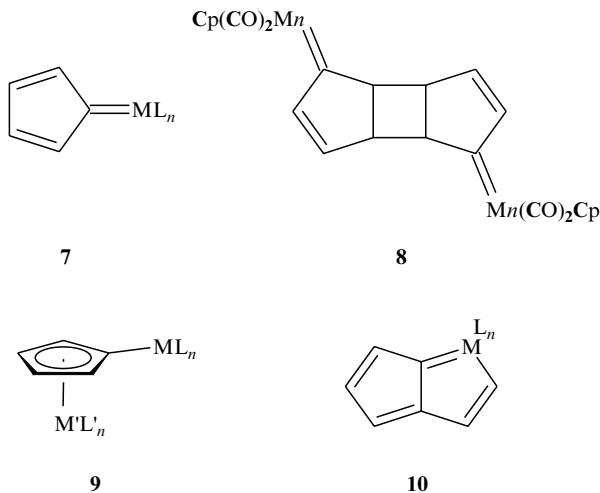


A certain degree of aromaticity has been ascribed to the metallabenzenes **2** [3]. Interestingly, much of the aromaticity seems to remain when benzene or a metallabenzene is centrally π -bonding to a metal ligand fragment (**4** and **5**) [1,4]. Pentafulvene (**6**), an isomer of benzene, is adequately described in its ground state by the classical cross-conjugated structure **6(A)** [5]. The chemical reactivity of this polyolefin is however governed by a high polarizability in the direction of **6(B)** [6]. The description **6(C)** is inadequate, due to the antiaromaticity of the five-membered ring system.



Isolobal replacement [7] of the exocyclic methylene group of **6** by a transition metal ligand fragment generates a metallafulvene (**7**), which may be more conventionally called a cyclopentadiene carbene or cyclopentadienylidene complex. To my knowledge, no simple metallafulvene has been reported to date. The manganese complex **8** [8], a [2 + 2] cycloaddition product of **7**, comes closest to such a species. π -Complexes of **7** are known, most of them adequately described by the so-called $\eta^5:\eta^1$ structure **9** and perhaps more appropriately viewed as a centrally bound cyclopentadienyl, which has oxidatively added to a nearby second metal atom, thereby metallating one CH function [9].

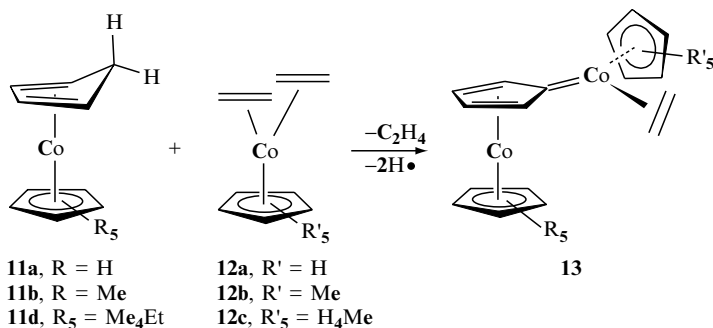
In this short review we will focus on a novel class of metallafulvene complexes, which are not well represented by formula **9**, and exhibit a high degree of charge separation. Reaction of these complexes with certain alkynes leads to the formation of a metallabicyclic ring system, and opens an entry into the hitherto unknown metallapentalene series **10**. Like fulvene, the parent hydrocarbon of these species, pentalene, is highly unstable and predicted to have a polyolefin structure [10].



2 COBALTAFULVENE COMPLEXES

Cobaltfulvenes are obtained in a surprisingly simple and clean reaction, which involves the twofold CH activation of the methylene group of η^4 -coordinated cyclopentadiene, brought about by the reactive ethylene complexes $[(\eta^5\text{-C}_5\text{R}_5)\text{Co}(\text{C}_2\text{H}_4)_2]$ (**12**) (Scheme 1 and Table 1) [11,12].

With the highly reactive Jonas reagent (**12a**), excellent yields of the cobaltfulvene complexes **13aa**, **13ba** and **13da** are obtained under very mild conditions (room temperature, 3–7 days). Reactions with the more robust complex **12b** require somewhat higher temperatures (40–60 °C). The high tendency of formation of the dinuclear species is nicely illustrated by the reaction of **12b** with cyclopentadiene. The cyclopentadiene complex **11b**, which is the first reaction

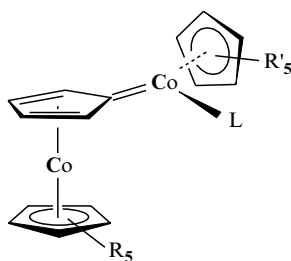


Scheme 1

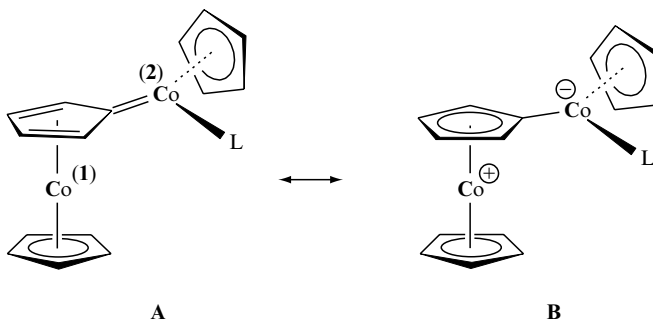
Table 1 Complexes with the cobaltfulvene ligand

Complex	C ₅ R ₅	C ₅ R' ₅	L	Complex	C ₅ R ₅	C ₅ R' ₅	L
13aa	C ₅ H ₅	C ₅ H ₅	C ₂ H ₄	13ab	C ₅ H ₅	C ₅ Me ₅	C ₂ H ₄
13ac	C ₅ H ₅	C ₅ H ₄ Me	C ₂ H ₄	13ba	C ₅ Me ₅	C ₅ H ₅	C ₂ H ₄
13bb	C ₅ Me ₅	C ₅ Me ₅	C ₂ H ₄	13da	C ₅ Me ₄ Et	C ₅ H ₅	C ₂ H ₄
14aa	C ₅ H ₅	C ₅ H ₅	CO	14ab	C ₅ H ₅	C ₅ Me ₅	CO
14ba	C ₅ Me ₅	C ₅ H ₅	CO	14bb	C ₅ Me ₅	C ₅ Me ₅	CO
15aa	C ₅ H ₅	C ₅ H ₅	^t BuNC	16aa	C ₅ H ₅	C ₅ H ₅	PMe ₃
16ab	C ₅ H ₅	C ₅ Me ₅	PMe ₃	17aa	C ₅ H ₅	C ₅ H ₅	PMe ₂ Ph
18aa	C ₅ H ₅	C ₅ H ₅	PMePh ₂	19aa	C ₅ H ₅	C ₅ H ₅	P(OMe) ₃

product, can only be isolated, still along with substantial amounts of **13bb**, when the reaction is carried out in neat cyclopentadiene. In a more dilute solution, **13bb** is exclusively formed, even in the presence of a large excess of cyclopentadiene.

**14–19**

Treatment of the ethylene complexes **13** with donor ligands L (L = CO, ^tBuNC, P(OMe)₃, PR₃) gives the substituted derivatives **14–19** (see Table 1). The complexes **13–19** are very air-sensitive, crystalline turquoise-green (**13–18**) or blue (**19**) solids.



The simple valence structure **A** for complexes **13–19** satisfies the 18-valence-electron rule for both cobalt atoms. Here, the cobaltafulvene moiety is η^4 -coordinated to Co(1) via the 1,3-diene system of the five-membered ring. However, a second 'resonance structure' **B** can be drawn, which involves a dipolar form of the cobaltafulvene, very similar to **6(C)** above. η^5 -Coordination of the five-membered ring generates a substructure which is very related to the well-known cobaltocenium ion. Effectively, **B** amounts to a zwitterion with the charges of opposite sign more or less localized on the two cobalt atoms.

The X-ray crystal structures of five derivatives of the cobaltafulvene complexes have been determined. The gross structural features are similar in all the derivatives studied. Two typical molecules are shown in Figures 1 and 2. A few important bond lengths and other relevant geometrical data are collected in Table 2.

Clearly, neither **A** or **B** suffice to describe the actual structures. Although not very pronounced, there is a definite trend in the molecular geometry, depending on the donor/acceptor properties of the ligand L on Co(2). As can be seen from Figure 1 and Table 2, the acceptor ligand CO causes the cobaltafulvene to flatten and the 'carbene' carbon C(1) to more closely approach Co(1). In contrast, in complex **16aa**, with the strong donor ligand PMe_3 , an increased folding of the cobaltafulvene away from Co(1) is noticeable (Figure 2 and Table 2). In other words, the carbon monoxide ligand pulls electron density away from Co(2), and increases the zwitterionic character. This is also apparent from the IR spectra of the carbonyl derivatives, which show the CO stretch at low wavenumbers ($1903\text{--}1875\text{ cm}^{-1}$). The opposite process is operative with the phosphine donor, thus shifting the actual structure more towards the limit **A**.

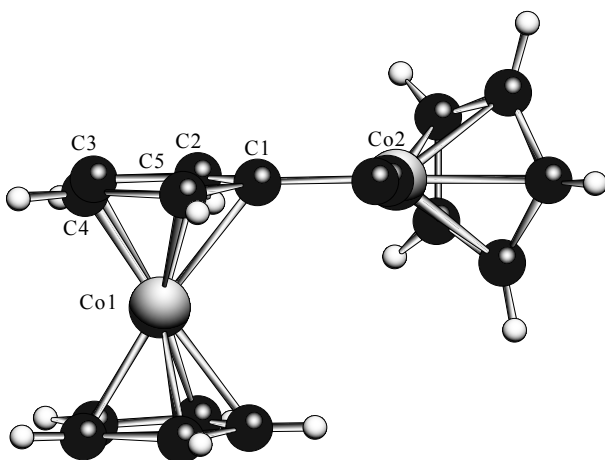


Figure 1 Molecular structure of complex **14aa**

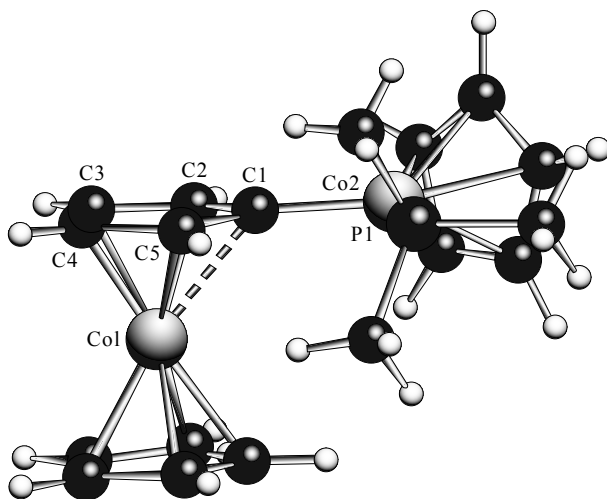


Figure 2 Molecular structure of complex **16aa**

Table 2 Important geometrical parameters (angles in degrees, distances in Å) for the complexes **13aa** ($R = R' = H$), **13ab** ($R = H, R' = Me$), **13ba** ($R = Me, R' = H$), **14aa** ($R = R' = H$), and **16aa** ($R = R' = H$)

Complex	13aa	13ab	13ba	14aa	16aa
Ligand	C ₂ H ₄	C ₂ H ₄	C ₂ H ₄	CO	PMe ₃
Co(1)–C(1)	2.188	2.228	2.202	2.156	2.240
Co(2)–C(1)	1.861	1.865	1.874	1.871	1.880
Co(1)···Co(2)	3.69	3.75	3.77	3.64	3.74
ϕ^a	5.8	7.2	5.2	2.7	7.7

^a Fold angle along C(2)–C(5).

As a further complication, spin equilibria are operative in the phosphine derivatives. This is revealed by the temperature-dependence of the NMR (¹H, ³¹P) resonances, which are shifted progressively on heating. The effects become less pronounced along the series, L = PMe₃ – PMe₂Ph – PMePh₂, and are not noticeable with other derivatives. The observed behaviour of the proton chemical shifts can be analysed in terms of the thermodynamics (ΔH^0 and ΔS^0) of the spin equilibrium between two isomers with total spin quantum numbers of $S = 0$ and 1 , respectively. Unfortunately, a unique solution for ΔH^0 and ΔS^0 cannot be achieved, due to the flatness of the hypersurface. A range of $24 \leq \Delta H^0 \leq 32 \text{ kJmol}^{-1}$ and $45 \leq \Delta S^0 \leq 74 \text{ Jmol}^{-1}\text{K}^{-1}$ is indicated by the obtained fits (Figure 3) [12].

Despite the ambiguities, one may safely conclude that the singlet-state species is the thermodynamically stable isomer in solution ($\Delta H^0 > 0$). The

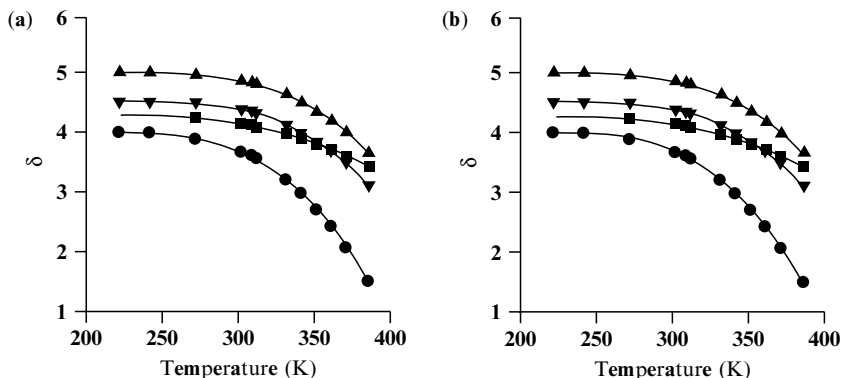
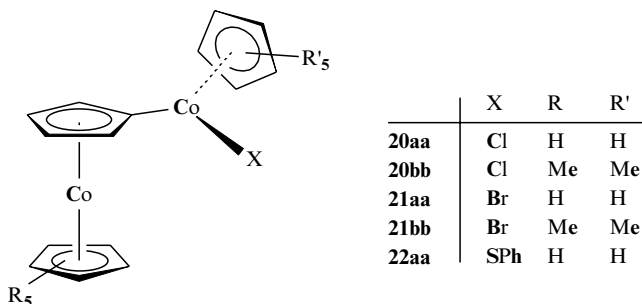


Figure 3 Temperature-dependence of the C_5H_5 and CH 1H NMR resonances of complex **16aa**, showing fits with (a) $\Delta H^0 = 27 \text{ kJ mol}^{-1}$, $\Delta S^0 = 45 \text{ J mol}^{-1} \text{ K}^{-1}$, and (b) $\Delta H^0 = 32 \text{ kJ mol}^{-1}$, $\Delta S^0 = 74 \text{ J mol}^{-1} \text{ K}^{-1}$. Reproduced by permission of Wiley-VCH from H. Wadepohl, W. Galm, H. Pritzkow and A. Wolf, *Chem. Eur. J.*, **2**, 1453 (1996)

concentration of the paramagnetic species remains low, even at elevated temperature (less than 30 % at 390 K).

In accord with the high sensitivity to air, cyclic voltammetry indicates facile one-electron oxidation of the cobaltfulvene complexes. At very negative potentials (beyond -1.2 V , versus SCE), the monoanions can also be generated reversibly. Careful chemical oxidation of the ethylene derivatives gives the paramagnetic neutral species **20–22** [13,14].



The molecular structure of **21bb** has been determined; it is similar to those of the diamagnetic derivatives, but shows a different rotational orientation of the two parts of the molecule around the bond $C1-Co2$ (Figure 4).

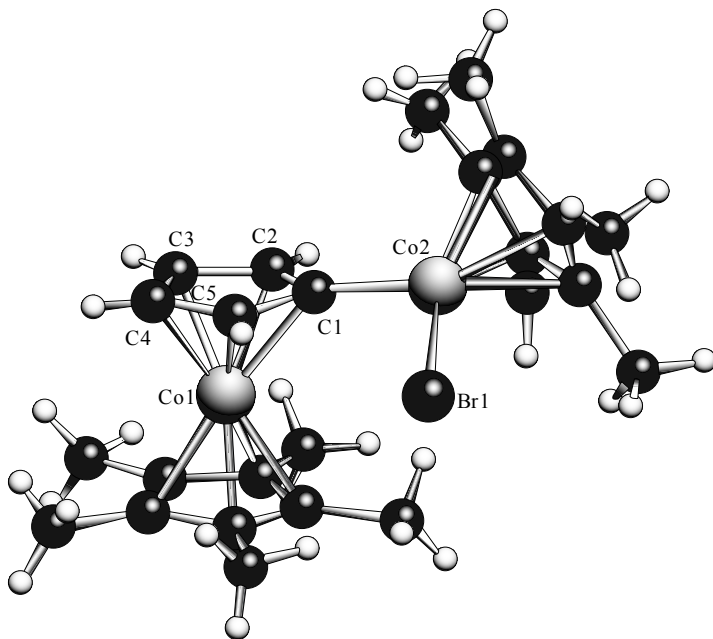
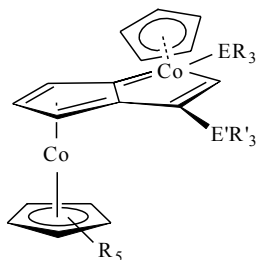


Figure 4 Molecular structure of complex **21bb**

3 COBALTAPENTALENE COMPLEXES

When the cobaltfulvene complexes **13aa** or **13ba** are heated with certain silyl or germyl substituted alkynes, an unusual cycloaddition reaction takes place. The purple products **23–30** (Table 3) are cyclopentadienyl cobalt complexes of the bicyclic cobaltapentalene ring system [15]. The carbonyl, trimethylphosphine and trimethylphosphite derivatives, **14aa**, **16aa** and **19aa**, respectively, can also be used for the reaction. However, with these substrates higher temperatures have to be used, and product yields are lower.



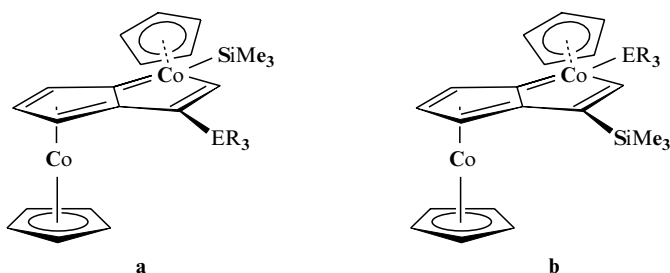
23 - 30

Table 3 Complexes with the cobaltapentalene ligand

Complex	C ₅ R ₅	ER ₃	E'R' ₃	Complex	C ₅ R ₅	ER ₃	E'R' ₃
23a	C ₅ H ₅	SiMe ₃	SiMe ₃	23b	C ₅ Me ₅	SiMe ₃	SiMe ₃
23c	C ₅ Me ₄ Et	SiMe ₃	SiMe ₃	24	C ₅ H ₅	SiMe ₂ Et	SiMe ₂ Et
25	C ₅ H ₅	SiMeEt ₂	SiMeEt ₂	26a	C ₅ H ₅	SiMe ₃	SiEt ₃
26b	C ₅ H ₅	SiEt ₃	SiMe ₃	27a	C ₅ H ₅	SiMe ₃	SiMe ₂ ^t Bu
27b	C ₅ H ₅	SiMe ₂ ^t Bu	SiMe ₃	28	C ₅ H ₅	SiMe ₃	CMe ₃
29a	C ₅ H ₅	SiMe ₃	GeMe ₃	29b	C ₅ H ₅	GeMe ₃	SiMe ₃
30	C ₅ H ₅	GeMe ₃	GeMe ₃				

In the reaction of **13aa** with the series of disilyl alkynes (Me_{3-n}Et_n)₂C₂ (*n* = 0 – 3), the product yield decreases from 80 % (*n* = 0) to 65 % (*n* = 1) to 35 % (*n* = 2), and higher temperatures have to be used in every case (45, 50 and 65 °C, respectively). With (SiEt₃)₂C₂ (*n* = 3) and **13aa**, no cobaltapentalene complex is formed, even at 75 °C. Hence, steric hindrance seems to play a crucial role. Indeed, molecular dynamics simulations indicate that in (SiEt₃)₂C₂ the silicon carbon bonds and even the carbon–carbon triple bond are effectively shielded by two ethyl groups, which are bent ‘backwards’ toward the centre of the molecule.

Similarly, the asymmetric alkyne Me₃SiC₂SiEt₃ gives two isomeric products **26a** and **26b** in a total yield of 80 %. When the reaction is carried out at 45 °C, the product **26a** with the smaller trimethylsilyl group on the cobalt is formed preferentially (67 %, **26a**; 33 %, **26b**). At higher temperatures (100 °C) both isomers are generated in approximately equal amounts. Similar results are obtained with Me₃SiC₂SiMe₂^tBu, but the dependence on temperature of the ratio of the products **27a** and **27b** was less pronounced.



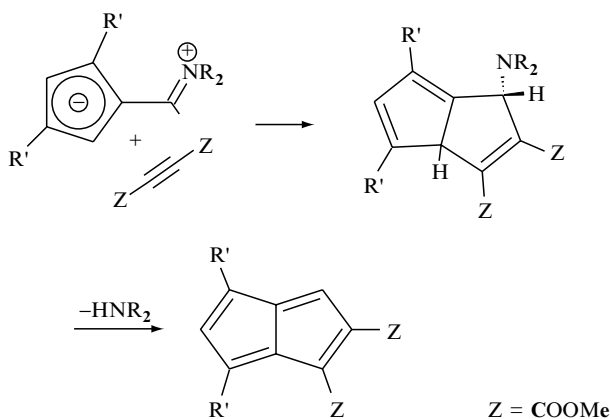
26, ER₃ = SiEt₃
27, ER₃ = SiMe₂^tBu
29, ER₃ = GeMe₃

When heated with **13aa** at 40 °C, the silyl/germyl alkyne Me₃SiC₂GeMe₃ nearly exclusively gave the product **29a** (70 % yield). Here the stronger carbon–silicon bond (rather than the weaker carbon–germanium bond) is

cleaved, and the silyl group becomes attached to cobalt. An increase of the reaction temperature (90 °C) again causes formation of both isomers **29a** and **29b** in about equal amounts. In contrast, $\text{Me}_3\text{SiC}_2^t\text{Bu}$ and **13aa** always give only one product, i.e. **28**, with the silyl group on the cobalt atom. Heating of **29a** to 80 °C for several hours does not result in isomerization, and no **29b** is formed.

The pairs of isomeric products, **26a** and **26b**, **27a** and **27b**, and **29a** and **29b**, cannot be separated. They are, however, clearly distinguished by their ^{29}Si NMR spectra, which show characteristic broad resonances at low field ($40 \leq \delta \leq 30$) for the silyl groups on cobalt [14].

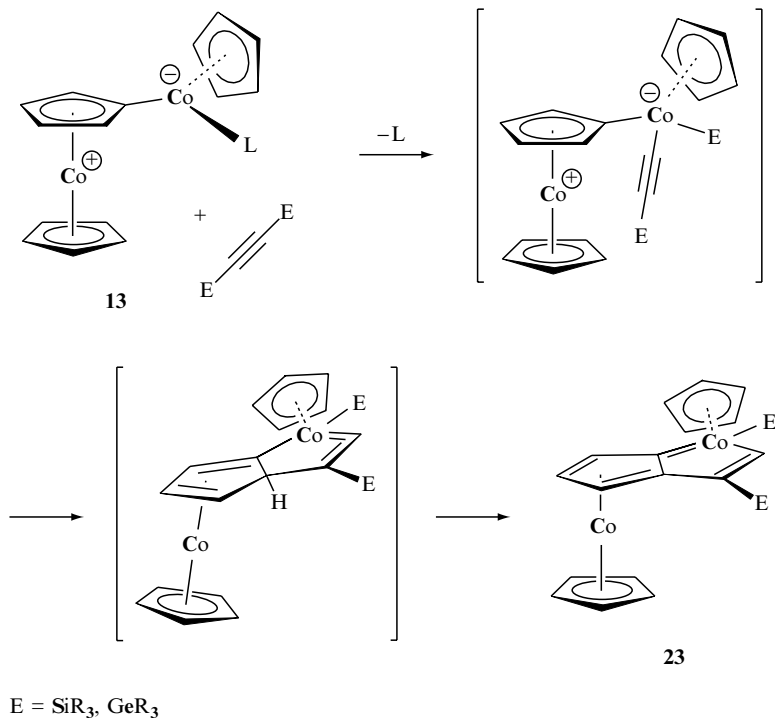
The formation of the cobaltapentalene bicyclic ring system from a metallafulvene and an alkyne is somewhat reminiscent of a cycloaddition reaction with an activated alkyne in organic fulvene chemistry. Electrophilic addition of acetylene dicarboxylic acid dimethyl ester to certain 6-aminofulvenes generates a pentalene derivative, probably via a dihydropentalene intermediate (Scheme 2) [16].



Scheme 2

However, electrophilic addition is not likely to be involved with the electron-rich alkynes used for the generation of the cobaltapentalenes. We believe that the reaction is initiated by an oxidative addition of the alkyne to the cobalt atom of the cobaltfulvene (Scheme 3). Nucleophilic attack of the cobaltfulvene by the β -carbon atom of the newly formed acetylide generates the metal-bicyclic ring system, which is then converted into the final cobaltapentalene by a 1,3-hydrogen shift.

This proposal is in line with the experimental results described above. In particular, of the two carbon–element (Si, Ge) bonds in $\text{Me}_3\text{SiC}_2\text{GeMe}_3$, the carbon–silicon bond is more polar and expected to more readily undergo



Scheme 3

oxidative addition, despite its higher bond energy. This would explain why **29a** with a cobalt–silicon bond is formed more easily than the Co–Ge isomer, **29b**. A sterically demanding transition state for oxidative addition of the alkyne also accounts for the observed distribution of isomers in the products of the reactions of **13aa** with $(\text{Me}_{3-n}\text{Et}_n\text{Si})_2\text{C}_2$.

The molecular structure of the cobaltapentalene complex **23c** is shown in Figure 5. The cobalt-containing part of the cobaltapentalene is completely planar, positioned at an angle of 6° to the other half of the bicyclic ring system. The pattern of endocyclic bond lengths is shown in Figure 6. There is more variation within the C₅Co moiety, but the cobalt carbon bonds are equal and quite short (1.88 Å).

As with the cobaltafulvene complexes **13–22**, the experimental molecular geometry cannot be explained satisfactorily by a single valence structure. Similar to structures **A** and **B** above, the resonance structures **C**, **D** and **E** can be drawn. Again, a considerable contribution from the dipolar structure **E** has to be assumed.

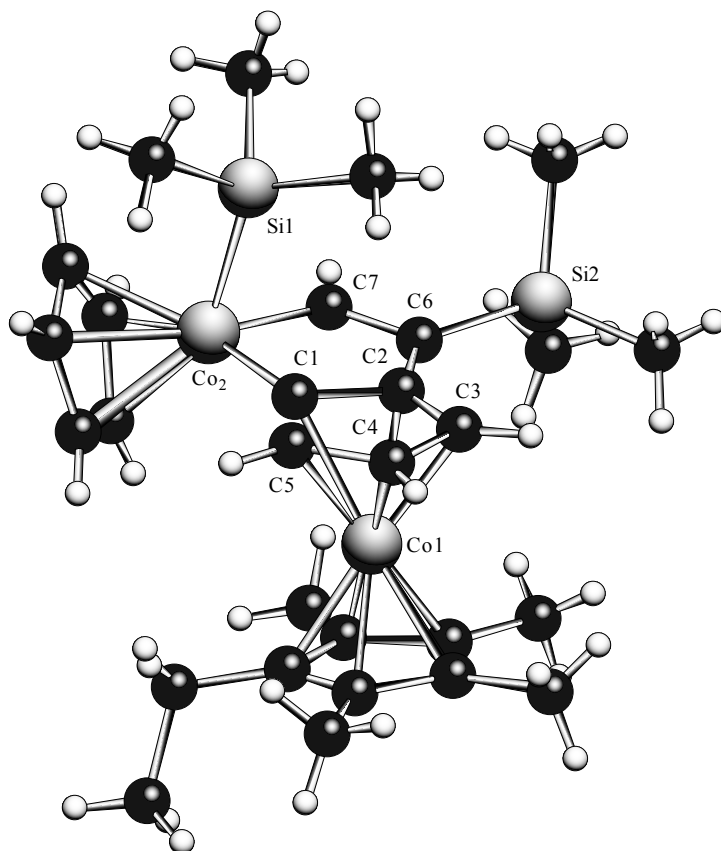
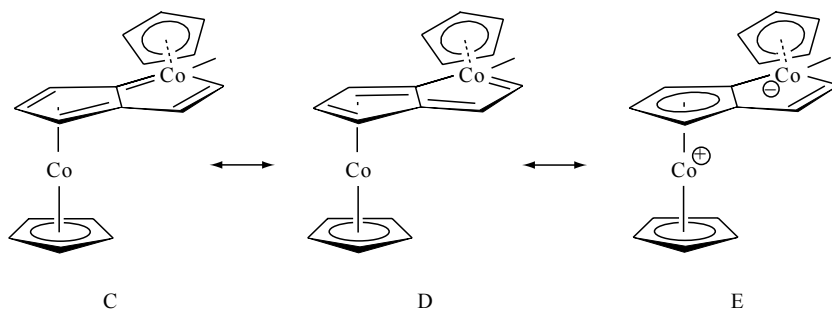


Figure 5 Molecular structure of complex 23c

4 CONCLUSIONS

For an understanding of the unusual structures of the complexes presented in this paper, isolobal relationships [7] are quite useful. This concept is based on

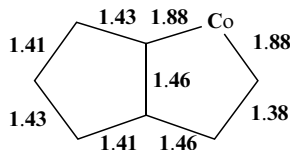
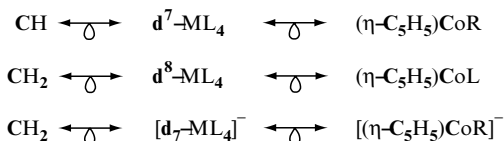


Figure 6 Bond lengths (Å) in the cobaltfulvene ligand in complex **23c**

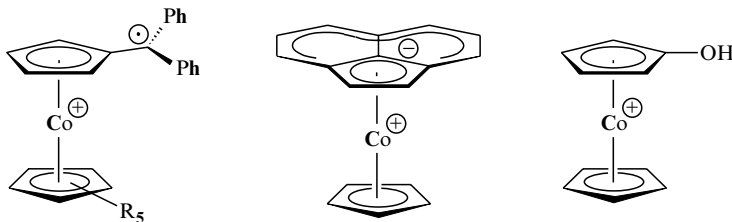


Scheme 4

similarities of the frontier orbitals of certain organic and organometallic fragments. In several places, we have already used isolobality to relate the organometallic fragments $(\eta\text{-C}_5\text{H}_5)\text{Co(L)}$ and $(\eta\text{-C}_5\text{H}_5)\text{Co(R)}$ to methylene CH_2 and methyne CH , respectively (Scheme 4).

Isolobality is however not a 1:1 relationship; for example, CH_2 is also isolobal to the anionic fragment $[(\eta\text{-C}_5\text{H}_5)\text{Co(R)}]^-$ Scheme 4. In Scheme 5, some of these relationships are translated into chemical compounds.

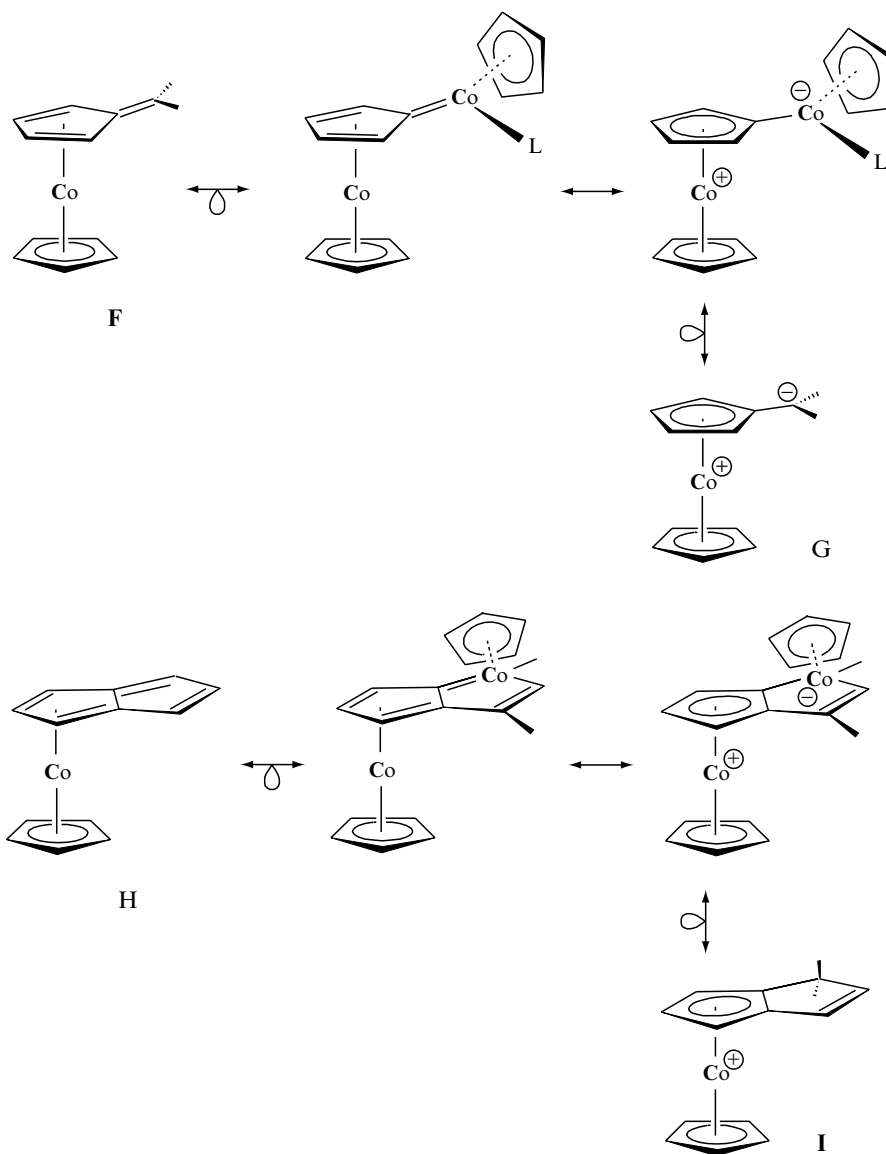
A variety of cyclopentadienyl cobalt complexes of organic fulvenes have been reported; invariably, η^4 -fulvene structures (**F**) are adopted [18–20]. There is no tendency for the neutral derivatives to form the zwitterions (**G**). However, the cations $[(\eta\text{-C}_5\text{R}_5)\text{Co}(6;6\text{-diphenylfulvene})]^+$ (**31**) have been shown to correspond to cobaltocenium-ion-substituted carbon-centered radicals [19]. A mono-nuclear cyclopentadienyl cobalt complex (**H**) of pentalene is unknown. The diamagnetic $[(\eta\text{-C}_5\text{Me}_5)\text{Co}]_2(\text{pentalene})$ has been prepared; unfortunately, the structure of this complex has not yet been determined [21]. Some complexes closely related to **I** have been reported and show indeed a η^5 -coordination of the hydropentalenyl ligand [22].



31a, R = H
31b, R = Me

32

33



Scheme 5

The cobaltfulvene and cobaltapentalene complexes discussed in this paper owe much of their stability and unusual properties to their (at least partial) zwitterionic structure. A cobaltocenium ion substructure is formed, which on its own is a highly preferred and stable moiety. A similar effect was

noted in the complex $[(\eta\text{-C}_5\text{H}_5)\text{Co}(\text{acenaphthylene})]$ (**32**), which also has a zwitterionic structure [23]. The products **33** [24] and **31** [19], derived from protonation of $[(\eta\text{-C}_5\text{H}_5)\text{Co}(\eta^4\text{-cyclopentadienone})]$ and oxidation of $[(\eta\text{-C}_5\text{R}_5)\text{Co}(\eta^4\text{-6,6-diphenylfulvene})]$, respectively, also gain their high stability from the cobaltocenium cation substructure.

5 ACKNOWLEDGEMENTS

This work was supported by the Deutsche Forschungsgemeinschaft, the Sonderforschungsbereich 247 and the Fonds der Chemischen Industrie. The award of a Heisenberg Fellowship is gratefully acknowledged.

6 REFERENCES

1. W. Lin, S. R. Wilson and G. S. Girolami, *Organometallics*, **16**, 2356 (1997).
2. (a) J. B. Collman, L. S. Hegedus, J. R. Norton and R.-G. Finke, *Principles and Applications of Organotransition Metal Chemistry*, University Science Books, Mill Valley, CA, 1987. (b) G. Wilke, *Pure Appl. Chem.*, **60**, 677 (1978). (c) G. Wilke, *Angew. Chem.*, **100**, 189 (1978).
3. D. L. Thorn and R. Hoffmann, *Nouv. J. Chem.*, **3**, 39 (1979).
4. P. v. R. Schleyer, B. Kiran, D. V. Simion and T. S. Sorensen, *J. Am. Chem. Soc.*, **122**, 510 (2000).
5. D. Lloyd, *Non-Benzenoid Conjugated Carbocyclic Compounds*, Elsevier, Amsterdam, 1984.
6. (a) P. A. Straub, D. Meuche and E. Heilbronner, *Helv. Chim. Acta*, **49**, 517 (1966). (b) E. D. Bergmann, *Chem. Rev.*, **68**, 41 (1968).
7. (a) R. Hoffmann, *Science (Washington)*, **211**, 995 (1981). (b) R. Hoffmann, *Angew. Chem.*, **94**, 725 (1982).
8. W. A. Herrmann, J. Plank, M. L. Ziegler and K. Weidenhammer, *Angew. Chem.*, **90**, 817 (1978).
9. W. A. Herrmann, G. Kriechbaum, C. Bauer, E. Guggolz and M. L. Ziegler, *Angew. Chem.*, **93**, 838 (1981).
10. N. C. Baird and R. M. West, *J. Am. Chem. Soc.*, **93**, 3072 (1972).
11. H. Wadepohl and H. Pritzkow, *Angew. Chem.*, **99**, 132 (1987).
12. H. Wadepohl, W. Galm, H. Pritzkow and A. Wolf, *Chem. Eur. J.*, **2**, 1453 (1996).
13. H. Wadepohl, W. Galm, H. Pritzkow and A. Wolf, *J. Chem. Soc., Chem. Commun.*, 1459 (1993).
14. A. Wolf, *PhD Dissertation*, Universität Heidelberg, Heidelberg, Germany, 1994.
15. H. Wadepohl, W. Galm, H. Pritzkow and A. Wolf, *Angew. Chem.*, **104**, 1050 (1992).
16. K. Hafner and M. Suda, *Angew. Chem.*, **88**, 341 (1976).
17. M. Elian, M. M. L. Chen, D. M. P. Mingos and R. Hoffmann, *Inorg. Chem.*, **15**, 1148 (1976).
18. H. Wadepohl and H. Pritzkow, *Acta Crystallogr., Sect. C*, **47**, 2061 (1991).
19. H. Wadepohl, F.-J. Paffen and H. Pritzkow, *J. Organomet. Chem.*, **579**, 391 (1999).
20. D. Rau and U. Behrens, *J. Organomet. Chem.*, **387**, 219 (1990).

21. E. E. Bunel, L. Valle, N. L. Jones, P. J. Carroll, C. Barra, M. Gonzalez, N. Munoz, G. Visconti, A. Aizman and J. M. Manriquez, *J. Am. Chem. Soc.*, **110**, 6596 (1988).
22. (a) T. J. Katz and M. Rosenberger, *J. Am. Chem. Soc.*, **85**, 2030 (1963). (b) T. J. Katz and J. J. Mrowca, *J. Am. Chem. Soc.*, **89**, 1105 (1967).
23. K. Jonas, *J. Organomet. Chem.*, **400**, 165 (1990).
24. J. E. Sheats, G. Hlatky and R. S. Dickson, *J. Organomet. Chem.*, **73**, 107 (1979).

9 Novel Highly Nucleophilic Ylidic Ligands for the Preparation of Unusually Stable Metal Complexes

NORBERT KUHN and MARTIN GÖHNER

Institut für Anorganische Chemie der Universität Tübingen, Auf der Morgenstelle 18, D-72076, Tübingen, Germany

and

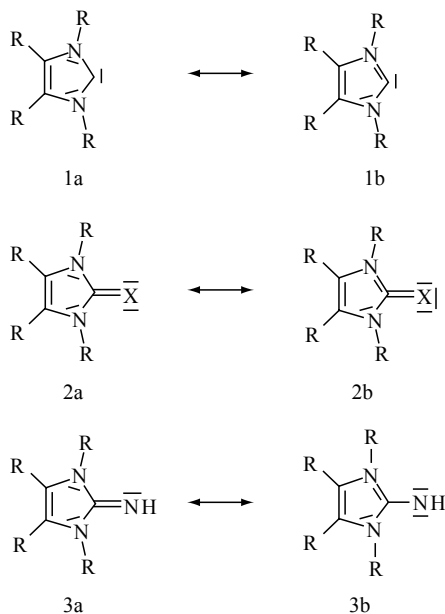
GERNOT FRENKING and YU CHEN

Fachbereich Chemie, Philipps-Universität Marburg, Hans-Meerwein-Strasse, D-35032 Marburg, Germany

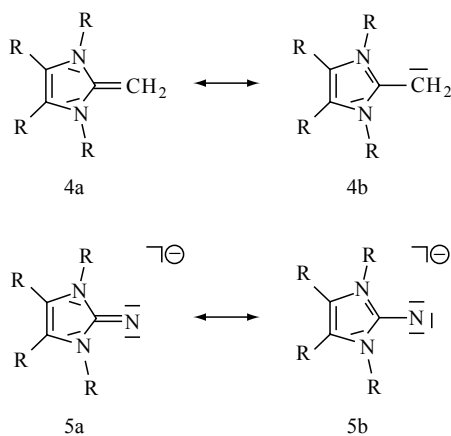
1 INTRODUCTION

There has been much interest in imidazole-derived bases in the past few years. For example, 2,3-dihydroimidazol-2-ylidenes (**1**) form stable carbenes, apparently as a consequence of the ability of the heterocyclic ring to stabilize formal positive charges [1]. For similar reasons, 2-chalcogenoimidazolines (**2**, X = Se [2], Te [3]) may be regarded as electroneutral selenolates or tellurolates from their coordination chemistry [4], as well as from their reactions with electrophilic main group centres [5,6].

Replacing the chalcogen atoms in **2** with methylene or imino fragments leads to the title compounds **3** and **4**, in which the exocyclic groups attached at C2 should also bear a negative formal charge. In the following, we will give an insight into the coordination chemistry of these interesting molecules, which have been investigated in our laboratories. We have also carried out DFT calculations using B3LYP and 6-31G (d,p) basis sets in order to investigate the geometries and electronic structures of the molecules [7,8]. The analysis of the bonding situation was carried out by using the natural bond orbital (NBO) method [9].



Scheme 1a



Scheme 1b

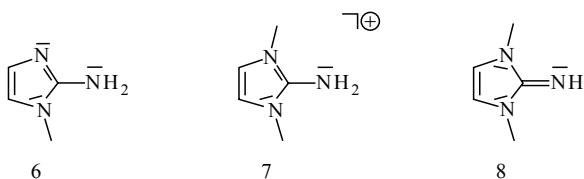
2 IMINOIMIDAZOLINES

2.1 SYNTHESIS AND STRUCTURE

As outlined above, 2-methyleneimidazolines should act as electroneutral amides R_2N^- , owing to the ylide-type resonance structure **3b**. Similarly, the deprotonated imidoimidazolinone species **5** may be compared with the imide

dianion RN^{2-} . Surprisingly, there are only rare examples of investigations of the chemistry of 2-iminoimidazolines [10]. This finding contrasts strongly with the rapidly developing chemistry of tetramethylguanidine derivatives [11], presumably as a consequence of problems with their syntheses.

In fact, all attempts to prepare 2-methyleneimidazolines from 2-chloroimidazolium cations and potassium amide have failed so far [12]. Reacting the basic type (**1**) carbenes with HN_3 leads exclusively to imidazolium azide salts instead of dinitrogen emission [13]. A simple and convenient route to 1,3-dimethyl-2-iminoimidazoline (**8**) (ImNH) starts from 1-methylimidazolamine (**6**) and methyl iodide, followed by deprotonation of the resulting 2-aminoimidazolium salt **7** with potassium hydride [14]. This method is unfortunately restricted to 3-methyl-2-iminoimidazolines as a consequence of side reactions, apparently deprotonation, when using alkyl iodides other than MeI. A promising synthetic route currently being investigated by us may be the cyclization of β -diketodiimines with trimethylsilyl thiocyanate under reduction conditions, followed by alcoholysis.



Scheme 2

The crystal structure analysis of **8** (Figure 1) reveals a short exocyclic CN bond (1.296(2) Å) which may indicate, together with the ‘in plane’ orientation of the NH fragment, the dominance of the ylène-type electron distribution [14]. From Wittig ylide structures, however, we know about the risks of this argument [15]. The angle N(2)–C(1)–N(3) (104.6(1)°) is clearly in the range of imidazoline derivatives containing double-bonded substituents at C2 [2,3,16]. Comparing the structure of **7** (chloride salt, Figure 2) we see the expected lengthening of the exocyclic CN bond (1.332(5) Å) in this case [14].

2.2 BONDING IN 2-IMINOIMIDAZOLINES

In order to elucidate the electronic structure and bonding situation in 2-iminoimidazolines, we carried out DFT calculations at the B3LYP/6-31G(d,p) level of theory [7] of molecules **6**, **7**, **8**. Figure 3 shows the theoretically predicted equilibrium geometries of the compounds, which are in very good agreement with the experimental values [14]. The results of the NBO analyses are given in Table 1.

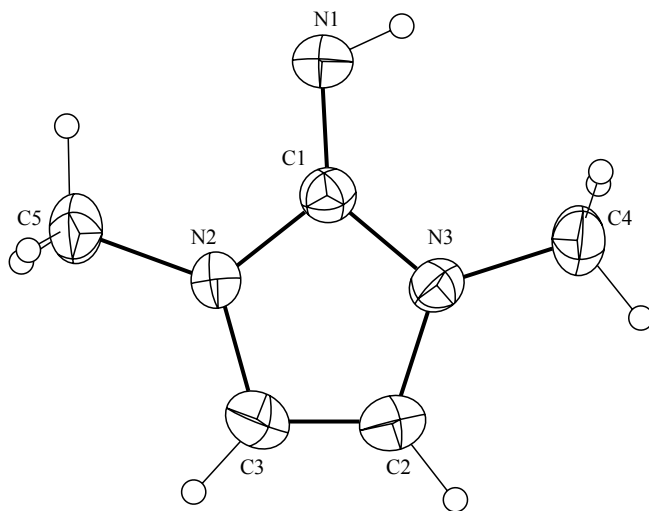


Figure 1 The crystal structure of $C_5H_9N_3$ (**8**). Selected bond lengths (Å) and angles ($^\circ$): C(1)–N(1) 1.296(2), C(1)–N(2) 1.375(2), N(2)–C(3) 1.392(2), C(3)–C(2) 1.330(2), C(2)–N(3) 1.390(2), N(3)–C(1) 1.371(2); N(1)–C(1)–N(2) 123.9(1), N(1)–C(1)–N(3) 131.4(1), N(2)–C(1)–N(3) 104.6(1), C(1)–N(1)–H 110.3(17); N(2)–C(1)–N(1)–H(1) 4.2. Reproduced by permission of Verlag der Zeitschrift für Naturforschung from N. Kuhn, R. Fawzi, M. Steimann, J. Wiethoff, D. Bläser and R. Boese, *Z. Naturforsch., B*, **50**, 1779 (1995)

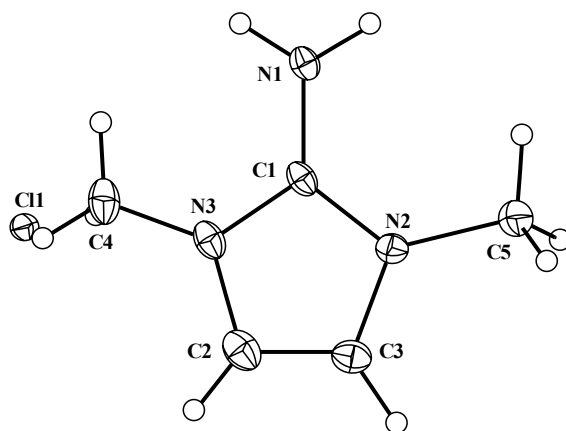


Figure 2 The crystal structure of $C_5H_{10}ClN_3$ (**7**). Selected bond lengths (Å) and angles ($^\circ$): C(1)–N(1) 1.332(5), C(1)–N(2) 1.336(5), N(2)–C(3) 1.397(5), C(3)–C(2) 1.344(7), C(2)–N(3) 1.384(6), C(1)–N(3) 1.354(5); N(2)–C(1)–N(3) 108.1(3), N(1)–C(1)–C(2) 126.4(3), N(1)–C(1)–C(3) 125.4(4), H(1)–N(1)–H(1') 108.2; N(2)–C(1)–N(1)–H(1) 1.6. Reproduced by permission of Verlag der Zeitschrift für Naturforschung from N. Kuhn, R. Fawzi, M. Steimann, J. Wiethoff, D. Bläser and R. Boese, *Z. Naturforsch., B*, **50**, 1999 (1995)

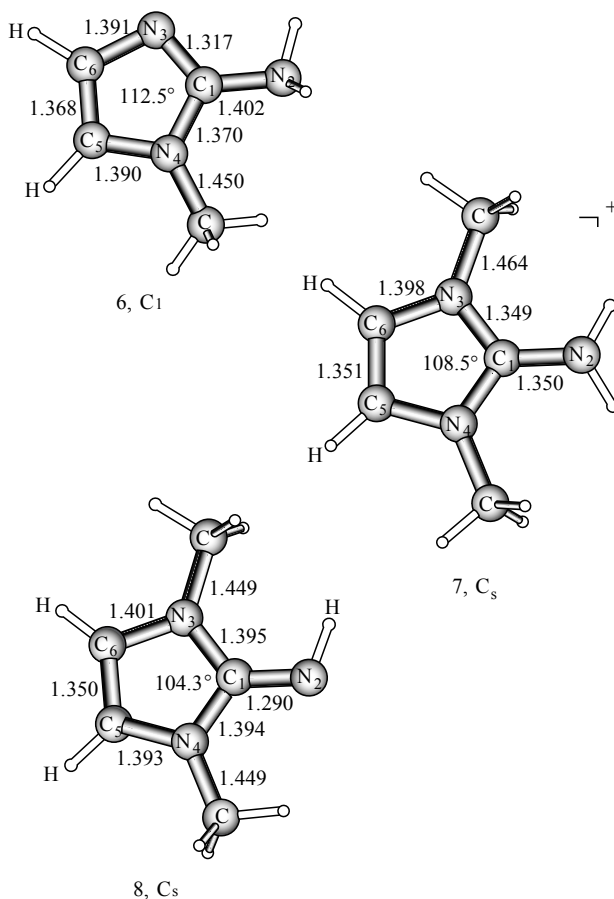


Figure 3 Calculated geometries of complexes **6**, **7** and **8**; bond lengths in Å, and angles in degrees

The NBO analysis of 1,3-dimethyl-2-iminoimidazoline (**8**) shows, as expected, that the weight of the Lewis structure **3a** (Scheme 1a) is higher than **3b**. The bond orders P_{AB} indicate partial double-bond character for the exocyclic C₁–N₂ bond (1.66), while the endocyclic C₁–N₃ and C₁–N₄ bonds are single bonds (1.08). The C₁–N₂ p-bond is polarized towards the nitrogen end (33.5% at the carbon atom). The C₁–N₂ s-bond is also polarized towards the N atom. We want to point out that there is a very large charge polarization of the C₁–N₂ bond. The atomic partial charges are +0.606 (C₁) and –0.845 (N₂). Protonation of **8** gives the Y-conjugated cation **7**. The NBO results (Table 1) suggest that the endocyclic C₁–N₃ and C₁–N₄ bonds in **7** have nearly the same π -bonding character as the exocyclic C₁–N₂ bond. This is given by the calculated bond orders which are only slightly higher for the former bonds (1.24)

Table 1 NBO results obtained for compounds **6**, **7**, **8**, **9**⁻, **9Li**, **10**⁺ and **18M** at B3LYP/6-31G(d,p)^a

Com- pound	<i>q</i>												<i>P_{AB}</i>								<i>C_i</i> (%)			
	<i>C</i> ₁	<i>N</i> ₂	<i>N</i> ₃	<i>N</i> ₄	<i>C</i> ₁	<i>N</i> ₂	<i>N</i> ₃	<i>N</i> ₄	<i>C</i> ₁ - <i>N</i> ₂	<i>C</i> ₁ - <i>N</i> ₃	<i>C</i> ₁ - <i>N</i> ₄	<i>σ</i> (<i>C</i> ₁ - <i>N</i> ₂)	<i>σ</i> (<i>C</i> ₁ - <i>N</i> ₃)	<i>σ</i> (<i>C</i> ₁ - <i>N</i> ₄)	<i>σ</i> (<i>C</i> ₁ - <i>N</i> ₃)	<i>σ</i> (<i>C</i> ₁ - <i>N</i> ₄)	<i>σ</i> (<i>C</i> ₁ - <i>N</i> ₃)	<i>σ</i> (<i>C</i> ₁ - <i>N</i> ₄)	<i>π</i> (<i>C</i> ₁ - <i>N</i> ₃)	<i>π</i> (<i>C</i> ₁ - <i>N</i> ₄)				
6	0.562	-0.902	-0.548	-0.413	0.998	—	1.278	1.582	1.08	1.51	1.16	59.72	41.62	36.25	40.21	—	—	—	—	—	—			
7	0.664	-0.842	-0.383	-0.383	0.936	1.757 ^b	1.568	1.568	1.22	1.24	1.24	40.93	38.29	38.29	25.48	—	—	—	—	—	—			
8	0.606	-0.845	-0.451	-0.433	0.947	1.464	1.657	1.646	1.66	1.07	1.08	43.25	37.00	37.17	—	—	—	—	—	—	33.45			
9 ⁻	0.435	-0.805	-0.531	-0.531	1.016	1.149	1.665	1.665	2.27	0.82	0.82	43.59	35.08	35.08	—	—	—	—	—	—	46.72			
9Li	0.591	-1.234	-0.450	-0.450	0.939	1.425	1.648	1.648	1.77	1.02	1.02	42.68	36.43	36.43	—	—	—	—	—	—	34.57			
10 ⁺	0.658	-1.073	-0.431	-0.421	0.919	1.515	1.427	1.427	1.55	1.09	1.10	41.31	37.02	37.16	—	—	—	—	—	—	29.55			
18M	0.640	-0.743	-0.381	-0.381	0.929	1.397	1.560	1.561	1.36	1.17	1.16	42.23	37.35	37.33	—	—	—	—	—	—	—			

^a An ECP with a (441/2111/41) valence basis set was used for Ti.

^b Calculated with enforced planarity of the *C*₁-*NH*₂ moiety.

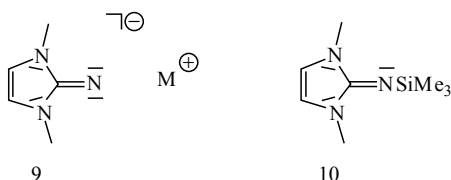
than for the latter (1.22). The endocyclic C_1-N_3 π -bond in **7** is more polarized towards the nitrogen end (25.5 % at carbon) than the exocyclic C_1-N_2 π -bond in **8**. The proton affinity (PA) of **8** is very high. The calculated value at B3LYP/6-31G(d,p) is 253.4 kcal mol⁻¹ [8]. This is even higher than the PA of guanidine. The theoretically predicted value at B3LYP/6-31G(d,p) for the PA of guanidine is only 244.2 kcal mol⁻¹.

Table 1 shows also the NBO results for 1-methylimidazolamine (**6**), which are given for comparison with **7** and **8**. Compound **6** has a C_1-N_3 double bond ($P_{AB} = 1.51$) which is less polarized toward the nitrogen end (40.2 % at C) than the carbon–nitrogen double bonds of **7** and **8**.

2.3 METALATION AND SILYLATION

Commonly, amines and imines are transferred into a more reactive state by metalation. In the case of **8**, the lithio [17], sodio [12], and potassio [12,18] derivatives ImNM (**9**) are obtained through reaction with MeLi, NaH, KH or MeK as colourless, air-sensitive solids of apparently polymeric nature. Soluble compounds are obtained by the addition of crown ethers, and a crystal structure investigation of [K(18-crown-6)][ImN] is currently in progress [19].

Although slightly soluble in acetonitrile, the structure of (ImN)₂Mg [20] obtained from Bu₂Mg and **8** is, as yet, unknown. A very soluble and highly reactive imidoimidazoline transfer reagent is conveniently accessible through the reaction of **8** with chlorotrimethylsilane; the resulting silyl compound (**10**) may be purified by distillation *in vacuo* and reacts rapidly with covalent inorganic chlorides (see below).



Scheme 3

2.4 BONDING IN 2-IMIDOIMIDAZOLINES

We calculated the structure and bonding situation of the free 2-imidoimidazoline anion **9**⁻ and the lithium derivative **9**Li at B3LYP/6-31G(d). Figure 4 shows the theoretically predicted geometries of the molecules. The NBO results are given in Table 1.

The calculations predict a rather short C_1-N_2 distance (1.224 Å) for the parent anion **9**⁻ while the C_1-N_3 and C_1-N_4 distances (1.518 Å) indicate single bonds. The geometrical parameters are supported by the calculated bond

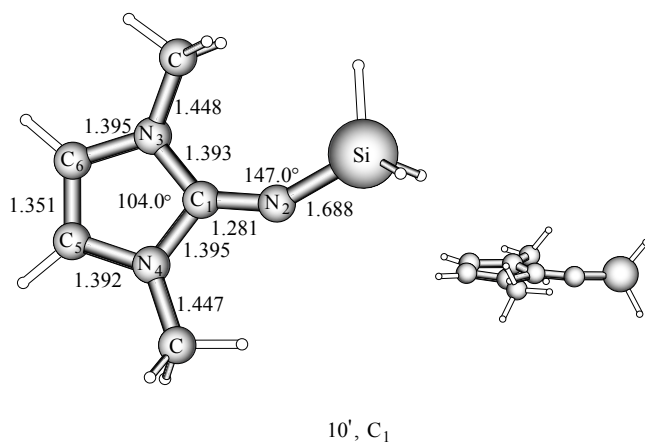
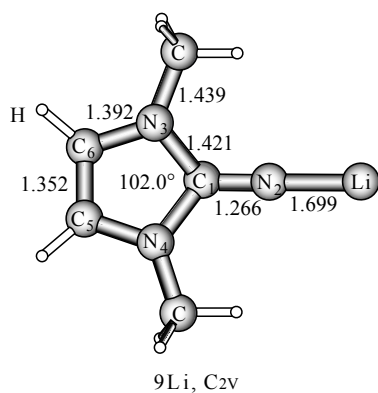
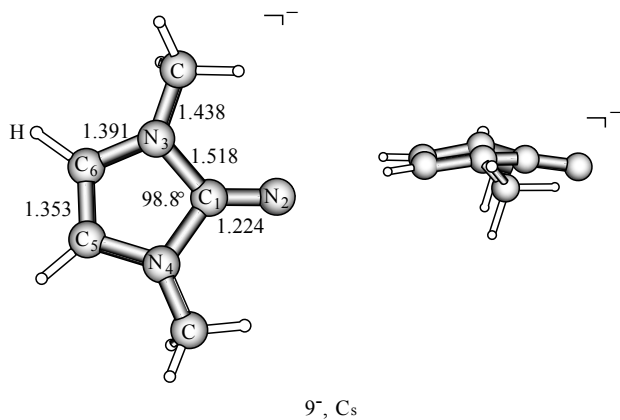


Figure 4 Calculated geometries of 9⁻, 9Li and 10'; bond lengths in Å, and angles in degrees

orders. The P_{AB} value for the C_1-N_2 bond (2.27) suggest even some bonding contributions from the in-plane π -orbital, i.e. partial triple-bond character. We wish to point out that the out-of-plane π -bond of C_1-N_2 is only slightly polarized towards the nitrogen end (46.7 % at C_1). The bond orders for the endocyclic C_1-N_3 and C_1-N_4 bonds (0.82) suggest single-bond character. The calculations predict that the ring structure of $\mathbf{9}^-$ is not perfectly planar. The deviation from planarity, which is caused by the repulsion between the methyl hydrogen atoms and N_2 , is not very large. We also want to point out that the population of the $p(\pi)$ orbital of N_2 (1.149 e) in $\mathbf{9}^-$ is significantly less than in $\mathbf{8}$ (Table 1). This means that the C_1-N_2 bond of $\mathbf{9}^-$ does not have the ylidic character as has been found for $\mathbf{8}$.

The calculated geometry and the results of the NBO analysis of $\mathbf{9Li}$ show that the bonding situation of the ring structure in the lithium derivative of 2-imidoimidazoline resembles that of compound $\mathbf{8}$. The main difference is that in the former molecule, the nitrogen atom N_2 carries a much higher negative charge (-1.234 e) than in the latter molecule (-0.845 e). The C_1-N_2-Li linkage of $\mathbf{9Li}$ is linear, while the C_1-N_2-H moiety of $\mathbf{8}$ is bent. The C_1-N_2 bond is shorter and the $C_1-N_{3/4}$ bonds are longer in $\mathbf{9Li}$ than in $\mathbf{8}$. We wish to emphasize here that $\mathbf{9Li}$ is a model compound which cannot directly be compared with the experimental structure of the true lithium derivative, because the latter compound has a polymeric structure, while the lithium atom in $\mathbf{9Li}$ is only mono-coordinated.

We have also carried out calculations for the silyl derivative $ImNSiH_3$ ($\mathbf{10}'$) which is a model system for the compound $\mathbf{10}$. Figure 4 shows the optimized geometry, and Table 1 the NBO data. The silyl group changes the ring structure of the parent compound $\mathbf{8}$ only very little. This becomes obvious when the calculated geometries and the NBO data of the molecules are compared. The exocyclic C_1-N_2 bond of $\mathbf{10}'$ is slightly shorter than in $\mathbf{8}$. The former compound has a more negatively charged nitrogen atom (N_2) than the former.

2.5 THE STRUCTURE OF $[Li_{12}O_2Cl_2(ImN)_8]$

The unusual coordination properties of the anion ImN^- are best documented by the structure of the cage compound $[Li_{12}O_2Cl_2(ImN)_8(THF)_4]$ ($\mathbf{11}$) obtained from $\mathbf{8}$ and $MeLi$ in tetrahydrofuran in the presence of air [17]. Commonly, the structures of organolithium compounds follow a limited number of ring, ladder and prismatic cage types [21]. The centrosymmetric structure (Figure 5) consists of a folded $Li_4N_2O_2$ ladder in which the central O_2^{2-} ion is connected to two Li centres. The two adjacent Li_4ClN_3 layers are connected with the central $Li_4N_2O_2$ unit via LiO and LiN interactions. The cage contains imidoimidazoline ligands coordinated at 3 ($N1, N21, N31$) and 4 ($N11$) Li centres ($LiN, 1.978(6)-2.183(6) \text{ \AA}$). There are only rare examples of molecular metal amide and imide structures containing nitrogen in a coordination state higher than four [22]: this demonstrates the high charge density at the imido nitrogen atoms discussed above.

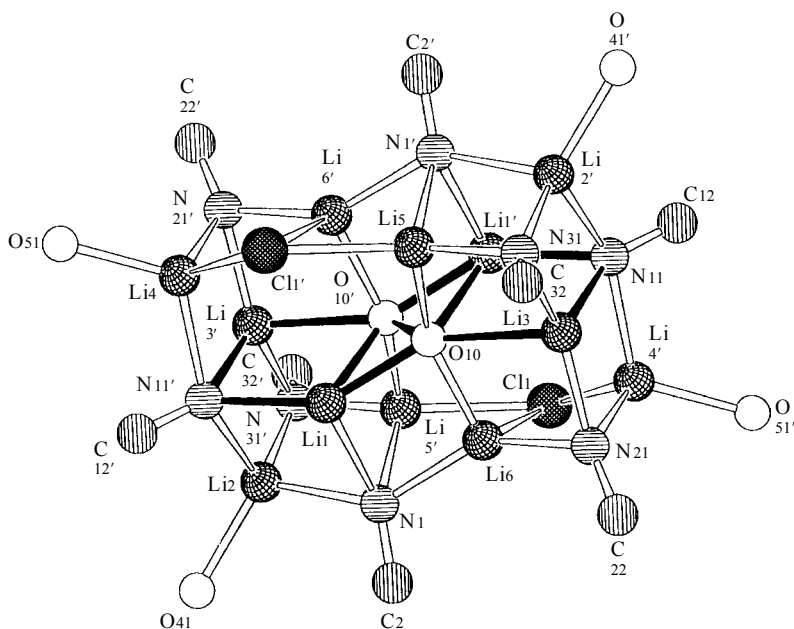
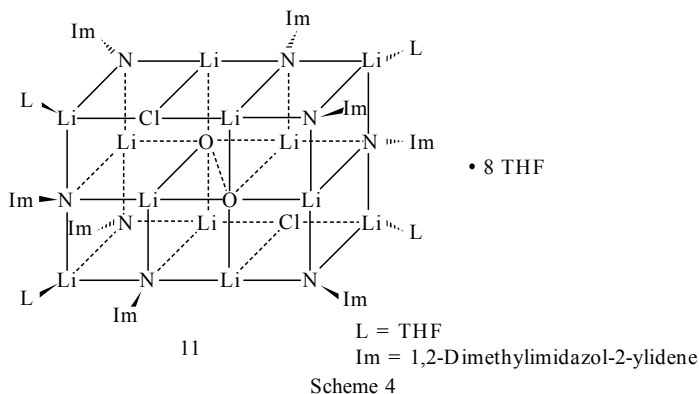


Figure 5 The crystal structure of $C_{56}H_{96}Cl_2Li_{12}N_{24}O_6 \cdot 8THF$ (**11**, $Li_{12}Cl_2N_8O_2$ core and atoms attached thereon). Selected bond lengths (Å) and angles ($^\circ$): $C-N_{cage}$ 1.260(4)–1.263(4), $N-Li$ 1.953(6)–2.183(6), $Li-Cl$ 2.385(6)–2.396(6), $Li-O$ 1.917(6)–2.593(5), $O(10)-O(10A)$ 1.544(4); ($N-C-N$)_{ring} 101.3(3)–101.6(3). Reproduced by permission of Wiley-VCH from N. Kuhn, U. Abram, C. Maichle-Mößmer and J. Wiethoff, *Z. Anorg. Allg. Chem.*, **623**, 1121 (1997)

2.6 IMINOIMIDAZOLINE PHOSPHANES

The ability of the imidoimidazoline substituent to transfer π -electron density from the exocyclic CN bond to an electrophilic centre makes this

ligand an interesting fragment of phosphorus compounds. Reaction of the silyl compound **10** with PCl_3 affords the dichlorophosphane **12** in which PN π -interaction has been discussed both from the unusual short PN bond (P(1)–N(1), 1.579(2) Å) and the relative orientation of the C(1)N(1)P(1) and N(2)C(1)N(3) planes (interplanar angle, $85.8(1)^\circ$ (Figure 6)) [23]. As a consequence of negative hyperconjugation [24], the PCl bonds are markedly elongated (P(1)–Cl(1), 2.207(1); P(1)–Cl(2), 2.151(1) Å), and the PNCl angles are widened in view of the ClPCl angle (Cl(1)–P(1)–N(1), $106.85(7)^\circ$; Cl(2)–P(1)–N(1), $104.16(8)^\circ$; Cl(1)–P(1)–Cl(2), $93.49(3)^\circ$). In fact, MO calculations (see below) clearly demonstrate the molecular geometry to be dominated by PN charge attraction, with no PN π -bonding being present. Apparently, a dicationic dimer is formed from **12** and AlCl_3 .

Subsequent substitution of the remaining chloro substituents of **12** is best achieved by use of the alkali iminoimidazolides mentioned above [25]. The properties of **13** and **14** also indicate high π -electron shifts from the imidazolyl ring to the adjacent PN moiety. As a consequence of nitrogen basicity, **13** is polymeric, while in **14** efficient PN π -bonding apparently enhances the phosphorus basicity, which is demonstrated by reactions with various electrophiles being currently under investigation [26].

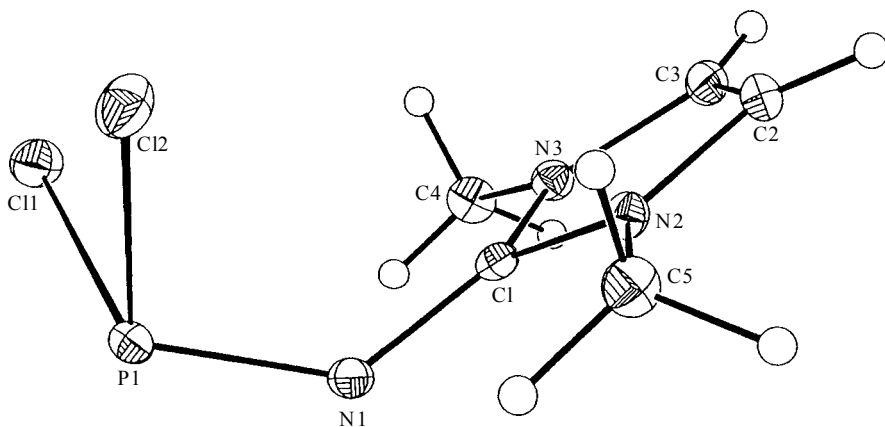
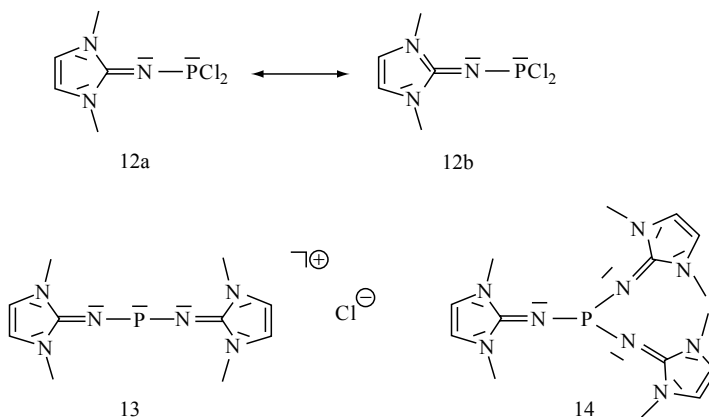


Figure 6 The crystal structure of $\text{C}_5\text{H}_8\text{Cl}_2\text{N}_3\text{P}$ (**12**). Selected bond lengths (Å) and angles ($^\circ$): P(1)–Cl(1) 2.207(1), P(1)–Cl(2) 2.151(1), P(1)–N(1) 1.579(2), N(1)–C(1) 1.341(3), C(1)–N(2) 1.352(3), N(2)–C(2) 1.384(3), C(2)–C(3) 1.332(4), C(3)–N(3) 1.384(3), N(3)–C(1) 1.348(3); Cl(1)–P(1)–Cl(2) $93.49(3)^\circ$, Cl(1)–P(1)–N(1) $106.85(7)^\circ$, Cl(2)–P(1)–N(1) $104.16(8)^\circ$, P(1)–N(1)–C(1) $130.5(2)^\circ$, N(1)–C(1)–N(2) $126.3(2)^\circ$, N(1)–C(1)–N(3) $126.7(2)^\circ$, N(2)–C(1)–N(3) $106.9(2)^\circ$, C(1)–N(1)–P(1)–Cl(1) 65.5° , C(1)–N(1)–P(1)–Cl(2) 32.6° , N(2)–C(1)–N(1)–P(1) 88.6° . Reproduced by permission of Wiley-VCH from N. Kuhn, R. Fawzi, M. Steimann and J. Wiethoff, *Chem. Ber.*, **129**, 479 (1996)



Scheme 5

2.7 BONDING IN IMINOIMIDAZOLINE PHOSPHANES

Figure 7 shows the calculated equilibrium geometries of two conformations of the iminoimidazoline phosphane **12** which have been found as minima on the

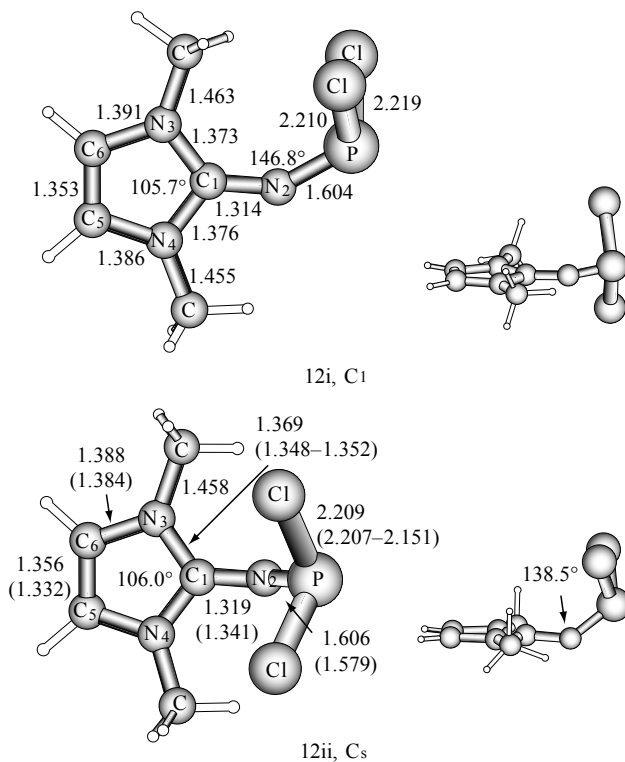


Figure 7 (cont.)

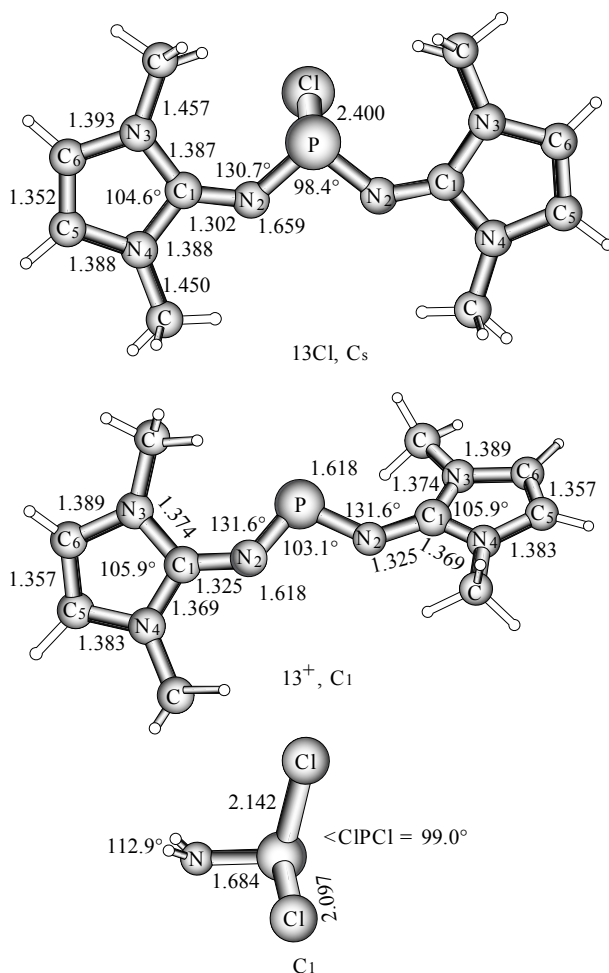


Figure 7 Calculated geometries of **12i**, **12ii**, **13Cl**, **13⁺** and H_2NPCl_2 ; bond lengths in Å, and angles in degrees

potential energy surface. The two conformations **12i** and **12ii** are energetically nearly degenerate. The isomeric form **12i** is < 0.1 kcal mol⁻¹ lower in energy than **12ii**. This is a strong argument against significant π -bonding of the P–N bond of **12**, because the C₁–N₂ bond π -plane of the NPCl₂ substituent of **12i** is orthogonal to the ring plane. Another argument against N–P π -bonding comes from the calculated bond order. The P_{N-P} values for **12i** (1.10) and **12ii** (1.11) suggest essentially a single bond. A bond order value $P_{N-P} = 0.95$ was calculated for the reference compound H_2N-PCl_2 . The slightly larger bond order of **12i** and **12ii** is caused by the shorter P–N₂ bonds rather than by π -contributions. The rather short P–N bond in **12** is due to the strong charge attraction between the negatively charged nitrogen atom and the positively charged

Table 2 NBO results obtained for compounds **12i**, **12ii**, **13Cl**, **13⁺** and H₂NPCl₂ at B3LYP/6-31G(d)

Com- pound	<i>q</i>										<i>P_{AB}</i>				<i>C₁(%)</i>					
	C ₁	N ₂	N ₃	N ₄	P	C ₁	C ₁	N ₂	N ₃	N ₄	C ₁ -N ₂	C ₁ -N ₃	C ₁ -N ₄	N ₂ -P	σ(C ₁ -N ₂)	σ(C ₁ -N ₃)	σ(C ₁ -N ₄)	π(C ₁ -N ₃)	π(C ₁ -N ₂)	
12i	0.663	-1.031	-0.391	-0.387	1.070	0.920	1.559	1.567	1.574	1.34	1.18	1.17	1.10	1.10	41.10	37.55	37.29	—	—	24.57
12ii	0.665	-1.043	-0.384	-0.384	1.064	—	—	—	—	1.30	1.19	1.19	1.11	1.11	41.49	37.22	37.22	—	—	20.58
13Cl	0.648	-0.974	-0.417	-0.404	1.170	0.922	1.499	1.591	1.590	1.47	1.13	1.12	0.97	0.97	41.90	37.25	37.11	—	—	29.16
13⁺	0.637	-0.952	-0.389	-0.371	1.163	0.911	1.464	1.497	1.489	1.33	1.17	1.19	1.18	1.18	41.60	37.34	37.44	25.86 ^a	—	—
H ₂ NPCl ₂	—	-1.209	—	—	1.020	—	—	—	—	—	—	—	0.95	—	—	—	—	—	—	—

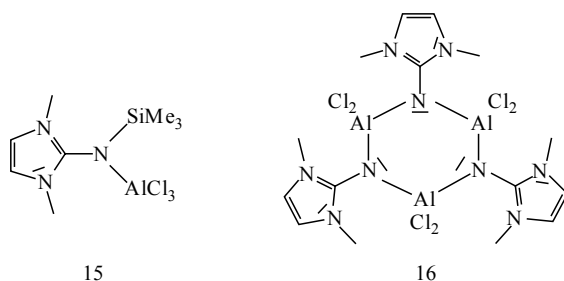
^a C₁-N₄.

phosphorus (Table 2). Thus, the bonding situation in **12** is best described by the Lewis structure **12a** shown in Scheme 5. This is also supported by the NBO values given in Table 2. The NBO analysis gives a partial C_1-N_2 double bond for **12i** ($P_{AB} = 1.34$) and **12ii** ($P_{AB} = 1.30$) and lone-pair orbitals at N_3 and N_4 . The C_1-N_2 π -bond is clearly polarized, however, toward the nitrogen end (24.6 % C_1 for **12i** and 20.6 % C_1 for **12ii**).

Figure 7 also shows the calculated geometries of $(ImN)_2PCl$ (**13Cl**) and $(ImN)_2P^+$ (**13⁺**). The structure of these molecules could only be studied theoretically because they exist in the solid state only as polymers. The theoretically predicted bond lengths indicate that in **13Cl** the $P-N_2$ bond is significantly longer and the C_1-N_2 bond is shorter than in **12i** and **12ii**. The cation **13⁺** also has a $P-N_2$ bond that is slightly longer than in **12i** and **12ii**, while the C_1-N_2 bond becomes slightly longer in the former compound. Note that the N_2-P-N_2 linkage in **13⁺** remains bent. The bending angle in **13⁺** (131.3°) is slightly larger than in **13Cl** (120.5°).

2.8 ALUMINIUM AND TITANIUM IMINOIMIDAZOLIDES

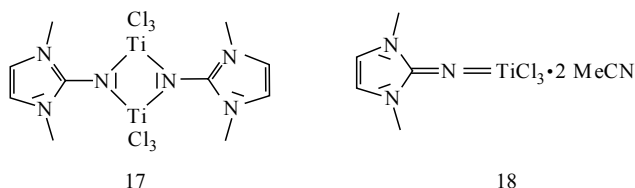
EN π -bonding in metal or metaloid iminoimidazolides should be best realized by use of electron-deficient centres E. There are numerous aluminium ring and cage compounds derived from aluminium amides and imides as their oligomers, as a consequence from electron deficiency [27]. Compound **10** reacts even at $0^\circ C$ with $AlCl_3$ to give the adduct **15** in almost quantitative yield. The stability of **15** is quite surprising in view of the low basicity of silylated amines and imines. At $180^\circ C$, **15** eliminates chlorotrimethylsilane to give the trimeric alane **16**. The structure of $[(ImN)AlCl_2]_3$ consists of a non-planar 'boat-like' Al_3N_3 ring (Figure 8) [20]. On comparison with the structure of the dimeric ketimide $[Al(NCPh_2)_3]_2$ [28], the AlN ring distances are significantly shortened in **16** (AlN 1.829(3)–1.849(2) Å).



Scheme 6

Similarly, **10** reacts with $TiCl_4$ to give the dinuclear titanium complex **17**. The X-ray structure (Figure 9) reveals a planar four-membered ring for the Ti_2N_2 unit, whose plane is almost perpendicular to those of the heterocyclic ring planes. The TiN distances are short, but not in the range of the true

double bond (Ti(1)–N(1) 1.958(2), Ti(1)–N(1A) 1.962(2) Å). Acetonitrile adds to **17** to give the mononuclear complex **18**, in which a linear ImNTi fragment indicates strong TiN π -interaction (Figure 10) [29], apparently in the direction of TiN double bonding (Ti(1)–N(1) 1.741(2) Å, Ti(1)–N(1)–C(1) 175.0(3) $^\circ$) [30].



Scheme 7

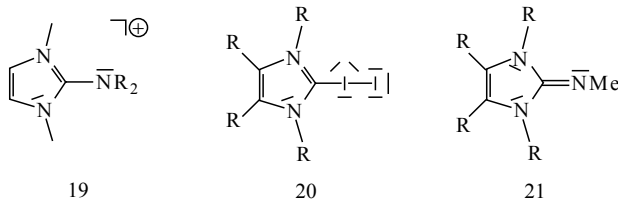
2.9 BONDING IN TITANIUM IMINOIMIDAZOLIDES

We investigated the bonding situation in the TiCl_3 complex **18M** in order to see if the acetonitrile ligands have a significant influence on the structure of the parent compound. We also wanted to study the extent of Ti–N π -bonding in the molecule. Figure 11 shows the calculated structure of **18M**, with the NBO data being given in Table 1.

The calculations predict that the parent compound **18M** also has a linear $\text{C}_1\text{–N}_2\text{–Ti}$ linkage as in **18**. A comparison of the calculated bond lengths and angles of **18M** with the experimental data of **18** shows very good agreement. This indicates that the octahedral coordination sphere of **18** does not significantly change the ImN–Ti bonding situation of **18M**. Note that the $\text{C}_1\text{–N}_2$ bond of **18M** (1.307 Å) is *longer* than in the parent compound **8** (1.291 Å), while the SiH_3 compound **10'** (1.281 Å) and the lithium compound **9Li** (1.266 Å) have *shorter* bonds than in **8**. Thus, the calculated geometries indicate that the Ti–N₂ bond might have some π -contribution. This is supported by the Ti–N bond order. The calculated value of $P_{\text{Ti–N}} = 1.27$ clearly shows that the titanium–nitrogen bond of **18M** has a significant degree of $d(\text{Ti})\text{–}p(\text{N})$ π -bonding, although this is still far away from a Ti–N double bond. We want to point out that the bond order for the $\text{C}_1\text{–N}_2$ bond of **18M** (1.36) is significantly lower than in **8** (1.66), although the former compound has a linear $\text{C}_1\text{–N}_2\text{–X}$ ($\text{X} = \text{Ti}$) moiety, while the $\text{C}_1\text{–N}_2\text{–X}$ ($\text{X} = \text{H}$) linkage of the latter is strongly bent.

2.10 ALKYLATION AND ACYLATION

Owing to the high nucleophilicity of **8** and its anion, we were unable to obtain *N*-alkylated iminoimidazolines from their reaction with convenient alkylating reagents, the dialkylaminoimidazolium cations **19** being formed instead. Similarly, the reaction of the iodine adduct **20** with primary amines failed, and **21** is accessible from **1** and MeN_3 only in poor yield.



Scheme 8

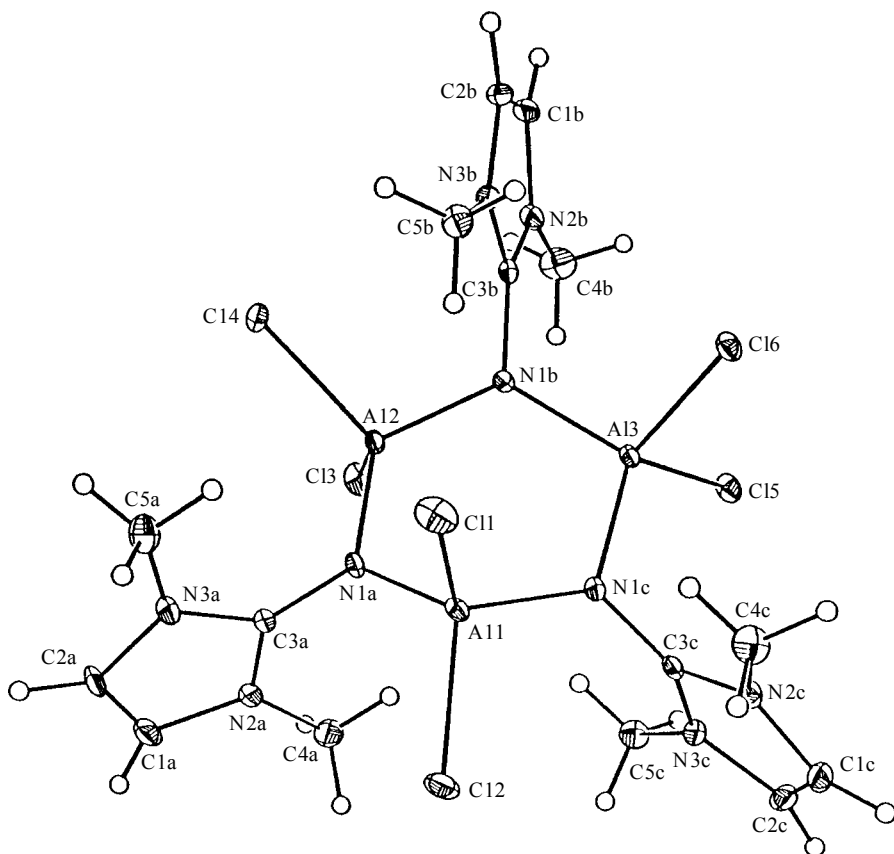


Figure 8 The crystal structure of $C_{15}H_{24}Al_3Cl_6N_9$ (**16**). Selected bond lengths (Å) and angles ($^\circ$): Al–N 1.829(3)–1.849(2), N(1)–C(3) 1.354(4)–1.362(4), C(3)–N(2,3) 1.346(4)–1.355(4), Al–Cl 2.1561(12)–2.1807(12); Al–N–Al' 119.81(13)–126.93(13), N–Al–N' 107.87(10)–110.02(11), N(2,3)–C(3)–N(1) 126.2(3)–127.5(3), N(2)–C(3)–N(3) 106.2(3)–106.4(3), Cl–Al–Cl' 103.32(5)–108.28(5), C(3)–N(1)–Al 116.3(2)–121.7(2); N(2a)–C(3a)–N(1a)–Al(1) -93.7 , N(2b)–C(3b)–N(1b)–Al(2) -92.0 , N(2c)–C(3c)–N(1c)–Al(3) 91.3 . Reproduced by permission of Wiley-VCH from N. Kuhn, R. Fawzi, M. Steimann and J. Wiethoff, *Z. Anorg. Allg. Chem.*, **623**, 554 (1997)

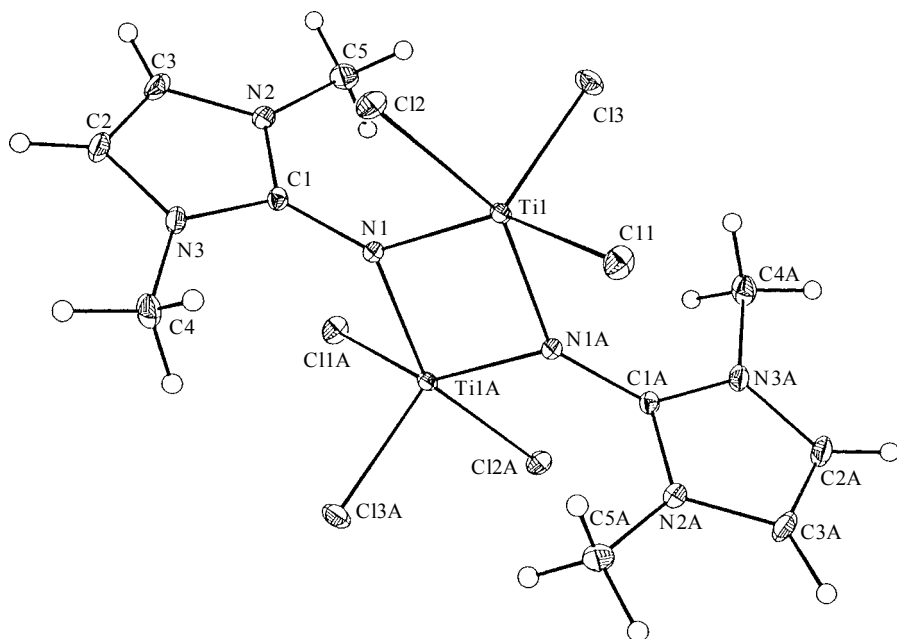
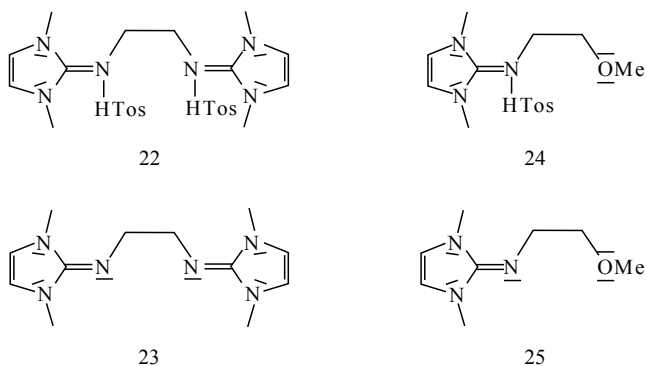


Figure 9 The crystal structure of $C_{10}H_{16}Cl_6N_6Ti_2$ (**17**). Selected bond lengths (Å) and angles ($^\circ$): Ti(1)–N(1) 1.958(2), Ti(1)–N(1A) 1.962(2), N(1)–C(1) 1.351(3), C(1)–N(2) 1.347(3), C(1)–N(3) 1.353(3), Ti–Cl 2.2249–2.3291, Ti(1)–Ti(1A) 3.0403(10); Ti(1)–N(1)–Ti(1A) 101.74(10), C(1)–N(1)–Ti(1) 128.7(2), C(1)–N(1)–Ti(1A) 129.5(2), N(1)–C(1)–C(2) 126.9(2), N(1)–C(1)–C(3) 126.4(3), N(2)–C(1)–N(3) 106.7(2); N(2)–C(1)–N(1)–Ti(1) 80.4. Reproduced by permission of Wiley-VCH from N. Kuhn, R. Fawzi, M. Steimann and J. Wiethoff, *Z. Anorg. Allg. Chem.*, **623**, 769 (1997)

A more satisfying result was obtained from the reaction of **8** with ethane-1,2-ditosylate. The isolatable adduct **22** was transferred into the bis(imino)ethane **23**



Scheme 9

by treatment with KH in good yields [31]. In a similar reaction, the methoxy (imino)ethane (**25**) is obtained from the reaction of **8** with 2-methoxyethyltosylate and subsequent deprotonation of **24** [32].

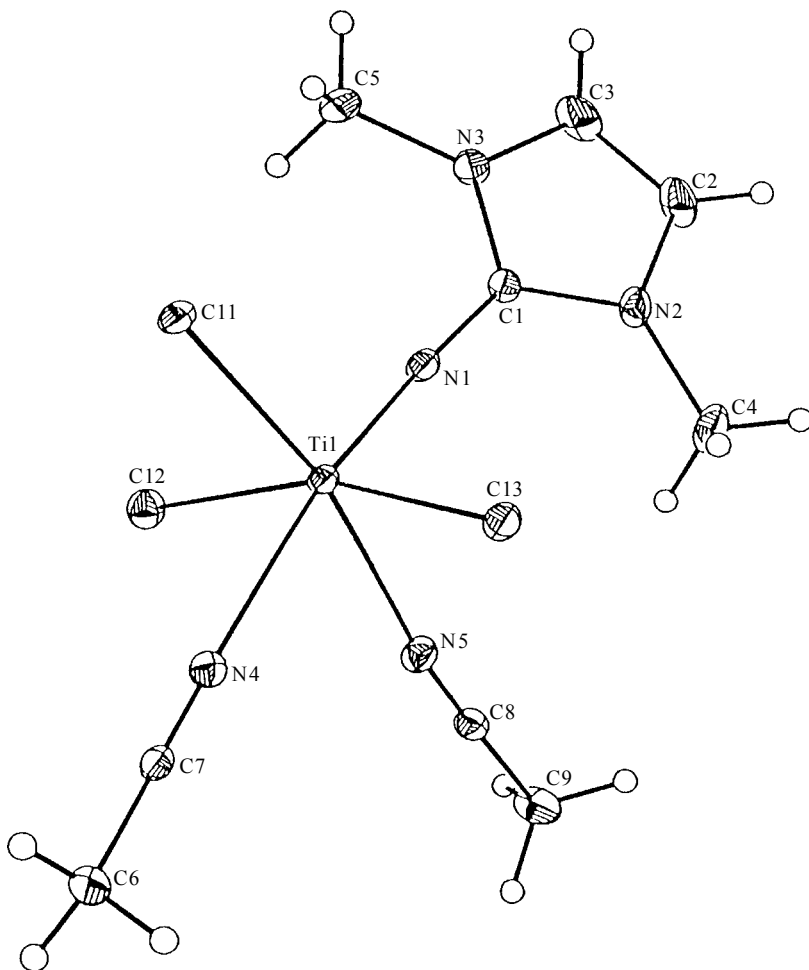


Figure 10 The crystal structure of $C_9H_{14}Cl_3N_5Ti$ (**18**). Selected bond lengths (Å) and angles ($^\circ$): Ti(1)–N(1) 1.741(2), Ti(1)–N(4) 2.343(2), Ti(1)–N(5) 2.212(3), Ti(1)–Cl(1) 2.3574(9), Ti(1)–Cl(2) 2.3567(11), Ti(1)–Cl(3) 2.3926(11), N(1)–C(1) 1.318(4), C(1)–N(2) 1.352(4), C(1)–N(3) 1.354(4); N(1)–Ti(1)–N(4) 171.69(10), N(1)–Ti(1)–N(5) 91.99(11), N(1)–Ti(1)–Cl 95.17(10)–100.02(9), Ti(1)–N(1)–C(1) 175.0(3), N(1)–C(1)–N(2) 127.4(3), N(1)–C(1)–N(3) 126.0(3), N(2)–C(1)–N(3) 106.6(3); N(2)–C(1)–N(1)–Ti(1) 34.9. Reproduced by permission of Wiley-VCH from N. Kuhn, R. Fawzi, M. Steimann and J. Wiethoff, *Z. Anorg. Allg. Chem.*, **623**, 769 (1997)

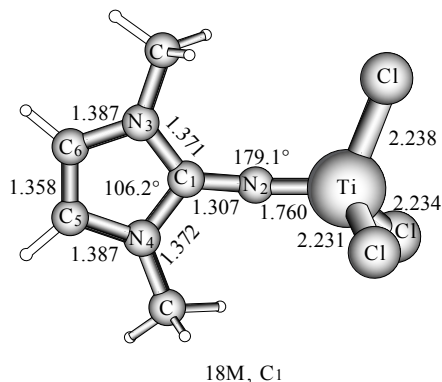
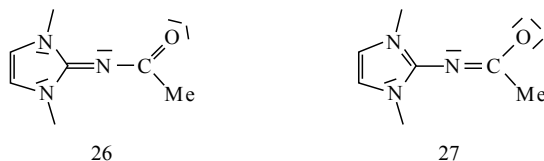


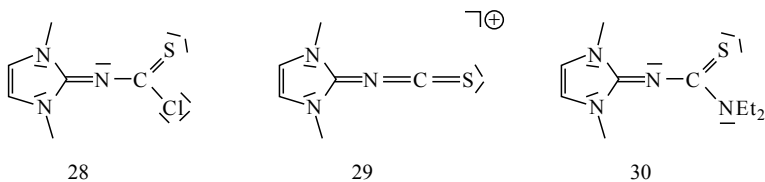
Figure 11 Calculated geometry of **18M**; bond lengths in Å, and angles in degrees

Acylation of **8** occurs immediately with acetyl chloride to give the acetylimino compound **26**. As expected from the ability of the heterocyclic ring to shift π -electron density into the acylimino fragment, the betaine structure **27** predominates, as indicated by NMR data [33].



Scheme 10

Compound **10** reacts with CSCl_2 to give the stable thiocarbonic chloride **28**, whose reactions are currently under investigation. The π -donor ability of the imino fragment is best documented by the formation of the stable cationic thiocyanate **29**. Similarly, lithiated **8** reacts with $\text{Et}_2\text{NC(S)Cl}$ to give the thiourea derivative **30**, whose X-ray structure (Figure 12) clearly demonstrates π -electron



Scheme 11

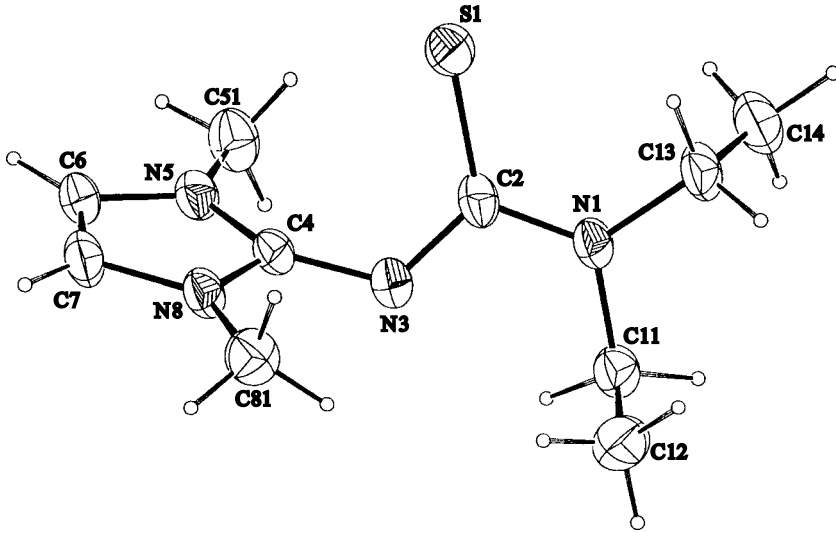
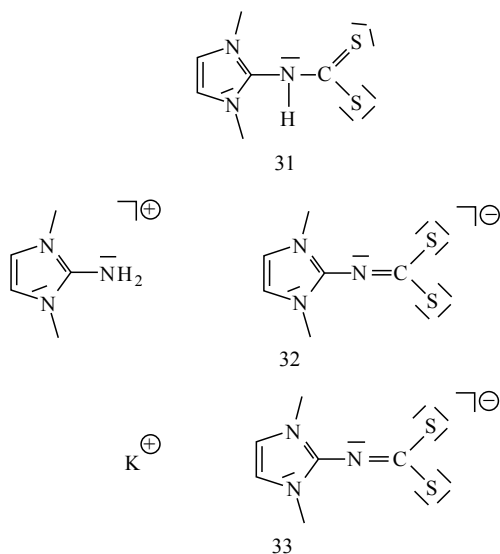


Figure 12 The crystal structure of $C_{10}H_8N_4S$ (**30**). Selected bond lengths (Å) and angles ($^\circ$): N(1)–C(2) 1.358(7), C(2)–S(1) 1.718(6), C(2)–N(3) 1.340(7), N(3)–C(4) 1.347(7), C(4)–N(5) 1.344(7), C(4)–N(8) 1.355(7); C(11)–N(1)–C(13) 115.5(4), C(11)–N(1)–C(2) 120.7(4), C(13)–N(1)–N(2) 123.3(5), N(1)–C(2)–S(1) 121.2(4), N(1)–C(2)–C(3) 114.6(5), S(1)–C(2)–N(3) 124.2(4), C(2)–N(3)–C(4) 120.2(5), N(3)–C(4)–N(5) 130.6(5), N(3)–C(4)–N(8) 122.6(5), N(5)–C(4)–N(8) 106.1(4); N(5)–C(4)–N(8)–C(2) 70.3. Reproduced by permission of Verlag der Zeitschrift für Naturforschung from N. Kuhn, R. Fawzi, C. Maichle-Mößner, M. Steimann and J. Wiethoff, *Z. Naturforsch., B*, **52**, 1055 (1997)

delocalization in the NC(S)N' fragment (N(3)–C(4) 1.347(7), N(3)–C(2) 1.340(7), C(2)–N(1) 1.358(7) Å; C(2)N(3)C(4)/N(5)C(4)N(8) 70.35 $^\circ$; the fragments Me₂N and NC(S) are coplanar) [34].

With CS₂, **8** forms a stable adduct (**31**) which models the mechanism of the well-known thioketone formation from the reaction of ketimines with CS₂. Apparently, the enhanced basicity of **8** allows the reaction to take place at moderate conditions, thus allowing the intermediate to be isolated. Species **31** is deprotonated by the strong base **8** to give the imidazolium salt **32** [35]. Its potassium salt (**33**) is obtained directly through the reaction of potassio imidoimidazoline (see above) with CS₂. The interesting structure (Figure 13) reveals the presence of K₂ units doubly bridged by dithioformimidate ligands. Their imino nitrogen atoms connect the K₂S₄ cages to the neighbouring units via KN interaction, thus demonstrating the high negative charge at these nitrogen centres [36].

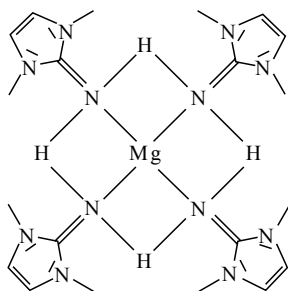


Scheme 12

2.11 COORDINATION OF 2-IMINOIMIDAZOLINES AT METAL CENTRES

As outlined above, 2-iminoimidazolines are strong nucleophiles, and thus being predestined to form stable metal complexes. In contrast to tertiary phosphanes, they are not sensitive towards oxygen, and therefore their metal complexes may be of interest in catalysis.

The only known complex of the parent iminoimidazoline $C_5H_9N_3$ (**8**) itself is the compound $[(C_5H_9N_3)_4Mg]Cl_2$ (**34**) [20]. The imino NC distances are only slightly elongated on coordination owing to the lack of π -electron transfer here. Apparently, the imino nitrogen atoms are connected via hydrogen bridges; no interionic interaction could be detected (Figure 14).



34

Scheme 13

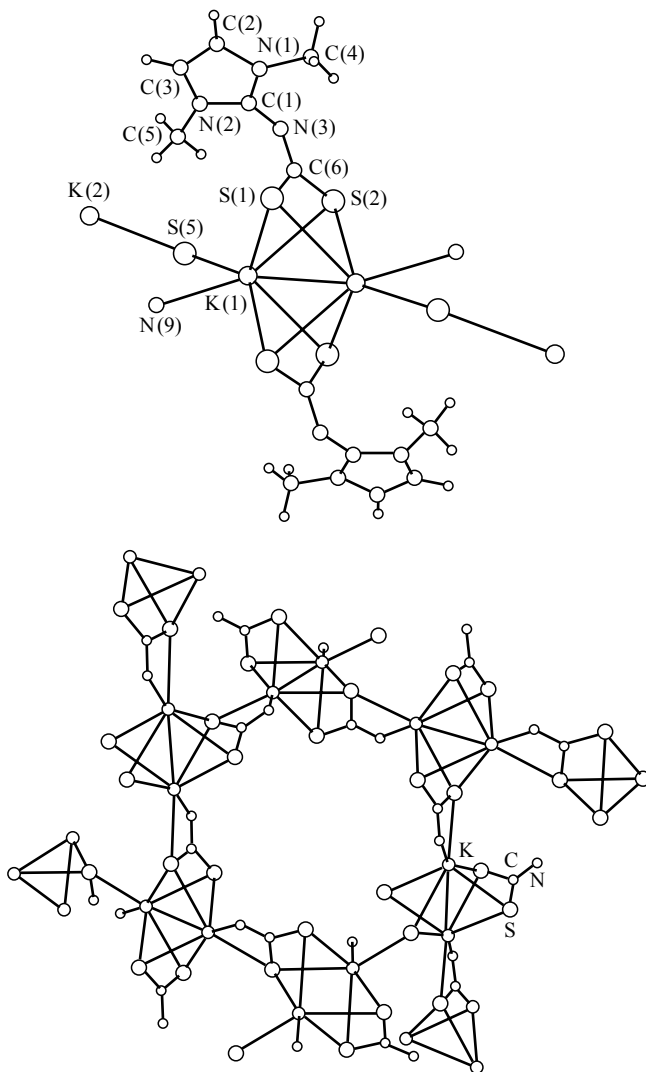
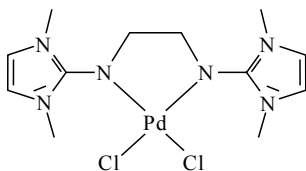


Figure 13 The crystal structure of $C_6H_8N_3S_2K \cdot 1/6 \text{ MeCN}$ (**33** \cdot 1.6 MeCN). Selected bond lengths (Å) and angles ($^\circ$): C(6)–S(1) 1.739(14), C(6)–S(2) 1.754(12), C(6)–N(3) 1.289(10), N(3)–C(1) 1.369(16), C(1)–N(1) 1.337(21), C(1)–N(2) 1.368(18); N(1)–C(1)–N(2) 107.5(11), C(1)–N(3)–C(6) 118.3(11), S(1)–C(6)–S(2) 119.4(5); N(1)–C(1)–N(3)–C(6) 90.6. Reproduced by permission of Wiley-VCH from N. Kuhn, R. Fawzi, M. Steimann, J. Wiethoff and G. Henkel, *Z. Anorg. Allg. Chem.*, **623**, 1577 (1997)

The bifunctional imine ligand **23** forms the palladium complex **35** in which the relative orientation of the imidazole and CN–Pd planes indicates the absence of imine CN π -bonding (Figure 15). According to the high energies of the empty metal orbitals, no NPd π -bonding could be detected. One of the

coordinating nitrogen atoms is clearly pyramidal, with the sum of the angles at N(5) being 344° as a consequence of high electron density [31].



35

Scheme 14

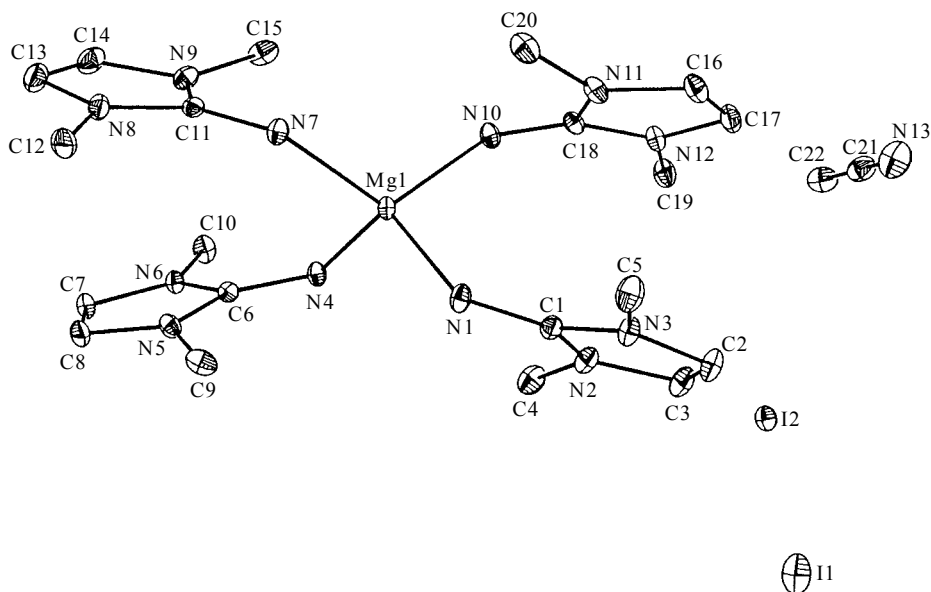
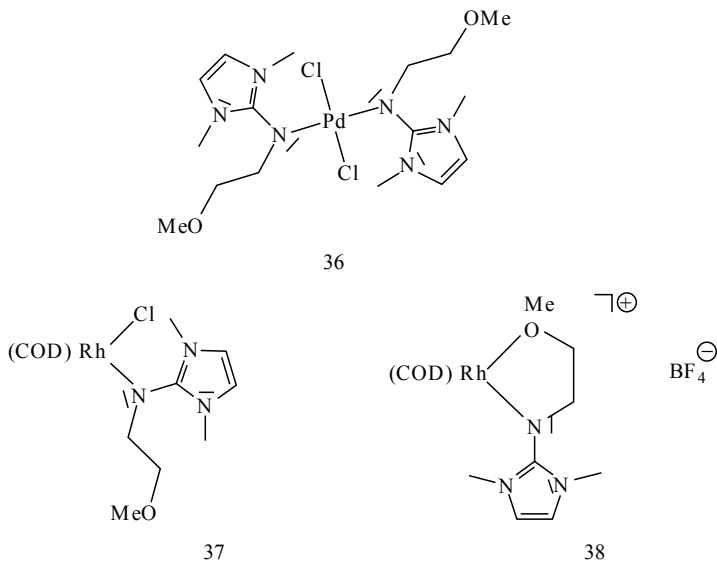


Figure 14 The crystal structure of $C_{20}H_{36}I_2MgN_{12}$ (**34**). Selected bond lengths (Å) and angles ($^\circ$): Mg–N 2.051(2)–2.063(2), $N_{Mg}-C_{Im}$ 1.318(3)–1.321(3), $(C-N)_{Im}$ 1.360(3)–1.366(3); N–Mg–N' 103.31(9)–117.31(9), Mg–N–C 123.6(2)–127.6(2), $(N-C-N')_{Im}$ 105.5(2)–106.1(2). Reproduced by permission of Wiley-VCH from N. Kuhn, R. Fawzi, M. Steimann and J. Wiethoff, *Z. Anorg. Allg. Chem.*, **623**, 554 (1997)

In view of the catalytic properties of hemilabile coordinating ligands, we have investigated the coordination properties of the bifunctional imine ligand **25**. With $(PhCN)_2PdCl_2$, **25** gives the imine complex **36** in which the ligands are attached at the metal centre via their imino nitrogen atoms only (Figure 16). Similarly, the rhodium complex **37** is obtained from $[(COD)RhCl]_2$ (Figure 17). In both compounds, a significant torsion angle between the CNC and CNM ($M = Pd, Rh$) planes indicating lack of CN π -bonding is observed. The compound **37** is transferred into the chelate complex **38**, through the reaction with $NaSbF_6$ with its structure currently being under investigation [32].



Scheme 15

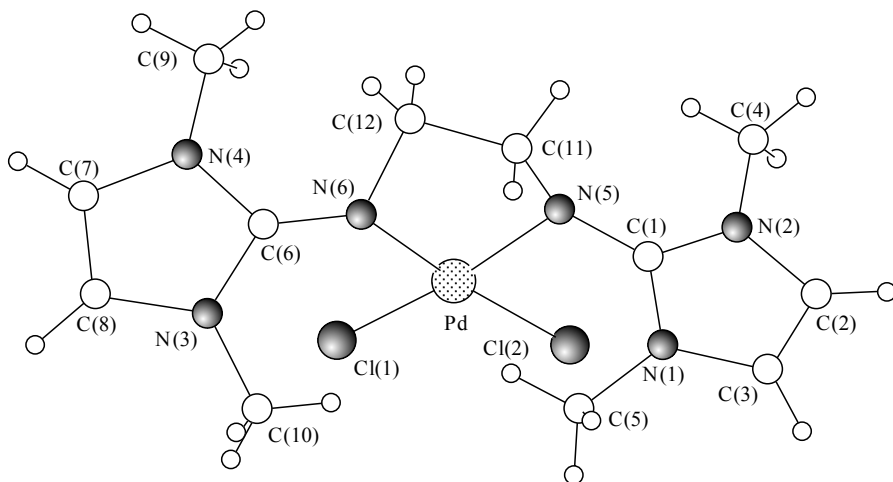
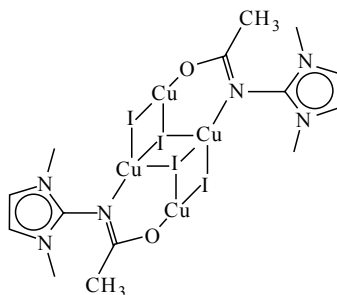


Figure 15 The crystal structure of $C_{14}H_{23}Cl_2N_7Pd$ (**35** • MeCN). Selected bond lengths (Å) and angles ($^\circ$): Pd–N(5) 2.017(3), Pd–N(6) 2.028(3), Pd–Cl(1) 2.351(1), Pd–Cl(2) 2.335(1), N(5)–C(1) 1.347(5), C(1)–N(1) 1.354(5), C(1)–N(2) 1.351(5), N(6)–C(6) 1.330(5), C(6)–N(3) 1.362(5), C(6)–N(4) 1.351(5); N(1)–C(1)–N(2) 106.0(3), N(3)–C(6)–N(4) 106.4(3), C(1)–N(5)–C(11) 114.4(3), C(1)–N(5)–Pd 117.9(3), C(11)–N(5)–Pd 112.1(2), C(6)–N(6)–C(12) 119.8(3), C(6)–N(6)–Pd 127.9(3), C(12)–N(6)–Pd 107.9(3); Pd–N(5)–C(1)–N(1) 84.4, Pd–N(6)–C(6)–N(3) 65.9. Reproduced by permission of Verlag der Zeitschrift für Naturforschung from N. Kuhn, M. Grathwohl, M. Steimann, and G. Henkel, *Z. Naturforsch., B*, **53**, 997 (1998)

The acetylmino ligand **26** forms, with CuI, the surprisingly stable tetranuclear stepped cubane-type complex **39** in which the short C(5)–N(3) distance confirms the azaenolate nature of the coordinated ligand as a consequence of π -electron delocalization (Figure 18) [33].



39

Scheme 16

3 METHYLENEIMIDAZOLINES

3.1 SYNTHESIS AND STRUCTURE

In enamines [37], the C–C double bond is strongly polarized by the mesomeric electron donation of the amino groups. This effect is best demonstrated by the chemistry of the cyclic endiamine **40** [38]. The process of π -electron transfer to the exocyclic methylene carbon atom should be enhanced by the incorporation of the nitrogen atoms into a heteroaromatic imidazole ring system.

The synthesis of the 2-methylene imidazoline **4** [39] is best achieved by deprotonation of the imidazolium cation **41** [40] by use of KH. The compound **4** is obtained as air-sensitive colourless crystals in good yield.

The X-ray structure analysis of **4** (Figure 19) reveals a planar five-membered ring system containing an exocyclic double bond, only slightly elongated in view of the expected range (C(1)–C(4), 1.357(3) Å). This finding parallels our structural results of the imine compound **8** discussed above. Information about an unusual ylide-type electron distribution (**4b**) comes from the ^{13}C NMR shift of the methylene carbon atom (δ , 40.2) which is at the upfield end of the sp^2

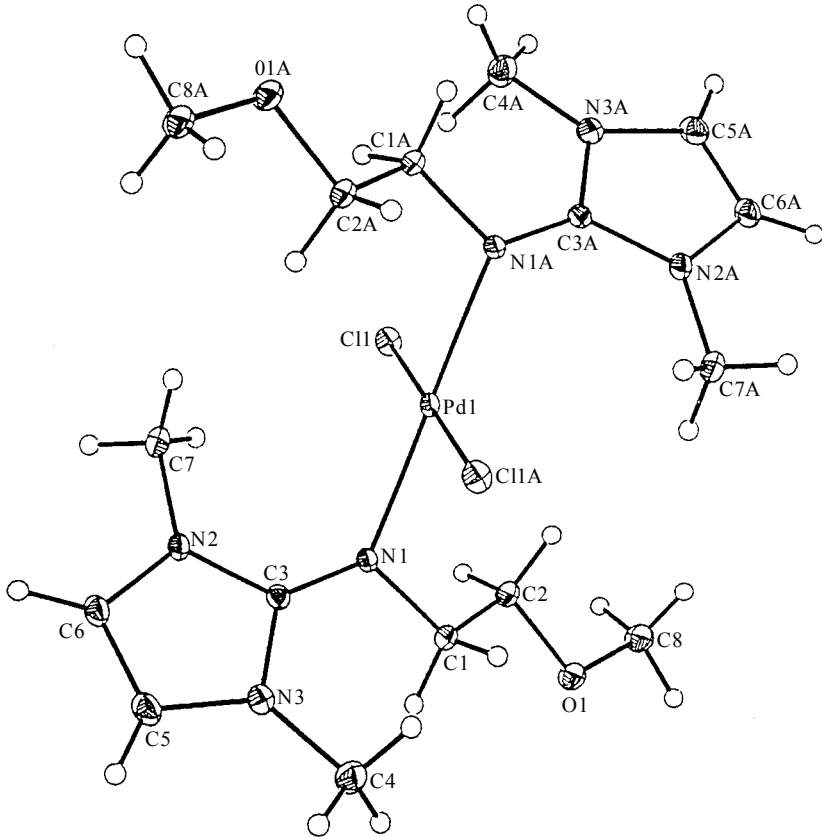
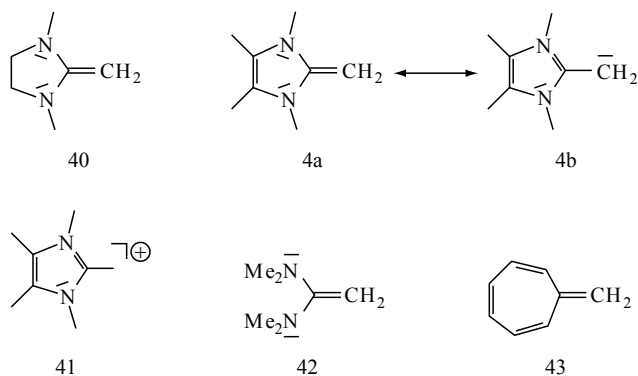


Figure 16 The crystal structure of $C_{16}H_{30}Cl_2N_6O_2Pd$ (**36**). Selected bond lengths (Å) and angles ($^\circ$): Pd(1)–N(1) 2.0617(13), Pd(1)–Cl(1) 2.3279(9), N(1)–C(1) 1.4630(19), N(1)–C(3) 1.3323(18), C(3)–N(2) 1.3627(18), C(3)–N(3) 1.370(2); N(1)–Pd(1)–N(1A) 180.00(7), Pd(1)–N(1)–C(3) 118.58(9), Pd(1)–N(1)–C(1) 114.64(10), N(1)–C(3)–N(2) 124.27(14), N(1)–C(3)–N(3) 129.79(13), C(3)–N(1)–C(1) 117.13(13), N(2)–C(3)–N(3) 105.84(13); N(2)–C(3)–N(1)–Pd(1) 59.7. Reproduced by permission of Verlag der Zeitschrift für Naturforschung from N. Kuhn, M. Grathwohl and Ch. Nachtigal, *Z. Naturforsch., B*, **56**, 704 (2001).

carbon range [41]. Comparison with other polarized methylene compounds (**40**, **42**, **43**) by use of their NMR shifts and calculated electron densities at CH_2 (AM1) [42] clearly demonstrates the top position of **4** in this series (Figure 20).



Scheme 17

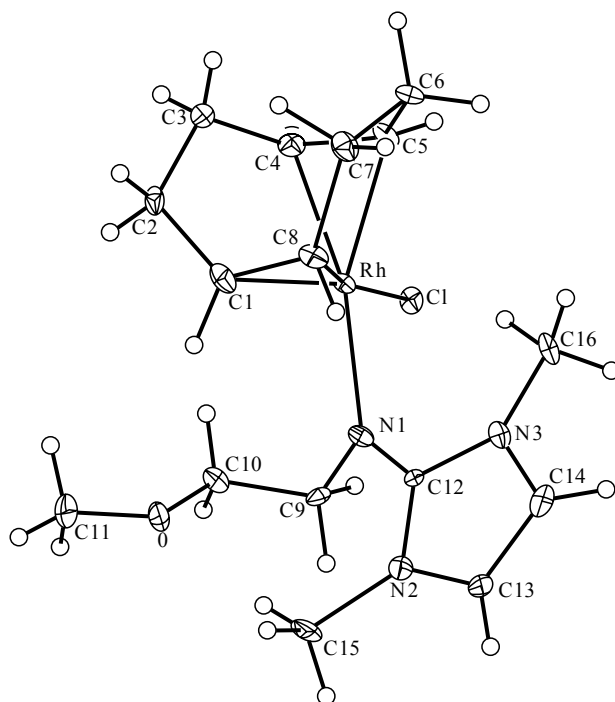


Figure 17 The crystal structure of $C_{16}H_{27}ClN_3ORh$ (**37**). Selected bond lengths (Å) and angles ($^\circ$): Rh–Cl 2.3957(18), Rh–C 2.090(7)–2.148(1), Rh–N(1) 2.130(9), N(1)–C(9) 1.463(9), N(1)–C(12) 1.328(11), C(12)–N(2) 1.360(11), C(12)–N(3) 1.364(8); Rh–N(1)–C(9) 118.2(6), Rh–N(1)–C(12) 123.7(5), N(1)–C(12)–N(2) 130.1(6), N(1)–C(12)–N(3) 123.5(8), N(2)–C(12)–N(3) 106.3(7), C(12)–N(1)–C(9) 117.9(8); N(2)–C(12)–N(1)–Rh 146.2. Reproduced by permission of Verlag der Zeitschrift für Naturforschung from N. Kuhn, M. Grathwohl and Ch. Nachtigal, *Z. Naturforsch., B*, **56**, 704 (2001).

3.2 BONDING IN 2-METHYLENEIMIDAZOLINES AND RELATED COMPOUNDS

We have analysed the electronic structure of 2-methyleneimidazoline (**4i**) and compared the bonding situation of **4i** (ImX, X = CH₂) with the results which we obtained for **8** (ImX, X = NH) and with the chalcogen derivates **2O** (ImX, X = O), **2S** (ImX, X = S), and **2Se** (ImX, X = Se). The calculated geometries of **2O**, **2S**, **2Se** and **4i** are shown in Figure 21, with the NBO results being given in Table 3.

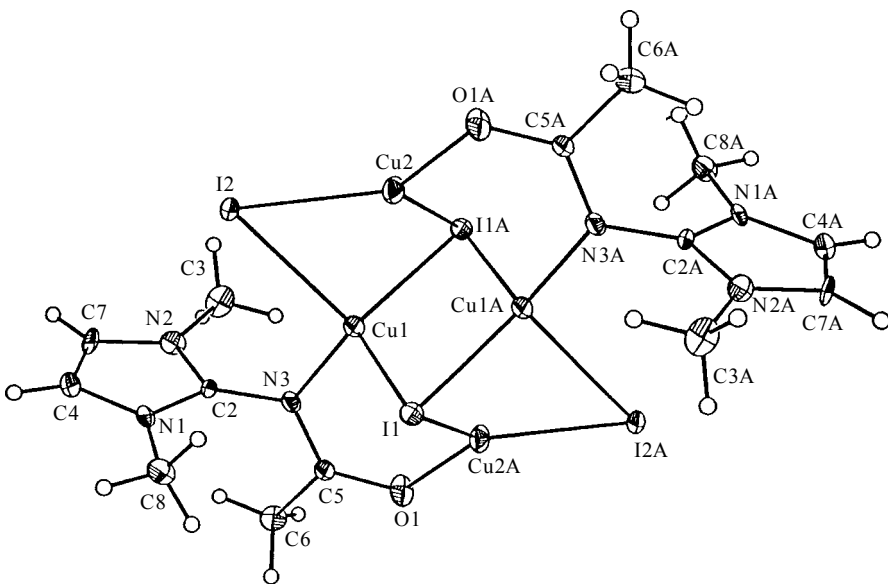


Figure 18 The crystal structure of C₁₄H₂₂Cu₄I₄N₆O₂ (**39**). Selected bond lengths (Å) and angles (°): Cu–I 2.520(2)–2.843(3), Cu(1)–N(3) 2.019(10), N(3)–C(2) 1.351(14), C(2)–N(1) 1.35(2), C(2)–N(2) 1.37(2), N(3)–C(5) 1.346(14), C(5)–O(1) 1.31(2), O(1)–Cu(2A) 1.918(10), N(1)–C(2)–N(2) 106.2(9); C(2)–N(3)–C(5) 120.3(10), C(2)–N(3)–Cu(1) 115.4(9); N(1)–C(2)–N(3)–C(5) 96.4, C(2)–N(3)–C(5)–O(1) 8.5, N(3)–C(5)–O(1)–Cu(2A) 9.0, N(1)–C(2)–N(3)–Cu(1) –81.0. Reproduced by permission of Wiley-VCH from N. Kuhn, R. Fawzi, M. Grathwohl, H. Kotowski and M. Steimann, *Z. Anorg. Allg. Chem.*, **624**, 1937 (1998)

A comparison of the experimental geometry of **4** with the calculated bond lengths and angles of **4i**, which has hydrogen atoms instead of methyl groups at C₅ and C₆, shows nearly perfect agreement between theory and experiment.

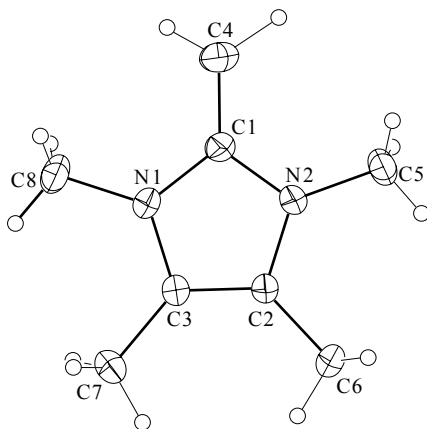


Figure 19 The crystal structure of $C_8H_{14}N_2$ (**4**). Selected bond lengths (Å) and angles ($^\circ$): C(1)–C(4) 1.357(3), C(1)–N(1) 1.382(3), C(1)–N(2) 1.376(3); N(1)–C(1)–N(2) 105.2(2); N(1)–C(1)–C(4)–H(1) 1.1. From N. Kuhn, H. Bohnen, J. Kreutzberg, D. Bläser and R. Boese, *J. Chem. Soc., Chem. Commun.*, 1136 (1993). Reproduced by permission of The Royal Society of Chemistry

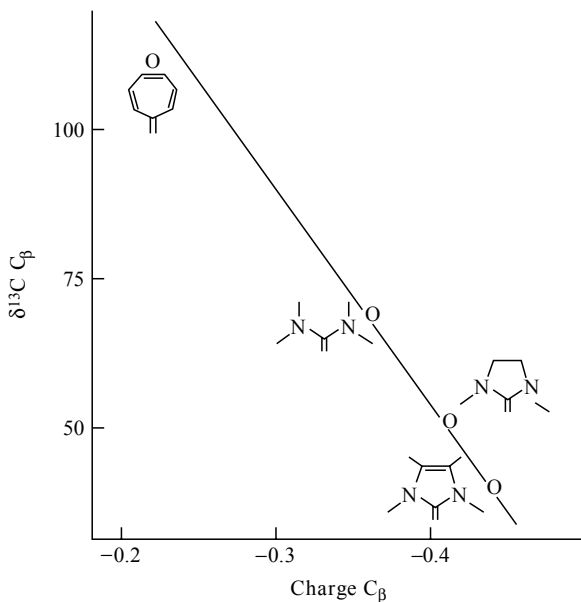
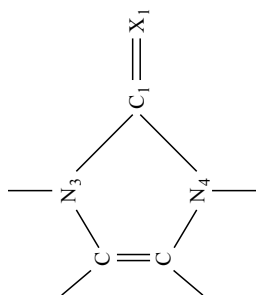


Figure 20 The variation of ^{13}C -NMR shift with charge density (CH_2) of **4** and related compounds

Table 3 NBO results obtained for compounds **20**, **2S**, **2Se**, **4i** and **8** at B3LYP/6-31G(d)



Com- pound	<i>q</i>					<i>P_{AB}</i>					<i>C_i</i> (%)					
	<i>C₁</i>	<i>X₂</i>	<i>N₃</i>	<i>N₄</i>	<i>C₁</i>	<i>X₂</i>	<i>N₃</i>	<i>N₄</i>	<i>C₁-X₂</i>	<i>C₁-N₃</i>	<i>C₁-N₄</i>	<i>σ(C₁-X₂)</i>	<i>σ(C₁-N₃)</i>	<i>σ(C₁-N₄)</i>	<i>π(C₁-N₃)</i>	<i>π(C₁-X₂)</i>
20	0.811	-0.682	-0.459	-0.459	0.884	1.586	1.633	1.633	1.59	1.08	1.08	35.45	36.15	36.15	—	26.79
2S	0.219	-0.294	-0.394	-0.394	0.991	1.633	1.571	1.571	1.45	1.15	1.15	60.19	36.99	36.99	—	26.19
2Se	0.152	-0.250	-0.389	-0.389	0.986	1.670	1.560	1.560	1.33	1.17	1.17	65.20	36.75	36.75	—	24.03
4i	0.371	-0.255	-0.426	-0.426	1.017	1.339	1.664	1.664	1.63	1.07	1.07	52.80	37.75	37.75	—	39.94
8	0.606	-0.484	-0.451	-0.433	0.947	1.464	1.657	1.646	1.66	1.07	1.08	43.25	37.00	37.17	—	33.45

The theoretically predicted geometries of the chalcogen complexes **2O**, **2S**, **2Se** are also in good agreement with the experimental data. The calculated geometries and the NBO data make it possible to analyse the trend in the bonding situation for ImX with $\text{X} = \text{CH}_2$ (**4i**), $\text{X} = \text{NH}$ (**8**) and $\text{X} = \text{O}$ (**2O**), and along the chalcogen series with $\text{X} = \text{O}$, S and Se. The effect of the exocyclic $\text{C}_1\text{-X}_2$ bond on the bonding in the cyclic moiety manifests itself by the calculated $\text{C}_1\text{-N}_3$ and $\text{C}_1\text{-N}_4$ distances, which show the order **4i** = **8** > **2O** > **2S** > **2Se**. Table 3 shows that the bond order of the $\text{C}_1\text{-N}_3$ and $\text{C}_1\text{-N}_4$ bonds increases following the same sequence as the bond length decreases. The exocyclic $\text{C}_1\text{-X}_2$ bond exhibits a trend of decreasing bond order P_{AB} for X_2 with the order **4i** > **8** > **2O** > **2S** > **2Se**. The $\text{C}_1\text{-X}_2$ π -bond becomes more polarized in the order **4i** > **8** > **2O** > **2S** > **2Se**.

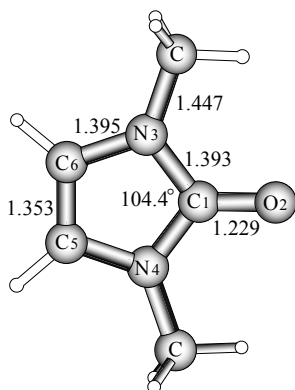
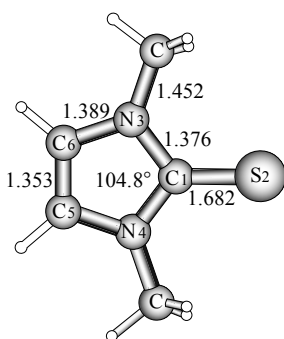
2O, C_{2v} 2S, C_{2v}

Figure 21 Calculated geometries of **2O**, **2S**, **2Se** and **4i**; bond lengths in Å, and angles in degrees

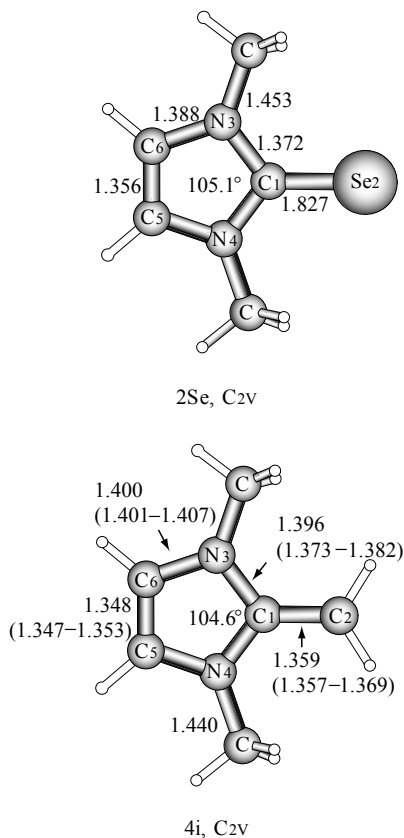
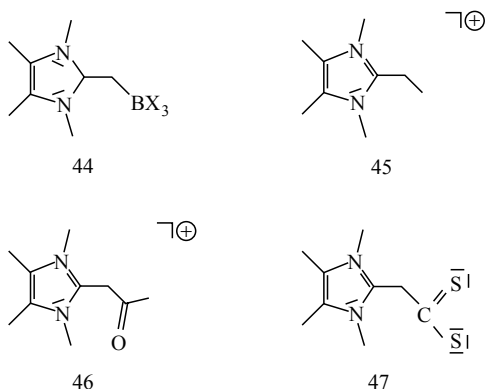


Figure 21 (continued)

3.3 REACTIONS WITH MAIN GROUP ELEMENT ELECTROPHILES

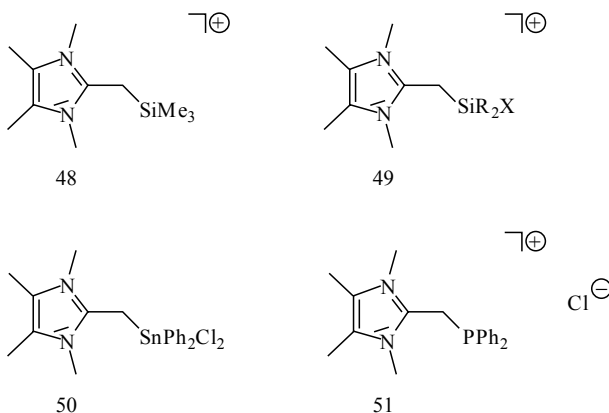
Compound **4** reacts with a wide variety of main group electrophiles to give element-alkyl compounds. Formation of C₂ ring carbon-element bonds is not found in any of these cases.

With boranes BX₃, electroneutral alkylborates **44** (X = H, F) are obtained in good yields. Similar reactions with alanes and gallanes are currently under investigation. Compound **4** is alkylated with MeI to give the 2-ethylimidazolium salt **45**. Similarly, the acyl compound **46** is obtained with acetyl chloride. With CS₂, the electroneutral dithiocarboxylate **47** is obtained [43].



Scheme 18

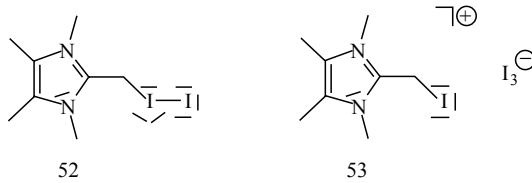
Silylation yielding **48** and **49** occurs with Me_3SiCl and R_2SiCl_2 ($\text{R} = \text{Me}, \text{Ph}$), respectively. Similarly, Ph_2SnCl_2 gives the stannyl compound **50**, whose X-ray structure analysis (Figure 22) reveals a hypervalent molecule containing tin in the coordination number 5. According to the VSEPR rule [44], the electronegative chlorine ligands occupy the axial positions, and the ylide substituent forms a classical tin-to-carbon alkyl bond ($\text{Sn-C}(8) 2.177(3) \text{ \AA}$) [43]. Ph_2PCl gives the cationic triorganophosphane **51** [45].



Scheme 19

With iodine, the adduct **52** is formed. Unfortunately, we have not been able to obtain single crystals suitable for X-ray structure analysis. Adduct **52** reacts

with further iodine to give the triiodide salt **53**, whose structure analysis (Figure 23) reveals weak interionic interaction (I(3)–I(4) 4.071(1) Å); the geometry of the iodomethyl substituent is in the normal range (C(8)–I(4) 2.161(5) Å) [43].



Scheme 20

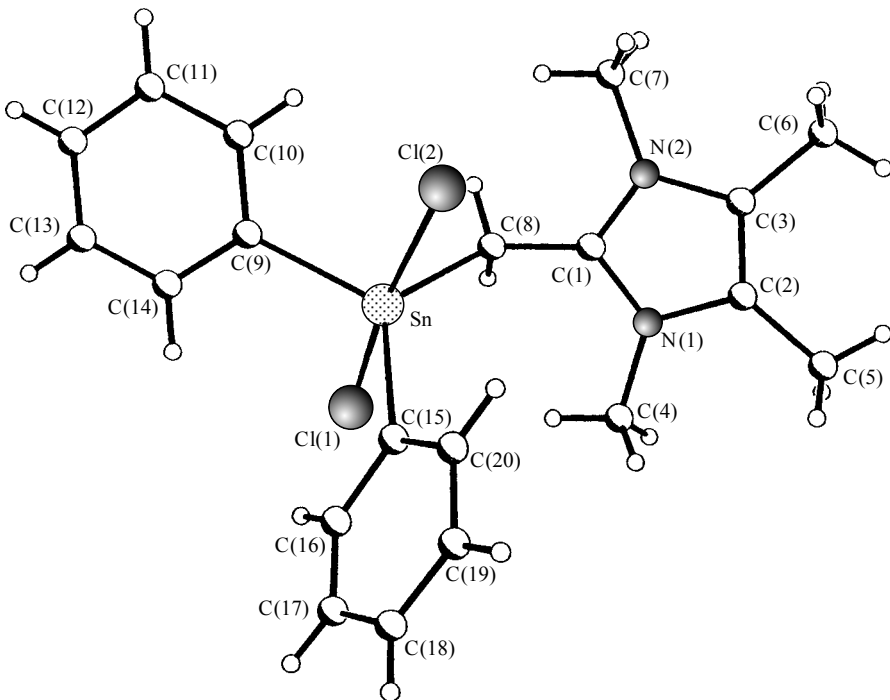


Figure 22 The crystal structure of $C_{20}H_{24}Cl_2N_2Sn$ (**50**). Selected bond lengths (Å) and angles ($^\circ$): Sn–Cl(1) 2.642(1), Sn–Cl(2) 2.550(1), Sn–C(8) 2.177(3), Sn–C(9) 2.139(3), Sn–C(15) 2.144(3), C(1)–C(8) 1.466(4), C(1)–N(1) 1.342(3), C(1)–N(2) 1.335(3); N(1)–C(1)–N(2) 106.5(2), C(1)–C(8)–Sn 119.9(2), C(8)–Sn–C(9) 112.8(1), C(9)–Sn–C(15) 119.4(1), C(15)–Sn–C(8) 127.5(1), Cl(1)–Sn–Cl(2) 171.7(1). Reproduced by permission of Verlag der Zeitschrift für Naturforschung from N. Kuhn, H. Bohnen, G. Henkel and J. Kreutzberg, *Z. Naturforsch., B*, **51**, 1267 (1996)

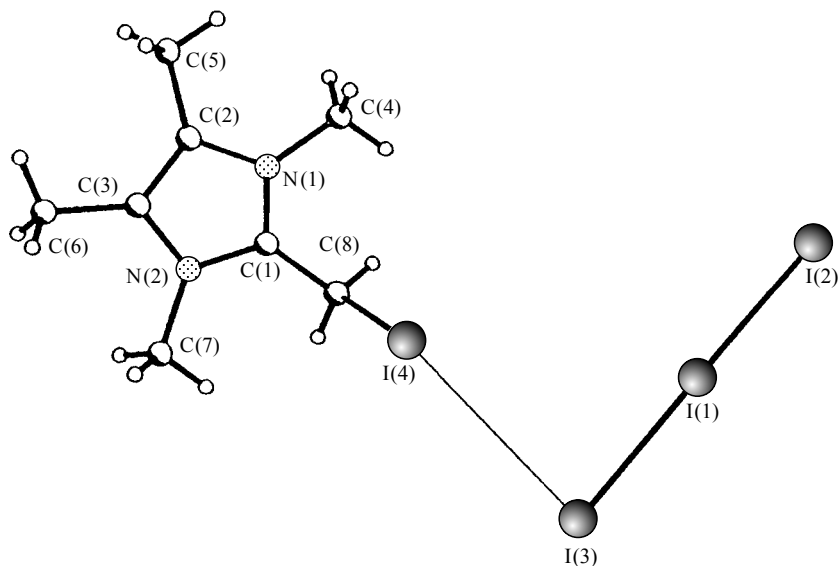


Figure 23 The crystal structure of $C_8H_{14}I_4N_2$ (**53**). Selected bond lengths (Å) and angles ($^\circ$): C(1)–C(8) 1.468(6), C(1)–N(1) 1.326(5), C(1)–N(2) 1.347(5), C(8)–I(4) 2.161(5), I(1)–I(2) 2.872(1), I(1)–I(3) 2.975(1), I(3)–I(4) 4.071(1); N(1)–C(1)–N(2) 107.5(4), C(1)–C(8)–I(4) 112.8(4), C(8)–I(4)–I(3) 143.0(2), I(4)–I(3)–I(1) 84.1(1), I(3)–I(1)–I(2) 177.9(1). Reproduced by permission of Verlag de Zeitschrift für Naturforschung from N. Kuhn, H. Bohnen, G. Henkel and J. Kreutzberg, *Z. Naturforsch., B*, **51**, 1267 (1996)

3.4 BONDING IN IODINE COMPLEXES

We were interested in the structure and bonding situation of the iodine complex **52**. Therefore, we optimized the geometry of the model compound **52M** which is shown in Figure 24.

The geometry optimization of **52M** yielded a very long C₂–I distance which is too long to be considered as a carbon–iodine bond. The geometry of the 2-methyleneimidazoline moiety of **52M** is nearly the same as that calculated for compound **4i**. We conclude that the bonding interactions between methyleneimidazolines and iodine are rather weak and that the experimentally observed compound is a dipole-induced dipole complex. Because weak interactions are poorly described by DFT methods, it is not a surprise that the geometry optimization of **52M** gave basically a non-bonded species.

We also carried out calculations for the iodomethyl compound **53M**. The calculated structure is also shown in Figure 24. The bonding of I⁺ to the methylene group of **4i** has a strong influence on the bonding situation. The exocyclic C₁–C₂ bond in **53M** is much longer (1.473 Å) than in **4i** (1.359 Å).

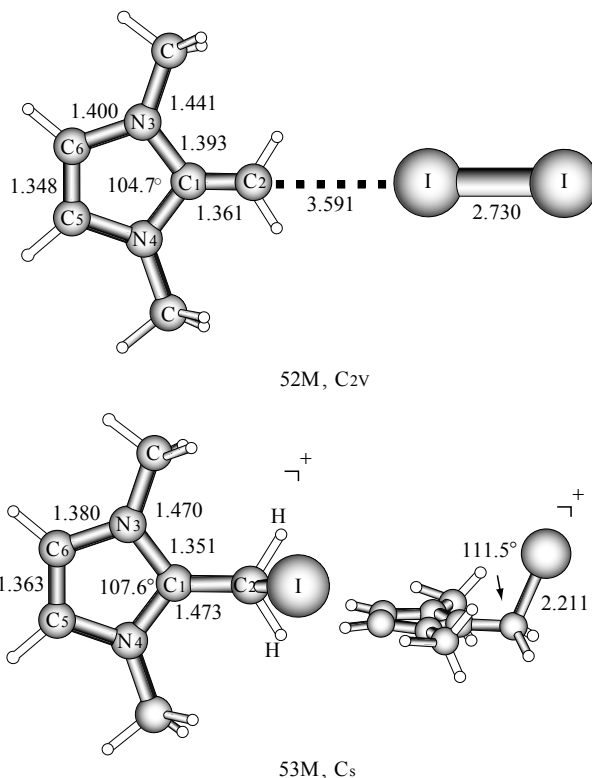


Figure 24 Calculated geometries of **52M** and **53M**: bond lengths in Å, and angles in degrees

The NBO data (Table 4) reveal that the C_1-C_2 bond of the former compound is essentially a single bond ($P_{C_1-C_2} = 1.08$), while the parent compound has a double bond ($P_{C_1-C_2} = 1.63$, see Table 3). In addition, the endocyclic bond lengths of **53M** are clearly different from those of **4i**.

3.5 TRANSITION METAL COMPLEXES

Commonly, olefins coordinate η^2 (side-on) at metal centres which causes significant back donation of π -electrons [46]. In the pentacarbonyl metal complexes **54**, however, both NMR and IR data indicate the ylide to act as a strong donor ligand. The X-ray structure of the molybdenum complex (Figure 25) demonstrates η^1 (edge-on) coordination ($Mo-C(6)$, 2.380(4); $Mo-C(7)$, 3.175 Å). The lack of electron acceptance by the olefin ligand is also indicated by a comparison of the metal-to-carbonyl bond lengths which exhibits the shortening of $Mo-C(5)$ (1.969(4) Å), being *trans* to the olefin [47].

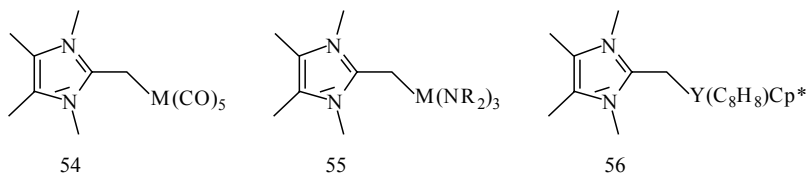
Table 4 NBO results obtained for compounds **53M**, **60M** and **61M** at B3LYP/6-31G(d,p)

Com- pound	q				$p(\pi)$				P_{AB}				$C_1(\%)$				
	C ₁	C ₂	N ₃	N ₄	C ₁	C ₂	N ₃	N ₄	C ₁ -C ₂	C ₁ -N ₃	C ₁ -N ₄	$\sigma(C_1-C_2)$	$\sigma(C_1-N_3)$	$\sigma(C_1-N_4)$	$\pi(C_1-N_3)$	$\pi(C_1-C_2)$	
53M ^a	0.456	-0.688	-0.334	-0.334	0.980	—	1.425	1.425	1.08	1.27	1.27	51.51	37.52	37.52	29.89	—	—
60M ^b	0.471	-0.477	-0.354	-0.354	0.894	—	1.509	1.509	1.00	1.25	1.25	52.71	37.23	37.23	26.59	—	—
61M ^c	0.155	-0.299	-0.474	-0.474	1.241	1.048	1.626	1.621	1.63	0.93	0.93	51.32	36.79	36.79	—	—	57.49

^a Charge: C/CH₂I in **53M**, -0.688/0.084.

^b Charge: CS₂ in **60M**, -0.729.

^c Charge: CS₂ in **61M**, -1.577.



Scheme 21

With lanthanoid centres, η^1 -coordination of compound **4** also takes place. The complexes **55** are obtained by addition of **4** to $(R_2N)_3M$ ($M = La, Nd$; $R = Me_3Si$). The X-ray structure of the neodymium compound (Figure 26) confirms the same coordination type discussed above for the molybdenum complex, including the significant lengthening of the olefinic double bond ($C(19)-C(20)$ 1.421(8) Å). A similar result is obtained from the X-ray structure

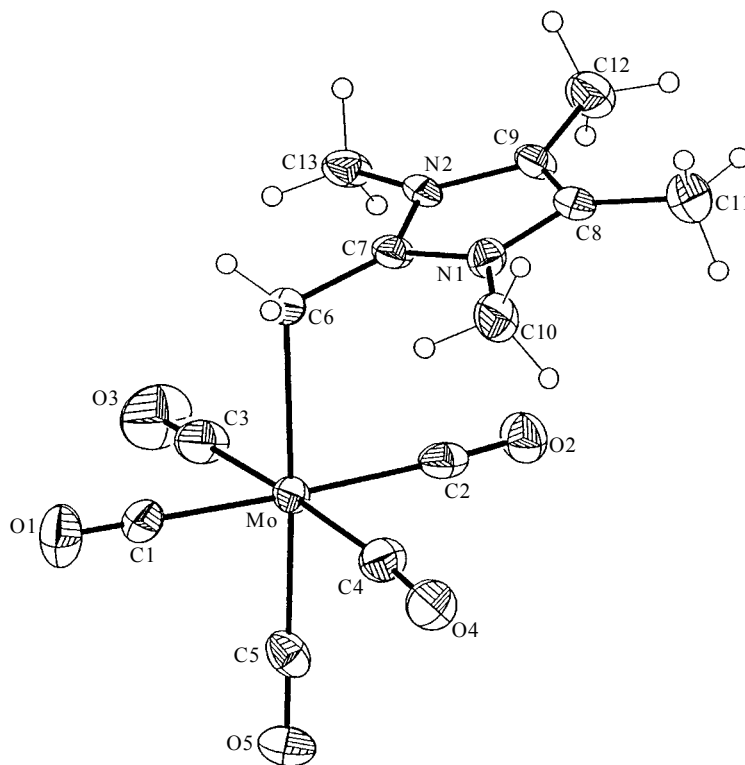


Figure 25 The crystal structure of $C_{13}H_{14}MoN_2O_5$ (**54**). Selected bond lengths (Å) and angles ($^\circ$): $C(7)-C(6)$ 1.431(5), $C(7)-N(1)$ 1.371(5), $C(7)-N(2)$ 1.352(5), $C(6)-Mo$ 2.380(4), $Mo-C(1)$ 2.048(4), $Mo-C(2)$ 2.059(4), $Mo-C(3)$ 2.068(6), $Mo-C(4)$ 2.048(5), $Mo-C(5)$ 1.969(4); $N(1)-C(7)-N(2)$ 105.9(3), $C(7)-C(6)-Mo$ 110.4(3), $C(6)-Mo-C(5)$ 175.6(1). Reproduced by permission of Wiley-VCH from N. Kuhn, H. Bohnen, D. Bläser and R. Boese, *Chem. Ber.*, **127**, 1405 (1994)

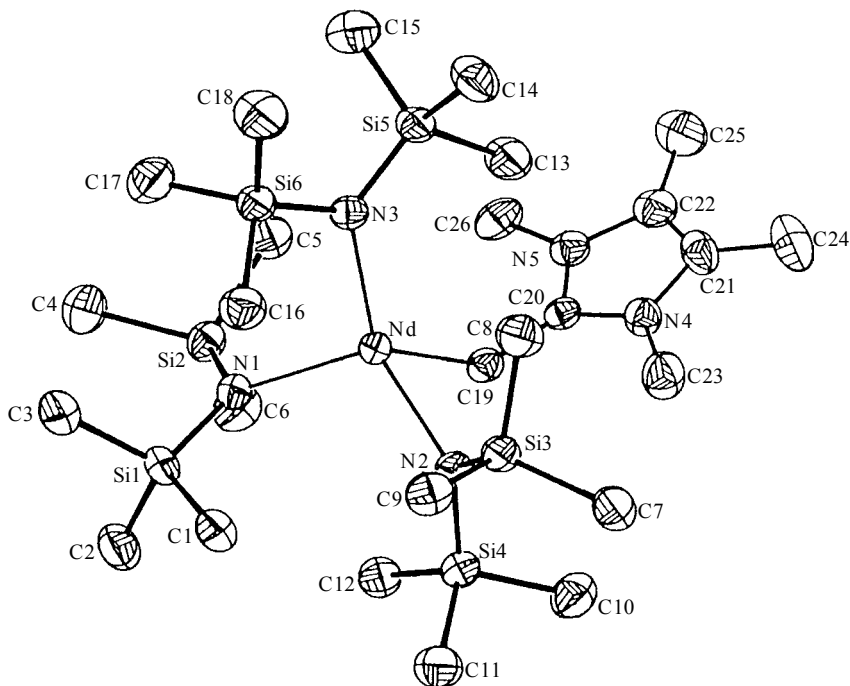


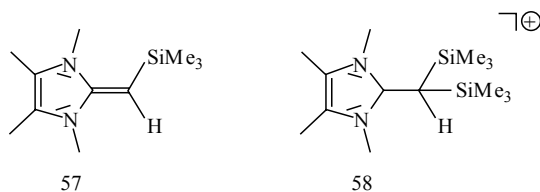
Figure 26 The crystal structure of $C_{26}H_{68}N_5Si_6Nd$ (**55**). Selected bond lengths (Å) and angles ($^\circ$): Nd–N(1) 2.323(5), Nd–N(2) 2.352(5), Nd–N(3) 2.351(5), Nd–C(19) 2.691(6), C(19)–C(20) 1.421(8), C(20)–N(4) 1.355(7), C(20)–N(5) 1.349(7); N(4)–C(20)–N(5) 105.1(5), Nd–C(19)–C(20) 126.2(4). Reprinted from *J. Organomet. Chem.*, **493**, H. Schumann, M. Glanz, J. Winterfeld, H. Hemling, N. Kuhn, H. Bohnen, D. Bläser and R. Boese, Ylidartige Olefinkoordination in Komplexen dreiwertiger f-Elemente, C14–C18, Copyright (1995), with permission from Elsevier Science

of the yttrium complex **56**, prepared by the reaction of **4** with $Cp^*Y(C_8H_8)$ (Figure 27) (C(2)–C(10) 2.410(13) Å). Interestingly, the carbon-to-metal bonds in both compounds are significantly elongated on comparison with conventional alkyl derivatives. This fact, and the small coordination shift in the ^{13}C -NMR spectra of **55** ($M = Ln$) and **56**, is interpreted in terms of the electrostatic nature of the ligand-to-metal interaction in this case [48].

3.6 C-SUBSTITUTED 2-METHYLENEIMIDAZOLINES

As is well known from Wittig ylide chemistry, their stability is increased by π -electron-withdrawing substituents at the methylene carbon atom. Surprisingly, we have not, as yet, been able to obtain stabilized ylids from compound **46**. The silylated ylid **57**, obtained from **48**, is rather unstable in contrast to its doubly silylated cationic derivative **58**. Deprotonation of **58** does not proceed even with strong organometallic bases [43]. We interpret this result as a consequence

of steric interactions between the *N*-methyl substituents and the mutually 'in-plane' orientated methylene C substituents.



Scheme 22

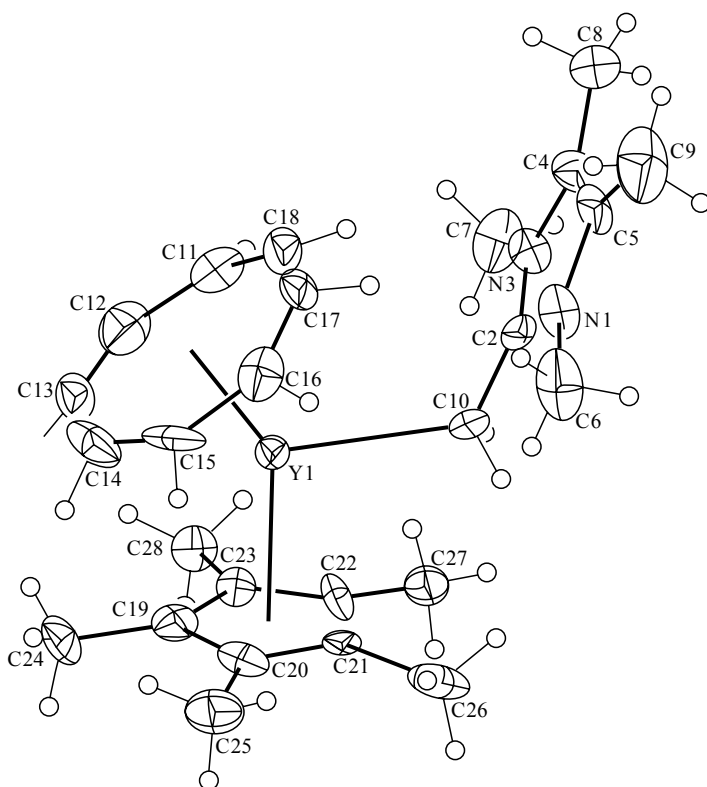
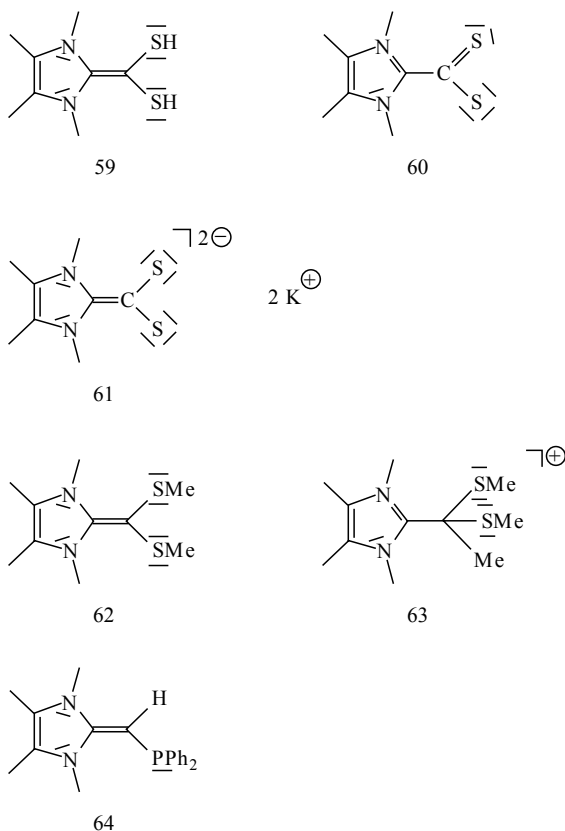


Figure 27 The crystal structure of $C_{26}H_{36}N_2Y$ (**56**). Selected bond lengths (Å) and angles ($^\circ$): Y(1)–C(10) 2.624(11), C(10)–C(2) 1.431(17), C(2)–N(1) 1.364(17), C(2)–N(3) 1.309(16); Y(1)–C(10)–C(2) 123.1(8), N(1)–C(2)–N(3) 107.2(10). Reprinted from *J. Organomet. Chem.*, **493**, H. Schumann, M. Glanz, J. Winterfeld, H. Hemling, N. Kuhn, H. Bohnen, D. Bläser and R. Boese, Ylidartige Olefinkoordination in Komplexen dreiwertiger f-Elemente, C14–C18, Copyright (1995) with permission from Elsevier Science

On the other hand, stable derivatives of the di(thiohydroxy)methyleneimidazole (**59**) could be obtained, starting with potassium reduction of the betaine **60** [49]. The resulting bis(1,1-dithiolate) dianion (**61**) ($R = iso\text{-}Pr$) has been characterized as an oligomeric cage compound in which a central K_6S_6 prism is surrounded by a K_6S_6 ring (Figure 28). In the dianion, the orientation of the ring and CS_2 planes is parallel. On comparison with **4**, the olefinic double bond is slightly elongated ($C(1)\text{--}C(12)$ 1.375(13) Å) presumably as a consequence of the steric interaction between the isopropyl groups and the sulfur atoms (Figure 29) [50]. The influence of the steric demand of the *N*-alkyl substituents has also been revealed by electrochemical investigations of the reduction process [51,52]. The stable thiolate **62**, obtained from **61** and MeI, is still reactive and may be further alkylated to give the cation **63** [51].

The cationic triorganophosphane **51** is deprotonated with excess **4** to give the vinyl phosphane **64** (Figure 30). The X-ray structure of **64** reveals an elongated olefinic bond, accompanied by a short PC bond ($C(13)\text{--}C(14)$ 1.397(8); $P(1)\text{--}C(13)$ 1.761(6) Å), which implies PC π -bonding [45].



Scheme 23

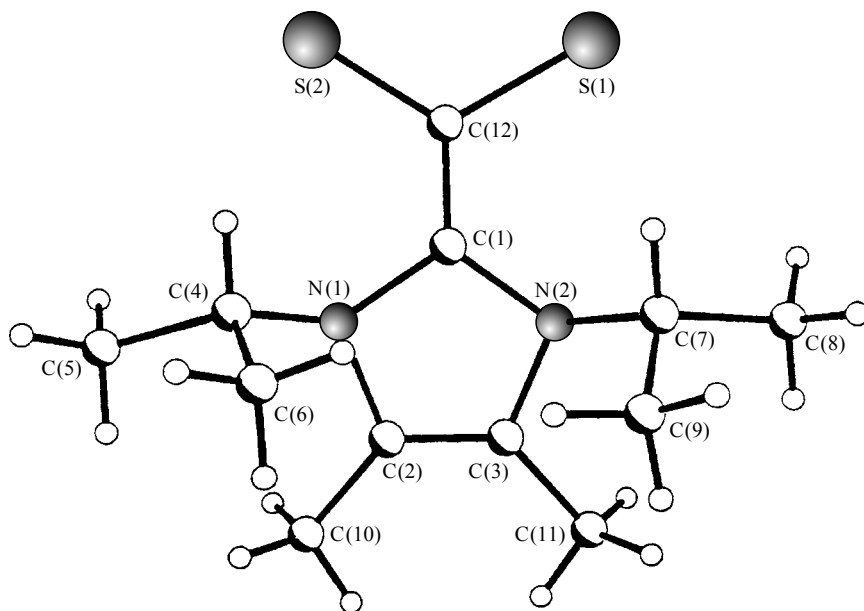


Figure 28 The structure of the 1,1-dithiolate anion in crystals of **61**•2THF•1/3 K₂S₂. Selected bond lengths (Å) and angles (°): C(1)–C(12) 1.375(13), C(1)–N(1) 1.455(10), C(1)–N(2) 1.428(15), C(12)–S(1) 1.803(8), C(12)–S(2) 1.764(11); N(1)–C(1)–N(2) 109.3(7), S(1)–C(12)–S(2) 117.6(5); S(1)–C(12)–C(1)–N(2) –8.3, S(2)–C(12)–C(1)–N(2) 4.7. From N. Kuhn, G. Weyers and G. Henkel, *J. Chem. Soc., Chem. Commun.*, 627 (1997). Reproduced by permission of The Royal Society of Chemistry

3.7 BONDING IN Im-CS₂ AND Im-CS₂²⁻

We have calculated the equilibrium geometries of the neutral compound **60M** and the dianion **61M** which can be used as model compounds for **60** and **61**, respectively. The structures are shown in Figure 31, with the results of the NBO analysis being given above in Table 4.

The calculated data provide interesting information about the structures and bonding situations of the two compounds. The CS₂ moiety of the neutral compound **60M** is perpendicular to the ring plane. The long (1.485 Å) C₁–C₂ bond is a single bond (P_{C₁–C₂} = 1:00), and the C₂–S bonds are very short (1.684 Å). The C₁–N_{3/4} bonds, as well as the N_{3/4}–C_{6/5} bonds, of **60M** are shorter than in 2-methyleneimidazoline (**4i**). The structure of **61M** is very interesting. The CS₂ moiety is in the same plane as the imidazole ring, which is in agreement with the X-ray structure of **61**. The most interesting result is that the methyl groups of **61M** are not in the ring plane. The nitrogen atoms of the dianion have a pyramidal coordination sphere. The NBO analysis gives electron lone-pairs at N₃ and N₄, and carbon–nitrogen single bonds for the ring moiety. The exocyclic C₁–C₂ bond is a double bond (P_{C₁–C₂} = 1.63).

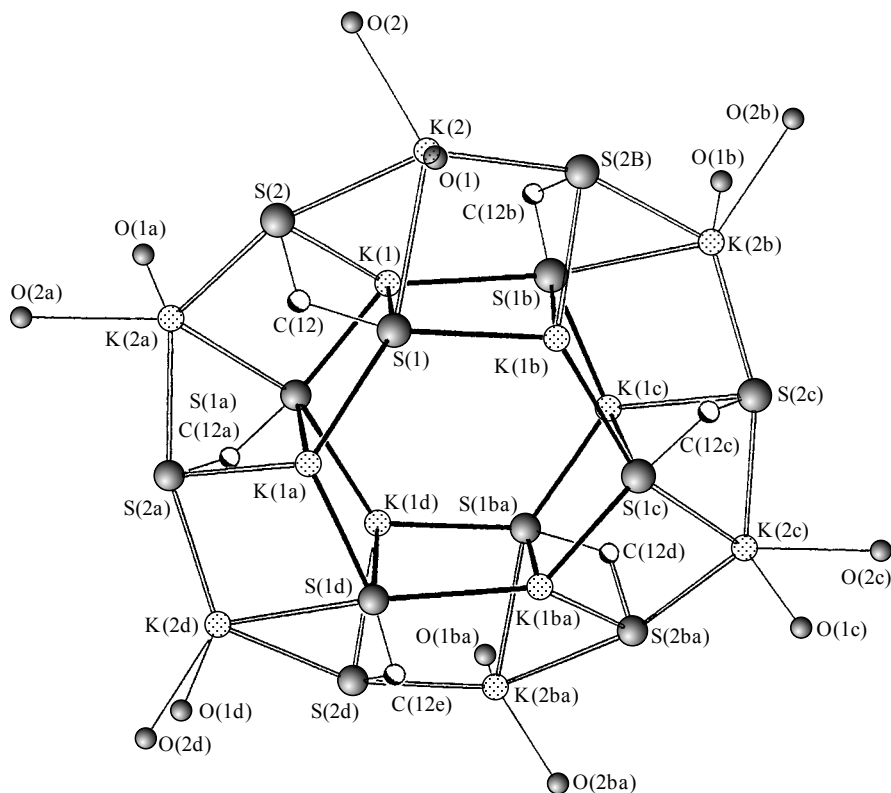
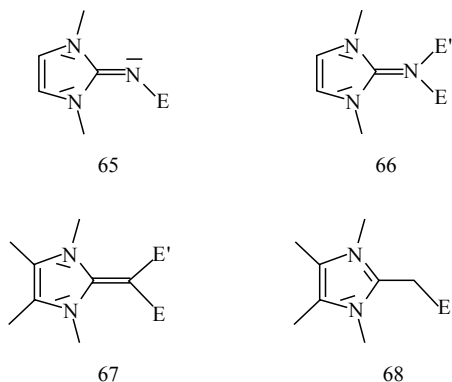


Figure 29 The $K_{12}S_{12}O_{12}$ core in crystals of $61 \cdot 2THF \cdot 1/3 K_2S_2$. Selected bond lengths (Å): K–K' 3.107(4)–4.212(4), K–S 3.023(3)–3.308(5). From N. Kuhn, G. Weyers and G. Henkel, *J. Chem. Soc., Chem. Commun.*, 627 (1997). Reproduced by permission of The Royal Society of Chemistry

4 CONCLUSIONS

Owing to the marked tendency of the heterocyclic ring to stabilize a positive formal charge, imino and methylene imidazoline (**3** and **4**) ligands exhibit strong donor properties as coordinating ligands, as demonstrated by spectroscopy. Comparison of their structural parameters (**65**–**68**) may be helpful for a deeper understanding of this situation (Scheme 24).

As expected from the near coplanar orientation of their imidazole and NH_n planes, the parent compounds **7** and **8** exhibit the shortest exocyclic CN bond lengths (Table 5 and 6) of this series. However, upon enhancing the torsion angles, $N_{ring}-C-N-E$, up to 90° , there is only a moderate lengthening of this bond in the imide-type compounds **65** and **66**, with the geometry of the



Scheme 24

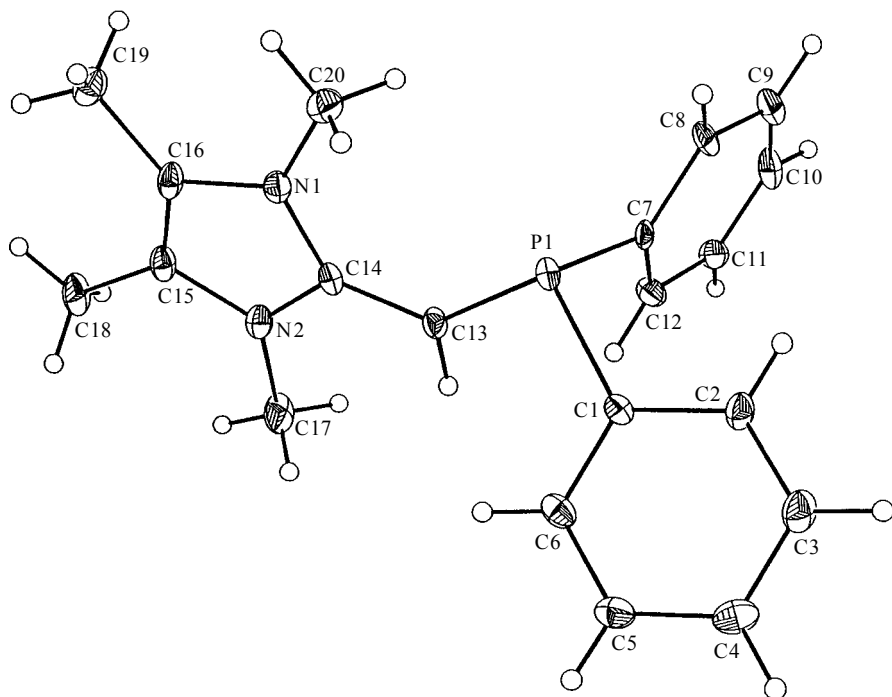


Figure 30 The crystal structure of $C_{20}H_{23}N_2P$ (**64**). Selected bond lengths (Å) and angles ($^\circ$): C(13)–C(14) 1.397(8), C(14)–N(1) 1.382(7), C(14)–N(2) 1.364(8), C(13)–P(1) 1.761(6), P(1)–C(1) 1.844(6), P(1)–C(7) 1.840(3); N(1)–C(14)–N(2) 105.4(5), C(14)–C(13)–P(1) 129.3(4), C(1)–P(1)–C(7) 98.5(2), C(1)–P(1)–C(13) 101.6(3), C(7)–P(1)–C(13) 104.2(2), C(14)–C(13)–H 115.4; N(1)–C(14)–C(13)–P(1) -3.3 . Reproduced by permission of Wiley-VCH from N. Kuhn, M. Göhner and M. Steimann, *Z. Anorg. Allg. Chem.*, 628, 896 (2002)

Table 5 Bond lengths (Å) and distances (°) of type-**65** compounds^a

Compound	(C–N) _{ring}	C–N _{exo}	(N–C–N) _{ring}	C–N–E	N–C–N–E
8	1.373	1.296	104.6	110.3	4.2
12	1.350	1.341	106.9	130.5	88.6
18	1.353	1.318	106.6	175.0	34.9
30	1.350	1.347	106.1	120.2	70.3
33	1.353	1.369	107.5	118.3	90.6

^a Mean values.**Table 6** Bond lengths (Å) and angles (°) of type-**66** compounds^a

Compound	(C–N) _{ring}	C–N _{exo}	(N–C–N) _{ring}	C–N–E(E')	N–C–N–E(E')
7	1.345	1.332	108.1	125.9	1.6
16	1.350	1.358	106.3	118.8	87.7
17	1.350	1.351	106.7	129.1	80.4
34	1.364	1.320	105.8	125.6	45.2
35	1.355	1.339	105.8	117.9	59.7
36	1.366	1.332	105.8	117.9	59.7
37	1.362	1.328	106.3	120.8	33.8
39	1.36	1.351	106.2	117.9	81.0

^a Mean values.**Table 7** Bond lengths (Å) and angles (°) of type-**67** compounds^a

Compound	(C–N) _{ring}	C(2)–C _{exo}	(N–C–N) _{ring}	C(2)–C–E(E')	N–C–C–E(E')
4	1.379	1.357	105.2	120.8	1.1
61 ^b	1.441	1.375	109.3	121.2	6.6
64	1.373	1.397	105.4	122.4	1.9

^a Mean values.^b R(N_{ring}) = *iso*-C₃H₇.

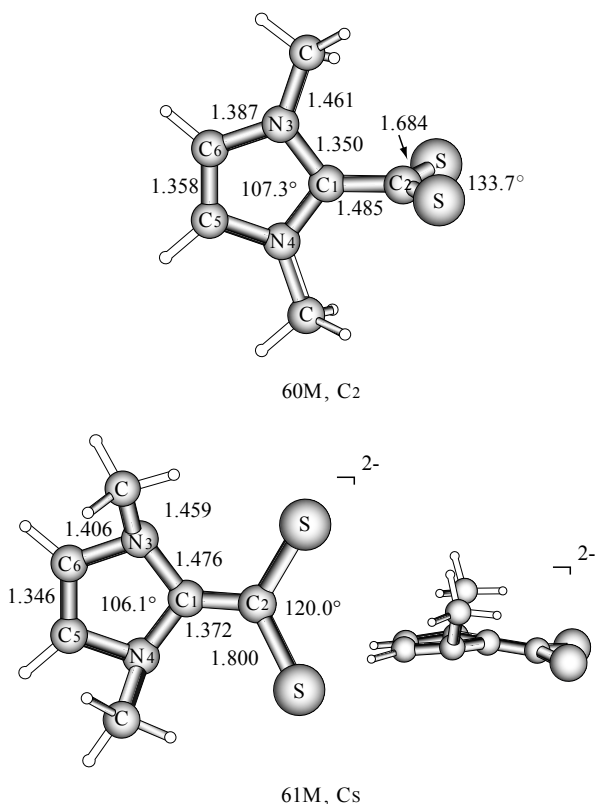
five-membered ring fragments, especially (C₂–N)_{ring} and (N–C–N)_{ring}, being almost unchanged. No direct correlation of the C–N–E angles and further parameters could be detected.

Going from the imine derivatives to the methylene ones (**67**) results in a slight lengthening of the (C₂–N)_{ring} bonds, with the marked increase observed for **61** apparently being influenced by the bulky isopropyl substituents (Table 7). In contrast to the phosphane imine derivative **12**, the methylene analogue **64** also exhibits a near coplanar orientation of the imidazole and phosphino fragments.

Coordination of the 2-methyleneimidazoline **4** gives the cationic alkyl derivatives **68**, in which the positive charge is located at the heterocyclic ring. The change of the bond angle (C₂–C–E) (Table 8) apparently does not markedly influence the ligand geometry.

Table 8 Bond lengths (Å) and angles (°) of type-**68** compounds^a

Compound	(C–N) _{ring}	C(2)–C _{exo}	(N–C–N) _{ring}	C(2)–C–E
68 (E = H ⁺) ^b	1.335	1.48	106.2	—
50	1.339	1.466	106.5	119.9
53	1.337	1.468	107.5	112.8
54	1.362	1.431	105.9	110.4
55	1.352	1.421	105.1	126.2
56	1.337	1.431	107.2	123.1

^a Mean values.^b See Reference [53].**Figure 31** Calculated geometries of **60M** and **61M**; bond lengths in Å, and angles in degrees

Analysis of the unusual bonding situation of these compounds by using quantum-chemical methods demonstrates the strength of combining theory and experiment in order to obtain a coherent understanding of the structures and reactivities of the molecules. The information which is available from

modern experimental and theoretical methods compliment each other, and thus gives a complete picture of the chemistry of the ylidic compounds.

5 ACKNOWLEDGEMENTS

The authors wish to express their gratitude to their co-workers for their skillfull experimental assistance. Financial support by the *Deutsche Forschungsgemeinschaft* and the *Fonds der Chemischen Industrie* is gratefully acknowledged.

6 REFERENCES AND NOTES

1. For an overview, see (a) M. Regitz, *Angew. Chem., Int. Ed. Engl.*, **35**, 725 (1996). W. A. Herrmann and Ch. Köcher, *Angew. Chem., Int. Ed. Engl.*, **36**, 2162 (1997).
2. (a) N. Kuhn, G. Henkel and Th. Kratz, *Z. Naturforsch., B*, **48**, 973 (1993). (b) D. J. Williams, M. R. Fawcett-Brown, R. R. Raye, D. VanDerveer, Y. T. Pang and R. L. Jones, *Heteroatom Chem.*, **4**, 409 (1993).
3. N. Kuhn, G. Henkel and Th. Kratz, *Chem. Ber.*, **126**, 2047 (1993).
4. N. Kuhn, R. Fawzi, Th. Kratz, M. Steimann and G. Henkel, *Phosphorus Sulfur Silicon*, **108**, 107 (1996).
5. (a) N. Kuhn, G. Henkel and Th. Kratz, *Chem. Ber.*, **127**, 849 (1994). (b) N. Kuhn, R. Fawzi, Th. Kratz, M. Steimann and G. Henkel, *Phosphorus Sulfur Silicon*, **112**, 225 (1996). (c) N. Kuhn, Th. Kratz and G. Henkel, *Z. Naturforsch., B*, **51**, 295 (1996).
6. (a) M. C. Aragoni, M. Arca, F. A. Devillanova, A. Garau, F. Isaia, V. Lippolis and G. Verani, *Coord. Chem. Rev.*, **184**, 271 (1999). (b) P. Deplano, J. R. Ferraro, M. L. Mercuri and E. F. Trogu, *Coord. Chem. Rev.*, **188**, 71 (1999).
7. B3LYP: (a) A. D. Becke, *J. Chem. Phys.*, **98**, 5648 (1993). (b) C. Lee, W. Yang and R. G. Parr, *Phys. Rev., B*, **3**, 785 (1988). (c) We employed 6-31G (d,p) basis sets for the main group elements and a small-core ECP with a (441/2111/41) valence basis set for Ti: P. J. Hay and W. R. Wadt, *J. Chem. Phys.*, **82**, 299 (1985). (c) The calculations were carried out with the program package *Gaussian 98*: M. J. Frisch, G. W. Trucks, H. B. Schlegel, G. E. Scuseria, M. A. Robb, J. R. Cheeseman, V. G. Zakrzewski, J. A. Montgomery, R. E. Stratmann, J. C. Burant, S. Dapprich, J. M. Milliam, A. D. Daniels, K. N. Kudin, M. C. Strain, O. Farkas, J. Tomasi, V. Barone, M. Cossi, R. Cammi, B. Mennucci, C. Pomelli, C. Adamo, S. Clifford, J. Ochterski, G. A. Petersson, P. Y. Ayala, Q. Cui, K. Morokuma, D. K. Malick, A. D. Rabuck, K. Raghavachari, J. B. Foresman, J. Cioslowski, J. V. Ortiz, B. B. Stefanov, G. Liu, A. Liashenko, P. Piskorz, I. Komaromi, R. Gomberts, R. L. Martin, D. J. Fox, T. A. Keith, M. A. Al-Laham, C. Y. Peng, A. Nanayakkara, C. Gonzalez, M. Challacombe, P. M. W. Gill, B. G. Johnson, W. Chen, M. W. Wong, J. L. Andres, M. Head-Gordon, E. S. Replogle and J. A. Pople, Gaussian Inc., Pittsburgh, PA, 1998.
8. G. Frenking, Y. Chen and N. Kuhn, unpublished results.
9. A. E. Reed, L. A. Curtiss and F. Weinhold, *Chem. Rev.*, **88**, 899 (1988).
10. See, for example, H. Quast and S. Hünig, *Chem. Ber.*, **101**, 435 (1968).
11. See, for example, (a) J. Münchenberg, O. Böge, A. K. Fischer, P. G. Jones and R. Schmutzler, *Phosphorus Sulfur Silicon*, **86**, 103 (1994). (b) J. Münchenberg, A. K. Fischer, J. Thönnessen, P. G. Jones and R. Schmutzler, *J. Organomet. Chem.*, **529**,

- 361 (1997). (c) J. V. Plack, J. Münchenberg, H. Thönnessen, P. G. Jones and R. Schmutzler, *Eur. J. Inorg. Chem.*, 865 (1998), and references cited therein.
12. N. Kuhn, J. and Wiethoff, unpublished results.
 13. N. Kuhn, and Th. Kratz, unpublished results.
 14. N. Kuhn, R. Fawzi, M. Steimann, J. Wiethoff, D. Bläser and R. Boese, *Z. Naturforsch., B*, **50**, 1779 (1995).
 15. (a) A. W. Johnson, *Ylides and Imines of Phosphorus*, Wiley, New York, 1993. (b) O. I. Kolodiazhnyi, *Phosphorus Ylides*, Wiley-VCH, Weinheim, 1999.
 16. N. Kuhn, J. Fahl, R. Fawzi and M. Steimann, *Z. Kristallogr. NCS*, **213**, 434 (1998).
 17. N. Kuhn, U. Abram, C. Maichle-Mößmer and J. Wiethoff, *Z. Anorg. Allg. Chem.*, **623**, 1121 (1997).
 18. N. Kuhn, R. Fawzi, M. Steimann, J. Wiethoff and G. Henkel, *Z. Anorg. Allg. Chem.*, **623**, 1577 (1997).
 19. For the structural chemistry of alkali phosphaneiminato compounds see S. Chitsaz, B. Neumüller and K. Dehnicke, *Z. Anorg. Allg. Chem.*, **625**, 9 (1999).
 20. N. Kuhn, R. Fawzi, M. Steimann and J. Wiethoff, *Z. Anorg. Allg. Chem.*, **623**, 554 (1997).
 21. For an overview, see (a) R. E. Mulvey, *Chem. Soc. Rev.*, **20**, 167 (1991). (b) A. M. Sapse and P. von R. Schleyer, *Lithium Chemistry*, Wiley, New York 1994. (c) D. S. Wright and M. A. Beswick, *Comprehensive Organometallic Chemistry II*, Vol. 1, G. Wilkinson (Ed.), Elsevier, Oxford, UK, 1995, pp. 1–34.
 22. See, for example, H. Nöth, H. Sachdev, M. Schmidt and H. Schwenk, *Chem. Ber.*, **128**, 105 (1995).
 23. N. Kuhn, R. Fawzi, M. Steimann and J. Wiethoff, *Chem. Ber.*, **129**, 479 (1996).
 24. A. E. Reed and P. von R. Schleyer, *J. Am. Chem. Soc.*, **112**, 1434 (1990).
 25. N. Kuhn, H. Kotowski and J. Wiethoff, *Phosphorus Sulfur Silicon*, **133**, 237 (1998).
 26. For further information on ketimidophosphanes, see Reference [8], and (a) A. Schmidpeter and W. Zeiß, *Chem. Ber.*, **104**, 1199 (1971). (b) R. F. Swindell, D. P. Babb, T. J. Quелlette and J. M. Shreeve, *Inorg. Chem.*, **11**, 242 (1972). (c) B. Hall, J. Keable, R. Snaith and K. Wade, *J. Chem. Soc., Dalton Trans.*, 986 (1978).
 27. See G. H. Robinson (Ed.), *Coordination Chemistry of Aluminum*, VCH, New York, 1993.
 28. S. J. Bryan, W. Clegg, R. Snaith, K. Wade and E. H. Wong, *J. Chem. Soc. Chem. Commun.*, 1223 (1987).
 29. N. Kuhn, R. Fawzi, M. Steimann and J. Wiethoff, *Z. Anorg. Allg. Chem.*, **623**, 769 (1997).
 30. For an overview, see D. E. Wigley, *Prog. Inorg. Chem.*, **42**, 239 (1994).
 31. N. Kuhn, M. Grathwohl, M. Steimann and G. Henkel, *Z. Naturforsch., B*, **53**, 997 (1998).
 32. N. Kuhn, M. Grathwohl, Ch. Nachtigal and M. Steimann, *Z. Naturforsch., B*, **56**, 704 (2001).
 33. N. Kuhn, R. Fawzi, M. Grathwohl, H. Kotowski and M. Steimann, *Z. Anorg. Allg. Chem.*, **624**, 1937 (1998).
 34. N. Kuhn, R. Fawzi, C. Maichle-Mößmer, M. Steimann and J. Wiethoff, *Z. Naturforsch., B*, **52**, 1055 (1997).
 35. N. Kuhn, R. Fawzi, M. Steimann and J. Wiethoff, *Z. Naturforsch., B*, **52**, 609 (1997).
 36. N. Kuhn, R. Fawzi, M. Steimann, J. Wiethoff and G. Henkel, *Z. Anorg. Allg. Chem.*, **623**, 1577 (1997).
 37. For an overview, see (a) A. G. Cook, *Enamines*, Marcel Dekker, New York, 1988. (b) Z. Rappoport (Ed.), *The Chemistry of Enamines*, Wiley, Chichester, UK, 1994.

38. See, for example, U. Gruseck and M. Heuschmann, *Chem. Ber.*, **120**, 2053 (1987).
39. N. Kuhn, H. Bohnen, J. Kreutzberg, D. Bläser and R. Boese, *J. Chem. Soc., Chem. Commun.*, 1136 (1993).
40. N. Kuhn, G. Henkel and J. Kreutzberg, *Z. Naturforsch., B*, **46**, 1706 (1991).
41. See, H.-O. Kalinowski, S. Berger and S. Braun, *¹³C-NMR-Spektroskopie*, Georg Thieme, Stuttgart, 1984.
42. N. Kuhn and J. Kreutzberg, unpublished results.
43. N. Kuhn, H. Bohnen, G. Henkel and J. Kreutzberg, *Z. Naturforsch., B*, **51**, 1267 (1996).
44. R. J. Gillespie and I. Hargittai, *The VSEPR Model of Molecular Geometry*, Allyn and Bacon, Boston, MA, 1991.
45. N. Kuhn, M. Göhner and M. Steimann, *Z. Anorg. Allg. Chem.*, **628**, 688 (2002).
46. See, for example, D. M. P. Mingos, in *Comprehensive Organometallic Chemistry*, Vol. 3, G. Wilkinson (Ed.), Pergamon Press, Oxford, UK, 1982, pp. 1–88.
47. N. Kuhn, H. Bohnen, D. Bläser and R. Boese, *Chem. Ber.*, **127**, 1405 (1994).
48. H. Schumann, M. Glanz, J. Winterfeld, H. Hemling, N. Kuhn, H. Bohnen, D. Bläser and R. Boese, *J. Organomet. Chem.*, **493**, C14 (1995).
49. N. Kuhn, H. Bohnen and G. Henkel, *Z. Naturforsch., B*, **49**, 1473 (1994).
50. N. Kuhn, G. Weyers and G. Henkel, *J. Chem. Soc., Chem. Commun.*, 627 (1997).
51. N. Kuhn, G. Weyers, S. Dümmling and B. Speiser, *Phosphorus Sulfur Silicon*, **128**, 45 (1997).
52. S. Dümmling, B. Speiser, N. Kuhn and G. Weyers, *Acta Chem. Scand.*, **53**, 876 (1999). Further information on **52**[54], cyanimino [55] and phosphorylmethylene [56] imidazolines has been published recently.
53. N. Kuhn, G. Henkel and J. Kreutzberg, *Z. Naturforsch., B*, **46**, 1706 (1991).
54. N. Kuhn, M. Göhner, M. Steimann, *Z. Anorg. Allg. Chem.*, **627**, 2048 (2001).
55. N. Kuhn, M. Grathwohl, M. Steimann, *Z. Naturforsch., B*, **56**, 1015 (2001).
56. N. Kuhn, M. Göhner, M. Steimann, *Z. Anorg. Allg. Chem.*, **628**, 1108 (2002).

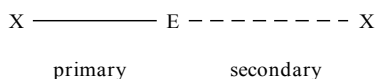
10 Supramolecular Interactions in Structures of Organic Antimony and Bismuth Compounds

GABOR BALÁZS and HANS JOACHIM BREUNIG

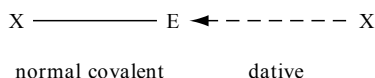
*Institut für Anorganische und Physikalische Chemie der Universität Bremen,
Fb 2, D-28334 Bremen Germany*

1 INTRODUCTION

Some examples of main group organometallic compounds of the type R_2EX , REX_2 , $(R_2E)_2Y$, $(R_2E)_2$ ($E = Sb, Bi$; $X = \text{halogen}$; $Y = O, S$; $R = \text{monovalent alkyl, aryl}$) and other organo antimony and organo bismuth compounds in the oxidation states I–III where strong intermolecular interactions lead to supramolecular [1–3] arrays are discussed in this present chapter. We have considered supramolecular interactions when a crystal structure consists of associated molecules or molecular units with intermolecular contact distances shorter than the sum of the van der Waals radii of the respective elements (r_{vdw} Sb 2.2, Bi 2.4, F 1.5, Cl 1.8, Br 1.9, I 2.1, O 1.5, S 1.8, Se 1.9 Å) [4]. In some cases, the association is so close that individual molecules cannot be distinguished and extended structures with almost homogeneous bonds in the backbone of chains or in the basic nets of layers result. Supramolecular interactions are generally more intense than normal van der Waals bonds, and have preferential orientations. In this aspect, they resemble hydrogen bonds and in fact there are close structural relationships between hydrogen-bonded systems and supramolecular architectures where Sb, Bi, and halogens or chalcogens are involved. Usually, the interactions occur *trans* to internal (*primary*) bonds of a molecule and correspond to *secondary* bonds according to the definition of Alcock [5,6].



Another conception is to consider the Lewis-acid-base properties and to describe the bonds between the molecules as being donor-acceptor interactions or dative bonds. It is generally accepted that σ^* orbitals of the normal covalent E-X bonds may serve as acceptor orbitals. The interactions usually increase with the polarity of the E-X bond and ultimately lead to homogeneous bond lengths.



The resulting hypervalent moieties, X-E-X, may be described with a 'three-centre-four-electron' bonding model where the bond order per bond is 0.5. This model rationalizes the general trend that stronger secondary bonds lead to weaker primary bonds.

Considerable interactions also occur sometimes between molecules of low polarity. Examples include distibines or dibismuthines, which are associated through close contacts between the heavy pnictogen atoms to linear chains of the type $(\text{ER}_2-\text{ER}_2\cdots\text{ER}_2-\text{ER}_2\cdots)_x$. Bonds between distibines or dibismuthines have been discussed in terms of particularly strong closed-shell interactions [7].

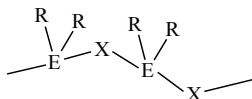
Intermolecular interactions have been known for a long time in the chemistry of inorganic antimony or bismuth compounds. The crystal structures of the trichlorides or tribromides of Sb and Bi consist of the well-defined molecules SbCl_3 (Sb-Cl, 2.34 Å) and BiCl_3 (Bi-Cl, 2.50 Å), although there are close intermolecular contacts to five chlorine atoms of the neighbouring molecules, thus enlarging the trigonal pyramidal coordination to the bicapped trigonal prismatic form (3 + 5 coordination). It is remarkable that the intermolecular contact distances are longer for SbCl_3 (Sb \cdots Cl, 3.46–3.74 Å) than for BiCl_3 (Bi \cdots Cl, 3.24–3.36 Å) [8].

The organometallic derivatives discussed here belong to the group of organic-inorganic compounds which combine an extended inorganic framework with organic species. Some of these hybrid materials are involved in fundamental and applied studies related to their optical, magnetic, thermochromic and electrical properties. With an appropriate coupling between organic and inorganic components, even further new physical properties, such as excitonic superconductivity, may be envisaged [9]. In the case of the organoantimony and -bismuth compounds discussed here, very little is known of the physical properties and therefore mainly recent advances in the structural chemistry are summarized. For earlier reviews in this field, see References [3,6,10–15]. The intensity of the intermolecular contacts in organometallic Sb(III) or Bi(III) compounds depends mainly on the number of organic groups. There is no doubt that interactions increase in the series $\text{R}_3\text{E} < \text{R}_2\text{EX} < \text{REX}_2 < \text{EX}_3$ (X = halogen). In fact, no structures of *tert*-stibanes or bismuthanes, R_3E , with

considerable intermolecular interactions are known. Organoelement dihalides (REX_2), on the other hand, display interactions even when the molecular units are protected by bulky organic groups. Diorganoelement halides, R_2EX , take an intermediate position.

2 DIORGANOELEMENT HALIDES AND RELATED IONIC COMPOUNDS

The crystal structures of three diphenyl antimony halides, i.e. Ph_2SbX ($\text{X} = \text{Cl}$ [10,16], Br [17], I [18]), and several diorganoelement chlorides, (R_2SbCl ($\text{R} = (\text{Me}_3\text{Si})_2\text{CH}$ [19]) and, R_2BiCl ($\text{R} = (\text{Me}_3\text{Si})_2\text{CH}$ [20] and 2, 4, 6-(CF_3)₃ C_6H_2 [21]) consist of molecules with contact distances longer than the sum of the van der Waals radii of the corresponding elements. Intermolecular interactions have been observed in the crystal structures of two antimony compounds, namely Me_2SbI [19] and Ph_2SbF [22], and two bismuth derivatives, i.e. Ph_2BiCl [23], Mes_2BiBr [24]. These structures consist of zigzag or helical chains with halogen bridges between the Sb or Bi atoms.



The chains may be considered as coordination polymers with dative bonds between the halogen donors and the Sb or Bi acceptors, with the Lewis acidic sites being *trans* to the $\text{E}-\text{X}$ bond. The bending of the chains at the halogen atoms and the (distorted) ψ -trigonal bipyramidal coordination of the Sb or Bi centres correspond to the predictions of the VSEPR model. Because of the small number of known crystal structures, only a preliminary consideration of the influence of the nature of the groups and atoms is possible. The trends that emerge now are not surprising and can be rationalized easily. Intermolecular contacts between the R_2EX molecules are stronger for bismuth than for antimony compounds; they decrease with bulky organic groups and are much closer for diphenylantimony fluoride when compared with the corresponding chloride, bromide or iodide.

A more detailed inspection of the structures reveals differences resulting mainly from the various possibilities for the orientation of the organic groups and the variations in the bond lengths. There is an interdependency between the chain structure and the packing of the chains in the crystal.

In the dimethylantimony iodide chain (Figure 1) the short and long $\text{Sb}-\text{I}$ bonds are clearly differentiated. The chain atoms lie almost in a plane, while the methyl groups are directed to one side of this plane. The reverse side is exposed to neighbouring chains with inter-chain $\text{Sb}\cdots\text{I}$ contacts close to the van der

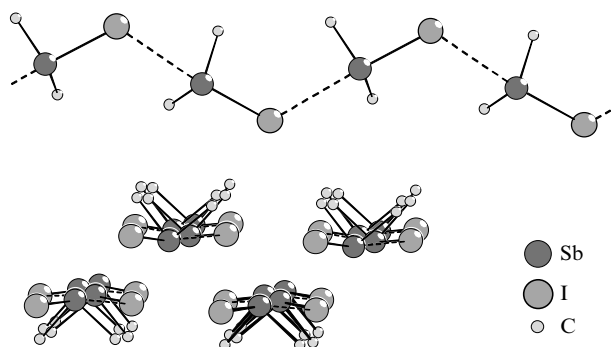


Figure 1 Chain structure of Me_2SbI . Distances (Å) and angles ($^\circ$): Sb–I 2.799(1), Sb··I (in the chain) 3.666(1), Sb··I (between the layers) 4.024(1)–4.167(1); I–Sb··I 171.87(4), Sb–I··Sb 116.83(3)

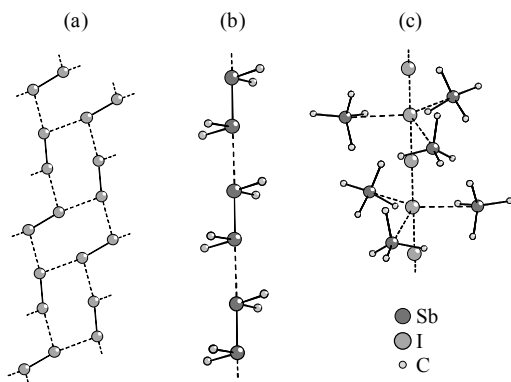


Figure 2 Molecular structures of (a) I_2 , (b) Me_4Sb_2 and (c) $(\text{Me}_4\text{Sb})_3\text{I}_8$. Distances (Å) and angles ($^\circ$): I_2 , I–I 2.715; I··I 3.496; I–I··I 170.11, 105.72; Me_4Sb_2 , Sb–Sb 2.830(1); Sb··Sb 3.709(1); Sb–Sb··Sb 178.80(1); $(\text{Me}_4\text{Sb})_3\text{I}_8$, I··I 3.296(4), 3.285(4); Sb··I 4.129(4); I··I··I 180.00(1); Sb··I··Sb 118.81(4)

Waals border. This type of chain packing leads to a system of inorganic and organic double layers.

Dimethylantimony iodide (Figure 1) is related to I_2 (Figure 2(a)) [8] and to $\text{Me}_2\text{SbSbMe}_2$ (Figure 2(b)) [25,26]. A comparison of the structures of these molecules in the solid state may be instructive for consideration of the influence of bond polarity and the role of methyl groups. All three structures consist of closely associated molecules. Tetramethyldistibine and dimethylantimony iodide have various features in common. In both structures there is only one close intermolecular contact per heavy atom. The resulting single chains are almost rectilinear in the crystals of the distibine but have a zigzag arrangement in solid Me_2SbI .

In contrast, there are two close contacts per iodine atom in the case of crystalline I_2 and the known layer structure (Figure 2(a)) results. A linear chain of iodine atoms exists, however, in the structure of the polyiodide $(Me_4Sb)_3I_8$ (Figure 2(c)) [27]. The orientation of the methyl groups in the case of Me_4SbI allows association of the chains to two double layers of the heavy atoms. In contrast, the antimony chain in Me_4Sb_2 is surrounded by the methyl groups, because the molecules adopt the antiperiplanar conformation. The ratio, $E \cdot E/E-E$, between the bond lengths for the (shortest) secondary and the primary bonds is often used as a measure for the intensity of the intermolecular contacts. For Me_2SbI , the ratio is 1.31, for I_2 1.29, while for Me_4Sb_2 the ratios 1.30 and 1.28 have been reported [25,26]. These values show that the intensities of the closest contacts between these molecules are very similar.

Much more intense interactions exist in crystalline diphenylantimony fluoride (Figure 3) [22]. The Sb-F bond lengths in the chain are almost equal and secondary and primary bonds can hardly be distinguished. The chain atoms do not lie in a plane and a helical arrangement results. The phenyl groups are orientated around the Sb-F chain. The environment of the antimony atoms is distorted ψ -trigonal bipyramidal.

Another example of a structure with almost homogeneous bonds is diphenylbismuth chloride [23]. The environment of the bismuth atoms in Ph_2BiCl is an almost ideal ψ -trigonal bipyramidal one. As in Me_2SbI , the heavy atoms are all in a plane and a perfect zigzag chain results (Figure 4). The phenyl groups lie pair-wise on both sides of the plane.

As expected, the bond lengths in the Ph_2BiCl chain (mean Bi-Cl, 2.755 Å) are considerably larger than in $[(Me_3Si)_2CH]_2BiCl$ (Bi-Cl, 2.530 Å), a molecular compound without supramolecular interactions [20]. Under the influence of the mesityl substituents, the association in the chain of Me_2SbBr molecules (Figure 5) is only loose. There are different bond lengths in the chain and also the distortions of the ψ -trigonal bipyramidal environment of the bismuth atoms

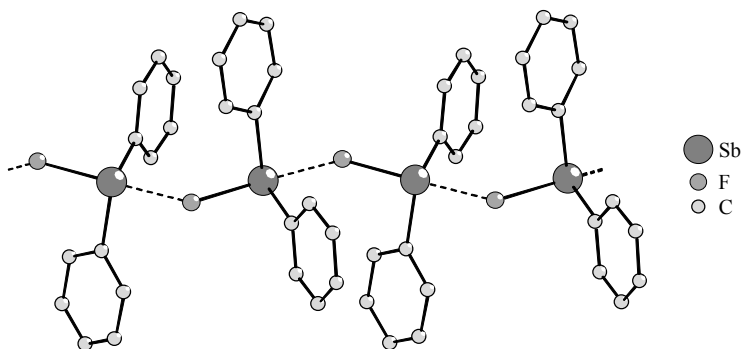


Figure 3 Chain structure of Ph_2SbF . Distances (Å) and angles ($^\circ$): Sb-F 2.166(2), Sb-F 2.221(3), Sb-F \cdots Sb 140.21(2), F-Sb \cdots F 165.06(2)

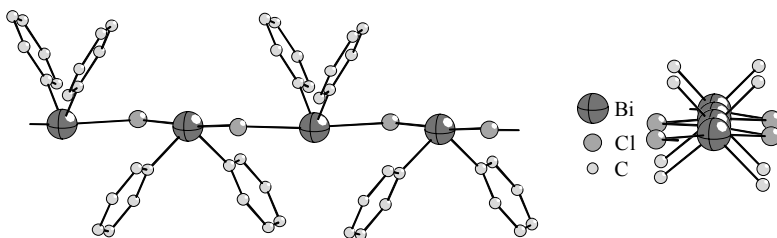


Figure 4 Chain structure of Ph_2BiCl . Distances (Å) and angles ($^\circ$): Bi–Cl 2.746–2.763; Bi–Cl–Bi 100.56(1); Cl–Bi–Cl 175.22(1), 175.61(1)

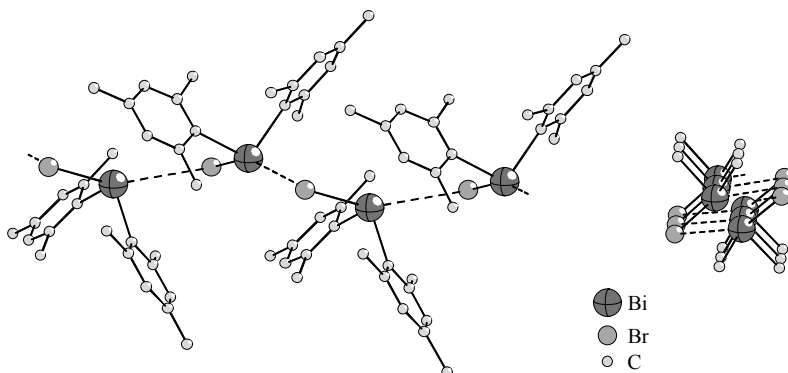


Figure 5 Chain structure of Mes_2BiBr . Distances (Å) and angles ($^\circ$): Bi–Br 2.689(2), Bi–Br 3.795(3), Br–Bi–Br 156.09(2), Bi–Br··Bi 96.69(1)

are considerable. The Bi–Br chains are helical. There are no close interactions between the chains which are protected from all sides by the mesityl groups.

The chain structures of diorganoelement halides, R_2EX , are closely related to the structures of the hypervalent anions $[\text{X}-\text{ER}_2-\text{X}]^-$, which likewise have a ψ -trigonal bipyramidal environment at the pnictogen atoms, with halogen atoms in the axial, with the lone pair of electrons and the organic substituents in the equatorial positions. In fact, the association of diorganoelement halides to chains may be envisaged as the first step of the formation of an ionic form, $\text{ER}_2^+[\text{X}-\text{ER}_2-\text{X}]^-$. Such an ionic form has not been observed in the structures of pure diorganoelement halides. However, a related ionic compound, which may be considered as a donor-stabilized derivative of an ionic form of dimethylantimony bromide, $\text{D} \rightarrow \text{SbMe}_2^+[\text{Br}-\text{SbMe}_2-\text{Br}]^-$ ($\text{D} = \text{Me}_4\text{Sb}_2$), is known [28]. The structure of the anion corresponds to the coordination sphere of the antimony atoms in Me_2SbI . The comparison of the cation $\text{Me}_2\text{Sb}-\text{SbMe}_2-\text{SbMe}_2^+$ (Sb–Sb 2.8203(4) Å, Sb–Sb–Sb $116.19(2)^\circ$) with the $\text{Me}_2\text{Sb}-\text{SbMe}_2 \cdots \text{SbMe}_2$ fragment in the chain structure of Me_4Sb_2 (Sb–Sb 2.830(3), Sb··Sb 3.709(1) Å; Sb–Sb··Sb $(178.80(1)^\circ)$) reveals major differences.

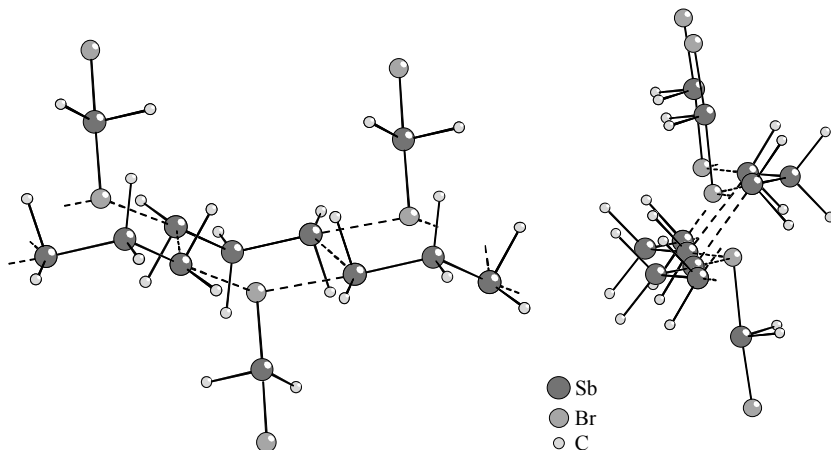


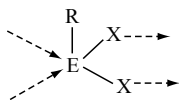
Figure 6 Molecular structure of $[\text{Me}_6\text{Sb}_3][\text{Me}_2\text{SbBr}_2]$. Distances (Å) and angles ($^\circ$): Sb–Sb 2.8203(4), Sb–Br 2.6999(11)–2.9773(10), Sb··Br 3.4693(8), Sb··Sb 3.8145(8), Sb–Sb–Sb 116.19(2), Sb··Br··Sb 125.83(1), Sb–Sb··Sb 118.88(1)

The Sb–Sb bond lengths in the cation are homogeneous and the coordination of the central antimony atom is distorted tetrahedral. In fact, the cation is more related to stibonium ions of the type R_4Sb^+ . In the crystal structure, there are close Sb··Br contacts between the anions and the cations, thus leading to zigzag $(\text{Sb}–\text{Sb}–\text{Sb}··\text{Br})_x$ chains with the methyl groups on both sides of the plane of the heavy atoms. These chains are associated pairwise through Sb··Sb contacts between the cationic Sb_3 units (Figure 6), and infinite antimony chains of the type $(\text{SbMe}_2–\text{SbMe}_2–\text{SbMe}_2··)_x$ can be distinguished.

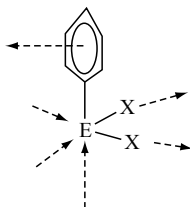
Other compounds with known crystal structures featuring hypervalent anions $[\text{X}–\text{ER}_2–\text{X}]^-$ are $\text{M}^+\text{Ph}_2\text{SbCl}_2^-$ ($\text{M} = \text{Me}_4\text{N}$ [29], Cp_2Co [30]), and $\text{M}^+\text{Ph}_2\text{SbI}_2^-$ ($\text{M} = \text{Et}_4\text{N}$) [31].

3 ORGANOELEMENT DIHALIDES

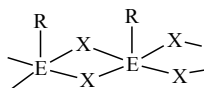
Observing the stronger Lewis acidity of organoelement dihalide molecules which contain two electronegative groups and are less protected by only one organic group it is easy to understand that intermolecular association occurs much more frequently when compared to diorganoelement halides. Such molecules have two donor sites at the halogen atoms and two acceptor sites *trans* to the element–halogen bond.



The coordination geometry and the tendency to form coordination polymers with bridging halogen atoms may easily be anticipated. Additional weak interactions *trans* to the alkyl groups are also possible, and under the influence of bulky organic groups, or when one of the acceptor sites is blocked by an external donor ligand, only one of the halogen atoms is involved in the supra-molecular framework. For the phenyl derivatives, the situation is more complex because interactions between the pnictogen atoms and the aryl groups may also occur and the acceptor strength *trans* to the phenyl group is possibly increased by the π -donation.



A general type of structure possesses linear chains of E_2X_2 rings sharing opposite vertices which are occupied by the Sb or Bi atoms in distorted square pyramidal environments. The alkyl groups are directed to one side of the chain.



The family of methylantimony dihalides (Cl, Br, I) and alkylbismuth diiodides belong to this type. The individual examples differ mainly in the positions of the longer and shorter bonds. In the structure of $MeSbI_2$ [32] and $MeSbBr_2$ [33] (Figure 7), the chain consists of trigonal pyramidal molecules which are connected through *secondary* bonds. The SbX_2 ($X = Br, I$) angles of the molecules open in the chain direction. The orientation of the methyl group to one side allows the pairwise association of the chains. The resulting system of inorganic and organic double layers is closely related to the structure of Me_2SbI .

The association of the molecules in the $MeSbX_2$ chains is weaker for the bromide when compared to the iodide ($MeSbBr_2$: $Sb \cdots Br/Sb-Br = 1.3$; $MeSbI_2$: $Sb \cdots I/Sb-I = 1.2$). Alkylbismuth diiodides have related double-chain structures with almost homogenous bond lengths between Bi and I. The structure of methylbismuth diiodide [9,34] is depicted in Figure 8.

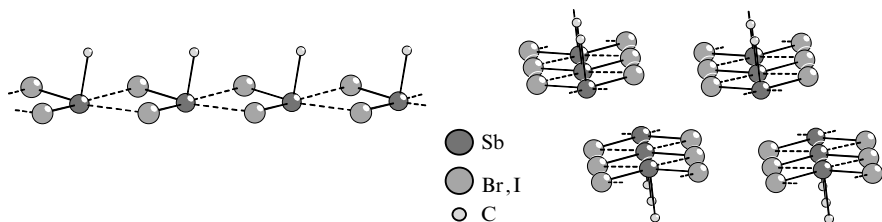


Figure 7 Isotypic structures of MeSbBr_2 and MeSbI_2 . Distances (Å) and angles ($^\circ$): MeSbBr_2 , Sb–Br 2.564(3), 2.583(3); Sb \cdots Br (in the chain) 3.299(3), 3.382(3); Sb \cdots Br (between the layers) 3.872(4), 4.015(4); Br–Sb–Br 97.6(1); Br \cdots Sb \cdots Br 70.84(2); Br–Sb \cdots Br 94.22(2), 166.12(3); MeSbI_2 , Sb–I 2.762(2)–2.799(2); Sb \cdots I (in the chain) 3.397(2), 3.469(2); Sb \cdots I (between the layers) 4.108(3); I–Sb–I 99.13(9); I \cdots Sb \cdots I 76.11(6); Sb–I \cdots Sb 91.10(7), 93.27(8)

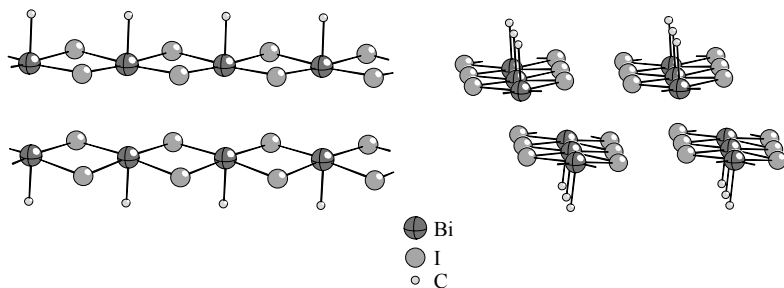


Figure 8 Molecular structure of MeBiI_2 . Distances (Å) and angles ($^\circ$): Bi–I 3.0870(10) 3.1279(10), I–Bi–I 88.07(3) 176.06(4), Bi–I–Bi 88.07(3), 89.55(3), Bi \cdots I (between the layers) 4.1549(11)

Related chains exist in crystals of $\text{C}_2\text{H}_5\text{BiI}_2$ and $n\text{-C}_4\text{H}_9\text{BiI}_2$ [34]. There are double chains in the structure of the ethyl derivative, but single chains in the crystals of the butyl compound (Figure 9).

The structure of pure MeSbCl_2 is not known. However, a mixed phase, $\text{MeSbCl}_2 \cdot 0.6 \text{SbCl}_3$, was analysed by X-ray diffraction [33]. The crystals contain alternating layers, where one layer consists of double chains of MeSbCl_2 molecules. Compared with MeSbBr_2 or MeSbI_2 , the orientation of the molecules is different. The SbCl_2 angles of neighbouring molecules open in opposite directions perpendicular to the chain. The second layer is partly disordered, where three quarters of the molecules are SbCl_3 , and a quarter are MeSbCl_2 . Close intermolecular contacts in the respective layers and between them result in a (3 + 5) coordination of the Sb atoms in both molecules (Figure 10).

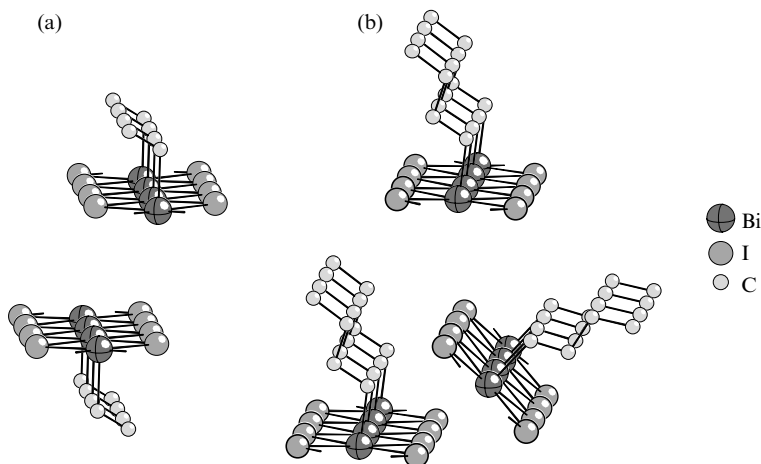


Figure 9 Chain structures of (a) EtBiI_2 , and (b) $n\text{-BuBiI}_2$. Distances (Å) and angles ($^\circ$): EtBiI_2 , Bi–I 3.1082(15), 3.1071(15); Bi–I 4.289(2); I–Bi–I 88.83(4), 179.00(7); Bi–I–Bi 88.83(5), 88.87(5); $n\text{-BuBiI}_2$, Bi–I 3.1347(15), 3.0883(15); Bi–I 4.1936(17); I–Bi–I 87.79(4), 178.09(5); Bi–I–Bi 87.79(5), 89.45(5)

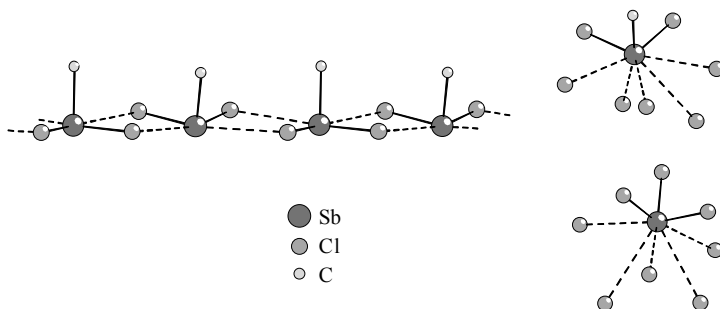


Figure 10 Section of a MeSbCl_2 chain and coordination of the molecules in the structure of $\text{MeSbCl}_2 \cdot 0.6 \text{SbCl}_3$. Distances (Å) and angles ($^\circ$): Sb–Cl 2.368(2)–2.430(3), $\text{Sb} \cdots \text{Cl}$ 3.337(3)–3.865(3), Sb–Cl–Sb (in the chain) 102.9(1)

The structure of MeBiCl_2 is a unique among the alkylpnictogen dihalides. Instead of a one-dimensional chain there is a puckered net of methyl bismuth units and chlorine atoms (Figure 11) with the methyl groups directed to one side. The meshes of the net consist of eight-membered $(\text{CH}_3\text{Bi})_4\text{Cl}_4$ heterocycles. The bismuth atoms are five-coordinate in square pyramidal environments, with basal chlorine atoms and apical methyl groups [35].

Under the protection of a bulky alkyl or aryl substituent, not all of the donor and acceptor sites are occupied and free E–X functions, not involved in the supramolecular framework remain. This is observed in the crystal structures

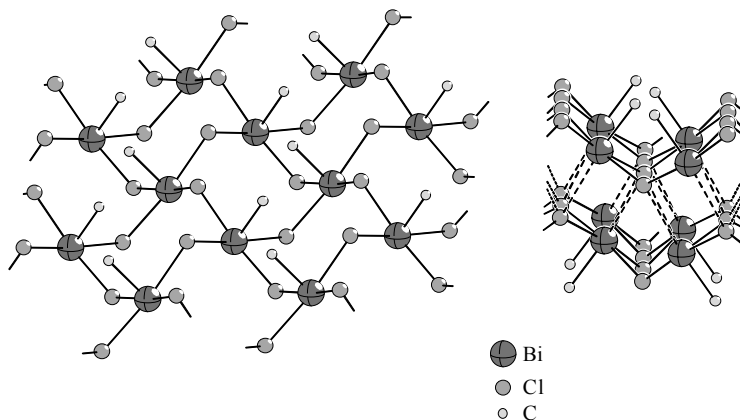
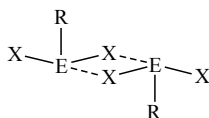


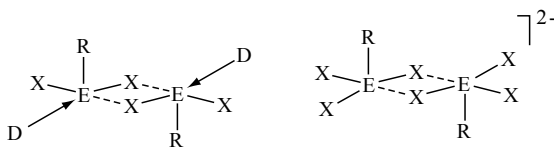
Figure 11 Molecular structure of MeBiCl_2 . Distances (Å) and angles ($^\circ$): Bi–Cl 2.741(1) 2.755(1), Bi–Cl 3.684(1), Bi–Cl–Bi 122.60(1) 134.32(1), Cl–Bi–Cl 88.49(1)–91.40(1), Bi–Cl–Bi 81.48

of RSbCl_2 ($\text{R} = \text{}^t\text{Bu}$ [36], $(\text{Me}_3\text{Si})_2\text{CH}$ [37,38], 2,4,6- $\text{Ph}_3\text{C}_6\text{H}_2\text{BiCl}_2$ [39] and 2,4,6- $\text{Me}_3\text{C}_6\text{H}_2\text{BiBr}_2$ [40]). Non-bridging chlorine atoms also exist in the crystal structure of $(\text{Me}_3\text{Si})_2\text{CHBiCl}_2 \cdot 0.5 \text{Et}_2\text{O}$ [41]. $(\text{Me}_3\text{Si})_2\text{CHSbCl}_2$ [37,38] is only weakly associated to dimers ($\text{Sb} \cdots \text{Cl}$, 3.518(1) Å). Analogous dimers are also formed in the case of 2,4,6- $\text{Ph}_3\text{C}_6\text{H}_2\text{BiCl}_2$ [39].



$\text{E} = \text{Sb}$, $\text{R} = (\text{Me}_3\text{Si})_2\text{CH}$; $\text{E} = \text{Bi}$, $\text{R} = 2,4,6\text{-Ph}_3\text{C}_6\text{H}_2$; $\text{X} = \text{Cl}$

Dimeric structures also result when Lewis acidic sites in organoelement dihalides are blocked by additional intramolecular coordination, as in 2- $\text{Me}_2\text{NCH}_2\text{C}_6\text{H}_4\text{BiI}_2$ [42], with neutral ligands, as in $(\text{Me}_3\text{Si})_2\text{CHBiCl}_2(\text{THF})$ [43] or $\text{PhBiBr}_2(\text{D})$ ($\text{D} = N, N'$ -dimethylpropyleneurea (dmpu), Ph_3PO) [44], or with anionic ligands, as in $(\text{PhSbI}_3)_2^{2-}$ [45] related complexes [14,15].



An example for a polymer where only one of the two halogen atoms is involved is $(\text{Me}_3\text{Si})_2\text{CHBiCl}_2 \cdot 0.5\text{Et}_2\text{O}$ [20] (Figure 12), a compound where a helical chain structure is stabilized by diethyl ether molecules in bridging positions *trans* to the alkyl groups.

A related chain structure is adopted by MesBiBr_2 [40] (Figure 13), where Bi and bridging Br atoms are arranged as a zigzag chain. The non-bridging bromine atoms lie on one side, with the mesityl groups on the other side of the plane as defined by the positions of the chain atoms. The structure is stabilized by weak π -interactions between the mesityl groups and the bismuth atoms.

When one of the acceptor functions is blocked by coordination of a neutral ligand *trans* to an E–X bond, not only the formation of dimers, as in PhBiBr_2 (dmpu) or $\text{PhBiBr}_2(\text{Ph}_3\text{PO})$ [44], but also polymerization may occur. Examples

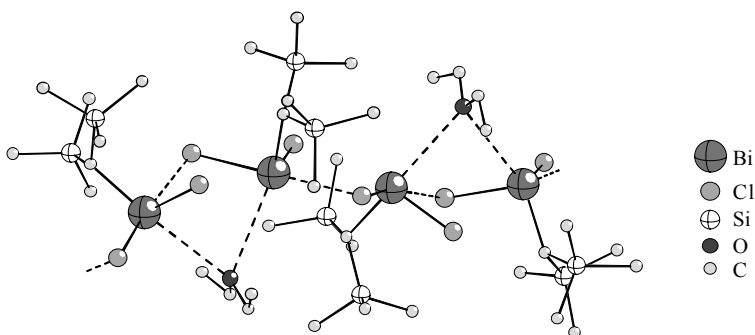


Figure 12 Chain structure of $(\text{Me}_3\text{Si})_2\text{CHBiCl}_2:0.50\text{Et}_2\text{O}$. Distances (Å) and angles ($^\circ$): Bi–Cl 2.522(5)–2.729(5), Bi··Cl 2.824(4) 2.851(4), Bi··O 3.431(11) 3.557(11), Cl–Bi··Cl (*trans*) 160.77(15), Bi–Cl··Bi 98.91(17) 109.03(18)

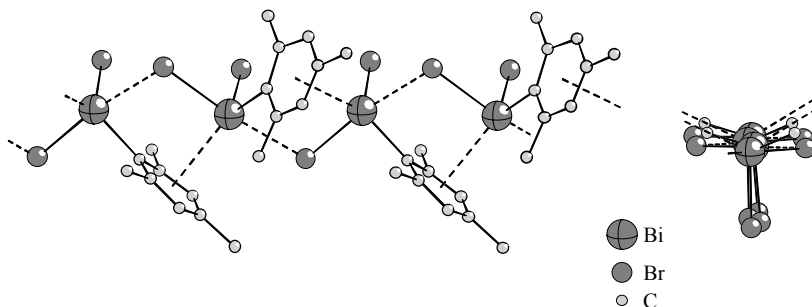


Figure 13 Chain structure of MesBiBr_2 . Distances (Å) and angles ($^\circ$): Bi–Br 2.619–2.818(3), Bi··Br 3.017(3) 3.022(3), Bi–centre of the mesityl ring 3.195(28) 3.301(11), Bi··Br··Bi 99.87(9) 101.04(9), Br–Bi–Br 92.99(11) 92.73(11), Br–Bi··Br (*trans*) 172.44(9)

of such coordination polymers are the mono-tetrahydrofuran adducts of phenylbismuth dihalides, $\text{PhBiX}_2(\text{thf})$ ($X = \text{Cl}$ [46], Br [47], I [47], thf = tetrahydrofuran) which form zigzag chains stabilized by π -interactions *trans* to the Bi–C bonds. The *ipso* carbon atoms of the phenyl groups lie in the plane of the polymeric chain. The thf ligands and the non-bridging halogen atoms occupy alternating positions on both sides of the plane. The structure of $\text{PhBiI}_2(\text{thf})$ [47] is depicted in Figure 14.

All of the bromine atoms are involved in the rather complex polymeric association in unsolvated PhBiBr_2 [48] (Figure 15). The polymeric chain is composed of square pyramidal PhBiBr_4 units connected through bridging bromine atoms. The structure contains folded Bi_2Br_2 rings, as well as planar

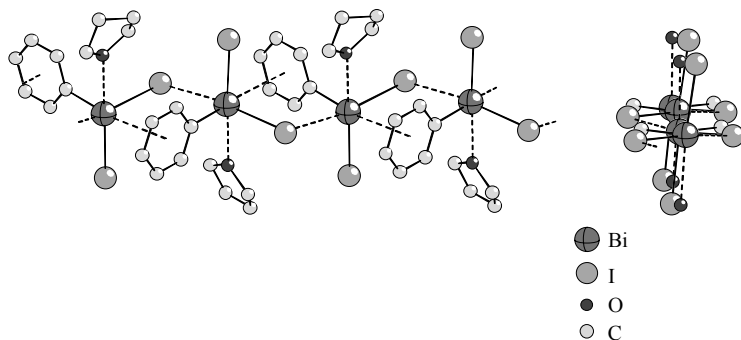


Figure 14 Chain structure of $\text{PhBiI}_2(\text{thf})$. Distances (Å) and angles ($^\circ$): Bi–I 2.883(3)–3.079(2), Bi··I 3.211(3)–3.226(2), Bi··O 2.809(16) 2.812(16), Bi··centre of C_6H_6 3.530 3.551, I–Bi··I (*trans*) 172.78(8), I–Bi–I 93.90(7)–94.85(7), Bi–I··Bi 100.33(7) 101.12(7)

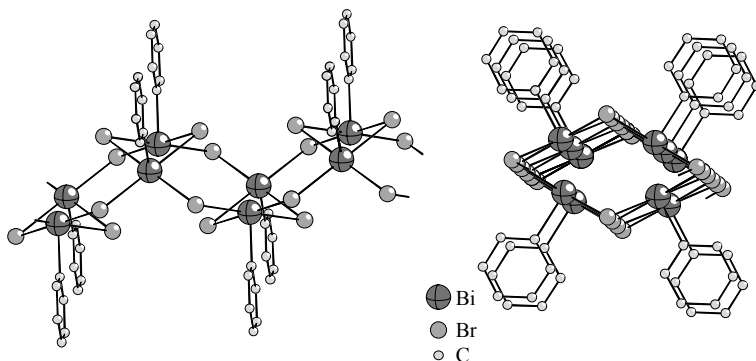


Figure 15 Molecular structure of PhBiBr_2 . Distances (Å) and angles ($^\circ$): Bi–Br 2.8802(13) 2.9251(16), Br–Bi–Br 84.49(4) 178.93(3), Bi–Br–Bi 81.83(4) 100.30(3)

Bi_4Br_4 rings, combining motifs of the architecture of both CH_3BiI_2 (see Figure 8) and CH_3BiCl_2 (see Figure 11). All of these REX_2 structures are based on REX_4 square pyramids and represent different ways of connecting these units. The resulting polymer chains and the packing of the chains result in the formation of inorganic–organic double layers in the case of the methyl compounds. In contrast, there is a tube-like arrangement in PhBiBr_2 , with the phenyl groups attached to the outer wall of the tube (see Figure 15).

A two-dimensional polymeric structure is also adopted by the association of the molecules in the isotypical crystals of phenylantimony dihalides, PhSbX_2 ($\text{X} = \text{Cl}, \text{Br}, \text{I}$) [49] (Figure 16, $\text{X} = \text{Br}$). The coordination around Sb is distorted octahedral with two intermolecular $\text{Sb}\cdots\text{X}$ contacts, with one of them *trans* to the phenyl groups, and one $\text{Sb}\cdots\text{arene}$ interaction. The PhSbX_2 molecules can easily be distinguished in the supramolecular framework. They are associated to dimers through strong secondary $\text{Sb}\cdots\text{X}$ interactions *trans* to intramolecular $\text{Sb}-\text{X}$ bonds.

The alignment of the dimeric units occurs through much weaker interactions *trans* to the $\text{Sb}-\text{C}$ bonds. The two-dimensional arrangement is established through $\text{Sb}\cdots\text{arene}$ interactions between different chains.

In crystals of ${}^t\text{BuSbCl}_2$ [36] (Figure 17), the molecules are associated to give a tube-like Sb, Cl framework which is surrounded by ${}^t\text{Bu}$ groups and terminal Cl atoms. Distorted cubes formed of four molecules can be distinguished as the basic building blocks. The antimony atoms are present in a distorted octahedral environment.

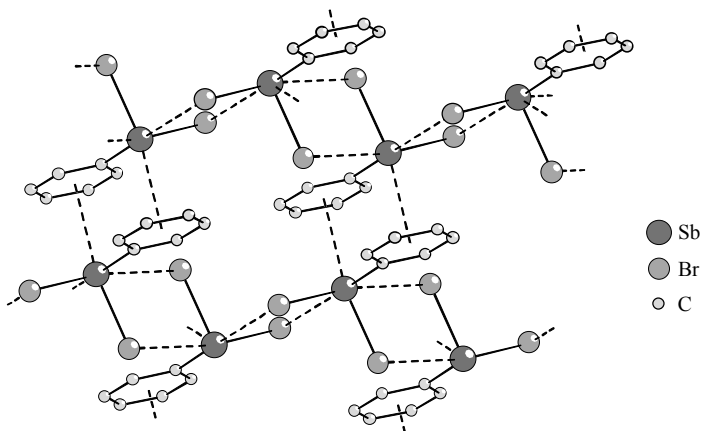


Figure 16 Molecular structure of PhSbBr_2 . Distances (Å) and angles ($^\circ$): $\text{Sb}-\text{Br}$ 2.5258(11) 2.5628(11), $\text{Sb}\cdots\text{Br}$ 3.6204(13) 4.0573(14) $\text{Sb}\cdots\text{centre of C}_6\text{H}_5$ 3.273(7), $\text{Br}-\text{Sb}\cdots\text{Br}$ 78.10(3) 166.91(4), $\text{Br}\cdots\text{Sb}\cdots\text{Br}$ 79.14(4)

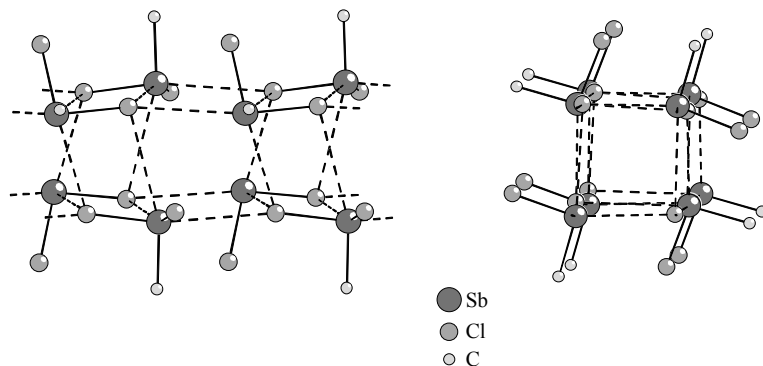


Figure 17 Molecular structure of $t\text{-BuSbCl}_2$. Distances (Å) and angles ($^\circ$): Sb–Cl 2.3878(19)–2.3731(16), Sb \cdots Cl 3.5082(16)–3.9913(16), Cl–Sb–Cl 95.40(5), Cl–Sb \cdots Cl 67.92(3)–159.26(5), Sb–Cl \cdots Sb 99.86(3)–165.40(3). The CH_3 groups are omitted for clarity

4 ORGANOMETALLIC COMPOUNDS WITH Sb–Sb OR Bi–Bi BONDS

The supramolecular architecture and the unusual colour phenomena resulting from the close intermolecular Sb \cdots Sb or Bi \cdots Bi contacts have already been reviewed several times [10–13,15] and only a few representative examples are presented here. The linear arrangement of distibines and dibismuthines has received considerable attention. A beautiful example is given by tetramethyl-distibine (Figures 2(b) and 18(a)), a red crystalline compound where almost rectilinear chains of antimony atoms with alternating short and long distances are surrounded by methyl groups [25,26]. Only very weak intermolecular Sb \cdots Sb contacts exist in the crystal structures of yellow distibines such as Ph_4Sb_2 [50] (Figure 18(b)).

The counterparts of the red distibines are the green dibismuthines, R_4Bi_2 [13,15], which are equally aligned to chains.

Three molecular compounds with *cyclo*- Sb_3 units are known where supramolecular interactions play a significant role, namely $\text{MeC}(\text{CH}_2)_3\text{Sb}_3$ [51], $\text{C}_5\text{H}_5(\text{CO})_2\text{MoSb}_3$ [52] and $\text{C}_5\text{Me}_5(\text{CO})_2\text{MoSb}_3$ [52] (Figure 19). All of these compounds are related to the Sb_4 molecule, which is stable only in the gas phase and rearranges to give grey antimony on condensation. The first steps of this process are intermolecular contacts between antimony atoms which are mimicked in the crystal structures of the *cyclo*- Sb_3 derivatives.

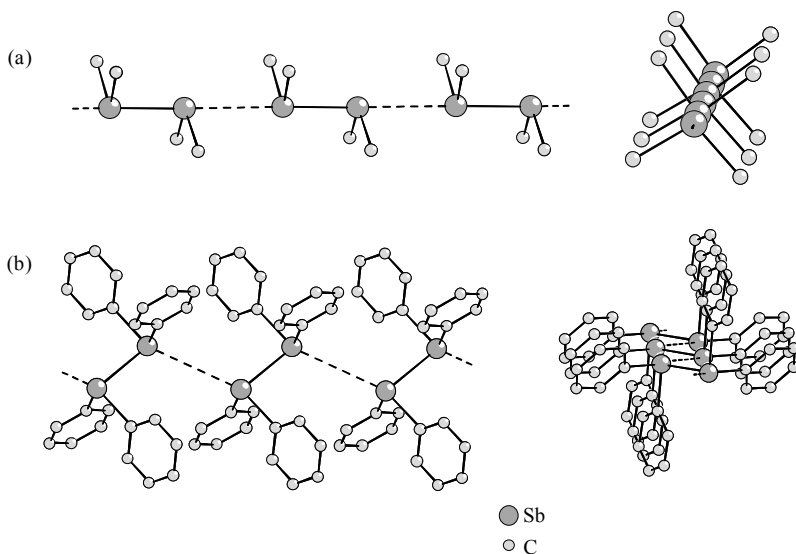


Figure 18 Chain structures of (a) Me_4Sb_2 , and (b) Ph_4Sb_2 . Distances (Å) and angles ($^\circ$): Me_4Sb_2 , $\text{Sb}-\text{Sb}$ 2.830(1); $\text{Sb} \cdots \text{Sb}$ 3.709(1); $\text{Sb}-\text{Sb} \cdots \text{Sb}$ 178.80(1); Ph_4Sb_2 , $\text{Sb}-\text{Sb}$ 2.84(3); $\text{Sb} \cdots \text{Sb}$ 4.28(3); $\text{Sb}-\text{Sb} \cdots \text{Sb}$ 108.11(1)

Monocyclic stibanes $(\text{RSb})_n$ ($n = 3-6$) are usually stabilized by bulkier organic groups, which hinder intermolecular contacts between the antimony atoms. The tetrastibetane, $\text{Mes}_4\text{Sb}_4 \cdot \text{C}_6\text{H}_6$, is the only antimony monocycle with a supramolecular chain structure [53] (Figure 20). The intermolecular contacts are of medium strength, existing between ring atoms in 1,3 positions and leading to a unique type of folded chain composed of Sb_4 units. The benzene molecules are weakly associated to one of the antimony atoms which is not involved in the chain formation.

Rather weak intermolecular $\text{Sb} \cdots \text{Sb}$ contacts exist in crystals of Sb_6 rings. Examples include the solvates of Ph_6Sb_6 [13] or six-membered tolylantimony rings [54]. These arylantimony rings crystallize as stacks of Sb_6 units surrounded by the aryl substituents and the solvate molecules. Four atoms of each ring are in bridging positions between two antimony atoms of the neighbouring molecules in the stack (3 + 2 coordination). It is instructive to compare this loose association ($\text{Sb} \cdots \text{Sb}$, 4.2 Å) with the structure of elemental antimony, which consists of layers of condensed Sb_6 rings in the chair conformation with very close contacts ($\text{Sb} \cdots \text{Sb}$, 3.36 Å) to three atoms of the neighbouring layer (3 + 3 coordination). A view of a stack of the ring molecules of $\text{Ph}_6\text{Sb}_6 \cdot \text{C}_6\text{H}_6$ is given in Figure 21. The stacking of the rings in the crystal is significant for the stability of the six-membered rings. They exist only in the crystalline state and transform to pentamers on dissolution.

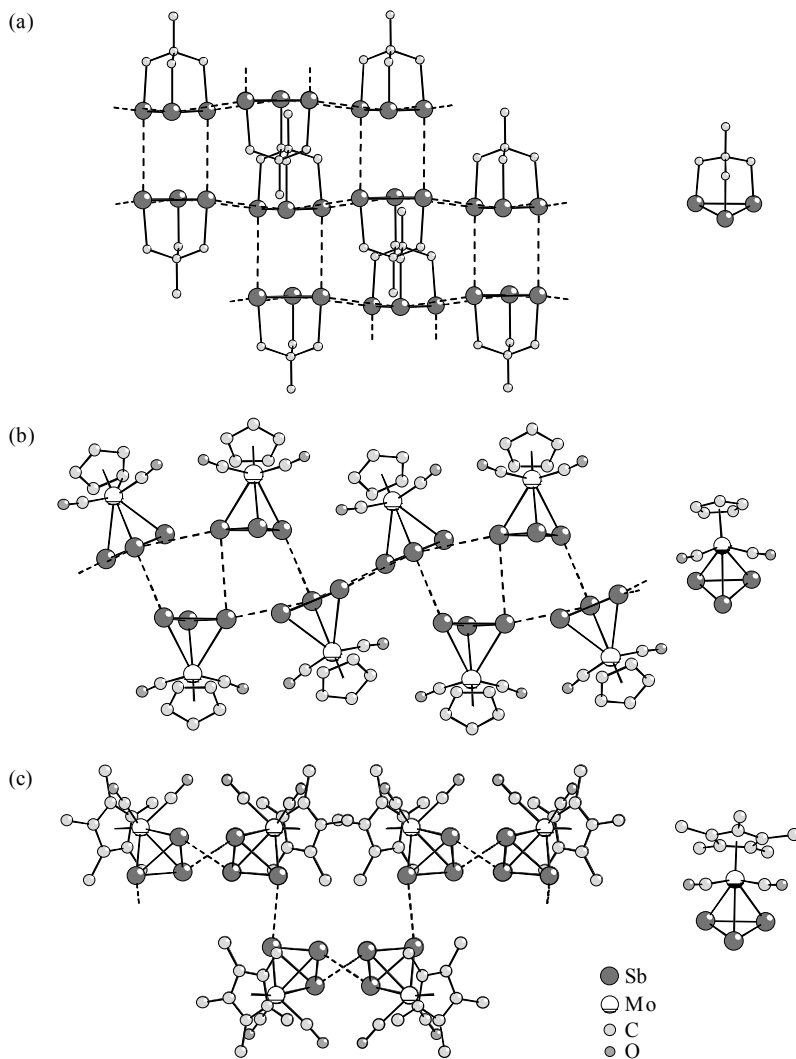


Figure 19 Molecular structures of (a) $\text{MeC}(\text{CH}_2)_3\text{Sb}_3$, (b) $\text{C}_5\text{H}_5(\text{CO})_2\text{MoSb}_3$ and (c) $\text{C}_5\text{Me}_5(\text{CO})_2\text{MoSb}_3$. Distances (Å) and angles ($^\circ$): $\text{MeC}(\text{CH}_2)_3\text{Sb}_3$, Sb–Sb 2.7955(17) 2.8173(17); Sb··Sb 3.9663(18) 4.0119(19); Sb··Sb··Sb 90.94(3) 116.887(2); $\text{C}_5\text{H}_5(\text{CO})_2\text{MoSb}_3$, Sb–Sb 2.7344(12)–2.7805(12); Sb··Sb 3.8381(12)–4.1268(13); Sb··Sb··Sb 73.09(2)–84.27(2); $\text{C}_5\text{Me}_5(\text{CO})_2\text{MoSb}_3$, Sb–Sb 2.7397(9)–2.7682(8); Sb··Sb 3.7450(9) 3.8343(9); Sb··Sb··Sb 101.73(2)–157.05(2)

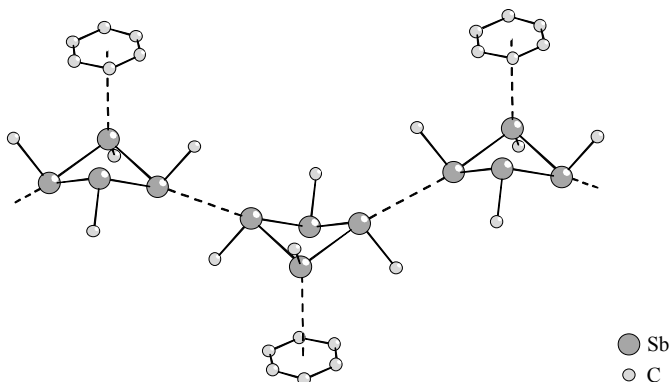


Figure 20 Molecular structure of $\text{Mes}_4\text{Sb}_4:\text{C}_6\text{H}_6$. Distances (Å) and angles ($^\circ$): Sb–Sb 2.8527(6)–2.8545(6), Sb··Sb 3.8634(7)–3.9065(7), Sb··centre of C_6H_6 3.831(14), Sb–Sb··Sb 124.93(1)–158.12(1). Only the ipso carbon atoms are shown for clarity

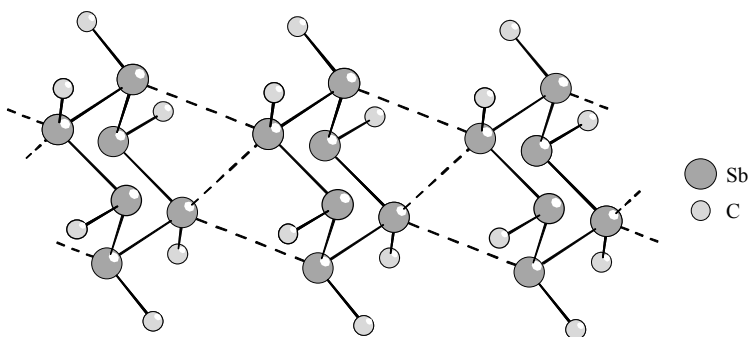


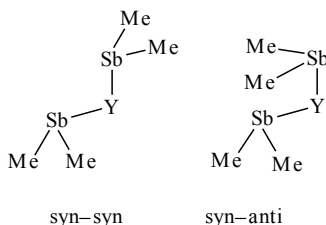
Figure 21 Chain structure of Ph_6Sb_6 1,4-dioxane. Distances (Å) and angles ($^\circ$): Sb–Sb 2.8355(11)–2.8386(10), Sb··Sb 4.2162(12)–4.2335(12), Sb–Sb··Sb 86.82(3)–93.65(3), Sb··Sb··Sb 58.64(1). Only the ipso carbon atoms are shown for clarity

5 ORGANOMETALLIC CHALCOGEN AND NITROGEN DERIVATIVES OF Sb OR Bi

Representative examples of organometallic compounds with E–chalcogen or E–N bonds (E = Sb, Bi) in supramolecular architectures comprise $(\text{Me}_2\text{Sb})_2\text{O}$ [55], $(\text{Me}_2\text{Sb})_2\text{S}$ [55], $\text{Me}_2\text{Sb–S–P(S)Me}_2$ [56], $(\text{MeSe})_3\text{Sb}$ [57], Et_2BiOPh [58], Me_2BiN_3 [59] and various other derivatives which have been included in recent reviews [3,15].

An inspection of the structures of bis(dimethylantimony)oxide and sulfide is especially instructive because these compounds have similar molecular structures. The supramolecular arrangement in the solid state is, however, essentially

different. The structures of the molecules were not only determined in the crystal under the influence of intermolecular contacts, but also in the gas phase. Theoretical calculations and electron diffraction techniques revealed that the molecules exist in the gas phase as 1:1 mixtures of two conformers, i.e. the *syn-syn* and the *syn-anti* form [60,61].



Crystals of $\text{Me}_2\text{SbOSbMe}_2$ contain molecules exclusively in a conformation close to the *syn-anti* form. The molecules are arranged to give zigzag chains (Figure 22), via weak intermolecular $\text{Sb}\cdots\text{O}$ interactions, making use, however, of only one Me_2Sb moiety. As expected from the different coordination of the two dimethylantimony fragments, the $\text{Sb}-\text{O}$ distances within a single molecule are not uniform. Whereas the bond not involved in the chain is found to be nearly as short as in the gaseous state (1.988(5) versus 1.976(14) Å [60]), the other is elongated to a length of 2.099(6) Å. Primary and secondary bond lengths and angles agree well with corresponding values found for valentinite, the orthorhombic modification of Sb_2O_3 .

Molecules of bis(dimethylantimony)sulfide adopt an approximate *syn-syn* conformation in the crystalline state, and owing to the coordination numbers (3 + 1) for the antimony atoms of both Me_2Sb groups and (2 + 2) for the sulfur atom, they build up a three-dimensional net of double helices which are linked

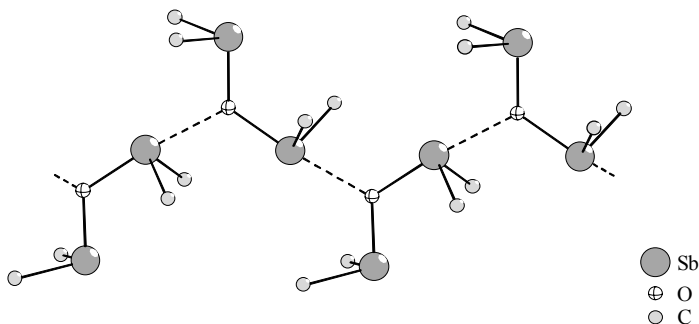


Figure 22 Chain structure of $\text{Me}_2\text{SbOSbMe}_2$. Distances (Å) and angles ($^\circ$): $\text{Sb}-\text{O}$ 1.988(1) 2.099(1), $\text{Sb}\cdots\text{O}$ 2.585(1), $\text{Sb}-\text{O}-\text{Sb}$ 123.02(1), $\text{Sb}-\text{O}\cdots\text{Sb}$ 117.75(1) 118.51(1), $\text{O}\cdots\text{Sb}-\text{O}$ 173.5(1)

together by Sb··S contacts (Figure 23). The molecular packing of $\text{Me}_2\text{SbSSbMe}_2$ is related to the structures of relevant inorganic solids, especially to that of β -quartz.

Crystals of $\text{Me}_2\text{SbS}_2\text{PMe}_2$ [56] consist of molecules which are associated to polymeric chains (Figure 24) through weak intermolecular Sb··S contacts (3.822(2) Å) to a terminal sulfur atom of a dithiophosphinato group of a neighbouring molecule. There are also intramolecular contacts with Sb··S distances of 3.158(2) Å, and a zigzag chain of the unique type $(\text{Sb}\cdots\text{S}\cdots)_x$ results.

The crystal structure of $(\text{MeSe})_3\text{Sb}$ [57] consists of molecules with trigonal pyramidal SbSe_3 units. Intermolecular Sb··Se contacts lead to a considerably distorted octahedral (3 + 3) coordination at Sb. The association of the molecules results in the formation of a two-dimensional layer structure where all

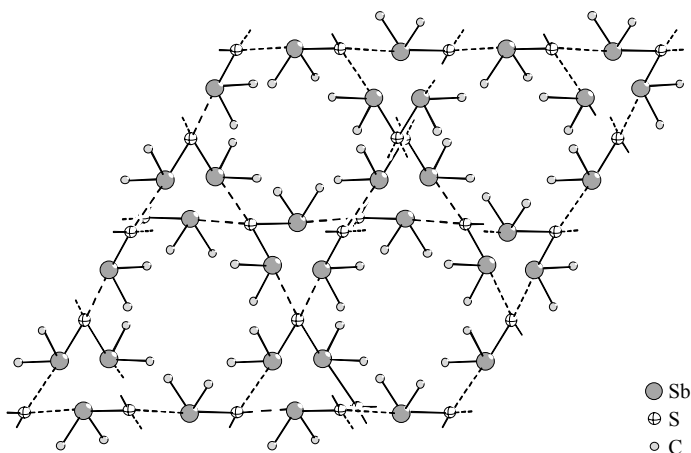


Figure 23 Molecular structure of $\text{Me}_2\text{SbSSbMe}_2$. Distances (Å) and angles ($^\circ$): Sb–S 2.498(1), Sb··S 3.164(1), Sb–S–Sb 92.35(1), Sb–S··Sb 109.90(1) 133.96(1), Sb··S··Sb 83.35(1), S–Sb··S 176.80(1)

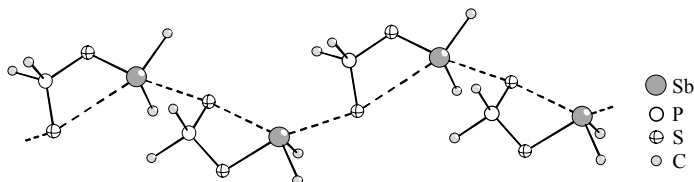


Figure 24 Chain structure of $\text{Me}_2\text{SbS}_2\text{PMe}_2$. Distances (Å) and angles ($^\circ$): Sb–S 2.555(2), Sb··S (intramolecular) 3.822(2) Sb··S (intermolecular) 3.158(2), S··Sb··S 127.80(5), Sb··S··Sb 164.49(1), S–Sb··S 60.72(1) 166.56(1)

heavier atoms are involved in the secondary bonding system and four-membered heterocycles can be distinguished (Figure 25).

A beautiful example for a helical-chain arrangement of alternating oxygen and bismuth atoms is given by Et_2BiOPh (Figure 26) [58]. The Bi–O bond lengths are homogeneous and the O–Bi–O units are very close to linearity. There are no individual molecules; Et_2Bi and PhO are in perfectly bridging positions. The chain is surrounded by the organic groups on all sides.

Crystals of Me_2BiN_3 consist of perfect zigzag chains of alternating bismuth and nitrogen atoms with bonds of equal lengths in the chain (Figure 27). Only

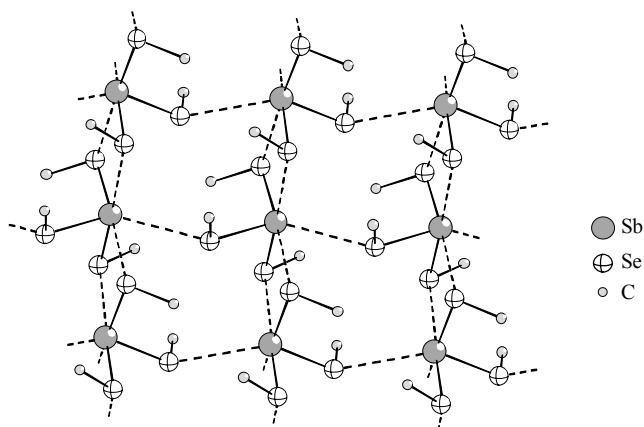


Figure 25 Molecular structure of $(\text{MeSe})_3\text{Sb}$. Distances (Å) and angles ($^\circ$): Sb–Se 2.5679(14)–2.5883(15), Sb··Se 3.6362(17)–3.6585(16), Se–Sb–Se 82.47(5)–102.10(5), Se–Sb··Se 86.39(3) 174.14(4)

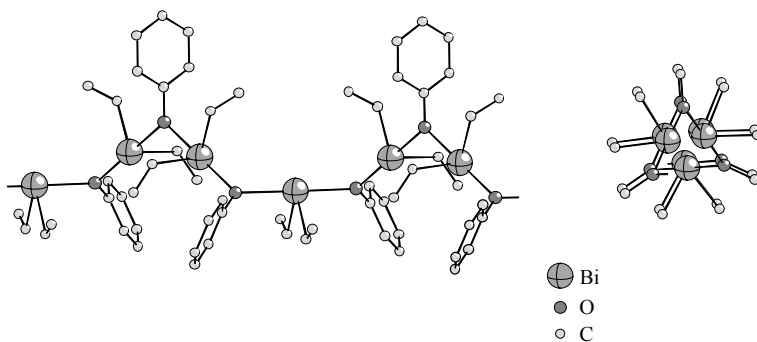


Figure 26 Chain structure of Et_2BiOPh . Distances (Å) and angles ($^\circ$): Bi–O 2.376(5), Bi–O–Bi 115.37(3), O–Bi–O 179.03(3)

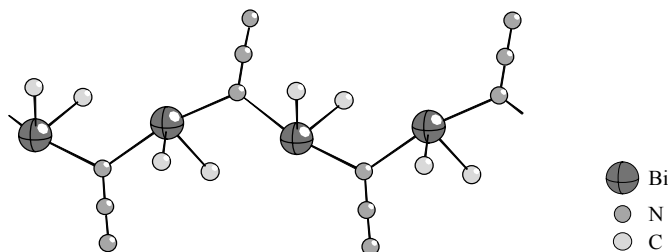


Figure 27 Chain structure of Me_2BiN_3 . Distances (Å) and angles ($^\circ$): Bi–N 2.48(6) 2.50(6), N–Bi–N 168.8(19), Bi–N–Bi 123.0(2)

the α -nitrogen atoms of the azido ligands are involved in the bridges between the bismuth atoms. The environment of Bi is distorted ψ -trigonal bipyramidal, with equatorial methyl groups and an N–Bi–N angle of 168.8(14) $^\circ$.

6 REFERENCES

1. J.-M. Lehn, *Angew. Chem.*, **100**, 91 (1988); *Angew. Chem. Int. Ed. Engl.*, **27**, 89 (1989).
2. F. Vögtle, *Supramolekulare Chemie*, Teubner, Stuttgart, 1992.
3. I. Haiduc and F. T. Edelmann, *Supramolecular Organometallic Chemistry*, Wiley-VCH, Weinheim, 1999.
4. N. Wiberg, *Holleman-Wiberg Lehrbuch der Anorganischen Chemie*, de Gruyter, Berlin, 1995.
5. N. W. Alcock, *Adv. Inorg. Radiochem.*, **15**, 1 (1972).
6. G. A. Landrum and R. Hoffmann, *Angew. Chem.*, **110**, 1989 (1998); *Angew. Chem. Int. Ed. Engl.*, **37**, 1887 (1998).
7. P. Pykkö, *Chem. Rev.*, **97**, 597 (1997).
8. A. F. Wells, *Structural Inorganic Chemistry*, Clarendon Press, Oxford, 1984.
9. S. Wang, D. B. Mitzi, G. A. Landrum, H. Genin and R. Hoffmann, *J. Am. Chem. Soc.*, **119**, 724 (1997).
10. G. Becker and O. Mundt, in *Unkonventionelle Wechselwirkungen in der Chemie metallischer Elemente*, B. Krebs (Ed.), VCH, Weinheim, 1992, pp. 199–217.
11. H. J. Breunig and S. Gülec, in *Unkonventionelle Wechselwirkungen in der Chemie metallischer Elemente*, B. Krebs (Ed.), VCH, Weinheim, 1992, pp. 218–230.
12. A. J. Ashe, *Adv. Organomet. Chem.*, **30**, 77 (1990).
13. (a) H. J. Breunig, in *The Chemistry of Organic Arsenic, Antimony and Bismuth Compounds*, S. Patai (Ed.), Wiley, Chichester, UK, 1994, pp. 441–456. (b) H. J. Breunig and R. Rösler, *Coord. Chem. Rev.*, **163**, 33 (1997).
14. H. J. Breunig, M. Denker and K. H. Ebert, in *Trends in Organometallic Chemistry*, Research Trends, Vol. 1, Trivandrum, India, 1994, pp. 323–334.
15. C. Silvestru, H. J. Breunig and H. Althaus, *Chem. Rev.*, 3277 (1999).
16. G. Becker, O. Mundt, H. Sachs, H. J. Breunig, E. Lork and J. Probst, *Z. Anorg. Allg. Chem.*, **627**, 699 (2001).
17. P. L. Millington and D. B. Sowerby, *J. Organomet. Chem.*, **480**, 227 (1994).
18. G. Alonzo, H. J. Breunig, M. Denker, K. H. Ebert and W. Offermann, *J. Organomet. Chem.*, **522**, 237 (1996).

19. H. J. Breunig, H. Althaus, R. Rösler and E. Lork, *Z. Anorg. Allg. Chem.*, **626**, 1137 (2000).
20. H. Althaus, H. J. Breunig, R. Rösler and E. Lork, *Organometallics*, **18**, 328 (1999).
21. K. H. Whitmire, D. Labahn, H. W. Roesky, M. Noltemeyer and G. M. Sheldrick, *J. Organomet. Chem.*, **402**, 55 (1991).
22. S. P. Bone and D. B. Sowerby, *J. Chem. Soc., Dalton Trans.*, 143 (1979).
23. R. Hillwig, F. Kunkel, K. Harms, B. Neumüller and K. Dehnicke, *Z. Naturforsch., B*, **52**, 149 (1997).
24. K. H. Ebert, R. E. Schulz, H. J. Breunig, C. Silvestru and I. Haiduc, *J. Organomet. Chem.*, **470**, 93 (1994).
25. A. J. Ashe, III, E. G. Ludwig, Jr, J. Oleksyszyn and J. C. Huffman, *Organometallics*, **3**, 337 (1984).
26. O. Mundt, H. Riffel, G. Becker and A. Simon, *Z. Naturforsch., B*, **39**, 317 (1984).
27. U. Behrens, H. J. Breunig, M. Denker and K. H. Ebert, *Angew. Chem.*, **106**, 1023 (1994); *Angew. Chem. Int. Ed. Engl.*, **33**, 987 (1994).
28. H. J. Breunig, M. Denker and E. Lork, *Angew. Chem.*, **108**, 1081 (1996); *Angew. Chem. Int. Ed. Engl.*, **35**, 1005 (1996).
29. M. Hall and D. B. Sowerby, *J. Organomet. Chem.*, **347**, 59 (1988).
30. F. Calderazzo, F. Marchetti, F. Ungari and M. Wieber, *Gazz. Chim. Ital.*, **121**, 93 (1991).
31. W. S. Sheldrick and C. Martin, *Z. Naturforsch., B*, **26**, 639 (1991).
32. H. J. Breunig, K. H. Ebert, S. Gülec, M. Dräger, D. B. Sowerby, M. J. Begley and U. Behrens, *J. Organomet. Chem.*, **427**, 39 (1992).
33. H. J. Breunig, M. Denker and K. H. Ebert, *J. Organomet. Chem.* **470**, 87 (1994).
34. D. B. Mitzi, *Inorg. Chem.*, **35**, 7614 (1996).
35. H. Althaus, H. J. Breunig and E. Lork, *Organometallics*, **20**, 586 (2001).
36. Y. Mourad, A. Atmani, Y. Mugnier, H. J. Breunig and K. H. Ebert, *J. Organomet. Chem.*, **476**, 47 (1994).
37. M. A. Mohammed, H. J. Breunig and K. H. Ebert, *Z. Naturforsch., B*, **51**, 149 (1996).
38. A. H. Cowley, N. C. Norman, M. Pakulski and D. L. Bricker, *J. Am. Chem. Soc.*, **107**, 8211 (1985).
39. E. V. Avtomonov, X.-W. Li and J. Lorberth, *J. Organomet. Chem.*, **530**, 71 (1997).
40. G. Becker, J. Eigner, M. Meiser, O. Mundt and J. Weidlein, *Z. Anorg. Allg. Chem.* **623**, 941 (1997).
41. H. Althaus, H. J. Breunig, R. Rösler and E. Lork, *Organometallics*, **18**, 328 (1999).
42. C. J. Carmalt, A. H. Cowley, R. D. Culp, R. A. Jones, S. Kamepalli and N. C. Norman, *Inorg. Chem.*, **36**, 2770 (1997).
43. H. J. Breunig and H. Althaus, *Phosphorus Sulfur Silicon*, **168**, 127 (2001).
44. C. J. Carmalt, A. H. Cowley, A. Decken and N. C. Norman, *Organometallics*, **17**, 1711 (1988).
45. H. J. Breunig, M. Denker and E. Lork, *Z. Anorg. Allg. Chem.*, **625**, 117 (1999).
46. W. Clegg, R. J. Errington, G. A. Fisher, R. J. Flynn and N. C. Norman, *J. Chem. Soc., Dalton Trans.*, 637 (1993).
47. W. Clegg, R. J. Errington, G. A. Fisher, D. C. R. Hockless, N. C. Norman, A. G. Orpen and S. E. Stratford, *J. Chem. Soc., Dalton Trans.*, 1967 (1992).
48. W. Clegg, M. R. J. Elsegood, R. J. Errington, G. A. Fisher and N. C. Normann, *J. Mater. Chem.*, **4**, 891 (1994).
49. O. Mundt, H. Stadelmann and H. Thurn, *Z. Anorg. Allg. Chem.*, **617**, 59 (1992).
50. K. V. Deuten and D. Rehder, *Cryst. Struct. Commun.*, **9**, 167 (1980).
51. J. Ellermann, E. Köck and H. Burzlaff, *Acta Crystallogr., Sect. C*, **41**, 1437 (1985).

52. H. J. Breunig, R. Rösler and E. Lork, *Angew. Chem.*, **109**, 2941 (1997); *Angew. Chem. Int. Ed. Engl.*, **36**, 2819 (1997).
53. M. Ates, H. J. Breunig, S. Gülec, W. Offermann, K. Häberle and M. Dräger, *Chem. Ber.*, **122**, 473 (1989).
54. H. J. Breunig, K. H. Ebert, S. Gülec and J. Probst, *Chem. Ber.*, **128**, 599 (1995).
55. H. J. Breunig, E. Lork, R. Rösler, G. Becker, O. Mundt and W. Schwarz, *Z. Anorg. Allg. Chem.*, **626**, 1595 (2000).
56. K. H. Ebert, H. J. Breunig, C. Silvestru and I. Haiduc, *Polyhedron*, **13**, 2531 (1994).
57. H. J. Breunig, S. Gülec, B. Krebs and M. Dartmann, *Z. Naturforsch., B*, **14**, 1351 (1989).
58. K. H. Whitmire, J. C. Hutchinson, A. L. McKnight and C. M. Jones, *J. Chem. Soc., Chem. Commun.*, 1021, (1992).
59. J. Müller, U. Müller, A. Loss, L. Lorberth, H. Donath and W. Massa, *Z. Naturforsch., B*, **40**, 1320 (1985).
60. A. Haaland, V. I. Sokolov, H. V. Volden, H. J. Breunig, M. Denker and R. Rösler, *Z. Naturforsch., B*, **52**, 296 (1997).
61. A. Haaland, D. J. Shorokhov, H. V. Volden, H. J. Breunig, M. Denker and R. Rösler, *Z. Naturforsch., B*, **53**, 381 (1998).

Index

- acetylenes
 - adsorbed 193–4
 - solid-state studies 197–8, **197**
 - metal complexes **180**
- actinides 121
- agostic interactions 78
- alkali metal compounds
 - alkalide anions 65
 - carbides 174, **175**
 - organolithium compounds 65–6, 66, 67
- alkaline earth compounds
 - carbides 175–6, **175**
- aluminium
 - iminoimidazolides 351, 351, 353
 - NMR properties of quadrupolar nuclei **55**
 - pentamethylcyclopentadienyl compounds 74
- antiferromagnetism 223, 224
 - antiferromagnetically coupled diradicals 268
- antimony
 - NMR properties of quadrupolar nuclei **55**
 - supramolecular interactions in organic structures 387–9
 - diorganic halides and related ionic compounds 389–93, 390, 391, 393
 - organoelement dihalides 393–400, 395, 396, 400, 401
 - organometallic chalcogen derivatives 404–8, 405, 406, 407
 - organometallic compounds with Sb–Sb bonds 401–2, 402, 403, 404
- arsenic
 - NMR properties of quadrupolar nuclei **55**
- barium carbide
 - carbon chemical shift tensors **175**
- benzene 297–9, 297
 - adsorption sites 298
 - cluster complexes
 - structure and dynamic behaviour 304–12, 304
 - synthesis 299–303
 - nucleus-independent chemical shift (NICS) 314
- beryllium
 - NMR properties of quadrupolar nuclei **55**
- bismuth
 - NMR properties of quadrupolar nuclei **56**
 - supramolecular interactions in organic structures 387–9
 - diorganic halides and related ionic compounds 389–93, 390, 392
 - organoelement dihalides 393–400, 395, 396, 397, 398, 399
 - organometallic chalcogen derivatives 404–8, 407, 408
 - organometallic compounds with Bi–Bi bonds 401–2
- Bleaney–Bowers law 234, 245, 246
- Borden's criterion 226–7
- boron
 - boron–nitrogen compounds 90–2
 - boron–oxygen compounds 99–100, 100
 - chemical shifts 92
 - complexes with transition metals 72–3, 73, 74
 - hydrides (boranes) 58–9, 59, 64, 66–8, 67
 - methyleneboranes 70
 - nido-hexaboranes 76
 - polyhedral 70, 71

- boron (*continued*)
 triferrocenylborane 68
 NMR properties of quadrupolar nuclei **55**
 structure of boron compounds 66–72, 67
- bromine
 NMR properties of quadrupolar nuclei **55**
- cadmium
 NMR properties of spin-1/2 nuclei **54**
 organometallic complexes 119–20
- caesium
 alkali anion 65
 NMR properties of quadrupolar nuclei **56**
 promoters 196
- calcium carbide
 carbon chemical shift tensors **175**
- calcium
 NMR properties of quadrupolar nuclei **55**
- carbide-containing transition metal
 carbonyl clusters 2
 $[\text{Co}_{13}(\text{C})_2(\text{CO})_{24}]^{4-}$ 3, 5, 5
 $[\text{Co}_3\text{Ni}_9(\text{C})(\text{CO})_{20}]^{3-}$ 2, 4, 4
 $[\text{Fe}_4(\text{C})(\text{CO})_{12}]^-$ 9
 redox couples 2–3
 $\text{Ru}_6(\text{C})(\text{CO})_{17}$ 7
 $[\text{Ru}_6(\text{C})(\text{CO})_{16}]^{2-}$ 5, 6, 6
 $[\text{Rh}_{12}(\text{C})_2(\text{CO})_{23}]^{4-}$ 3, 4, 4
- carbon
 carbene complexes 77
 carbenium ions 75, **75**
 carbides 79, 79
 carbocations 60, 61, 76
nido-structures 76
 carbon–nitrogen compounds 92–3
 carbyne complexes 77
 CS tensors 173, 186–8
 alkali metal carbides 174, **175**
 alkaline earth carbides 175–6, **175**
 comparison 176
 copper–olefin complexes **178–9**, 182–3
 iron–cyclopentadiene complexes **186**
 metal–1, 5-cyclooctadiene complexes **179**, 183
 metal–acetylene complexes **180**, 184–5
 metal–cyclopentadienyl complexes **187**, 188–91
 metal–olefin complexes **179–80**, 183–4
 platinum–olefin complexes **178**, 180–2, 182
 η^6 -coordinated complexes **187**
 dioxide 99
 fullerenes 74–5
 hydrogen bonding, C–H π interaction 62, 62
 monoxide 99
 NMR properties of spin-1/2 nuclei **54**
 chemical shift anisotropy (CSA) relaxation 113
 chiral derivatization agents (CDAs) 116–17
- chlorine
 NMR properties of quadrupolar nuclei **55**
- chromium
 chromium– η^6 -coordinated complexes **187**, 191, 191, 193
 cluster complexes
 $[(\text{CO})_3\text{Cr}(\eta\text{-C}_6\text{H}_6)]$ 313, 314
 $[\text{Cr}(\eta\text{-C}_6\text{H}_6)_2]$ 314
 NMR properties of quadrupolar nuclei **55**
 (RC = CR')_n-bridged ditopic polyradicals 275, 275
- cobalt
 carbonyl clusters
 $[\text{Co}_{13}(\text{C})_2(\text{CO})_{24}]^{4-}$ 3, 5, 5
 $[\text{Co}_3\text{Ni}_9(\text{C})(\text{CO})_{20}]^{3-}$ 2, 4, 4
 cluster complexes 306
 $[\{\eta\text{-C}_5\text{H}_5\text{Co}\}_3(\mu_3\text{-1, 1-diphenylethane})]$ 305, 310, **310**, 311
 $[\{\eta\text{-C}_5\text{H}_5\text{Co}\}_3(\mu_3\text{-C}_6\text{H}_6)]$ 314
 $[\{\eta\text{-C}_5\text{H}_5\text{Co}\}_3(\mu_3\text{-}m\text{-methylstyrene})]$ 310, 311
 $[\{\eta\text{-C}_5\text{H}_5\text{Co}\}_3(\mu_3\text{-}\beta\text{-methylstyrene})]$ 305, **310**
 bond length distribution 309, **310**

- facial benzene 299, 299, 300, 301
cobalttafulvene complexes 323–7, 324, 324, 325, 326, 326, 327, 328, 332–5, 333
cobaltapentalene complexes 328–31, 328, 329, 329, 331, 332–5, 332
cobalt–cyclopentadienyl complexes 187, 191
heteronuclear cobalt–nickel clusters
[Co₂Ni₁₀(C)(CO)₂₀]²⁻ 41–4, 43
[Co₃Ni₇(C)₂(CO)₁₅]³⁻ 44
[Co₃Ni₇(C)₂(CO)₁₆]²⁻ 44
[Co₃Ni₉(C)(CO)₂₀]²⁻ 41–4
[Co₆Ni₂(C)₂(CO)₁₆]²⁻ 41–4, 44
heteronuclear rhodium–cobalt clusters
[Rh₆Co(N)(CO)₁₅]²⁻ 45
homonuclear clusters
[Co₆(C)(CO)₁₃]²⁻ 27
[Co₆(C)(CO)₁₄]⁻ 23
[Co₆(C)(CO)₁₅]²⁻ 21–2, 22
[Co₆(C)(CO)₁₈]⁻ 21–2, 23
[Co₆(N)(CO)₁₅]⁻ 21–2, 22
[Co₆(P)(CO)₁₆]⁻ 21–2, 22
[Co₇(N)(CO)₁₅]²⁻ 22–4
[Co₇(N)(CO)₁₅]²⁻ 25
[Co₈(C)(CO)₁₈]²⁻ 24, 26
[Co₉(C)₂(CO)₁₉]²⁻ 27
[Co₉(P)(CO)₂₁]⁻ 24, 27
[Co₁₀(N)₂(CO)₂₉]⁴⁻ 28
[Co₁₀(P)(CO)₂₂]³⁻ 24, 27, 28
[Co₁₁(C)₂(CO)₂₂]²⁻ 27
[Co₁₃(C)₂(CO)₂₄]⁴⁻ 24–6, 28
[Co₁₃(N)₂(CO)₂₄]³⁻ 24–6, 28
[Co₁₄(N)₃(CO)₂₆]³⁻ 28
NMR properties of quadrupolar nuclei 55
organometallic complexes 114
copper
copper–acetylene complexes 180
copper–1, 5-cyclooctadiene complexes 179, 183
copper–dimethylacetylene complexes 180
copper–diphenylacetylene complexes 180
copper–olefin complexes 178–9, 182–3
copper–bis-(trimethylsilyl) acetylene complexes 180
2-iminoimidazolines 362, 362, 365
NMR properties of quadrupolar nuclei 55
organometallic complexes 118
cross-polarization (CP) NMR 170
Curie–Weiss law 231, 234, 235, 240, 246
1,5-cyclooctadiene (cod)
metal complexes 179, 183
1,3,5,7-cyclooctatetraene (cot)
metal complexes 180, 185, 186
decamethylferrocene
Mössbauer effect spectroscopy 210–11, 212
density functional theory (DFT) 170
bonding and superexchange in
C_{2n}-bridged diradicals 260, 261
redox chemistry of C_{2n}-bridged diradicals 267–8
deuterium NMR studies 149
asymmetry parameter 150
deuterium quadrupole (Q)
nucleus 149–51
Larmor frequency 154
relaxation times 155
deuterium quadrupole coupling constant (DQCC) 147, 150, 151
determination methods 151
molecular orbital calculations 153
solid-state NMR
spectroscopy 151–3, 151
spin–lattice relaxation in
solution 153–4
transition metal hydrides 154–61, 156, 158
1,3-dimethyl-2-iminoimidazoline 339, 339, 340, 341–3, 341, 342
dimethylacetylene (dma)
metal complexes 180
1,1-dimethylferrocene 208
diphenylacetylene (dpa)
metal complexes 180, 184–5
[(η²-diphos)(η⁵-C₅Me₅)Fe]⁺
mononuclear complexes 237–9
polynuclear complexes 239–40
ditopic diradicals 227–9, 228
experimental determination of magnetic interactions 229–37

- effective core potentials (ECPs) 170
- electron spin resonance (ESR)
spectroscopy 230, 231–3, 243
anisotropy 240, **241**, **243**
- enantiomeric composition of
mixtures 116–17
- ethenyloctamethylferrocene 212
- ethynyloctamethylferrocene 212
Mössbauer effect spectroscopy 214–16
- ethynyloctamethylferrocenium
hexafluorophosphate
Mössbauer effect spectroscopy 214–16
- Evan's method 230–1, 242
- exchange coupling parameter **244**
- Fermi contact term 57
- ferrocene **186**, 188–90, *189*, *190*, 191–2,
207
- ferrocenylacetonitrile 208
- ferrocenylmethanol *210*
- ferromagnetism 223, *224*
- fluorine
NMR properties of spin-1/2 nuclei **54**
NMR studies
simple compounds 104–5, *105*
transition metal fluorides 105, *106*
- fullerenes 74–5, 193, *193*
- fullerides 176–7
- gallium
NMR properties of quadrupolar
nuclei **55**
- germanium
NMR properties of quadrupolar
nuclei **55**
organogermanium compounds 86–7,
88
- gold
NMR properties of quadrupolar
nuclei **56**
- Gol'danskii–Karyagin effect
(GKE) 207–8
- hafnium
hafnium–cyclopentadienyl
complexes 193
NMR properties of quadrupolar
nuclei **56**
- Heisenberg–Dirac–van Vleck
Hamiltonian 223–5
- hexamethyl dewar benzene (hmdb)
metal complexes **180**
- homoleptic transition metal carbonyl
clusters 1
- Hund's rule 225, 256
- hydrocarbons
unusual chemical shifts 59, *60*
- hydrogen
hydrogen bonding with N, O or F 60–2
hydrogen bonding, C–H π
interaction 62, *62*
NMR properties of quadrupolar
nuclei **55**
NMR properties of spin-1/2 nuclei **54**
- hydroxymethylferrocene 208
Mössbauer effect spectroscopy 209–10,
209
- hyperconjugation 69
- iminoimidazolines 357
bonding 339–43, **342**, 343–5
coordination at metal
centres 358–62, 358, *360*, *361*,
362, *363*, *364*, *365*
alkylation and acylation 352–7
aluminium iminoimidazolides 351, *351*,
353
iminoimidazoline phosphanes 346–7,
347, *348*
bonding 348–51, *348*–9, **350**
2-iminoimidazolines
metalation and silylation 343, *343*,
344
synthesis and structure 338–9, *338*, *340*,
341
[Li₁₂O₂Cl₂(ImN)₈] 345–6, *346*
titanium iminoimidazolides 351–2, *352*,
354, *355*, *356*
bonding 352
- indium
NMR properties of quadrupolar
nuclei **55**
- interstitial atoms 1
- iodine
methyleneimidazolines 370–1, *371*, *372*,
373

- NMR properties of quadrupolar nuclei **55**
- iridium
- heteronuclear iron–iridium clusters
 - $[\text{Fe}_5\text{Ir}(\text{N})(\text{CO})_{15}]^{2-}$ 38
 - heteronuclear rhodium–iridium clusters
 - $[\text{Rh}_6\text{Ir}(\text{N})(\text{CO})_{15}]^{2-}$ 45
 - hydrides 63
 - iridium–1,5-cyclooctadiene complexes **179**
 - NMR properties of quadrupolar nuclei **56**
- iron
- $(\text{RC} = \text{CR}')_n$ -bridged ditopic polyradicals 270–1, 270
 - crystallographic data **270**
 - C_{2n} -bridged ditopic triradicals 264–5
 - crystallographic data **265**
 - chemical shift anisotropy (CSA) relaxation 113
 - diradicals with 1,3-diethynylphenyl units 281
 - diradicals with 2,5-diethynylthienyl units 280–1
 - ditopic polyradicals
 - with 1,4-diethynylphenyl units 279–80
 - heteronuclear iron–iridium clusters
 - $[\text{Fe}_5\text{Ir}(\text{N})(\text{CO})_{15}]^{2-}$ 38
 - heteronuclear iron–mercury clusters
 - $\{\mu_4\text{-Hg}[\text{Fe}_5(\text{C})(\text{CO})_{14}]_2\}^{2-}$ 39–40, **40**
 - heteronuclear iron–molybdenum clusters
 - $[\text{Fe}_3\text{Mo}_3(\text{N})(\text{CO})_{18}]^{3-}$ 36
 - heteronuclear iron–nickel clusters
 - $[\text{Fe}_6\text{Ni}_6(\text{N})_2(\text{CO})_{24}]^{2-}$ 38–9, 38, 39
 - heteronuclear iron–platinum clusters
 - $[\text{Fe}_5\text{Pt}(\text{C})(\text{CO})_{15}]^{2-}$ 39
 - heteronuclear iron–rhodium clusters
 - $[\text{FeRu}_3(\text{N})(\text{CO})_{12}]^-$ 36
 - $[\text{Fe}_3\text{Rh}_3(\text{C})(\text{CO})_{15}]^-$ 36
 - $[\text{Fe}_4\text{Rh}(\text{C})(\text{CO})_{14}]^{2-}$ 36
 - $[\text{Fe}_4\text{Rh}_2(\text{N})(\text{CO})_{15}]^-$ 36, 37
 - $[\text{Fe}_5\text{Rh}(\text{C})(\text{CO})_{16}]^-$ 36
 - $[\text{Fe}_5\text{Rh}(\text{N})(\text{CO})_{15}]^{2-}$ 36, 37
 - homonuclear clusters
 - $[\text{Fe}_4(\text{C})(\text{CO})_{12}]^-$ 9
 - $[\text{Fe}_4(\text{C})(\text{CO})_{12}]^{2-}$ 6–8, 9
 - $\text{Fe}_4(\text{C})(\text{CO})_{13}$ 6–8, 9
 - $[\text{Fe}_4(\text{N})(\text{CO})_{11}(\text{PPh}(\text{C}_5\text{H}_4\text{FeC}_5\text{H}_5)_2)]^-$ 10, **10**
 - $[\text{Fe}_4(\text{N})(\text{CO})_{12}]^-$ 6–8
 - $[\text{Fe}_4(\text{N})(\text{CO})_{13}(\text{PMe}_2\text{Ph})]^-$ **10**
 - $[\text{Fe}_4(\text{N})(\text{CO})_{13}(\text{PPh}_3)]^-$ **10**
 - $\text{Fe}_5(\text{C})(\text{CO})_{12}(\text{PMe}_2\text{Ph})_3$ **12**
 - $[\text{Fe}_5(\text{C})(\text{CO})_{14}]^{2-}$ 11–13, **11**
 - $\text{Fe}_5(\text{C})(\text{CO})_{15}$ 11–13
 - $\text{Fe}_5(\text{C})(\text{CO})_{15}$ **11**
 - $\text{Fe}_5(\text{C})(\text{CO})_{15}$ **12**
 - $[\text{Fe}_5(\text{N})(\text{CO})_{14}]^-$ 11–13, **11**, **13**
 - $[\text{Fe}_6(\text{C})(\text{CO})_{16}]^{2-}$ 13–14, **13**, **14**
 - $[\text{Fe}_6(\text{N})(\text{CO})_{15}]^{3-}$ 13–14, **13**, **14**
 - hydrides 63–4, **64**
 - iron–1,3,5,7-cyclooctatetraene complexes 185, **186**
 - iron–cyclopentadienyl complexes **186**, 188–90, **189**, **190**, 191–2
 - iron– η^6 -coordinated complexes **187**
 - magnetic interactions in cationic organoiron polyradicals 237
 - $[(\eta^2\text{-diphos})(\eta^5\text{-C}_5\text{Me}_5\text{Fe})\text{Fe}]^+$ mononuclear complexes 237–9
 - $[(\eta^2\text{-diphos})(\eta^5\text{-C}_5\text{Me}_5\text{Fe})\text{Fe}]^+$ polynuclear complexes 239–40
 - polynuclear diradicals 241–8, 250–1
 - polynuclear monoradicals 240–1
 - polynuclear triradicals 248–50, **248**
 - metal atom motion 207–8
 - baseline studies 208–16
 - decamethylferrocene 210–11, **212**
 - experimental procedure 216
 - hydroxymethylferrocene 209–10, **209**
 - nonamethylferrocene 211–14, **213**
 - nonomethylferrocenium hexafluorophosphate 214–16
 - NMR properties of spin-1/2 nuclei **54**
 - organometallic complexes 112–13, **113**
 - piano-stool complexes 237–8, **238**, **264**
 - triradicals with 1,3,5-phenylene units 285–6, **286**
- isomer shift (IS) 207
- Jonas reagent 300, 323, 323
- Lamb term 56
- lanthanides 121

- lanthanum
 methyleneimidazolines 375
 NMR properties of quadrupolar nuclei **56**
- Larmor frequency 154
- lead
 chemical shifts 80–1, 80, 85, 86, 87
 NMR properties of spin-1/2 nuclei **54**
 organolead compounds 80–3
 tetra-coordinate nuclei 84
- lithium
 amides 90, 91
 carbide
 carbon chemical shift tensors **175**
 [Li₁₂O₂Cl₂(ImN)₈] 345–6, 346
 NMR properties of quadrupolar nuclei **55**
 organolithium compounds 65–6, 66, 67
- magic-angle hopping (MAH) 173
 magic-angle spinning (MAS) NMR 170
 chemical shift tensors 173
 magic-angle turning (MAT) 173
- magnesium
 2-iminoimidazolines 358, 358, 360
 magnesium–cyclopentadienyl complexes **187**, 190
 NMR properties of quadrupolar nuclei **55**
- magnetic communication 220–3, 221, 289–90
 magnetic interactions in cationic organoiron polyradicals 237
 (η^2 -diphos)(η^5 -C₅Me₅)Fe⁺
 mononuclear complexes 237–9
 polynuclear diradicals 241–8
 polynuclear monoradicals 240–1
 polynuclear triradicals 248–50, 248, 250–1
- magnetic interactions in polyradicals
 antiferro- and ferromagnetic exchange interactions 223, 224
 ESR determination 231–3
 experimental determinations 229–37
 ground state derivation 225–7
 Heisenberg–Dirac–van Vleck Hamiltonian 223–5
 NMR determination 230–1
- solid-state susceptibility measurements 233–7
 structural changes between spin states in ditopic diradicals 227–9, 228
- structural implications 251–2
 bonding and superexchange in (RC=CR')_n-bridged diradicals 272–5, 273
 bonding and superexchange in C_{2n}-bridged diradicals 256–62, 257, 258, 259, 261
 bonding and topology-dependent superexchange in diethyl-(hetero)aryl diradicals 282–5, 283, 284
 diradicals with 1,3-diethynylphenyl units 281, 280–1
 ditopic polyradicals with 1,4-diethynylphenyl units 279–80
 hetero(aryl)-bridged diradicals 277–86
 redox chemistry of C_{2n}-bridged diradicals 266–9, 267
 redox chemistry of (RC=CR')_n-bridged diradicals 276–7, 278
 results for C_{2n}-bridged ditopic triradicals 264–6
 S/T gap in C_{2n}-bridged diradicals 262–3
 simple aryl-bridged ditopic polyradicals 278–9
 spin isomers in C_{2n}-bridged diradicals 252–6, **253**
 spin isomers in (RC=CR')_n-bridged ditopic polyradicals 270–2, **270**
 spin transitions in (RC=CR')_n-bridged diradicals 276, 277
 spin-exchange induced structural changes 287–9
 triradicals with 1,3,5-phenylene units 285–6
- manganese
 bonding and superexchange in C_{2n}-bridged diradicals 260, 261
 C_{2n}-bridged ditopic triradicals 265–6, 266
 crystallographic data **265**

- NMR properties of quadrupolar nuclei **55**
 organometallic complexes 109–11, *111*, *112*
 (RC=CR')-bridged ditopic polyradicals 270, 270
 crystallographic data **270**
 spin isomers in C_{2n}-bridged diradicals 255
 crystallographic data **253**
- Maryland convention 169
 mean-square-amplitude of vibration (MSAV) 207–8
- mercury
 heteronuclear iron–mercury clusters
 $\{\mu_4\text{-Hg}[\text{Fe}_5(\text{C})(\text{CO})_{14}]_2\}^{2-}$ 39–40, *40*
 heteronuclear osmium–mercury clusters
 $[\text{Os}_{18}\text{Hg}_2(\text{C})_2(\text{CO})_{42}]^{2-}$ 40–1
 $[\text{Os}_{18}\text{Hg}_2(\text{C})_2(\text{CO})_{42}]^{4-}$ 40–1, *42*
 $[\text{Os}_{18}\text{Hg}_3(\text{C})_2(\text{CO})_{42}]^{2-}$ 40–1, *41*, *42*
 heteronuclear ruthenium–mercury clusters
 $\{\mu_4\text{-Hg}[\text{Ru}_6(\text{C})(\text{CO})_{16}]_2\}^{2-}$ 40
 $\{\text{Hg}_3[\text{Ru}_9(\text{C})(\text{CO})_{21}]_2\}^{2-}$ 40
 hydrides 64
 NMR properties of spin-1/2 nuclei **54**
 organometallic complexes 120–1
- metallocenes 185–6
 ferrocene **186**, 188–90, *189*, *190*, 191–2, 207
- methyleneimidazolines
 bonding in Im-CS₂ and Im-CS₂²⁻ 379
 C-substituted 2-
 methyleneimidazolines 376–8, *379*
 iodine complexes 370–1, *371*, 372–3, 372, *373*
 2-methyleneimidazolines
 bonding 365–8, **374**
 reactions with main group element
 electrophiles 369–71, *371*
 synthesis and structure 362–3, *366*, **367**, 368–9
 transition metal complexes 373–6, *375*, 376, *377*
- molecular cluster complexes 297–9, *297*, 316
 electronic structure 312–14
 reactivity 314
 structure and dynamic behaviour 304–12, *304*
 activation parameters for arene rotation **311**
 bond length distribution *309*, **310**
 synthesis 299–303
 molecular wires 222
- molybdenum
 heteronuclear iron–molybdenum clusters
 $[\text{Fe}_3\text{Mo}_3(\text{N})(\text{CO})_{18}]^{3-}$ 36
 methyleneimidazolines 373, *375*
 molybdenum–cyclopentadienyl complexes **187**, 190
 molybdenum–η⁶-coordinated complexes 193
 NMR properties of quadrupolar nuclei **55**
 organometallic complexes 107
 triradicals with 1,3,5-phenylene units 286, *286*
- Mössbauer effect spectroscopy 207–8, 237–8, **238**, **242**
 baseline studies 208
 decamethylferrocene 210–11, *212*
 ethynyloctamethylferrocene and ethynyloctamethylferrocenium
 hexafluorophosphate 214–16
 hydroxymethylferrocene 209–10, **209**
 nonamethylferrocene and nonomethylferrocenium
 hexafluorophosphate 211–14, *213*
 experimental procedures 216
- neodymium
 methyleneimidazolines 375, *376*
- nickel
 carbonyl clusters
 $[\text{Co}_3\text{Ni}_9(\text{C})(\text{CO})_{20}]^{3-}$ 2, 4, *4*
 heteronuclear cobalt–nickel clusters
 $[\text{Co}_2\text{Ni}_{10}(\text{C})(\text{CO})_{20}]^{2-}$ 41–4, *43*
 $[\text{Co}_3\text{Ni}_7(\text{C})_2(\text{CO})_{15}]^{3-}$ 44
 $[\text{Co}_3\text{Ni}_7(\text{C})_2(\text{CO})_{16}]^{2-}$ 44
 $[\text{Co}_3\text{Ni}_9(\text{C})(\text{CO})_{20}]^{2-}$ 41–4
 $[\text{Co}_6\text{Ni}_2(\text{C})_2(\text{CO})_{16}]^{2-}$ 41–4, *44*
 heteronuclear iron–nickel clusters
 $[\text{Fe}_6\text{Ni}_6(\text{N})_2(\text{CO})_{24}]^{2-}$ 38–9, 38, *39*

nickel (*continued*)

homonuclear clusters

- $[\text{Ni}_7(\text{C})(\text{CO})_{12}]^{2-}$ 34
- $[\text{Ni}_8(\text{C})(\text{CO})_{16}]^{2-}$ 34
- $[\text{Ni}_9(\text{C})(\text{CO})_{17}]^{2-}$ 32, 32
- $[\text{Ni}_{10}(\text{C}_2)(\text{CO})_{16}]^{2-}$ 34
- $[\text{Ni}_{11}(\text{C}_2)(\text{CO})_{15}]^{4-}$ 34
- $[\text{Ni}_{12}(\text{C}_2)(\text{CO})_{16}]^{4-}$ 34
- $[\text{Ni}_{16}(\text{C})_4(\text{CO})_{23}]^{4-}$ 34
- $[\text{Ni}_{32}(\text{C})_6(\text{CO})_{36}]^{6-}$ 32–4, 33
- $[\text{Ni}_{38}(\text{C})_6(\text{CO})_{42}]^{6-}$ 34, 35
- $[\text{Ni}_{38}(\text{H})(\text{C})_6(\text{CO})_{42}]^{6-}$ 34, 34

NMR properties of quadrupolar nuclei **55**

niobium

hydrides

- niobocene silyl hydrides 64, 64

NMR properties of quadrupolar nuclei **55**

nitrogen

chemical shifts 89, 92

NMR properties of quadrupolar nuclei **55**NMR properties of spin-1/2 nuclei **54**

NMR studies 87–9

- boron–nitrogen compounds 90–2
- carbon–nitrogen compounds 92–3
- lithium amides 90, 91
- simple compounds 89–90
- transition metal–nitrogen compounds 93–4

nonamethylferrocene

- Mössbauer effect spectroscopy 211–14, 213

nonomethylferrocenium

hexafluorophosphate

- Mössbauer effect spectroscopy 211–14

norbornadiene (nbd)

metal complexes **179–80**

nuclear magnetic resonance (NMR)

spectroscopy 51–3, 121–2

acoustic ringing 113

adsorbed acetylenes 193–4

solid-state studies 197–8

adsorbed olefins 193–4

solid-state studies 194–7, **195**adsorbed η -coordinated organometallics 198

alkali metal compounds

- alkalide anions 65
- organolithium compounds 65–6, 66, 67

aluminium compounds

- pentamethylcyclopentadienyl compounds 74

boron compounds

- structure of boron compounds 66–72, 67

transition metal–boron

- complexes 72–3, 73, 74

chemical shift (CS) tensor

- nuclear magnetic shielding and chemical shift 167–8

principal axis system (PAS) 167

Ramsey theory 168

chemical shifts (δX) 54–7

boron 92

carbenium ions **75**

lead 80, 85, 86, 87

nitrogen 89, 92, 93

phosphorus 96

tin 80, 85, 86, 87

coupling constants ${}^nJ(\text{A},\text{X})$ 57–8

deuterium studies 149–51, 161–2

experimental techniques 170–1

- chemical shift (CS) tensor for isolated spin-1/2 nucleus 171, 172

chemical shift (CS) tensors MAS spectra 173

cross-polarization (CP) 170

dipolar chemical shift method 171–3, 173

magic-angle spinning (MAS) 170

sample size 174

fluorine compounds

simple compounds 104–5, 105

transition metal fluorides 105

group 14 element chemistry

- carbon atoms in unusual surroundings 74–9

organosilicon, -germanium, -tin, -lead compounds 79–87

hydrides 58, 145–7

applications 147–9

boron (boranes) 58–9, 59

carbocations 60, 61

- hydrocarbons, unusual chemical shifts 59, 60
 - hydrogen bonding with N, O or F 60–2
 - hydrogen bonding, C–H π interaction 62, 62
 - transition metals 62–4
 - lanthanides and actinides 121
 - ligand nuclei in organometallic compounds 165–6, 198
 - ligand–metal bonding 166–7, 167
 - magic-angle hopping (MAH) 173
 - magic-angle turning (MAT) 173
 - magnetic interactions in polyradicals 230–1
 - magnetic shielding tensors 169–70
 - density functional theory (DFT) 170
 - effective core potentials (ECPs) 170
 - metal carbides 174
 - carbon CS tensors for alkali metal carbides 174
 - carbon CS tensors for alkaline earth metal carbides 175–6
 - comparison of CS tensors 176
 - fullerides 176–7
 - metallocenes 185–6
 - carbon CS tensors 186–91
 - other solid-state studies 191–3
 - metal–olefin and metal–acetylene complexes 177
 - carbon-13 studies 178–85, **178–80**
 - solid-state studies of internal dynamics 185
 - Zeise's anion 177, 177
 - nitrogen compounds 87–9
 - boron–nitrogen compounds 90–2
 - carbon–nitrogen compounds 92–3
 - lithium amides 90
 - simple compounds 89–90
 - transition metal–nitrogen compounds 93–4
 - notation 168–9
 - Nucleus-Independent Chemical Shift (NICS) 59
 - organotransition metal complexes 106–7
 - cadmium 119–20
 - cobalt 114
 - copper 118
 - iron 112–13, 113
 - manganese 109–11, 111, 112
 - mercury 120–1
 - molybdenum 107
 - osmium 114
 - platinum 115–18, 117, 118, 119
 - rhodium 114, 115, 116
 - ruthenium 113
 - silver 118–19, 120
 - technetium 111
 - tungsten 108–9, 110
 - vanadium 107, 108, 109
 - oxygen compounds
 - boron–oxygen compounds 99–100, 100
 - simple compounds 98–100
 - transition metal carbonyl compounds 99, 100
 - transition metal complexes 101
 - para*-hydrogen induced polarization (PHIP) 64
 - phosphorus compounds 94–8
 - properties of quadrupolar nuclei **55–6**
 - properties of spin-1/2 nuclei **54**
 - screening constant $\sigma(X)$ 56
 - selenium compounds 101–3, 104
 - tellurium compounds 101–3
 - tin compound mixture 52
 - xenon 105–6
- nucleus-independent chemical shift (NICS) 313, 314
- octamethylferrocene (OMF) 212
- olefins
 - adsorbed 193–4
 - solid-state studies 194–7, **195**
 - metal–olefin complexes
 - copper **178–9**, 182–3, 183
 - iridium **179**
 - platinum **178, 179**
 - platinum 180–2, 181, 182, 183
 - rhodium **179**
 - silver **179, 183**
- osmium
 - cluster complexes
 - $[(CO)_3Os]_3(\mu_3-C_6H_6)$ **310**, 313, 314, 315

- osmium (*continued*)
 $[\text{Os}_3(\text{CO})_7(\text{NCMe})(\text{C}_2\text{H}_4)(\mu_3\text{-C}_6\text{H}_6)]$
 312, 312
 $[\text{Os}_6(\text{CO})_{11}(\mu\text{-H})_2(\eta\text{-C}_6\text{H}_6)$
 $(\mu_3\text{-C}_6\text{H}_6)]$ **310**
 facial benzene 299, 299, 302–3, 302,
 303
 heteronuclear osmium–mercury clusters
 $[\text{Os}_{18}\text{Hg}_2(\text{C})_2(\text{CO})_{42}]^{2-}$ 40–1
 $[\text{Os}_{18}\text{Hg}_2(\text{C})_2(\text{CO})_{42}]^{4-}$ 40–1, 42
 $[\text{Os}_{18}\text{Hg}_3(\text{C})_2(\text{CO})_{42}]^{2-}$ 40–1, 41, 42
 homonuclear clusters
 $[\text{Os}_4(\text{N})(\text{CO})_{12}]^-$ 20
 $[\text{Os}_5(\text{C})(\text{CO})_{14}]^{2-}$ 18, 18
 $\text{Os}_5(\text{C})(\text{CO})_{15}$ 18, 18
 $\text{Os}_5(\text{C})(\text{CO})_{16}$ 20
 $[\text{Os}_6(\text{P})(\text{CO})_{18}]^-$ 18–19, 19
 $[\text{Os}_{10}(\text{C})(\text{CO})_{24}]^{2-}$ 19–20, 19, 20
 $[\text{Os}_{10}(\text{H})_4(\text{CO})_{24}]^{2-}$ 20, 21
 NMR properties of spin-1/2 nuclei **54**
 organometallic complexes 114
 Ovchinnikov rule 226–7, 288–9
 Overhauser effect 52
 oxygen
 NMR properties of quadrupolar
 nuclei **55**
 NMR studies
 boron–oxygen compounds 99–100,
 100
 simple compounds 98–100
 transition metal carbonyl
 compounds 99, 100
 transition metal complexes 101
 ozone 99
 palladium
 bifluoride complex 63
 2-iminoimidazolines 359–60, 360, 361,
 363
 phosphorus
 chemical shifts 96
 NMR properties of spin-1/2 nuclei **54**
 NMR studies 94–8
 piano-stool complexes 237–8, 238,
 264
 platinum
 bifluoride complex 63
 cluster complexes
 $[\text{Ru}_6\text{Pt}_3(\text{CO})_{18}(\mu_3\text{C}_6\text{H}_5(\text{CH}_2)_2\text{Ph})$
 $(\mu_3\text{-H})_4]$ 307, **310**, 312
 facial benzene 303, 304
 heteronuclear iron–platinum clusters
 $[\text{Fe}_5\text{Pt}(\text{C})(\text{CO})_{15}]^{2-}$ 39
 heteronuclear rhodium–platinum
 clusters
 $[\text{Rh}_{10}\text{Pt}(\text{N})(\text{CO})_{21}]^{3-}$ 44
 heteronuclear ruthenium–platinum
 clusters
 $\text{PtRu}_5(\text{C})(\text{CO})_{16}$ 40
 NMR properties of spin-1/2 nuclei **54**
 organometallic complexes 115–18, 117,
 118, 119
 platinum–1,5-cyclooctadiene
 complexes **179**, 183
 platinum–diphenylacetylene
 complexes **180**, 184–5
 platinum–norbornadiene
 complexes **179–80**
 platinum–olefin complexes **178**, 180–2,
 181, 182
 potassium
 alkali anion 65
 carbide
 carbon chemical shift tensors **175**
 2-iminoimidazolines 359
 NMR properties of quadrupolar
 nuclei **55**
 principal axis system (PAS) 167
 quadrupole splitting (QS) 207
 Ramsey theory 168
 rhenium
 homonuclear clusters
 $[\text{Re}_6(\text{C})(\text{CO})_{19}]^{2-}$ 36
 $[\text{Re}_7(\text{C})(\text{CO})_{21}]^{3-}$ 35–6, 35
 $[\text{Re}_8(\text{C})(\text{CO})_{24}]^{2-}$ 35–6, 35
 NMR properties of quadrupolar
 nuclei **56**
 spin isomers in C₂n-bridged diradicals
 crystallographic data **253**
 rhodium
 carbonyl clusters
 $[\text{Rh}_{12}(\text{C})_2(\text{CO})_{23}]^{4-}$ 3, 4, 4
 cluster complexes
 $[(\eta\text{-C}_5\text{H}_5)\text{Rh}]_3(\mu_3\text{-C}_6\text{H}_6)]$ **310**

- $[(\eta\text{-C}_5\text{Me}_5)\text{Rh}]_3(\mu_2\text{-H})_3(\mu_3\text{-C}_6\text{H}_6)]$ 308, **310**
 $[(\eta\text{-C}_5\text{Me}_5)\text{Rh}]_3(\mu_2\text{-H})_3(\mu_3\text{-C}_6\text{H}_6)]^{2+}$ 309, **310**
 facial benzene 299–300, 300, 301
 heteronuclear iron–rhodium clusters
 $[\text{Fe}_3\text{Rh}_3(\text{C})(\text{CO})_{15}]^-$ 36
 $[\text{Fe}_4\text{Rh}(\text{C})(\text{CO})_{14}]^{2-}$ 36
 $[\text{Fe}_4\text{Rh}_2(\text{N})(\text{CO})_{15}]^-$ 36, 37
 $[\text{Fe}_5\text{Rh}(\text{C})(\text{CO})_{16}]^-$ 36
 $[\text{Fe}_5\text{Rh}(\text{N})(\text{CO})_{15}]^{2-}$ 36, 37
 heteronuclear rhodium–cobalt clusters
 $[\text{Rh}_6\text{Co}(\text{N})(\text{CO})_{15}]^{2-}$ 45
 heteronuclear rhodium–iridium clusters
 $[\text{Rh}_6\text{Ir}(\text{N})(\text{CO})_{15}]^{2-}$ 45
 heteronuclear rhodium–platinum clusters
 $[\text{Rh}_{10}\text{Pt}(\text{N})(\text{CO})_{21}]^{3-}$ 44
 heteronuclear rhodium–silver clusters
 $\{\text{Ag}[\text{Rh}_6(\text{C})(\text{CO})_{15}]_2\}^{3-}$ 45
 homonuclear clusters
 $[\text{Rh}_6(\text{C})(\text{CO})_{13}]^{2-}$ 31
 $[\text{Rh}_6(\text{C})(\text{CO})_{15}]^{2-}$ 29–30, 29
 $[\text{Rh}_6(\text{N})(\text{CO})_{15}]^-$ 29–30, 29
 $[\text{Rh}_7(\text{N})(\text{CO})_{15}]^{2-}$ 30, 30
 $\text{Rh}_8(\text{C})(\text{CO})_{19}$ 31
 $[\text{Rh}_9(\text{P})(\text{CO})_{21}]^{2-}$ 32
 $[\text{Rh}_{10}(\text{P})(\text{CO})_{22}]^{3-}$ 32
 $[\text{Rh}_{12}(\text{C})_2(\text{CO})_{24}]^{2-}$ 30–1
 $\text{Rh}_{12}(\text{C})_2(\text{CO})_{25}$ 32
 $[\text{Rh}_{12}(\text{N})_2(\text{H})(\text{CO})_{23}]^{3-}$ 32
 $[\text{Rh}_{14}(\text{C})_2(\text{CO})_{33}]^{2-}$ 32
 $[\text{Rh}_{14}(\text{N})_2(\text{CO})_{25}]^{2-}$ 32
 $[\text{Rh}_{15}(\text{C})_2(\text{CO})_{28}]^{2-}$ 32
 $[\text{Rh}_{23}(\text{N})_4(\text{CO})_{38}]^{3-}$ 32
 $[\text{Rh}_{28}(\text{N})_4(\text{H})_2(\text{CO})_{41}]^{4-}$ 32
 2-iminoimidazolines 360, 361, 364
 metallaquinone 77, 77
 NMR properties of spin-1/2 nuclei **54**
 organometallic complexes 114, 115, 116
 rhodium–1,5-cyclooctadiene complexes **179**
 rhodium–1,3,5,7-cyclooctatetraene complexes **180**
 rhodium–hexamethyl dewar benzene complexes **180**
 rhodium–norbornadiene complexes **179**
- rubidium
 alkali anion 65
 NMR properties of quadrupolar nuclei **55**
- ruthenium
 $(\text{RC}=\text{CR}')_n$ -bridged ditopic polyradicals 272, 272, 275, 275
 C_{2n} -bridged ditopic triradicals 266, 266
 carbonyl clusters
 $(\text{Ru}_6(\text{C})(\text{CO})_{16})(\text{PPh}_2\text{Et})$ 8
 $[\text{Ru}_6(\text{C})(\text{CO})_{16}]^{2-}$ 5, 6
 $\text{Ru}_6(\text{C})(\text{CO})_{17}$ 7
 $[\text{Ru}_6(\text{C})(\text{CO})_{18}]^{2-}$ 7
 cluster complexes 304
 $\{[(\text{CO})_3\text{Ru}]_3(\mu_3\text{-C}_6\text{H}_6)\}$ **310**
 $[\text{Ru}_5\text{C}(\text{CO})_{12}(\mu_3\text{-C}_6\text{H}_6)]$ 306, **310**
 $[\text{Ru}_6\text{C}(\text{CO})_{11}(\eta\text{-C}_6\text{H}_5\text{Me})(\mu_3\text{-C}_6\text{H}_5\text{Me})]$ 311, 312
 $[\text{Ru}_6\text{C}(\text{CO})_{11}(\eta\text{-C}_6\text{H}_6)(\mu_3\text{-C}_6\text{H}_6)]$ **310**
 $[\text{Ru}_6\text{Pt}_3(\text{CO})_{18}(\mu_3\text{-C}_6\text{H}_5(\text{CH}_2)_2\text{Ph})(\mu_3\text{-H})_4]$ 307, **310**, 312
 facial benzene 299, 299, 302–3, 302, 303, 304
 heteronuclear iron–ruthenium clusters
 $[\text{FeRu}_3(\text{N})(\text{CO})_{12}]^-$ 36
 heteronuclear ruthenium–mercury clusters
 $\{\text{Hg}_3[\text{Ru}_9(\text{C})(\text{CO})_{21}]_2\}^{2-}$ 40
 $\{\mu_4\text{-Hg}[\text{Ru}_6(\text{C})(\text{CO})_{16}]_2\}^{2-}$ 40
 heteronuclear ruthenium–platinum clusters
 $\text{PtRu}_5(\text{C})(\text{CO})_{16}$ 40
 homonuclear clusters
 $[\text{Ru}_4(\text{N})(\text{CO})_{12}]^-$ 18
 $\text{Ru}_5(\text{C})(\text{CO})_{15}$ 15, 15
 $[\text{Ru}_5(\text{N})(\text{CO})_{14}]^-$ 15, 15
 $[\text{Ru}_6(\text{C})(\text{CO})_{16}]^{2-}$ 18
 $\text{Ru}_6(\text{C})(\text{CO})_{17}$ 18
 $[\text{Ru}_8(\text{P})(\text{CO})_{22}]^-$ 15–16, 16
 $[\text{Ru}_{10}(\text{C})(\text{CO})_{24}]^{2-}$ 16–17, 17
 $[\text{Ru}_{10}(\text{C})_2(\text{CO})_{24}]^{2-}$ 18
 $[\text{Ru}_{10}(\text{N})(\text{CO})_{24}]^-$ 18
 hydrides 63
 NMR properties of quadrupolar nuclei **55**
 organometallic complexes 113

- ruthenium (*continued*)
 ruthenium–cyclopentadienyl complexes **187**, 190
 spin isomers in C_{2n} -bridged diradicals 254
 crystallographic data **253**
 spin-exchange induced structural changes 287, 287
- scandium
 NMR properties of quadrupolar nuclei **55**
- selenium
 NMR properties of spin-1/2 nuclei **54**
 NMR studies 101–3, 104
- semiconducting quantum interface device (SQUID) susceptometry 233–7
- semi-interstitial atoms 1
- silicon
 NMR properties of spin-1/2 nuclei **54**
 organosilicon compounds 79–80, 83–4, 85
- silver
 heteronuclear rhodium–silver clusters $\{Ag[Rh_6(C)(CO)_{15}]_2\}^{3-}$ 45
 NMR properties of spin-1/2 nuclei **54**
 organometallic complexes 118–19, 120
 silver–1,5-cyclooctadiene complexes **179**, 183
- singlet–triplet (S/T) energy gap 229–30, 231, 234, 242
 magnitude in C_{2n} -bridged diradicals 262–3
- singly occupied molecular orbitals (SOMOs) 223, 226, 282–4
 bonding and superexchange in C_{2n} -bridged diradicals 256–62, 257, 258, 259, 261
- sodium
 alkali anion 65
 carbide
 carbon chemical shift tensors **175**
 NMR properties of quadrupolar nuclei **55**
- spin-echo double resonance (SEDOR) 196
- strontium carbide
 carbon chemical shift tensors **175**
- sulphur
 NMR properties of quadrupolar nuclei **55**
- tantalum
 agostic interactions 78
 bonding and superexchange in C_{2n} -bridged diradicals 260, 261
 NMR properties of quadrupolar nuclei **56**
 spin isomers in C_{2n} -bridged diradicals 252
 crystallographic data **253**
- technetium
 NMR properties of quadrupolar nuclei **55**
 organometallic complexes 111
- tellurium
 NMR properties of spin-1/2 nuclei **54**
 NMR studies 101–3
 temperature-independent paramagnetism (TIP) 234–5, 236–7
 1,1,4,4-tetraphenylbutatriene 268, 269, 269
- thallium
 NMR properties of spin-1/2 nuclei **54**
- tin
 chemical shifts 80–1, 80, 85, 86, 87
 methyleneimidazolines 370, 371
 NMR properties of spin-1/2 nuclei **54**
 organotin compounds 80–3
 tetra-coordinate nuclei 84
 tin–nitrogen heterocubane 82
- titanium
 borane complexes 72–3
 complexes with catalytic activity 78–9
 iminoimidazolides 351–2, 352, 354, 355, 356
 bonding 352
 NMR properties of quadrupolar nuclei **55**
 spin isomers in C_{2n} -bridged diradicals 252, 253
 crystallographic data **253**
 titanium–cyclopentadienyl complexes **187**, 190, 192
- transition metal carbonyl clusters 1, 2–6
 heteronuclear cobalt–nickel clusters

- $[\text{Co}_2\text{Ni}_{10}(\text{C})(\text{CO})_{20}]^{2-}$ 41–4, 43
 $[\text{Co}_3\text{Ni}_7(\text{C})_2(\text{CO})_{15}]^{3-}$ 44
 $[\text{Co}_3\text{Ni}_7(\text{C})_2(\text{CO})_{16}]^{2-}$ 44
 $[\text{Co}_3\text{Ni}_9(\text{C})(\text{CO})_{20}]^{2-}$ 41–4
 $[\text{Co}_6\text{Ni}_2(\text{C})_2(\text{CO})_{16}]^{2-}$ 41–4, 44
 heteronuclear iron–iridium clusters
 $[\text{Fe}_5\text{Ir}(\text{N})(\text{CO})_{15}]^{2-}$ 38
 heteronuclear iron–mercury clusters
 $\{\mu_4\text{-Hg}[\text{Fe}_5(\text{C})(\text{CO})_{14}]_2\}^{2-}$ 39–40, 40
 heteronuclear iron–molybdenum clusters
 $[\text{Fe}_3\text{Mo}_3(\text{N})(\text{CO})_{18}]^{3-}$ 36
 heteronuclear iron–nickel clusters
 $[\text{Fe}_6\text{Ni}_6(\text{N})_2(\text{CO})_{24}]^{2-}$ 38–9, 38, 39
 heteronuclear iron–platinum clusters
 $[\text{Fe}_5\text{Pt}(\text{C})(\text{CO})_{15}]^{2-}$ 39
 heteronuclear iron–rhodium clusters
 $[\text{Fe}_3\text{Rh}_3(\text{C})(\text{CO})_{15}]^{3-}$ 36
 $[\text{Fe}_4\text{Rh}(\text{C})(\text{CO})_{14}]^{2-}$ 36
 $[\text{Fe}_4\text{Rh}_2(\text{N})(\text{CO})_{15}]^{3-}$ 36, 37
 $[\text{Fe}_5\text{Rh}(\text{C})(\text{CO})_{16}]^{3-}$ 36
 $[\text{Fe}_5\text{Rh}(\text{N})(\text{CO})_{15}]^{2-}$ 36, 37
 heteronuclear iron–ruthenium clusters
 $[\text{FeRu}_3(\text{N})(\text{CO})_{12}]^{3-}$ 36
 heteronuclear osmium–mercury clusters
 $[\text{Os}_{18}\text{Hg}_2(\text{C})_2(\text{CO})_{42}]^{2-}$ 40–1
 $[\text{Os}_{18}\text{Hg}_2(\text{C})_2(\text{CO})_{42}]^{4-}$ 40–1, 42
 $[\text{Os}_{18}\text{Hg}_3(\text{C})_2(\text{CO})_{42}]^{2-}$ 40–1, 41, 42
 heteronuclear rhodium–cobalt clusters
 $[\text{Rh}_6\text{Co}(\text{N})(\text{CO})_{15}]^{2-}$ 45
 heteronuclear rhodium–iridium clusters
 $[\text{Rh}_6\text{Ir}(\text{N})(\text{CO})_{15}]^{2-}$ 45
 heteronuclear rhodium–platinum clusters
 $[\text{Rh}_{10}\text{Pt}(\text{N})(\text{CO})_{21}]^{3-}$ 44
 heteronuclear rhodium–silver clusters
 $\{\text{Ag}[\text{Rh}_6(\text{C})(\text{CO})_{15}]_2\}^{3-}$ 45
 heteronuclear ruthenium–mercury clusters
 $\{\text{Hg}_3[\text{Ru}_9(\text{C})(\text{CO})_{21}]_2\}^{2-}$ 40
 $\{\mu_4\text{-Hg}[\text{Ru}_6(\text{C})(\text{CO})_{16}]_2\}^{2-}$ 40
 heteronuclear ruthenium–platinum clusters
 $\text{PtRu}_5(\text{C})(\text{CO})_{16}$ 40
 homonuclear cobalt clusters
 $[\text{Co}_6(\text{C})(\text{CO})_{13}]^{2-}$ 27
 $[\text{Co}_6(\text{C})(\text{CO})_{14}]^{3-}$ 23
 $[\text{Co}_6(\text{C})(\text{CO})_{15}]^{2-}$ 21–2, 22
 $[\text{Co}_6(\text{C})_2(\text{CO})_{18}]$ 21–2, 23
 $[\text{Co}_6(\text{N})(\text{CO})_{15}]^{3-}$ 21–2, 22
 $[\text{Co}_6(\text{P})(\text{CO})_{16}]^{3-}$ 21–2, 22
 $[\text{Co}_7(\text{N})(\text{CO})_{15}]^{2-}$ 22–4, 25
 $[\text{Co}_8(\text{C})(\text{CO})_{18}]^{2-}$ 24, 26
 $[\text{Co}_9(\text{C})_2(\text{CO})_{19}]^{2-}$ 27
 $[\text{Co}_9(\text{P})(\text{CO})_{21}]^{2-}$ 24, 27
 $[\text{Co}_{10}(\text{N})_2(\text{CO})_{29}]^{4-}$ 28
 $[\text{Co}_{10}(\text{P})(\text{CO})_{22}]^{3-}$ 24, 27, 28
 $[\text{Co}_{11}(\text{C})_2(\text{CO})_{22}]^{2-}$ 27
 $[\text{Co}_{13}(\text{C})_2(\text{CO})_{24}]^{4-}$ 24–6, 28
 $[\text{Co}_{13}(\text{N})_2(\text{CO})_{24}]^{3-}$ 24–6, 28
 $[\text{Co}_{14}(\text{N})_3(\text{CO})_{26}]^{3-}$ 28
 homonuclear iron clusters
 $[\text{Fe}_4(\text{C})(\text{CO})_{12}]^{2-}$ 6–8, 9
 $\text{Fe}_4(\text{C})(\text{CO})_{13}$ 6–8, 9
 $[\text{Fe}_4(\text{N})(\text{CO})_{11}(\text{PPh}(\text{C}_5\text{H}_4\text{FeC}_5\text{H}_5)_2)]^{3-}$ 10, 10
 $[\text{Fe}_4(\text{N})(\text{CO})_{12}]^{3-}$ 6–8, 9
 $[\text{Fe}_4(\text{N})(\text{CO})_{13}(\text{PMe}_2\text{Ph})]^{3-}$ 10
 $[\text{Fe}_4(\text{N})(\text{CO})_{13}(\text{PPh}_3)]^{3-}$ 10
 $\text{Fe}_5(\text{C})(\text{CO})_{12}(\text{PMe}_2\text{Ph})_3$ 12
 $[\text{Fe}_5(\text{C})(\text{CO})_{14}]^{2-}$ 11–13, 11
 $\text{Fe}_5(\text{C})(\text{CO})_{15}$ 11–13, 11, 12
 $[\text{Fe}_5(\text{N})(\text{CO})_{14}]^{3-}$ 11–13, 11, 13
 $[\text{Fe}_6(\text{C})(\text{CO})_{16}]^{2-}$ 13–14, 13, 14
 $[\text{Fe}_6(\text{N})(\text{CO})_{15}]^{3-}$ 13–14, 13, 14
 homonuclear nickel clusters
 $[\text{Ni}_7(\text{C})(\text{CO})_{12}]^{2-}$ 34
 $[\text{Ni}_8(\text{C})(\text{CO})_{16}]^{2-}$ 34
 $[\text{Ni}_9(\text{C})(\text{CO})_{17}]^{2-}$ 32, 32
 $[\text{Ni}_{10}(\text{C})_2(\text{CO})_{16}]^{2-}$ 34
 $[\text{Ni}_{11}(\text{C})_2(\text{CO})_{15}]^{4-}$ 34
 $[\text{Ni}_{12}(\text{C})_2(\text{CO})_{16}]^{4-}$ 34
 $[\text{Ni}_{16}(\text{C})_4(\text{CO})_{23}]^{4-}$ 34
 $[\text{Ni}_{32}(\text{C})_6(\text{CO})_{36}]^{6-}$ 32–4, 33
 $[\text{Ni}_{38}(\text{C})_6(\text{CO})_{42}]^{6-}$ 34, 35
 $[\text{Ni}_{38}(\text{H})(\text{C})_6(\text{CO})_{42}]^{6-}$ 34, 34
 homonuclear osmium clusters
 $[\text{Os}_{10}(\text{C})(\text{CO})_{24}]^{2-}$ 19–20, 19, 20
 $[\text{Os}_{10}(\text{H})_4(\text{CO})_{24}]^{2-}$ 20, 21
 $[\text{Os}_4(\text{N})(\text{CO})_{12}]^{3-}$ 20
 $[\text{Os}_5(\text{C})(\text{CO})_{14}]^{2-}$ 18, 18
 $\text{Os}_5(\text{C})(\text{CO})_{15}$ 18, 18
 $\text{Os}_5(\text{C})(\text{CO})_{16}$ 20
 $[\text{Os}_6(\text{P})(\text{CO})_{18}]^{3-}$ 18–19, 19
 homonuclear rhenium clusters
 $[\text{Re}_6(\text{C})(\text{CO})_{19}]^{2-}$ 36

transition metal (*continued*)[Re₇(C)(CO)₂₁]³⁻ 35–6, 35[Re₈(C)(CO)₂₄]²⁻ 35–6, 35

homonuclear rhodium clusters

[Rh₆(C)(CO)₁₃]²⁻ 31[Rh₆(C)(CO)₁₅]²⁻ 29–30, 29[Rh₆(N)(CO)₁₅]²⁻ 29–30, 29[Rh₇(N)(CO)₁₅]²⁻ 30, 30Rh₈(C)(CO)₁₉ 31[Rh₉(P)(CO)₂₁]²⁻ 32[Rh₁₀(P)(CO)₂₂]³⁻ 32[Rh₁₂(C)₂(CO)₂₄]²⁻ 30–1Rh₁₂(C)₂(CO)₂₅ 32[Rh₁₂(N)₂(H)(CO)₂₃]³⁻ 32[Rh₁₄(C)₂(CO)₃₃]²⁻ 32[Rh₁₄(N)₂(CO)₂₅]²⁻ 32[Rh₁₅(C)₂(CO)₂₈]²⁻ 32[Rh₂₃(N)₄(CO)₃₈]³⁻ 32[Rh₂₈(N)₄(H)₂(CO)₄₁]⁴⁻ 32

homonuclear ruthenium clusters

[Ru₄(N)(CO)₁₂]⁻ 18Ru₅(C)(CO)₁₅ 15, 15[Ru₅(N)(CO)₁₄]⁻ 15, 15[Ru₆(C)(CO)₁₆]²⁻ 18Ru₆(C)(CO)₁₇ 18[Ru₈(P)(CO)₂₂]⁻ 15–16, 16[Ru₁₀(C)₂(CO)₂₄]²⁻ 18[Ru₁₀(N)(CO)₂₄]⁻ 18

transition metals

carbonyl compounds 99, 100

complexes with boron 72–3, 73, 74

complexes with nitrogen 93–4

complexes with oxygen 101

fluorides 105, 106

hydrides 62–4, 145–7

deuterium studies 149–51

DQCC determination 154–61

NMR applications 147–9

metal-to-carbon p-bonding 321–2, 322

methyleneimidazoline complexes 373–6

organotransition metal complexes

106–7

cadmium 119–20

cobalt 114

copper 118

iron 112–13, 113

manganese 109–11, 111, 112

mercury 120–1

molybdenum 107

osmium 114

platinum 115–18, 117, 118, 119

rhodium 114, 115, 116

ruthenium 113

silver 118–19, 120

technetium 111

tungsten 108–9, 110

vanadium 107, 108, 109

bis-(trimethylsilyl) acetylene (btsa)metal complexes **180**

tritopic polyradicals 229–37

tungsten

NMR properties of spin-1/2 nuclei **54**

organometallic complexes 108–9, 110

uranium

simple aryl-bridged ditopic

polyradicals 278

vanadium

ditopic polyradicals with

1,4–diethynylphenyl units 279

NMR properties of quadrupolar
nuclei **55**

organometallic complexes 107, 108, 109

(RC=CR')_n-bridged ditopic

polyradicals 271–2, 271, 274, 275

crystallographic data **270**

simple aryl-bridged ditopic

polyradicals 278–9

xenon

NMR properties of spin-1/2 nuclei **54**

NMR studies 105–6

ylidic ligands 337, 338, 380–4

bond lengths and angles **382**, **383**, **383**

iminoimidazolines

alkylation and acylation 352–8

aluminium iminoimidazolides 351

bonding in 2-imidoimidazolines

343–5, 339–43

coordination at metal centres 358–62

metalation and silylation 343

phosphanes 346–51

structure of [Li₁₂O₂Cl₂(ImN)₈] 345

synthesis and structure 338–9

- titanium iminoimidazolides 351–2
- methyleneimidazolines
 - bonding in Im-CS₂ and Im-CS₂²⁻ 379
 - bonding in iodine complexes 372–3
 - bonding in
 - 2-methyleneimidazolines 365–9
 - C-substituted
 - 2-methyleneimidazolines 376–9
 - reactions with main group element electrophiles 369–72
 - synthesis and structure 362–4
 - transition metal complexes 373–6
- ytterbium
 - NMR properties of spin-1/2 nuclei **54**
- yttrium
 - methyleneimidazolines 376, 377
 - NMR properties of spin-1/2 nuclei **54**
- Zeeman effect 53, 232
- Zeise's anion 177, 177
- Zeise's dimer 177, 181
- Zeise's salt 181, 181, 185
- zero-field splitting 232–3, 233
- zinc
 - NMR properties of quadrupolar nuclei **55**
- zirconium
 - complexes with catalytic activity 78–9
 - NMR properties of quadrupolar nuclei **55**
 - zirconium–cyclopentadienyl complexes 193